Design of polymetallic uranium assemblies for the development of single molecule magnets

Lucile Chatelain

Communauté
UNIVERSITÉ Grenoble Alpes

THÈSE

Pour obtenir le grade de

DOCTEUR DE LA COMMUNAUTÉ UNIVERSITÉ DE GRENOBLE ALPES

Spécialité **Chimie Inorganique et Bio-inorganique**

Arrêté ministériel : 7 août 2006

Présentée par

Lucile CHATELAIN

Thèse dirigée par **Marinella MAZZANTI** et
codirigée par **Philippe MOISY**
préparée au sein du **Laboratoire de Reconnaissance Ionique et Chimie de Coordination** du **Service de Chimie Inorganique et Biologique, INAC, CEA-Grenoble / Groupe de Chimie de Coordination, ISIC, EPFL**
dans **l'Ecole Doctorale Chimie Sciences Du Vivant**

Conception d'assemblages polymétalliques d'uranium pour le développement de molécules aimants

Soutenance prévue le **20 juillet 2016**, devant le jury composé de :

Pr. Richard WINPENNY
Professeur à l'Université de Manchester (Rapporteur)
Dr. Gregory NOCTON
Chargé de recherche à l'Ecole Polytechnique (Rapporteur)
Pr. Kay SEVERIN
Professeur à l'Ecole Polytechnique Fédérale de Lausanne (Examinateur)
Dr. Carole DUBOC
Directrice de recherche à l'Université Grenoble Alpes (Président)
Pr. Marinella MAZZANTI
Directrice de recherche à l'Ecole Polytechnique Fédérale de Lausanne (Directrice de thèse)
Dr. Philippe MOISY
Directeur de recherche au CEA-Marcoule (co-Directeur de thèse)

Communauté
UNIVERSITÉ Grenoble Alpes

THESIS

For obtaining the degree of

DOCTOR OF PHILOSOPHY OF COMMUNAUTÉ UNIVERSITÉ DE GRENOBLE ALPES

Specialty : **Inorganic and Bio-Inorganic Chemistry**

Arrêté ministériel : 7 août 2006

Presented by

Lucile CHATELAIN

Thesis directed by **Marinella MAZZANTI** and
codirected by **Philippe MOISY**
Thesis prepared in the **Laboratoire de Reconnaissance Ionique et Chimie de Coordination** du **Service de Chimie Inorganique et Biologique, INAC, CEA-Grenoble** / **Group of Coordination Chemistry, ISIC, EPFL**
In the **École Doctorale Chimie Sciences de Vivant**

Design of polymetallic uranium assemblies for the development of single molecule magnets

Thesis scheduled the **20 july 2016**, in presence of :
Prof. Richard WINPENNY
Professor at the University of Manchester (Rapporteur)
Dr. Gregory NOCTON
Chargé de recherche à l'Ecole Polytechnique (Rapporteur)
Prof. Kay SEVERIN
Professeur à l'Ecole Polytechnique Fédérale de Lausanne (Examinateur)
Dr. Carole DUBOC
Directrice de recherche à l'Université Grenoble Alpes (Président)
Prof. Marinella MAZZANTI
Directrice de recherche à l'Ecole Polytechnique Fédérale de Lausanne (Directrice de thèse)
Dr. Philippe MOISY
Directeur de recherche au CEA-Marcoule (co-Directeur de thèse)

Résumé

L'étude de la chimie des actinides est essentielle dans le cadre de la technologie nucléaire pour le développement de nouveaux combustibles, pour l'étude du retraitement des déchets nucléaires et la migration des actinides dans l'environnement mais aussi pour la compréhension fondamentale des interactions actinide/ligand et la formation de liaisons multiples. Les propriétés magnétiques des molécules polymétalliques d'actinides sont particulièrement intéressantes pour explorer la communication magnétique entre différents centres métalliques. De plus, ces molécules ont été identifiées comme particulièrement prometteuses pour la conception de molécules aimants. L'uranium a une grande réactivité redox notamment due à ses multiples degrés d'oxydation accessibles et forme aisément des assemblages polynucléaires. Néanmoins, très peu de synthèses contrôlées de complexes polymétalliques d'uranium et de neptunium ont été décrites dans la littérature. La première approche de ce travail repose sur la synthèse de clusters oxo/hydroxo d'uranium à partir de l'hydrolyse contrôlée d'uranium tétravalent en présence d'un ligand organique rencontré dans l'environnement. Cette étude a mené à une famille de clusters aux géométries originales, dont la taille varie en fonction des conditions réactionnelles employées. Cependant les clusters obtenus ne mènent pas à des propriétés de molécules aimants. Dans le but de favoriser une plus grande interaction entre les métaux par le ligand pontant, l'interaction cation-cation a été utilisée pour la synthèse rationnelle d'assemblages d'uranyle(V). Par le passé, peu de complexes d'uranyle(V) ont été isolés à cause de son instabilité vis-à-vis de la dismutation ; cependant, l'optimisation du ligand organique et des conditions de synthèse ont finalement permis de stabiliser l'uranyle(V). Nous avons utilisé des complexes stables d'uranyle(V) comme brique de base pour former des molécules hétéronucléaires avec des métaux 3d et 4f. Un réglage fin des conditions de réactions a mené à une conception rationnelle d'assemblages discrets ou polymériques. L'étude des propriétés magnétiques de ces assemblages d'uranium a mis en valeur des propriétés de molécules ou chaînes aimants avec de hautes valeurs d'énergie de relaxation. L'uranyle(V) a également été utilisé comme modèle structural du neptunium qui est plus radioactif permettant d'isoler un complexe isostructural homométallique de neptunyle(V) grâce à des conditions réactionnelles similaires. Finalement, des ligands nitrures favorisant la formation de liaison multiples uranium-ligand, ont été utilisés pour construire de nouveaux complexes binucléaires d'uranium supportés par des ligands silanols. De nouvelles molécules, sans précédent, contenant des nitrures comme ligand pontant associés à de l'uranium au degré d'oxydation +III ont été isolées et caractérisées.

Mots-clés

uranium, uranyle(V), neptunyle(V), interaction cation-cation, CCI, cluster, magnétisme, molécule aimant, SMM, chaine aimant, SCM, acide benzoïque, nitrure, silanol

Discipline

Chimie Inorganique

Laboratoires

- Laboratoire de Reconnaissance Ionique et Chimie de Coordination Service de Chimie Inorganique et Biologique, UMR-E3 CEA-UJF Institut Nanosciences et Cryogénie, CEA Grenoble 17 Rue des Martyrs, 38054 Grenoble Cedex, France
- Ecole polytechnique fédérale de Lausanne
Institut des sciences et ingénierie chimiques
Groupe de Chimie de Coordination
CH-1015 Lausanne, Suisse

Abstract

The study of actinide chemistry is not only essential for the development of nuclear fuel, nuclear fuel reprocessing or environmental clean up, but also for the understanding of fundamental actinide/ligand interactions and multiple bounding. The magnetic properties of polynuclear actinide molecules are of significant interest to investigate the magnetic communication between the metallic centres. Furthermore, they are highly promising for the design of molecular magnets. Uranium undergoes redox reactions due to a wide range of available oxidation states and easily forms polynuclear assemblies. However, only a few controlled synthetic routes towards these polynuclear uranium assemblies are described in the literature. In this context, the first part of this work was dedicated to the synthesis of oxo/hydroxo uranium clusters from the controlled hydrolysis of tetravalent uranium in the presence of an environmentally relevant ligand. This led to the synthesis of clusters with novel geometries, for which size could be varied as a function of the reaction conditions employed. However, the obtained clusters do not behave as SMM. In order to gain a stronger interaction between metallic centres, the cation-cation interaction was used to rationally design polynuclear uranyl(V) complexes. The isolation of uranyl(V) complexes had been limited in the past by its disproportionation, however, a fine tuning of the organic ligand and reaction conditions finally allowed to stabilise uranyl(V). We used stable uranyl(V) units as building block to form heteronuclear complexes with 3d and 4f metals with polymeric or discrete structures. The study of the magnetic properties of the uranium polynuclear assemblies was carried out and revealed single molecule or chain magnet behaviours with high energy barriers. The uranyl(V) unit was also used as a structural model for the more radioactive neptunium element, allowing the isolation of an isostructural trinuclear neptunyl(V) assembly in similar reaction conditions. Finally, the use of a nitride ligand as a bridging unit, allowing the formation of uranium-ligand multiple bonds, was explored to build novel di-uranium complexes supported by siloxy ligands. Nitride molecules containing unprecedented uranium in the +III oxidation state were isolated and characterised.

Keywords

uranium, uranyl(V), neptunyl(V), cation-cation interaction, CCI, cluster, magnetism, single molecule magnet, SMM, single chain magnet, SCM, benzoic acid, nitride, silanol

Specialty

Inorganic Chemistry

Laboratories

- Laboratoire de Reconnaissance Ionique et Chimie de Coordination
Service de Chimie Inorganique et Biologique, UMR-E3 CEA-UJF
Institut Nanosciences et Cryogénie, CEA Grenoble
17 Rue des Martyrs, 38054 Grenoble Cedex, France
- Ecole polytechnique fédérale de Lausanne Institut des sciences et ingénierie chimiques Groupe de Chimie de Coordination
CH-1015 Lausanne, Switzerland

Acknowledgements
Remerciements

First of all I would like to thank all the members of my committee for accepting to review this thesis work.

I would like to acknowledge my supervisor Prof. Marinella Mazzanti for sharing her passion for coordination chemistry and research with me, encouraging me to pursue my PhD. I am grateful for her support and the various opportunities she has given me to develop through a wide variety of projects and different laboratory settings! I would like to thank my co-supervisor Dr Philippe Moisy for supporting my desire to handle transactinide elements and allowing me to spend few months in the CEA of Marcoule.

A lot of people from various laboratories have been extremely helpful throughout my PhD and deserve my gratitude. Au sein du RICC/SCIB du CEA-Grenoble, je tiens à remercier particulièrement Jacques Pécaut, toujours prêt à partager ses connaissances de cristallographie, son sourire et son soutien, qui ont continué même après le déménagement à l'EPFL. Je voudrais aussi remercier Jean-François Jacquot pour son aide lors des mesures de magnétisme, Colette Lebrun, pour la spectrométrie de masse, Pierre-Alain Bayle pour la spectroscopie RMN, Serge Gambarelli pour les mesures de RPE, Lydia Plassais pour les synthèses organiques et un grand merci à Lionel Dubois pour ses précieux conseils. Merci également à Pascale Maldivi pour m'avoir accueillie au sein de son laboratoire et à Zohra Termache, secrétaire hors pair.

Many thanks to all the members of the RICC group, with whom I shared my office, the glovebox and everyday laboratory life, for all their help and support and for making my time in the lab so enjoyable during my master internship and two first years of PhD: Maria, Marie, Julie, Clément, Valentin, Gaylord, Yves, Céline, Oliver, Sebastiano, Jennifer, Matthieu and Johannes. Special thanks to Victor, who introduced me to uranium chemistry and contributed to my choice of pursuing this PhD.

Au CEA-Marcoule, je voudrais remercier Marie-Christine Charbonnel pour m'avoir accueillie au sein de son laboratoire. J'aimerais remercier toute l'équipe du LN1 qui m'a accordée beaucoup de temps pour que mes deux mois se déroulent au mieux et toujours dans la bonne humeur. Je voudrais remercier Laëtitia Guérin, Nathalie Boubals, Thomas Dumas et particulièrement Matthieu Autillo et Christelle Tamain.

I had the pleasure and privilege to spend almost a month at the University of Manchester with Dr. Floriana Tuna for the ac magnetic measurements. I would like to thank her for her time and for teaching me so many things about magnetism. I am also very thankful to Prof. Roberto Caciuffo and his group for the ac magnetic measurements of the neptunium compounds in ITU Karlsruhe.

Au sein du groupe GCC de l'EPFL, je voudrais particulièrement remercier Anne-Sophie Chauvin pour son soutien, toujours prête à nous accorder du temps. Je tiens à remercier Euro Solari pour son expertise et son aide, notamment dans la collecte de nos cristaux, Rosario Scopelliti pour la résolution de nos structures, Pascal Mieville pour les études RMN, Yoann Dind pour sa précieuse aide pour que nos ordinateurs fonctionnent et un grand merci à Nadia Gauljaux toujours prête à résoudre nos problèmes administratifs.

And I would like to thank all the members of the GCC team, with whom I shared my office, the glovebox and everyday laboratory life for the last two years of my PhD: Marta, Rory, Sarah, Anna, Joshua, Mathieu, Vipul, and a special thanks to Julie, again, for moving with me to the EPFL, for her support, her help, her friendship and the car-sharing, most of the time in good mood!

Je tiens à remercier mes amis rencontrés au fil des années depuis mon village d'enfance, au lycée, à l'université, à l'ENS Lyon, la prépa agrég et mon équipe de TREC, qui ont su me soutenir au cours de ces années, notamment, Noémie, Clemence, Lydie, Aline, Chloé, Emilie, Sara(h), Claire, Elodie, Anaïs et Cécile.

Un immense merci à ma famille, pour leurs encouragements et précieux soutien tout au long de ces longues années d'études, particulièrement mes parents, sans qui tout cela n'aurait jamais été possible, Thomas, Loïc et leurs familles qui se sont agrandies au cours de cette thèse.

Enfin, à celui qui par son soutien infaillible a largement contribué à la réussite de mes études, un grand merci à toi, Arnaud.

Table of contents

CHAPTER I. INTRODUCTION

I.1) The Actinides

Among the actinide family, uranium and thorium are the two most studied elements. Notably, these two elements (also with the protactinium element) are naturally found in significant quantities in the earth's crust whereas the transuranic atoms are man-made. Consequently, uranium and thorium were discovered earlier than the transuranic elements in 1789 and 1829, respectively, while the other actinide elements were discovered in the 20th century as a consequence of the Manhattan project and the work of Glenn Seaborg. One common property of the actinides is their radioactivity, with huge discrepancies in lifetime and activities. With their fissile abilities, uranium and plutonium have been extensively used in the nuclear applications. For processing nuclear fuels and weapons and radioactive-waste clean up, it is critical to understand the fundamental chemistry and speciation of actinides.[1] These chemical elements exhibit unique characteristics and have the potential to accomplish chemistry not possible with d-transition metals. The following part summarises some of the properties of 5f-element coordination chemistry.[2,3]

I.1.1) Fundamental properties

The bonding in 5f actinide elements lies in between the two extremes defined by the d-block elements and the lanthanides. The radial extension of the 5f orbitals is larger than for the 4f orbitals, as highlighted by comparing the radial distribution of the orbitals of Nd^{3+} and U^{3+} (Figure I- 1).[4,5] Consequently, in contrast to the lanthanides, the actinide-ligand interaction presents a much greater degree of covalency. Due to mostly ionic interactions, a weak stereochemical preference and a labile coordination sphere occur for actinides as for lanthanides, leading to variable coordination numbers (from 3 to 12) and geometries.[6] In contrast to lanthanide complexes, the sensitivity of the spectroscopic and magnetic properties to the coordination environment is larger due to the greater degree of covalent character of actinide-ligand interactions. It should also be noted that due to the larger size of the actinides compared to the lanthanides, relativistic effects are also increased for actinides. The combination of ligand-field and spin-orbit coupling considerably complicates the

electronic structure of actinide coordination compounds. Magnetic and spectroscopic properties are thus challenging to interpret.[7]

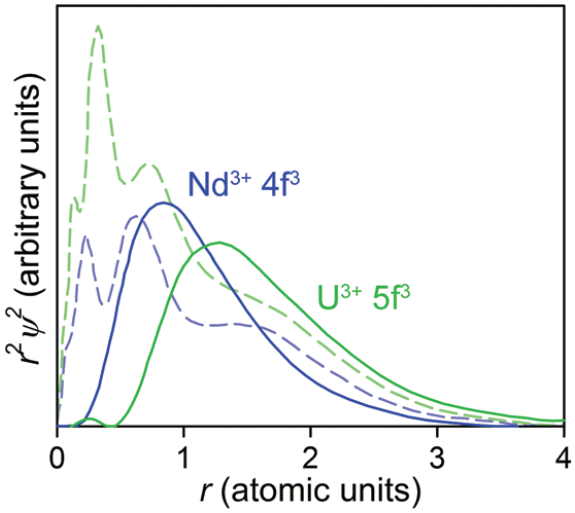

Figure I- 1 Radial probability distribution functions for trivalent neodymium and uranium. Solid blue and green lines represent the probability distributions for the three valence f electrons of Nd^{3+} and U^{3+} respectively, relative to their core electrons (dashed lines).[8]

The redox chemistry of 5f-element complexes also displays intermediate features between the lanthanide and d-block metals. The lighter actinide elements have many characteristics in common with d-block elements, such as multiple accessible oxidation states from +II to +VII, exhibiting rich redox chemistry. On the other hand, similarly to the lanthanides, the chemistry of the heavier actinides is dominated by the trivalent oxidation state (Table I- 1).[2,5]

Table I- 1 Oxidation states of the actinides. The most stable states are shown in red. Adapted from [9]

Ac	Th	Pa	U	Np	Pu	Am	Cm	Bk	Cf	Es	Fm	Md	No	Lr
	2		2			2			2	2	2	2	2	
3			3	3	3	3	3	3	3	3	3	3	3	3
	4	4	4	4	4	4	4	4	4					
		5	5	5	5	5								
			6	6	6	6								
				7	7	7								

Within the accessible oxidation states, two different behaviours exist. The compounds of actinides in low oxidation states usually contain An^{n+} (n = 2, 3, 4) cations, while the higher oxidation states are mostly encountered as actinyl moieties AnO_2^{+} and AnO_2^{2+}. In actinyls, the actinide centre is bound linearly to two oxygen atoms, resulting in an ion with an overall charge of +1 or +2. The additional ligands are coordinated in the equatorial plane of the

actinyl ion, with 4 to 6 coordination sites. In contrast, the An^{n+} ions do not tend to exhibit geometric preferences and a large array of coordination numbers are observed (from 3 to 12). The effective charge of the actinide centre decreases along the series: $An^{4+}>AnO_2^{2+}>An^{3+}>AnO_2^{+}>An^{2+}$.[10]

Actinides and lanthanides are Pearson hard acids. They bind preferentially to hard acids like negative oxygen and fluoride donors rather than to soft donors. However, the increased covalency of the actinides with respect to the lanthanides results in a slightly higher affinity for soft electron donors, such as aromatic amines. This increased affinity for soft donors has been used to develop selective extractants for the separation of minor actinides (such as Am^{3+}) from lanthanides in spent nuclear fuel reprocessing.[11-13]

During this work, I have mainly investigated the chemistry of uranium under anhydrous conditions. I also had the chance to perform some studies with neptunyl(V). Consequently, the introduction focuses mostly on the chemistry of these two elements in anhydrous conditions.

I.1.2) Survey of oxidation states

I.1.2.1) +VI oxidation state

Hexavalent actinides are mainly present in the form of the actinyl(VI) AnO_2^{2+}. Uranyl(VI) is the main species observed in the +VI oxidation state in the actinide series and is found naturally in the environment. The coordination chemistry of uranyl(VI) has been extensively studied both in aqueous[14,15] and organic solution[16-18] since it represents the most stable species of uranium. A wide variety of mononuclear and polynuclear complexes, both in aqueous or organic media, has been characterised with various ligands, some of which include: multidentate N-donor ligands (Schiff base salicylaldehyde-derivatives: salophen, salen),[19] compartmental ligands,[20] carbonates,[21] carboxylates,[22] and selenates.[23,24] The increasing number of characterised polynuclear peroxide-bridged uranyl(VI) clusters should also be highlighted. The size of the clusters, containing from 16 to 120 uranium atoms, can be modulated by using different alkali cations to balance the charge of the clusters, or by varying the pH of the solution.[15]

The most common uranium(VI) precursors used for the synthesis of compounds in anhydrous conditions are uranyl halide derivatives. One of the most used is the $[UO_2Cl_2(THF)_3]$ complex.[25] This complex results from the treatment of $UO_2Cl_2(OH_2)_n$ obtained from the dissolution of UO_3 in aqueous HCl, with an excess of Me_3SiCl in THF.[26] In the group

we also use the iodide precursor $[UO_2I_2(Py)_3]$, which can be prepared from the oxidation of trivalent iodide uranium with pyridine N-Oxide in pyridine.[27]

I.1.2.2) +V oxidation state

As stated before, actinyl-type complexes, built around the AnO_2^+ moiety, dominate the chemistry of the actinides in the +V oxidation state. Neptunium in NpO_2^+ is stable while plutonyl(V) complexes can only be observed transiently.

Uranyl(V) is stable thermodynamically in aqueous solution only in a very small pH region (pH= 2-5), over a very limited range of potential,[28] in concentrated carbonate media,[21,29,30] or in reducing environments at mineral surfaces.[31-33] The low stability of uranyl(V) is due to its rapid disproportionation to UO_2^{2+} and U^{4+} as described in the equation: [9]

$$2\,UO_2^{+}{}_{(aq)} + 4H^+ \longrightarrow UO_2^{2+}{}_{(aq)} + U^{4+}{}_{(aq)} + 2\,H_2O$$

The formation of a binuclear uranyl(V) intermediate through the coordination of one oxo group to the equatorial plane of another actinyl moiety has been shown to be a key step in the disproportionation reaction.[34-37]

In order to prepare stable pentavalent uranyl complexes, non-aqueous solvents and bulky ligands can be used to exclude the presence of protons and to prevent the formation of the dimeric intermediate, respectively.

In 2003, Ikeda and co-workers reported spectroscopic evidence (IR, UV-visible) that uranyl(V) compounds were electrochemically produced from the reduction of uranyl(VI) in the presence of ligands of various denticity (mono, bi- tetra- or pentadentate) such as β-diketonates and Schiff bases (salen, salophen, saldien) using the aprotic solvents dmso or dmf over a large range of potential (-0.52 V to -1.67 V (vs. Fc^+/Fc couple)).[38-46] In these systems, dmso or dmf probably acts as a ligand preventing the aggregates formation leading to electron transfer.[47,48] These electrochemical studies suggest that the choice of an appropriate ligand could stabilise UO_2^+ in solution. However, these complexes were not isolated in the solid state and were only characterised by UV and IR spectroscopies.

The first pentavalent uranyl $[UO_2(OPPh_3)_4](OTf)$ complex characterised by single crystal X-ray diffraction studies was serendipitously isolated by Ephritikhine et al.[49] However, attempts to synthesise this complex by reduction of the hexavalent analogue through chemical or photochemical methods failed.

The first reproducible synthesis of a uranyl(V) complex was developed in our group in 2006, using a different approach, instead of reducing a uranyl(VI) compound, a two electron

oxidation of U(III) was performed to give a UO_2^+ complex. The pentavalent uranyl coordination polymer $\{[UO_2(Py)_5][KI_2(Py)_2]\}_n$, was reproducibly synthesised by oxidation of $[UI_3(THF)_4]$ with a mixture of pyridine N-Oxide and water.[27] The molecular structure of the coordination polymer was determined by X-ray diffraction, as presented in Figure I- 2. A second route for synthesising this compound was later reported by Ephritikhine et al., which consisted of the reduction of $[UO_2I_2(THF)_3]$ with KC_5R_5 (R = Me, H) in pyridine.[50]

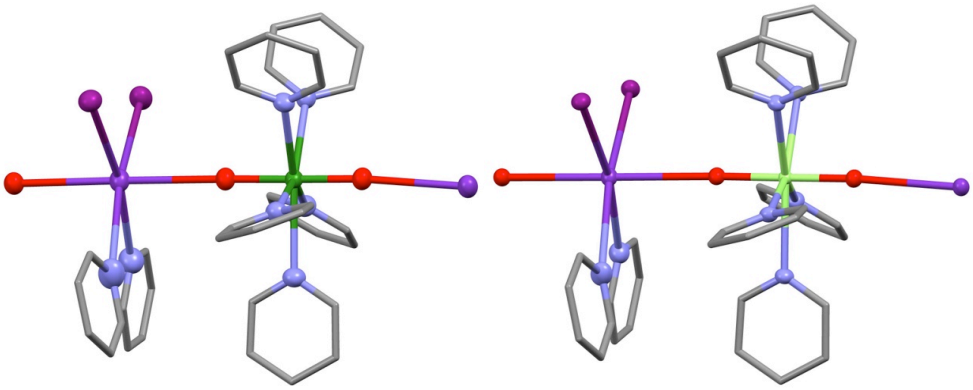

Figure I- 2 Molecular structures of $\{[UO_2(Py)_5][KI_2(Py)_2]\}_n$ (left) and $\{[NpO_2(Py)_5][KI_2(Py)_2]\}_n$ (right) (H were omitted; ligands are represented with pipes for clarity, C are represented in grey, O in red, K in purple, N in blue, Np in light green and U in green)

Recently, an analogous neptunyl(V) $\{[NpO_2(Py)_5][KI_2(Py)_2]\}_n$ polymer was reported, isostructural with $\{[UO_2(Py)_5][KI_2(Py)_2]\}_n$ (Figure I- 2).[51] This complex represents the first practical precursor for the anhydrous study of the coordination chemistry of NpO_2^+. The $\{[NpO_2(Py)_5][KI_2(Py)_2]\}_n$ complex was prepared by boiling dry ‘‘NpO_2Cl’’ in anhydrous pyridine solution, and subsequent addition of KI.

The synthesis of $\{[UO_2(Py)_5][KI_2(Py)_2]\}_n$ provides a very convenient starting material and opened up a new field of exploration for the development of the coordination chemistry of uranyl(V). In our group, the reaction of this polymer with bulky Schiff base ligands in pyridine led to the isolation of stable mononuclear uranyl(V) complexes (Scheme I- 1 (A)).[52-54] In parallel, Hayton and coworkers reported the synthesis of stable uranyl(V) complexes obtained from the reduction of bulky β-diketiminate or diketonate uranyl(VI) complexes (Scheme I- 1 (B))[55-57] and Arnold and coworkers reported the reductive silylation of the uranyl(VI) cation in a macrocyclic ligand (Scheme I- 1 (C)), presented in Chapter III.[58,59]

Scheme I- 1 Representation of ligands stabilising uranyl(V) complexes

A) Mazzanti

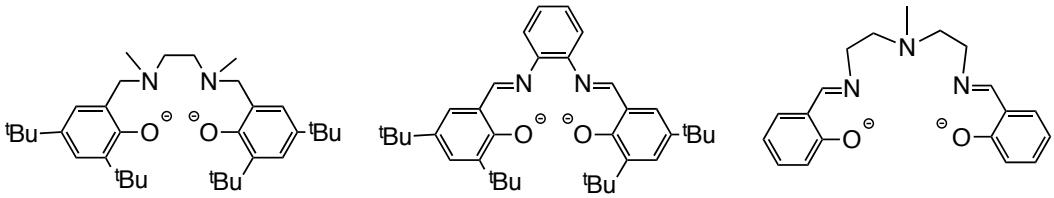

C) Arnold 2008

B) Hayton 2008

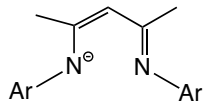

Ar: 2,6-$iPr_2C_6H_3$

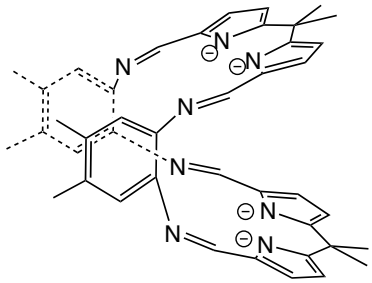

We can finally note that several non-uranyl compounds of U(V) have been characterised with halide and alkoxide ligands more than forty years before the development of uranyl(V) chemistry.[60] Several mononuclear uranium(V) complexes with imido[61-69] or terminal oxo[66,70-72] ligands have also been isolated from the oxidation of low-valent uranium complexes.[73]

I.1.2.3) +IV oxidation state

The +IV oxidation state of uranium is common as it is stable in anaerobic aqueous solutions and is found in the environment.

The mostly used U(IV) precursors in anaerobic and anhydrous conditions are uranium halides. Uranium tetrachloride has been prepared by different methods over the years.[74-77] A popular but dangerous method consists of the reaction of UO_3 with hexachloropropene to produce [UCl_4] as an emerald green solid in quantitative yield.[25] As chloride is not always the optimal halide for salt elimination reactions, the tetraiodides have also received great attention. However, UI_4 decomposes to UI_3 and I_2 at room temperature.[78] Different solvent adducts are known [$UI_4(S)_n$] (S = Py, n = 3 ; S = MeCN, n = 4; S = PhCN, n = 4;[79,80] S = Et_2O, n = 4;[81] S = 1,4-dioxane, n = 2)[82] and they possess increased stability. Depending on the reactivity investigated, the best solvent adduct is used. Thus, the nitrile adducts have found application in the synthesis of nitride-azide clusters[83] but their use is limited by the reactivity of the unsaturated nitrile linkage. The ether adducts [$UI_4(OEt_2)_2$] and [UI_4(1,4-dioxane)$_2$]

represent more versatile iodide precursors as the uranium bound solvents are non-redox active. Each of them is prepared by reacting uranium turnings with iodine in diethylether[81] or 1,2-dioxane.[82]

As for uranyl(VI), uranium(IV) chemistry is well-developed and numerous mononuclear or polynuclear complexes have been reported,[4,18,25] containing a wide variety of ligand such as: multidentate N-donor ligands,[19] carbonates,[21] amides,[84], cyanides,[85] cyclopentadienyl and derivatives,[86] oxo and hydroxo groups.[87]

I.1.2.4) +III oxidation state

Trivalent uranium complexes are less common than their tetravalent counterparts due to the strongly reducing nature of U(III). The uranium(III) ion is highly reactive with oxygen or traces of water. Moreover, the choice of the ligand is crucial in stabilising U(III) as it can react with redox-active ligands, leading to its oxidation or it can disproportionate to U(IV) and U(0).[86,88]

Currently, the THF-solvated uranium triiodide $[UI_3(THF)_4]$ is the most commonly used starting material for accessing low-valent uranium derivatives.[25,89] Different synthetic routes to $[UI_3(THF)_4]$ have been described.[90,91] A convenient and efficient synthesis of the dioxane adduct $[UI_3(1,4\text{-dioxane})_{1.5}]$ was reported recently that consists of the oxidation of uranium turnings with I_2 in 1,4-dioxane.[82] The analogous THF-solvated compound can be obtained upon extraction of $[UI_3(1,4\text{-dioxane})_{1.5}]$ with THF. Another useful precursor is the highly sterically hindered amide $[U\{N(SiMe_3)_2\}_3]$ complex, synthesised from the salt exchange metathesis of $[UI_3(THF)_4]$ with 3 equiv. of $KN(SiMe_3)_2$.[89,91] The amido ligands are easily protonated and the reaction with protonated ligands leads to a reaction mixture free of alkali metal cations and halide anions that could interfere in the complex reactivity. Moreover, this precursor is soluble in hydrocarbon solvents, preventing undesired reactions with oxygenated solvents.

Suitable ligands for the preparation of stable U(III) complexes should provide enough steric bulk and electronic saturation. At first, U(III) chemistry was widely explored with organometallic ligands such as cyclopentadienyl derivatives.[86] In parallel, a few U(III) complexes with bulky monodentate oxygen-donor and nitrogen-donor ligands such as alkoxide, aryloxide,[92] imide,[93] and silylamide[94] (Scheme I- 2 (A)) was reported. More recently, tripodal polydentate O-donor and N-donor ligands have been successfully employed to stabilise U(III) (Scheme I- 2 (B)).[12,95-97]

Scheme I- 2 Selected monodentate and multidentate ancillary ligands employed to support U(III) chemistry

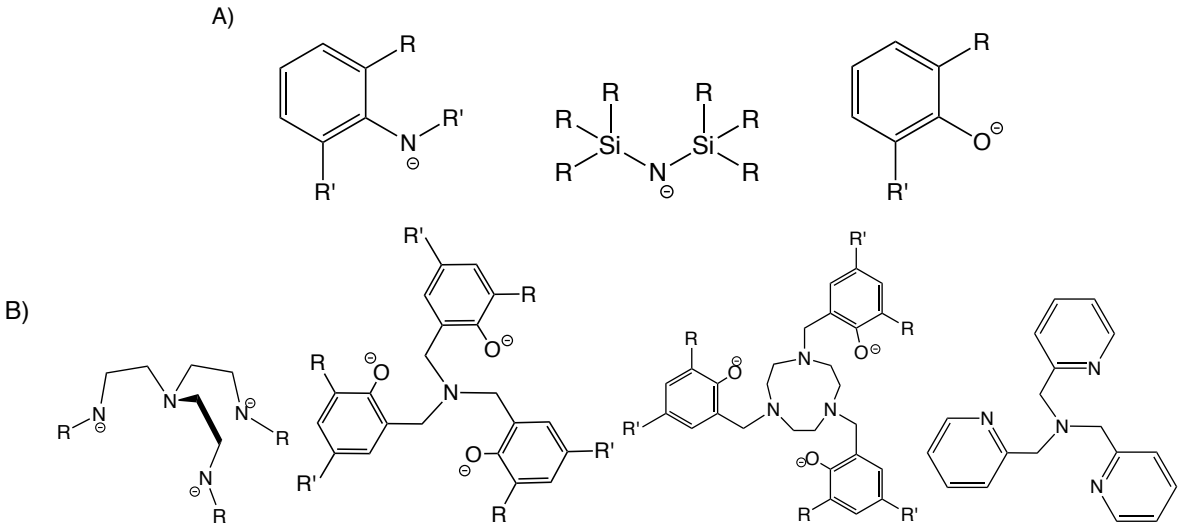

In our group, the use of the tris(tertbutoxy)siloxide ligand, which is bulky, highly soluble in hydrocarbon solvents, cheap and commercially available, has led to the isolation of several uranium(III) complexes.[69,98,99] This ligand allows multiple coordination modes and can also lead to polymetallic assemblies (Scheme I- 3).

Scheme I- 3 Common coordination modes for the $[OSi(O^tBu)_3]^-$ ligand: (a) monodentate (terminal mode); (b) bidentate; (c) monodentate bridging; (d) bidentate bridging.

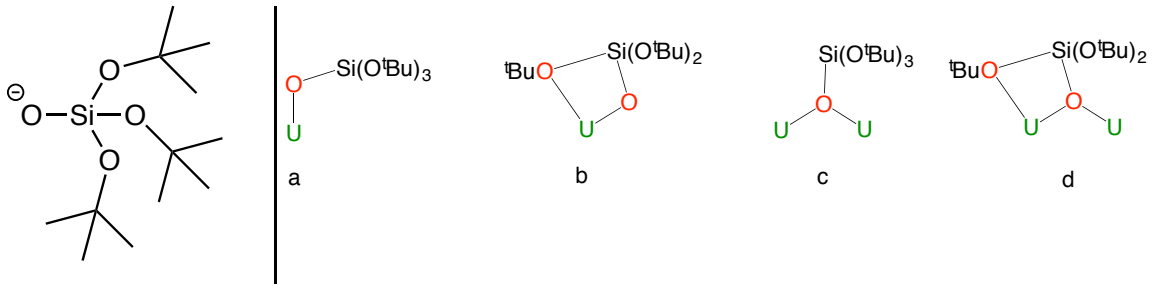

I.1.2.5) +II oxidation state

Very recently, six examples of uranium(II) have also been reported. In these complexes, the U(II) is coordinated by three sterically hindered cyclopentadienyl or by chelating tris(aryloxide) arene ligands (Scheme I- 4) forming ion pairs. The use of [2.2.2-cryptand] or crown ethers to encapsulate the alkali metal cations plays a role in the stability of the complexes.[100-102]

Scheme I- 4 Scheme of the uranium(II) complex [K(2.2.2-crypt)][((^{Ad,Me}ArO)$_3$mes)U] reported by the Meyer group[101]

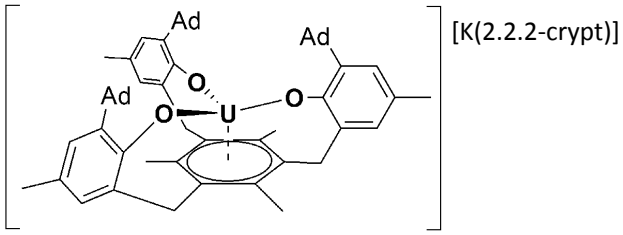

I.1.3) Magnetic properties under static field

Since uranium possesses three common paramagnetic oxidation states ($5f^1$ U(V), $5f^2$ U(IV), and $5f^3$ U(III)), a commonly used analytical method to support the assignment of uranium oxidation state is measurement of magnetic susceptibilities.[103] However, no models describe accurately the magnetic properties of actinides, which is why the evaluation of the magnetic moment of uranium complexes is not as straightforward as it is for transition metal or lanthanide complexes. For any metal, the magnetic moment mostly results from the contributions of the ground state and the low-lying thermally accessible excited states. For d^n transition metals, a good estimation of room-temperature magnetic moment is given by the spin-only formula, $\mu_{eff} = 2\sqrt{S(S+1)}$. For $4f^n$ lanthanides, spin-orbit coupling is large and ligand field splitting is small due to the limited radial extension of the 4f orbitals. In consequence, the Russell-Saunders scheme becomes an accurate model and allows the determination of the ground state defined by a $^{2S+1}L_J$ term. For most of the 4f elements, room-temperature magnetic moments can be approximated by $\mu_{eff} = g_J\sqrt{J(J+1)}$ and correlated with oxidation state.[6] With a greater radial extension of the 5f orbitals meaning that ligand field effects cannot be ignored, combined with large spin-orbit coupling, the actinides are intermediate between the lanthanides and transition metals. Consequently, no simple theoretical scheme used for transition metal or lanthanide complexes can be applied for the actinides.[6,25]

The Russell-Saunders coupling scheme is commonly used as an approximate starting point as it provides a simple model on which to base free ion actinide electronic structure. In this scheme, the ground state of free ions is given by the $^{2S+1}L_J$ terms and some are reported in the Table I- 2. Differences in magnetic properties are observed for actinide complexes in solid-state or in aqueous solutions. Although we are interested in this work by

solid-state magnetic properties of molecular complexes, the magnetic properties of actinide elements in aqueous solutions are currently investigated.[104-106]

Table I- 2 Magnetic moments calculated in the LS scheme for some electronic configuration of uranium, compared to the experimental range of magnetic moments reported for uranium complexes[103]

Configuration	Ground state (free ion)	g_J	μ_{eff} calc. (μ_B)	χT calc. ($cm^3.K.mol^{-1}$)	$\mu_{eff(U)}$ exp. (μ_B)[103]
f^0 (U^{VI})	$^1S_0$	-	-	-	-
f^1 (U^{V})	$^2F_{5/2}$	6/7	2.54	0.80	1.24-3.77
f^2 (U^{IV}, Np^{V})	$^3H_4$	4/5	3.58	1.60	1.36-3.79
f^3 (U^{III})	$^4I_{9/2}$	8/11	3.62	1.64	1.75-3.8

with g_J and μ_{eff} calculated as follow: $g_J = \frac{3}{2} + \frac{(S(S+1)-L(L+1)}{2J(J+1)}$ and $\mu_{eff} = g_J\sqrt{J(J+1)}$

The magnetic moments calculated for the free U(III), U(IV), U(V), Np(V) ions in the LS coupling scheme at room temperature are reported in Table I- 2 together with the range of measured room-temperature magnetic moments for solid uranium complexes in the oxidation states +V, +IV, +III.[103] We can observe that the range is large and the overlap between the different oxidation states is considerable. At room temperature, the experimental value of the magnetic moment may be not sufficient to assign a formal oxidation state. However, in mononuclear complexes of uranium, the shapes of the magnetic moment or χT vs. temperature plots are distinct and more helpful in differentiating different oxidation states.[107-109] Examples of variable-temperature plots for mononuclear (^{R}ArO)$_3$tacn uranium complexes in the +III, +IV and +V oxidation states are represented in Figure I- 3.[107]

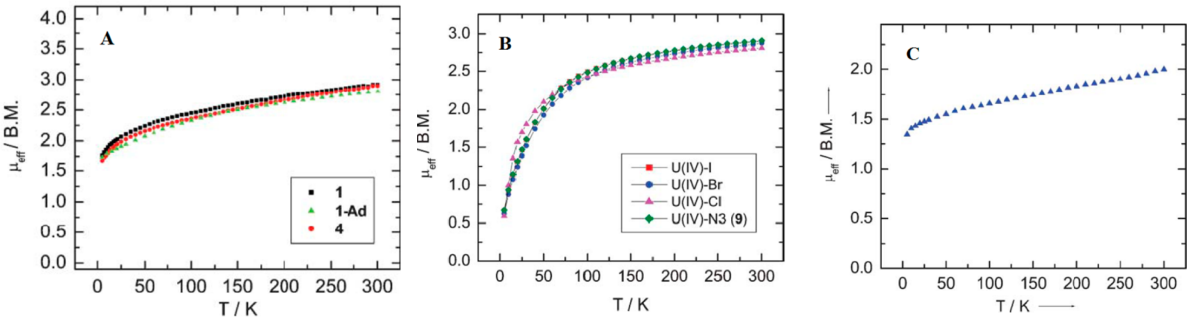

Figure I- 3 Examples of magnetic moments versus temperature plots for a series of related (^{R}ArO)$_3$tacn complexes containing uranium in the A) +III, B) +IV and C) +V oxidation states.[107]

Typically, uranium(III) and uranium(V) magnetic moments decrease slowly with temperature and drop at low temperature, as low-lying states are depopulated. However, appreciable magnetic moments of the half integral spin systems U(III) and U(V) remained at

2 K as they adopted an orbital doublet ground state.[6,25,103] In contrast to U(III) and U(V), the magnetic moment of uranium(IV) complexes usually decreases significantly with temperature. In most of the uranium(IV) complexes, the magnetic moment tends to zero, indicative of a singlet ground state at low temperatures (typically around 50 K). The electronic energy states of uranium(IV) showing successively the effects of electrostatic repulsion, spin-orbit and crystal field splitting (for the ground state) are represented in Figure I- 4.[25] Temperature-independent paramagnetism (TIP) is often observed in uranium(IV) complexes and arises from the coupling of low-lying crystal-field excited states with the ground state.[6,110] This TIP leads to non-zero magnetic moment at 2 K. Such TIP can also be observed in diamagnetic f^0 uranium(VI) compounds where it arises from the coupling of paramagnetic excited states with the ground state.[6]

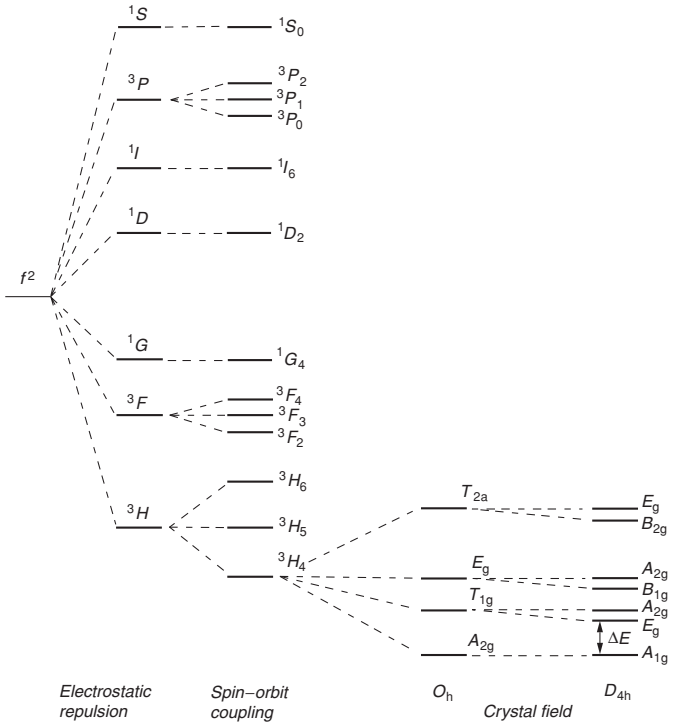

Figure I- 4 Qualitative energy-level diagram for the uranium(IV) ion showing successively the effects of electrostatic repulsion, spin-orbit and crystal field splitting only for the ground state.[6]

Very limited magnetic data on discrete complexes of transactinide and neptunium, in particular, are available. To our knowledge, only one structurally characterised discrete complex of neptunium(IV) has been measured under dc field.[111] The χT vs T plot of this $5f^3$ $[Np(COT)_2]$ complex presented a similar trend to that of $5f^3$ uranium(III) complexes. For neptunium(V), only the magnetic data of a mixed-valent neptunyl(V)-neptunyl(VI) complex, presented in section I.3.1.1.2) have been reported.[112] Magnetic studies have otherwise mostly focused on neptunyl(V) 3D networks.[113,114]

A full understanding of the actinide magnetic properties is not straightforward due to the complexity of the electronic structure of these ions. It is even more complicated in polymetallic assemblies. The combination of different oxidation states and the possibility of magnetic exchange render the interpretation of the magnetic properties of polymetallic complexes of actinides challenging.

I.2) Single Molecule, Ion and Chain Magnets

I.2.1) d-block and lanthanide based molecular magnets

In 1993, Sessoli and coworkers discovered the presence of slow relaxation of the magnetisation in a dodecanuclear manganese $[Mn_{12}O_{12}(O_2CMe)_{16}(H_2O)_4]$ cluster for the first time.[115,116] This molecule possessed the ability to retain magnetisation for relatively long periods of time under a temperature, called the blocking temperature, in the absence of an applied magnetic field. Molecules with these characteristic properties were called single-molecule magnets (SMMs). Ten years later, the same phenomenon was surprisingly observed for a mononuclear lanthanide complex $[LnPc_2]^-$ (Ln = Tb, Dy; Pc^{2-} = phtalocyanine dianion)[117] and these kinds of molecules were called single ion magnets (SIMs). These discoveries drastically changed the field of molecular magnetism and a significant amount of progress has occurred since these early results. The interest in single-molecule magnets is largely due to their potential use in applications such as high density information storage and quantum computing.[118-120]

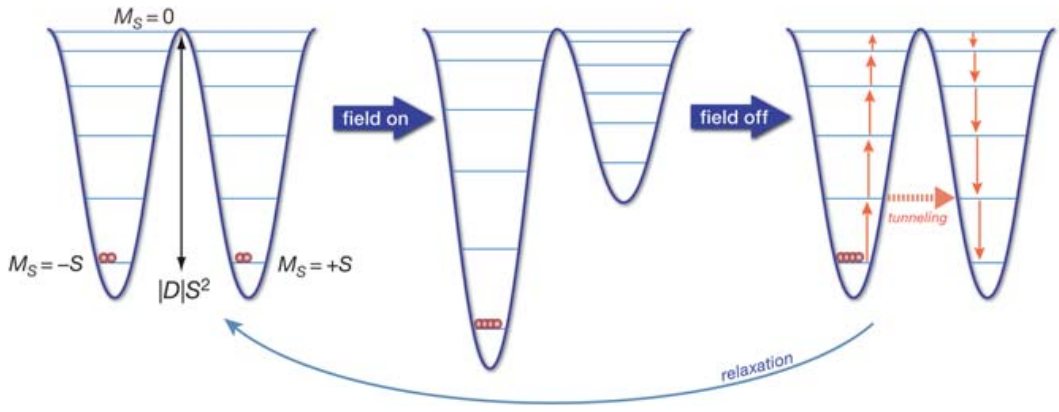

Figure I- 5 Schematic diagram demonstrating the magnetisation and magnetic relaxation processes in a Single Molecule Magnet, taken from ref [121]

Traditionally, the magnetisation and relaxation processes of SIMs or SMMs are described by the 'double-well' diagram of Figure I- 5. The $\pm M_S$ states are plotted on two different wells, separated by an energy barrier $\Delta E=|D|S^2$. The magnitude of the relaxation

barrier is directly proportional to the spin ground state and the magnetic anisotropy, quantified by the axial zero-field splitting parameter. At zero field, the $\pm M_S$ states are equally populated, resulting in zero magnetisation. In the presence of an external magnetic field parallel to the magnetisation axis, the $+M_S$ levels are destabilised while the $-M_S$ levels are stabilised and remain populated. After removal of the external magnetic field, the system returns to the thermal equilibrium. The larger the spin-reversal barrier $\Delta E=|D|S^2$ is, more long will be the relaxation time for the return to thermal equilibrium. This barrier is therefore one critical determinant for the observation of single-molecule magnetism. Experimentally, the pair (τ, T) (with τ the relaxation time associated to the temperature T) is usually determined thanks to magnetic measurements under an oscillating field. The relaxation time follows an Arrhenius law in the thermal regime, $\tau = \tau_0 * \exp(\Delta E/k_B T)$, allowing a quantification of ΔE.

To use SMMs in applications, a much higher relaxation barrier and blocking temperature must be attained. An increase of the relaxation barrier necessitates the maximisation of both S and D. Molecules that possess high spin ground states with a large magnetic anisotropy have been designed. Two different approaches have been investigated in parallel in the past years.

At first, most efforts were devoted to the design of large clusters of d-block transition metals to maximise magnetic exchange between metal ions and the total spin of the ground state.[122-128] Polynuclear transition metal complexes with high spin values were reported up to a record value of S = 83/2.[129,130] However, no significant improvement on the anisotropy barriers for such high-spin systems have been reported due to low magnetic anisotropy. In this context, the Mn_{12} clusters remained the best SMMs for several years ($\Delta E \approx 64$ K, $T_B = 4$ K). The introduction of lanthanide metal ions, which display strong magnetic anisotropy, was investigated and led to considerable improvements. Several studies focused on the synthesis of polynuclear lanthanide clusters[125,131,132] or on the 3d-4f approach, where first-row transition-metal ions are associated with lanthanide ions.[133,134] In these systems, magnetic relaxation was mostly dominated by single ion anisotropy due to the limited radial extension of the 4f orbitals and the essentially electrostatic lanthanide-ligand interactions, limiting the possibility of magnetic exchange. Radical ligands revealed their ability to promote magnetic exchange between lanthanide ions, leading to a considerable rise of the blocking temperature to 14 K.[135-137]

In parallel, another route investigated is the design of mononuclear molecules behaving as SIMs. The first SIM, a terbium complex, indeed displayed a larger anisotropy barrier than large polymetallic clusters. During the course of this PhD, numerous SIMs were reported that exhibited considerably high anisotropy barriers, with a recent record of 1025 K for a mono-dysprosium complex, and blocking temperatures (maximum 20 K).[138-142] These

consequent increases arose from a better understanding of the importance of the symmetry to maximise magnetic anisotropy.[143,144] The strategies have since been focused on ligand design to favoured coordination geometries around the metallic centre, improving the magnetic anisotropy. Interestingly, these principles were also recently applied to mononuclear transition metal complexes, leading to improved SIM behaviours.[145-149] A few examples of SMMs and SIMs are reported in Table I- 3.

Table I- 3 Relaxation barrier and blocking temperature for selected SMMs and SIMs of bloc d and 4f elements

	ΔE (K)	τ_0 (s)	T_B (K)	H_{coer} (T) (sweep rate, $T.s^{-1}$)
SMM				
$[Mn_{12}O_{12}(CH_3COO)_{16}(H_2O)_4]$ [115]	61	$2.1.10^{-7}$	4	1 at 2.2 K
$[Mn_6O_2(sao)_6(O_2CPh_2)(EtOH)_6]$ [150]	86.4	2.10^{-10}	4.5	1.5 at 2.9 K (0.14)
$[\{[(Me_3Si)_2N]_2(THF)Dy\}_2N_2]^-$ [135]	177	8.10^{-9}	8.3	1.5 at 2 K (0.08)
$[\{[(Me_3Si)_2N]_2(THF)Tb\}_2N_2]^-$ [136]	326.6	$8.2.10^{-9}$	14	5 at 11 K (0.009)
$[(Cp'_2Dy)\{\mu\text{-}P(H)Mes\}]_3$ [151]	300	$6.53.10^{-9}$	4.4	0
$[Cr^{III}_2Dy^{III}_2(OMe)_2(O_2CPh)_4(mdea)_2(NO_3)_2]$ [152]	77	$5.1.10^{-8}$	3.7	2.8 at 1.8 K (0.003)
$[Fe_2Dy(L)_2(H_2O)]ClO_4$ [153]	459	$1.11.10^{-11}$	-	-
SIM				
$[TbPc_2]TBA$ [117]	330.9	$6.25.10^{-8}$	1.7	0
$[DyPc_2]TBA$ [117]	40.3	$6.26.10^{-6}$	1.7	0
$[Dy(BIPM^{TMS})_2][K(18C6)(THF)_2]$ [140]	721 /813	$1.11.10^{-12}$ / $5.65.10^{-13}$	10	0.8 at 1.8 K (0.0035)
$[Dy_4K_2O(O^tBu)_{12}]$ [125]	692	$6.6.10^{-11}$	5	0.15 at 0.03 K (0.14)
$[Dy(Cy_3PO)_2(H_2O)_5]Br_3$ [141]	543	2.10^{-11}	20	1.25 at 2 K (0.02)
[Dy(bbpen)Br] [142]	1025	$4.21.10^{-12}$	14	0.6 at 2 K (0.02)
$[Fe(C(SiMe_3)_3)_2]^-$ [145]	325	1.33×10^{-9}	4.5	0

Meanwhile, in 2001, a 1D polymeric molecule displaying slow relaxation of the magnetisation was reported.[154] Such polymeric molecular magnets were called single chain magnets (SCMs). A chain can behave as a magnet if large uniaxial anisotropy, strong intra-chain magnetic interactions between high-spin magnetic units of the 1D arrangement and negligible inter-chain magnetic interaction are combined.[155] [118,156-160] As for SIMs and SMMs, the SCM properties can be compared to each other through the height of their energy barrier and blocking temperature. However, the relaxation mechanism is different compared to SMMs. A simple model consists of considering a chain of spins for which only two orientations are possible, defining an Ising system. The relaxation process begins with the reversal of one spin in the chain, which costs energy equal to $4JS^2$, due to the magnetic exchange interactions (J) between two neighbouring spins.[155] The propagation mechanism is called a random walk as at any spin flip step, it has equal probability to advance or to travel

back (Figure I- 6). As the initiation of the relaxation magnetisation depends on J, improved SCMs should display the highest possible intrachain coupling. A few examples of SCMs containing d-block and lanthanide metals are reported in Table I- 4.

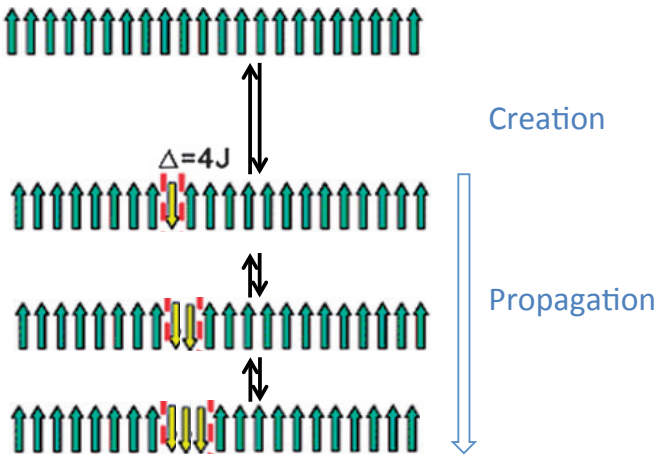

Figure I- 6 Basic mechanism of the magnetisation dynamics in SCMs, adapted from ref[155]

Table I- 4 Relaxation barrier and blocking temperature for selected SCMs of bloc d and 4f elements

SCM	ΔE (K)	τ_0 (s)	T_B (K)	H_{coer} (T)
$[Co(hfac)_2(NITPhOMe)]_n$ [154]	154	$3.0.10^{-11}$	6	0.1 at 2 K
$[Co(hfac)_2PyrNN]_n$ [161]	377 / 396	7.10^{-10} / 6.10^{-12}	14	3.2 at 8 K
$[Co(hfac)_2NaphNN]_n$ [162]	398	$4.0.10^{-12}$	13.2	3 at 8 K
$[Mn_2(saltmen)_2Ni(pao)_2(py)_2](ClO_4)_2$ [163]	72	$5.5.10^{-11}$	14	0.05 at 1.8 K
$[Dy(hfac)_3\{NIT(C_6H_4OPh)\}]$ [164]	46 / 69	$5.6.10^{-10}$ / $1.9.10^{-12}$	2.6	-

I.2.2) Actinide-based molecular magnets

Actinides have been identified as good candidates for the development of molecular magnets due to their physicochemical properties. Notably, the greater radial extension of the 5f over the 4f orbitals introduces the possibility of higher covalency and magnetic exchange compared to the lanthanides.[7,8] Moreover, actinide ions present a higher axial magnetic anisotropy with respect to transition metals. The low radioactivity of natural and depleted uranium associated to its large availability from the nuclear industry renders it the actinide ion most suitable for potential applications.

The first example of an actinide SIM was reported by Long and coworkers in 2009 and consisted of a simple trigonal prismatic uranium(III) complex, with

diphenylbis(pyrazolylborate) Ph_2BPz_2 ligands.[165] Since then, a few SIMs and SMMs have been reported (Table I- 5) and contain U(III) ($5f^3$, J = 9/2), U(V) ($5f^1$, J = 5/2), Np(IV) ($5f^3$), and Pu(III) ($5f^5$, J = 5/2) ions. The odd number of electrons in these configurations leads to a magnetic ground state. Two recent reviews cover all actinide-based SMMs or SIMs and these examples are reported in Table I- 5.[8,166]

Table I- 5 Relaxation barrier and blocking temperature for selected actinide SMM and SIM

	ΔE in K (H_{dc} in T)	**τ_0 (s)**	**T_B (K)**	**H_{coer} (T)** (sweep rate)
SIM $5f^1$				
$[UO(Tren^{TIPS})]$ [72]	21.5 (0.1)	$2.6.10^{-7}$	1.8	0
SIM $5f^2$				
$[\{(SiMe_2NPh)_3tacn\}U(bipy)]$ [167]	14.1 (0.1)		1.7	0
SIM $5f^3$				
$[U(Ph_2BPz_2)_3]$ [165]	28.8	1.10^{-7}	-	-
$[U(H_2BPz_2)_3]$ [168,169]	22.9	4.10^{-7}	-	-
$[U(Tp)_3]$ [170]	5.4 (0.01)	7.10^{-5}	-	-
$[U(Bc^{Me})_3]$ [171]	31.6 (0.075)	$1.0.10^{-7}$	-	-
$[U(TpMe_2)_2]I$ [172]	30 (0.05)	$1.8.10^{-7}$	3.5	0
$[U(TpMe_2)_2(bipy)]I$ [173]	26.2 (0.5)	$1.4.10^{-7}$	4.5	0
$[U(TpMe_2)_2(bipy)]$ [174]	28.5	$3.28.10^{-7}$	0.33	0
$[U(BIPM^{TMS})I_2(THF)]$ [175]	23.4 (0.2)	$2.9.10^{-7}$	-	-
$[UI_3(THF)_4]$ [175]	18.6 (0.2)	$6.4.10^{-7}$	-	-
$[U(N(SiMe_3)_2)_3]$ [175]	31 (0.2)	1.10^{-11}	-	-
$[U(N(Si^tBuMe_2)_2)_3]$ [176]	21.4 (0.06)	$3.1.10^{-7}$	1.8	0
$[U(N(SiMe_3)_2)_4][K(18C6)]$ [174]	23	$2.2.10^{-8}$	-	-
$[U(OSi(OtBu)_3)_4][K(18C6)]$ [174]	26	$2.6.10^{-7}$	-	-
$[U(COT'')_2][Li(THF)_4]$ [177]	27 (0.1)	$4.6.10^{-6}$	-	-
$[Np(COT)_2]$ [111]	41 (0.5)	$1.1.10^{-5}$	1.8	0
SIM $5f^5$				
$[Pu(Tp)_3]$ [178]	26.3 (0.01)	$2.9.10^{-7}$	-	-
SMM				
$[(U(BIPM^{TMS}H)I)_2(\mu\text{-}\eta^6\text{:}\eta^6\text{-}C_6H_4CH_3)]$ [179]	-	-	1.8	0
$\{[Np^{VI}O_2Cl_2][Np^{V}O_2Cl(THF)_3]_2$ [112]	140	-	-	-
$[\{[UO_2(salen)]_2Mn(Py)_3\}_6]$ [180]	142	3.10^{-12}	4.5	1.5 at 2.25 K ($4\ mT.s^{-1}$)

Most of the reported examples in the literature consists of mononuclear uranium in the +III oxidation state with poly(pyrazolyl)borate ligands.[165,168-170,172,173] [172] [171,174] Complexes of U(III) with siloxide, silylamide,[174-176] iodide or tridentate methanide ligands[175] with different coordination numbers and geometries have also shown SIM properties. The energy barriers of these complexes are relatively low and range between 5.5 and 32 K. The application of a dc field is often necessary to observe slow relaxation in ac measurements.

Very recently, Almeida and coworkers described the first uranium(IV) complex exhibiting SIM properties.[167] The complex contains an azobenzene radical ligand and the exchange of the uranium(IV) with the radical allowed for the formation of a magnetic ground state leading to SIM behaviour. The energy of spin reversal is close to the uranium(III) SIMs.

However, the potential of actinide in the development of SMMs remains largely unexplored. One successful approach in the design of actinide single-molecule magnets may arise from the study of exchange-coupled systems with an appropriate superexchange pathway. One example of a reported dinuclear uranium(III) SMM consisted of a toluene uranium(III) sandwich compound. However, the maximum in the out-of-phase component was observed only for the highest ac frequencies, which precluded the extraction of an energy barrier.[179] Moreover, in this example, the magnetic coupling is ambiguous and no clear conclusion on the origin of the slow relaxation of the magnetisation could be given. To date, two polymetallic actinyl assemblies, built on the direct coordination of an oxo group of an actinyl moiety to another metallic centre (designated as a cation-cation interaction (CCI)) have led to SMM behaviour. The first multinuclear actinide complex to demonstrate both superexchange and slow magnetic relaxation was assembled through cation-cation interactions. This molecule consists of a trinuclear neptunyl(V/VI) cluster (Table I- 5), in which oxo bridges between actinide metals promotes a pathway for the magnetic communication.[112,181] The second example of polymetallic actinide SMMs was reported in our group and consists on a cluster of uranyl(V) and manganese(II) connected through CCI (Table I- 5).[180] The structures of these two molecules are described in section I.3.1.1.2) and Chapter III, respectively.

I.3) Routes to homo- and heteropolymetallic actinide assemblies

Polynuclear actinide assemblies have good potential to display SMM properties. However, the controlled preparation of polymetallic actinide complexes is a great challenge due to the multiple accessible oxidation states and coordination geometries leading to the relatively unpredictable chemical properties of these elements. Recent reviews described the reported polynuclear actinide assemblies.[15,87,182]

Three main strategies have been developed to build polynuclear actinide assemblies: the redox reactivity of actinides, the use of innocent bridging ligands and the cation-cation interaction. Only a few examples of polymetallic actinide compounds classified by the nature of the bridging group are discussed here: oxygen, nitrogen or carbon-based bridging ligands.

In these three classes, clusters based on the different strategies used to build these polymetallic complexes are presented. In particular, the focus is on compounds for which magnetic exchange coupling between actinide centres occurred.

I.3.1) Oxygen-based bridging ligands

A wide variety of ligands containing oxygen-donor atoms acting as bridges have been reported in actinide chemistry, such as oxo, hydroxo,[87] carboxylate,[22,183] phosphate,[184] sulphate, alkoxide,[185] or ether ligands. These ligands are possible building blocks to support the formation of polynuclear structures. It is interesting to note that polynuclear assemblies of transition metals or lanthanides metal ions with such bridging ligands displayed SMM behaviour with high anisotropy barriers.[115,116,125,131,132,150,186]

I.3.1.1) Oxo bridging ligands

Actinide ions are hard Lewis acids, and consequently they easily form oxo compounds. They are easily hydrolysed, leading to the formation of oxo/hydroxo aggregates. A full review of these species produced in hydrolysis reactions was recently presented by Soderholm.[87] The oxo bridges are particularly interesting for the building of polymetallic assemblies with various geometries as they can bridge 2, 3, 4 and even 5 or 6 metallic centres.[96,132,187-189] Despite its environmental relevance, the isolation of polynuclear assemblies in aqueous solution is very difficult due to the complexity of hydrolysis/redox chemistry in water and the formation of mixture of species.

A few controlled synthetic routes in organic solvents are known to lead to the formation of polynuclear oxo/hydroxo assemblies. Such synthetic strategies are important for the design of new functional actinide materials. We can note that serendipitous reactivity of actinides with oxygenated solvent (THF, DME, Et_2O) or water/oxygen traces has led to the formation polynuclear complexes containing bridging μ-oxo, μ_3-oxo or μ_4-oxo ligands.[188,190-194] The observation of hydrolysis in organic media highlights the possibility to synthesise actinide oxo clusters from the controlled hydrolysis of low-valent precursors in strictly anhydrous organic media. The addition of stoichiometric amounts of water to low-valent actinide precursors in the presence of organic ligands in strictly anhydrous solutions has led to the reproducible isolation of several polynuclear oxo/hydroxo clusters. This synthetic strategy is described in Chapter II. Two additional strategies have led to oxo clusters: controlled redox reactions (oxidation, reduction, disproportionation or comproportionation) of actinides(III/IV/V/VI) and the use of cation-cation interaction of actinyl(V/VI) units.

I.3.1.1.1) Redox reactivity

I.3.1.1.1.1) Oxidations with O_2/O-atom transfer agents

Reaction with O_2 or with oxo group donors (Me_3NO, Py-NO, N_2O, NO, CO_2) has been widely investigated with tri- and tetra-valent uranium complexes and has been reviewed in the past few years.[16,70,109,187,195-199] Most of the oxo complexes isolated by reaction with O^{2-} donors presented a dimeric structure with uranium(IV) atoms bridged by one linear μ-oxo or two μ-oxo groups with a diamond core structure, while only one example of an hexanuclear U(V) cluster with a U_6O_{13} core was isolated in the Andersen group.[189] For this cluster, no unambiguous magnetic exchange coupling between the 6 U(V) centres was reported.

Contrary to the hexanuclear cluster reported by Andersen, in the past few years, the group of Meyer have isolated several mono and bis μ-oxo U(IV) or U(V) complexes displaying unambiguous magnetic communication between the uranium atoms. The reaction of the trivalent complexes [(($^{t\text{-Bu}}$ArO)$_3$mes)U], [((^{Ad}ArO)$_3$N)U] or [((^{tBu}ArO)$_3$tacn)U], supported by polydentate ligands comprising of three aryloxide arms anchored on triazacyclononane, amine or mesityl groups, with an excess of N_2O or CO_2 yielded mono-oxo dimeric uranium(IV) compounds.[187,195,197] Instead, the addition of Py-NO or Me_3NO to [((^{Ad}ArO)$_3$N)U] or [((^{nP,Me}ArO)$_3$tacn)U] yielded uranium(V) bis-μ-oxide complexes [{((^{Ad}ArO)$_3$N)U}$_2$(μ-O)$_2$] and [{((^{nP,Me}ArO)$_3$tacn)U}$_2$(μ-O)$_2$], respectively. Both complexes display a diamond-shaped [U(μ-O)$_2$U] structural motif.[187,199] Due to the steric hindrance of the polydentate ligands used, assemblies of higher nuclearity than two could not be achieved. Interestingly, a series of related bis-oxo dimeric U^{IV}/U^{IV} and U^{V}/U^{IV} complexes supported by the (^{nP,Me}ArO)$_3$tacn ligand has been described by the same authors recently thanks to the controlled reduction of the dimeric U(V) complex.[199]

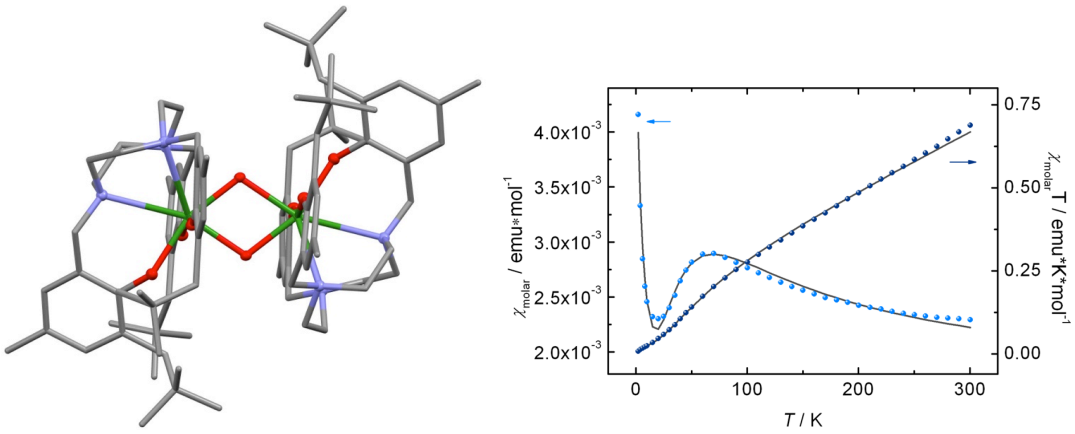

Figure I- 7 (left) Molecular structure of [{((^{nP,Me}ArO)$_3$tacn)U}$_2$(μ-O)$_2$] (right) (H were omitted for clarity, ligands are represented with pipes . Atoms: C in grey, N in blue, O in red, U in green). (right) Temperature-dependent SQUID magnetisation data for [{((^{nP,Me}ArO)$_3$tacn)U}$_2$(μ-O)$_2$], fit are represented in black lines (J = -65 cm^{-1}).[199]

The magnetic properties of these species were investigated and revealed that the presence of magnetic coupling is strongly influenced by the environment around the uranium atoms. The bis-oxo uranium(V) complex [{((^{nP,Me}ArO)$_3$tacn)U}$_2$(μ-O)$_2$] possesses an unambiguous antiferromagnetic coupling at 70 K with strong exchange coupling constant of -65 cm^{-1} (Figure I- 7) whereas the two uranium(V) ions in [{((^{Ad}ArO)$_3$N)U}$_2$(μ-O)$_2$] did not show the unambiguous presence of magnetic coupling.[187,199] Interestingly, the related U^{IV}/U^{IV} and U^{V}/U^{IV} complexes supported by the (^{nP,Me}ArO)$_3$tacn ligand did not reveal magnetic coupling.

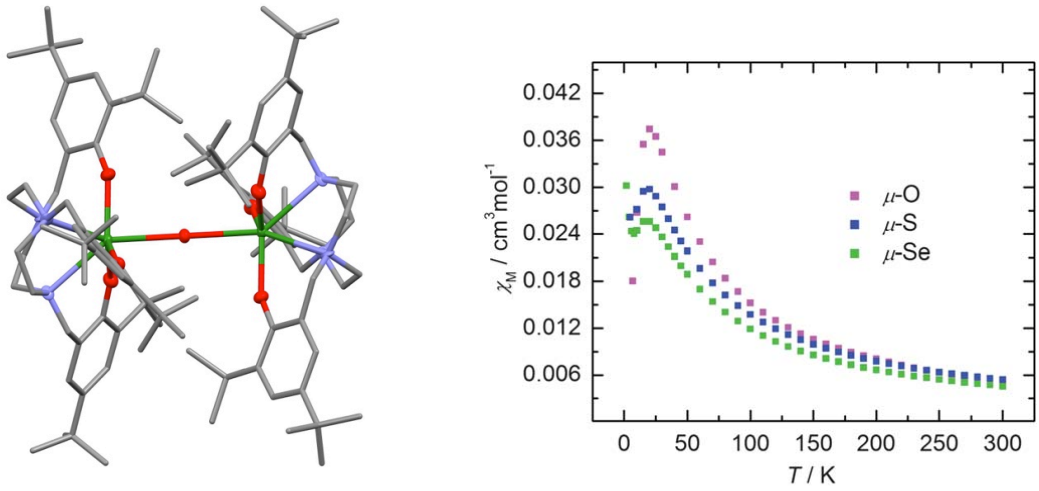

Figure I- 8 (left) Molecular structure of [{((^{tBu}ArO)$_3$tacn)U}$_2$(μ-O)] (H and coordinated DME molecules were omitted for clarity, ligands are represented with pipes . Atoms: C in grey, N in blue, O in red, U in green). (right) Temperature-dependent SQUID magnetisation data for [{((^{tBu}ArO)$_3$tacn)U}$_2$(μ-E)] (E= O, S, Se).[187]

An unusual antiferromagnetic coupling between uranium(IV) atoms occurs in [{((^{tBu}ArO)$_3$tacn)U}$_2$(μ-O)], with a maximum in the magnetic susceptibility observed at 20 K (Figure I- 8) while the dimeric uranium(IV) complex [{((^{Ad}ArO)$_3$N)U}$_2$(μ-O)] do not show any coupling.[187] We can also note that analogous dinuclear uranium(IV) (^{tBu}ArO)$_3$tacn complexes with sulphide and selenide bridges also displayed antiferromagnetic coupling at 20 K.[187]

To our knowledge, the only other example of unambiguous antiferromagnetic coupling between two uranium(IV) centres, also mediated by an oxo bridging ligand, was reported by Liddle (T_N = 3 K). The product of the reaction between the trivalent [U(Tren^{DMSB})] complex (Tren^{DMSB} = N(CH$_2$CH$_2$NSiMe$_2$^{t}Bu)$_3$] and CO yields a dimeric uranium(IV) complex bridged by a linear $^-$O-CC-O$^-$ ligand, which is quantitatively converted into a μ-oxo bis-uranium(IV) complex at high temperature.[200] As the thermolysis led to the insertion of the ethyne diolate group into one of the N-Si bonds of the Tren^{DMSB} ligand (Scheme I- 5), the authors suggested that the oxo-bridge came from the glass reaction vessel.

Scheme I- 5 Synthesis of the oxo dinuclear U(IV) product (R: $SiMe_2{}^tBu$).

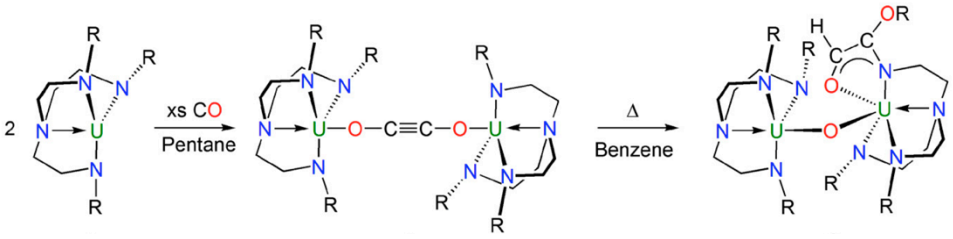

I.3.1.1.1.2) Reduction of actinyl units

The uranyl moiety provides a convenient alternative oxide precursor for the synthesis of polynuclear uranium oxo assemblies. Several hexanuclear oxo compounds have been reported from the comproportionation reaction between uranyl(VI) and trivalent or tetravalent uranium complexes[201,202] or by the reduction of uranyl(VI).[203] They all displayed a U_6O_8 core consisting of six uranium(IV) ions placed at the vertices of an octahedron where 8 oxo (or hydroxo) cap the triangular faces of the octahedron. The magnetic properties of these large assemblies were not reported.

Recently, using a similar strategy, Arnold et al. described the reductive silylation of the uranyl(VI) pacman (Pcm^{4-} a tetra-anionic pyrrole-imine macrocycle) complex with the uranyl(VI) silylamide salt $[UO_2(N(SiMe_3)_2)_2]$.[204] The resulting binuclear uranium(V) dioxo complex $[\{(Me_3SiO)U(\mu\text{-}O)\}_2(Pcm)]$, derived from two trans-uranyl dications, features a multiply bonded U_2O_2 core, and two silylated exo-oxo groups (Figure I- 9).

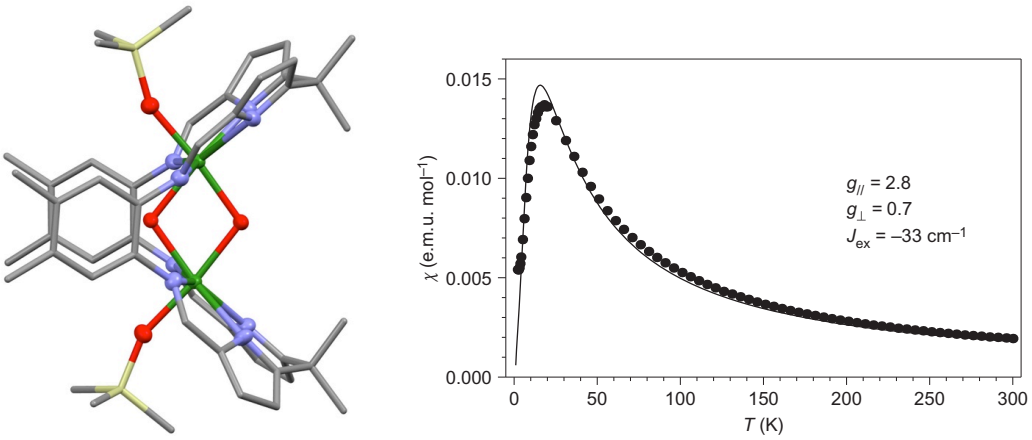

Figure I- 9 (left) Molecular structure of the butterfly-shaped dimer $[\{(Me_3SiO)U(\mu\text{-}O)\}_2(Pcm)]$ (H atoms were omitted for clarity. Ligands are represented with pipes, C are represented in grey, O in red, N in blue, Si in light yellow and U in green.). (right) Solid state magnetic behaviour of $[\{(Me_3SiO)U(\mu\text{-}O)\}_2(Pcm)]$ between 2 and 300 K. The line shows the calculated fit to the data.[204]

Interestingly, a clear signature of antiferromagnetic coupling between the uranium centres was observed with a maximum in the magnetic susceptibility curve at 17 K. The

magnetic susceptibility was fitted and afforded a large value of the exchange coupling constant of -33 cm^{-1} (Figure I- 9).

A series of dinuclear bridging oxo-U^{V}/U^{V}, U^{IV}/U^{IV}, U^{VI}/U^{VI} were synthesised form the controlled oxidation or reduction of the $[\{(Me_3SiO)U(\mu\text{-}O)\}_2(Pcm)]$ complex.[205] The complexes displaying the functionalization of the exo oxo groups of $[\{OU^{V}(\mu\text{-}O)\}_2(Pcm)]^{2-}$ with lithium, potassium and tin were also isolated.[206] However, the magnetic data of these assemblies were not reported.

I.3.1.1.1.3) Disproportionation of uranyl(V)

Recently, a few oxo polymetallic assemblies were isolated in our group from the induced disproportionation reaction of uranyl(V). The disproportionation reaction of uranyl(V) compounds in aprotic solvents leads to a uranyl(VI) complex and polynuclear uranium(IV) species connected with μ-oxo groups. The disproportionation reaction may be induced in aprotic solvents by the use of protons or highly charged cations.

The treatment of the uranyl(V) complex $\{[UO_2(Py)_5][KI_2(Py)_2]\}_n$ with two equivalents of benzoic acid in pyridine immediately yielded a 1:1 mixture of the uranyl(VI) complex $[UO_2(PhCOO)_2(Py)_2]$ and a hexanuclear uranium(IV) cluster $[U_6O_4(OH)_4(PhCOO)_{12}(Py)_3]$ according to Scheme I- 6.[207] This later complex has a U_6O_8 core.

Scheme I- 6 Induced disproportionation of uranyl(V) with benzoic acid

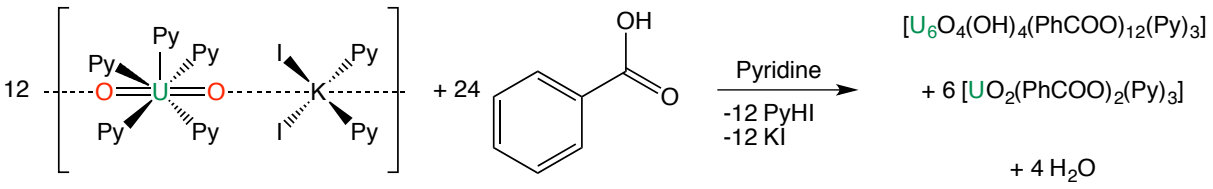

Further studies in our group have shown that the disproportionation of uranyl(V) may be induced by the presence of uranium(IV) complexes. The addition of the U(IV) salt $[UI_4(Et_2O)_2]$ to uranyl(V) $[UO_2(Mesaldien)K]_n$ (Mesaldien = N,N'-(2-aminomethyl)diethylenebis(salicylidene imine)) in the presence of MesaldienK_2 led to partial disproportionation of the uranyl(V) affording the linear tetramer U(V/IV) $\{[UO_2(Mesaldien)\text{-}(U(Mesaldien)]_2(\mu\text{-}O)\}$ and uranyl(VI) complex $[UO_2(Mesaldien)]_n$.[54] The structure of $\{[UO_2(Mesaldien)\text{-}(U(Mesaldien)]_2(\mu\text{-}O)\}$ presents UO_2^{+}-U^{4+} interactions (Figure I- 10 top).

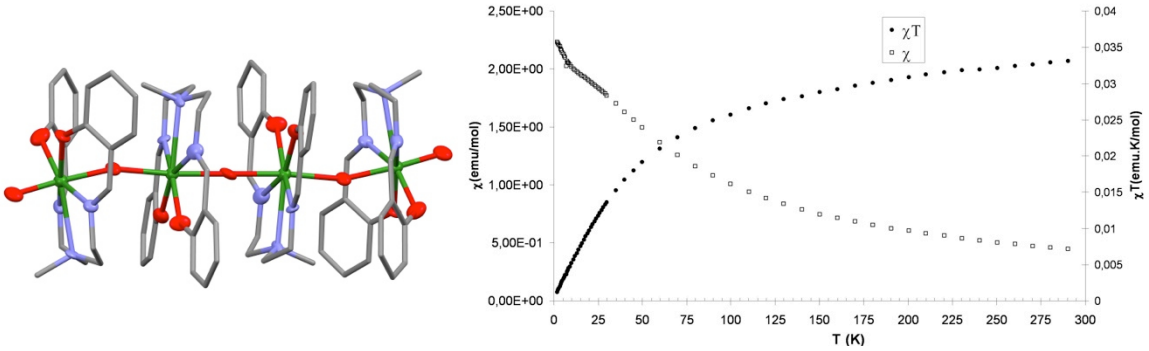

Figure I- 10 (left) Molecular structure of {[UO_2(Mesaldien)-(U(Mesaldien)]$_2$(μ-O)} (H are omitted for clarity, ligands are represented as pipe. Atoms : C in grey, O in red, N in blue, U in green); (right) Temperature-dependent magnetic susceptibility data for {[UO_2(Mesaldien)-(U(Mesaldien)]$_2$(μ-O)} in the range of 2-300 K in a 1 T field.[208]

No clear magnetic exchange was observed for this mixed-valent U(IV)/U(V) cluster. The inflexion point around 18 K in the slope of the magnetic susceptibility vs T might indicate a superimposition of the paramagnetism of the U(V) centres with the TIP behaviour of the U(IV) present below this temperature (Figure I- 10 bottom).[208]

The controlled formation of polynuclear uranium oxo complexes via the induced disproportionation of uranyl(V) is not a viable method, as yields of the uranium(IV) oxo product will always be less than 50%. However, the actinyl moieties may lead to polymetallic assemblies connected by oxo ligand through the cation-cation interaction, presented in the section below.

I.3.1.1.2) Cation-cation actinyl clusters

I.3.1.1.2.1) Cation-cation interaction

The oxygen atoms of the actinyl(V) moieties are strong Lewis bases and can coordinate other metal ions. The direct linkage of two actinyl ions via the oxo group from one actinyl moiety has been designated as a cation-cation interaction (CCI). The interaction of any metallic ion with one oxo group of an actinyl moiety is also called CCI. The stability of An(V) cation-cation (CC) complexes decreases in the series UO_2^+ > NpO_2^+ > PuO_2^+.[209,210] This interaction is exceedingly rare in actinyl(VI) chemistry due to the low Lewis basicity of the two oxo atoms of the actinyl(VI) moieties. This interaction can occur with different geometries as shown in Scheme I- 7[211] leading to the formation of polynuclear complexes of actinides with different geometries.

Scheme I- 7 Different types of cation-cation interactions encountered with actinyl ions. M represent another metal cation.

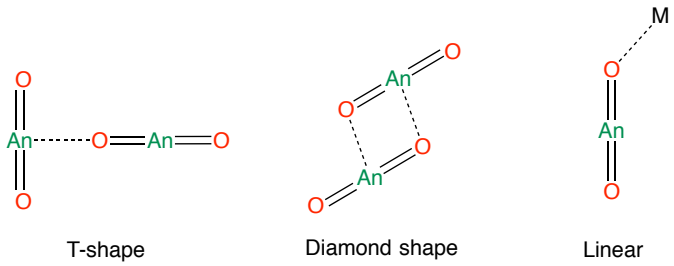

Despite the early observation of CCI in uranyl(V) aqueous solution,[212] preparation of compounds with mutual coordination of UO_2^+ was not observed until 2006 due to the easy disproportionation of uranyl(V). This interaction is however well-established for the stable neptunyl(V) unit, as numerous examples of CCI have been structurally characterised. Most of the CC compounds consist of materials with extended network structures (NpO_2^+,[113,114,211,213-215] NpO_2^{2+},[216], UO_2^{2+}),[17,211,217-230] while a very limited number of finite CC complexes have been reported. The neptunyl(V) and uranyl(V) discrete CC complexes are presented in the next sections. We can note that a few examples of discrete uranyl(VI) CC complexes have been reported,[17,231] in which the uranium centre is coordinated to strong donor ligands[231,232,233] or multi-nucleating ligands.[234,235] However, as uranyl(VI) ion is diamagnetic, these assemblies are not of interest in magnetic studies.

I.3.1.1.2.2) Neptunyl(V)

Two dimeric neptunyl(V) complexes have been reported in the literature : $[(NpO_2)_2(C_6H_4F(COO))_2(bipy)_2]$ (Figure I- 11 left)[236] and $[(NpO_2)_2(C_6H_5(COO))_2(bipy)_2]$.[237] These three complexes present a similar core, with neptunyl(V) ions connected through a diamond-shaped cation-cation interaction and bridged by bidentate benzoate ligands. An average lengthening of the Np-O bond involved in the cation-cation interaction of 0.06 Å with respect to the unbound Np-O is usually encountered with neptunyl(V) cation-cation assemblies. We can notice the rare example of the CC plutonyl(V) complex $[(PuO_2)_2(C_6H_5(COO))_2(bipy)_2]$ with a core and structure similar to that of $[(NpO_2)_2(C_6H_5(COO))_2(bipy)_2]$ (Figure I- 11 right).[237]

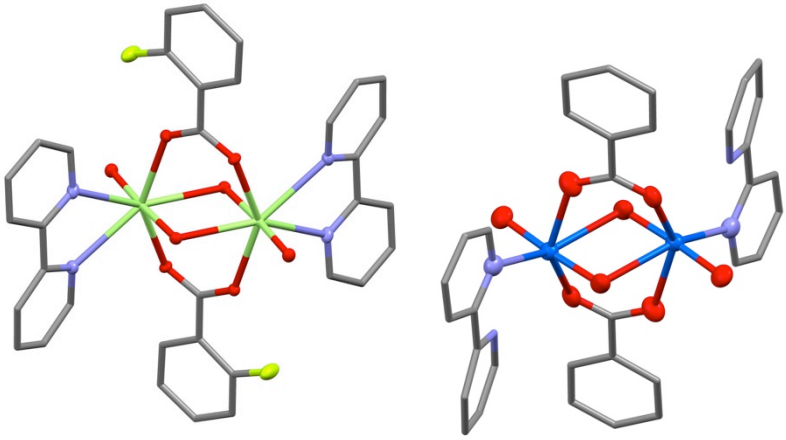

Figure I- 11 Molecular structures of $Na_4[(NpO_2)_2(C_6(COO)_6)]$ and $[(PuO_2)_2(C_6H_5(COO))_2(bipy)_2]$ (H atoms are omitted and ligands are represented with pipes for clarity, C are represented in grey, O in red, N in light blue, F in yellow, Np in light green and Pu in blue) [236,237]

Only one discrete trinuclear CC complex of neptunyl has been reported so far. In 2009, May and co-workers described the synthesis of the mixed-valent neptunyl(V)/neptunyl(VI) complex $[\{Np^{VI}O_2Cl_2\}\{Np^{V}O_2Cl(THF)_3\}_2]$ (Figure I- 12).[181] This trinuclear complex was obtained by reduction of the hexavalent neptunyl precursor $[NpO_2Cl_2(THF)_2]$ in THF solution. This complex consists of a trinuclear core with neptunyl atoms placed at the edge of a triangle. One oxo group of each neptunyl(V) coordinates the equatorial plane of the neptunyl(VI) through a cation-cation interaction, while the two neptunyl(V) moieties are linked via two bridging chlorides. This trimeric complex was the first neptunyl cluster isolated in organic solution.

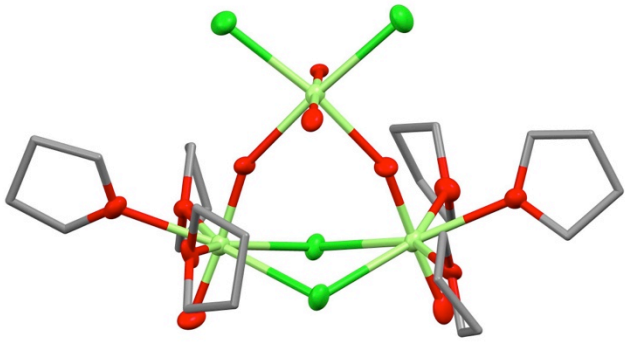

Figure I- 12 Molecular structure of the mixed-valent neptunyl(V/VI) assembly $[\{Np^{VI}O_2Cl_2\}\{ Np^{V}O_2Cl(THF)_3\}_2]$ (H atoms are omitted and ligands are represented with pipes for clarity, C are represented in grey, O in red, Cl in green, and Np in light green)[181]

Magnetic studies of the trinuclear $[\{Np^{VI}O_2Cl_2\}\{Np^{V}O_2Cl(THF)_3\}_2]$ complex revealed that this complex displays significant exchange coupling between the 5f centres (Np^{V} / Np^{VI} J

= 7.51 cm^{-1} , Np^{V}/Np^{V} J = 0.39 cm^{-1}) (Figure I- 13 left).[112] Moreover, this complex displayed slow relaxation of magnetisation with an energy barrier of 140 K (Figure I- 13 right).

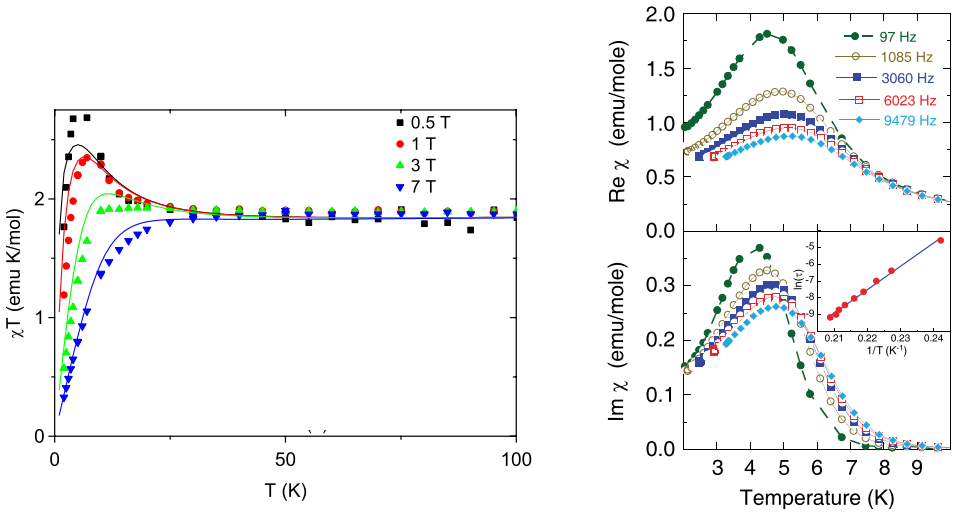

Figure I- 13 (left) Plot of cT vs T for $[\{Np^{VI}O_2Cl_2\}\{Np^{V}O_2Cl(THF)_3\}_2]$ collected with applied field values of 0.5, 1,3 and 7 T. Solid lines result of calculations. (right) Real (top panel) and imaginary (bottom panel) part components of the ac magnetic susceptibility of $[\{Np^{VI}O_2Cl_2\}\{Np^{V}O_2Cl(THF)_3\}_2]$ as a function of temperature, measured at different frequencies f of the driving field. The natural logarithm of the relaxation time is plotted in the inset as function of 1/T.[112]

A tetranuclear mixed valent Np(IV)-Np-(V) assembly $[BuMeIm]_5[(NpO_2)_3Np(H_2O)_6Cl_{12}]$ was isolated in 2010, in Moisy's group (Figure I- 14).[238] This complex, isolated from an ionic liquid, is constituted of three neptunyl(V) $[NpO_2Cl_4]^{3-}$ molecules connected through their oxygen atoms to a Np(IV) $[Np(H_2O)_6]^{4+}$ complex (Figure I- 14) However, magnetic characterisation of this complex was not reported.

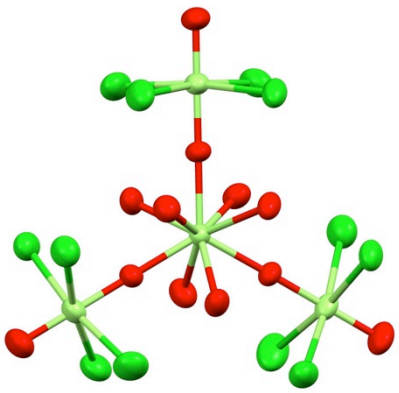

Figure I- 14 Molecular structure of $[(NpO_2)_3Np(H_2O)_6Cl_{12}]^{5-}$ (H toms are omitted. Cl are represented in green, O in red, and Np in light green)[238]

Finally, a second CC assembly containing four neptunyl(V) assembled in a square shape has been isolated and it is presented in the Chapter III.[239]

I.3.1.1.2.3) Uranyl(V)

Uranyl(V), stabilised in aprotic and anaerobic media with suitable organic ligands, is also able to build polynuclear assemblies via CCI.[47,58,231,240-244] Cation-cation polynuclear compounds of uranyl(V) are described in detail in Chapter III. However, we can note that the first example of uranyl(V) CC complex $\{[UO_2(dbm)_2]_4[K_6(Py)_{10}]\}I_2Py_2$ was reported in our group from the reaction of the dibenzoylmethanate (dbm^-) ligand with the uranyl(V) precursor $\{[UO_2(Py)_5][KI_2(Py)_2]\}_n$ in pyridine (Scheme I- 8).[47,240] The addition of 18-crown-6 (18c6) displaced the potassium ions and led to the formation of a dinuclear assembly $[UO_2(dbm)_2K(18C6)]_2$. In $\{[UO_2(dbm)_2]_4[K_6(Py)_{10}]\}I_2Py_2$ the four uranyl(V) units are arranged in a square geometry with T-shaped CCI while in $[UO_2(dbm)_2K(18C6)]_2$ the two uranyl(V) units formed a diamond-shaped CCI.

Scheme I- 8 Synthesis of $\{[UO_2(dbm)_2]_4[K_6(Py)_{10}]\}I_2Py_2$ and $[UO_2(dbm)_2K(18C6)]_2$

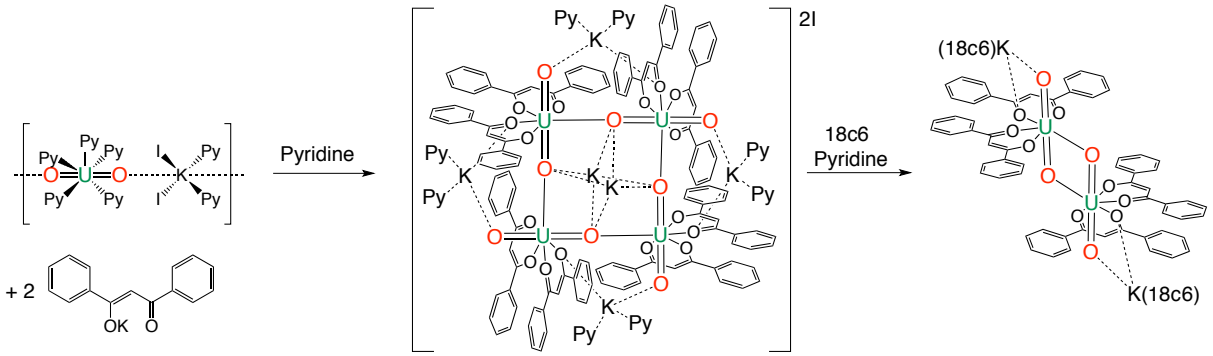

An unambiguous antiferromagnetic coupling with a Neel temperature of 5 K was revealed in the magnetic susceptibility vs T plot of $[UO_2(dbm)_2K(18C6)]_2$, indicating that the oxo bridge formed through the CCI might provide a pathway for magnetic communication between the uranium(V) centres. Notably, unambiguous antiferromagnetic coupling with Neel temperatures ranging from 5 to 12 K[48,231,242] and uranyl(V)-Mn(II) exchange-coupled SMM[180] have been reported in our group for various uranyl(V) CC geometries.

We have reported the different strategies to form oxo bridging ligands in actinide chemistry. Although a lot of different ligands displaying oxygen as bridging unit exist, the focus in the next two parts is on two examples of dinucleating Schiff base and siloxide ligands as the resulting assemblies revealed magnetic exchange.

I.3.1.2) Dinucleating ligands with phenoxide bridges

Compartmental ligands are extensively used to build polynuclear assemblies.[20] The Ephritikhine group investigated the formation of heterometallic compounds by the strategic use of hexadentate compartmental Schiff base ligands. Several trinuclear assemblies with the general formula $U^{IV}L^{i}_{2}M^{II}_{2}(Py)_{n}$ (M = Co, Ni, Cu, Zn; Py = pyridine, L^{i} = Schiff-base bridging ligands, see Figure I- 15) have been successfully synthesised.[245-248] The first step of the formation of these clusters consisted of the coordination of the transition metal into the inner N_2O_2 site of the hexadentate compartmental Schiff base, followed by the addition of uranium(IV) [U(acac)$_4$] (acac = acetylacetonate), which binds the oxygen atoms of the salicylidene fragments of two different $L^{i}M$ units, forming four M-O-U bridges overall. Interestingly, the coordination environment around the U(IV) ion remains invariant with changes in the bridging compartmental ligand, suggesting that differences in the magnetic behaviour across the series are not due to differences in the ligand field of the uranium ion.

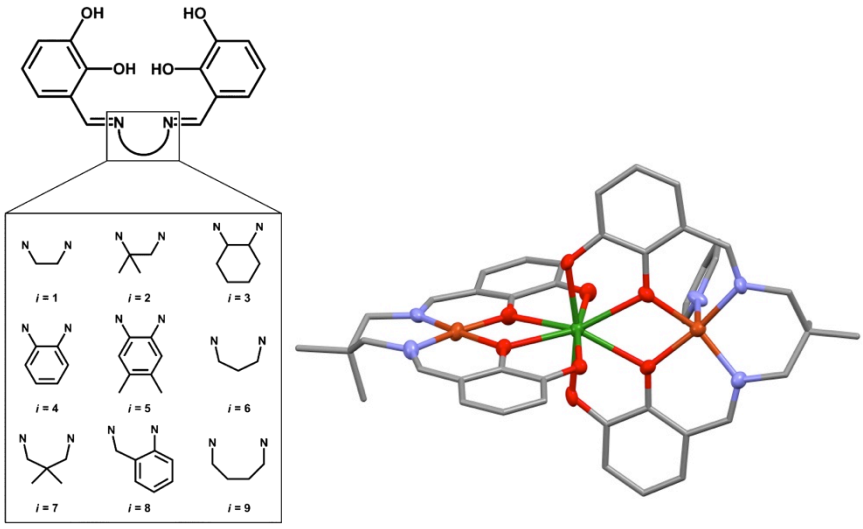

Figure I- 15 (left) Schematic representation of the ligand precursors H_4L^{i}. Note the two-carbon backbone for i) 1-5, three-carbon backbone for i) 6-8, and four-carbon backbone for i) 9. (right) Structure of $UL^{7}_{2}Cu_2(Py)$. (H atoms omitted and ligands represented in pipes. Atoms: C (grey), O (red), N (light blue), Cu (orange) and U (green)).

The isolation of isostructural diamagnetic zinc analogues enabled the use of a subtraction method for the analysis of the magnetic interactions between the U(IV) and M(II) ions. Systems with Cu(II) have been the most studied. The subtraction of the UZn_2 magnetic data from the UCu_2 magnetic data (see Figure I- 16) removes any contribution from the U(IV) ion and only leaves the spin contribution of the two Cu(II) ions together with any vestiges of magnetic exchange coupling. The authors performed this analysis, but they did not attempt to quantify the magnitude of the interaction.[245-248] Only a qualitative determination of the sign of the exchange constant was performed: a ferromagnetic coupling (J > 0) is observed when

$\Delta\chi_M T$ rises with decreasing temperature to reach a maximum, while an antiferromagnetic exchange interaction (J < 0) occurred otherwise.

The nature of the exchange appears to be highly dependent on the identity of the bridging Schiff base: for L^i (i = 6-9), a ferromagnetic coupling occurred, while for L^i (i = 1-5), an antiferromagnetic coupling is present. The shift from antiferromagnetic to ferromagnetic coupling may arise from of an increase in the Cu···U distance, which is associated with a lengthening in the diimino chain; however, not all of the UCu_2 clusters have been structurally characterised, precluding a systematic magneto-structural study. The magnetic data of the copper-uranium assemblies have been fitted few years later by Prof. Long to estimate the strength of the uranium-copper interaction.[7] The exchange coupling constants are reported in Figure I- 16 right and the sign obtained is in agreement with the qualitative observation of the subtracted magnetic curves.

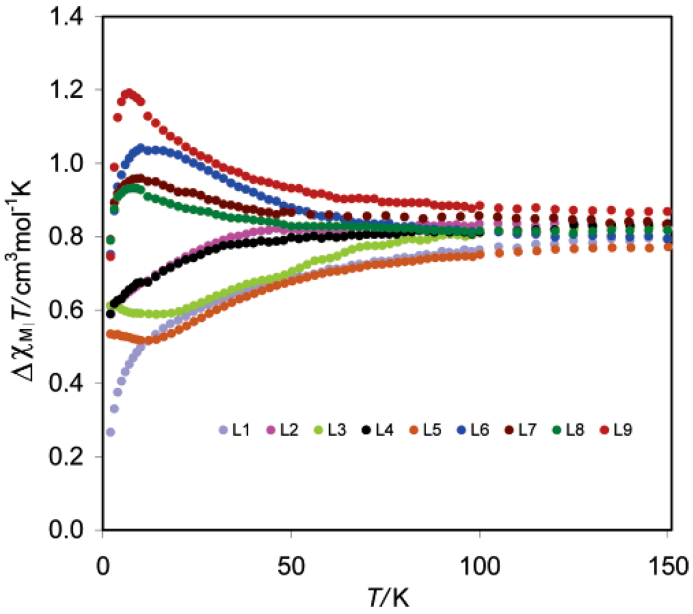

	J_{min} (cm^{-1})
$UL^1{}_2Cu_2(py)$	−1.5
$UL^2{}_2Cu_2(py)$	−0.8
$UL^3{}_2Cu_2(py)$	−1.8
$UL^4{}_2Cu_2(py)$	−0.5
$UL^5{}_2Cu_2(py)$	−1.3
$UL^6{}_2Cu_2(py)$	+2.6
$UL^7{}_2Cu_2(py)$	+0.8
$UL^8{}_2Cu_2(py)$	+0.7
$UL^9{}_2Cu_2(py)$	+1.9

Figure I- 16 (left) Variable-temperature magnetic susceptibility data obtained by subtracting the $UL^i{}_2Zn_2$ data from the corresponding $UL^i{}_2Cu_2$ data; (right) Exchange constants for $UL^i{}_2Cu_2$ clusters from ref [7]

In an attempt to obtain similar heterometallic assemblies with uranium(V), the Ephritikhine group oxidised the $U^{IV}L^i{}_2M_2$ clusters (M = Cu, Zn; i = 6,9) with silver nitrate.[249] The $U^VL^9{}_2Zn_2$ was obtained cleanly, while the other clusters with copper and L^6 ligand yielded mixtures of species.

I.3.1.3) Bridging siloxide ligand

Interest in siloxides ligands for 4f [250,251] and 5f [69,98,99,252-254] elements complexes has developed in the past few years, and their use has led to the stabilisation of low-valent complexes that can react with small molecules (N_2, CO_2, CS_2). In the group, a significant body of work has been carried out on the tris-(tertbutoxy)siloxide ligand, which has the ability to adopt mono- or bidentate binding modes and act as bridging ligand, leading to a wide variety of possible oligomeric structures (Scheme I- 3). Despite the high interest in polymetallic uranium(III) systems for the design of SMM, the number of isolated complexes is very limited and the tris-(tertbutoxy)siloxide ligand offered an opportunity to build polymetallic uranium(III) complexes.

The first U(III) complex supported by the tris-(tertbutoxy)siloxide ligand was isolated from the reaction of $[U\{N(SiMe_3)_2\}_3]$ with 3 equivalents of tris-(tert-butoxy)silanol $HOSi(O^tBu)_3$ in hexane at -40°C, resulting in the U(III) complex $[U(OSi(O^tBu)_3)_2(\mu\text{-}OSi(O^tBu)_3)]_2$ (Figure I-17 left).[98] The two U(III) ions are bridged by two siloxide ligands, forming a centrosymmetric assembly. Magnetic susceptibility temperature dependence for $[U(OSi(O^tBu)_3)_2(\mu\text{-}OSi(O^tBu)_3)]_2$ revealed the presence of a clear antiferromagnetic coupling of the U(III) cations with an unambiguous maximum in the plot of χ versus T at 16 K.[253,255]

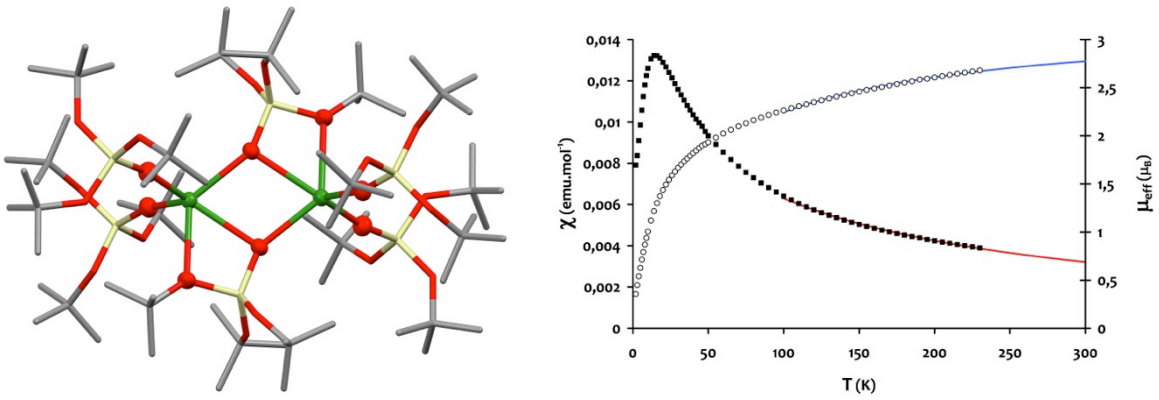

Figure I- 17 (left) Solid-state molecular structure of $[U(OSi(O^tBu)_3)_2(\mu\text{-}OSi(O^tBu)_3)]_2$ crystallised from hexane. Hydrogen atoms are omitted for clarity. Uranium (green), oxygen (red), silicon (yellow) and carbon (grey) atoms are represented with 50% probability ellipsoids, ligands represented in pipes; (right) Temperature-dependent SQUID magnetisation data (0.5 T) for complex of $[U(OSi(O^tBu)_3)_2(\mu\text{-}OSi(O^tBu)_3)]_2$ (data per U centre) plotted as χ (black squares) and μ_{eff} (open circles) versus temperature. Curie-Weiss fit : red and blue curves.[253,255]

I.3.2) Nitrogen-bridged actinide clusters

Polynuclear actinide complexes assembled through nitrogen-containing bridges have been isolated through redox or non-redox processes. We can distinguish pure nitrogen bridging ligands such as nitride N^{3-}, nitrogen N_2, reduced nitrogen N_2^{2-}, azide N_3^- and bridging ligands containing nitrogen as the donor atom linked to a carbon skeleton. The large palette of nitrogen-containing bridging ligand (nitrile, cyanide, amine, amide, imine, imide, aromatic N-heterocycle, pyrazole…) has led to polynuclear complexes with various geometries.

Very rare examples of dinuclear complexes with nitrogen bridging ligands have been reported so far. They usually resulted from the reaction of nitrogen gas with highly reactive U(III) complexes[256,257] [198,254,258] [93] However, no magnetic properties were reported for these few dinuclear assemblies. The azide and nitride ligands are presented in Chapter IV, while polymetallic assemblies obtained with organic ligands containing nitrogen as the bridging atom are presented in the next sections. The presentation is organised according to the nature of the bridging ligand, and to the synthetic strategy employed, which includes the direct association with a bridging ligand or a redox reaction leading to the formation of polymetallic assemblies.

I.3.2.1) Neutral and mono-anionic N-donor ligands

In this part, different examples of neutral bridging ligands containing imine or nitrile groups and mono-anionic N-donor ligands as amido or reduced N-heterocyclic ligands are presented.

I.3.2.1.1) Uranium complexation

Edelstein and coworkers were the first to investigate polynuclear uranium amino complexes and reported dinuclear,[259] trinuclear[260,261] and tetranuclear[262] uranium(IV) complexes with $^-NEt_2$ and N,N'-dimethylethylenediamine ligands (Figure I- 18). No evidence of metal-metal interactions was observed for the dinuclear $[U(NEt_2)_4]_2$ and trinuclear $[U_3(CH_3NCH_2CH_2NCH_3)_6]$ complexes.

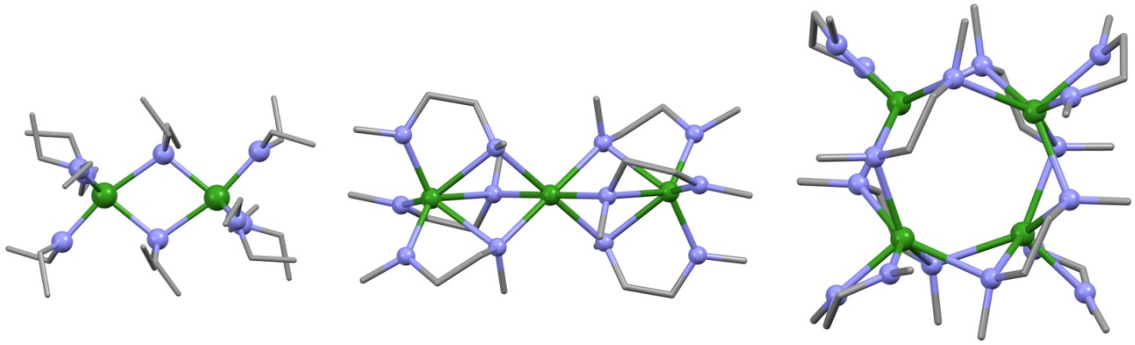

Figure I- 18 Molecular structures of the $[U(NEt_2)_4]_2$ (left), $[U_3(CH_3NCH_2CH_2NCH_3)_6]$ (middle) and $[U_4(CH_3NCH_2CH_2NCH_3)_8]$ (right) complexes.(H atoms were omitted for clarity. Ligands are represented with pipes, C are represented in grey, N in blue and U in green.) [260,261]

The group of Long described the synthesis of polynuclear uranium complexes with the 3,5-dimethylpyrazolate ligand. The reaction of Me_2PzK with $[UCl_4]$ afforded the binuclear complex $[U(Me_2Pz)_4]_2$ (Me_2Pz^- = 3,5-dimethylpyrazolate). The structure of the dimer consists of two U(IV) centres connected through two bridging Me_2Pz^- ligands (Figure I- 19 left).[262] It should be noted that the addition of $M(cyclam)Cl_2$ (M = Co, Ni, Cu, Zn; cyclam = 1,4,8,11-tetraazacyclotetradecane) to $[U(Me_2Pz)_4]_2$ cleaved the dimeric structure, inserting one $(cyclam)MCl_2$ complex into $[U(Me_2Pz)_4]_2$ to yield the heterotrimetallic 3d-5f clusters $(cyclam)M[(\mu\text{-}Cl)U(Me_2Pz)_4]_2$ (CuU_2 represented in Figure I- 19 right).[262,263]

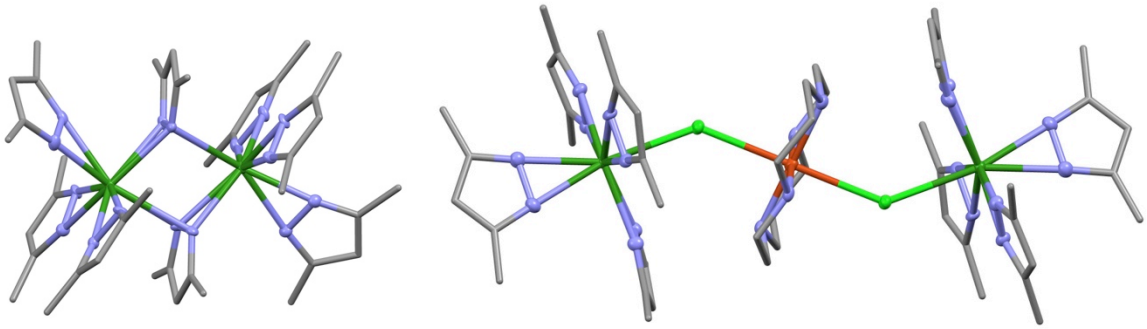

Figure I- 19 Molecular structures of the uranium assemblies $[U(Me_2Pz)_4]_2$ (left) and $(cyclam)Cu[(\mu\text{-}Cl)U(Me_2Pz)_4]_2$ (right) (H atoms were omitted for clarity. Ligands are represented with pipes, C are represented in grey, N in blue, Cl in light green, Cu in orange and U in green.)[262]

While the magnetic properties of $[U(Me_2Pz)_4]_2$ were not reported, the heterometallic MU_2 assembly revealed rare magnetic 3d-5f interactions. The invariance in the coordination geometry of the U(IV) centres in the different $(cyclam)M[(\mu\text{-}Cl)U(Me_2Pz)_4]_2$ clusters, and the existence of the ZnU_2 molecule, with the diamagnetic zinc, enabled the authors to use a subtraction method to quantify the exchange interaction (Figure I- 20). Ferromagnetic exchange coupling constants J were obtained for CoU_2 ranging from 15 to 48 cm^{-1}, weaker

for the NiU_2 cluster ($2.8 < J < 19$ cm^{-1}) and inexistent interactions were observed for CuU_2.[262,263] These ferromagnetic constants are much larger than the one reported by Ephritikhine for the UM_2L^i assemblies with binucleating ligands.[245-248] The nature of the bridging linear chloride vs two phenolate may considerably influence the strength of the interaction.

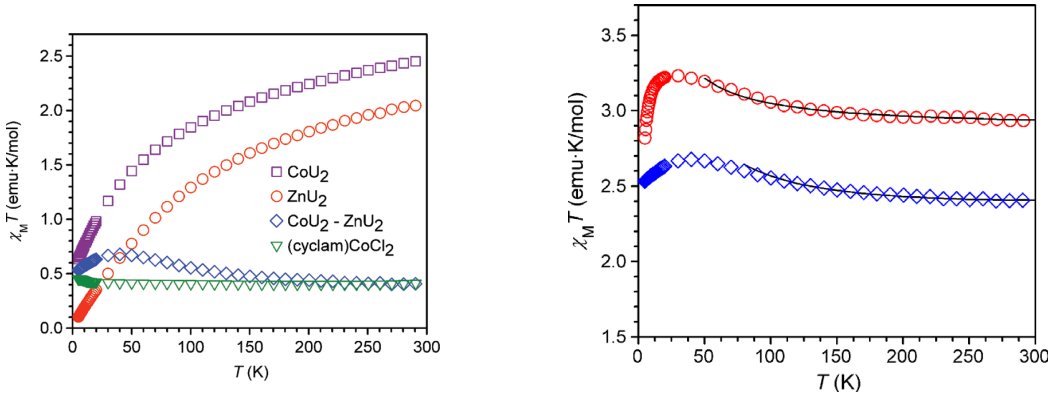

Figure I- 20 Variable temperature magnetic susceptibility data for CoU_2 and ZnU_2 and the subtracted data CoU_2-ZnU_2 (Magnetic data for the precursor complex (cyclam)$CoCl_2$ are depicted in comparison) (left) and the subtracted χT data of CoU_2-ZnU_2 (blue diamonds) and NiU_2-ZnU_2 (red circle) with the straight lines correspond to the best calculated fits.[262,263]

Kiplinger et al used more elaborate bridging ligands, allowing for the synthesis of homo- and hetero-metallic (U, Th, Yb) assemblies. [264] [265] [266] [267] Despite the presence of the π-system of the bridging ligand in these assemblies, no significant metal-metal coupling was observed in the magnetic data. However, electrochemical evidences of electronic communication within the assemblies were reported. The authors attempted to deconvolute the magnetic data of the heterometallic UYb_2 complex in order to extract information regarding potential exchange interactions between the U(IV) and Yb(III) centres.[264]

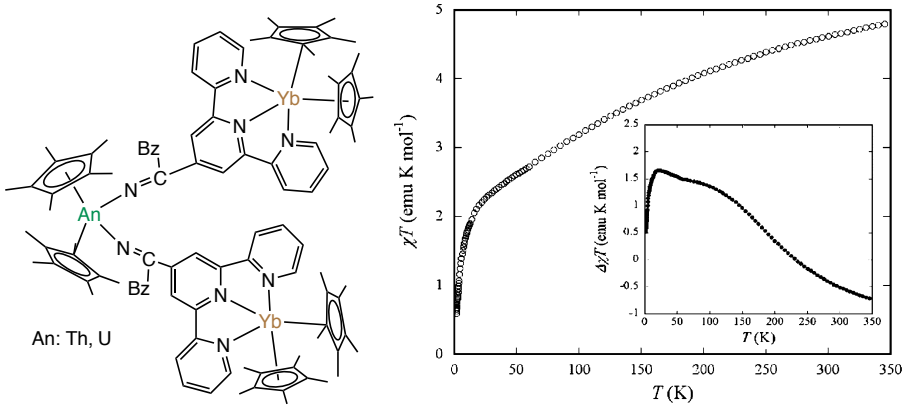

Figure I- 21 (left) Representation of $[Cp^*_2An\{N=C(Bz)(tpy\text{-}YbCp^*_2)\}_2]$ (An = Th, U); (right) variable-temperature magnetic susceptibility data for UYb_2. Inset: Variable temperature magnetic susceptibility data obtained upon subtraction of data for $Cp^*_2U[(N=C(Bz)tpy)_2$ and $ThYb_2$ from the UYb_2 data.[264]

The $[Cp^*_2An\{N=C(Bz)(tpy\text{-}YbCp^*_2)\}_2]$, $AnYb_2$ complexes (Figure I- 21) were obtained from the reaction of $[Cp^*_2An\{N=C(Bz)(tpy)\}_2]$ (An = Th, U) (Bz = CH_2Ph, tpy = terpyridyl) with two equivalents of $[Cp^*_2Yb(OEt_2)]$.[264] The structures of these complexes consist of a central $[Cp^*_2An^{IV}]^{2+}$ unit connected through N=C(Bz)tpy bridges to $Cp^*_2Yb^{II}$tpy and $Cp^*_2Yb^{III}$tpy$^{\bullet}$ in $AnYb_2$. Kiplinger and coworkers employed subtraction methods with the use of the magnetic data of the precursor $[Cp^*_2U\{N=C(Bz)(tpy)\}_2]$ and the diamagnetic Th(IV) analogue $ThYb_2$. The $\Delta\chi_M T$ vs T plot revealed the presence of a maximum interpreted as evidence of exchange coupling within the cluster (Figure I- 21). However, the specific nature of the coupling remains unclear due to the complexity of this system containing three distinct paramagnetic centres (U(IV), Yb(III) ions and the terpyridine radical).

I.3.2.1.3) Redox reactivity

The number of uranium(IV)-uranium(IV) assemblies exhibiting magnetic interactions is very limited. Few synthetic efforts have dealt with the formation of polymetallic assemblies based on uranium(III) to increase the strength of the magnetic exchange.

Notably, the Long group reported an attempt to synthesise an analogous di-uranium(III) complex of the pyrazolate dinuclear uranium(IV) $[U(Me_2Pz)_4]_2$ (Me_2Pz^- = 3,5-dimethylpyrazolate) species. Interestingly, the reaction of potassium dimethylpyrazolate with the uranium(III) complex $[UI_3(THF)_4]$ led to the unanticipated reductive cleavage of the Me_2Pz^- ligand into the ketimidopent-2-ene-2-imido ($kipi^{3-}$) ligand (Scheme I- 9).[268]

Scheme I- 9 Reduction of 3,5-dimethylpyrazolate

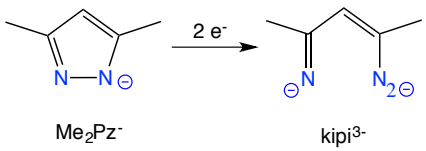

A series of three tetranuclear uranium clusters incorporating the bridging $kipi^{3-}$ and Me_2Pz^- ligands was isolated. One tetranuclear uranium(IV) $[U_4(Me_2Pz)_{10}(kipi)_2]$ and two mixed-valent U(III)-U(IV) $[U_4(Me_2Pz)_8(kipi)_2]$ and $[U_4(Me_2Pz)_{11}(kipi)]$ complexes were structurally characterised. From these clusters, only the mixed-valent $[U_4(Me_2Pz)_{11}(kipi)]$ assembly (core represented in Figure I- 22 left) was isolated in large enough quantities to perform magnetic susceptibility measurements (Figure I- 22 right). Antiferromagnetic coupling may be present between the two U(III) atoms of the mixed-valent cluster as the magnetic moment fell well below the level expected for a ground state featuring two

independent uranium(III) centres. However, due to the absence of a clear signature in the magnetic data, no clear conclusions about the presence of magnetic coupling were reported.

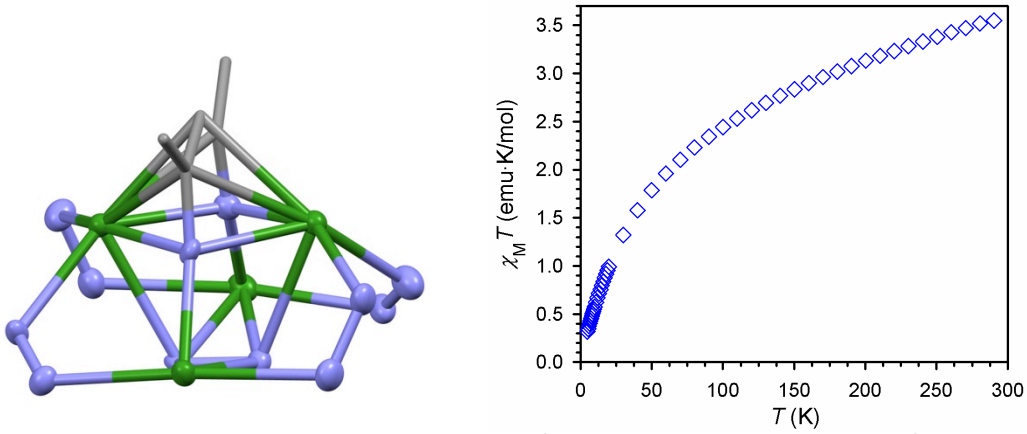

Figure I- 22 (left) Molecular structure of the core of $[U_4(Me_2Pz)_{11}(kipi)]$ (Carbon of the Me_2Pz^- ligands and non bridging Me_2Pz^- ligands removed for clarity. H atoms were omitted for clarity. Ligands are represented with pipes, C are represented in grey, N in blue and U in green.) and (right) χT vs T plot of $[U_4(Me_2Pz)_{11}(kipi)]$.[268]

I.3.2.2) Imido ligands

Imido ligands consist of NR^{2-} anions, which can coordinate one, two or three metallic centres. Double deprotonations of primary amines, reductive breaking of diazene compounds or two-electron reduction of organic azides can all afford these ligands. In the first section, the formation of polynuclear uranium complexes from the reaction of precursor of imido ligands with uranium complexes is presented, followed by the redox reactivity of mononuclear imido uranium complexes leading to the formation of assemblies.

I.3.2.2.1) Formation of polynuclear imido uranium complexes

The formation of imido-bridged di-uranium(IV) complexes from the reaction of primary amines RNH_2 with organoalkyl uranium(IV) complexes were described by the groups of Diaconescu and Liddle,[269,270] while the group of Boncella described the reaction of LiN(H)R (R = 2,6-^{i}Pr$_2$C$_6$H$_3$, 2-^{t}BuC$_6$H$_4$) with $[UCl_4]$ affording mono(arylimido) complexes with the general formula $[U(\mu\text{-}NR)(Cl)_2(THF)_2]_2$.[271] All these complexes contain a diamond-shaped (U-μ-NR)$_2$ core. The magnetic properties of these three molecules were investigated, but no magnetic exchange between the uranium(IV) atoms was observed.

Cummins and coworkers reported the four-electron reduction of azobenzene by the low-valent di-uranium(III) μ-η^6,η^6-toluene inverted sandwich complex $(\mu\text{-}C_7H_8)[U(N[R]Ar)_2]_2$ (R

= ^{t}Bu, Ar = 3,5-$C_6H_3Me_2$), yielding the uranium(IV) phenylimido-bridged dimer [U(μ-NPh)(N[R]Ar)$_2$]$_2$.[272] The magnetic properties of this dinuclear compound, with a diamond (U-μ-NPh)$_2$ core were not reported.

In contrast, the first imido compound displaying interesting magnetic properties was reported in 1990 by Andersen and coworkers. Exploiting the reactivity of trivalent uranium with diorganoazide, they isolated binuclear complexes of uranium(V) through the oxidative elimination of N_2. Two bis-imido uranium(V) complexes [$(MeC_5H_4)_3U]_2$(μ-1,4-$N_2C_6H_4$) and [$(MeC_5H_4)_3U]_2$(μ-1,3-$N_2C_6H_4$) were isolated (Scheme I- 10).[62]

Scheme I- 10 Synthesis of bimetallic uranium imido dimers

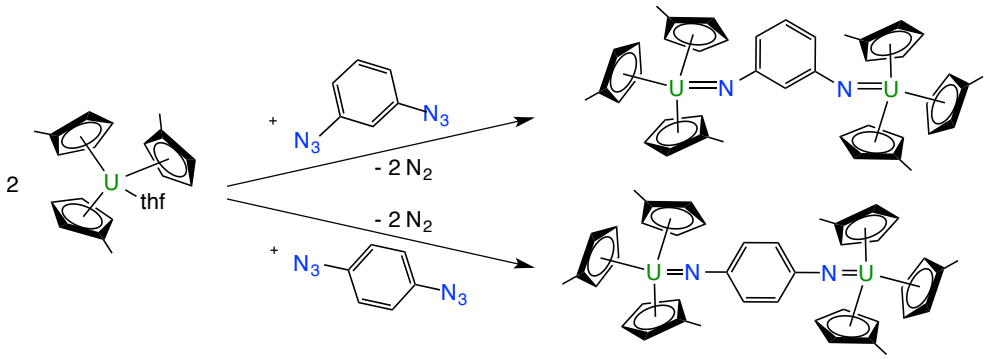

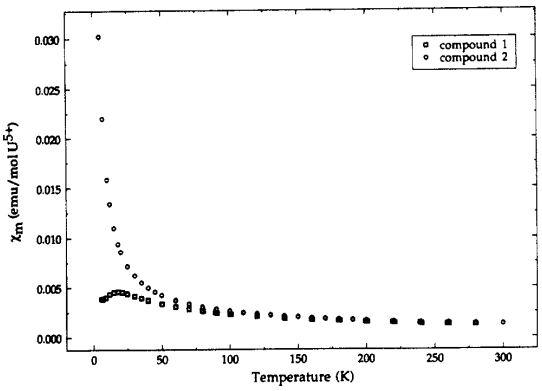

Figure I- 23 Experimental magnetic susceptibility data of [Cp'$_3$U]$_2$[μ-1,4-$N_2C_6H_4$] (Compound 1) and [Cp'$_3$U]$_2$[μ-1,3-$N_2C_6H_4$] (Compound 2) [62]

The magnetic properties of the two [$(MeC_5H_4)_3U]_2$(μ-1,4-$N_2C_6H_4$) and [$(MeC_5H_4)_3U]_2$(μ-1,3-$N_2C_6H_4$) complexes displayed strong differences (Figure I- 23). An unambiguous antiferromagnetic coupling between the two U(V) ions with a maximum at 20 K was observed for the [1,4-$N_2C_6H_4$] bridged complex while the [1,3-$N_2C_6H_4$]-bridged

uranium(V) ions behave as two independent paramagnets. This study was one of the first probing the possible magnetic communication between two uranium metals and the estimated exchange coupling constant amounted to -19 cm^{-1}.[62]

I.3.2.2.2) Redox reactivity of imido uranium complexes

In the section above, the formation of imido bridged polynuclear uranium complexes is discussed. However, imido ligands can also bind one metallic centre, yielding mononuclear complexes.[273] The redox reactivity of such mononuclear complexes has resulted in the formation of polynuclear assemblies in three separate cases.

Boncella and coworkers were the first to isolate and characterise a mononuclear trans-imido analogue of uranyl(VI).[274,275] During their investigation of the reactivity of such units, they discovered that the reduction of the mononuclear bis(imido) uranium(VI) complex, $[U(N^tBu)_2(^tBu_2bipy)I_2]$ with NaC_5Me_5 led to the dimeric $[U(N^tBu)_2I(^tBu_2bipy)]_2$ complex (Scheme I- 11).[276] The two uranyl-like $[U(N^tBu)_2I]$ complexes are connected through a diamond-shaped cation-cation interaction (Figure I- 24 left). Interestingly, a clear antiferromagnetic coupling between the uranium centres occurs at 13 K, and an exchange coupling between the two uranium(V) of -12cm^{-1} was calculated (Figure I- 24 right).

Scheme I- 11 Synthesis of $[\{U(N^tBu)_2I(^tBu_2bipy)\}_2]$

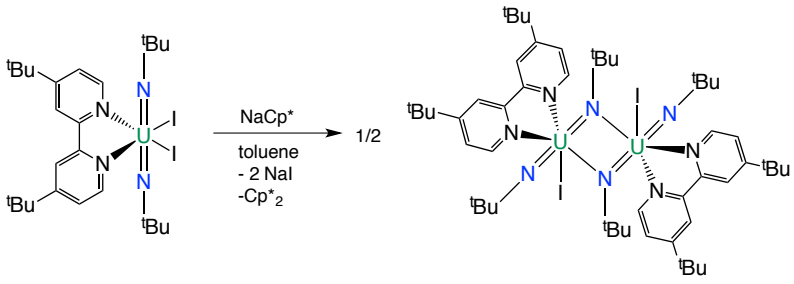

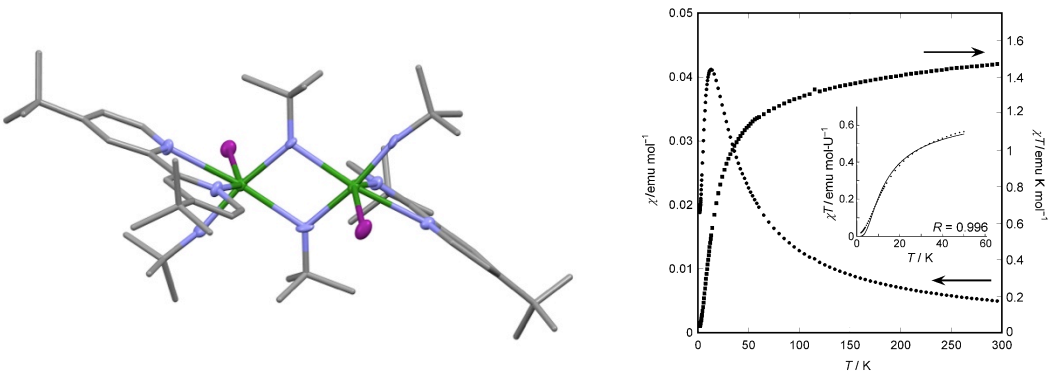

Figure I- 24 Molecular structure of the uranium dimer $[\{U(N^tBu)_2I(^tBu_2bipy)\}_2]$.(H atoms were omitted for clarity. Ligands are represented with pipes, C are represented in grey, N in blue, I in purple and U in green.) (left) and

molar temperature-dependent magnetic behaviour of [{U(N^{t}Bu)$_2$I(^{t}Bu$_2$bipy)}$_2$] recorded in the range 2-300 K (right).[276]

Recently, the group of Bart investigated the formation of uranium(VI) tris(imido) complexes and their reactivity.[277,278] Notably, the uranium(VI) [U(NDIPP)$_3$] (DIPP = 2,6-diisopropylphenyl) complex can be reduced with potassium graphite by a single-electron transfer to yield a tris(imido) uranium(V) complex, which self-assembled to form a dinuclear complex {[K(Et$_2$O)]$_2$[U(NDIPP)$_2$(μ-NDIPP)]$_2$} (Figure I- 25 left).[278] No unambiguous AF coupling was identified for {[K(Et$_2$O)]$_2$[U(NDIPP)$_2$(μ-NDIPP)]$_2$} (Figure I- 25 right), despite the short U-U distance (3.597(1) Å) close to the one found in [U(N^{t}Bu)$_2$(I)(^{t}Bu$_2$bpy)]$_2$ (3.577(1) Å) (T_N = 13 K).[276]

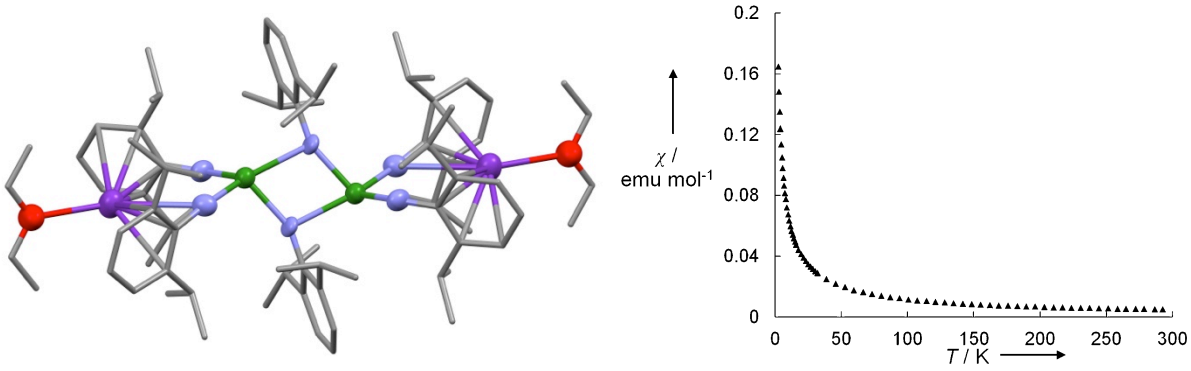

Figure I- 25 (left) Molecular structure of {[K(Et$_2$O)]$_2$[U(NDIPP)$_2$(μ-NDIPP)]$_2$} (H atoms omitted for clarity. Ligands are represented with pipes, C are represented in grey, N in blue, O in red, K in purple and U in green.) and (right) χ versus T of the temperature dependent magnetic data collected at 1.0 T for {[K(Et$_2$O)]$_2$[U(NDIPP)$_2$(μ-NDIPP)]$_2$}[278]

These examples show that the reduction of uranium(VI) imido complexes can lead to the formation of U(V) based polynuclear assemblies.

Andersen et al. have also shown that the comproportionation of the mononuclear uranium(V) imido complex [U^V(MeC$_5$H$_5$)$_2$(NR)] (R = Ph, SiMe$_3$) with the uranium(III) [U^{III}(MeC$_5$H$_5$)$_3$(THF)] complex can afford binuclear uranium(IV) complexes with diamond (U-μ-NR)$_2$ cores.[279] The magnetic properties of these complexes were not reported.

I.3.3) Carbon-bridged actinide clusters

Pure bridging carbon ligands are rare in actinide chemistry as carbanionic species are highly basic and readily react with traces of water or protons. In strictly aprotic conditions, alkenes, alkynes, carbenes, carbides, reduced aromatic cycles can promote the formation of polymetallic assemblies. Only two different examples of carbon-based bridging ligands, reduced arene and multi-ethynyl ligands are presented here.

I.3.3.1) Ethynyl ligands

Shores and co. were interested in the study of the magnetic communication between trigonal bipyramidal uranium(IV) complexes in polynuclear assemblies through conjugated organic ligands.[280] To achieve these objectives, they used the uranium(IV) ion coordinated to a bulky tripodal trianionic ligand (NN'_3 = $[N(CH_2CH_2NSi^tBu\text{-}Me_2)_3]$) and poly-ethynylbenzene ligands, which have been demonstrated to be efficient communicators of spin information between paramagnetic transition metal species.[281] They reported that the reaction of the monodeprotonated complex $[(bit\text{-}NN'_3)U]$ ($bit\text{-}NN'_3$ = $[N\text{-}(CH_2CH_2NSi^tBuMe_2)_2(CH_2CH_2Si^tBuMeCH_2]$) with the appropriate acetylenes led to di- or trinuclear complexes through the reprotonation of the triamidoamine ligand by the acetylene and the coordination of the acetylide anion formed in situ (Scheme I- 12).

Scheme I- 12 Synthesis of $[(NN'_3)_2U_2(m\text{-}DEB)]$, $[(NN'_3)_2U_2(p\text{-}DEB)]$ and $[(NN'_3)_3U_3(TEB)]$

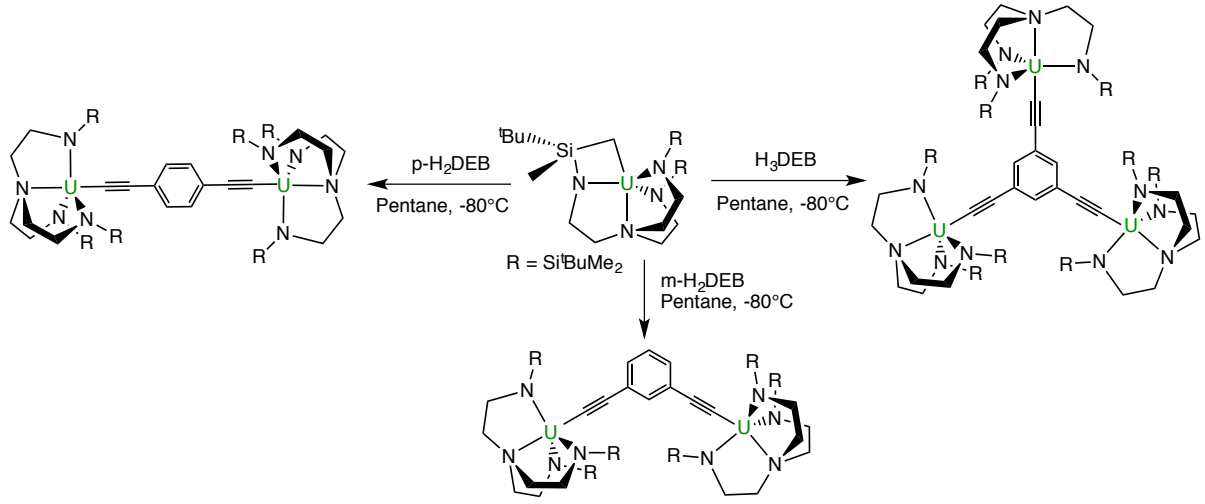

The uranium(IV) ions in the complexes $[(NN'_3)_2U_2(m\text{-}DEB)]$ ($m\text{-}DEB^{2-}$ = 1,3-diethynylbenzene), $[(NN'_3)_2U_2(p\text{-}DEB)]$ ($p\text{-}DEB^{2-}$ = 1,4-diethynylbenzene) and

$[(NN'_3)_3U_3(TEB)]$ (TEB^{3-} = 1,3,5-triethynylbenzene) formed with this strategic synthesis are in the expected coordination geometry, while the salt exchange reaction of $[(NN'_3)UCl]$ with 0.5 equiv of Li_2(p-DEB) resulted in the formation of a dinuclear U(IV) complex $[(NN'_3)_2U_2$(p-DEB)$(THF)_2]$.

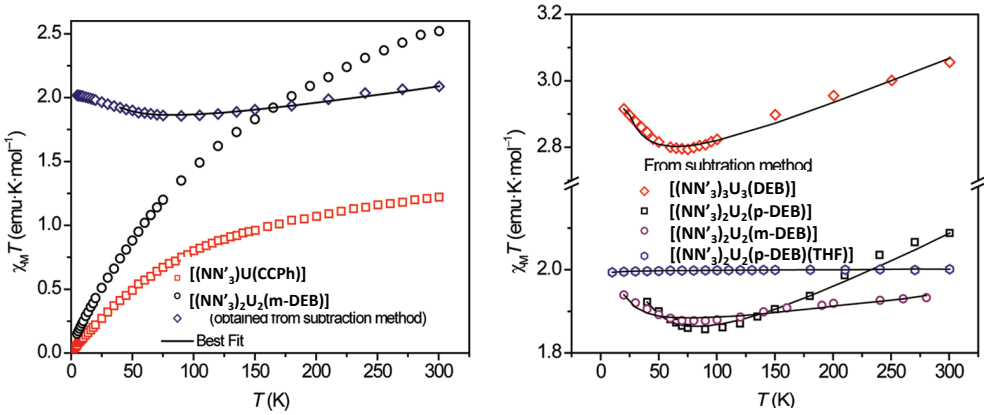

Figure I- 26 (left) Temperature dependence of the magnetic susceptibility for compounds $[(NN'_3)U(CCPh)]$ and $[(NN'_3)_2U_2$(m-DEB)] (1 kG); and fit of the data obtained from the subtraction method for $[(NN'_3)_2U_2$(m-DEB)]; (right) solid lines give best fits to the data obtained from the subtraction method for di and trinuclear complexes.[280]

Clear magnetic coupling between the uranium centres was not observed for any of the $[(NN'_3)_2U_2$(p-DEB)$(THF)]$, $[(NN'_3)_2U_2$(m-DEB)], $[(NN'_3)_2U_2$(p-DEB)] and $[(NN'_3)_3U_3$(TEB)] complexes.[280] The subtraction method was employed to evaluate if some magnetic interactions between the uranium(IV) centres were present and their strength (Figure I- 26). The magnetic susceptibility data for di- and trinuclear complexes were subtracted at each temperature by the paramagnetic susceptibility of a mono-acetylide species $[(NN'_3)U(CCPh)]$ (two times for dinuclear complexes, three times in the case of trinuclear species) and a temperature-independent value to account for the spin-only contribution of the U(IV) centre was added. The resulting data possess curvature, suggesting the presence of U-U magnetic interactions in the pentacoordinate uranium(IV) species, while no interaction is observed for $[(NN'_3)_2U_2$(p-DEB)$(THF)_2]$. Despite the fact that all the compounds presented in this study give non-magnetic ground states at low temperature, fits to the adjusted magnetic susceptibility data point to weak ferromagnetic communication between the uranium centres in the di- and trinuclear pentacoordinate U(IV)-containing compounds $[(NN'_3)_2U_2$(m-DEB)] (J = 4.8(2) cm^{-1}), $[(NN'_3)_2U_2$(p-DEB)] (J = 2.8(1) cm^{-1}) and $[(NN'_3)_3U_3$(TEB)] (J = 1.1(2) cm^{-1}), consistent with exchange coupling constants previously reported for actinide ions. AC susceptibility measurements were carried out on the $[(NN'_3)_2U_2$(m-DEB)] complex, showing the strongest ferromagnetic interaction, but did not reveal SMM properties.

I.3.3.2) Arene ligands

I.3.3.2.1) μ-η^1:η^1-Ar

The Liddle group reported an unexpectedly strong ferromagnetic exchange coupling in a dinuclear uranium(IV) complex. The reduction of [U(Ts^{Xy})(Cl)(THF)] (Ts^{Xy} = HC(SiMe$_2$NAr)$_3$; Ar = 3,5-Me$_2$C$_6$H$_3$] with KC$_8$ in hexane yielded the dinuclear uranium(IV) [U{HC(SiMe$_2$Ar)$_2$(SiMe$_2$-μ-N)}(μ-η^1:η^1-Ar)U-(Ts^{Xy})] complex. As a result of reductive C-N bond activation, the [U{HC(SiMe$_2$Ar)$_2$(SiMe$_2$-μ-N)}(μ-η^1:η^1-Ar)U-(Ts^{Xy})] complex features one bridging aryl group and one bridging imido group (Figure I- 27). Magnetisation data for this complex reveal an unusual ferromagnetic interaction with an exchange coupling constant estimated at J = + 20 cm^{-1}.[282]

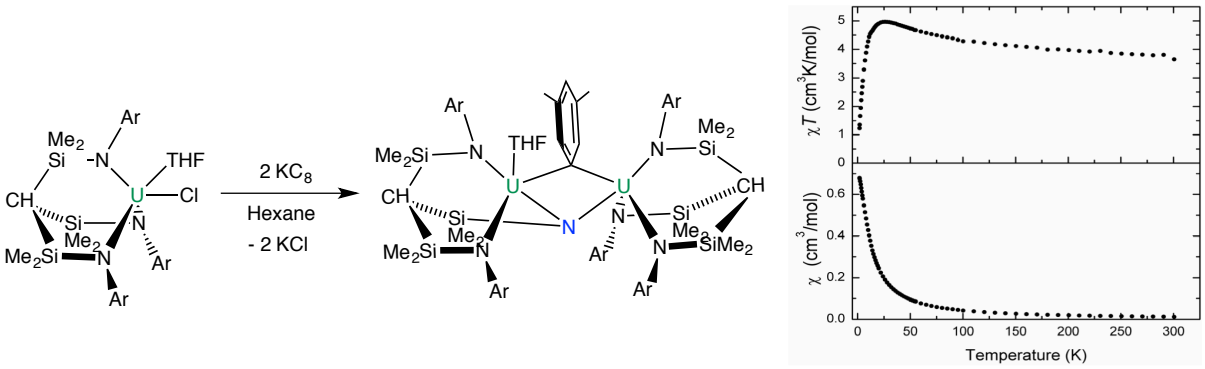

Figure I- 27 (left) Synthesis of [U{HC(SiMe$_2$Ar)$_2$(SiMe$_2$-μ-N)}(μ-η^1:η^1-Ar)U-(Ts^{Xy})]; (right) temperature-dependent magnetic susceptibility data of [U{HC(SiMe$_2$Ar)$_2$(SiMe$_2$-μ-N)}(μ-η^1:η^1-Ar)U-(Ts^{Xy})] in the temperature range 2-300 K (right).[282]

I.3.3.2.2) μ-η^6:η^6-Ar

Several studies report the synthesis of inverted sandwich compounds in which an arene molecule bridges two uranium ions in a symmetrical fashion such as η^6,η^6 for C$_6$ arene. Liddle recently reviewed the inverted sandwich arene complexes of uranium[182] and only two examples presenting interesting magnetic properties are highlighted here.

The first diuranium inverted C$_6$-arene sandwich complexes were prepared by the Cummins group from the treatment of [U(I)(N[R]Ar)$_3$] (Ar = C$_6$H$_3$-3,5-Me$_2$); R = ^{t}Bu, adamantyl) with excess KC$_8$ in toluene (Figure I- 28 left).[272] These reactions afforded the sandwich complexes [{U(N[R]Ar)$_2$}$_2$(μ:η^6-η^6-C$_6$H$_5$Me)] with concomitant elimination of KI and one amide ligand per uranium, probably as its potassium salt. Only the structure of [{U(N[Ad]Ar)$_2$}$_2$(μ:η^6-

η^6-C_6H_5Me)] was determined by X-ray diffraction. Short U-C_{Tol} distances (mean 2.593(9) Å) and theoretical calculations highlighted the strong uranium-arene interactions. Oxidation state assignments are not straightforward for such reduced arene species and investigations of the electronic structure revealed the U^{III}-Tol^{2-}-U^{III} state as the best formulation.[283]

The magnetic susceptibility data of the [{U(N[^{t}Bu]Ar)$_2$}$_2$(μ:η^6-η^6-C_6H_5Me)] complex were reported, but not compared to the structurally characterised Ad complex. A maximum at 110 K, characteristic of the presence of an antiferromagnetic coupling between the uranium centres in [{U(N[^{t}Bu]Ar)$_2$}$_2$(μ:η^6-η^6-C_6H_5Me)] was observed (Figure I- 28 right). This Neel temperature of 110 K is the highest reported so far for a molecular complex of uranium.[283]

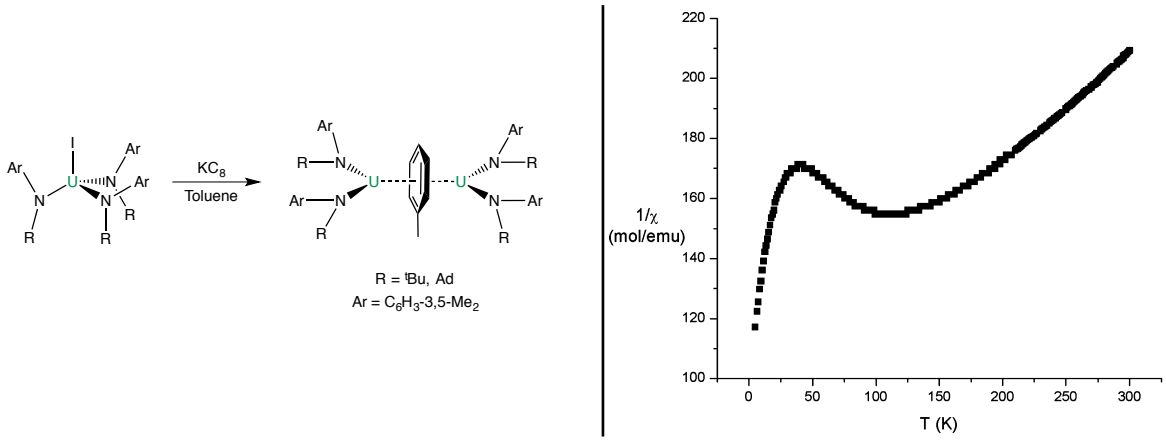

Figure I- 28 (left) Synthesis of [{U(N[R]Ar)$_2$}$_2$(μ:η^6-η^6-C_6H_5Me)] and (right) plot of the inverse of the magnetic susceptibility versus T for [{U(N[^{t}Bu]Ar)$_2$}$_2$(μ:η^6-η^6-C_6H_5Me)].[283]

Despite the increasing number of characterised arene-bridged diuranium complexes and the strong antiferromagnetic coupling observed in [{U(N[^{t}Bu]Ar)$_2$}$_2$(μ:η^6-η^6-C_6H_5Me)], very few magnetic studies have been reported so far for such assemblies.[179,255,283] From these compounds, one example revealed SMM behaviour. Liddle et al reported the reduction of the uranium(IV) [U(BIPM^{TMS})(μ-I)(I)]$_2$ complex (BIPM^{TMS} = C(PPh$_2$NSiMe$_3$)$_2$) with potassium graphite in the presence of toluene, in THF leading to the inverted-sandwich arene-bridged diuranium complex [(U(BIPM^{TMS}H)(I))$_2$(μ- η^6-η^6-$C_6H_5CH_3$)] (Scheme I- 13).[179] Similarly to the arene-bridged diuranium complexes of Cummins, the two uranium atoms of [(U(BIPM^{TMS}H)(I))$_2$(μ-η^6-η^6-$C_6H_5CH_3$)] are the trivalent oxidation state, bound to a bridging toluene^{2-} ligand.

Scheme I- 13 Synthesis of $[(U(BIPM^{TMS}H)(I))_2(\mu\text{-}\eta^6\text{-}\eta^6\text{-}C_6H_5CH_3)]$

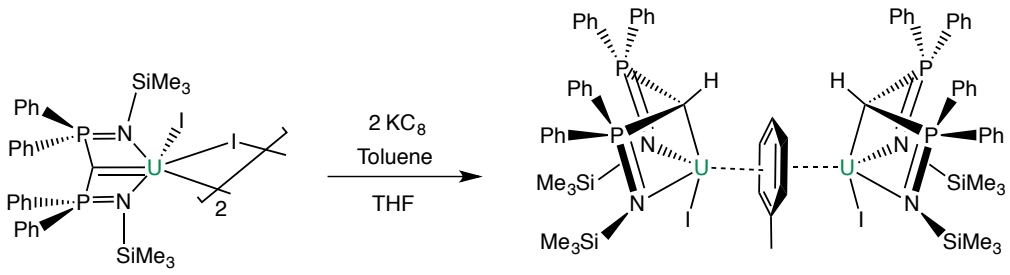

In contrast to $[\{U(N[^tBu]Ar)_2\}_2(\mu{:}\eta^6\text{-}\eta^6\text{-}C_6H_5Me)]$, no strong antiferromagnetic exchange interactions are present in $[(U(BIPM^{TMS}H)(I))_2(\mu\text{-}\eta^6\text{-}\eta^6\text{-}C_6H_5CH_3)]$. This complex showed SMM properties.[179] A butterfly-shaped hysteresis and frequency-dependent out-of-phase signals (under an external dc field of 1 kG) were observed (Figure I- 29), demonstrating the presence of slow relaxation of the magnetisation. However, the maximum in the out-of-phase component was observed only for the highest ac frequencies, precluding the extraction of an energy barrier.

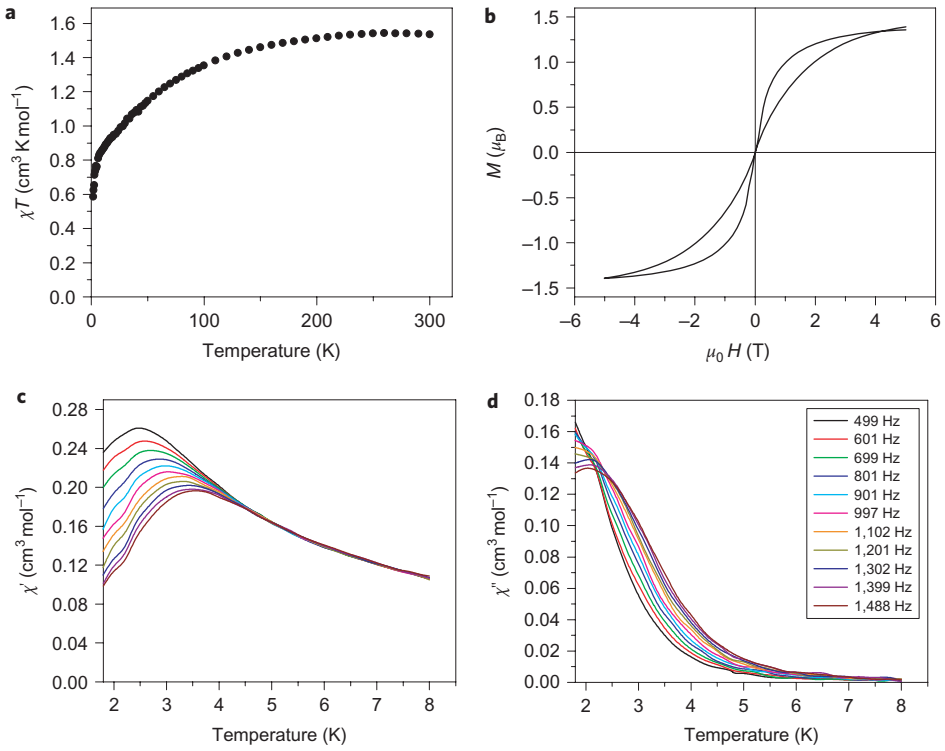

Figure I- 29 (a) Susceptibility-temperature product at applied fields of 0.1 T (T < 50 K) and 1 T (T > 40 K); (b) magnetic hysteresis at 1.8 K at a sweep rate of 2.6 $mT.s^{-1}$; (c) in-phase component of the ac susceptibility at different frequencies at an applied dc field of 1 kG; (d) out-of-phase component of the ac susceptibility at different frequencies at 1 kG oft he $[(U(BIPM^{TMS}H)(I))_2(\mu\text{-}\eta^6\text{-}\eta^6\text{-}C_6H_5CH_3)]$ complex.[179]

Great differences are observed in the magnetic properties of the two inverted sandwich arene complexes of uranium [{U(N[^{t}Bu]Ar)$_2$}$_2$(μ:η^6-η^6-C$_6$H$_5$Me)] and [(U(BIPM^{TMS}H)(I))$_2$(μ-η^6-η^6-C$_6$H$_5$CH$_3$)]. However, the reason for such a difference is not resolved and is complicated by the absence of the crystal structure of the dinuclear [{U(N[^{t}Bu]Ar)$_2$}$_2$(μ:η^6-η^6-C$_6$H$_5$Me)] complex. Moreover, it is still not clear whether the observed phenomena for [(U(BIPM^{TMS}H)(I))$_2$(μ-η^6-η^6-C$_6$H$_5$CH$_3$)] originates from poly- or single-ion behaviour, even though theoretical calculations revealed some degree of electronic communication mediated by δ-bonds.[179]

I.3.4) Summary

An overview of the synthetic strategies employed to design polynuclear actinide clusters and the reported examples of magnetic exchange in actinide-containing molecules is contained in this chapter. Although other bridging ligands have been used to design actinide cluster (halides,[9,284-287] hydrides,[9,288,289] chalcogenides,[187,272] pnictogen and derivatives,[182,290,291] cyanide,[85] oxalate,[292] and bridging ligands arising of small molecule activation[109] we chose to focus on the assemblies showing magnetic exchange. It is apparent that strong differences occur for each of the three paramagnetic oxidation states of uranium: +III, +IV, +V.

- **Uranium(III):** Although mononuclear uranium(III) complexes may behave as SIMs in multiple coordination environments,[165,168-170,172,173,175 171 174,176] the anisotropy barriers remain weak (5-33 K). The design of polynuclear assemblies of uranium(III) might be a good way to improve the slow relaxation of the magnetisation. Only one dinuclear uranium(III) complex, [(U(BIPM^{TMS}H)(I))$_2$(μ-η^6-η^6-C$_6$H$_5$CH$_3$)], single molecule magnet has been reported so far. However, the reason of this is still uncertain, and may be attributed to a single ion effect or to a magnetic exchange through the bridging arene.[179] To our knowledge, only two unambiguous exchange-coupled uranium(III) complexes have been reported and revealed antiferromagnetic coupling, with Neel temperatures of 16 K for the [U(OSi(O^{t}Bu)$_3$)$_2$(μ-OSi(O^{t}Bu)$_3$)]$_2$ complex[253,255] and 110 K for the [{U(N[^{t}Bu]Ar)$_2$}$_2$(μ:η^6-η^6-C$_6$H$_5$Me)] complex.[272,283] It is worth reiterating that this last example exhibis the highest Neel temperature for molecular uranium systems to date. The lack of knowledge on exchange-coupled uranium(III) is strongly correlated to the extremely limited number of polymetallic assemblies of uranium(III) due to the high reactivity and instability of U(III) compounds. The [U(OSi(O^{t}Bu)$_3$)$_2$(μ-OSi(O^{t}Bu)$_3$)]$_2$ complex displays a U$_2$O$_2$ diamond core bridged through the anionic oxygen of the tert(tristerbutyl)siloxide ligand (U1-O1=2.398 Å, U1-O1A=2.549 Å, U-U

3.9862(2) Å, U-O-U=107.4°).[253,255] The U-U distance in [{U(N[Ad]Ar)$_2$}$_2$(μ:η^6-η^6-C$_6$H$_5$Me)] (related to the [{U(N[^{t}Bu]Ar)$_2$}$_2$(μ:η^6-η^6-C$_6$H$_5$Me)] complex, U-U: 4.320 Å)[272,283] is significantly longer than in [U(OSi(O^{t}Bu)$_3$)$_2$(μ-OSi(O^{t}Bu)$_3$)]$_2$, but the coordination of the reduced arene to the uranium(III) leads to stronger U-C interactions than the siloxide ligands. The pathway for the magnetic communication is probably more efficient through a bridging arene, leading to high antiferromagnetic coupling. It could be anticipated that in order to provide efficient magnetic exchange between several uranium(III) ions, bridging ligands than can support multiple bonding should be investigated to generate a strong uranium-ligand interaction and promote superexchange pathway.

• **Uranium(V)/Neptunyl(V):** The first example of exchange-coupled actinide compounds reported (T_N = 20 K, J = -19 cm^{-1}) consists of the dinuclear uranium(V) imido complex [(MeC$_5$H$_4$)$_3$U]$_2$(μ-1,4-N$_2$C$_6$H$_4$), in which the two uranium(V) ions are coupled through the π-conjugated organic ion [μ-1,4-N$_2$C$_6$H$_4$]$^{4-}$.[62] A few examples of cation-cation complexes of uranyl(V) revealing antiferromagnetic coupling in diamond-shaped[47] or T-shaped[48,231,242] assemblies followed, with Neel temperatures ranging from 5 to 12 K. A mixed-valent cation-cation complex of neptunyl has even shown ferromagnetic neptunyl(VI)-neptunyl(V) interaction (+7.5 cm^{-1}) leading to SMM properties.[112,181] These preliminary results indicate that the cation-cation interaction of actinyl moieties provides a good pathway for magnetic communication.

A particular unit found in most of the di-uranium(V) complexes displaying antiferromagnetic coupling, is the diamond-shaped U$_2$E$_2$ (E= N, O) core (Figure I- 30). The bridging imido and oxo ligands yield strong uranium-ligand interactions and provide a pathway for the magnetic communication of the uranium(V) ions.[47,199,204,276] Neel temperatures ranging from 5 to 70 K have been reported for these complexes. The [{(((^{nP,Me}ArO)$_3$tacn)U}$_2$(μ-O)$_2$] complex displays the highest Neel temperature (70 K) reported for two coupled uranium(V) ions.[199] However, not all of the di-uranium(V) complexes with a diamond-shaped core reveal clear antiferromagnetic coupling. Notably, no unambiguous antiferromagnetic coupling was observed in {[K(Et$_2$O)]$_2$[U(NDIPP)$_2$(μ-NDIPP)]$_2$} [278] and [{((^{Ad}ArO)$_3$N)U}(μ-O)$_2${U((^{Ad}ArO)$_3$N)(PyNO)}] [187] (Figure I- 30). Slight structural changes in the diamond-core or in the coordination geometry of the U(V) ions may limit the magnetic communication and lead to the stabilisation of the high spin rather than the low spin magnetic ground state. It is very difficult to understand the different properties due to the lack of theoretical models and examples to rely on.

$[U(N^tBu)_2I(^tBu_2bipy)]_2$ [276]	**$\{[K(Et_2O)]_2[U(NDIPP)_2(\mu\text{-}NDIPP)]_2\}$** [278]
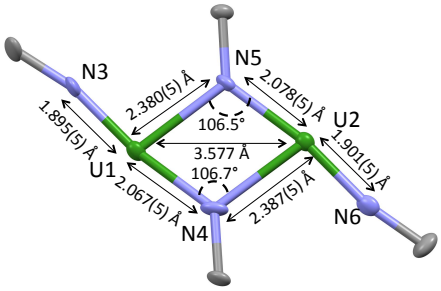	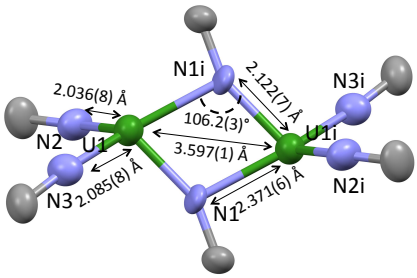
T_N=13 K, J=-12cm^{-1}	No AF
U1, U2: Pseudo octahedral	U1, U2: Distorded tetrahedral
$[UO_2(dbm)_2K(18C6)]_2$ [47]	**$[\{(Me_3SiO)U(\mu\text{-}O)\}_2(Pcm)]$** [204]
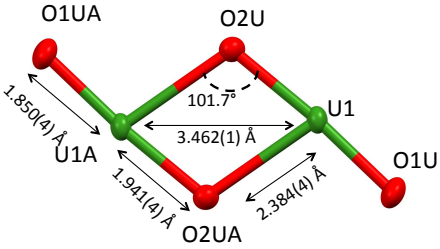	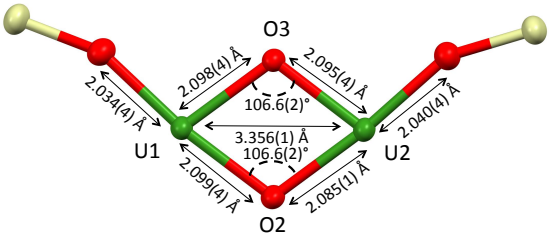
T_N=5 K	T_N=17 K, J=-33cm^{-1}
U1, U2: Distorded pentagonal bipyramidal	U1, U2: Distorded pentagonal bipyramidal
$[\{((^{nP,Me}ArO)_3tacn)U\}_2(\mu\text{-}O)_2]$ [199]	**$[\{((^{Ad}ArO)_3N)U\}(\mu\text{-}O)_2\{U((^{Ad}ArO)_3N)(PyNO)\}]$** [187]
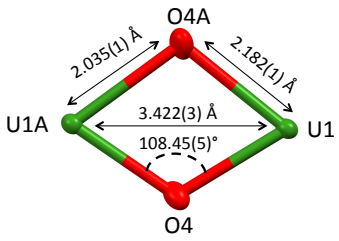	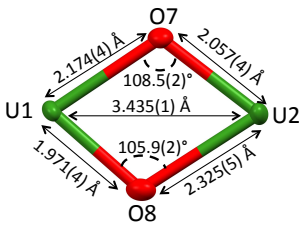
T_N=70 K	No AF
U1, U2: Trigonal dodecahedral	U1: pseudo-octahedral / U2: distorted mono-capped trigonal prismatic

Figure I- 30 Diamond cores and structural parameters of dinuclear uranium(V) complexes

However, from these examples, we can remark that the interaction of uranium through bridging ligands seems to require uranium-ligand multiple bonds, found with imido or oxo ligands.

• **Uranium(IV):** Uranium(IV) compounds have been the most investigated due to their stability and ease of handling. However, the magnetism of uranium(IV) is strongly correlated to its coordination geometry. In contrast to U(III) and U(V), the $5f^2$ ions display a singlet ground state in most reported complexes and a limited number of examples of U(IV) complexes displaying magnetic exchange has been reported.

To our knowledge, only four examples of complexes presenting unambiguous antiferromagnetically coupled uranium(IV) ions have been reported so far and they consist of the $[\{((^{tBu}ArO)_3tacn)U^{IV}\}_2(\mu\text{-}E)]$ (E: O, S, Se)[187] and $[\{U(Tren^{DMSB})\}(\mu\text{-}O)\{U(Tren^{DMSB\text{-}C2O2})\}]$ [200] complexes. In each of them, the two uranium(IV) ions are coupled through a linear chalcogenide bridge.

Ferromagnetic interactions have been reported in a few homometallic uranium(IV) complexes. Weak ferromagnetic interactions have been estimated ranging from +1.1 to +4.8 cm^{-1} in di- and tri-nuclear uranium(IV) assemblies, in which the uranium ions are bridged through conjugated ethynylbenzene ligands[280] while a stronger ferromagnetic exchange coupling constant of J = +20 cm^{-1} was estimated in the complex $[U\{HC(SiMe_2Ar)_2(SiMe_2\text{-}\mu\text{-}N)\}(\mu\text{-}\eta^1\text{:}\eta^1\text{-}Ar)U\text{-}(Ts^{Xy})]$,[282] displaying a distorted UNCU diamond core (UCU angle of 89.2°).

Finally, a few examples of heterometallic transition metal-uranium(IV) complexes have been reported that displayed ferromagnetic or antiferromagnetic coupling interactions. Very weak coupling constants were reported for the $U^{IV}L^i{}_2M^{II}{}_2(Py)_n$ (M = Co, Ni, Cu, Zn; L^i = Schiff-base bridging ligands) complexes (U(IV)-Cu(II): +0.7/+2.6 cm^{-1} and -0.5/-1.8 cm^{-1} depending on the nature of the Schiff base ligand) [7,245-248] in which the uranium ion and the transition metals are connected through the bridging phenolate of the compartmental ligand, while stronger ferromagnetic coupling interactions were reported in the $(cyclam)M[(\mu\text{-}Cl)U(Me_2Pz)_4]_2$ clusters (CoU_2 = +15/+48 cm^{-1}, NiU_2 = +2.8/+19 cm^{-1}) in which the uranium ions and the transition metal are connected through a chloride bridge.[262,263]

No single molecule magnet behaviour has been reported for these ferromagnetically coupled uranium(IV) homo or heterometallic clusters.[262,263,287] However, in 2015, the first uranium(IV)-based SMM was reported thanks to the coupling of a uranium(IV) ion with an organic radical ligand.[167] This result clearly suggests that in the right environment, and coupled with paramagnetic species, polynuclear uranium(IV) SMMs may be reachable.

I.4) Purpose and objectives of the project

A crucial prerequisite for the application of SMMs is the observation of hysteresis at reasonable temperatures. In this quest, chemists and physicists face huge synthetic challenges. The high magnetic anisotropy of the uranium ion over a range of oxidation states, combined with its ability to engage in magnetic exchange interactions with other metal centres, makes it particularly promising for the development of improved SMMs. Moreover, the low radioactivity of natural and depleted uranium, and its large availability from the nuclear industry, renders it the actinide element most suitable for potential applications. The objectives of this PhD work were the development of new synthetic strategies to prepare well-defined high nuclearity homo-polymetallic and heteropolymetallic uranium clusters and to implement magnetic exchange between metal ions in these assemblies with the final target to design improved single molecule magnets. In order to design uranium based exchange-coupled single molecule magnets, better knowledge of the magnetic communication in actinide-based molecules is also essential.

In this context, we will develop novel synthetic strategies to build polynuclear actinides complexes assembled via different bridging ligands. The oxo ligands are able to bind multiple metallic centres leading to a wide variety of geometries. Moreover, magnetic communication through oxo groups has been reported in polymetallic actinide complexes and has led to strong antiferromagnetic or ferromagnetic interactions. The first objective of this PhD work was to explore the formation of large uranium(IV) oxo/hydroxo clusters, possibly with high spin numbers. To build these new oxo compounds, we will use a synthetic method developed in our lab involving the controlled hydrolysis of low-valent uranium precursors in organic solution. These reactions will be carried out in presence of environmentally relevant ligands. Polynuclear oxo assemblies are indeed involved in the environmental actinide migration. The small oxo clusters formed under controlled conditions can be seen as simple models of the species involved in the environment. This study may lead to a better understanding of the formation of the aggregates, which is particularly relevant in the clean-up of radioactive waste. To design and isolate large poly-uranium clusters with possible SMM properties and with the objective of a better understanding of the parameters directing the cluster formation and geometry, we will explore the influence of the reaction parameters such as the solvent, the temperature, the stoichiometry of the organic ligand and the nature of the uranium precursor.

In the second part, we will investigate another route to oxo-bridged polymetallic assemblies. We will take advantage of the ability of uranyl(V) cations to bind other metal ions through the oxo group for the development of poly-homometallic and poly-heterometallic

complexes. We will use cation-cation interactions to provide a rational route to the assembly of polymetallic complexes. Combined with the single ion anisotropy of the uranyl(V) ion, the obtained cation-cation complexes have great potential to act as single molecule magnets. Subtle ligand tuning and carefully chosen synthetic methods will be developed to prevent disproportionation of the UO_2^+ cation and to promote self-assembly through cation-cation interactions. Furthermore, we will control the nuclearity of the resulting assemblies to design selectively 1D polymeric structures or discrete compounds. A wide variety of transition metals or lanthanide ions will be used to form exchange-coupled 3d-5f or 4f-5f heteropolymetallic assemblies. High spin-inversion barriers and hysteresis temperatures should result from associating the anisotropic UO_2^+ cation and d-block and f-block metal cations with a high total spin. Moreover, the simple $5f^1$ electronic structure is an excellent starting point for the development of magnetic models, an essential step for understanding the structure-properties relation. In parallel, we will investigate the coordination chemistry of neptunyl(V) in the group of Dr. Moisy at Marcoule. Using the knowledge accumulated in our lab on uranyl(V) chemistry, similar working conditions will be used with the neptunyl(V) moiety to access novel discrete complexes. For each novel polynuclear assembly synthesised, we will investigate the magnetic properties, notably the presence of slow relaxation of the magnetisation, characteristic of single molecule magnet behaviour, to rationalise the structure-properties relationship.

Finally, we will explore the chemistry of bridging nitride ligands to design polynuclear uranium assemblies. Nitride bridges may lead to uranium-ligand multiple bonds and provide a pathway for magnetic interactions. Moreover the uranium-nitride systems are particularly relevant for the development of new nuclear fuels, N-atom transfer catalysts, as well as gaining a better understanding of f-orbital implication in actinide-ligand multiple bonds. We will develop new synthetic routes to nitrido bridged di-uranium complexes in which uranium ions are held in close proximity to each other by the presence of U-N multiple bonding. These ligands may provide attractive starting materials for the synthesis of magnetically coupled uranium(III) systems. The rational design of exchange-coupled SMM based on uranium(III) presents significant synthetic challenges. We will explore the possibility of accessing U(III)-nitride from the chemical reduction of previously reported uranium(IV) nitrido bridged complexes. In parallel, we will develop synthetic methods to access bis-uranium bis-nitrido compounds from the reductive and selective transformation of inorganic azides to investigate the impact of subtle change on the uranium coordination environment and U-N-U angles on the magnetic properties.

CHAPTER II. OXO/HYDROXO POLYNUCLEAR COMPLEXES OF URANIUM

II.1) Context

Oxide and hydroxide are suitable ligands to utilise in the preparation of polymetallic assemblies. These ligands are indeed able to bridge from two to six metallic centres, leading to various geometries and unexpected polymetallic assemblies. Moreover, these oxo/hydroxo bridges favour strong magnetic communication between metallic centres required in the design of SMMs. The first SMM reported in 1993 by Sessoli and coworkers, $[Mn_{12}O_{12}(CH_3COO)_{16}(H_2O)_4]$, consisted of a $Mn_{12}O_{12}$ core where the twelve manganese ions were connected by μ_3-oxo ligands.[115,116] Since then, several oxo/hydroxo clusters with 3d or 4f metals displaying SMM behaviour, exhibiting high energy barriers of the magnetisation have been reported.[125,130,150,186,293,294] Furthermore, the strong magnetic communication in polynuclear uranium oxo complexes is reported in the Introduction chapter.[47,187,199,204,231,242] Since oxo ligands are efficient bridging ligands providing a path for magnetic communication, we were interested in investigating the assembly of large polymetallic clusters.

A second interesting property of oxo/hydroxo actinide assemblies is their environmentally relevance, as oxide nanoparticles of actinides can be formed in natural waters. A few general aspects of the actinides in the environment are presented in the next part.

II.1.1) Oxide nanoparticles formed in the environment

The highly toxic and radioactive actinide contaminants present naturally or from human activities in the environment pose a long-term health risk if they are ingested or inhaled.[295] That is why the study of actinide speciation in the environment is an active research area.[296-299]

Actinide speciation strongly depends on the pH conditions and redox potentials as several oxidation states can co-exist in natural waters under normal conditions: uranium exists both in the +VI and the +IV oxidation states, neptunium is present in the +V and +IV oxidation states whereas the +III, +IV, +V and +VI oxidation states of plutonium can co-exist.[28] The speciation of actinides also depends on the natural ligands and minerals present

in the media.[31-33,300-303] As each local soil is unique, a prediction of the spread through the environment is complicated.

Actinides have been found to migrate in the environment under different forms: as small complexes adsorbed onto mobile particles,[298,304-306] as soluble complexes with natural ligands, and as, polynuclear or colloidal assemblies.[21,299,307-311] The size of the actinide particles or colloids strongly influences the solubility: a small particle (sub-micrometric size) has high apparent solubility, facilitating actinide migration in the environment.

Polynuclear actinide oxide assemblies have been observed in natural waters and can be formed from the easy hydrolysis of An^{4+} over a wide range of pH values through olation and oxolation reactions, as highlighted Scheme II- 1.[21,87,296]

Scheme II- 1 Hydrolysis, olation and oxolation reactions of tetravalent actinides

Hydrolysis of An(IV) ions $\quad An^{4+} + n\ H_2O \rightleftharpoons [An(OH)_n]^{(4-n)+} + n\ H^+$

Olation reaction $\quad [An(OH)_n]^{(4-n)+} + [An(H_2O)_n]^{4+} \rightleftharpoons$ "An-OH-An" $+ H_2O$

Oxolation reaction $\quad 2\ [An(OH)_n]^{(4-n)+} \rightleftharpoons$ "An-O-An" $+ H_2O$

Moreover, in 1991 Lovley and coworkers discovered that anaerobic bacteria could convert dissolved uranyl(VI) complexes into precipitated tetravalent uranium, mainly as uraninite UO_2.[312] This microbial activity is being actively investigated as a method of in situ bioremediation of uranium-contaminated groundwater, assuming that the formation of highly insoluble uraninite will inhibit the mobilisation of uranium. Reviews in the literature have given detailed accounts of the microbial communities associated with bioremediation of uranium-contaminated groundwater.[313-315]

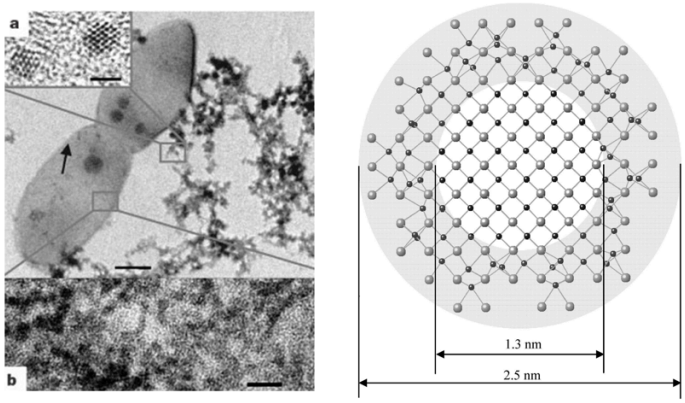

Figure II- 1 Characterisation of bioreduced uraninite (UO_2) nanoparticles by TEM[316] (left) and EXAFS structural determination of biogenic uraninite nanoparticles[317] (right, U atoms were represented in grey, O atoms in black).

However, in 2002, Suzuki and coworkers observed that uraninite, secreted outside the bacteria cell, was nanometer-sized (Figure II- 1).[316-319] Consequently, due to their small size (diameter less than 2nm), these uraninite nanoparticles are mobile in aqueous solution.

The reduction of UO_2^{2+} by anaerobic microorganisms is via direct enzymatic pathways or indirectly via biogenerated Fe(II). The formation of a pentavalent uranyl intermediate was observed in the course of the bioreduction mediated by *Geobacter sulfurreducens*.[320-322] This observation supports the hypothesis of a single electron transfer to uranyl(VI), forming uranyl(V), which disproportionates and produces UO_2. However, this uranyl(V) intermediate is not systematically observed. Moreover, it has been recently demonstrated that non-uraninite uranium(IV) can also be formed as a result of direct microbial activity.[323] The speciation and solubility of this non-crystalline uranium(IV) strongly depend on the presence of complexing surfaces and inorganic ligands.[306,324-327] A full understanding of actinide bioreduction may lead to the development of new approaches for the remediation of uranium-contaminated sites.

The synthesis of simple molecular models can help to understand the separate parameters influencing polynuclear assembly formation in complicated media such as the environment. Notably, oxo and hydroxo uranium species may form simple models of the uraninite nanoparticle found in the environment.

II.1.2) Oxo/hydroxo clusters: aqueous solution

Oxolation and olation reactions of actinide(IV) compounds easily take place in aqueous solution, resulting in the formation of polynuclear oxo/hydroxo assemblies.[87] However, these reactions often lead to complicated mixtures of compounds, and only a few clusters have been structurally characterised from aqueous solution. Most of the clusters structurally characterised in acidic aqueous conditions consist of assemblies of six uranium(IV) atoms placed at the corners of an octahedron. Each of the eight triangular faces are capped with triply bridging oxo or hydroxo ligands, resulting in a $U_6O_4(OH)_4$ core. Carboxylate or sulfonate ligands bridge two adjacent uranium centres, stabilising the assembly.[328-330] One example for uranium is represented in Figure II- 2.[329] Clusters presenting the same hexanuclear core have also been reported for Th(IV),[329-331] Np(IV)[330,332] and Pu(IV) ions.[333]

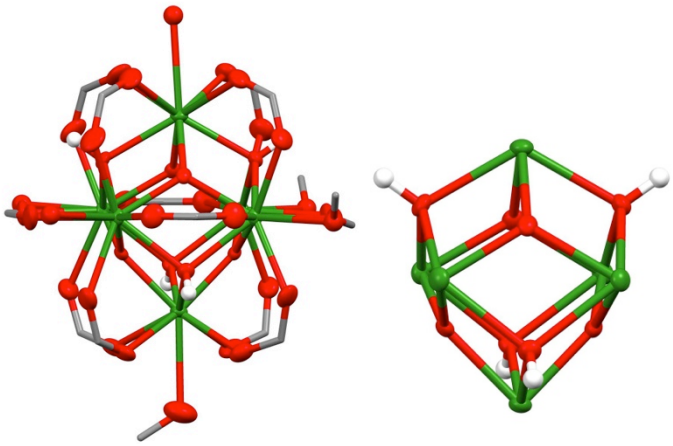

Figure II- 2 Molecular structure of $[U_6O_4(OH)_4(HCOO)_{12}(H_2O)_6]$ (left), $U_6O_4(OH)_4$ core (right) (right; H were not determined in the crystal structure) (Ligands are represented with pipes for clarity, C are represented in grey, O in red, H in white, and U in green) [329]

In 2008, Soderholm et al. first isolated a disrete plutonium cluster $Li_{12}[Pu_{38}O_{56}Cl_{42}(H_2O)_8](H_2O)_x$ with a $Pu_{38}O_{56}$ core (Figure II- 3) from an aqueous solution containing plutonium colloids. More recently, the same group reported that the neutralisation of a Pu(IV) solution in concentrated HCl with LiOH while the solution is boiling yields to the similar cluster. Recrystallisation from an aqueous solution of HCl/LiCl afforded $Li_2[Pu_{38}O_{56}Cl_{42}(H_2O)_{20}](H_2O)_{15}$. In both clusters, the $[Pu_{38}O_{56}]^{40+}$ core is decorated with chloride anions and consists of 38 plutonium(IV) atoms assembled via μ_3- and μ_4-oxo ligands with a fluorite-type structural packing.[334,335]

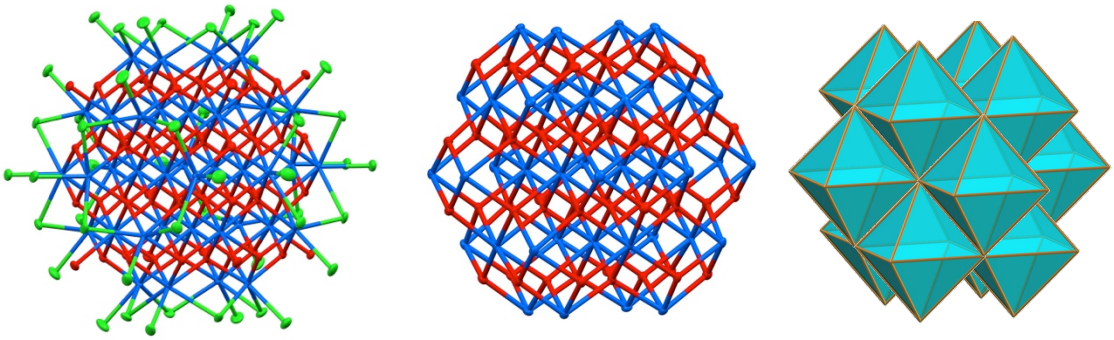

Figure II- 3 Molecular structure of the $Li_{12}[Pu_{38}O_{56}Cl_{54}(H_2O)_8](H_2O)_x]$ cluster and $Pu_{38}O_{56}$ cluster core (H and Li atoms were not determined in the crystal structure. Cl are represented in green, O in red and Pu in blue) [334,335]

Despite its environmental relevance, the isolation of polynuclear assemblies in aqueous solution is very difficult due to the complexity of hydrolysis/redox actinide chemistry. Organic solvents have been used to gain better control of the reaction conditions involved in the oxo/hydroxo cluster synthesis, most notably for the design of SMMs.

II.1.3) Controlled hydrolysis of low-valent uranium in organic solution

In organic media, controlled oxidation of low-valent uranium complexes with O_2 or with oxo group donors (Me_3NO, Py-NO, N_2O, NO, CO_2) provides a route to bridging oxo polymetallic compounds of uranium. Some examples are presented in the Introduction chapter.[70,187,189,195,197-199]

Oxo or hydroxo complexes of uranium from low-valent uranium complexes in anhydrous solution have also been reported as the outcome of adventitious traces of water.[188,192,336] In contrast, Andersen et al. reported 20 years ago that the reaction of stoichiometric amounts of water with the trivalent uranium hydride complex $[U(Cp^+)_2(\mu_2\text{-}H)]_2$ (Cp^+: $1,3(Me_3C)_2C_5H_3$) afforded the isolation of the dinuclear hydroxo cluster $[U(Cp^+)_2(\mu_2\text{-}OH)]_2$, which can be converted quantitatively to the oxide analogue after heating at 100°C (Scheme II- 2). In the $[U(Cp^+)_2(\mu_2\text{-}OH)]_2$ and $[U(Cp^+)_2(\mu_2\text{-}O)]_2$ complexes, the two uranium centres are bridged by two μ_2-hydroxo or μ_2-oxo ligands.[337] The magnetic properties of these two hydroxo and oxo complexes were not reported by the authors.

Scheme II- 2 Hydrolysis of $[Cp^+_2U(\mu_2\text{-}H)]_2$

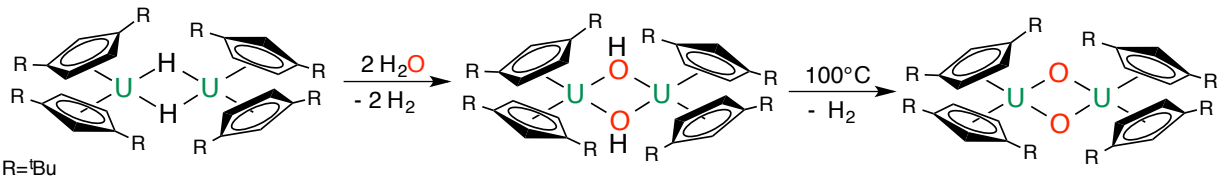

In 2003, Mazzanti et al. demonstrated that such controlled hydrolysis reactions could be extended to U(III) complexes containing different supporting ligands. Notably, the reaction of stoichiometric amounts of water with the trivalent uranium TPA complex $[U(TPA)_2]I_3$ led to the loss of protonated TPA and the formation of the trinuclear U(IV) oxo complex $\{[U(TPA)(\mu_2\text{-}O)I]_3(\mu_3\text{-}I)\}I_2$.[96] The three uranium atoms in $\{[U(TPA)(\mu_2\text{-}O)I]_3(\mu_3\text{-}I)\}I_2$ form a triangular unit and are connected by three bridging μ_2-O placed along the edges of the triangle. One TPA ligand remained coordinated to each uranium atom, suggesting that the TPA ligand probably prevents the formation of larger assemblies (Figure II- 4).

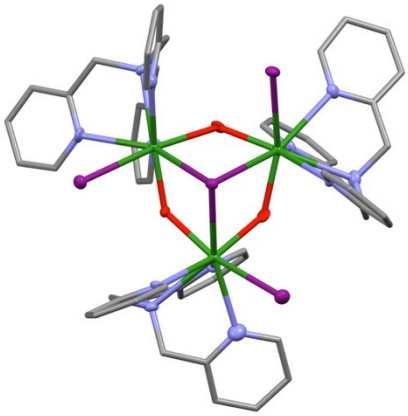

Figure II- 4 Molecular structure of $\{[U(tpa)(\mu_2\text{-}O)I]_3(\mu_3\text{-}I)\}^{2+}$ (H atoms, co-crystallised solvent molecules and non-coordinated iodide counterions were omitted for clarity. Ligands are represented with pipes. C are represented in grey, O in red, N in blue, I in purple and U in green.) [96]

Based on the observation that bulky ligands may prevent the formation of larger clusters, the Mazzanti group performed the controlled hydrolysis of non-sterically crowded trivalent uranium complexes. The reaction of $[UI_3(THF)_4]$ with two equivalents of water in the presence of potassium triflate in acetonitrile yielded a dodecanuclear mixed-valent uranium(IV/V) cluster $[U_{12}(\mu_3\text{-}OH)_8(\mu_3\text{-}O)_{12}I_2(\mu_2\text{-}OTf)_{16}(CH_3CN)_8]$ with a $U_{12}O_{20}$ core (Scheme II- 3).[338,339] In this complex, the 12 uranium atoms are arranged as a double-decker square-antiprism, in which two stacked distorted square-antiprisms share the plane formed by four uranium ions. Bond valence sum analysis and magnetic measurements revealed the presence of ten U(IV) centres and two U(V) ions, with a positive charge delocalised on the cluster core. Interestingly, crystallisation before completion of the reaction led to a mixture of the $U_{12}O_{20}$ cluster together with different intermediate products: $\{[U_6(\mu_3\text{-}O)_7(\mu_3\text{-}OH)(\mu_2\text{-}OTf)_8(\eta\text{-}OTf)_5(CH_3CN)_5]K_6(\mu_3\text{-}OTf)(CH_3CN)_3\}_n$ ($U_6O_8K_6$), $\{[U_6(\mu_3\text{-}O)_8(\mu_2\text{-}OTf)_{12}(H_2O)_{3.5}][K_4(\mu_2\text{-}H_2O)_2(H_2O)_4].4.5H_2O\}_n$ ($U_6O_8K_4$), $[U_6(\mu_3\text{-}O)_8(\mu_2\text{-}OTf)_8(\eta_2\text{-}OTf)_4]K_2$ ($U_6O_8K_2$) and $[U_6(\mu_3\text{-}O)_8(\mu_2\text{-}OTf)_{12}(H_2O)_3].23H_2O$ (U_6O_8) (Scheme II- 3). X-ray crystal structure analysis of these compounds revealed the presence of a U_6O_8 core in all cases. The six uranium atoms are situated at the vertices of an octahedron with the eight triangular faces of the octahedron bridged by μ_3-oxo groups. The potassium ions present in the $U_6O_8K_6$, $U_6O_8K_4$ and $U_6O_8K_2$ units bridge discrete U_6O_8 clusters units to afford extended networks.

To compare the influence of the oxidation state of the uranium precursor, similar hydrolysis was carried out with $[UI_4(PhCN)_4]$ in presence of potassium triflate in acetonitrile. The $U_{12}O_{20}$ cluster was not isolated, instead the two extended networks $U_6O_8K_2$ and $U_6O_8K_6$ presenting the U_6O_8 cluster core were characterised (Scheme II- 3). This result highlights the difference of reactivity between uranium(III) and uranium(IV) towards water.[339]

Scheme II- 3 Hydrolysis of $[UI_3(THF)_4]$ (left) and $[UI_4(PhCN)_4]$ (right) in the presence of potassium triflate in acetonitrile.

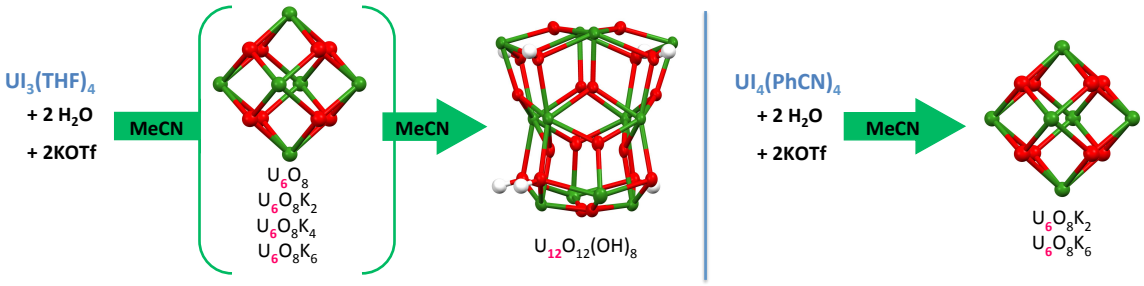

When the hydrolysis reaction is carried out with $[U(OTf)_3(CH_3CN)_3]$ instead of the uranium(III) tris(iodide) precursor, the formation of clusters larger than U_6O_8 is not observed and only the $U_6O_8K_6$, $U_6O_8K_4$, $U_6O_8K_2$ and U_6O_8 clusters are formed (Scheme II- 4).[338,339]

Scheme II- 4 Hydrolysis of $[U(OTf)_3(CH_3CN)_3]$ in the presence of potassium triflate in acetonitrile.

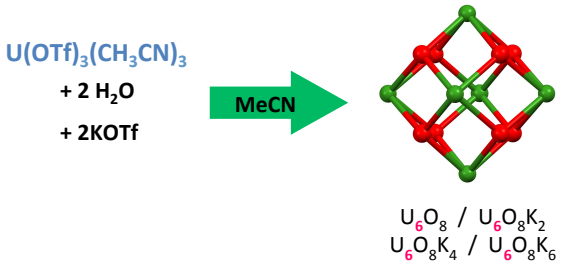

Different cluster nuclearities are obtained from the hydrolysis of $[UI_3(THF)_4]$ and $[U(OTf)_3(CH_3CN)_3]$ in the presence of potassium triflate due to the presence of the iodide ligands (Scheme II- 3 and Scheme II- 4). This highlights the important role of the ligands in directing the formation of the clusters. Ligands also have an important role in the cluster stability. Notably, ligand exchange studies were carried out with $U_{12}O_{20}$, $U_6O_8K_6$, $U_6O_8K_4$, $U_6O_8K_2$ and U_6O_8.

When the bridging triflate ligands coordinated to the uranium cations in these clusters are replaced by bidentate dibenzoylmethanate (dbm) ligands, the cluster $[U_6O_4(OH)_4(\eta\text{-}dbm)_{12}]$ is formed.[340] In the presence of dbm ligand, the dodecanuclear $U_{12}O_{20}$ cluster is cleaved into a smaller U_6O_8 assembly (Scheme II- 5). The six uranium centres in $[U_6O_4(OH)_4(\eta\text{-}dbm)_{12}]$ are placed at the vertices of an octahedron and are in the +IV oxidation state. While the triflate/iodide clusters are stable in solution over time, the dbm cluster decomposed to form a mononuclear U(IV) complex $[U(dbm)_4]$. This difference reflects the necessity of having ancillary bridging ligands such as the triflate ligands, which bridged

adjacent uranium ions, compared to the diketonate ligand, which coordinated only one uranium centre.

Scheme II- 5 Reaction of $U_{12}O_{20}$ and U_6O_8 clusters with dbmK.

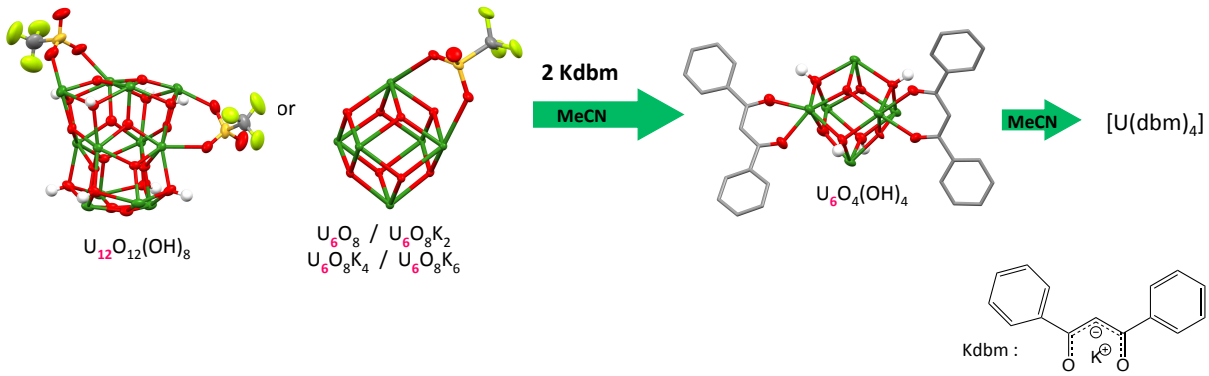

The magnetic properties of the two clusters $U_{12}O_{20}$ and $[U_6O_4(OH)_4(\eta\text{-dbm})_{12}]$ were measured (Figure II- 5). The plot of the magnetic susceptibility vs. T of $[U_6O_4(OH)_4(\eta\text{-dbm})_{12}]$ reveals a plateau between 20 and 6 K (Figure II- 5 right), attributed to temperature independent paramagnetism (TIP) of uranium(IV) due to coupling between a non-magnetic ground state and low-lying excited states through a Zeeman perturbation.[340] Such a clear plateau was not observed for $U_{12}O_{20}$, however an inflexion point at 50 K (Figure II- 5 left) is present, and may arise from the combination of TIP for uranium(IV) and paramagnetic uranium(V) ions.[339] However, the magnetic data of $U_{12}O_{20}$ are not very clear and further magnetic characterisations of this mixed-valent U(IV)/U(V) cluster should be investigated. Notably, this complex is a potential SMM.

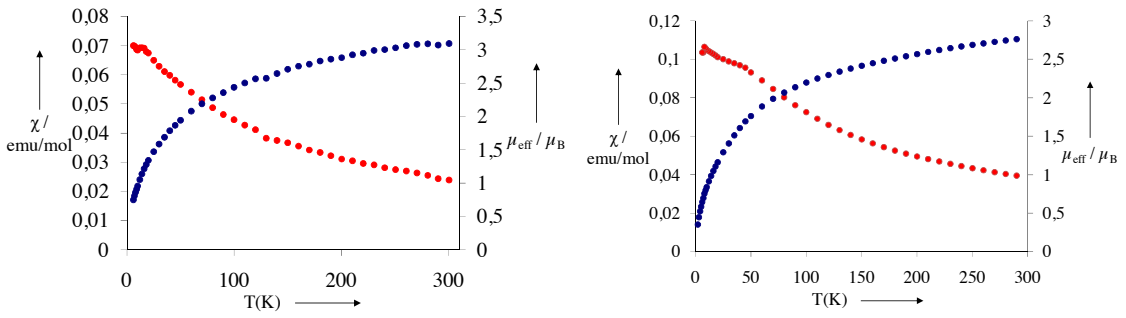

Figure II- 5 Temperature-dependent magnetic suscpetibility data (per uranium centre) of $[U_6O_4(OH)_4(\eta\text{-dbm})_{12}]$ (left) and $U_{12}O_{20}$ (right) (χ in red and μ_{eff} in blue)[339,340]

In view of the difference of stability observed between the oxo/hydroxo clusters supported by bridging triflate or non-bridging diketonate ligands, our group has also

investigated the ability of the benzoate ligand to stabilise larger clusters. Moreover, the benzoate ligand may be seen as a model for humic acid or organoacids found in soils. Consequently, the hydrolysis products supported by this ligand are environmentally relevant. The addition of the benzoate ligand to the product of the controlled hydrolysis of $[UI_3(THF)_4]$ with two equivalents of water was strongly influenced by the nature of the solvent (Scheme II- 6). In pyridine, a hexanuclear cluster $[U_6O_4(OH)_4(PhCOO)_{12}(Py)_3]$ with a U_6O_8 core is formed while in acetonitrile a mixture of $[U_{10}O_8(OH)_6(PhCOO)_{14}I_4(H_2O)_2(MeCN)_2]$ and $[U_{10}O_8(OH)_6(C_6H_5COO)_{12.82}I_{3.18}(H_2O)_4(MeCN)_3]I_2.5MeCN$ with a $U_{10}O_{14}$ core is formed.[207,341] The use of a less coordinating solvent than pyridine, e.g. acetonitrile, leads to larger polynuclear assemblies containing a higher number of hydroxide groups.

Scheme II- 6 Schematic representation of the synthetic correlations between the benzoate clusters

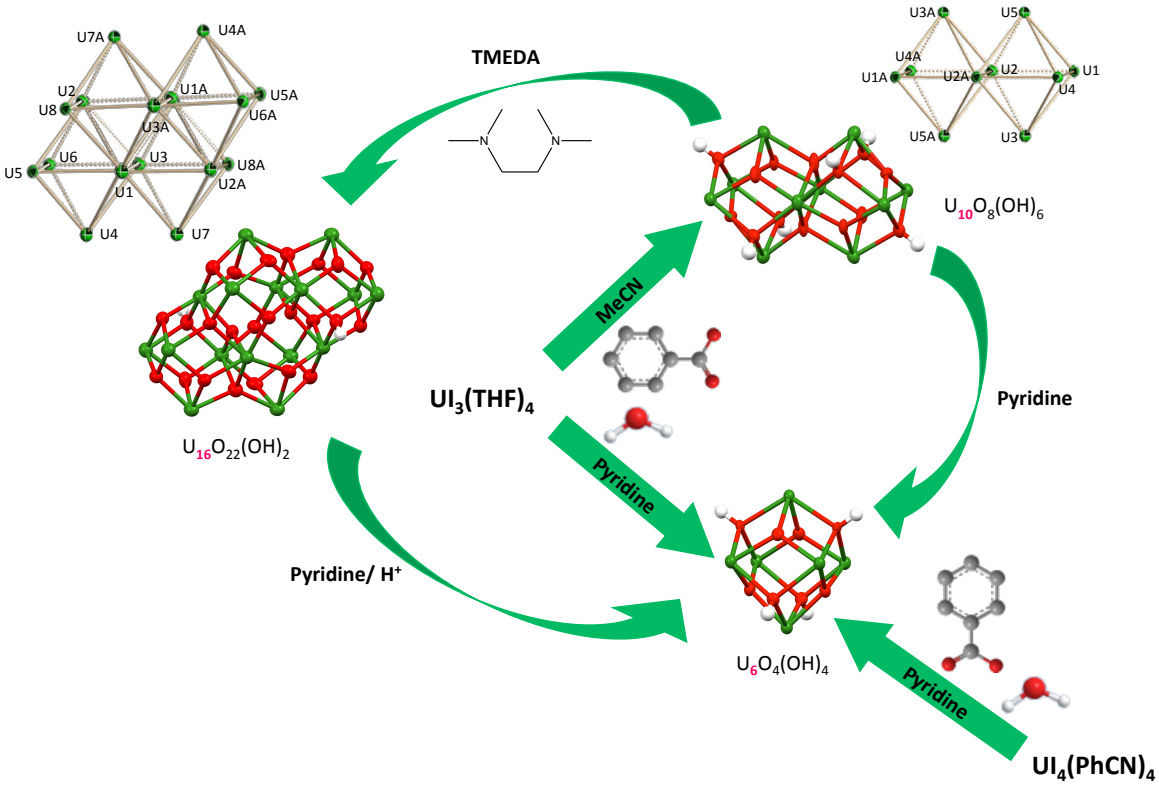

The benzoate ligands bridge two adjacent uranium ions, stabilising the structures in solution. This result highlights the fact that the nature of the bridging ligands is critical in the stabilisation of high nuclearity structures. All of the uranium atoms in these two clusters are in the +IV oxidation state. Interestingly, the addition of a Lewis base such as TMEDA to the reaction mixture in acetonitrile leads to the deprotonation of hydroxide groups, forming the $\{[K(MeCN)]_2[U_{16}O_{22}(OH)_2(PhCOO)_{24}]\}$ cluster with a $U_{16}O_{24}$ core that contains only 2

hydroxide ligands (Scheme II- 6). The calculated BVS for the uranium atoms is in agreement with the presence of 12 U(IV) and 4 localised U(V). These syntheses are represented in Scheme II- 6.

Reactivity studies showed that the $\{[K(MeCN)]_2[U_{16}O_{22}(OH)_2(PhCOO)_{24}]\}$ cluster can be converted into the $[U_6O_4(OH)_4(PhCOO)_{12}(Py)_3]$ cluster after addition of pyridinium chloride in pyridine in the presence of potassium benzoate via the reprotonation of the oxo groups and rearrangement of uranium atoms. We can indeed observe that the number of coordinated benzoate decreased in high nuclearity clusters ($PhCOO^-$/U ratio: 1.5 in $U_{16}O_{24}$, 1.3-1.4 in $U_{10}O_{14}$) compared to the U_6O_8 unit ($PhCOO^-$/U ratio: 2).

To compare the product of the controlled hydrolysis of uranium(III) and uranium(IV), the hydrolysis of the uranium(IV) precursor $[UI_4(PhCN)_4]$ with two equivalents of water in the presence of potassium benzoate was performed in pyridine and led to the hexanuclear cluster $[U_6O_4(OH)_4(PhCOO)_{12}(Py)_3]$.[207] Contrary to the hydrolysis of uranium(III) triiodide or uranium(IV) tetraiodide in the presence of triflate reported above,[338,339] the same species is obtained from the controlled hydrolysis of uranium(III) or uranium(IV) iodide with benzoate ligands in pyridine. These results highlight the strong influence of the reaction parameters on the nuclearity of the final structure.

The solid-state magnetic susceptibility χ_M of $[U_6O_4(OH)_4(PhCOO)_{12}(Py)_3]$ and $\{[K(MeCN)]_2[U_{16}O_{22}(OH)_2(PhCOO)_{24}]\}$ was measured and is plotted vs. T in Figure II- 6. The χ versus T values of $[U_6O_4(OH)_4(PhCOO)_{12}(Py)_3]$ increase with decreasing temperature but the temperature dependence is reduced below 10 K. This behaviour could be attributed to temperature independent paramagnetism (TIP) of uranium(IV) or magnetic coupling between the uranium ions.[208] To investigate the possibility of single molecule magnet properties, ac magnetic susceptibility and hysteresis cycle measurements were performed on polycrystalline samples of $[U_6O_4(OH)_4(PhCOO)_{12}(Py)_3]$. However, the in-phase and out-of-phase components of the ac susceptibility did not present any maximum and no open hysteresis loop was observed. These results clearly indicate the absence of slow magnetic relaxation. The χ versus T values of $\{[K(MeCN)]_2[U_{16}O_{22}(OH)_2(PhCOO)_{24}]\}$ increase with decreasing temperature and do not reveal clear magnetic coupling between the uranium centres.[341] Contrary to the uranium(IV) cluster $[U_6O_4(OH)_4(PhCOO)_{12}(Py)_3]$, the large size cluster $\{[K(MeCN)]_2[U_{16}O_{22}(OH)_2(PhCOO)_{24}]\}$ containing uranium in the +IV and +V oxidation states may be a good potential candidate for single molecule magnet properties.

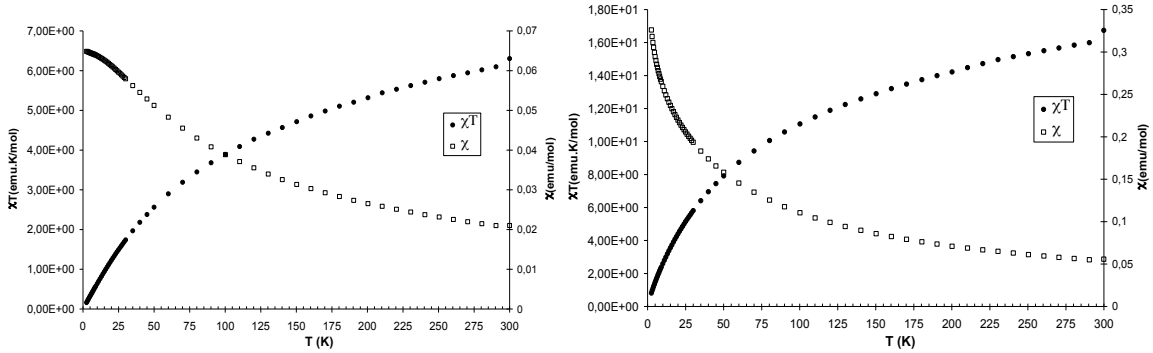

Figure II- 6 Temperature-dependent magnetic susceptibility data for $[U_6O_4(OH)_4(PhCOO)_{12}(Py)_3]$ (left) and $\{[K(MeCN)]_2[U_{16}O_{22}(OH)_2(PhCOO)_{24}]\}$ (right) from 2-300 K in a 1 T field.[208,341]

The examples of controlled hydrolysis of low-valent complexes, presented above, prove that quantitative and reproducible cluster syntheses can be accessed by this method. With these examples, we have seen that:

- The nature of the ligands (OTf^-, I^-, $PhCOO^-$) influenced the size as well as the stability of the assemblies, notably organic ligands, able to bridge two adjacent uranium ions, stabilised the oxo/hydroxo core of the cluster compared to non-bridging ligands.
- Acid/base conditions and either more (pyridine) or less (acetonitrile) coordinating solvents are able to tune the nuclearity of the clusters.
- The assembly of larger clusters, which appear to be the thermodynamic products, requires longer reaction times and proceeds through smaller cluster assembly.

II.2.) Synthesis of oxo/hydroxo clusters

II.2.1) Objectives

In order to design SMMs based on oxo/hydroxo uranium clusters, which can also act as simple model of the uraninite nanoparticles, we choose the strategy developed above, namely the controlled hydrolysis of low-valent uranium complexes. However, the hydrolysis of uranium complexes cannot be followed by proton NMR spectroscopy due to the broadness of the signals. Consequently, to characterise the hydrolysis product, we have to crystallise it. We know that oxo/hydroxo clusters supported with benzoate ligands crystallise quite easily and that bridging benzoate ligands stabilise high nuclearity clusters.[207,341] Moreover, this ligand is environmentally relevant as it may be seen as a model of humic acid or organoacids found in the environment. For these reasons, we decided to use the benzoate ligand as a bridging organic ligand.

Previous studies have shown that the nature of the uranium precursor (triflate, iodide/ uranium(III), uranium(IV)) in controlled hydrolysis reactions affected the size and the geometry of the assembly.[338,340] We decided to investigate the influence of the halide by using [UCl_4] as the low-valent uranium precursor, which has never been used for the controlled hydrolysis of uranium(IV). The presence of the chloride anions, which have a higher affinity for U(IV) compared to the iodide anions, should lead to the isolation of new cluster geometries. Moreover, high nuclearity plutonium clusters $Li_{12}[Pu_{38}O_{56}Cl_{42}(H_2O)_8](H_2O)_x$ and $Li_2[Pu_{38}O_{56}Cl_{42}(H_2O)_{20}](H_2O)_{15}$ were isolated from colloidal solutions of plutonium(IV), reported by Soderholm and coworkers, contained a $Pu_{38}O_{56}$ core decorated with chloride ligands.[334,335] It would be of high interest to see if such assemblies could be formed for uranium(IV) in the presence of chloride.

Therefore, we studied the controlled hydrolysis of different tetravalent uranium precursors, i.e. [UCl_4] and [$UI_4(OEt_2)_2$], in the presence of benzoate ligands to investigate the influence of the uranium precursor, the solvent, the stoichiometry of the benzoate ligand, and temperature, respectively, on the nuclearity of the products of hydrolysis.

II.2.2) Effect of the uranium precursor

II.2.2.1) Synthesis of $[U_6O_4(OH)_4(PhCOO)_{12}(Py)_3]$ and $[U_{16}O_{15}(OH)_8(PhCOO)_{26}(Py)_2]$

Previous work from our group showed that the reaction of uranium(III) triiodide or uranium tetraiodide with two equivalents of water and two equivalents of potassium benzoate in pyridine yields $[U_6O_4(OH)_4(PhCOO)_{12}(Py)_3]$ **1** in both cases, presenting a U_6O_8 core (Scheme II- 7).[207] X-ray quality crystals of **1** had been obtained in acetonitrile or in 1/5 mixture of pyridine/acetonitrile. In order to evaluate the impact of the presence of a more coordinating halide in the uranium precursor, the hydrolysis reaction of [UCl_4] under the same conditions was studied.

Scheme II- 7 Synthesis of **1** in pyridine from U(IV) chloride and U(IV) iodide precursors.

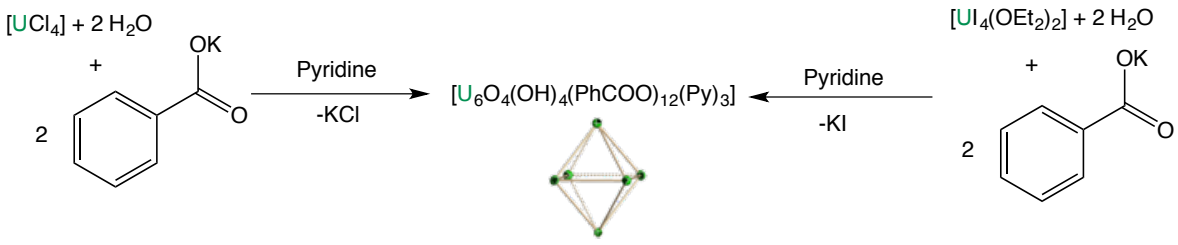

$[UCl_4]$ was first reacted with a solution of two equivalents of water in pyridine followed by the addition of two equivalents of benzoate in pyridine. After diffusion of DIPE into the reaction mixture in pyridine, big dark crystals of the previously reported $[U_6O_4(OH)_4(PhCOO)_{12}(Py)_3]$ **1** were obtained in 65% yield (Scheme II- 7). Proton NMR and UV-visible spectroscopy of the isolated product enabled the unambiguous identification of cluster **1**. The UV-visible spectra of the crude reaction mixture of the hydrolysis of $[UCl_4]$ in pyridine in the presence of benzoate show a larger, less resolved band that could suggest the presence of multiple species in solution (Figure II- 7).

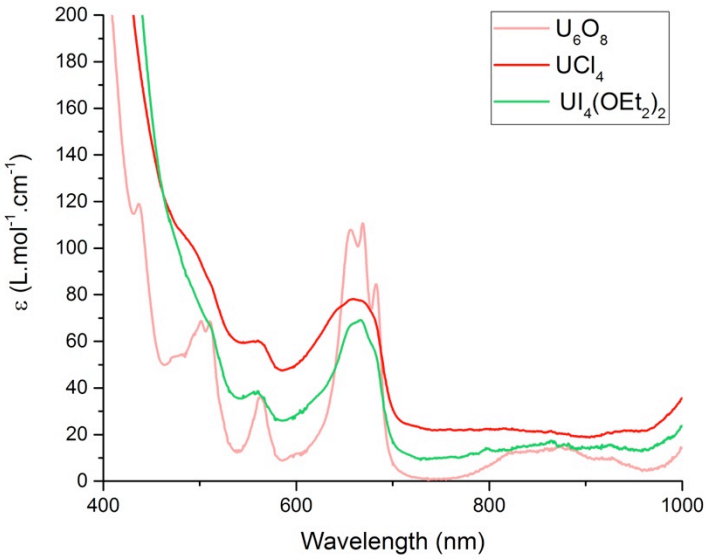

Figure II- 7 UV-visible spectra in pyridine of the reaction mixture of $[UCl_4]$ with 2 equivalents of water and 2 equivalents of potassium benzoate after 5 days (red line) and the reaction mixture of $[UI_4(OEt_2)_2]$ with 2 equivalents of water and 2 equivalents of potassium benzoate after 6 days (green line) compared to the UV-visible spectra of $[U_6O_4(OH)_4(PhCOO)_{12}(Py)_3]$ **1** (pink line).

We wanted to follow the hydrolysis reactions of $[UI_4(OEt_2)_2]$ or $[UCl_4]$ in the presence of potassium benzoate over time. Proton NMR spectroscopy is uninformative for such reaction mixtures and we chose electronic absorption spectroscopy to follow the evolution of these reactions (Figure II- 8), as it has been already used in previous studies in our group.[338] The hydrolysis of $[UI_4(OEt_2)_2]$ in the presence of potassium benzoate is immediate with a shift of the uranium(IV) band from 653 nm to 670 nm and no evolution is observed over time. In the case of $[UCl_4]$, the two fine bands at 655 and 673 nm disappear after the addition of water and potassium benzoate. However, the broad band shifts from 627 to 670 nm over the course of two days, by which time the reaction is complete.

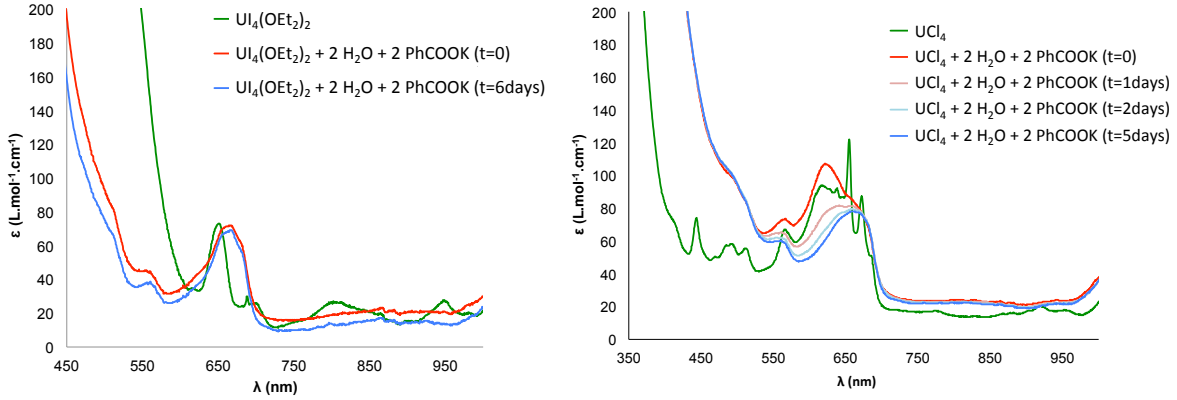

Figure II- 8 UV-visible spectra of $[UI_4(OEt_2)_2]$ (left) and $[UCl_4]$ (right) in pyridine and the evolution over time of the reaction mixtures from the hydrolysis of $[UI_4(OEt_2)_2]$ and $[UCl_4]$ in pyridine in the presence of potassium benzoate.

When conducting the first hydrolysis experiments of $[UCl_4]$ in the presence of 2 equiv. of potassium benzoate in pyridine, several crystallisation conditions were tested. Notably, recrystallisation of the reaction mixture from acetonitrile yielded a few crystals of a new cluster $[U_{16}O_{15}(OH)_8(PhCOO)_{26}(Py)_2]$ **2** with a novel $U_{16}O_{23}$ core geometry (Scheme II- 8). The reaction of $[UCl_4]$ with 1.7 equiv. of water and 1.7 equiv. of potassium benzoate, a stoichiometry based on the structure of **2** (ratio benzoate/U = 1.63), in acetonitrile with 4 equiv. of pyridine led to cluster **2** in 39% yield.

Scheme II- 8 Synthesis of clusters **1** and **2** in acetonitrile from U(IV) chloride, and synthesis of **1** from uranium(III) or uranium(IV) iodide precursors.

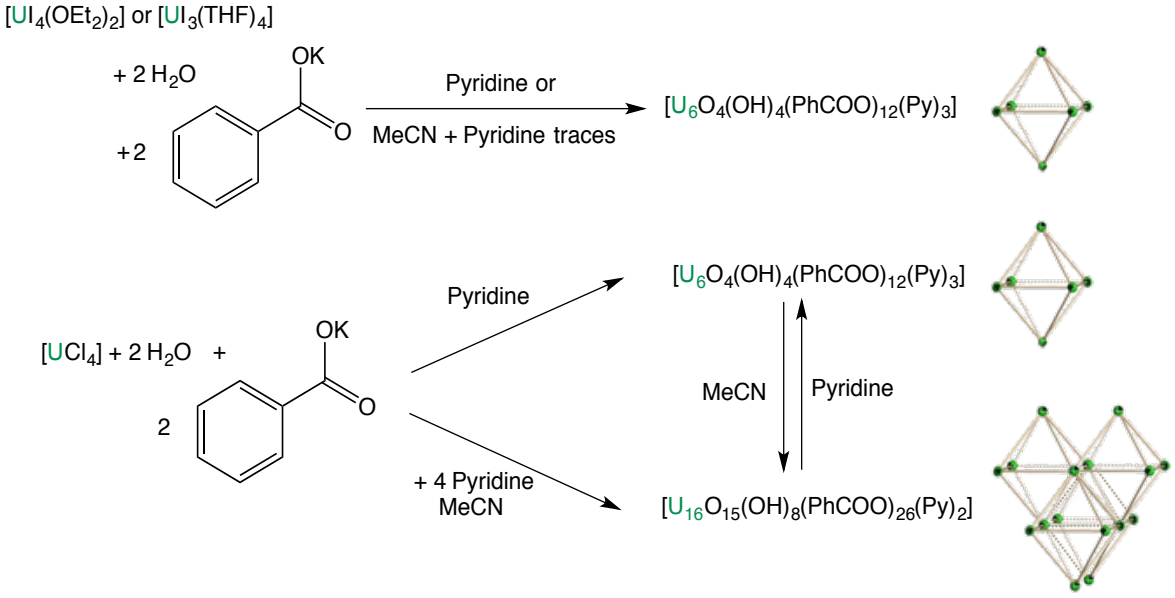

The X-ray crystal structure of $[U_{16}O_{15}(OH)_8(PhCOO)_{26}(Py)_2]$ **2** shows the presence of a discrete oxo/hydroxo cluster with a $U_{16}O_{23}$ core and a 1.6:1 benzoate/uranium ratio (Figure II- 9). The geometrical arrangement of the uranium atoms in the $U_{16}O_{23}$ core can be described as four fused octahedrons with sixteen crystallographically inequivalent uranium atoms (Figure II- 10). Each octahedron shares three edges of three different neighbouring octahedrons. Thus the centre of the four octahedrons forms a tetrahedron. The overall cluster size is approximately 22×20×20 $Å^3$ while the core structure is 7.65 Å wide (U7-U15 distance) and 8.59 Å high (U12-U14 distance).

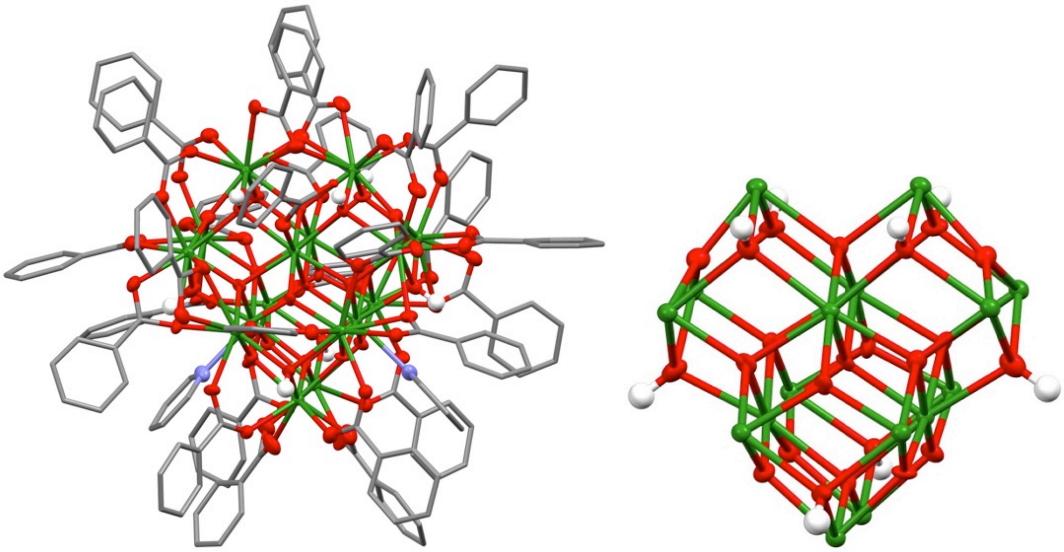

Figure II- 9 Molecular structure of cluster **2** and its core (ellipsoids are set at 30% probability). H atoms and solvent molecules are removed for clarity and the benzoate ligands are drawn as pipes. U green, O red, C gray, N blue, H white. Average bond lengths [Å] : U-μ_3O=2.241(2), U-μ_4O=2.371(2), U-μ_3OH=2.440(2), U-O_{Bz}=2.50(11), U-U=3.85(6).

The U1, U2, U3, U5, U11 and U13 atoms are eight coordinate with a cubic geometry for U1, U2, U3 and U5, and a bicapped trigonal prismatic geometry for U11 and U13 (Figure II- 10). The remaining uranium atoms are nine coordinate with a tricapped trigonal prismatic coordination geometry for U4, U7, U8 and U12, while U6, U9, U10, U14, U15 and U16 feature a capped square antiprismatic coordination geometry. The uranium atoms are connected by 15 oxo, 8 hydroxo and 26 benzoate ligands. 8 μ_3-O ligands and 8 μ_3-OH ligands cap 16 triangular faces of the octahedrons; and 7 μ_4-O ligands are located in the tetrahedral cavity formed by two or four adjacent octahedrons. The position of the hydroxo ligands in the crystal structure has been assigned on the basis of geometrical parameters. The mean U-O distance of the μ_3-O groups (2.241(2) Å) is significantly shorter than for the μ_3-OH groups (2.440(2) Å). The mean U-O distance is 2.371(2) Å for the μ_4-O groups. The calculated BVS for the uranium atoms is in agreement with the presence of 16U ions in the

+IV oxidation state. An overall positive charge of 64 for the cluster is consistent with the presence of 8 hydroxo and 15 oxo groups in the neutral complex. Fourteen benzoate ligands bridge two adjacent uranium(IV) centres of a same octahedron. Ten additional bidentate bridging benzoate ligands connect two uranium(IV) centres of two different octahedrons. Finally two more benzoate ligands are each monodentate but the non-coordinated oxygen is engaged in hydrogen bonding with a μ_3-hydroxo group. One pyridine molecule is found in the coordination spheres of U3 and U5, respectively.

The two structural arrangements of the uranium ions in the cluster $[U_{16}O_{15}(OH)_8(PhCOO)_{26}(Py)_2]$ **2** and in the previously reported $\{[K(MeCN)]_2[U_{16}O_{22}(OH)_2(PhCOO)_{24}]\}$,[341] are represented in Figure II- 10.

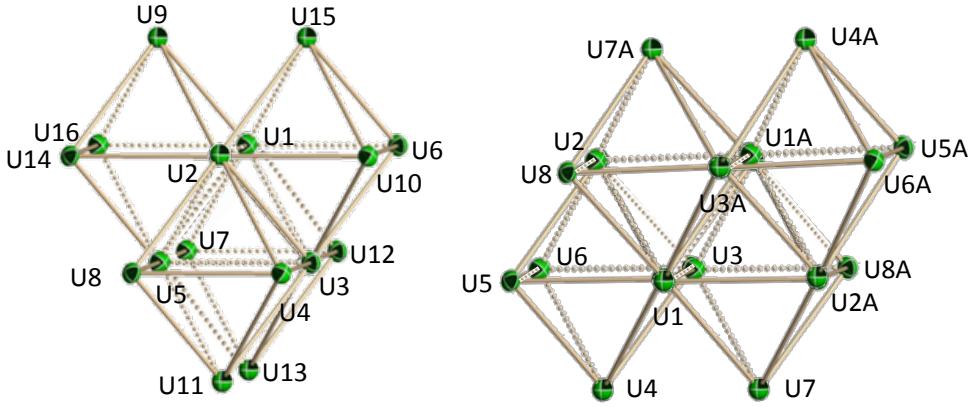

Figure II- 10 Arrangement of the octahedrons in $[U_{16}O_{15}(OH)_8(PhCOO)_{26}(Py)_2]$ **2** (left) and $\{[K(MeCN)]_2[U_{16}O_{22}(OH)_2(PhCOO)_{24}]\}$ (right) (atoms A are found with the inversion centre).

Both of them contain 16 uranium atoms arranged in 4 fused octahedrons sharing common edges. However, as highlighted in Figure II- 10 the two cores do not have the same geometry. In $\{[K(MeCN)]_2[U_{16}O_{22}(OH)_2(PhCOO)_{24}]\}$, the two external octahedrons share one edge with each one of the two adjacent octahedrons. Overall, each octahedron shares one edge with all of the neighbouring octahedrons. In **2**, each octahedron shares three edges of three different neighbouring octahedrons, forming a compact tetrahedron. As a result of the different structural arrangements, $\{[K(MeCN)]_2[U_{16}O_{22}(OH)_2(PhCOO)_{24}]\}$ (24 x 24 x 26 $Å^3$, 11.13 Å wide (U6-U6 distance) and 8.38 Å high (U8-U8 distance)) is larger than **2** (22×20×20 $Å^3$, 7.65 Å wide (U7-U15 distance) and 8.59 Å high (U12-U14 distance)). The asymmetric unit of $\{[K(MeCN)]_2[U_{16}O_{22}(OH)_2(PhCOO)_{24}]\}$ consists of eight crystallographically inequivalent uranium atoms related to their symmetry equivalents by an inversion centre (located in the middle of the U1-U1A and U3-U3A edges) while sixteen crystallographically inequivalent uranium atoms are present in **2**. The presence of twelve uranium(IV) ions and four uranium(V) ions (localised on U2 and U3) was confirmed with BVS calculations in

{[K(MeCN)]$_2$[$U_{16}O_{22}(OH)_2(PhCOO)_{24}$]} whereas the sixteen uranium atoms of **2** are in the +IV oxidation state. This difference probably arises from the different starting materials. The trivalent uranium precursor is very reactive and unstable towards water. Concomitant with its hydrolysis, U(III) is oxidised to form U(IV) or U(V), while the hydrolysis of U(IV) does not lead to a redox reaction.

^{1}H NMR studies show that the spectrum of [$U_{16}O_{15}(OH)_8(PhCOO)_{26}(Py)_2$] **2** in deuterated MeCN is broad, whereas in pyridine, well-defined signals assigned to the [$U_6O_4(OH)_4(PhCOO)_{12}(Py)_3$] cluster **1** appear (Figure II- 11). The UV-visible spectrum of [$U_{16}O_{15}(OH)_8(PhCOO)_{26}(Py)_2$] **2** in pyridine also confirmed the presence of the [$U_6O_4(OH)_4(PhCOO)_{12}(Py)_3$] **1** cluster with characteristic fine features in the 640-730 nm band. In pyridine, the [$U_{16}O_{15}(OH)_8(PhCOO)_{26}(Py)_2$] **2** compound is disrupted to give the [$U_6O_4(OH)_4(PhCOO)_{12}(Py)_3$] **1** cluster. A similar phenomenon has already been observed for a mixture of [$U_{10}O_8(OH)_6(PhCOO)_{14}I_4(H_2O)_2(MeCN)_2$] and [$U_{10}O_8(OH)_6(PhCOO)_{12.82}I_{3.18}(H_2O)_4(MeCN)_3$]$I_2$ in pyridine solution.[341]

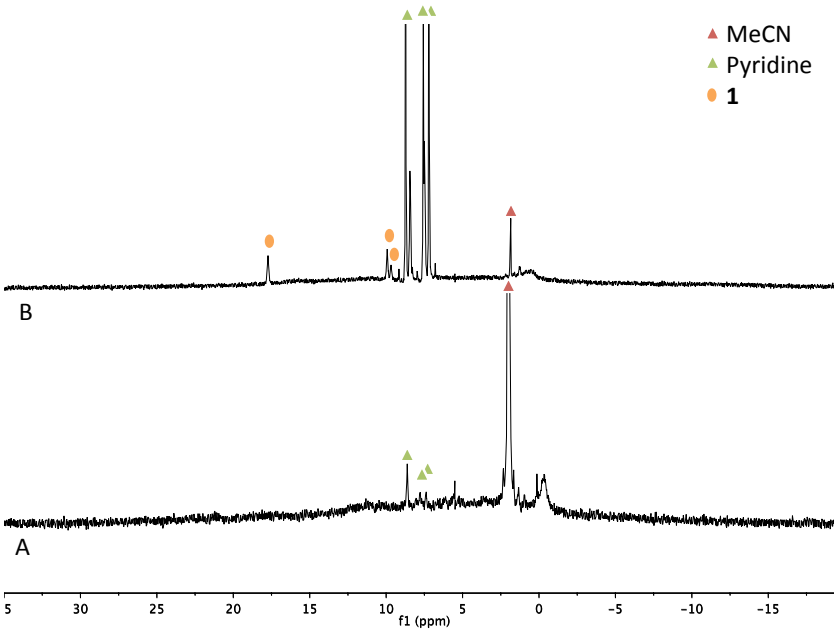

Figure II- 11 ^{1}H NMR (200 MHz, 298 K) spectra of [$U_{16}O_{15}(OH)_8(PhCOO)_{26}(Py)_2$] **2** in MeCN (A) and in pyridine (B), showing the characteristic peaks of the [$U_6O_4(OH)_4(PhCOO)_{12}(Py)_3$] cluster **1**.

We have been able to isolate two different clusters [$U_{16}O_{15}(OH)_8(PhCOO)_{26}(Py)_2$] **2** and [$U_6O_4(OH)_4(PhCOO)_{12}(Py)_3$] **1** from the hydrolysis of [UCl_4] in the presence of potassium benzoate depending of the solvents used for the crystallisation (Scheme II- 8). The ratio of coordinated pyridine/U is significantly lower in [$U_{16}O_{15}(OH)_8(PhCOO)_{26}(Py)_2$] **2** (2/16 = 0.125) than in [$U_6O_4(OH)_4(PhCOO)_{12}(Py)_3$] **1** (3/6 = 0.5). Based on these two examples of [UCl_4]

hydrolysis, we can observe that the presence of an excess of pyridine favoured smaller assemblies and that the use of small quantities of pyridine did not prevent the formation of a large cluster. This is very different from what was observed for the product of hydrolysis of $[UI_4(OEt_2)_2]$, as only the cluster **1** $[U_6O_4(OH)_4(PhCOO)_{12}(Py)_3]$ crystallised from an acetonitrile solution with traces of pyridine.[207] Thus, it is evident that the nature of the tetravalent uranium precursor has an influence on the product of the hydrolysis in the presence of potassium benzoate. Rather surprising is the fact that the different reactivity does not result in the coordination of either halides to the uranium centres.

II.2.2.2) Synthesis of $[U_{10}O_8(OH)_6(PhCOO)_{12.82}I_{3.18}(H_2O)_4(MeCN)_3]I_2$, $[U_{13}K_4O_{12}(OH)_4(PhCOO)_{12}Cl_{14}]Cl_2$ and $[U_{13}K_2O_9(OH)_7(PhCOO)_{12}Cl_{16}]Cl$

Previous studies in our group have shown that the controlled hydrolysis of low-valent uranium in solvents less coordinating than pyridine, such as acetonitrile, leads to the formation of larger oxo and hydroxo complexes.[341] In particular, the reaction of UI_3 with water in acetonitrile in presence of potassium benzoate led to the isolation of a cluster with a $U_{10}O_8(OH)_6$ core (Scheme II- 9). Therefore, we have investigated the reactions of $[UI_4(OEt_2)_2]$ and $[UCl_4]$ with two equivalents of water in the presence of potassium benzoate, also in acetonitrile, according to Scheme II- 9. The slow diffusion of DIPE into these two reaction mixtures in acetonitrile led to the isolation of X-ray quality crystals.

Scheme II- 9 Syntheses in acetonitrile of **3** from $[UI_4(OEt_2)_2]$ and $[UI_3(THF)_4]$ and clusters **4** and **5** from $[UCl_4]$.

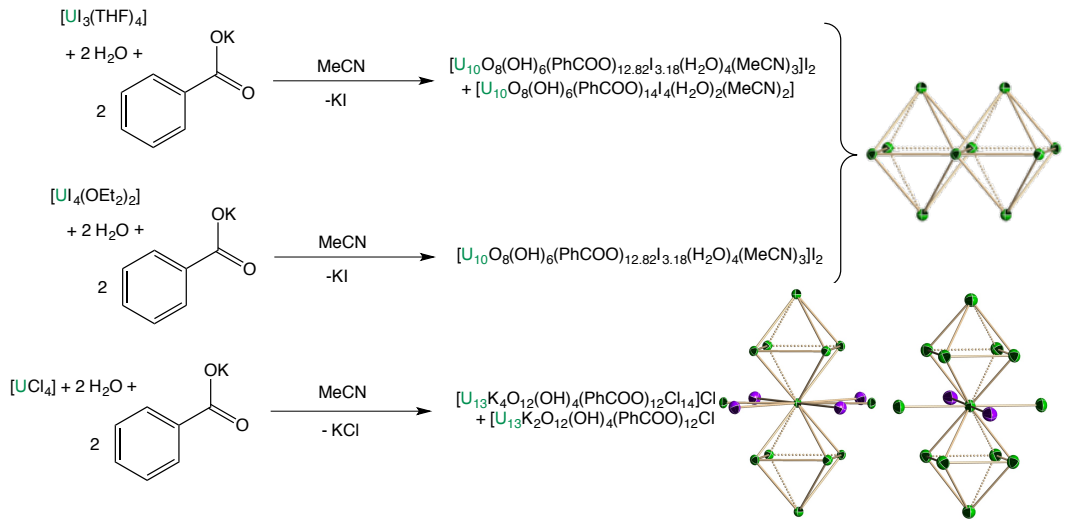

X-ray analysis of the single crystals of the hydrolysis of $[UI_4(OEt_2)_2]$ in the presence of potassium benzoate in acetonitrile revealed the presence of a cluster with the formula $[U_{10}O_8(OH)_6(PhCOO)_{12.82}I_{3.18}(H_2O)_4(MeCN)_3]I_2.5MeCN$, **3**, which contains a $U_{10}O_{14}$ core. This is a similar product to that formed from the hydrolysis of uranium triiodide (Figure II- 12).

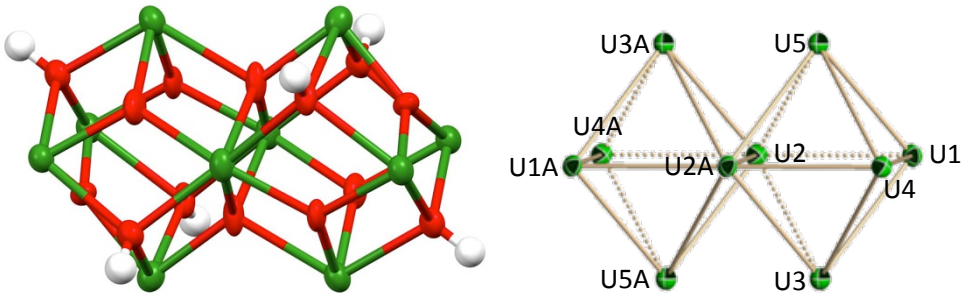

Figure II- 12 Molecular structure of $U_{10}O_{14}$ cluster core in $[U_{10}O_8(OH)_6(PhCOO)_{12.82}I_{3.18}(H_2O)_4(MeCN)_3]I_2.5MeCN$ **3** (ellipsoids are set at 30% probability). U green, O red, C gray, H white (atoms A are found with the inversion centre). Average bond lengths [Å] : U-μ_3O=2.230(17), U-μ_4O=2.389(18), U-μ_3OH=2.475(17), U-I_{term}=3.158(1), U-μ_2I=3.297(2), U-O_{Bz}= 2.37(3), U-U = 3.83(6).

Two different type of X-ray quality crystals were isolated from the hydrolysis of $[UCl_4]$ in the presence of potassium benzoate in acetonitrile. Independent X-ray diffraction studies revealed two new discrete oxo/hydroxo clusters with novel $U_{13}K_xO_{16}$ (x = 2 or 4) cores and the chemical formulas $[U_{13}K_4O_{12}(OH)_4(PhCOO)_{12}Cl_{14}]Cl_2$ **4** and $[U_{13}K_2O_9(OH)_7(PhCOO)_{12}Cl_{16}]Cl$ **5**, respectively. Crystals of these two species were isolated either from a concentrated acetonitrile solution or by slow diffusion of DIPE into an acetonitrile solution.

The structure of $[U_{13}K_4O_{12}(OH)_4(PhCOO)_{12}Cl_{14}]Cl_2$ **4** consists of 13 uranium atoms connected together by bridging oxide (12), hydroxide (4), chloride (14) and benzoate ligands (12) with 3.25 crystallographically different uranium ions (Figure II- 13). The cluster size is about 21×20×9 $Å^3$, with the largest U-U distance being 11.1 Å. The geometrical arrangement of the 13 uranium atoms can be described as two octahedrons sharing U4 as a common summit (inversion centre located on U4 at the intersection between a mirror and a 2-fold axis). Two additional uranium ions U5 are located in the plane between the two octahedrons, with a U5-U4-U5 angle of 180.0°. Four potassium ions are also present in this plane. The calculated BVS is in agreement with the presence of 13 U(IV) ions. Four triply bridging oxides and four triply bridging hydroxides alternatively cap eight triangular faces defined by the U1, U2, U3 atoms and their symmetry equivalents. The position of the hydroxo ligands in the crystal structure has been assigned on the basis of geometrical parameters. The mean U-O distances are 2.23(1) Å for the μ_3-O groups and 2.47(1) Å for the μ_3-OH groups. Four μ_5-oxides cap the faces of four octahedrons and they bridge three uranium atoms of the

octahedrons (mean U-μ_3O distance of 2.27(1) Å) and two potassium ions (mean K-O: 3.326(8) Å). Four other μ_6-oxo groups bridge the U5 atom to three uranium atoms of the octahedron and are also weakly bonded to two potassium ions (mean U-O distance of 2.36(1) Å, K-O 3.084(9) Å). Eight benzoate ligands bridge eight external edges of each octahedron while four additional benzoates bridge the U1, U1A and K2 atoms connecting one octahedron to the middle plane. Eight bridging chloride μ_2-Cl^- connect U1, U3 and their 6 equivalent positions to the closest potassium atom among K2, K2A, K2B or K2C atoms. Two chloride ligands bridge two potassium ions. Then four μ_3-Cl^- connect U3, K2 and U5 ions and their equivalent positions. The presence of 12 oxo ligands, 4 hydroxo ligands, 12 benzoates, 14 coordinated chlorides and two free chloride anions adds up to an overall charge of -56 for complex **4**, which is distributed over the 13 uranium(IV) centres. One acetonitrile molecule is also found in the coordination sphere of U2 in axial position.

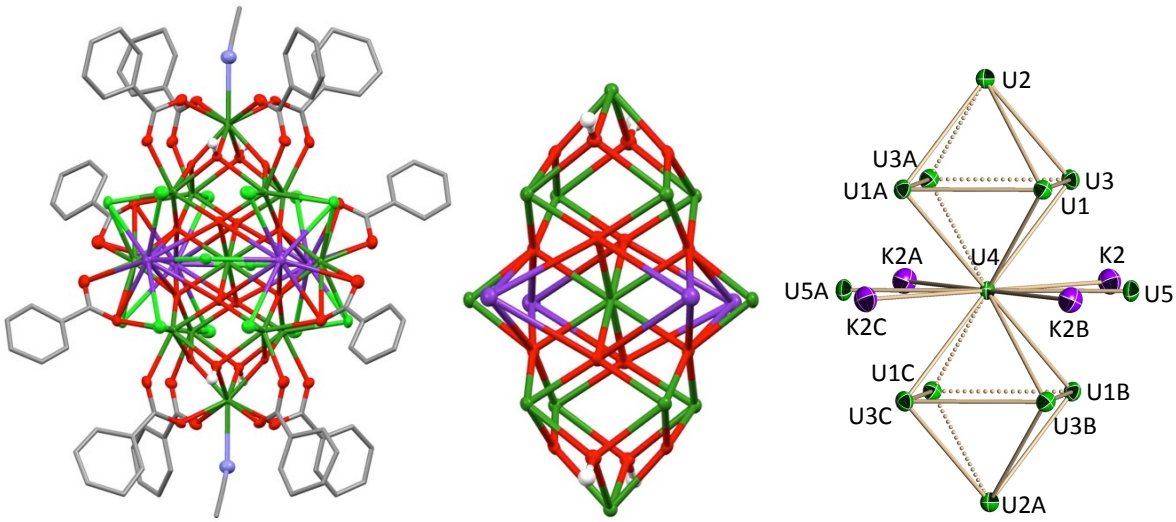

Figure II- 13 Molecular structure of **4** $[U_{13}K_4O_{12}(OH)_4(PhCOO)_{12}Cl_{14}]Cl_2$ cluster and $U_{13}K_4O_{16}$ core (ellipsoids are set at 30% probability). H atoms and solvent molecules are removed for clarity, ligands are represented in capped sticks. U green, O red, C gray, N blue, Cl light green, K purple, H white. (atoms A are found with the mirror, atoms B found with 2-fold rotational axis and atoms C found with the inversion centre). Average bond lengths [Å]: U-μ_3O=2.230(10), U-μ_5O(K)=2.269(9), U-μ_4O=2.365(9), U-μ_3OH=2.473(13), U-μ_2Cl(K)=2.696(4), U-μ_3Cl=2.859(4), K-μ_5O=3.326(8), K-μ_6O(U)=3.084(9), K-μ_2Cl(U)=3.414(6), K-μ_2Cl(K)=3.184(4), K-μ_3Cl=3.298(6), U-O_{Bz}=2.46(22), U-U=3.85(4).

The second type of crystals from the controlled hydrolysis of $[UCl_4]$ in the presence of potassium benzoate shows the presence of the oxo/hydroxo cluster $[U_{13}K_2O_9(OH)_7(PhCOO)_{12}Cl_{16}]Cl$ **5** with a $U_{13}K_2O_{16}$ core (Figure II- 14). The structure of the $U_{13}O_{16}$ core in **5** is similar to the one in **4**, consisting of 13 uranium atoms arranged as two octahedrons sharing U4 as a common summit and two other uranium U3 ions present in the middle plane between the two octahedrons. However, only two potassium ions are present in this plane, and they are perpendicular to the line U3-U4-U3 (U3-U4-U3 angle 180.0(0)°, U3-

U4-K1 angle 90.0(0)°). The uranium and potassium ions are connected by μ_3- and μ_4-oxide, μ_3-hydroxide, chloride and benzoate ligands. Only the position of four hydroxo ligands in the crystal structure has been assigned on the basis of geometrical parameters. The mean U-O distances are 2.23(4) Å for the μ_3-O groups and 2.43(9) Å for the μ_3-OH groups. Four μ_4-oxides cap the faces of four octahedrons and they bridge three uranium atoms of the octahedrons (mean U-μ_4O distance of 2.27(3) Å) and one potassium ion (K-O: 3.019(8) Å). Four other μ_4-oxo groups bridge the U3 atom to three uranium atoms of the octahedron (mean U-O distance of 2.36(1) Å). Eight benzoate ligands bridge eight external edges of each octahedron while four additional benzoates bridge the U3 and U5 atoms connecting one octahedron to the middle plane. Twelve bridging chloride ligands μ_2-Cl^- connect U2/U3, U2/K1 and U5/K1 and their equivalents. Then four μ_3-Cl^- ligands connect U2, U3 and K1 ions and their equivalents. The three extra negative charges found for the $\{[U_{13}K_2O_{12}(OH)_4(PhCOO)_{12}Cl_{16}]Cl\}^{3-}$ species may be compensated by the presence of three delocalised hydroxides ligands to form the neutral uranium(IV) compound $[U_{13}K_2O_9(OH)_7(PhCOO)_{12}Cl_{16}]Cl$ or of a mixed valent U(IV)/U(V) complex containing 10 U(IV) and 3 U(V). However, the bond valence sum calculation is in agreement with the presence of 13 U(IV).

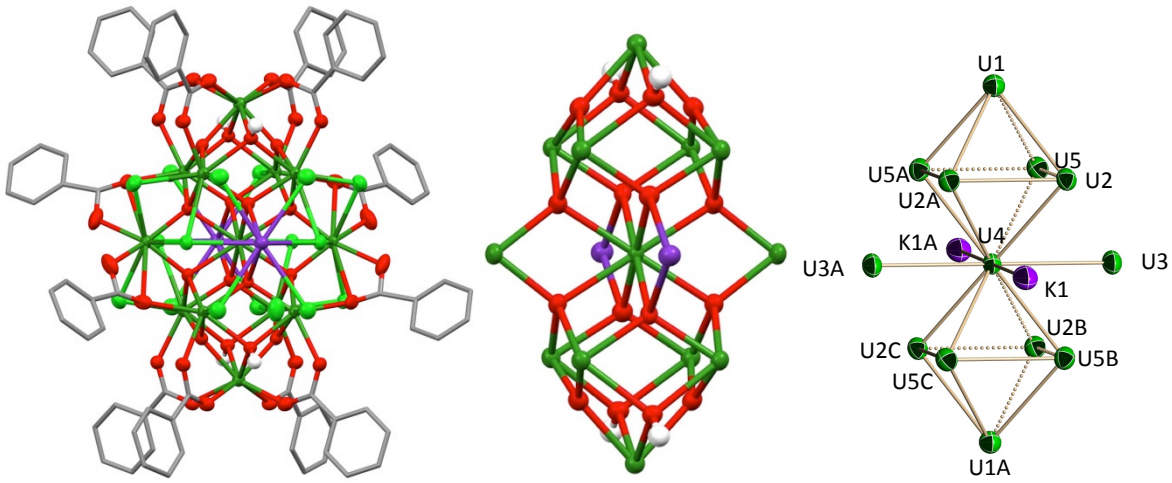

Figure II- 14 Molecular structure of $[U_{13}K_2O_9(OH)_7(PhCOO)_{12}Cl_{16}]Cl$ cluster **5** and $U_{13}K_2O_{16}$ core. (Ellipsoids are set at 30% probability). H atoms and solvent molecules are removed for clarity, ligands are represented as pipes. U green, O red, C gray, N blue, light green, K purple, H white. (Atoms A are found with the mirror, atoms B found with 2-fold rotational axis and atoms C found with the inversion centre).

Both X-ray crystal structures of **4** $[U_{13}K_4O_{12}(OH)_4(PhCOO)_{12}Cl_{14}]Cl_2$ and **5** $[U_{13}K_2O_9(OH)_7(PhCOO)_{12}Cl_{16}]Cl$ revealed the presence of discrete oxo/hydroxo clusters with the $U_{13}O_{16}$ core. The arrangements of the uranium and oxygen atoms are the same for both

structures, leading to very small differences in the structural parameters. However, the charge of the two clusters **4** and **5** is different due to differing number of potassium ions and chloride ligands decorating the $U_{13}O_{16}$ cores.

As the two clusters **4** and **5** crystallise under the same conditions, we have not been able to separate one cluster from the other. Moreover, only a very small amount of the crystalline mixture of **4** and **5** was reproducibly isolated (15% yield) from independent hydrolysis reactions of $[UCl_4]$ in acetonitrile in the presence of potassium benzoate. Attempts to isolate larger amounts led to a green powder, which does not have a well-defined proton NMR spectrum of **4** and **5**. These observations led us to think that a large mixture of species might be present in the acetonitrile reaction mixture.

The UV-visible spectrum of the mixture of the two clusters features a characteristic band assigned to uranium(IV) around 690nm.[80] The ^{1}H NMR spectrum of the reaction mixture of a stoichiometric amount of water with $[UCl_4]$ in the presence of potassium benzoate in acetonitrile is broad, whereas the isolated mixture of $[U_{13}K_4O_{12}(OH)_4(PhCOO)_{12}Cl_{14}]Cl_2$ **4** and $[U_{13}K_2O_9(OH)_7(PhCOO)_{12}Cl_{16}]Cl$ **5** gives a well-defined ^{1}H NMR spectrum in acetonitrile (Figure II- 15). Similar spectra have been obtained from different mixtures of **4** and **5** from different syntheses, however the integration ratios are slightly different, suggesting that the ratio between **4** and **5** is not always the same. After measurement of the diffusion coefficient with PFGSTE studies, no difference was observed between the different peaks. A diffusion coefficient of $9.04.10^{-10}$ m².s^{-1} and a hydrodynamic radii of 7.1 Å were calculated, close to the spherical radii estimated from the crystal structures (8.3 Å). The proton NMR spectrum of **4** and **5** in pyridine does not have well-defined peaks. The two clusters **4** and **5** may be disrupted or rearranged but not into cluster **1**, whereas we have observed that compound $[U_{16}O_{15}(OH)_8(PhCOO)_{26}(Py)_2]$ **2** was cleaved into the cluster **1** $[U_6O_4(OH)_4(PhCOO)_{12}(Py)_3]$ in pyridine. However, the ^{1}H NMR spectrum in acetonitrile after addition of pyridine leads to the characteristic peaks of **4** and **5**, showing that these clusters are reformed (Figure II- 15). The number of benzoate ligands is probably not sufficient to allow the cleavage of **5** and **6** into $[U_6O_4(OH)_4(PhCOO)_{12}(Py)_3]$ **1** in pyridine, as the ratio of benzoate/U in **1** (12/6 = 2) is higher than in **4** and **5** (12/13 = 0.9).

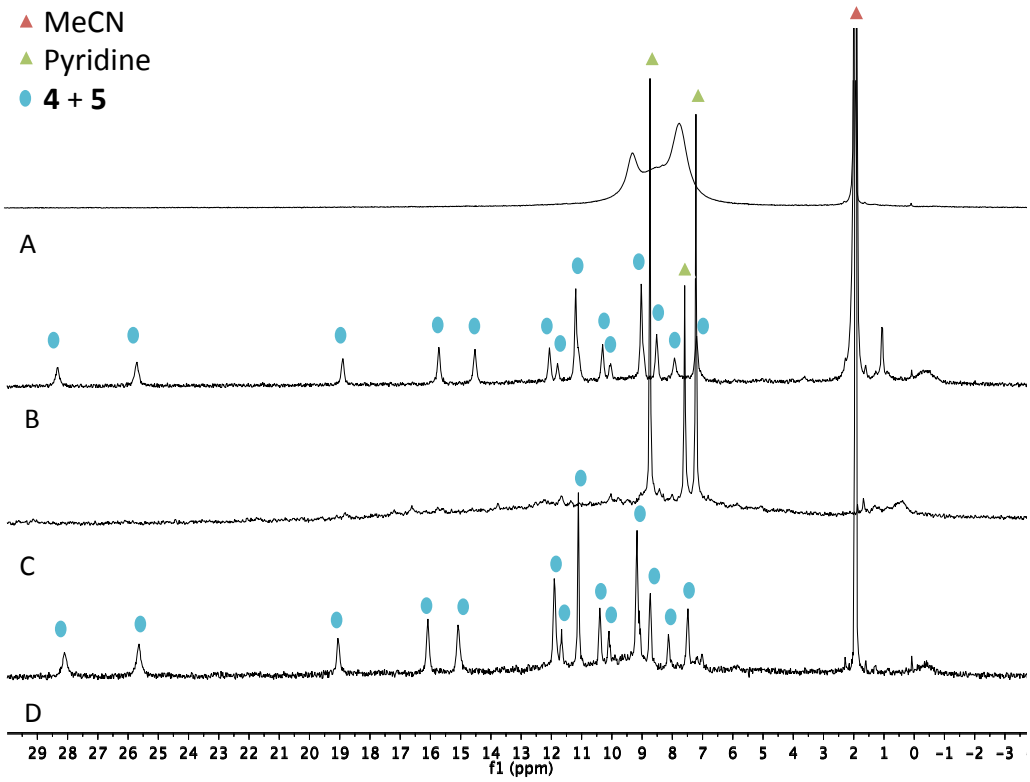

Figure II- 15 (A) ^{1}H NMR spectrum (200MHz, 298 K) of the reaction mixture of [UCl_4] with two equivalents of water in the presence of potassium benzoate in CD_3CN. (B, C, D) ^{1}H NMR spectra (200MHz, 298 K) of a mixture of **4** and **5** $[U_{13}K_4O_{12}(OH)_4(PhCOO)_{12}Cl_{14}]Cl_2$ and $[U_{13}K_2O_9(OH)_7(PhCOO)_{12}Cl_{16}]Cl$: (B) in CD_3CN; (C) in Py-d_5; (D) in CD_3CN after the proton NMR spectrum (C) recorded in Py-d_5.

These results show that the controlled hydrolysis of uranium tri- and tetra-iodide in the presence of potassium benzoate in acetonitrile leads to a mixture of discrete oxo/hydroxo clusters $[U_{10}O_8(OH)_6(PhCOO)_{14}I_4(H_2O)_2(MeCN)_2]$ and $[U_{10}O_8(OH)_6(PhCOO)_{12.82}I_{3.18}(H_2O)_4(MeCN)_3]I_2$ **3** with a $U_{10}O_{14}$ core; whereas the controlled hydrolysis of uranium tetrachloride in the presence of potassium benzoate in acetonitrile leads to a mixture of discrete oxo/hydroxo clusters $[U_{13}K_4O_{12}(OH)_4(PhCOO)_{12}Cl_{14}]Cl_2$ **4** and $[U_{13}K_2O_9(OH)_7(PhCOO)_{12}Cl_{16}]Cl$ **5** with $U_{13}K_xO_{16}$ cores. These products of hydrolysis displayed important structural differences. Notably, the clusters from the hydrolysis of [UCl_4] consist of an arrangement of 13 uranium atoms, while ten uranium atoms are present in the product of hydrolysis of the iodide uranium(III/IV) precursors. Moreover, chloride ligands bridge two or three uranium atoms in **4** and **5** whereas the iodide ligands bridge only two uranium atoms in $[U_{10}O_8(OH)_6(PhCOO)_{14}I_4(H_2O)_2(MeCN)_2]$ and $[U_{10}O_8(OH)_6(PhCOO)_{12.82}I_{3.18}(H_2O)_4(MeCN)_3]I_2$ **3**. The ratio between Cl/benzoate or I/benzoate is 1.17 (14/12) in **4** and **5**, and 0.25 (3.2/12.8) in **3**, respectively. The higher affinity of U(IV) for hard donors such as chloride and benzoate is probably the origin of the

observed outcome of the hydrolysis of $[UI_4(OEt_2)_2]$ and $[UCl_4]$. In the case of $[UCl_4]$, the chloride anions are less easily displaced by the benzoate ligands compared to the iodide anion in $[UI_4(OEt_2)_2]$, leading to different cluster geometries.

Thanks to these studies, we have observed that the geometry of the oxo/hydroxo clusters resulting of the hydrolysis of the uranium triiodide or tetraiodide (Scheme II- 6) are significantly different than from the uranium tetrachloride (Scheme II- 10).

Scheme II- 10 Schematic representation of the synthetic correlations between the benzoate clusters from the hydrolysis of $[UCl_4]$ at room temperature

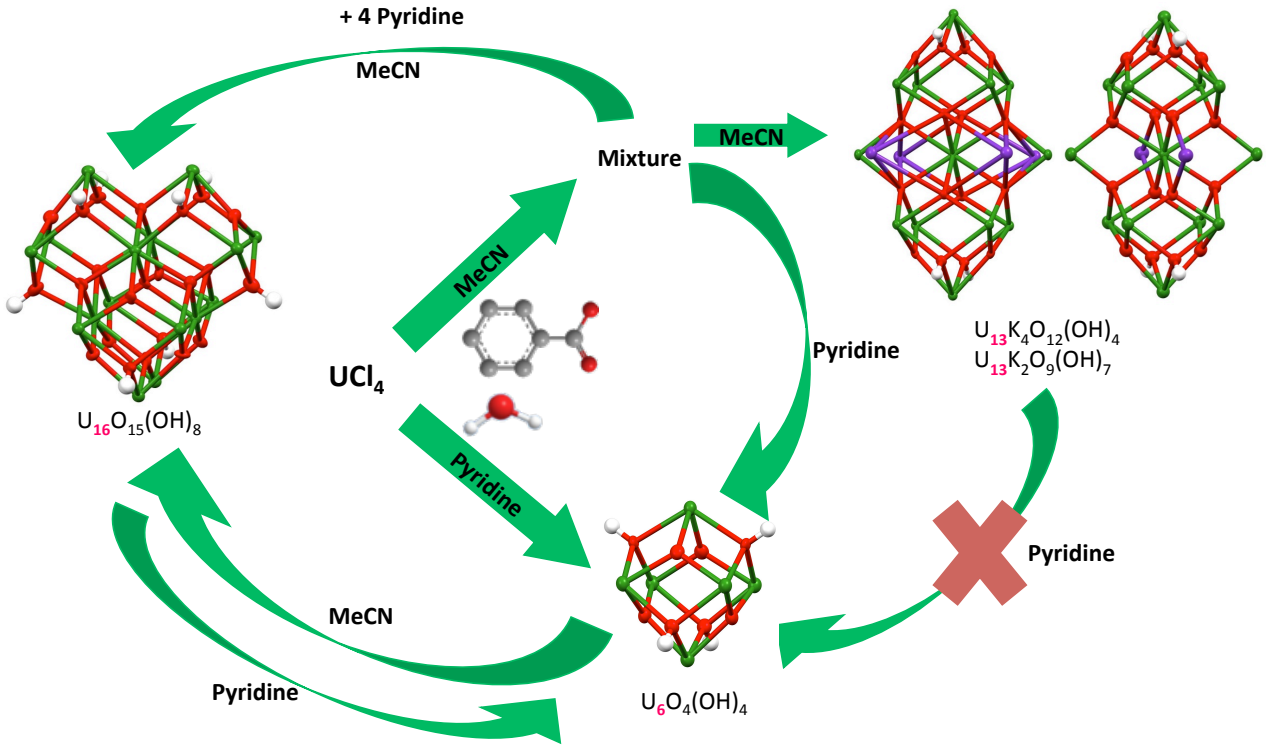

II.2.3) Effect of the excess of benzoate ligand

The reaction of $[UCl_4]$ and a stoichiometric amount of water (2 equivalents) in the presence of potassium benzoate (2 equivalents) leads to different cluster geometries depending on the solvent conditions as summed up in Scheme II- 10. Despite the use of 2 equivalents of potassium benzoate per uranium centre (ratio benzoate/U used = 2), the number of benzoate ligands coordinated to the product of hydrolysis is often lower than the stoichiometry used (ratio benzoate/U = 0.9 for **4** and **5**, 1.6 for **2**, 2 for **1**). A small excess of benzoate ligand in the reaction mixture did not lead to small oxo/hydroxo compounds. To

further study the influence of ligand excess on the resulting geometry, a large excess of benzoate was used in acetonitrile.

Scheme II- 11 Synthesis of the cluster $[U_6O_4(PhCOO)_{16}(Py)_4]$ **6**.

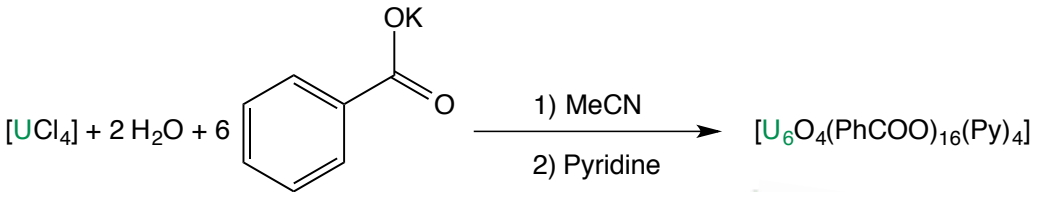

The reaction of one equivalent of $[UCl_4]$ with two equivalents of water followed by the addition of six equivalents of potassium benzoate in acetonitrile gave an insoluble green/white precipitate that is only soluble in pyridine (Scheme II- 11). Slow diffusion of DIPE into the pyridine solution allowed for the crystallisation of a new oxo compound $[U_6O_4(PhCOO)_{16}(Py)_4]$ **6** with a U_6O_4 core in 63% yield. The X-ray crystal structure of **7** reveals the presence of a discrete oxo cluster with a U_6O_4 core (Figure II- 16).

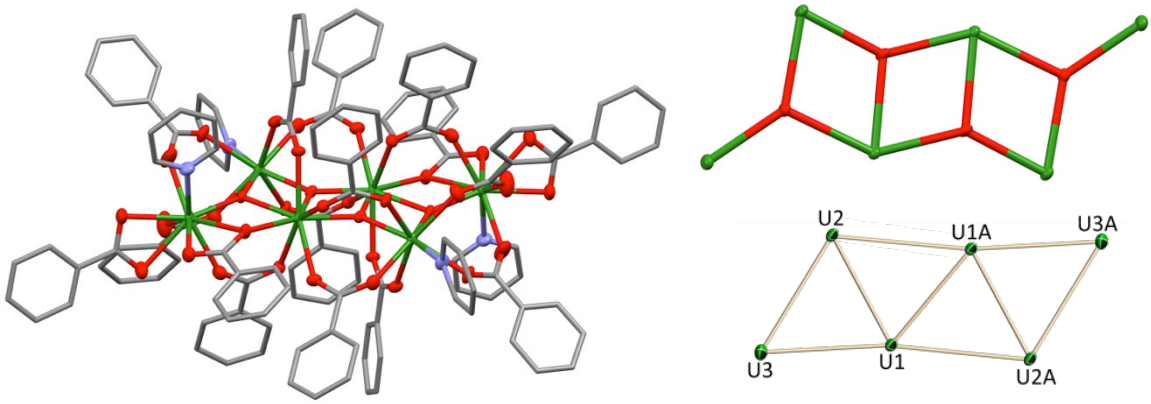

Figure II- 16 Molecular structure of **6** and U_6O_4 core. (Ellipsoids are set at 30% probability). H atoms, disorder and solvent molecules are removed for clarity, ligands represented as pipes. U green, O red, C gray, N blue, H white. (Atoms A are found with the inversion centre). Average bond lengths [Å]: U-μ_3O=2.245(4), U-O_{Bz}=2.42(8), U-U=3.9(2).

The structure consists of 6 uranium atoms connected by four oxide and 16 benzoate ligands with 3 crystallographically independent uranium ions. The cluster size is about 25×16×14 $Å^3$, with the largest U-U distance being 10.6 Å. The geometrical arrangement of the 6 uranium atoms can be described as four equilateral triangles with a side 3.9(1) Å long and sharing one edge with each other in almost the same plane (mean deviation from the plane: 0.09 Å). Four μ_3-oxides bridge the four triangular faces with a mean U-O distance of

2.24(1) Å. Eight bridging benzoate ligands bind the U1-U2 and U2-U3 atoms in the external longest side of the triangles. Two more bridging benzoates bridge U1 and U2 in the internal side of the triangle. Four bidentate bridging benzoate ligands bridge U1-U3 in the shortest side of the triangle and two bidentate benzoate ligands coordinate the U3 atoms. One pyridine molecule is found in the coordination sphere of the U3 atoms. U1 and U2 are eight coordinate, and U3 is nine coordinate. The calculated BVS is in agreement with the presence of 6 U(IV) ions.

Proton NMR studies of **6** $[U_6O_4(PhCOO)_{16}(Py)_4]$ revealed a well-defined spectrum (Figure II- 17) and show that cluster $[U_6O_4(PhCOO)_{16}(Py)_4]$ **6** is stable in pyridine solution for more than one month. Pulsed-Field Gradient Stimulated Echo (PFGSTE) diffusion NMR was used to measure the diffusion coefficient of **6** $[U_6O_4(PhCOO)_{16}(Py)_4]$ in pyridine solution ($D=3.09.10^{-10}$ $m^2.s^{-1}$).[342] The hydrodynamic radii (8.0 Å) calculated from this diffusion coefficient compared to the spherical radii (9.2 Å) evaluated from the crystal structure of **6** is in agreement with the presence of a hexanuclear cluster in solution.

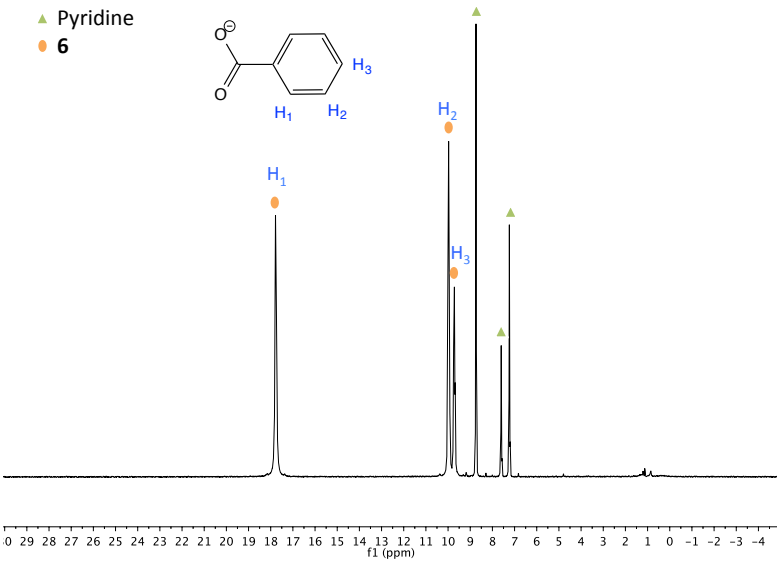

Figure II- 17 ^{1}H NMR spectrum (200M Hz, 298 K, Py-d_5) of **6**

The ratio of benzoate/uranium in **6** (16/6 = 2.7) has increased compared to **4** and **5** (12/13 = 0.9), **2** (26/16 = 1.6) and **1** (12/6 = 2). In the $[U_6O_4(PhCOO)_{16}(Py)_4]$ cluster **6**, the planar geometry of the oxo core allows the coordination of two bridging benzoate ligands between two adjacent uranium centres. In the $[U_6O_4(OH)_4(PhCOO)_{12}(Py)_3]$ cluster **1**, only one benzoate ligand bridges two adjacent uranium centres, probably due to sterical constraints.

II.2.4) Influence of the temperature

We have shown above that the nature of the uranium precursor (iodide or chloride), the nature of the solvent and the stoichiometry of the benzoate ligand can influence the geometry of the clusters obtained by controlled hydrolysis of low-valent uranium. The largest cluster obtained from controlled hydrolysis of low-valent uranium so far consists of an assembly of 16 uranium atoms. We then became interested in investigating the influence of the temperature on the size of the clusters.

Scheme II- 12 Synthesis of **7** in hot acetonitrile

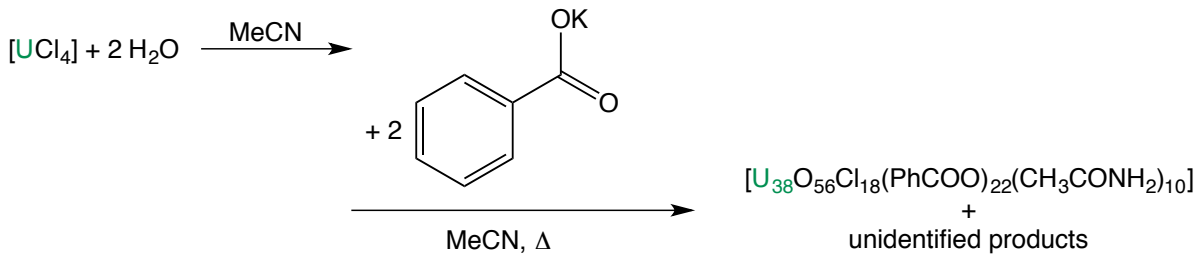

To study the influence of the temperature on these systems, the mixture of $[UCl_4]$ reacted with two equivalents of water and two equivalents of potassium benzoate in acetonitrile was refluxed for 32 hours at atmospheric pressure under argon (Scheme II- 12). A greenish, insoluble solid formed and could not be characterised. The slow diffusion of DIPE into the reaction solution yielded X-ray quality crystals of $[U_{38}O_{56}Cl_{18}(PhCOO)_{22}(CH_3CONH_2)_{10}]$ **7** combined to a green solid.

The X-ray crystal structure of $[U_{38}O_{56}Cl_{18}(PhCOO)_{22}(CH_3CONH_2)_{10}]$ **7** reveals the presence of a discrete oxo cluster with a $U_{38}O_{56}$ core, with a fluorite-type structural packing (Figure II- 18). The structure consists of 38 uranium atoms connected together by bridging oxides (56) forming the $U_{38}O_{56}$ core, surrounded by chloride (18), benzoate ligands (22) and acetamide (10) with 4.75 crystallographically inequivalent uranium ions. The cluster size is about 26×25×23 $Å^3$, with the largest U-U distance being 12.1 Å. The geometrical arrangement of the 38 uranium atoms in the structure can be described as thirteen fused octahedrons. Each external octahedron shares five edges of five different neighbouring octahedrons. Thus, the centre of the octahedrons forms a centred cuboctahedron and each external uranium ion is placed at the summit of a truncated octahedron (Figure II- 18).

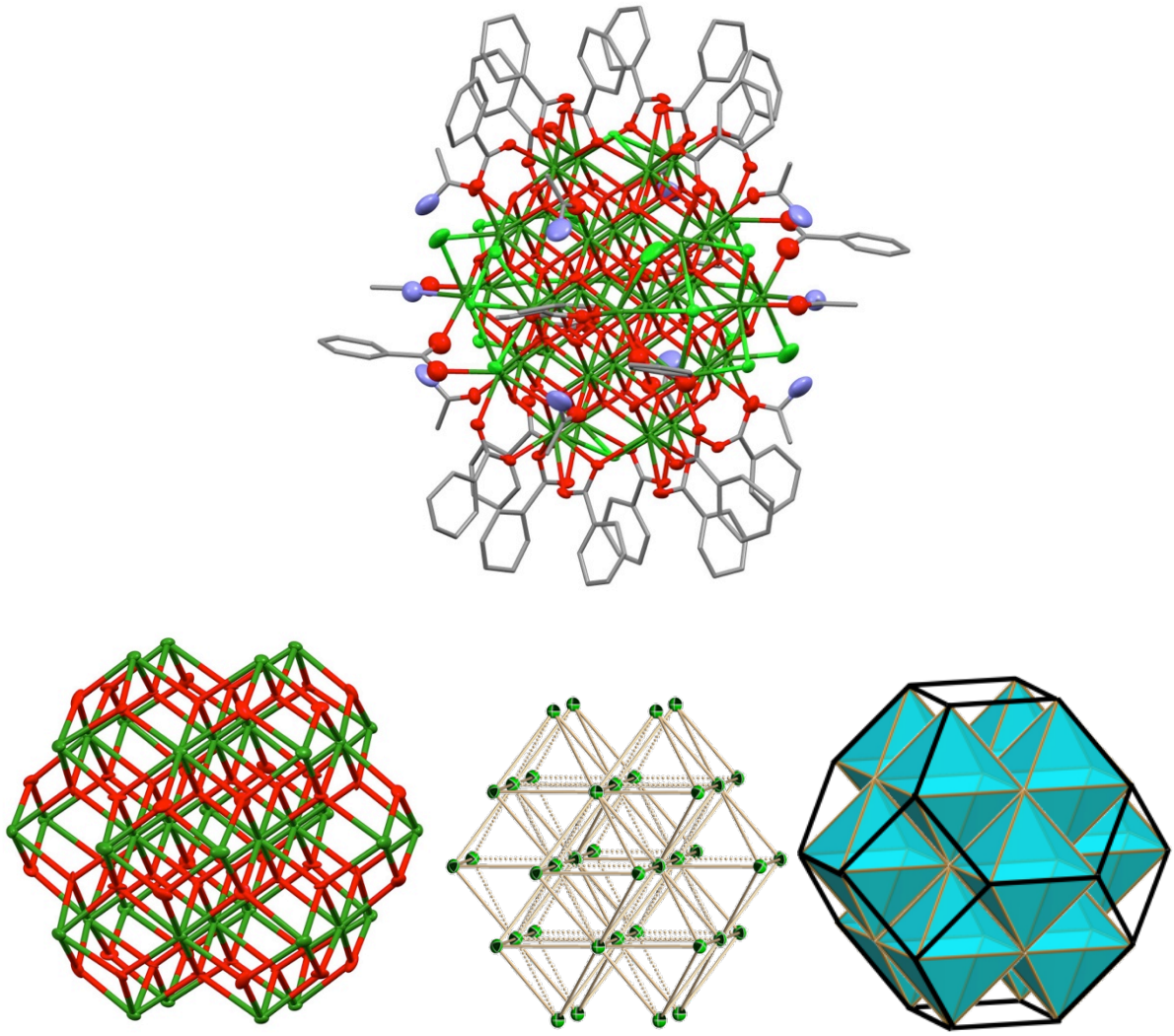

Figure II- 18 Molecular structure of $[U_{38}O_{56}Cl_{18}(PhCOO)_{22}(CH_3CONH_2)_{10}]$ **7** and arrangement of the octahedrons (Ellipsoids are set at 30% probability). H atoms are removed for clarity, ligands are represented as capped sticks. U green, O red, C gray, N blue, Cl light green, H white. Average bond lengths [Å]: U-μ_3O=2.248(9), U-μ_4O=2.364(10), U-Cl=2.694(15), U-μ_2Cl(U)=2.844(4), U-μ_4Cl(U)=3.066(3) U-O_{Bz}=2.43(12), U-U=3.80(10).

24 μ_3-O ligands cap 24 triangular faces of the octahedrons in the hexagonal faces of the truncated octahedron; 32 μ_4-O ligands are located in the tetrahedral cavity formed by two or four adjacent octahedrons. The calculated bond valence sum (BVS) is in agreement with the presence of 56 oxide oxygen atoms. The mean U-O distances are 2.25(1) Å for the μ_3-O and 2.36(1) Å for the μ_4-O atoms. Each square face is capped by a μ_4-Cl anion surrounded on the edge of the square either by 4 bridging benzoates in 2 facing squares or by 2 disordered μ_2-Cl anions with 2 bridging benzoates in the 4 remaining squares. The twelve edges between neighbouring hexagonal faces are occupied by 10 bridging benzoates and 2 bridging acetamides disordered with benzoates. Eight additional acetamides complete the coordination sphere of the uranium ions at the centre of the eight hexagonal faces. The

acetamide results from the partial hydrolysis of hot acetonitrile catalysed by H^+ released during the formation of the cluster. The calculated BVS is in agreement with the presence of 38 U(IV) ions. The presence of 56 oxo ligands, 22 benzoates and 18 chloride ions requires a corresponding positive charge of +152 for the complex, and this is distributed over the 38 U(IV) centres.

During the progress of my PhD, a similar cluster containing a $U_{38}O_{56}$ core was reported and was reproducibly prepared using solvothermal methods, in which both pressure and temperature were increased at the same time. Usually, such methods are used in the preparation of extended networks but the Loiseau group reported the formation of the discrete oxo-hydroxo cluster $[U_{38}O_{56}Cl_{18}(THF)_8(PhCOO)_{24}].8THF$ from the hydrolysis of $[UCl_4]$ with a controlled amount of water (6 equivalents) and benzoic acid (15.4 equivalents) in anhydrous THF under solvothermal conditions (130°C, 36h) (Scheme II- 13).[343] A very recent kinetic study of this reaction from the same group revealed that the uranium(IV) precursor is partially oxidised into a uranyl(VI) species after one hour of heating, and this remains in solution, while the $[U_{38}O_{56}Cl_{18}(THF)_8(PhCOO)_{24}].8THF$ cluster is present in the solid phase.[344] They also noticed the formation of smaller oxo species when the reaction time was not long enough to form the $U_{38}O_{56}$ cluster.

Scheme II- 13 Solvothermal synthesis of $[U_{38}O_{56}Cl_{18}(THF)_8(PhCOO)_{24}].8THF$.

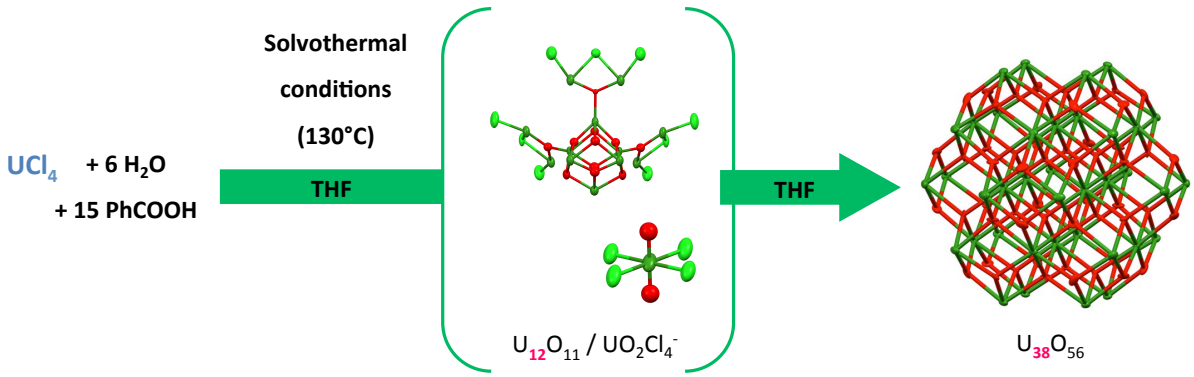

The structure of $[U_{38}O_{56}Cl_{18}(PhCOO)_{22}(CH_3CONH_2)_{10}]$ **7** is closely related to that of the $[U_{38}O_{56}Cl_{18}(PhCOO)_{24}(THF)_8]$ cluster isolated from the solvothermal hydrolysis of $[UCl_4]$ in THF in the presence of benzoic acid (Scheme II- 13),[343] and of the Pu(IV) nanoclusters $Li_{14}(H_2O)_n[Pu_{38}O_{56}Cl_{54}(H_2O)_8]$ and $Li_2[Pu_{38}O_{56}Cl_{42}(H_2O)_{20}]$, which were isolated from colloidal solutions of plutonium.[334,335] The structural arrangement of the uranium and oxygen atoms is similar in the two clusters $[U_{38}O_{56}Cl_{18}(PhCOO)_{22}(CH_3CONH_2)_{10}]$ **7** and $[U_{38}O_{56}Cl_{18}(PhCOO)_{24}(THF)_8]$.[343] The coordination mode of the chloride ligands surrounding

the core is also the same for both compounds. The coordination sphere of the uranium ions is completed by benzoate and THF ligands in $[U_{38}O_{56}Cl_{18}(PhCOO)_{24}(THF)_8]$ and by benzoate and acetamides in **7**. Another difference between the two $U_{38}O_{56}$ clusters is the charge and the oxidation state of the uranium atoms. Each uranium atom in $[U_{38}O_{56}Cl_{18}(PhCOO)_{22}(CH_3CONH_2)_{10}]$ **7** is in the +IV oxidation state. The previously reported $[U_{38}O_{56}Cl_{18}(PhCOO)_{24}(THF)_8]$ cluster is anionic ($[U_{38}O_{56}Cl_{18}(PhCOO)_{24}(THF)_8]^{2-}$) and therefore the presence of 2 delocalised U(V) and 36U(IV) was proposed.[343]

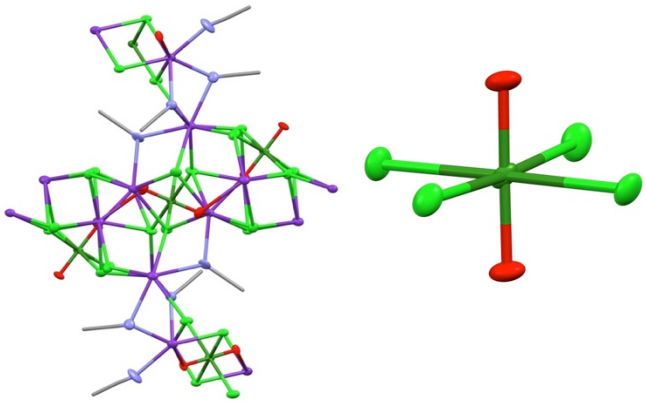

Figure II- 19 Molecular structure of $[UO_2K_2Cl_4(MeCN)_2]$ **8** and coordination around the uranyl(VI). (Ellipsoids are set at 30% probability). H atoms are removed for clarity, MeCN are represented as capped sticks. U green, O red, C gray, N blue, Cl light green, K purple. Average bond lengths [Å]: U-O_{yl}=1.769(17), U-Cl=2.653(16), K-Cl=3.28(11), U-U=7.83(1).

Serendipitous traces of oxygen in hydrolysis reactions of $[UCl_4]$ in the presence of potassium benzoate in acetonitrile yielded **7** together with crystals of a 3D network of uranyl(VI) chloride $[UO_2K_2Cl_4(MeCN)_2]$ **8** (Figure II- 19). The uranium atom is six coordinate with a slightly distorted octahedral coordination geometry formed by four chloride anions situated in the equatorial plane and by the two uranyl oxygen atoms in the axial positions. The mean U-O_{yl} and U-Cl bond distances are 1.769(17) Å and 2.653(16) Å respectively, and these are in the range of mean U-O_{yl} and U-Cl distances found in reported $[UO_2Cl_4]^{2-}$ units (U-O_{yl} : 1.76(1)-1.77(1) Å and U-Cl: 2.65(2)-2.68(1) Å).[345-348] Potassium cations are bound to oxo groups of the uranyl(VI), chloride ligands and bridging acetonitrile, leading to an extended network. The coordination of strong donor ligands in the equatorial plane of the uranyl(VI) weakens the U=O_{yl} bond, allowing for the coordination of the oxo group to another metal centre. A handful examples of extended networks[17,211,217-221,223-230] or discrete molecules[17,231-235] of uranyl(VI) have been reported, presenting homometallic or heterometallic CCIs.

The uranyl(VI) polymer was only isolated from the controlled hydrolysis of U(IV) in the presence of serendipitous traces of oxygen. On the other hand, uranyl(VI) is detected in solution in every solvothermal synthesis of $[U_{38}O_{56}Cl_{18}(PhCOO)_{24}(THF)_8]$.[344] The oxidation of U(IV) into uranyl(VI) in the study reported by Loiseau is not well explained but occurs quickly after one hour. The nature of the reduced species remains unclear.

Currently, the isolation of $[U_{38}O_{56}Cl_{18}(PhCOO)_{22}(CH_3CONH_2)_{10}]$ **7** in analytically pure form has not been possible, preventing us from performing further characterisations. Further experiments will be carried out to continue the investigation of the hydrolysis of $[UCl_4]$ in the presence of potassium benzoate at high temperatures in different solvent and with different stoichiometries in order to selectively synthesise **7**.

II.2.5) Structural comparison

A summary of structural parameters is reported in Table II- 1 for the complexes obtained from the controlled hydrolysis of $[UCl_4]$ in the presence of potassium benzoate. The hydroxo groups of **1**, **2**, **3**, **4** and **5** were assigned thanks to longer U-μ_3OH bond lengths (mean value 2.457(20) Å) compared to the mean U-O distances for the U-μ_3O groups (mean value 2.241(9) Å). These distances are in the range of previous U-μ_3OH and U-μ_3O distances reported for oxo/hydroxo clusters.[207,338,341] The clusters **2**, **3**, **4** and **5**, containing μ_4-oxo ligands, have U-μ_4O bond lengths (2.375(13) Å) that are 0.13 Å longer than the U-μ_3O bonds. The U-μ_4O distances found in these clusters are similar in length to the U-O bonds found in the UO_2 nanoparticle prepared in the laboratory or by bacterial reduction of uranyl(VI) (mean value of 2.346(6) Å).[317] The U-U distances in the discrete synthesised clusters lie in the same range as those in the UO_2 nanoparticle (synthetic UO_2: 3.867(4) Å and biogenic UO_2: 3.842(5) Å).[317]

Table II- 1 Average bond lengths cores compared to UO_2 [317] (in Å).

Compound	**1**	**2**	**3**	**4**	**5**	**6**	**7**	**UO_2 abiotic**	**UO_2 biogenic**
U-μ_3OH	2.439(4)	2.440(2)	2.475(17)	2.473(13)	2.432(92)	-	-	-	-
U-μ_3O	2.251(4)	2.241(2)	2.230(17)	2.230(10)	2.225(40)	2.245(4)	2.248(9)	-	-
U-μ_4O	-	2.371(2)	2.389(18)	2.360(10)	2.361(12)	-	2.364(10)	2.354(7)	2.345(5)
U-U	3.84(1)	3.85(6)	3.83(6)	3.85(4)	3.84(4)	3.89(21)	3.80(10)	3.867(4)	3.842(5)

The average diameter of UO_2 uraninite nanoparticles formed from the reduction of uranyl(VI) is 1.3 nm while the overall particle size is approximately 2.5 nm.[317,318] These structural parameters are really close to the cluster **7** that has a volume of 26×25×23 $Å^3$ (size with ligands around the core) with the largest U-U distance in the core of 12.1 Å (Figure II-20). The mean U-μ_4O distance is in the same range than in the UO_2 nanoparticle, whereas the U-U is shorter of 0.05 Å for **7**. This can be due to the distortion induced by the chloride and benzoate ligands surrounding the cluster core. These parameters show that **7** can be used as a good synthetic model of the environmental relevant uraninite nanoparticle.

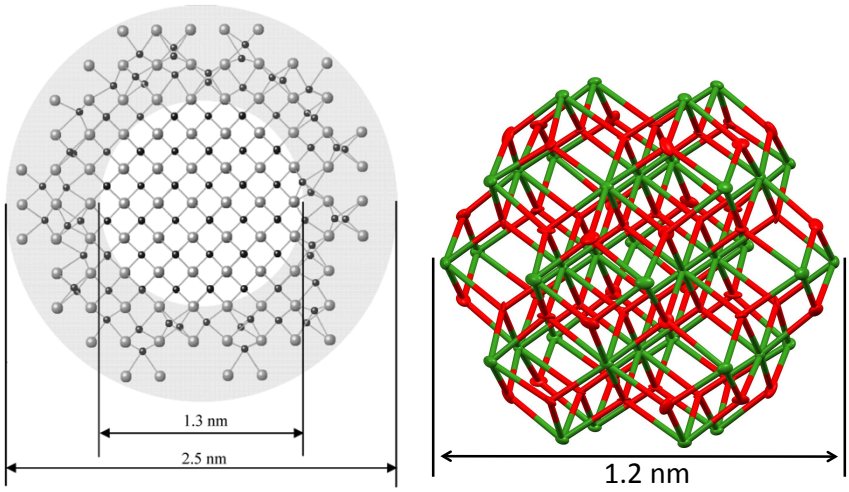

Figure II- 20 Structural model of nanobiogenic uraninite [317] (Atoms : O, black; U, grey) (left) and core of **7** (Atoms : O, red; U, green) (right).

II.2.6) Magnetic properties

The magnetic properties of the clusters $[U_{12}(\mu_3\text{-}OH)_8(\mu_3\text{-}O)_{12}I_2(\mu_2\text{-}OTf)_{16}(CH_3CN)_8]$, $[U_6O_4(OH)_4(\eta\text{-}dbm)_{12}]$, $[U_6O_4(OH)_4(PhCOO)_{12}(Py)_3]$ and $\{[K(MeCN)]_2[U_{16}O_{22}(OH)_2(PhCOO)_{24}]\}$ reported in the group have been measured and described in section II.1.3). The magnetic susceptibility of $[U_6O_4(OH)_4(\eta\text{-}dbm)_{12}]$ presented a TIP below 20 K,[340] while the $[U_6O_4(OH)_4(PhCOO)_{12}(Py)_3]$ cluster did not reveal TIP or slow relaxation of the magnetisation.[208] No clear magnetic coupling between the six uranium(IV) atoms was present in these two clusters, however very few examples of magnetic coupling involving U(IV) have been reported so far.[187,245,246,262,280,282]

We were interested in two clusters that were previously reported in our group, $[U_{12}(\mu_3\text{-}OH)_8(\mu_3\text{-}O)_{12}I_2(\mu_2\text{-}OTf)_{16}(CH_3CN)_8]$ [338] and $\{[K(MeCN)]_2[U_{16}O_{22}(OH)_2(PhCOO)_{24}]\}$.[341] Both their large sizes and the presence of uranium(IV) and uranium(V) motivated us to investigate the possibility of single molecule magnet properties.

The temperature dependence magnetic susceptibility (χ) of these two clusters has already been reported in a dc field. Both of them revealed an increase of χ with decreasing the temperature and an effective magnetic moment at 300 K of 2.79 μ_B and 2.89 μ_B per uranium for $[U_{12}(\mu_3\text{-}OH)_8(\mu_3\text{-}O)_{12}I_2(\mu_2\text{-}OTf)_{16}(CH_3CN)_8]$[338] and $\{[K(MeCN)]_2[U_{16}O_{22}(OH)_2(PhCOO)_{24}]\}$,[341] respectively. These values are slightly lower than the theoretical value calculated in the L-S coupling scheme for 10U(IV) and 2U(V) for $[U_{12}(\mu_3\text{-}OH)_8(\mu_3\text{-}O)_{12}I_2(\mu_2\text{-}OTf)_{16}(CH_3CN)_8]$ (μ_{eff} = 3.43 μ_B per U centre) and 12 U(IV) and 4 U(V) for $\{[K(MeCN)]_2[U_{16}O_{22}(OH)_2(PhCOO)_{24}]\}$ (μ_{eff} = 3.35 μ_B per U centre), but they are still in the range of reported experimental values.[103]

For both clusters, the magnetisation versus field curve at 2 K from -5 T to 5 T revealed the absence of an open hysteresis loop. To further investigate these mixed valent U(IV)/U(V) compounds, we performed ac magnetic susceptibility measurements with a 1.55 Oe ac field oscillating at a frequency (ν) varying from 1 to 1400 Hz under zero dc-field and a dc field of 0.1 T or 0.2 T for $[U_{12}(\mu_3\text{-}OH)_8(\mu_3\text{-}O)_{12}I_2(\mu_2\text{-}OTf)_{16}(CH_3CN)_8]$ (Figure II- 21) and for $\{[K(MeCN)]_2[U_{16}O_{22}(OH)_2(PhCOO)_{24}]\}$ (Figure II- 22).

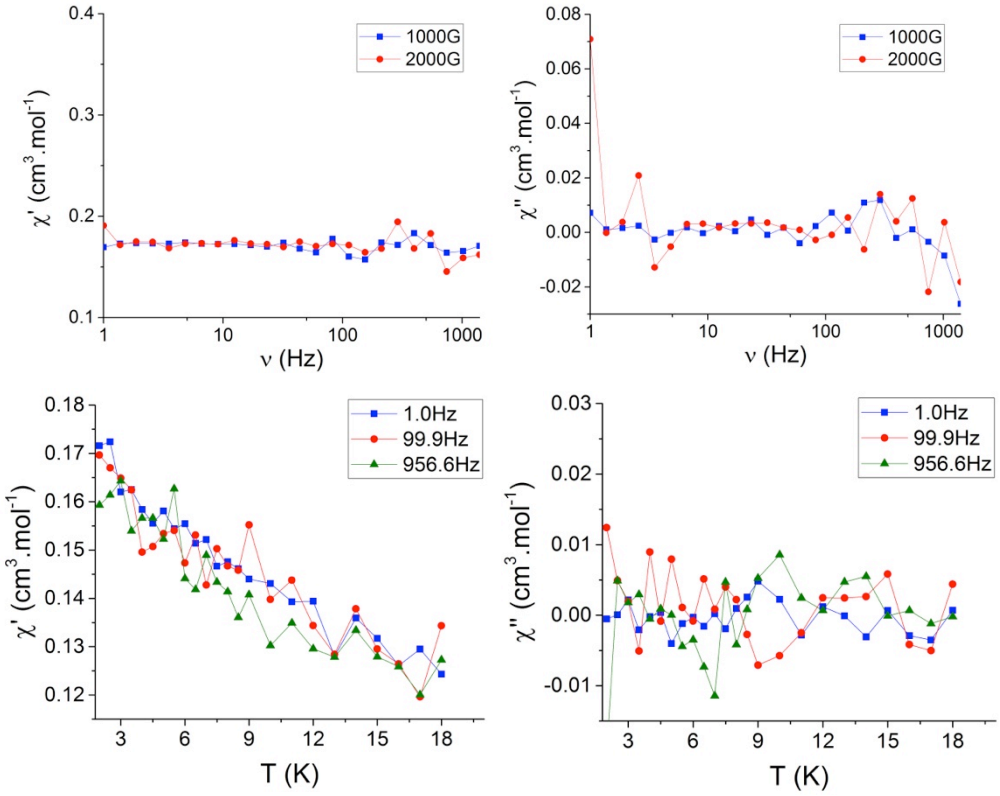

Figure II- 21 dc field dependence at 1.8 K of the in-phase (χ') (left up) and out-phase (χ'') (right up) ac susceptibility plotted vs. frequency of $[U_{12}(\mu_3\text{-}OH)_8(\mu_3\text{-}O)_{12}I_2(\mu_2\text{-}OTf)_{16}(CH_3CN)_8]$ recorded at 1.55 G ac field and temperature dependence of the (bottom left) in-phase and (bottom right) out-of-phase ac susceptibility components measured at 1.55 G ac field under 1000 G dc field.

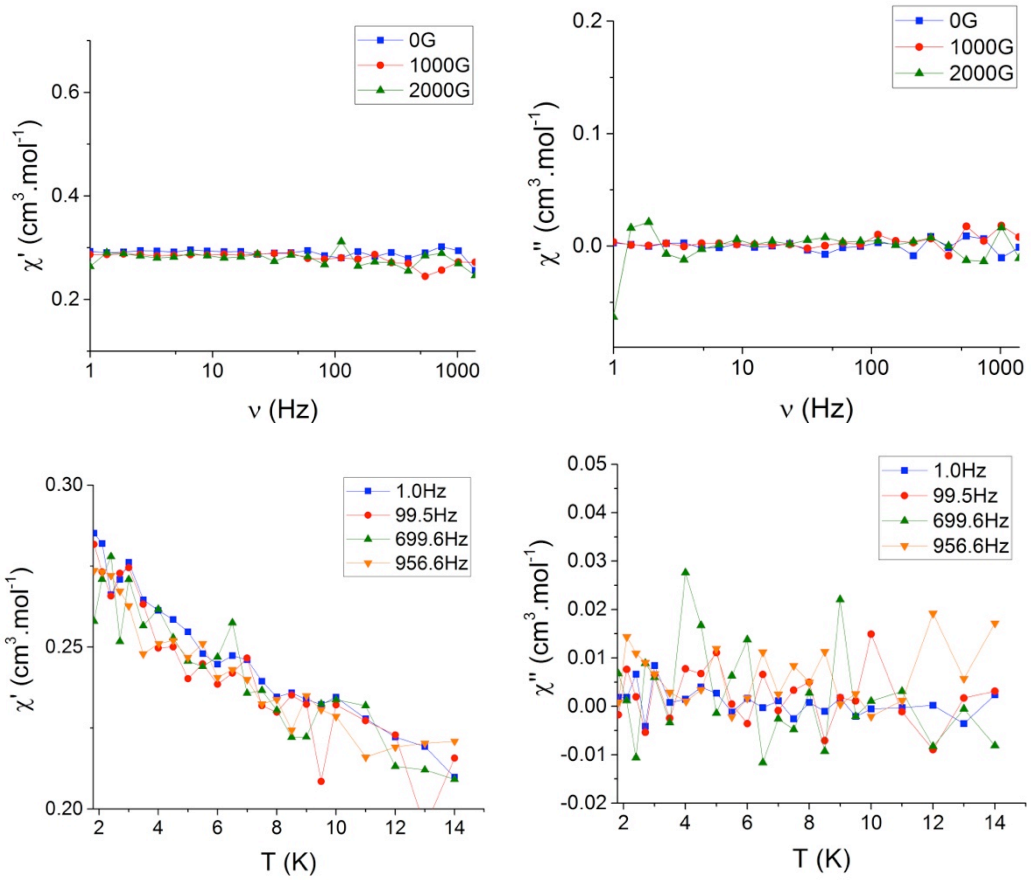

Figure II- 22 dc field dependence at 1.8 K of the in-phase (χ') (left up) and out-phase (χ'') (right up) ac susceptibility plotted vs. frequency of {[K(MeCN)]$_2$[U$_{16}$O$_{22}$(OH)$_2$(PhCOO)$_{24}$]} recorded at 1.55 G ac field and temperature dependence of the (bottom left) in-phase and (bottom right) out-of-phase ac susceptibility components measured at 1.55 G ac field under 1000 G dc field.

No frequency dependent peak was observed in any measurement. These results clearly indicate the absence of slow magnetic relaxation and ruled out the use of [U$_{12}$(μ$_3$-OH)$_8$(μ$_3$-O)$_{12}$I$_2$(μ$_2$-OTf)$_{16}$(CH$_3$CN)$_8$] and {[K(MeCN)]$_2$[U$_{16}$O$_{22}$(OH)$_2$(PhCOO)$_{24}$]} as potential single molecule magnets.

We have not observed the presence of magnetic communication between the uranium centres in the oxo/hydroxo clusters synthesised from controlled hydrolysis of low-valent uranium. However, oxo and hydroxo ligands are used extensively in molecular magnetism to assemble polymetallic compounds. Very few examples of magnetic coupling have been reported between uranium(IV) or uranium(V) bridged with oxo ligands. To our knowledge, two examples of unambiguous antiferromagnetic coupling (T_N = 3-20 K) between two U(IV) centres bridged linearly by a μ-O^{2-} ligand, were reported by the Meyer and Liddle groups (Table II- 2),[187,200] while three examples of antiferromagnetic coupling have been reported in pure U(V) complexes presenting a diamond core U$_2$(μ-O)$_2$ (Table II- 2).[47,199,204]

Table II- 2 Mean bond distances (Å) and angles (°) of selected oxo/hydroxo compounds.

Compound	Ox. state	M-μ_3OH	M-μ_2O	M-μ_3O	M-μ_4O	M-O-M	M-M	Magnetic properties
{[K(MeCN)]$_2$[U$_{16}$O$_{22}$(OH)$_2$(PhCOO)$_{24}$]} [341]	+IV/+V	2.29(9)	-	2.3(1)	2.4(1)	101.84-132.30	3.78(13)	-
[U$_{12}$(μ_3-OH)$_8$(μ_3-O)$_{12}$I$_2$(μ_2-OTf)$_{16}$(CH$_3$CN)$_8$] [338]	+IV/+V	2.52(8)	-	2.22(9)	-	99.75-122.68	3.82(9)	-
[{((tBuArO)$_3$tacn)U^{IV}}$_2$(μ-O)] [187]	+IV	-	2.110(4)	-	-	180	4.219	AF (20 K)
[{U(Tren^{DMSB})}(μ-O){U(Tren$^{DMSB\text{-}C2O2}$)}] [200]	+IV	-	2.127(3)	-	-	160.9	4.195(1)	AF (3 K)
[{((nP,MeArO)$_3$tacn)U^{V}}$_2$(μ-O)$_2$] [199]	+V	-	2.11(10)	-	-	108.45(5)	3.4222(3)	(AF 70 K)
[U^{V}O$_2$(dbm)$_2$K(18c6)]$_2$ [47]	+V	-	2.16(31)	-	-	105.8(2)	3.462(4)	(AF 5 K)
[(Me$_3$SiOU^{V}O)$_2$(Pcm)] [204]	+V	-	2.09(1)	-	-	106.5(2)	3.3557	(AF 17 K)

Compared to the other examples of exchange-coupled uranium oxo molecules displaying bridging μ_2-oxo ligands, it is possible that the interaction between uranium and the μ_3- or μ_4-oxo ligands in [U$_{12}$(μ_3-OH)$_8$(μ_3-O)$_{12}$I$_2$(μ_2-OTf)$_{16}$(CH$_3$CN)$_8$] and {[K(MeCN)]$_2$[U$_{16}$O$_{22}$(OH)$_2$(PhCOO)$_{24}$]} is not strong enough to promote magnetic interaction. Perhaps a multiple U-O bond is required to favour magnetic communication through the oxo ligand. Based on these results, we decided to not continue investigating these oxo/hydroxo clusters for the design of uranium-based SMMs.

II.3) Conclusion

The work presented in this chapter describes the preparation of polynuclear uranium hydroxo/oxo clusters. The synthetic approach exploited a method developed in our laboratory: the controlled hydrolysis of low-valent precursors. Notably, a comparison between the hydrolysis of the iodide and chloride uranium(IV) precursors in the presence of biologically relevant organic ligands has been studied. The reaction conditions have been tuned to build new polynuclear architectures. Five hydroxo/oxo clusters with unprecedented geometries and nuclearities have been isolated. Moreover, the study at high temperature led to the isolation of one of the biggest oxo clusters reported to date. This work has revealed the wide variety of possible geometries and expanded the family of hydroxo/oxo clusters reported with benzoate as a biologically relevant organic ligand.

Although these clusters have not proven to be of interest as potential uranium-based SMMs, the synthetic route based on the controlled hydrolysis of low-valent uranium complexes conceptually reproduces the aggregation phenomena observed in environmental and microbial uranium reduction. Indeed, these discrete hydroxo/oxo clusters can be seen as small models of the uraninite nanoparticles formed in the anaerobic bioreduction of uranyl(VI). The synthesis of these hydrolysed species may lead to a better understanding of

the formation of the uraninite nanoparticles in the environment and how their sizes are controlled. In the near future, studies will be directed to investigate the mechanism of the U(IV) hydrolysis and will focus on studies at high temperatures.

In order to design uranium SMMs, we have synthesised large homometallic clusters. However, the U-μ_3O bond is probably not strong enough to lead to unambiguous magnetic coupling between the uranium centres, while some reported complexes containing μ_2-O^{2-} bridging ligand did. Keeping in mind SMM synthesis as long term objective, we then focused on the synthesis of heteropolymetallic assemblies using the cation-cation interaction, which is known to promote magnetic interaction.

CHAPTER III. ACTINYL(V) POLYMETALLIC COMPLEXES

III.1) Context

The cation-cation interaction (CCI), defined as the coordination of other metal ions to the actinyl oxygen atom, leads to the formation of polynuclear complexes of actinides with different geometries, as described in the Introduction chapter.[211] This interaction is due to the strong Lewis basicity of the oxygen atoms of the AnO_2^+ moieties. The few examples of discrete neptunyl(V) complexes assembled via CCI are described in the Introduction chapter.

We have observed in the mixed-valent trinuclear $[\{Np^{VI}O_2Cl_2\}\{Np^{V}O_2Cl(THF)_3\}_2]$ complex that the building of supramolecular assemblies through CCI was a successful strategy to promote strong magnetic coupling between the actinide metallic centres with SMM poperties.[112,181] In contrast to neptunyl(V), uranyl(V) is much more unstable and readily disproportionates into uranyl(VI) and uranium(IV). The disproportionation mechanism of urany(V) involves the formation of a dimeric cation-cation intermediate quickly followed by a single-electron transfer and protonation steps.[34-37] Over the past ten years, a handful of stable mononuclear uranyl(V) complexes have been successfully isolated thanks to the use of bulky ligands and aprotic and anaerobic media.[52,55,58,180] The critical role of cation-cation interactions in the disproportionation reaction of uranyl(V) has largely limited the isolation of polynuclear complexes of this ion. However, the $5f^1$ configuration of the uranyl(V) cation is of first interest for the investigation of the magnetic properties of the polynuclear compound formed due to the absence of inter-electronic repulsion. Since the CCI is an efficient pathway for magnetic coupling and to build polynuclear assemblies with various geometries, we have been interested in the synthesis of uranyl(V) CC assemblies to design SMMs.

III.1.1) Towards the first CC uranyl(V) complex

The first CC complex of pentavalent uranyl $\{[UO_2(dbm)_2]_4[K_6(Py)_{10}]\}I_2Py_2$, already presented in the Introduction chapter, was isolated from the reaction of $\{[UO_2(Py)_5][KI_2(Py)_2]\}_n$ with 2 equivalents of dibenzoylmethanate (dbm^-) in pyridine (Scheme III- 1).[240] Another tetranuclear structure was isolated from an analogous reaction in acetonitrile solution, yielding $\{[UO_2(dbm)_2]_2[\mu\text{-}K(MeCN)_2][\mu_8\text{-}K]\}_2$ (Figure III- 1 right).[47] These two clusters are

constituted of four $[UO_2(dbm)_2]^-$ complexes, with each uranyl ion donating and accepting one T-shaped cation-cation interaction, forming a square. An average lengthening of the U-O bond involved in the CCI of 0.1 Å with respect to the unbound U-O is usually encountered with uranyl(V) CC assemblies. Two potassium ions located above and below the plane of the UO_2^+ tetramer, respectively, bind four different uranyl oxygens.

Scheme III- 1 Synthesis of $\{[UO_2(dbm)_2]_4[K_6(Py)_{10}]\}I_2Py_2$, $\{[UO_2(dbm)_2]_2[\mu\text{-}K(MeCN)_2][\mu_8\text{-}K]\}_2$ and $[UO_2(dbm)_2K(18c6)]_2$

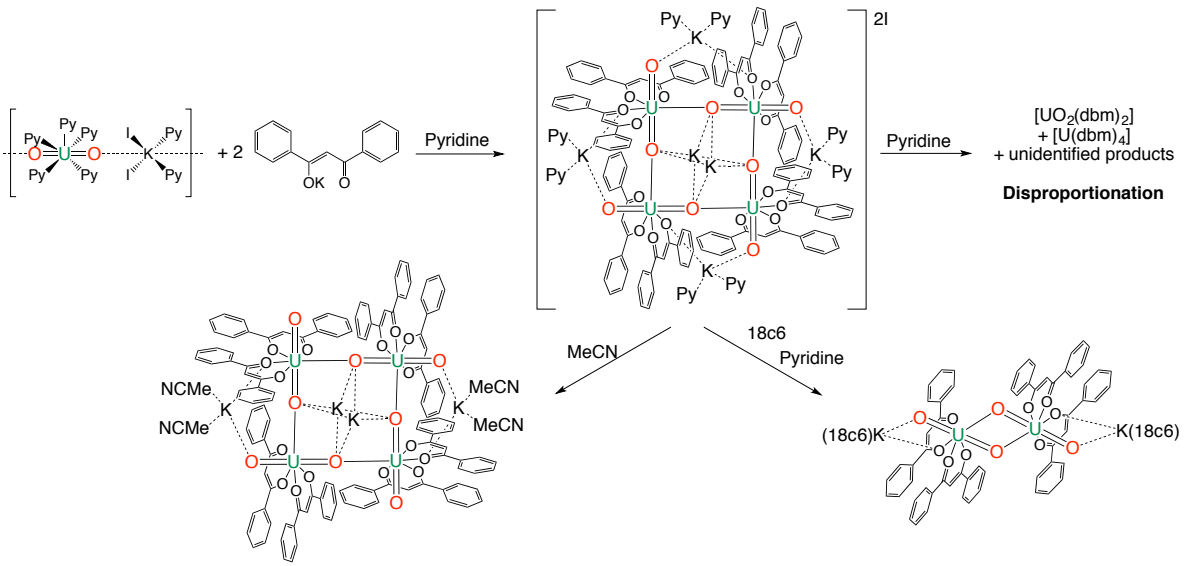

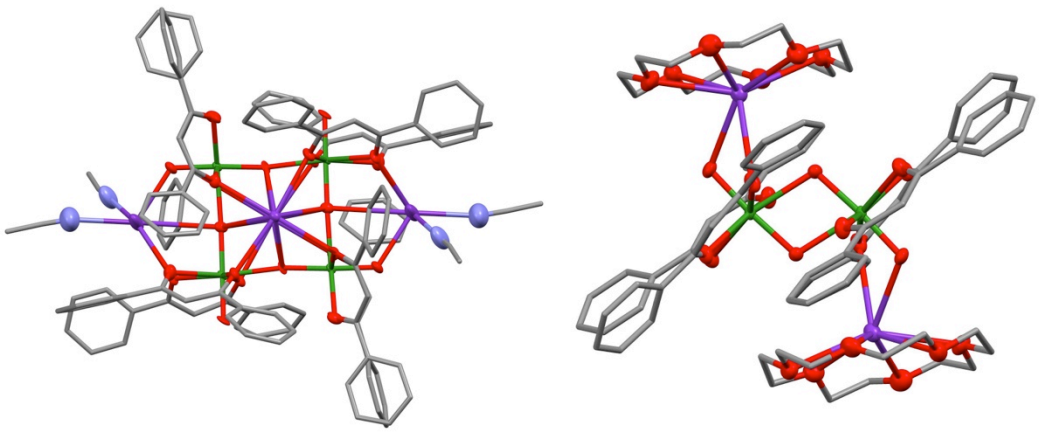

Figure III- 1 Molecular structures of $\{[UO_2(dbm)_2]_2[\mu\text{-}K(MeCN)_2][\mu_8\text{-}K]\}_2$ (left) and of $[UO_2(dbm)_2K(18c6)]_2$ (right). (H, I^- anions and co-crystallised pyridine molecules were omitted; ligands are represented with pipes for clarity, C are represented in grey, O in red, K in purple, N in blue and U in green).

To study the role of the coordinated potassium counterions, the reaction of the pyridine solvate $\{[UO_2(dbm)_2]_4[K_6(Py)_{10}]\}I_2Py_2$ with 18-crown-6 ether (18c6), known for its affinity for potassium cation, was investigated. The reaction yielded a centrosymmetric dimer

$[UO_2(dbm)_2K(18c6)]_2$, (Figure III- 1 right) in which both units are assembled through a diamond-shaped CCI (Scheme III- 1).[47]

The measured temperature-dependent magnetic susceptibility highlights the presence of unambiguous antiferromagnetic coupling between the two uranium centres of the $[UO_2(dbm)_2K(18c6)]_2$ dimer, with the appearance of a maximum in χ vs. T at 5 K, while $\{[UO_2(dbm)_2]_2[\mu\text{-}K(MeCN)_2][\mu_8\text{-}K]\}_2$ probably involves magnetic coupling at lower temperature (Figure III- 2).[47] These results provided the first example of magnetic coupling between uranium ions via uranyl(V) oxo bridges.

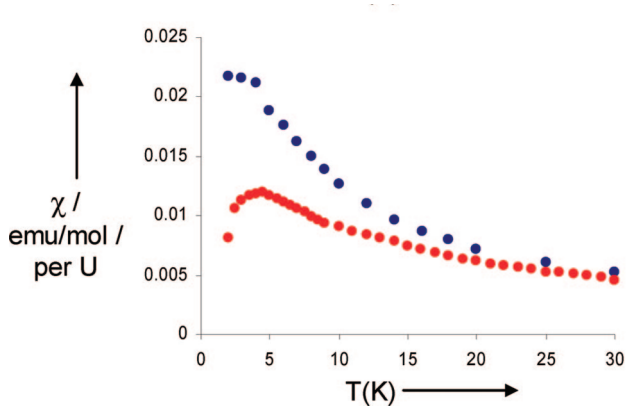

Figure III- 2 Temperature-dependent magnetic susceptibility data for $\{[UO_2(dbm)_2]_2[\mu\text{-}K(MeCN)_2][\mu_8\text{-}K]\}_2$ (blue circles) and $[UO_2(dbm)_2K(18c6)]_2$ (red circles) over the range 2-30 K.

In pyridine or THF solutions, these clusters disproportionate into the $[U(dbm)_4]$ and $[(UO_2(dbm)_2]$ complexes. This result seemed to validate the general assumption that the formation of cation-cation complexes would inevitably result in the disproportionation of the pentavalent uranyl species. However, stable CC complexes of uranyl(V) have been isolated with polydentate ligands such as the dinucleating macrocyclic ligand used in the Arnold group and tetradentate Schiff base ligands in our group.

III.1.2) Dinucleating macrocyclic ligand

Arnold and coworkers described the stable uranyl(V)-Fe(II) cation-cation complex $[UO(OSi(CH_3)_3)(THF)Fe_2I_2(Pcm)]$ (Pcm^{4-} a pyrrole-imine macrocycle called Pac-man) from the reductive silylation of the uranyl(VI) complex $[UO_2(THF)(PcmH_2)]$ in the presence of FeI_2 and the silylamide base $KN(Si(CH_3)_3)_2$ (Scheme III- 2). Similar procedures with zinc and other silylated bases yielded analogous uranyl(V) complexes (Scheme III- 2).[58] One coordination pocket of the macrocycle ligand is occupied by the uranyl moiety while the second

coordinates partially two metal centres (Figure III- 1 left). The endo-oxo group of the uranyl(V) is bound to one 3d metal. However, magnetic characterisation of the iron complex did not reveal magnetic coupling between the two high-spin Fe(II) ions and the f^1 U(V) ion.

Scheme III- 2 Synthesis of $[UO(OSi(CH_3)_3)(THF)M_2I_2(Pcm)]$, $[UO_2Ln(Py)_2(Pcm)]_2$ and $[(Py)_3LiOUO(\mu\text{-}Cl)Ln(Py)(Pcm)]$.

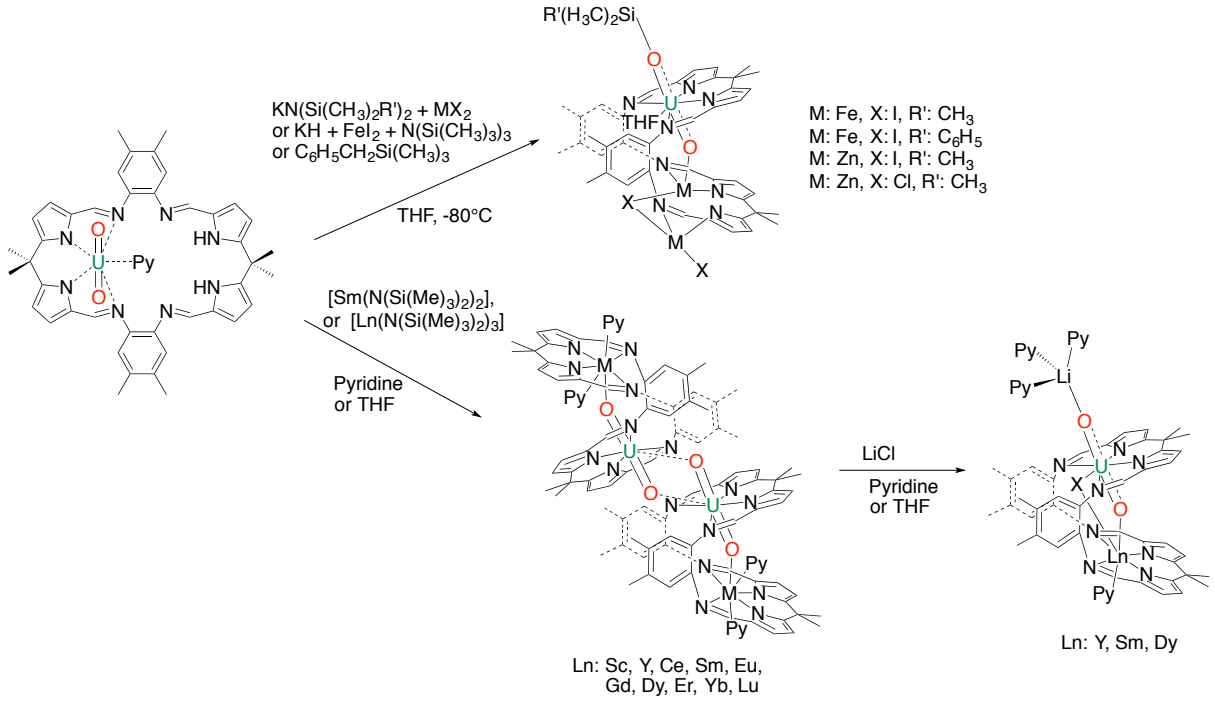

Surprinsingly, the direct reaction of $[UO_2(THF)(PcmH_2)]$ with transition metal silylamides $[M(N(Si(Me)_3)_2)_2]$ (M= Mn, Fe, Co) did not lead to the reduction of uranyl(VI) into uranyl(V), but instead, molecular cation-cation complexes are formed in which, uniquely, the transition metal bounds to the endo-uranyl oxygen atom and to the second coordination pocket of the Pcm ligand.[234] However, the use of the divalent lanthanide complex $[Sm(N(Si(Me)_3)_2)_2]$ [241] or trivalent lanthanide complex $[Ln(N(Si(Me_3)_2)_3]$ (Ln: Sc, Y, Ce, Sm, Eu, Gd, Dy, Er, Yb, Lu)[244], led to the reduction of the uranyl(VI) into uranyl(V) and the lanthanide ion bounds to the endo-uranyl oxygen atom and to the second coordination pocket of the Pcm ligand (Scheme III- 2). A single-electron transfer from the strongly reducing Sm(II) to the UO_2^{2+} group leads to reduction into uranyl(V), while with the trivalent lanthanide complexes the authors described a mechanism involving homolysis of a Ln(III)−$N(SiMe_3)_2$ bond, affording 1 equiv of $^{\cdot}N(SiMe_3)_2$. The resulting $[UO_2Ln(Py)_2(Pcm)]_2$ complexes exist as a dimer in the solid state, forming a diamond-shaped CCI between two uranyl(V) units. Addition of lithium chloride leads to the disruption of the dimeric

$[UO_2Ln(Py)_2(Pcm)]_2$ complexes, and the formation of monomeric complexes $[(Py)_3LiOUO(\mu\text{-}Cl)Ln(Py)(Pcm)]$, where the exo oxo group of the uranyl(V) is coordinated to a lithium ion.

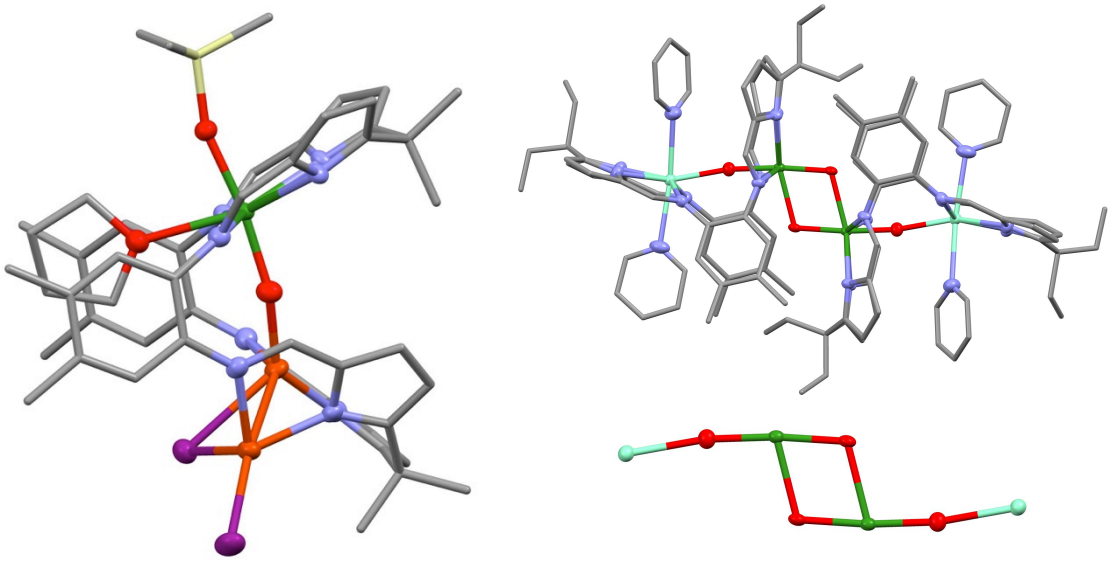

Figure III- 3 Molecular structures of $[UO(OSi(CH_3)_3)(THF)Fe_2I_2(Pcm)]$ (left) and $[UO_2Sm(Py)_2(Pcm)]_2$ (right) (H omitted for clarity and ligands represented in pipes. Atoms: C in grey, N in light blue, Fe in orange, Si in yellow, Sm in light green, O in red, and U in green)[241]

Magnetic coupling within some of these systems was investigated. The comparison of the magnetic properties of the dimeric samarium complex $[UO_2Sm(Py)_2(Pcm)]_2$ (Figure III- 3 right) with the properties of the diamagnetic yttrium analogue shows the influence of the lanthanide ion on the magnetic properties. The $[UO_2Sm(Py)_2(Pcm)]_2$ complex presents clear antiferromagnetic coupling with a maximum in the magnetic susceptibility observed around 10 K, while the yttrium analogues did not present any significant interaction.[241] The magnetic curves were fitted to a model that described a relatively large antiferromagnetic coupling between the U and Sm ions ($J = -10.5\ cm^{-1}$) and a small antiferromagnetic coupling between the two U ions ($J < -1\ cm^{-1}$) (Figure III- 4).[241] The magnetic data does not reveal clear antiferromagnetic coupling in the monomeric $[(Py)_3LiOUO(\mu\text{-}Cl)Sm(Py)(Pcm)]$ complex, but an antiferromagnetic exchange coupling of $-37cm^{-1}$ was calculated between the uranium(V) and the samarium(III) ions. Finally, the dimeric dysprosium $[UO_2Dy(Py)_2(Pcm)]_2$ complex revealed a butterly-shaped hysteresis cycle at 3 K, however this magnetic bistability was ascribed to the single-ion properties of Dy(III) rather than arising from intramolecular interactions.[244]

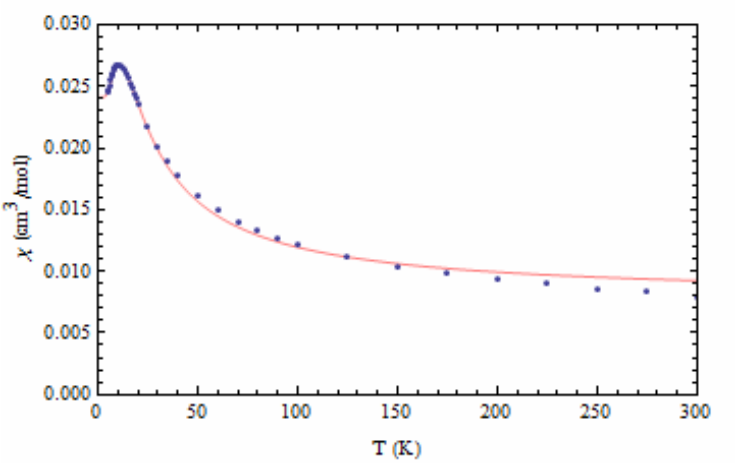

Figure III- 4 Variation of the magnetic susceptibility of the $[UO_2Sm(Py)_2(Pcm)]_2$ complex with temperature (dots: measurements, line: calculations).[241]

These studies performed in the Arnold group with a dinucleating macrocyclic ligand have led to stable CC uranyl(V) complexes with alkali metals, transition metals and lanthanides from the reduction of uranyl(VI).[58,241,244,349,350] Magnetic coupling was interpreted as a uranyl(V)-4f interaction, however no SMM properties have been reported.

III.1.3) Tetradentate Schiff base ligands

Subsequent to the first CC uranyl(V) complexes reported in our group with the dbm ligand, tetradentate Schiff base ligands have been used to avoid partial ligand loss leading to the disproportionation of the CC assemblies. These ligands stabilised uranyl(V) as highlighted by the electrochemical studies from Ikeda[40,41] and the recent uranyl(V) mononuclear complexes isolated in our laboratory.[52,53] Moreover, they leave open one coordination site in the equatorial plane of uranyl(V), leading to possible CC assemblies.

The reaction of the uranyl(V) polymer $\{[UO_2(Py)_5][KI_2(Py)_2]\}_n$ with salenK_2 in pyridine led to the formation of an insoluble complex of pentavalent uranyl. This solid was dissolved in the presence of 18-crown-6 ether (18c6) to yield the tetrameric pentavalent uranyl complex $\{[UO_2(salen)]_4[\mu_8\text{-}K]_2\}(K(18c6)(Py))_2$ (Scheme III- 3 and Figure III- 5 left), which has a similar square core to dbm CC assemblies.[231] In contrast to the dbm assemblies, this tetrameric structure is fully stable in pyridine solution and is retained even in dmso, suggesting a stronger CCI.[48] Cyclic voltammetry of the complex dissolved in pyridine demonstrated that a reversible one-electron oxidation does not destroy the structure of the cluster, and the oxidation of $\{[UO_2(salen)]_4[\mu_8\text{-}K]_2\}(K(18c6)(Py))_2$ with CuI yielded a mixed-valent uranyl(V)/uranyl(VI) tetranuclear $\{[UO_2(salen)]_4[\mu_8\text{-}K]_2\}(K(18c6)(Py))_2$ cluster.[231] Temperature dependent magnetic data of $\{[UO_2(salen)]_4[\mu_8\text{-}K]_2\}(K(18c6)(Py))_2$ revealed an unambiguous

antiferromagnetic coupling at 5 K. The observation of a stronger coupling in the salen tetramer compared to $\{[UO_2(dbm)_2]_2[\mu\text{-}K(MeCN)_2][\mu_8\text{-}K]\}_2$, in which the presence of magnetic coupling at temperature lower than 2 K had been suspected, could be the result of small differences in the structural parameters associated with the presence of a stronger UO_2^+---UO_2^+ interaction.

Scheme III- 3 Synthesis of $\{[AnO_2(salen)]_4[\mu_8\text{-}K]_2\}(K(18c6)(Py))_2$ (An: U, Np)

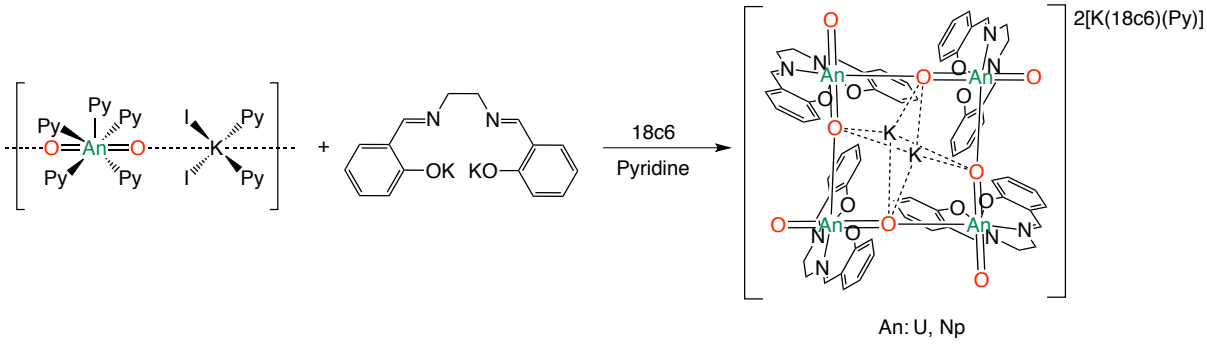

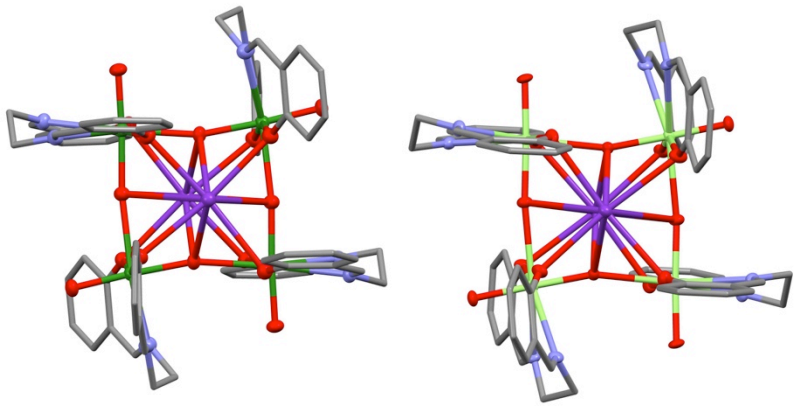

Figure III- 5 Molecular structures of $\{[UO_2(salen)]_4[\mu_8\text{-}K]_2\}^{2-}$ (left) and $\{[NpO_2(salen)]_4[\mu_8\text{-}K]_2\}^{2-}$ (right) (H were omitted for clarity, C are represented in grey, O in red, K in purple, N in blue, Np in light green and U in green)[231,239]

It should be noted that recently, an isotructural complex of $\{[UO_2(salen)]_4[\mu_8\text{-}K]_2\}(K(18c6)(Py))_2$ with neptunyl(V) was reported.[239] The reaction of the neptunyl(V) polymer $\{[NpO_2(Py)_5][KI_2(Py)_2]\}_n$ with salenK_2 in pyridine in presence of 18c6 gave the tetrameric pentavalent neptunyl complex $\{[NpO_2(salen)]_4[\mu_8\text{-}K]_2\}(K(18c6)(Py))_2$ (Scheme III- 3 and Figure III- 5 right). As for the uranium analogue, the tetrameric neptunyl(V) structure is retained in pyridine. This study shows one more time the analogous properties of neptunyl(V) and uranyl(V), demonstrating the potential use of uranyl(V) as a model of the coordination of neptunyl(V).

Recent studies in our group explored the importance of both the organic ligands and alkali-metal counterions in determining the stability of the uranyl(V)-based CC assemblies in pyridine solution.[48] The reactions of the more flexible acacen ligand and the more aromatic salophen ligands with uranyl(V) precursor in the presence of crown-ether or cryptand yielded three additional clusters $\{[UO_2(acacen)]_4[\mu_8\text{-}K]_2[K(18c6)(Py)]_2\}$ (Figure III- 6 left), $\{[UO_2(acacen)]_4[\mu_8\text{-}K]\}.2[K(222)(Py)]$ and $\{[UO_2(salophen)]_4[\mu_8\text{-}K]_2[\mu_5\text{-}KI]_2[(K(18c6)]_2\}.2[K(18c6)(THF)_2].2I$ (Scheme III- 4 and Figure III- 6 right), that are stable towards disproportionation. These three complexes contain the same uranium-oxygen core as the tetranuclear dbm and salen uranyl(V) assemblies.

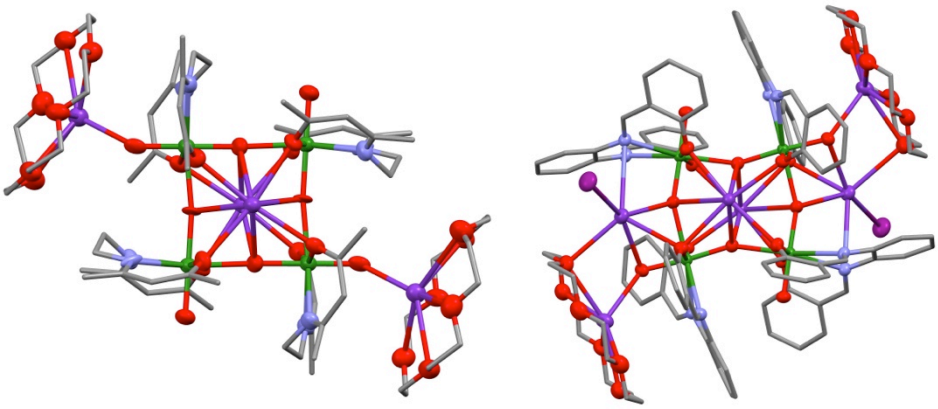

Figure III- 6 Molecular structures of $\{[UO_2(acacen)]_4[\mu_8\text{-}K]_2[K(18c6)(Py)]_2\}$ (left) and $\{[UO_2(salophen)]_4[\mu_8\text{-}K]_2[\mu_5\text{-}KI]_2[(K(18C6)]_2\}$ (right) (H were omitted for clarity, C are represented in grey, O in red, K in purple, N in blue and U in green) [48]

The salen and acacen clusters retained their tetrameric structures in pyridine. However, with the salophen ligand, diffusion coefficient measurements suggest the presence of a stable mononuclear species in pyridine (in the presence of 2 equivalents of 18c6), while the tetranuclear compound crystallised from THF solution (Scheme III- 4).[48] It should be noted that in the absence of crown ether, a complicated mixture of disproportionation products containing at least $[UO_2(salophen)(Py)]$ and $[U(salophen)_2]$ is formed in pyridine. The addition of a small excess of KI with respect to 18c6 (0.1 equivalents) in pyridine is sufficient to promote the complete disproportionation of the uranyl(V) salophen complex in 2 days (Scheme III- 4). However, the uranyl(V) complex formed with the bulkier ligand ^{t}Bu-salophen is stable, even in presence of free potassium. This highlighted the strong influence of the steric bulk on the stability of uranyl(V) complexes.

Scheme III- 4 The reaction of with Salophen K_2 in the presence or absence of 18c6 leads respectively to the stabilisation of U(V) or to the disproportionation.

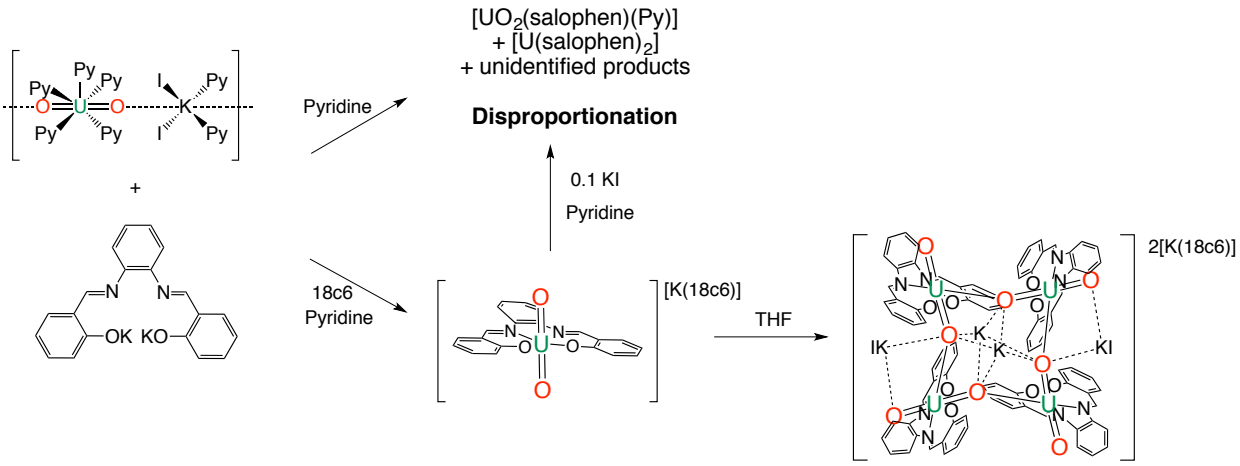

The potassium cation clearly plays a role in the structure and stability of the tetramers presented above. During my master's thesis, we studied the use of tetradentate monoanionic ligands to design homometallic complexes whereas every example of uranyl(V) CC clusters in the literature are heterometallic. The reaction of the UO_2^+ precursor $\{[UO_2(Py)_5][KI_2(Py)_2]\}_n$ with the potassium salt of the tetradentate aza β-diketiminate ligand, LK (L = 2-(4-Tolyl)-1,3-bis(quinolyl)malondiiminate) in pyridine led to the immediate formation of a trimeric uranyl(V) complex $[UO_2L]_3$ (Scheme III- 5).[242] The crystal structure shows a trimeric molecule consisting of three uranyl moieties coordinated to each other through CCI to form an equilateral triangle (Figure III- 7). This was the first example of CC assembly formed in the absence of alkali metal ions.

Scheme III- 5 Synthesis and reactivity of $[UO_2L]_3$

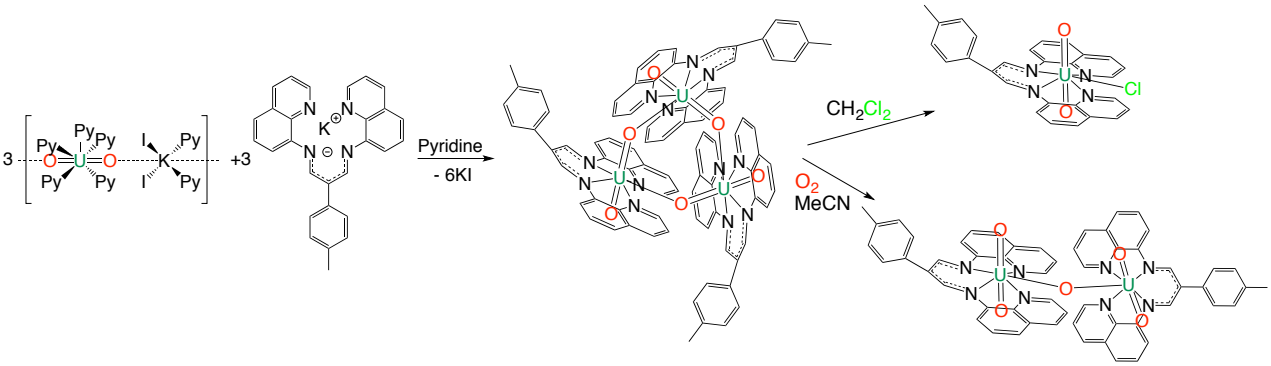

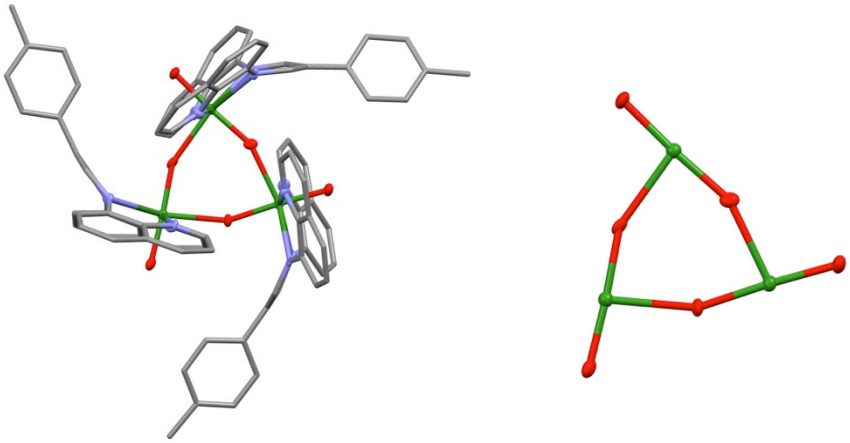

Figure III- 7 Molecular structure of $[UO_2L]_3$ (top left), of its uranyl core (right) (Ligands were represented in pipes, H and co-crystallised solvent molecules were omitted for clarity, C atoms are represented in grey, O in red, N in light blue and U in green.) [242]

The temperature dependent magnetic susceptibility was measured for the triangular shaped complex in the temperature range 2-300 K and clearly indicates the presence of an antiferromagnetic coupling between the f^1 ions with a maximum at 12 K (Figure III- 8). $[UO_2L]_3$ is characterised by a non-magnetic ground doublet corresponding to two oppositely twisted chiral arrangements of the uranium moments.[242,351]

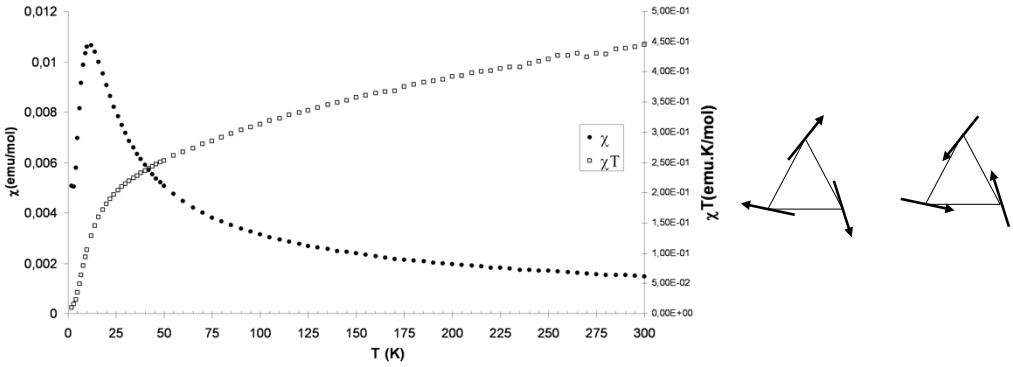

Figure III- 8 Temperature-dependent magnetic susceptibility data for $[UO_2L]_3$ in the range of 2-300 K (left) and schematic representation of the ground state of $[UO_2L]_3$ (right). [242,351]

This trimeric complex is highly stable with respect to disproportionation but reacts with oxidising agents.[242] A hexavalent complex $[UO_2LCl]$ is formed from the reaction between $[UO_2L]_3$ and CH_2Cl_2, probably through chloride abstraction from the solvent. $[UO_2L]_3$ reacted with dioxygen in acetonitrile solution to yield the dinuclear complex $\{[UO_2(L)]_2[\mu_2\text{-}O]\}$ where the two oxo-bridged uranyl(VI) complexes are arranged almost perpendicular to each other.

In order to gain further insight into the effect of the counterions on both structure and stability, a systematic study was carried out in the group on the very stable uranyl(V) salen complex by addition of different metallic salts. An alternative “potassium free” synthetic route was developed.[48] The reduction of the uranyl(VI) salen complex [(UO_2)(salen)(Py)] with Cp^*_2Co afforded the highly soluble complex of uranyl(V) [UO_2(salen)(Py)][Cp^*_2Co], which could not be isolated. The addition of one equivalent of KI and one equivalent of 18c6 afforded the tetrameric {[UO_2(salen)]$_4$[μ_8-K]$_2$}(K(18c6)(Py))$_2$ complex previously described from the reaction of the uranyl(V) polymer {[$UO_2(Py)_5$][$KI_2(Py)_2$]} and salenK_2. Consequently, the [UO_2(salen)(Py)][Cp^*_2Co] complex is a suitable starting material to study the influence of the counterions. Similar syntheses between [UO_2(salen)(Py)][Cp^*_2Co] and NaI or RbI in presence of 18c6 also gave stable tetrameric complexes [UO_2(salen)]$_4$[μ_8-M]$_2$[M(18c6)(Py)$_2$]$_2$ (M: Na, Rb) (Scheme III- 6). However, the reaction of [UO_2(salen)(Py)][Cp^*_2Co] and the iodide salt of the smaller Li^+ ion resulted in the slow disproportionation of the uranyl(V) complex, yielding a mixture of decomposition products containing [U(salen)$_2$] complex and [$U^{VI}O_2$(salen)(Py)] (Scheme III- 6). The lower stability of the UO_2^+ complex in the presence of Li^+ probably results from both steric and electronic effects associated with the higher charge/size ratio of Li^+ compared to Na^+, K^+ and Rb^+.

Scheme III- 6 Effect of the counter-ion

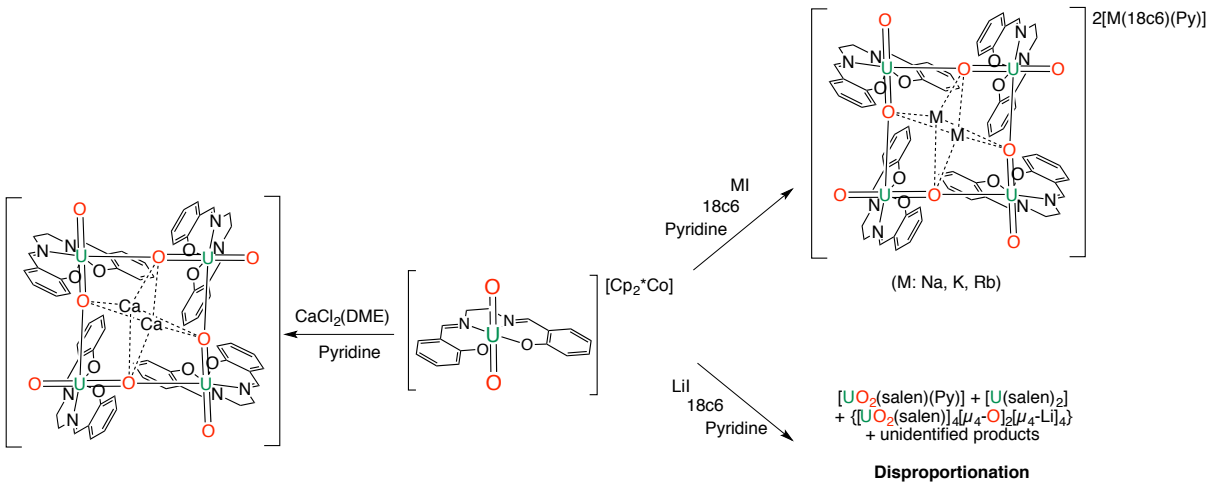

From the decomposition mixture, an oxo uranyl cluster {[UO_2(salen)]$_4$[μ_4-O]$_2$[μ_4-Li]$_4$} was isolated (Figure III- 9 left).[48] In this structure, two adjacent uranium atoms are bridged by an oxo anion while the internal oxygen atom of the uranyl groups are connected to the opposite oxo anion by a lithium cation, yielding a U_4Li_4 cubic cluster. The presence of the μ-

oxo groups in the structure accounts for the fate of the oxygen in the disproportionation reaction of pentavalent uranyl compounds in aprotic solvents.

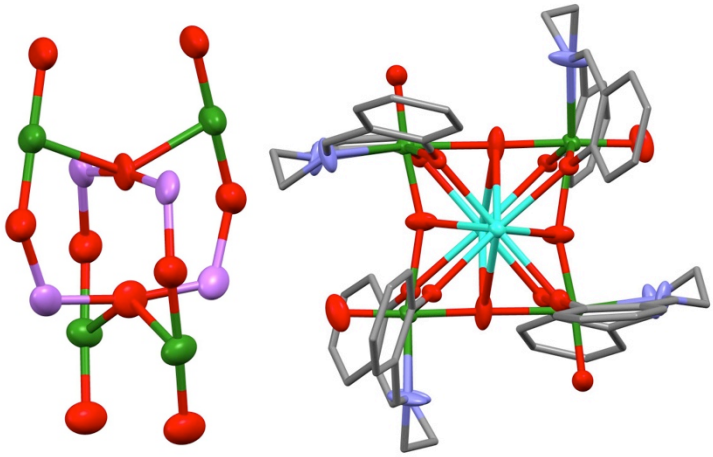

Figure III- 9 Molecular structures of the core of {[UO_2(salen)]$_4$[μ_4-O]$_2$[μ_4-Li]$_4$} (left) and {[UO_2(salen)]$_4$$Ca_2$} (right). (H were omitted and ligands were represented in pipes for clarity, C are represented in grey, O in red, Li in pink, N in blue, Ca in turquoise and U in green) [48,180]

To determine if the charge of the cation used had an influence on both the stability and the structure of the cluster formed, the same strategy was used with Ca^{2+}, an earth alkaline divalent cation which has a very close ionic radius to the previously studied Na^+ ion (ionic radius Ca^{2+} = 1.12 Å and Na^+ = 1.18 Å).[352] The reaction of two equivalents of the monomeric uranyl(V) complex [UO_2(salen)(Py)][Cp^*_2Co] with one equivalent of $CaCl_2$(DME) in pyridine resulted in the formation of the stable tetrameric complex {[UO_2(salen)]$_4$$Ca_2$} (Scheme III- 6and Figure III- 9 right).[180]

Unambiguous antiferromagnetic couplings are present at 5 K for [UO_2(salen)]$_4$[μ_8K]$_2$[K(18c6)(Py)$_2$]$_2$, at 11 K for [UO_2(salen)]$_4$[μ_8-Rb]$_2$[Rb(18c6)(Py)$_2$]$_2$ and at 7 K for {[UO_2(salen)]$_4$$Ca_2$}.[48,180] These results show the importance of the size of the cation on the stabilisation of the CC assembly, as well as the influence on the magnetic interaction, probably resulting from small structural changes within the tetrameric cores.

During my master's thesis, we studied the effect of manganese(II), a high spin paramagnetic transition metal, on structure geometry, stability and magnetic properties. The reaction of two equivalents of the monomeric uranyl(V) complex [UO_2(salen)(Py)][Cp^*_2Co] with one equivalent of $Mn(NO_3)_2$ in pyridine led to a dodecanuclear uranyl(V) complex containing six manganese(II) centres [{[UO_2(salen)]$_2$Mn(Py)$_3$}$_6$], $U_{12}Mn_6$, with a wheel geometry (Scheme III- 7).[180] The "potassium free" synthetic procedure was used to prevent the presence of both Mn(II) and K^+ in the reaction mixture. Moreover, the Cp_2*$CoNO_3$

complex formed during the reaction is soluble in pyridine while the $U_{12}Mn_6$ wheel is not, leading to easy separation of the two complexes.

Scheme III- 7 Synthesis of $[\{[UO_2(salen)]_2Mn(Py)_3\}_6]$

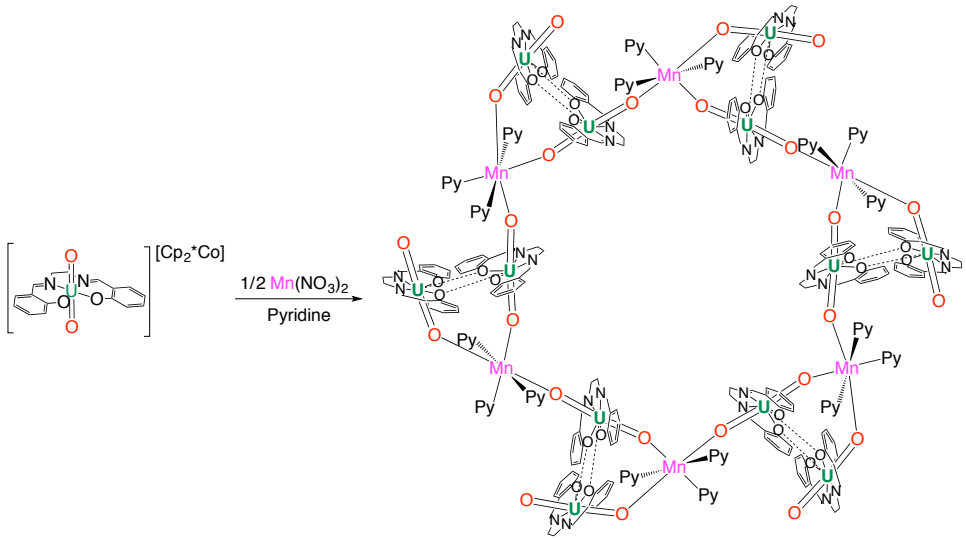

The structure of complex $[\{[UO_2(salen)]_2Mn(Py)_3\}_6]$ represents the largest uranyl(V) cluster reported to date and contains UO_2^+-Mn CCI without UO_2^+-UO_2^+ CCI (Figure III- 10).[180] The structure consists of a centrosymmetric hexamer assembled from six triangles of two salen bound UO_2^+ cations, mutually coordinated through two salen-phenolate bridges, which are both coordinated through the uranyl oxygen to the same Mn^{2+} ion. The six triangles are connected together to yield the final $U_{12}Mn_6$ wheel through the CCI of the manganese ion from one triangle with the uranyl oxygen of an adjacent triangle. The strong preference of the Mn^{2+} ion for an octahedral geometry, the UO_2^+: Mn^{2+} CCI and the 2:1 UO_2^+: Mn^{2+} ratio, all drive the final assembly shape.

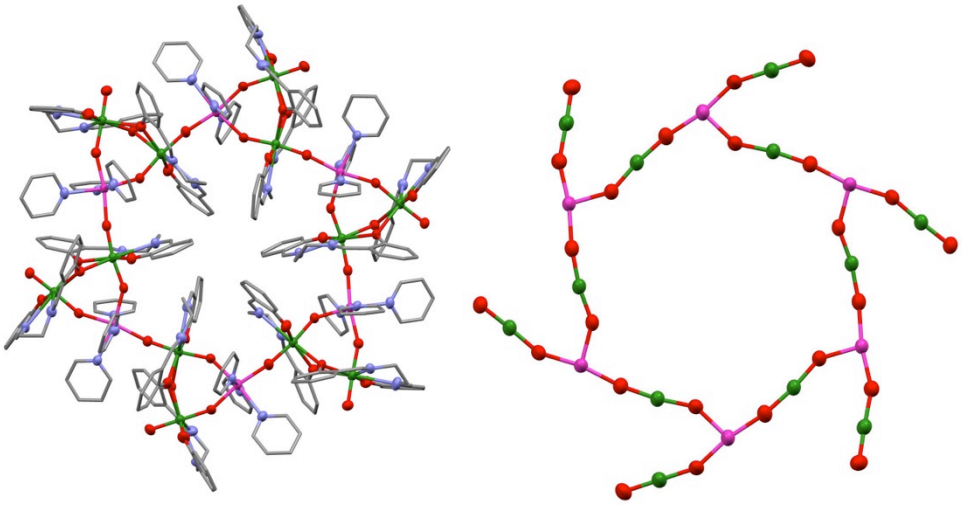

Figure III- 10 Molecular structures of [{[UO_2(salen)]$_2$Mn(Py)$_3$}$_6$] (left) and detail of the core (right) (Ellipsoid plots at 30 % probability. Co-crystallised pyridine molecules and H were omitted and ligands are represented with pipes for clarity, C are represented in grey, O in red, N in blue Mn in pink and U in green) [180]

Magnetic measurements on polycrystalline sample of [{[UO_2(salen)]$_2$Mn(Py)$_3$}$_6$] revealed interesting properties.[180] The observation of open hysteretic loops below 4.5 K, with a coercive field of 1.5T at 2.25 K, confirmed the presence of a magnetic ground state (Figure III- 11). A barrier to relaxation of 142 ± 7 K was extrapolated from the ac data analysis, arising of the interaction of 6 high spin Mn(II) (S = 5/2) ions and 12 anisotropic uranyl(V) units.

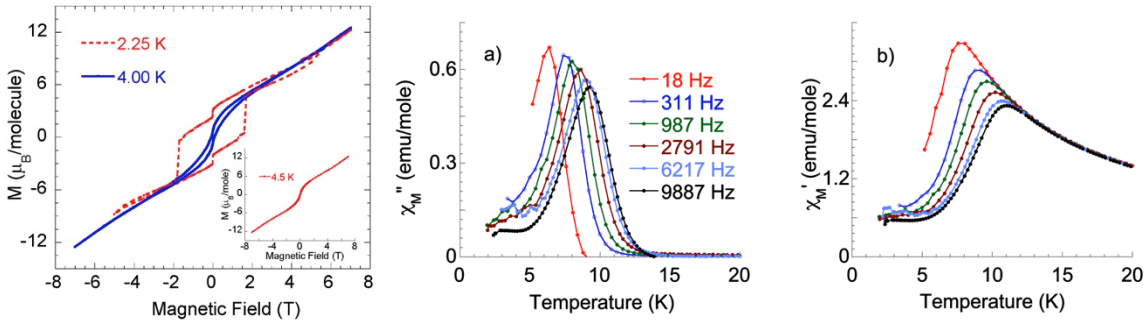

Figure III- 11 (left) Hysteresis cycles measured at 2.25 and 4 K between 7 and -7 T with a sweep rate of 0.004 T/s. (middle and right) Temperature dependence of the out-of-phase (χ_M'', a) and in-phase (χ_M', b) components of the ac magnetic susceptibility measured in a 10 G ac field oscillating at the indicated frequencies, under zero dc field.[180]

This $U_{12}Mn_6$ wheel was the first 5f-3d based molecular complex exhibiting single molecule magnet properties with an open magnetic hysteresis loop at low temperature, with a non-zero coercive field. Moreover, its relaxation barrier is one of the highest among any previously reported manganese assemblies or the few characterised uranium single-molecule magnet systems. The interesting magnetic properties of this $U_{12}Mn_6$ cluster suggest

that the use of the exchange-coupled 3d-uranium ions is a very promising path in the quest for single molecule magnets with improved properties.

In attempt to change the nature of the transition metal, similar syntheses with metallic salts containing Fe(II), Co(II), Ni(II) and Zn(II) were performed. However, none of them led to a similar assembly as the wheel obtained with Mn(II). Contrary to the $U_{12}Mn_6$ wheel, which is unsoluble in pyridine, mixtures of products were solubles as well as the soluble $[Cp_2^*Co]NO_3$ complex. Partial ligand scrambling was even observed between $[UO_2(salen)]^-$ and Co^{2+} as proton NMR spectroscopy revealed characteristic peaks corresponding to [Co(salen)]. However, the use of Cd(II) yielded a microcrystalline solid. This compound was characterised by X-ray powder diffraction and revealed similar unit cell parameters as the $U_{12}Mn_6$ wheel. This result may be due to the preference of Cd(II) for an octahedral geometry. Cd(II) is diamagnetic and the magnetic properties of this compound revealed an unambiguous antiferromagnetic coupling between the uranyl(V) ions at 6.5 K.

III.2) Synthesis of cation-cation assemblies of uranyl(V)

The results described above demonstrate that cation-cation interaction provides an effective strategy to build large homo or heterometallic assemblies with various geometries. The bridging oxo group between the actinide and another metal ion is strongly bound to the actinide centre, leading to an efficient pathway for intermetallic magnetic interaction. Notably, Sm(III)-U(V)[241,244] and Mn(II)-U(V)[180] magnetic exchanges have been reported, the latter displaying SMM behaviour.

In order to design SMMs based on uranyl(V), we decide to use the tunable CCI to synthesise heterometallic 5f-3d and 5f-4f assemblies with new geometries and good potential as single molecule magnets. We choose stable uranyl(V) complexes in which the uranyl(V) is coordinated to multidentate Schiff base ligands used in our group as builing blocks of CC assemblies.

III.2.1) Synthesis of polymeric chains of uranyl(V)

III.2.1.1) Choice of the ligand and of the metal

In the literature, some polymeric assemblies of uranyl(V) have been reported. The first example is the starting material $\{[UO_2(Py)_5][KI_2(Py)_2]\}_n$, where potassium cations bridge the uranyl oxo group via a CCI.[27,50] A few other examples of uranyl(V) polymeric structures, such as $[UO_2(salan\text{-}^tBu_2)(Py)K]_n$, $\{[UO_2(salophen\text{-}^tBu_2)(THF)]K(THF)_2\}_n$ and

$[UO_2(Mesaldien)K]_n$ has been reported.[52-54] In all the other reported polymers, the presence of the potassium cation also leads to polymeric structures. In order to investigate the possibility of assembling exchange-coupled uranium-based single chain magnets we have targeted the assembly of polymeric chains containing a paramagnetic transition metal bound to the uranyl(V) oxo group by cation-cation interaction. Mn(II) and Cd(II) were chosen. It was indeed previously observed that Mn(II) gave a stable wheel $U_{12}Mn_6$ with improved SMM properties.[180] The Cd(II) ion was also demonstrated to be a good choice to obtain an analogous heteropolymetallic complex structure due to its preference for octahedral geometry. This compound containing diamagnetic Cd was used as a model to analyse the magnetic exchange in the $U_{12}Mn_6$ wheel.

In order to prepare polymeric chains assembling uranyl(V) complexes and d-block ions through cation-cation interaction, the choice of supporting ligands and reaction conditions is extremely important. Ligands preventing UO_2^+---UO_2^+ interactions are ideal for the assembly of polymeric chains through UO_2^+---M^{n+} interactions. We therefore investigated the formation of polymeric chains using the pentadentate Mesaldien ligand that prevents UO_2^+---UO_2^+ interactions and is known to stabilise uranyl(V).[54] It is also worth investigating ligands that lead to stable UO_2^+---UO_2^+ interactions, such as the salen ligand, because it was found (in the $U_{12}Mn_6$ assembly) that in the presence of dicationic metals the UO_2^+---M^{n+} interaction is favoured over UO_2^+---UO_2^+ interactions.[180] A 1:1 stoichiometry of UO_2^+:M(II) (M: Mn, Cd) was used to favour the formation of polymeric chains over the assembly of discrete polymetallic units (the wheel $U_{12}Mn_6$ is formed at 1:0.5 stoichiometry UO_2^+:M(II)).

III.2.1.2) Polymer syntheses

III.2.1.2.1) Syntheses of $\{UO_2(salen)M\}_n$ (M: Mn, Cd)

The reaction of the monomeric uranyl(V) complex $[UO_2(salen)(Py)][Cp^*_2Co]$, (prepared in situ by reduction of $[U^{VI}O_2(salen)(Py)]$ with $[Cp^*_2Co]$[48,180] with one equivalent of $Mn(NO_3)_2$ in pyridine afforded the coordination polymer $\{[UO_2(salen)(Py)][Mn(Py)_4](NO_3)\}_n$, **10**-$\{UO_2(salen)Mn\}_n$, as a pink microcrystalline powder in 65% yield (Scheme III- 8). An analogous procedure with the diamagnetic cadmium salt produced $\{[UO_2(salen)(Py)][Cd(Py)_4](NO_3)\}_n$ **9**-$\{UO_2(salen)Cd\}_n$ in 65% yield (Scheme III- 8). The two complexes are stable in the solid state for months under argon atmosphere.

Similarly to the wheel $U_{12}Mn_6$, attempts to synthesise polymeric structures of uranyl(V) with iron, cobalt or nickel led to a complicated mixture of soluble products as

revealed by proton NMR spectroscopy and no further studies were conducted using these metals.

Scheme III- 8 Synthesis of $\{UO_2(salen)M\}_n$ (M: Mn, Cd)

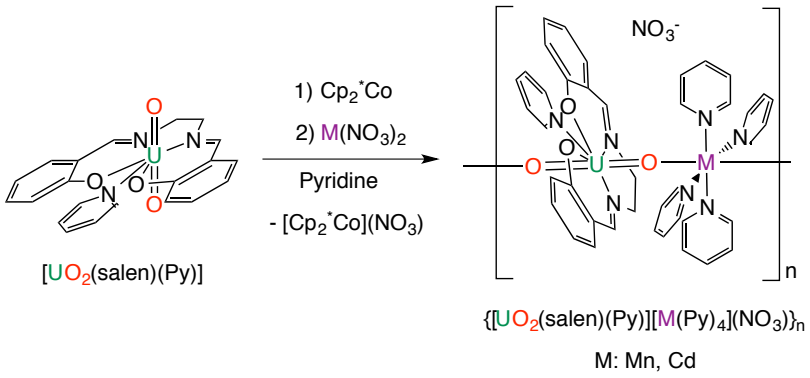

X-ray quality single crystals of **9**-$\{UO_2(salen)Cd\}_n$.2Py were obtained by a slow diffusion of pyridine solutions of the two reactants. Its structure revealed the presence of cationic dimetallic chains $\{[UO_2(salen)(Py)][Cd(Py)_4]\}_n^{n+}$ alternating with layers of NO_3^- anions (Figure III- 12 left). The asymmetric unit of **9**-$\{UO_2(salen)Cd\}_n$ contains three uranium and three cadmium ions that are crystallographically non-equivalent due to the non-linear arrangement of the UO_2^+ groups and Cd^{2+} ions along the chain (U-O-Cd angles range from 161.9(6)° to 175.2(6)°). Each oxygen of the uranyl(V) complexes $[UO_2(salen)(Py)]^-$ is connected through cation-cation interactions with a Cd^{2+} ion to form the cationic polymeric chain $\{[UO_2(salen)(Py)][Cd(Py)_4]\}_n^+$. The seven-coordinate uranium atom features a slightly distorted pentagonal bipyramidal coordination geometry. The two oxygen and the two nitrogen donor atoms of the salen ligand and a nitrogen of a coordinated pyridine are situated in the equatorial plane while the two uranyl oxygen are in axial positions. The cadmium ion has an octahedral coordination geometry and it is coordinated by four pyridine nitrogen atoms in the equatorial plane and by two uranyl(V) oxo groups in the apical positions. The U-O_{yl} distance (U-O_{yl} = 1.87(2) Å) is in the range of U-O_{yl} distances found for uranyl(V) oxo groups featuring cation-cation interactions.[27,48,53,58,231,242] No Cd-O_{yl}(U(V)) assemblies have ever been isolated but the mean Cd-O_{yl} distance of 2.28(2) Å is in the range of those found in a heterobimetallic U(VI)/Cd(II) carboxyphosphonates network with Cd^{2+} ions coordinated to the apical oxygen of the uranyl(VI) moieties (Cd-O_{yl} = 2.252(4) Å).[353]

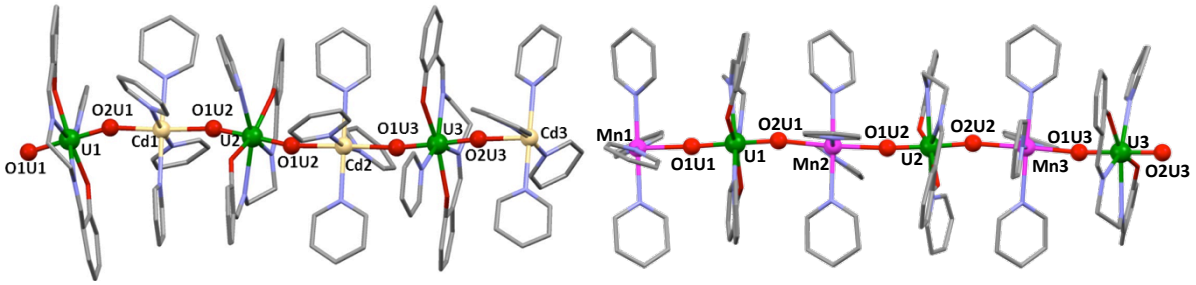

Figure III- 12 Molecular structures of the structure of **9**-$\{UO_2(salen)Cd\}_n$ (left) and **10**-$\{UO_2(salen)Mn\}_n$ (right) (ligands were represented in pipes, H and co-crystallised solvent molecules were omitted for clarity, C are represented in grey, O in red, Cd in cream, Mn in pink, N in light blue and U in green.)

X-ray analysis was also performed on single crystals of $\{[UO_2(salen)(Py)][Mn(Py)_4](NO_3)\}_n$. Although the quality of the crystals was poor, the connectivity was unambiguously determined and shows the presence of a coordination polymer isostructural with **9**-$\{UO_2(salen)Cd\}_n$ (Figure III- 12 right). To further prove the isostructurality of the two polymers, X-ray powder diffraction patterns were recorded for microcrystalline samples of both Cd and Mn polymers. These patterns are consistent with those calculated from the X-ray single crystal data and further support that both bulk samples contains isostructural homogeneous compounds (Figure III- 13).

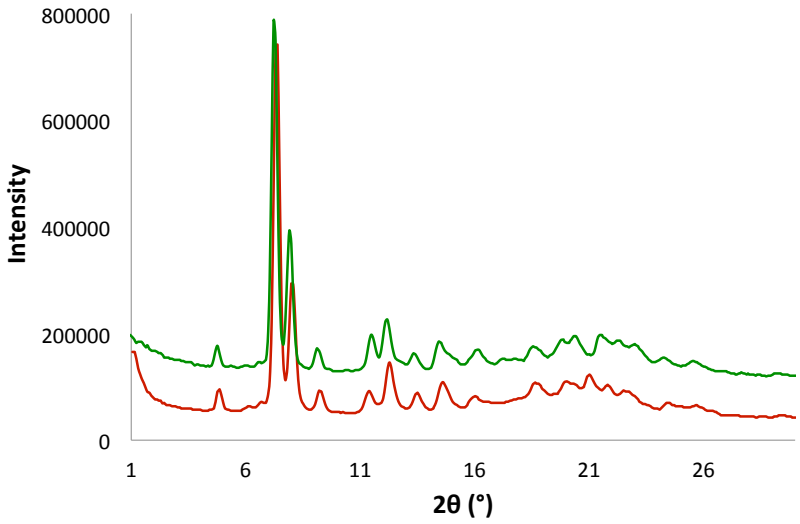

Figure III- 13 X-ray diffractogram of bulk compounds **9**-$\{UO_2(salen)Cd\}_n$.3.2(Py) (red line) and **10**-$\{UO_2(salen)Mn\}_n$.0.5(Py) (green line).

III.2.1.2.2) Synthesis of $\{UO_2(Mesaldien)Mn\}_n$

In order to investigate the influence of the ligand coordinated to the uranyl(V) unit on the geometry of the assembly, we used the pentadentate Schiff base ligand, reasoning that its use would lead to a different coordination geometry and different magnetic properties. The reduction of $[UO_2(Mesaldien)]$ with one equivalent of $[Cp^*_2Co]$ yielded the monomeric uranyl(V) complex $[UO_2(Mesaldien)][Cp^*_2Co]$, **11** (Scheme III- 9). In contrast to $[UO_2(salen)(Py)][Cp^*_2Co]$, which is unstable by addition of non-solvent, rendering its isolation difficult,[48] **11** crystallised easily by slow diffusion of hexane into a pyridine solution and it was isolated in high yield (90%). This complex is fully stable in the solid state and in acetonitrile or pyridine. The higher stability toward disproportionation of this Mesaldien complex compared to the salen analogue is consistent with previously reported spectroscopic and synthetic studies showing that pentadentate Schiff bases stabilise pentavalent uranyl by saturating the equatorial coordination sites,[45,46,54] thus preventing the formation of dimeric disproportionation intermediates.

Scheme III- 9 Synthesis of **12**-$\{UO_2(Mesaldien)Mn\}_n$

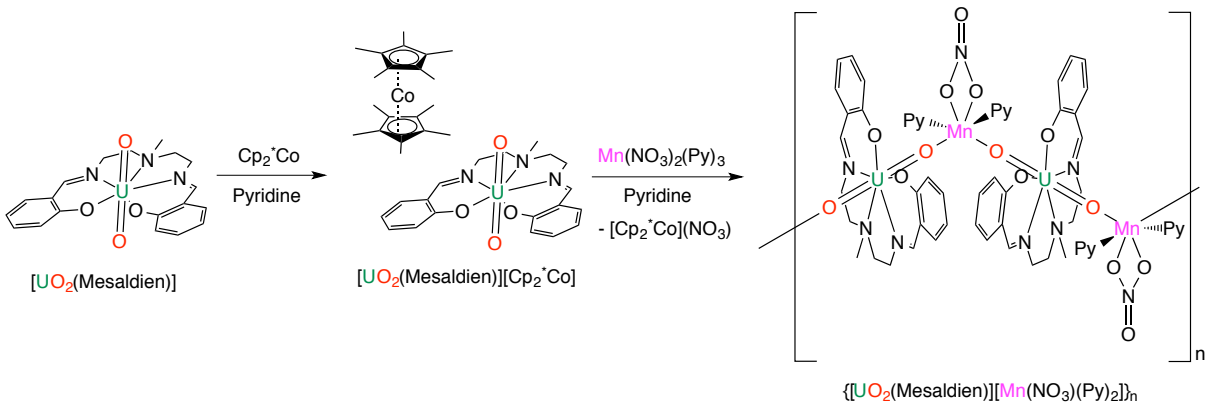

The reaction of $[UO_2(Mesaldien)][Cp^*_2Co]$, **11** with one equivalent of $Mn(NO_3)_2$ afforded the 1D polymer $\{[UO_2(Mesaldien)][Mn(NO_3)(Py)_2]\}_n$, **12**-$\{UO_2(Mesaldien)Mn\}_n$, as a pink microcrystalline powder in 66% yield (Scheme III- 9). X-ray quality single crystals of $\{[UO_2(Mesaldien)][Mn(NO_3)(Py)_2]\}.2Py$ were obtained from a dilute pyridine solution (5.4 mM) and the X-ray crystal structure is shown in Figure III- 14. Similar syntheses with $Cd(NO_3)_2$, $FeCl_2$ or $Co(NO_3)_2$ yielded amorphous solids and no single crystals suitable for X-ray diffraction were obtained. Studies employing these salts were then discontinued.

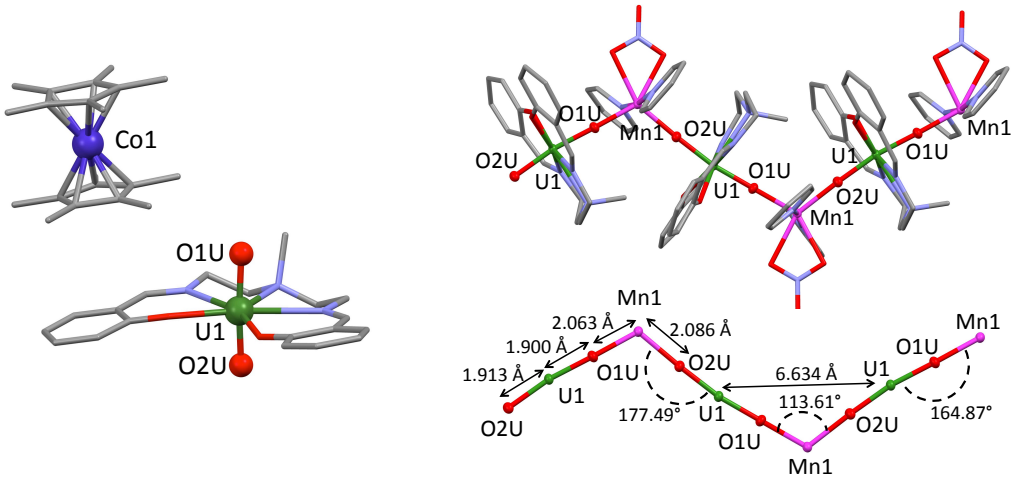

Figure III- 14 Molecular structures of $[UO_2(Mesaldien)][Cp^*_2Co]$, **11** (left) and $\{[UO_2(Mesaldien)][Mn(NO_3)(Py)_2]\}_n$ (right top) and enhanced view of the zig-zag core with associated distances and angles (right bottom) (ligands were represented in pipes, H and co-crystallised solvent molecules were omitted for clarity, C are represented in grey, O in red, N in light blue, Co in blue, Mn in pink and U in green.)

The structure of $[UO_2(Mesaldien)][Cp^*_2Co]$, **11** reveals an anionic mononuclear $[UO_2(Mesaldien)]^-$ uranyl(V) complex well separated from a cationic $[Cp^*_2Co]^+$ (Figure III- 14). In the structure of **12**-$\{UO_2(Mesaldien)Mn\}_n$ each oxo group of the uranyl(V), $[UO_2(Mesaldien)]^-$ units bridge two $[Mn(NO_3)(Py)_2]^+$ cations to yield a zig-zag one-dimensional chain through a linear cation-cation interaction. The asymmetric unit of **12**-$\{UO_2(Mesaldien)Mn\}_n$ contains only one uranium atom and one manganese atom, forming the neutral repeating entity $\{[UO_2(Mesaldien)][Mn(NO_3)(Py)_2]\}$. The U atom in $[UO_2(Mesaldien)]^-$ unit is seven coordinate, with a slightly distorted pentagonal bipyramidal coordination geometry formed by two trans oxo groups, three nitrogen atoms and two oxygen atoms from the Schiff base ligand. The manganese (II) ion is hexacoordinated by two oxygen atoms of two different uranyl(V), by two oxygen atoms of a bidentate nitrate ligand and by two nitrogen atoms of two pyridine molecules. The mean U=O bond distances in **11** (U1-O1U 1.846(6)Å and U1-O2U 1.847(6)Å) are shorter than in **12**-$\{UO_2(Mesaldien)Mn\}_n$ (U1-O1U 1.900(3) Å and U1-O2U 1.913(3)Å) due to the CCI, but lie in the range of the values typically observed for uranyl(V) complexes.[27,48,53,58,231,242] The mean Mn-O_{yl} (where O_{yl} is the uranyl oxygen) bond distance in **12**-$\{UO_2(Mesaldien)Mn\}_n$ is 2.075(3) Å, significantly shorter than that found in the $U_{12}Mn_6$ wheel-shaped uranyl(V) cluster (2.15(2) Å).[180] The U-O-Mn angles deviate slightly from linearity and range from 164.4(2)° to 177.2(2)°. A 2-fold screw axis along ¼, y, ¼ direction repeated the asymmetric unit resulting in a zig-zag geometry with a U-Mn-U angle of 113.62(3)°.

III.2.1.2.3) Structural comparison

The observed geometries of the two polymeric structures U-Mn are very different. In the case of $\{UO_2(salen)M\}_n$ (M: Mn, Cd), the uranyl(V) complexes of the tetradentate Schiff base salen and the M(II) units are pratically linear (mean U-M-U angle of 170.25(1.9)°) whereas the mean U-Mn-U angle in **12**-$\{UO_2(Mesaldien)Mn\}_n$ is 113.62(3)°, resulting in a zig-zag arrangement. The deviation from linearity in **12**-$\{UO_2(Mesaldien)Mn\}_n$ probably results from the presence of a bidentate nitrate ligand bonded to the manganese cation.

Due to the zig-zag geometry in **12-**$\{UO_2(Mesaldien)Mn\}_n$ the intra-chain separations between neighbouring U(V)-U(V) and M(II)-M(II) ions (respectively 6.6341(2) Å and of 7.897(1) Å) are much shorter than in the linear $\{UO_2(salen)M\}_n$ (mean distances M=Cd: U-U = 8.276(9) Å, Cd-Cd = 8.357(38) Å; M=Mn: U-U = 8.08(7) Å, Mn-Mn = 8.09(2) Å).

No evidence of significant inter-chain hydrogen bonding or pi-stacking interactions in the structure of the three polymers was observed. The chains are well separated with the shortest inter-chain U-U, U-M and M-M distances at 11.9682(12) Å and 10.9843(17) Å and 11.690(2) Å in **9**-$\{UO_2(salen)Cd\}_n$**,** 11.3838(9) Å, 10.9279(10) Å and 11.5126(10) Å in **10**-$\{UO_2(salen)Mn\}_n$ and 11.8812(4) Å, 10.4452(11) Å and 9.0183(19) Å in **12**-$\{UO_2(Mesaldien)Mn\}_n$, respectively. These features indicate the presence of magnetically isolated chains in the polymeric complexes[158,163] and magnetic properties were measured both under static and oscillating magnetic fields.

III.2.1.3) Magnetic properties

III.2.1.3.1) In static field

Temperature-dependent magnetic data between 2 and 300 K were performed on polycrystalline samples of $\{UO_2(salen)M\}_n$ (M: Mn, Cd) and **12**-$\{UO_2(Mesaldien)Mn\}_n$ at magnetic fields ranging from 0.01 to 5 T. The χT values at room temperature (Table III- 1) are coherent for these three molecules with one uranyl(V) alone or associated to one manganese(II) ion (S = 5/2, g = 2). The χT product of **9**-$\{UO_2(salen)Cd\}_n$ decreased rapidly below 25 K, which could be due to single-ion crystal field effects associated with U(V)[72] or possibly weak next-nearest neighbour antiferromagnetic exchange between uranium centres (Figure III- 15 left). For the uranyl(V)-Mn(II) polymers, the χT product is constant from 300 K to 80 K before reaching a field-dependent maximum indicating probable ferromagnetic interactions. After this maximum, the product drops rapidly at very low temperatures,

probably due to saturation effects, magnetic anisotropy and/or inter-chain antiferromagnetic interactions (Figure III- 15 right).

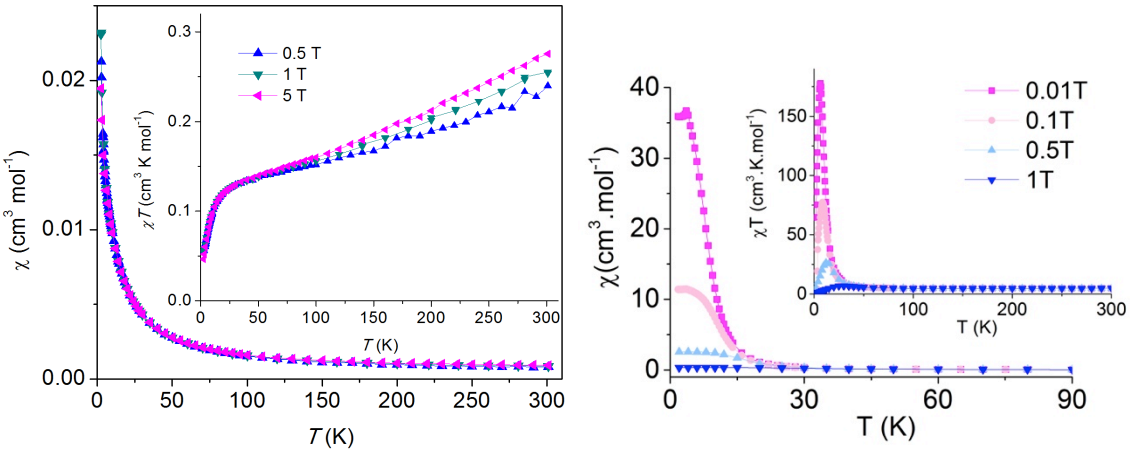

Figure III- 15 Temperature dependence of χ for **9**-{UO_2(salen)Cd}$_n$ (left) and **12**-{UO_2(Mesaldien)Mn}$_n$ (right) measured at three different fields between 0.01 and 5 T. Inset: Temperature dependence of χT for the same fields.

Table III- 1 χT values (in cm^3.K.mol^{-1}) at room temperature and at the maximum associated to the field (in T). Parameters obtained for the scaling of χT curves (Δ/k_B in K and C in cm^3.K.mol^{-1})

	9-{UO_2(salen)Cd}$_n$	**10-{UO_2(salen)Mn}$_n$**	**12-{UO_2(Mesaldien)Mn}$_n$**
$\chi T_{(300\ K)}$	0.3	4.3	4.8
$\mu_{eff(300\ K)}$	1.55	5.87	6.20
χT_{max} (H)	-	56.8 (0.01) / 43.1 (0.1)	177.29 (0.01) / 77.29 (0.1)
Δ/k_B / C_{eff}	-	45.5 / 1.98	42.8 / 2.28
Δ_1/k_B / C_1		45.5 / 1.98	44.0 / 2.13
Δ_2/k_B / C_2	-	-90.2± 9.4 / 2.73	-81.8 ± 5.9 / 3.05

The occurrence of a linear regime characteristic of Ising 1D systems is highlighted by the scaling of the χT data of **10**-{UO_2(salen)Mn}$_n$ (Figure III- 16) and **12**-{UO_2(Mesaldien)Mn}$_n$.[158,354] In both cases, the ln(χT) versus 1/T plot increases linearly between 45 and 16 K. The equation $\chi T = C_{eff} \exp(\Delta/k_B T)$ was used to fit the experimental data in the linear regime. This equation describes a ferromagnetically coupled infinite chain. Another fit between 16 and 300 K of the χT curves can be performed using the equation $\chi T = C_1 \exp(\Delta_1/k_B T) + C_2 \exp(\Delta_2/k_B T)$, where a second negative exponential that vanishes at 0 K is added to take into account the high-temperature crystal field effect or antiferromagnetic contribution.[355] Energy gaps and pre-exponential factors are reported in the Table III- 1. As expected, the high-temperature extrapolated Curie constants, $C = C_1 + C_2 = 4.71$ cm^3.K.mol^{-1} for **10**-{UO_2(salen)Mn}$_n$ and $C = C_1 + C_2 = 5.18$ cm^3.K.mol^{-1} for **12**-{UO_2(Mesaldien)Mn}$_n$, are close to the expected value for one Mn(II) ion and one U(V) ion.

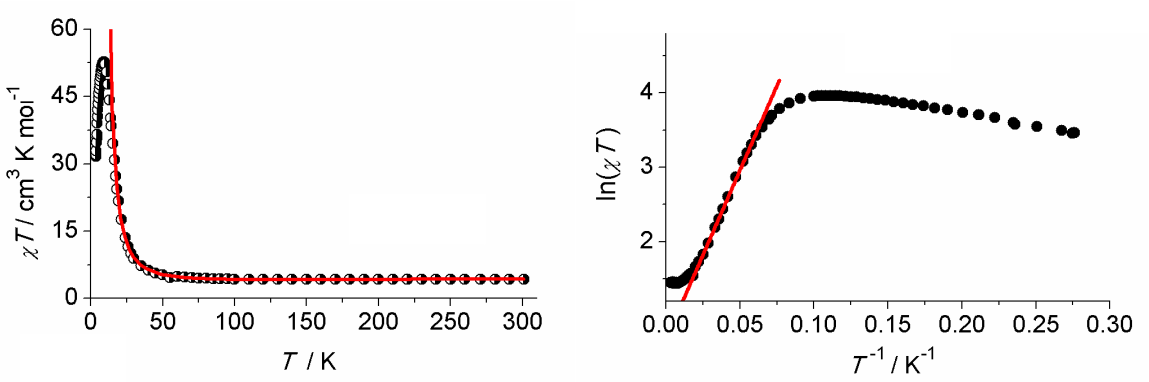

Figure III- 16 Plots of (top) χT versus T and (bottom) ln(χT) versus 1/T for a polycrystalline sample of **10**-$\{UO_2(salen)Mn\}_n$ measured at 0.05 T applied field with fit represented as red line.

Divergences between zero-field cooled and field cooled magnetisations as a function of temperature are observed below 6 and 3.5 K for **10**-$\{UO_2(salen)Mn\}_n$ and **12**-$\{UO_2(Mesaldien)Mn\}_n$, respectively. Under zero field, a remnant magnetisation (REM) of 1.7 μ_B is preserved for **10**-$\{UO_2(salen)Mn\}_n$ before vanishing after 5.8 K, whereas for **12**-$\{UO_2(Mesaldien)Mn\}_n$ the remnant magnetisation of 2.2 μ_B is conserved until 3 K corresponding to the blocking temperature of the material. The retention of the magnetisation is typical of a single chain magnet below its blocking temperature T_B. To further characterise these compounds, field-dependent (-7T +7T) magnetisation measurements were then performed at temperatures between 2 and 5 K. For both polymers, these measurements show an open hysteresis cycle below 3 K. A significant coercive field of 3.4 T is obtained at 2 K for **10**-$\{UO_2(salen)Mn\}_n$ compared to 1.75 T at 2 K for **12**-$\{UO_2(Mesaldien)Mn\}_n$. The coercive field in both cases decreases with increasing temperature (Figure III- 17). The presence of a magnetic ground state and magnetic bi-stability is consequently confirmed with these measurements.

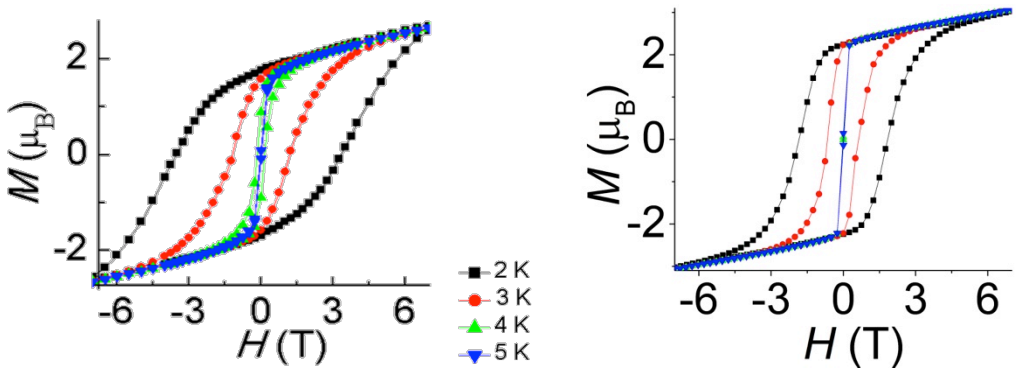

Figure III- 17 Hysteresis loops of **10**-$\{UO_2(salen)Mn\}_n$ (left) and **12**-$\{UO_2(Mesaldien)Mn\}_n$ (right) recorded at four different temperatures with a field sweep rate of 0.0061 $T.s^{-1}$.

III.2.1.3.2) In oscillating field

III.2.1.3.2.1) $\{UO_2(salen)Cd\}_n$

Zero-field ac susceptibility measurements on **9**-$\{UO_2(salen)Cd\}_n$ did not lead to a frequency dependent peak of the magnetic susceptibility. However, application of a permanent dc field of 0.1 T reveals frequency dependent components of the ac susceptibility in both the in-phase (χ') and out-of-phase (χ'') (Figure III- 18). The necessity of this small dc field can be useful if quantum tunnelling is present at zero-field, an observation often assessed in uranium single molecule magnets.[72,168] ac susceptibility measurements between 1.8 and 3 K were carried out at several frequencies between 1 and 1399 Hz with a 1.55 G ac field for **9**-$\{UO_2(salen)Cd\}_n$ under 0.1 T applied field.

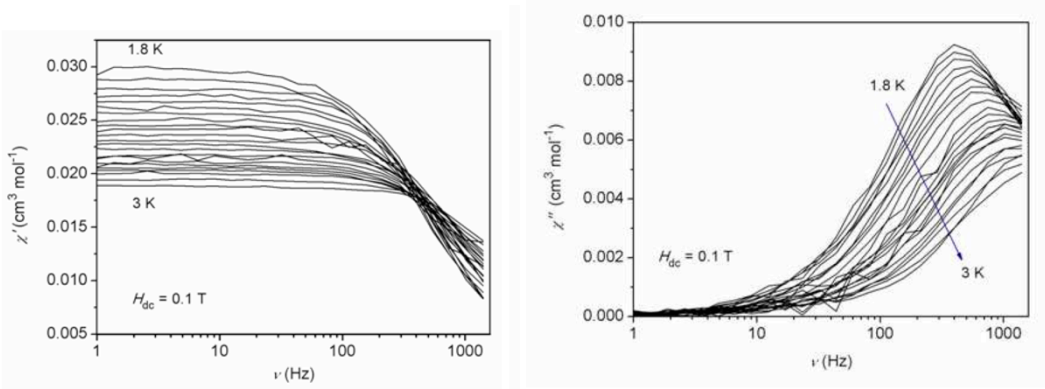

Figure III- 18 Frequency dependence of the (left) real (χ') and (right) imaginary (χ'') ac susceptibility for **9**-$\{UO_2(salen)Cd\}_n$ measured under 0.1 T dc field and 1.55 G ac field.

A generalised Debye model for one relaxation process was used to fit the frequency dependence of the in-phase (χ') and out-of-phase (χ'') components of the ac susceptibility.[356] The α parameter ranged between 0.12 and 0.16, revealing a narrow distribution of relaxation times. The relaxation times obtained from the ac experiments were fitted to the Arrhenius equation $\tau = \tau_0 \exp(\Delta E/k_B T)$, where τ is the relaxation time, ΔE is the energy barrier for the relaxation of the magnetisation and τ_0 is the pre-exponential factor. ΔE was established to be 7.5 ± 0.1 K and $\tau_0 = 7.3 \times 10^{-6}$ s. This result shows the anisotropy of pure U(V) units.

III.2.1.3.2.2) $\{UO_2(salen)Mn\}_n$ and $\{UO_2(Mesaldien)Mn\}_n$

In contrast to **9**-$\{UO_2(salen)Cd\}_n$, zero-field ac susceptibility measurements undoubtedly yielded clear χ'(T,f) and χ''(T,f) maxima (Figure III- 19). **10**-$\{UO_2(salen)Mn\}_n$ was measured between 2 and 15 K at several frequencies between 10 and 9887 Hz with a 10 G

ac field and between 0.1 and 1399 Hz with a 1.55 G ac field. **12**-{UO_2(Mesaldien)Mn}$_n$ was measured between 3.6 and 7.5 K at several frequencies between 0.1 and 1399 Hz with a 1.55 G ac field. In these temperature ranges, both the in-phase (χ') and out-of-phase (χ'') components of the ac susceptibility are strongly frequency dependent, precluding any tridimensional ordering. The relative variation of the temperature of the χ'' peak with respect to the frequency is measured by a parameter $\phi = (\Delta T_{max}/T_{max})/\Delta(\log f)$, the values of which are 0.13 for **10**-**10**-{UO_2(salen)Mn}$_n$ and 0.10 for **12**-{UO_2(Mesaldien)Mn}$_n$. They are in the range of normal superparamagnets, excluding the possible occurrence of a spin glass state.[357]

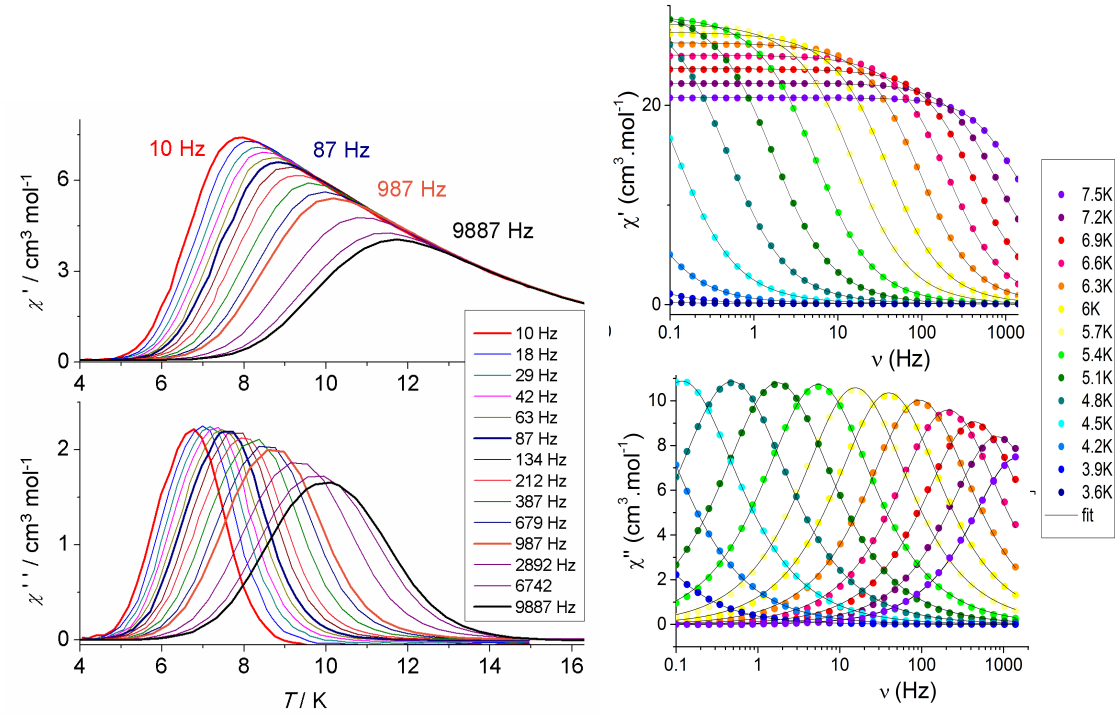

Figure III- 19 Temperature dependence of the (top) real (χ') and (bottom) imaginary (χ'') ac. susceptibility for **10**-{UO_2(salen)Mn}$_n$ measured at zero-dc field and 10 G ac field (left), and frequency dependence for **12**-{UO_2(Mesaldien)Mn}$_n$ measured at zero-dc field and 1.55 G ac field (right).

Both frequency dependence of the in-phase (χ') and out-of-phase (χ'') components of the ac susceptibility of **10**-{UO_2(salen)Mn}$_n$ and **12**-{UO_2(Mesaldien)Mn}$_n$ were fitted to a generalised Debye[356] model for one relaxation process, giving the following ranges of the α parameter: 0.20-0.43 and 0.11-0.20, respectively. These results revealed a narrow distribution of relaxation times. Below 10 K for **10**-{UO_2(salen)Mn}$_n$ and 7.2 K for **12**-{UO_2(Mesaldien)Mn}$_n$, respectively, semi-circular Cole-Cole plots (χ'' vs. χ') are obtained, confirming that only one relaxation process occurs. As for **9**-{UO_2(salen)Cd}$_n$, the magnetisation relaxation times obtained from the ac experiments as a function of temperature and frequency were fitted to the Arrhenius equation $\tau = \tau_0 \exp(\Delta E/k_B T)$ (Figure III- 20). The fit gives ΔE = 134.0 ± 0.8 K and τ_0 = 3.1 x 10^{-11} s for **10**-{UO_2(salen)Mn}$_n$. A

crossing in the Arrhenius plot occurs for **12**-{UO_2(Mesaldien)Mn}$_n$, giving two energy barriers: ΔE_1 = 122.1 ± 1.4 K and ΔE_2 = 107.0 ± 0.7 K respectively associated to $\tau_0^{(1)}$ = 6.2 x 10^{-12} s and $\tau_0^{(2)}$ = 7.4 x 10^{-11} s. Two activated regions have been already reported in other SCMs and may be due to finite-size effects.[156-158,358]

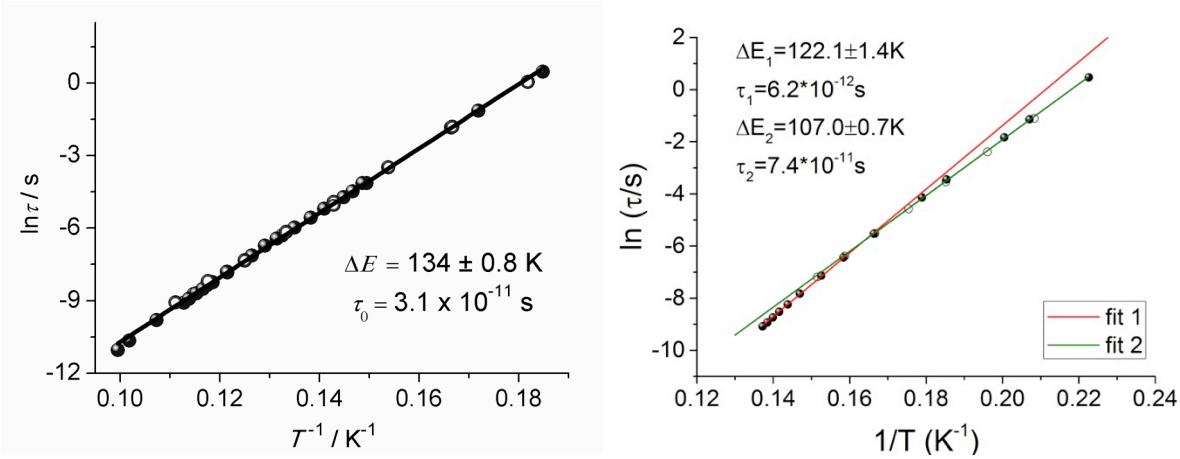

Figure III- 20 Arrhenius plot displaying T-dependence of the relaxation times for **10**-{UO_2(salen)Mn}$_n$ (left) and **12**-{UO_2(Mesaldien)Mn}$_n$ (right) (open circles : from frequency-dependent data; dots : from temperature-dependent data).

III.2.1.3.2.3) Discussion

Characteristic magnetic properties of the three studied chains are reported in Table III- 2.

Table III- 2 Blocking temperature, coercitive field and energy barriers for the three chains

	T_B (K)	H_{coer} (T) at 2 K ($0.0061T.s^{-1}$)	ΔE (K)
9-{UO_2(salen)Cd}$_n$	-	-	7.5 ± 0.1 (0.1T)
10-{UO_2(salen)Mn}$_n$	5.8	3.2	134.0 ± 0.8
12-{UO_2(Mesaldien)Mn}$_n$	3.5	1.75	122.1 ± 1.4 107.0 ± 0.7

Only a few rare examples of SMMa based on homometallic U(V) complexes have been reported so far. The only example of a monometallic U(V) terminal mono-oxo complex from Liddle has an energy barrier of 21 K (1kG),[72] which is clearly higher than the one found in **9**-{UO_2(salen)Cd}$_n$. However, even if the uranium ion has the same oxidation state in both systems, the coordination geometry is different and could induce strong changes.

The increase between the uranyl(V)-Cd(II) and uranyl(V)-Mn(II) polymers is unprecedented. From the value of 7.5 K measured for the Cd polymer, the energy barrier increases almost twenty times for the Mn(II) polymer. This increase cannot arise from the presence of the Mn(II) alone, because Mn(II) is isotropic and no examples of Mn(II) SMM or SIM based on the Mn(II) ion alone have ever been reported. This clearly shows that the U(V)-Mn(II) magnetic coupling through the cation-cation interaction is rather efficient and that magnetic communication occurs between the two metallic centres. The high relaxation barriers are most likely the result of the ferromagnetic intra-chain coupling associated to the large anisotropy of the uranyl group.[53]

In the two U-Mn chains, the effect of the geometry and of the ligand coordinated to the uranyl(V) onto the magnetic properties is emphasised by the observed differences in energy barrier, blocking temperature and coercive field. The ΔE barriers obtained from the ac data are larger than the energy gaps extracted from dc susceptibility measurements. This situation is often observed in SCMs of highly anisotropic repeating units.[158,358] The relaxation barrier experienced by individual magnetic units and magnetic correlations governed the dynamics of the magnetisation.[354] The polymeric chains **10**-$\{UO_2(salen)Mn\}_n$ and **12**-$\{UO_2(Mesaldien)Mn\}_n$ are the two first examples of actinide based SCMs. Furthermore, they demonstrate higher energy barriers and blocking temperatures than other SCMs based on f-elements.[156-158,163,164,355,359,360]

III.2.2) Synthesis of discrete assemblies based on uranyl(V)

III.2.2.1) Uranyl(V) and d-block metals

III.2.2.1.1) Control of the geometry

It is shown in the previous chapters that the use of a 1:1 uranyl(V)(salen):Mn(II) ratio leads to the formation of polymeric assemblies whereas the wheel U_6Mn_{12} is formed with the 1:0.5 uranyl(V)(salen):Mn(II) ratio.[180] However, these studies revealed the difficulty of changing the nature of the transition metal, as only manganese(II) and cadmium(II) yielded characterised CC complexes and the absence of ligand scrambling. The highly sophisticated character of the wheel assembly prevents the interpretation of magnetic data and renders the rational design of analogous structures containing different d-block ions difficult.

In order to rationally prepare simpler systems with lower nuclearity and to enlarge the number of $5f^1$-3d SMMs to other transition metals, we have developed a new synthetic strategy. We have used a chelating ligand to block the coordination sphere of the d-block

metallic centre to prevent the formation of coordination polymers. We chose a neutral tripodal tetradentate ligand TPA (TPA = tris(2-pyridylmethyl)amine) to coordinate the d-block transition metals M(II) (M: Cr, Mn, Fe, Co, Ni, Cu, Zn, Cd). Furthermore we chose the Mesaldien ligand, as the organic ligand for the uranyl(V). This ligand only allows linear UO_2^+---M^{n+} interactions due to the saturation of the equatorial plane of the uranyl(V). This strategy has allowed for the synthesis of a series of isostructural trinuclear $5f^1$-3d complexes, the study of their stability and of their magnetic properties. In contrast to the insoluble $U_{12}Mn_2$ wheel and the polymeric structures, these assemblies are soluble in pyridine. To avoid the presence of the $[Cp_2^*Co]^+$ complex and difficult separation by crystallisation, we used a salt exchange procedure starting from $[UO_2(Mesaldien)K]_n$[54] rather than the reduction of $[UO_2(Mesaldien)]$ with Cp_2^*Co. The interaction of the uranyl(V) towards M^{2+} is more favourable than UO_2^+---K^+ and leads selectively to heterometallic UO_2^+---M^{2+} formation.

III.2.2.1.2) TPA as chelating ligand

III.2.2.1.2.1) Syntheses of UMn_2-TPA-I, UMn_2-TPA-Cl, UFe_2-TPA and UCd_2-TPA

The reaction of two equivalents of $[M(TPA)I_2]$ (M = Mn, Cd) with the uranyl(V) complex $[UO_2(Mesaldien)K]_n$[54] in pyridine gave the trimetallic compounds $[\{[M(TPA)I][UO_2(Mesaldien)][M(TPA)I]\}I]$ (M: Mn, Cd), **13**-UMn_2-TPA-I and **14**-UCd_2-TPA in 60-65% yield (Scheme III- 10).

Scheme III- 10 Syntheses of **13**-UMn_2-TPA-I, **14**-UCd_2-TPA, **15**-UMn_2-TPA-Cl and **16**-UFe_2-TPA

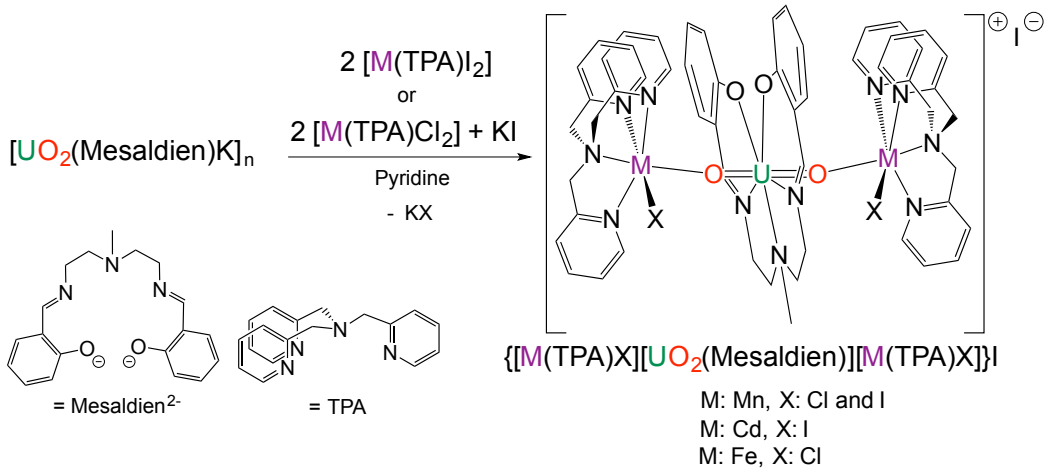

The analogous reaction carried out with $[Fe(TPA)I_2]$ always yielded intractable oils. However, the use of two equivalents of the chloride complex $[M(TPA)Cl_2]$ (M: Mn, Fe) in the

presence of KI afforded the trimetallic compounds [{[M(TPA)Cl][UO_2(Mesaldien)][M(TPA)Cl]}I] (M: Mn, Fe), **15**-UMn_2-TPA-Cl and **16**-UFe_2-TPA in yields of 80% and 43%, respectively. The presence of the iodide counter-ion is essential to obtain X-ray quality crystals of the **16**-UFe_2-TPA complex. X-ray quality crystals of all of these trimetallic species were obtained by slow diffusion of hexane into a pyridine solution. The solid-state structure of UM_2-TPA-X (M:Mn, Cd, X:I; M: Mn, Fe, X:Cl) contains two $[M(TPA)X]^+$ cations linked to the two oxo groups of the $[UO_2(Mesaldien)]^-$ anion through a linear cation-cation interaction (Figure III- 21).

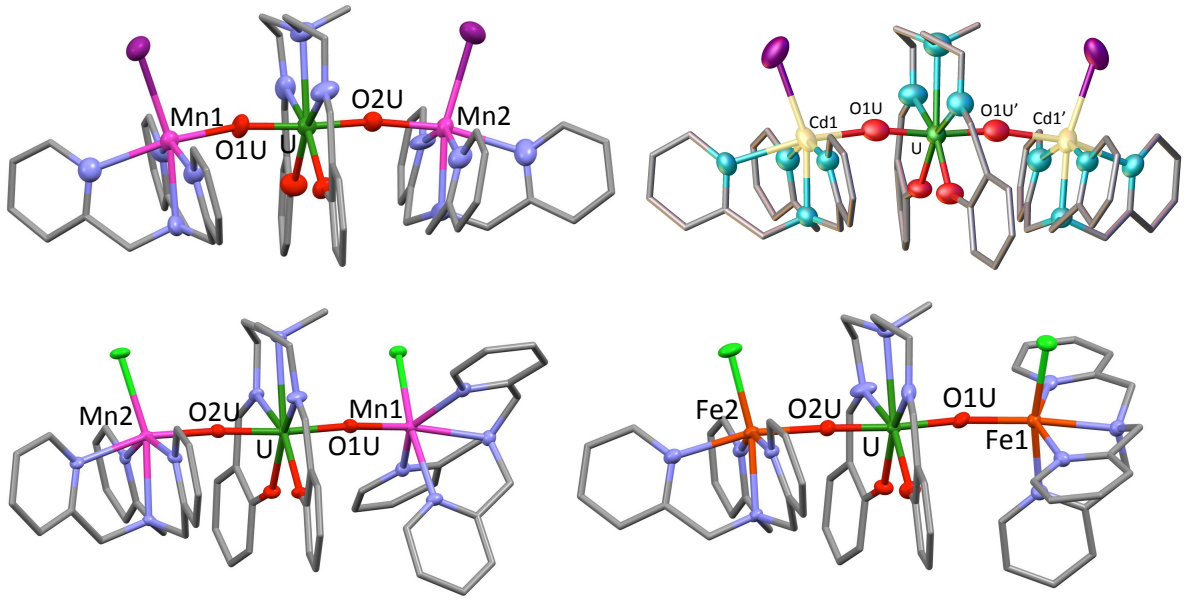

Figure III- 21 Crystallographic structure of **13**-UMn_2-TPA-I (top left), **14**-UCd_2-TPA (top right), **15**-UMn_2-TPA-Cl (bottom left) and **16**-UFe_2-TPA (bottom right) with hydrogen atoms, disorder and co-crystallised solvent molecules omitted for clarity (ellipsoids probability : 30%; ligands represented in capped sticks). Atoms: C (grey), O (red), Mn (pink), Fe (orange), Cd (light yellow), N (light blue), I (purple), Cl (light green) and U (green).

The seven-coordinate uranium atom in $[UO_2(Mesaldien)]^-$ has a slightly distorted pentagonal bipyramid coordination geometry, defined by the two oxygen and three nitrogen atoms of the $Mesaldien^{2-}$ ligand in the equatorial plane and the two uranyl oxygen atoms in the axial positions. The transition metals in $[M(TPA)X]^+$ are hexacoordinate, with a distorted octahedral coordination geometry formed by the four nitrogen atoms of the chelating TPA ligand, one oxygen atom from the uranyl(V) group, and a coordinated halogen anion.

III.2.2.1.2.2) Syntheses of UCo-TPA and UNi_2-TPA

In order to expand the range of $5f^1$-3d trinuclear complexes, the reactions of $[UO_2(Mesaldien)K]_n$ with two equivalents of Cr(II), Co(II), Ni(II) and Cu(II) TPA complexes were performed.

Interestingly, the reaction of $[UO_2(Mesaldien)K]_n$ with two equivalents of [Co(TPA)I]I did not yield a trimetallic entity, but instead a mixture of a bimetallic species [{[Co(TPA)][UO_2(Mesaldien)]}I] and of the [{[Co(TPA)I]I complex were isolated. The [{[Co(TPA)][UO_2(Mesaldien)]}I], **17**-UCo-TPA compex was obtained analytically pure and in a good yield (73%) from the reaction of $[UO_2(Mesaldien)K]_n$ and [Co(TPA)I]I in a 1:1 ratio in pyridine (Scheme III- 11). X-ray quality crystals of **17**-UCo-TPA**.**1Py were obtained by slow diffusion of hexane in a pyridine solution of **17**-UCo-TPA, and its crystal structure was determined by single crystal X-ray diffraction (Figure III- 22 left).

Scheme III- 11 Syntheses of **17**-UCo-TPA and **18**-UNi_2-TPA

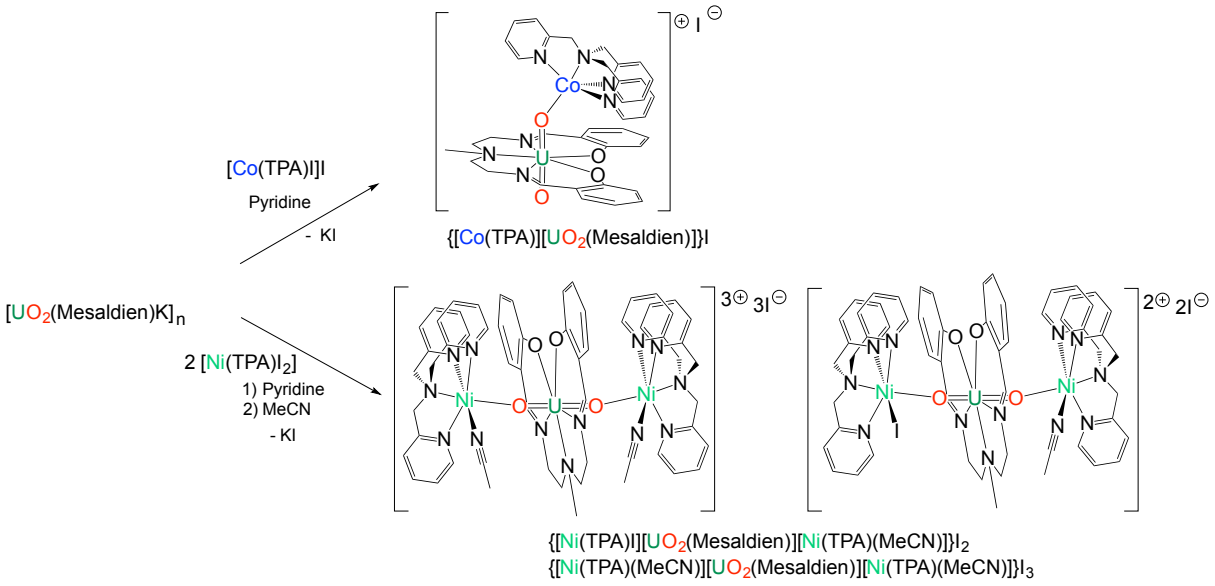

The addition of two equivalents of $[Ni(TPA)I_2]$ to the uranyl(V) complex $[UO_2(Mesaldien)K]_n$[54] in pyridine yielded a purple solution. Slow diffusion of hexane or DIPE into a pyridine solution of this mixture gave intractable oils. However, when pyridine was replaced by acetonitrile, X-ray diffraction crystals grew from slow diffusion of DIPE into the solution. The asymmetric unit contains two different complexes: [{[Ni(TPA)(MeCN)][UO_2(Mesaldien)] [Ni(TPA)(MeCN)]}I_2] and [{[Ni(TPA)(MeCN)][UO_2(Mesaldien)][Ni(TPA)(MeCN)]}I_3] (**18**-UNi_2-TPA) (Scheme III- 11 and Figure III- 22 right). These complexes were synthesised in 94% yield.

The structure of **17**-UCo-TPA (Figure III- 22 left) consists of one $[Co(TPA)]^{2+}$ cation bound to one oxo group of the $[UO_2(Mesaldien)]^-$ anion in a linear cation-cation interaction. In this bimetallic species, only one oxo group of the uranyl(V) is engaged in a linear cation-cation interaction. Co(II) is pentacoordinate, with a slightly distorted trigonal bipyramid

geometry defined by the four nitrogen atoms of the TPA ligand and one oxygen atom from the uranyl(V) group. In **18**-UNi_2-TPA (Figure III- 22 right), two six-coordinate Ni(II) complexes are linked to uranyl(V) oxo groups to form trimetallic assemblies. In **17**-UCo-TPA and **18**-UNi_2-TPA, the uranium atom is heptacoordinate with a slightly distorted pentagonal bipyramidal coordination geometry formed by the two uranyl oxygen atoms and five donor atoms of the Mesaldien^{2-} ligand in the equatorial plane.

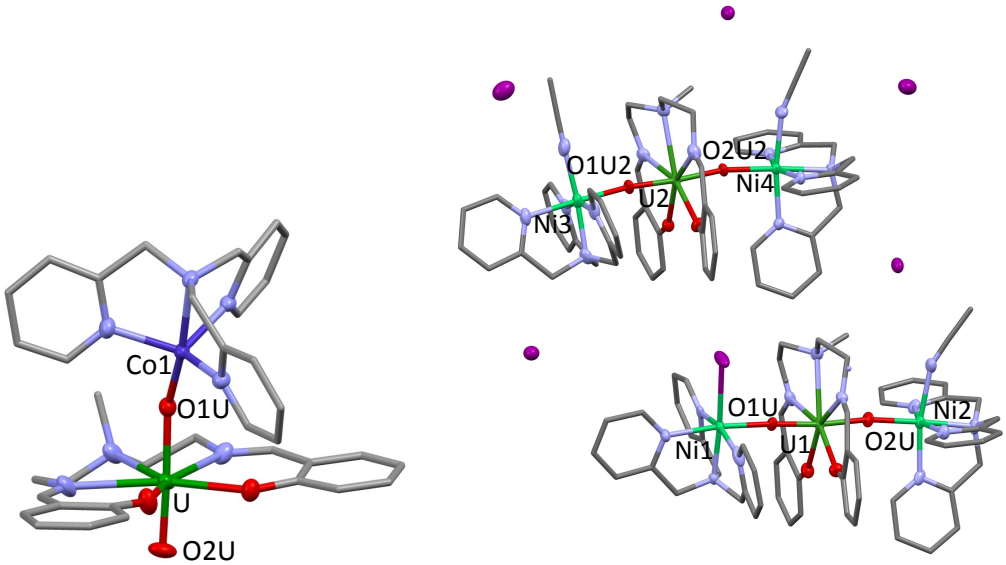

Figure III- 22 Solid-state molecular structure (left) of **17**-UCo-TPA (iodide counter-ion omitted) and the two complexes present in the asymmetric unit of **18**-UNi_2-TPA (right) (30% probability ellipsoids). (Ligands were represented in capped sticks, hydrogen, disorder and co-crystallised solvent molecules were omitted for clarity) Colour code: uranium (green), cobalt (blue), nickel (light green), oxygen (red), nitrogen (light blue), iodide (purple) and carbon (grey).

The difference between the two complexes of **18**-UNi_2-TPA (Figure III- 22 right) arises from a different coordination environment for the nickel ions. The first trimetallic complex contains two $[Ni(TPA)(MeCN)]^{2+}$ cations bound through cation-cation interactions to the two oxo groups of the uranyl while the second complex consists of one $[Ni(TPA)(MeCN)]^{2+}$ cation and one $[Ni(TPA)I]^{+}$ cation bonded to the oxo of the uranyl(V) Mesaldien complex forming an asymmetric assembly. It's interesting to note that **17**-UCo-TPA and **18**-UNi_2-TPA are the first examples of uranyl(V)-Co(II)/Ni(II) interactions probing the stability of uranyl(V) with these transition metals.

Compared to Co(II) and Ni(II), the reaction of $[UO_2(Mesaldien)K]_n$ with two equivalents of $[Cu(TPA)Cl_2]$ or $[Cr(TPA)Cl_2]$ did not lead to the stabilisation of a polymetallic entities. With Cu(II), the uranyl(V) complex was oxidised into uranyl(VI), as revealed by the characteristic proton NMR spectrum of $[UO_2(Mesaldien)]$.[54] The redox potential of the $U^{VI}O_2^{2+}/U^{V}O_2^{+}$ couple in pyridine, where the uranyl unit is coordinated to Schiff base ligands, ranges between -1.51

and -1.81 V vs the Fc^+/Fc reference,[53,231] while the reduction potential of Cu(II) TPA complexes range between -0.38 and -0.67 V vs the Fc^+/Fc couple.[361,362] Based on these differences in redox potentials, it is understandable why the uranyl(V) Mesaldien complex is oxidised by the Cu(II) TPA complex.

In the case of the reaction of $[UO_2(Mesaldien)K]_n$ with two equivalents of $[Cr(TPA)Cl_2]$, the proton NMR spectrum of the reaction mixture evolves over time and after two days, sharp shifted peaks characteristic of a uranium(IV) complex were observed (Figure III- 23). No signals corresponding to the uranyl(VI) $[UO_2(Mesaldien)]$ complex were observed, suggesting that $[UO_2(Mesaldien)K]_n$ is reduced into uranium(IV) in presence of Cr(II) and does not disproportionate. The reduction of uranyl(V) into uranium(IV) is not rapid and implies the breaking of the uranyl unit. The group of Hayton reported that the presence of Lewis acids or sylilated reagents facilitates the reduction in weakening the $U\text{-}O_{yl}$ bond. In these systems, the redox potential of the U(V)/U(IV) couple ranges from -0.72 to -1.21 V vs the Fc^+/Fc reference.[363,364] The redox potential of the Cr(III)/Cr(II) couple, in which the metallic centre is coordinated to a TPA ligand, ranges between -1.51 and -1.75 V vs the Fc^+/Fc.[365] The reduction of $[UO_2(Mesaldien)K]_n$ may occur with the reducing Cr(II) ion, however no crystal structure has been obtained from the reaction mixture to support this hypothesis.

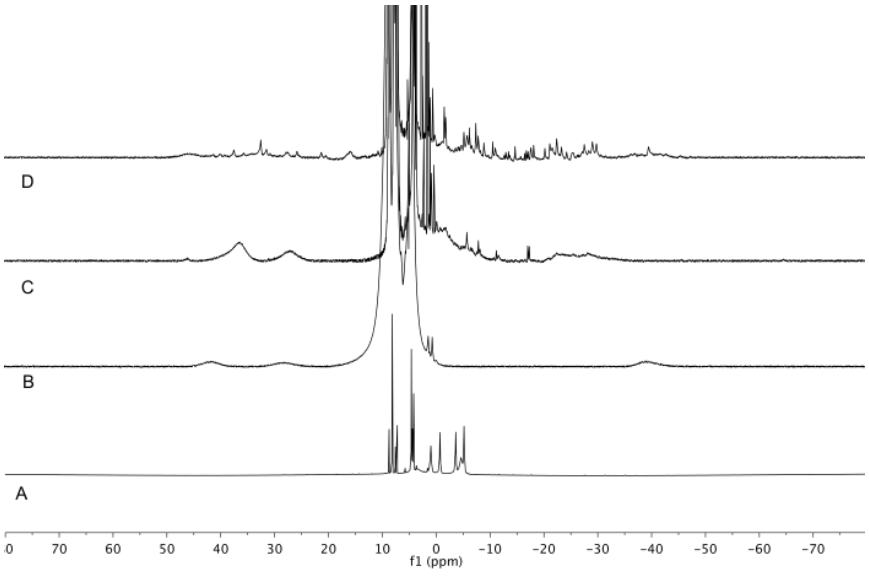

Figure III- 23 ^1H NMR spectrum (400M Hz, Py-d_5, 298 K) of (A) $[UO_2(Mesaldien)K]_n$, (B) $[Cr(TPA)Cl_2]$, (C) the reaction mixture 1:2 $[UO_2(Mesaldien)K]_n$:$[Cr(TPA)Cl_2]$ 10 minutes after the addition of $[Cr(TPA)Cl_2]$ to $[UO_2(Mesaldien)K]_n$ and (D) of the reaction mixture 1:2 $[UO_2(Mesaldien)K]_n$:$[Cr(TPA)Cl_2]$ after 2 days.

III.2.2.1.3) BPPA as chelating ligand: Syntheses of UM_2-BPPA (M: Mn, Fe, Co, Ni)

The adopted synthetic procedure allowed for the rational synthesis of Mn(II), Fe(II) and Ni(II) heterodimetallic trinuclear assemblies. In these complexes, the coordination sphere of the transition metal is not saturated by the TPA ligand and a sixth coordination site is occupied either by a halogen anion or by a coordinating solvent such as acetonitrile. In the case of Co(II), a dinuclear complex is formed, probably due to the lower affinity of the $[Co(TPA)]^{2+}$ complex for halide binding, which results in a higher residual charge of the $[Co(TPA)]^{2+}$ complex compared to $[M(TPA)X]^{+}$ or $[M(TPA)(MeCN)]^{2+}$. Such higher charge results in only one complex being bound to the uranyl(V) oxo group. In order to promote the formation of a trimetallic assembly and also to verify why in the case of the cobalt only a dimer was formed, we resorted to the use of monoanionic TPA analogue, the BPPAH ((bis(2-picolyl)(2-hydroxybenzyl)amine). In BPPAH, a pyridyl arm of the TPA is replaced with a phenolate arm, leading to a monoanionic tetradentate ligand after deprotonation.

The reaction of $[UO_2(Mesaldien)K]_n$ with two equivalents of [M(BPPA)I] (M = Mn, Fe, Co, Ni) in pyridine yielded [{[M(BPPA)(Py)][UO_2(Mesaldien)][M(BPPA)]}I] (M = Fe, Co), **20**-UFe_2-BPPA and **21**-UCo_2-BPPA, and [{[M(BPPA)(Py)][UO_2(Mesaldien)][M(BPPA)(Py)]}I] (M: Mn, Ni), **19**-UMn_2-BPPA and **22**-UNi_2-BPPA in high yields (70-92%) (Scheme III- 12).

Scheme III- 12 Syntheses of the trimetallic complexes **20**-UFe_2-BPPA, **21**-UCo_2-BPPA and **22**-UNi_2-BPPA.

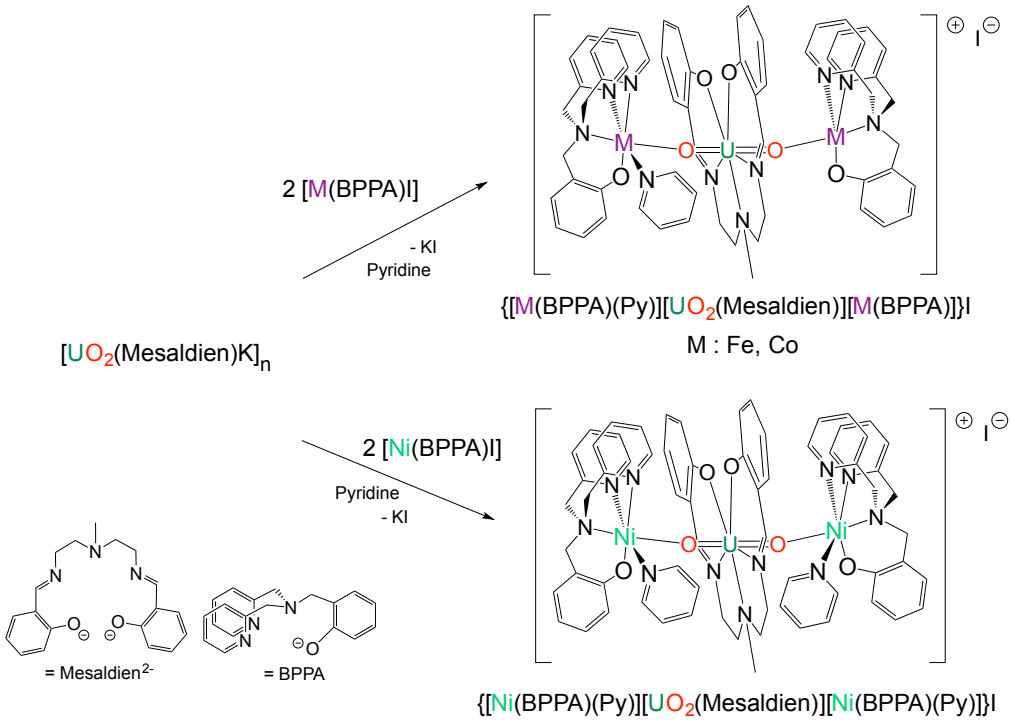

Single crystals of UM_2-BPPA (M: Fe, Co, Ni) were grown by slow diffusion of hexane into a pyridine solution of the respective complexes. In each of the UM_2-BPPA (M = Fe, Co, Ni) structures (Figure III- 24), the two oxo groups of the central $[UO_2(Mesaldien)]^-$ uranyl(V) are linked to two M(II) (M = Fe, Co, Ni) complexes, $[M(BPPA)(Py)]^+$ and $[M(BBPA)]^+$ in UM_2-BPPA (M = Fe, Co), or two $[Ni(BPPA)(Py)]^+$ cations in **22**-UNi_2-BPPA. The uranium atom in $[UO_2(Mesaldien)]^-$ has a slightly distorted pentagonal bipyramidal coordination geometry. In UM_2-BPPA (M = Fe, Co), the two d-block metals do not have the same environment due to the different coordination geometry. In $[M(BBPA)]^+$ the metal has a trigonal bipyramidal coordination geometry formed by the three nitrogen atoms and one oxygen atom of the BPPA ligand, and one uranyl(V) oxo group. However, the second is six-coordinate with a slightly distorted octahedral arrangement, as one nitrogen of a pyridine is present in the $[M(BPPA)(Py)]^+$ unit. This difference in the coordination environment is not present for Ni(II). Each nickel atom is hexacoordinated in a slightly distorded octahedral arrangement by three nitrogen atoms and one oxygen of the BPPA ligand, one nitrogen from a coordinated pyridine and one uranyl(V) oxo group. Thanks to the BPPA ligand, a single isomer for **22**-UNi_2-BPPA crystallised.

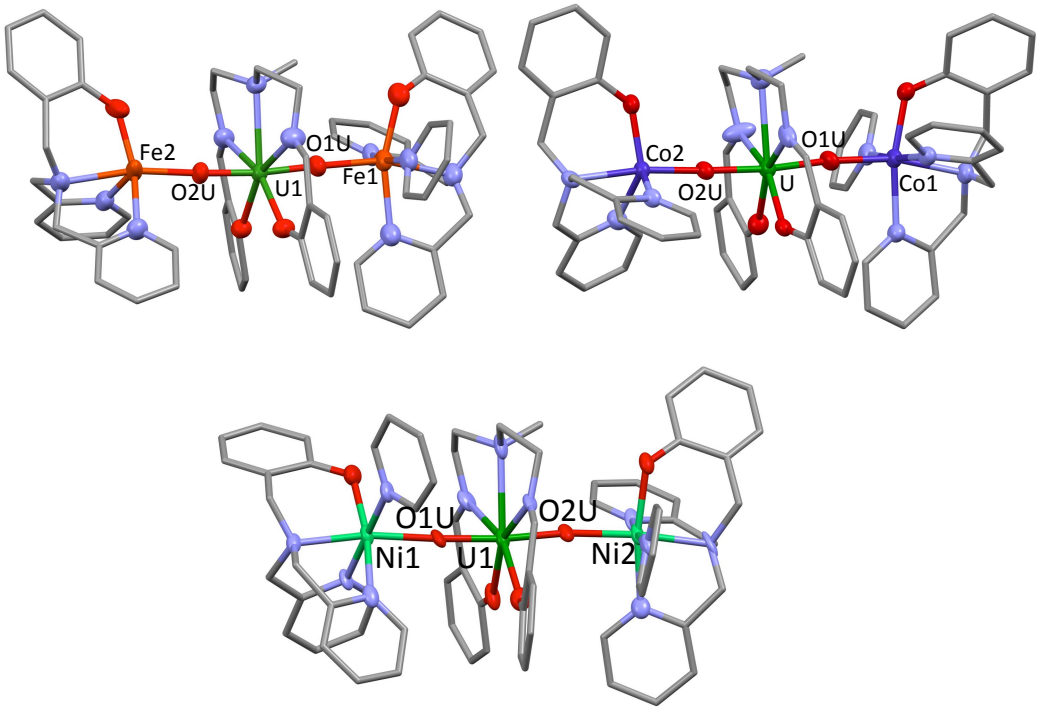

Figure III- 24 Crystallographic structure of **20**-UFe_2-BPPA (top left) **21**-UCo_2-BPPA (top right) and **22**-UNi_2-BPPA (bottom) (30% probability ellipsoids). (Ligands were represented in capped sticks, with hydrogen atoms, iodide couter-anion, disorder and solvent molecules omitted for clarity). Atoms: C (grey), O (red), Ni (light green), N (light blue), Co (blue) and U (green).

In contrast to the neutral tetradentate TPA ligand, where a bimetallic complex U-Co was obtained, a trimetallic assembly is formed with the monoanionic BPPA. As anticipated, the capping ligand has a strong effect on the nuclearity of the final structure. The nucleophilic character of the 3d cation can therefore be tuned by the charge of the coordinated ligand. The cobalt centre in $[Co(BPPA)]^+$ has a lower positive charge than in $[Co(TPA)]^{2+}$, allowing for the coordination of a second complex to the second oxo group.

In the case of Mn(II), no single crystals were obtained, even after a multitude of attempts and conditions tried. ESI/MS studies reveals a peak at m/z = 1311.3, which corresponds to the molecular cation $\{[Mn(BPPA)][UO_2(Mesaldien)][Mn(BPPA)]\}^+$ (Figure III-25). Elemental analysis of the solid is consistent with the formula $\{[Mn(BPPA)][UO_2(Mesaldien)][Mn(BPPA)]\}I.2Py.0.9KI$ (the presence of KI is explained as this complex is less soluble than the UMn_2-TPA analogue, rendering the complete removal of KI difficult), however, we cannot determine if the two pyridine molecules are coordinated to the Mn(II) centre. These two characterisations suggest the presence of a trimetallic assembly, **19**-UMn_2-BPPA.

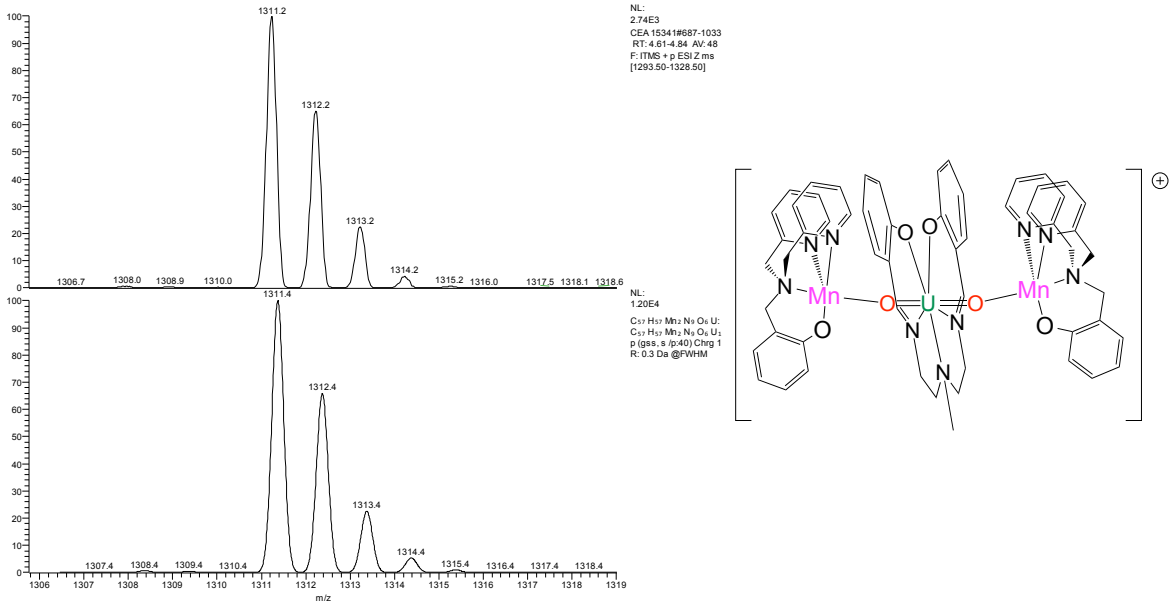

Figure III- 25 Zoom on the molecular peak (top) compared with the theoretical isotopic (bottom) profile calculated for $\{[Mn(BPPA)][UO_2(Mesaldien)][Mn(BPPA)]\}^+$.

All metallic salts Mn(II), Fe(II), Co(II), Ni(II) gave trimetallic assemblies with the use of the BPPA ligand. In order to compare the effect of the chelating ligand on the reaction of uranyl(V) Mesaldien with Cr(II), we performed the reaction of $[UO_2(Mesaldien)K]_n$ with two

equivalents of [Cr(BPPA)Cl]. The result was indeed not clear with TPA as no product was isolated.

After two days, the reaction mixture obtained from the reaction of $[UO_2(Mesaldien)K]_n$ with two equivalents of [Cr(BPPA)Cl] gave a broad proton NMR spectrum which displays sharp shifted peaks resembling a uranium(IV) complex (Figure III- 26 right). This result, as observed with $[Cr(TPA)Cl_2]$, suggests that the uranyl(V) group is reduced into uranium(IV) species. From the reaction of $[UO_2(Mesaldien)K]_n$ with two equivalents of [Cr(BPPA)Cl], we crystallised a mixed-valent Cr(II)/Cr(II) complex: $[\{Cr(BPPA)(\mu\text{-}O)\}_4Cr].2I$, **23**. The crystal structure of **23** is represented in Figure III- 26 (left) and consists of a pentanuclear assembly in which 4 Cr(III) BPPA complexes bridge through oxo ligands, forming a square. One Cr(II) is placed at the centre of the square, and it is linked to the four oxo groups. The μ-oxo groups in the structure probably arise from the uranyl(V) entity. This result shows that Cr(II) is able to reduce uranyl(V) to form uranium(IV) and Cr(III) complexes.

Scheme III- 13 Reaction of $[UO_2(Mesaldien)K]_n$ with two equivalents of [Cr(BPPA)Cl]

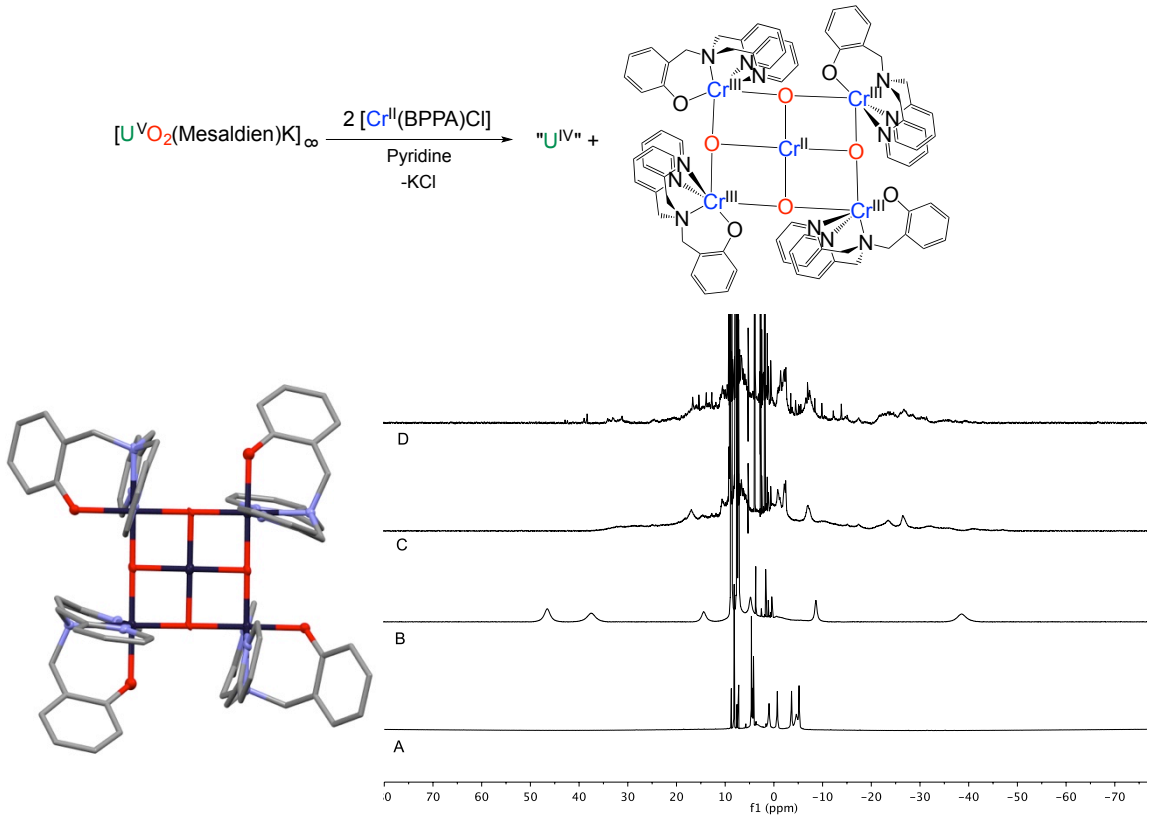

Figure III- 26 (left) Crystallographic structure of $[\{Cr(BPPA)(\mu\text{-}O)\}_4Cr].2I$, **23** (30% probability ellipsoids). (Ligands were represented in capped sticks, with hydrogen atoms, iodide couter-anion and solvent molecules omitted for clarity). Atoms: C (grey), O (red), N (light blue) and Cr (dark blue). (right) ^1H NMR (400MHz, Py-d_5, 298 K) spectrum of (A) $[UO_2(Mesaldien)K]_n$, (B) [Cr(BPPA)Cl], (C) the reaction mixture 1 :2 $[UO_2(Mesaldien)K]_n$:[Cr(BPPA)Cl] 10minutes after the addition of [Cr(BPPA)Cl] to $[UO_2(Mesaldien)K]_n$ and (D) of the reaction mixture 1 :2 $[UO_2(Mesaldien)K]_n$:[Cr(BPPA)Cl] after 2days.

Cr(II) cannot be used to form polymetallic assemblies with uranyl(V), however we have been able to isolate trimetallic assemblies with Mn(II), Fe(II), Co(II) and Ni(II). We decided to perform a similar synthesis with Cd(II) in order to obtain a diamagnetic model of the UM_2-BPPA assemblies. Although the Cd(II) ion was successfully used as diamagnetic analogue in the previous reported syntheses, attempts to synthesise the UCd_2-BPPA complex from the reaction of $[UO_2(Mesaldien)K]_n$ with two equivalents of [Cd(BPPA)I] failed. We then tried to use the diamagnetic Zn(II) ion. The reaction of $[UO_2(Mesaldien)K]_n$ with two equivalents of [Zn(BPPA)I] did not lead to the expected trimetallic assembly but instead {$[UO_2(Mesaldien)][Zn(BPPA)]$}, **24** was isolated. The crystal structure of **24** was determined by single crystal X-ray diffraction (Figure III- 27) and consists of one $[Zn(BPPA)]^+$ cation bound to one oxo group of the $[UO_2(Mesaldien)]^-$ anion in a linear cation-cation interaction. In this bimetallic species, only one oxo group of the uranyl(V) is engaged in a linear cation-cation interaction. The Zn(II) ion is pentacoordinate, with a slightly distorted trigonal bipyramidal coordination geometry defined by the three nitrogen atoms and one oxygen atom of the BPPA ligand, and one oxygen atom from the uranyl(V) group. As this dinuclear complex cannot be used as a diamagnetic model of the UM_2-BPPA complexes, we did not characterise this compound any further.

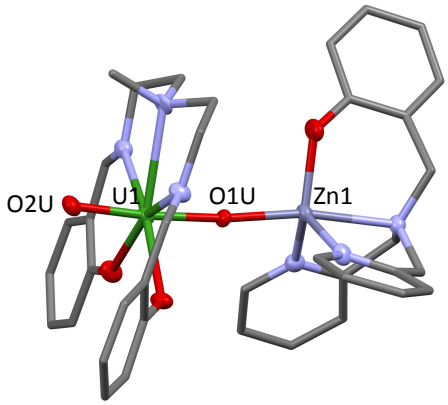

Figure III- 27 Solid-state molecular structure of {$[UO_2(Mesaldien)][Zn(BPPA)]$}, **24** (30% probability ellipsoids). (Ligands were represented in capped sticks, hydrogen, iodide counter-ions and co-crystallised solvent molecules were omitted for clarity) Colour code: uranium (green), zinc (grey-blue), oxygen (red), nitrogen (light blue) and carbon (grey).

III.2.2.1.4) TPEN as chelating ligand: Syntheses of UM_2-TPEN (M= Mn, Co)

The Co(II) complex of the monoanionic chelating ligand BPPA led to a trimetallic assembly. However, the coordination sphere of the two cobalt centres is not equivalent in **21**-UCo_2-BPPA. Pentacoordinate or hexacoordinate cobalt atoms have been found by X-ray diffraction. These differences can induce differences in the magnetic moments of the cobalt centres, leading to a more difficult interpretation of the magnetic properties.

We have also observed with the use of TPA or BPPA that the nucleophilic character of the 3d cation can be tuned by the charge of the capping ligand. The nucleophilic character can also be tuned by the denticity of the ligand. With higher denticity, no free coordination site is present on the metallic centre and only one geometrical environment around the metallic centre will be favoured. We thus decided to investigate the geometry of the assembly formed in the presence of d-block complexes of the hexadentate TPEN (tetrapyridylethylenediamine) ligand.

The reaction of $[UO_2(Mesaldien)K]_n$ with two equivalents of the complex $[M(TPEN)]I_2$ (M = Mn, Co) formed in situ in pyridine gave the trimetallic assemblies $[\{[M(TPEN)][UO_2(Mesaldien)][M(TPEN)]\}I_3]$ (M: Mn, Co), **25**-UMn_2-TPEN and **26**-UCo_2-TPEN in 63% and 49% yield, respectively (Scheme III- 14). Again, the formation of a trimetallic assembly was observed with cobalt thanks to the electron-rich TPEN ligand.

Scheme III- 14 Syntheses of **25**-UMn_2-TPEN and **26**-UCo_2-TPEN

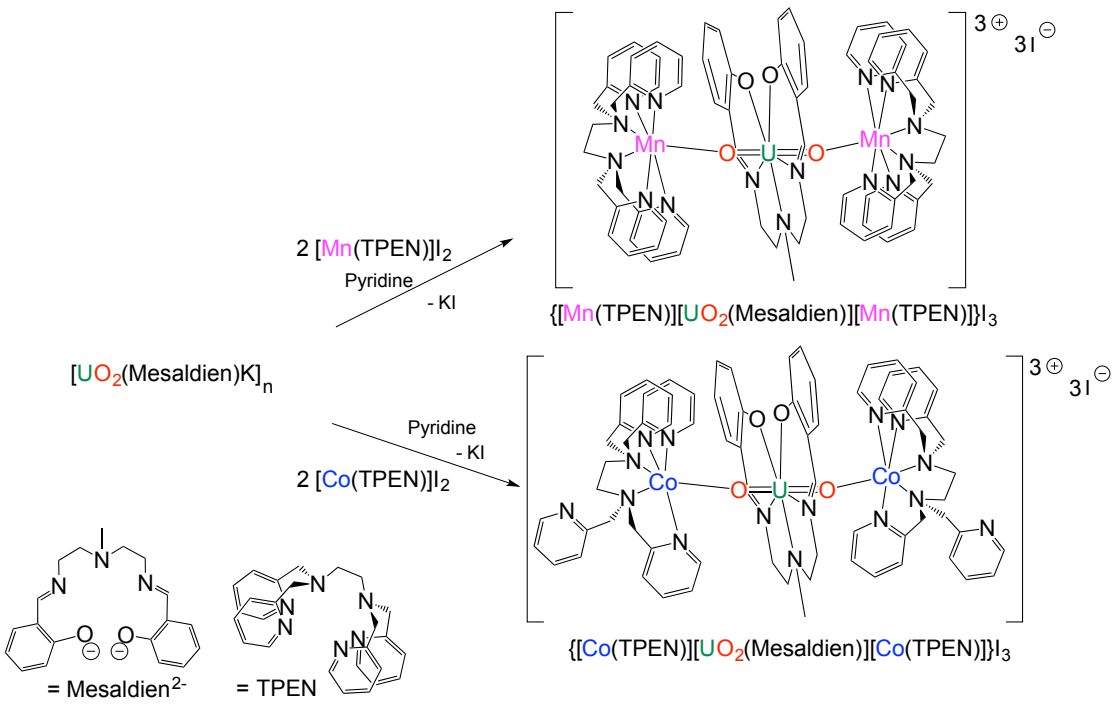

X-ray quality crystals of **25**-UMn_2-TPEN were grown from an acetonitrile solution of the complex layered with DIPE whereas the **26**-UCo_2-TPEN.3.5MeCN.2Pyridine crystals required slow diffusion of DIPE into a 2/3 Pyridine/MeCN solution containing the complex. Both crystals are represented in Figure III- 28. The solid-state structure of **25**-UMn_2-TPEN revealed two trimetallic complexes in the asymmetric unit (Figure III- 28 top). These two complexes displayed similar coordination environments but slight differences on the bond distances and angles. For both the **25**-UMn_2-TPEN and **26**-UCo_2-TPEN complexes, the two oxo groups of the central $[UO_2(Mesaldien)]^-$ uranyl(V) are linked to two $[M(TPEN)]^{2+}$ (M: Mn, Co) complexes. The asymmetric unit of **26**-UCo_2-TPEN contains half a uranium atom and one $[Co(TPEN)]^{2+}$ complex, as a 2-fold axis passes through the uranium atom and the central nitrogen atom of the Mesaldien ligand. Consequently, the two $[Co(TPEN)]^{2+}$complexes are similar. Each cobalt atom is six coordinate, and features a slightly distorded octahedral arrangement formed by five nitrogen atoms from the TPEN ligand and one oxo group of uranyl(V). We can observe that one pyridyl arm is not coordinated to the cobalt metallic centre. This is not encountered in the **25**-UMn_2-TPEN, as the Mn(II) in the $[Mn(TPEN)]^{2+}$ complex is coordinated to the 6 nitrogen atoms of the TPEN ligand and one oxygen atom of the uranyl(V).

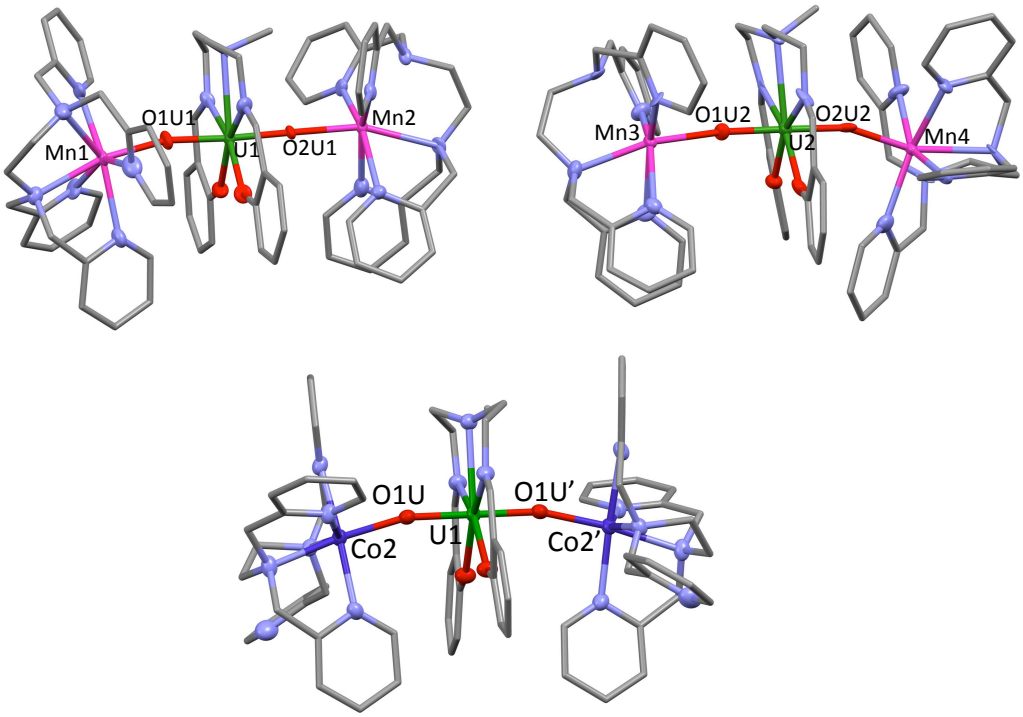

Figure III- 28 Solid-state molecular structure of **25**-UMn_2-TPEN (top) and **26**-UCo_2-TPEN (bottom) (30% probability ellipsoids). (Ligands were represented in pipes, hydrogen atoms, disorder and co-crystallised solvent molecules were omitted for clarity) Colour code: uranium (green), manganese (pink), cobalt (blue), oxygen (red), nitrogen (light blue) and carbon (grey).

The use of the TPEN ligand led to a symmetrical arrangement for the two cobalt complexes. Thanks to the use of BPPA and TPEN ligands, polymetallic assemblies of UO_2^+-Co(II)/Ni(II) have been synthesised with similar environments around the metal centres.

III.2.2.1.5) Stability and characterisation of the discrete assemblies

Each discrete assembly presented in section III.2.2.1) is stable in the solid state or in pyridine or acetonitrile solution for months under an argon atmosphere. ^{1}H proton NMR studies show that the spectrum of the polymetallic assembly differs significantly from the spectra of the independent $[UO_2(Mesaldien)K]_n$ and d-block complexes, indicating that the assembly is present in solution (example for **17**-UCo-TPA Figure III- 29, see Appendix). Furthermore, ESI/MS experiments in 90:10 acetonitrile:pyridine solutions indicate that all of these complexes retain their dimetallic or trimetallic form also in gas phase as molecular cations $\{[UO_2(Mesaldien)][Co(TPA)]\}^+$, $\{[M(TPA)X][UO_2(Mesaldien)][M(TPA)X]\}^+$ (M: Mn, Cd, Ni, X=I; M: Fe, Mn, X= Cl), $\{[M(BBPA)][UO_2(Mesaldien)][M(BBPA)]\}^+$ (M: Mn, Fe, Co, Ni) and $\{[M(TPEN)][UO_2(Mesaldien)][M(TPEN)]I_2\}^+$ (M: Mn, Co) are observed (example for **18**-UNi_2-TPA Figure III- 30, see Appendix). These studies both in solution and gas phase highlighted the strength of the cation-cation interaction between uranyl(V) and transition metals.

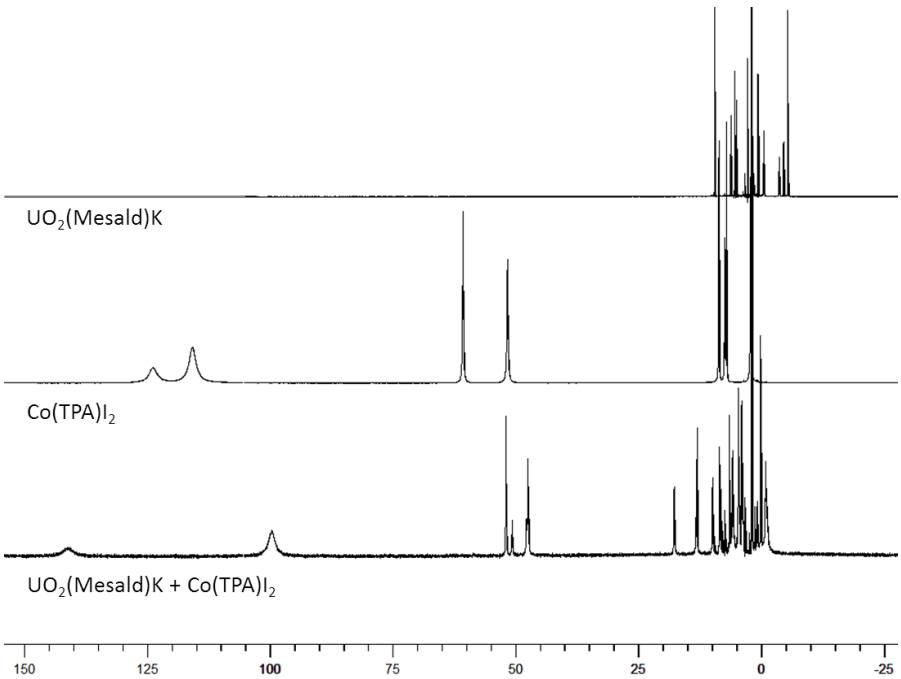

Figure III- 29 ^{1}H NMR spectra (200 MHz, CD_3CN, 298 K) (left) of complex $\{[Co(TPA)I][UO_2(Mesaldien)]\}I$ compared to [Co(TPA)I]I and $[UO_2(Mesaldien)K]_n$.

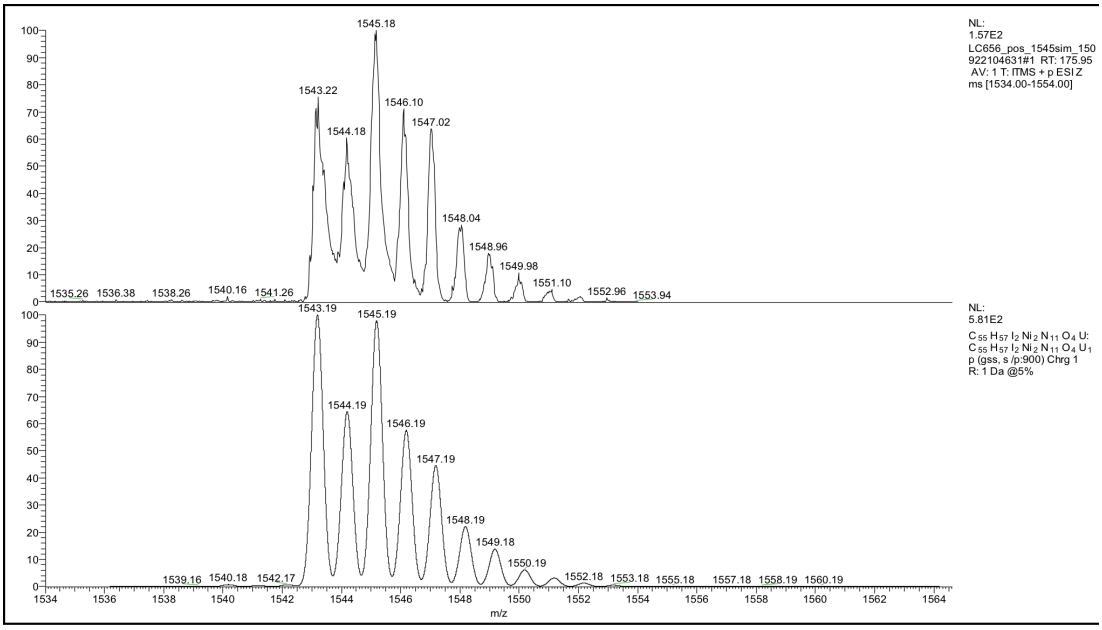

Figure III- 30 Zoom on the molecular peak (top) compared with the theoretical isotopic (bottom) profile calculated for $\{[Ni(TPA)][UO_2(Mesaldien)][Ni(TPA)]I_2\}^+$.

III.2.2.1.6) Structural comparison of discrete assemblies

Distances and angles for the crystallised complexes are reported in Table III- 3 and the cores of the structures are represented in Figure III- 31. The mean uranyl $U{=}O_{yl}$ bond distances lie in the range of the values typically observed for $U^V{=}O$ distances in the presence of cation-cation interactions (range: 1.837-1.934Å).[47,180,231,241,366] The mean $Mn–O_{yl}$ bond distances in **13**-UMn_2-TPA-I (2.055(6) Å) and **15**-UMn_2-TPA-Cl (2.093(37) Å) are close to the one found in the **12**-$\{UO_2(Mesaldien)Mn\}_n$ polymer (2.075(3) Å) but considerably shorter than that found in the heteronuclear $U_{12}Mn_6$ wheel (2.15(2) Å)[180] and in a heterodimetallic uranyl(VI)–Mn(II) complex (2.163(4) Å)[234] whereas the mean $Mn\text{-}O_{yl}$ bond distances in **25**-UMn_2-TPEN (2.153(10) Å) lies in the range of these last complexes. In the **14**-UCd_2-TPA complex, the mean $Cd\text{-}O_{yl}$ distance (2.201(16) Å) is slightly shorter than in the **9**-$\{UO_2(salen)Cd\}_n$ polymer complex (2.28(2) Å), or in a heterodimetallic U(VI)/Cd(II) system (2.252(4) Å).[353] The mean $Fe(II)\text{-}O_{yl}$ distance in **16**-UFe_2-TPA (2.07(7) Å) and **20**-UFe_2-BPPA (2.03(3) Å) are significantly longer than in the uranyl(V)–$Fe(II)_2$ Pacman complex (1.946(4) Å).[58] The mean $Co\text{-}O_{yl}$ distances in **21**-UCo_2-BPPA and **26**-UCo_2-TPEN are 2.010(1) Å and 2.025(4) Å, respectively, longer than the $Co\text{-}O_{yl}$ distance in the bimetallic **17**-UCo-TPA (1.924(3) Å) due to the weaker interaction between the oxo groups of the uranyl(V) and the two cobalt complexes. It is, however, significantly shorter than in the reported uranyl(VI)–Co(II) Pacman complex (2.084(6) Å).[234] The mean $Ni(II)\text{-}O_{yl}$ distance (2.047(2) Å) in **22**-UNi_2-

BPPA is similar to the one in **18**-UNi_2-TPA (2.021(33) Å). No furher comparison is available as no uranyl(VI) or uranyl(V) have ever been linked to Ni(II) through a cation-cation interaction. The arrangements of the three metal ions M-U-M are almost linear (162.06(5)-176.81(2)°).

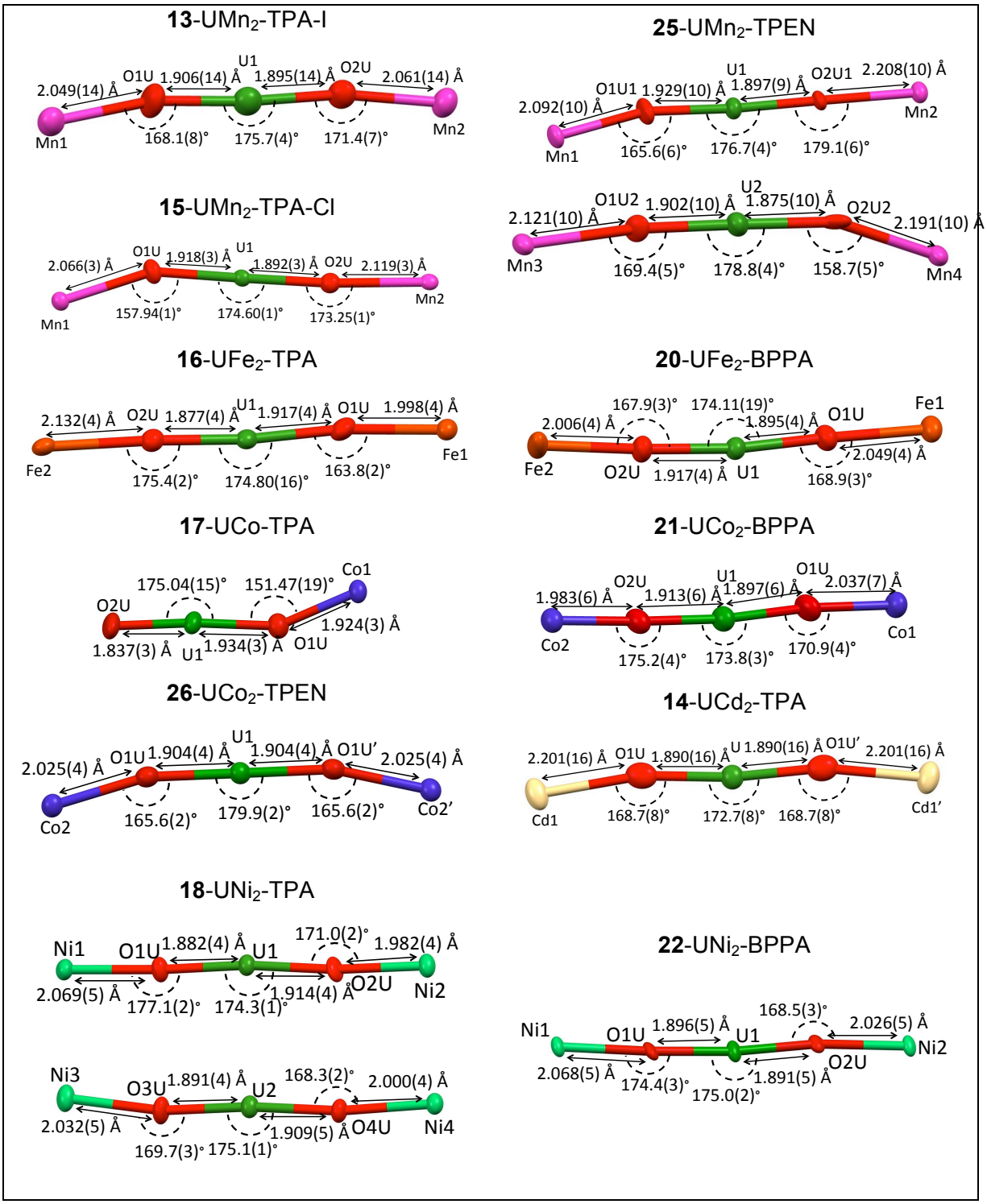

Figure III- 31 Structural parameters of the core of the discrete complexes.

Table III- 3 Intramolecular distances (Å) and angles (°) of the discrete complexes

M_x-O_x=U_x=O_{x+1}-M_{x+1}	U_x-M_x	U_x-M_{x+1}	M_x-M_{x+1}	M_x-U_x-M_{x+1}
13-UMn_2-TPA-I ($U_{x=1}$)	3.934(3)	3.944(3)	7.867(4)	173.77(5)
15-UMn_2-TPA-Cl ($U_{x=1}$)	3.910(1)	4.004(1)	7.891(1)	171.192(1)
25-UMn_2-TPEN ($U_{x=1}$)	3.990(2)	4.105(2)	8.090(3)	175.65(5)
25-UMn_2-TPEN ($U_{x=2}$)	4.006(3)	3.996(2)	7.904(3)	162.06(5)
16-UFe_2-TPA-Cl ($U_{x=1}$)	3.8762(9)	4.0054(9)	7.8691(12)	173.54(2)
20-UFe_2-BPPA ($U_{x=1}$)	3.9248(12)	3.9012(12)	7.8131(16)	173.42(2)
17-UCo-TPA ($U_{x=1}$)	3.7388(5)			
21-UCo_2-BPPA ($U_{x=1}$)	3.9209(17)	3.8927(15)	7.809(2)	175.97(3)
26-UCo_2-TPEN ($U_{x=1}$)	3.8988(7)	3.8988(7)	7.7337(15)	165.31(3)
18-UNi_2-TPA-I ($U_{x=1}$)	3.9493(12)	3.8839(10)	7.8301(14)	176.81(2)
18-UNi_2-TPA-I ($U_{x=2}$)	3.9064(12)	3.8889(10)	7.7873(14)	174.822(19)
22-UNi_2-BPPA ($U_{x=1}$)	3.9598(11)	3.8976(11)	7.8522(16)	175.81(3)
14-UCd_2-TPA ($U_{x=1}$)	4.0717(16)	4.0717(16)	8.135(3)	174.86(6)

No evidence of significant intermolecular hydrogen bonding or pi-stacking interactions in the structure of the d-block metals/uranyl(V) assemblies was observed. The molecules are well separated with similar values for the shortest intermetallic distances (Table III- 3 and Table III- 4). Only the intermetallic distances of **17**-UCo-TPA are reduced compared to the trimetallic assemblies. The distances are long enough to preclude any long-range interactions.

Table III- 4 Shortest intermolecular distances (Å) of the discrete complexes

	U-U	U-M	M-M
13-UMn_2-TPA-I	10.9469(4)	8.7589(4)	7.6296(4)
15-UMn_2-TPA-Cl	10.025(1)	9.526(1)	7.236(1)
25-UMn_2-TPEN	10.9084(4)	10.2933(4)	8.9152(4)
16-UFe_2-TPA-Cl	9.8358(4)	9.5228(8)	7.2977(12)
20-UFe_2-BPPA	10.2602(9)	9.1797(10)	7.9627(14)
17-UCo-TPA	8.31382(13)	7.26841(12)	8.14835(10)
21-UCo_2-BPPA	10.4919(14)	9.7639(11)	7.7742(7)
26-UCo_2-TPEN	12.3578 (7)	11.4417(9)	10.0136(15)
18-UNi_2-TPA-I	9.7869(8)	9.2856(9)	8.7694(13)
22-UNi_2-BPPA	11.148(1)	9.1476(12)	8.571(2)
14-UCd_2-TPA	11.0107(7)	8.6904(7)	7.4179(5)

III.2.2.1.7) Magnetic properties

III.2.2.1.7.1) In static field

Magnetic susceptibility measurements between 1.8 or 2-300 K in a static field were performed on polycrystalline samples of the different bi- and trimetallic assemblies (Figure III-32). Experimental χT values are reported in the Table III- 5 and are compared to the expected value at room temperature, calculated with the spin-only formula for each transition metal. The χT value for **14**-UCd_2-TPA at room temperature equals 0.32 cm^3 K mol^{-1} (μ_{eff} = 1.55 μ_B) per uranium ion (Cd(II) is diamagnetic). The measured value of the magnetic moment for U(V) is significantly smaller with respect to the free-ion value (2.54μ_B) probably by the combined ligand field effects and spin-orbit coupling.[53,103]

Based on this value, all the χT values measured at room temperature for the Mn, Fe, Ni polynuclear complexes are in agreement with two high-spin non-interacting transition metals and one uranyl(V) for the trimetallic species, and with one high-spin cobalt(II) associated to one uranyl(V) for **17**-UCo-TPA. For UMn_2, UFe_2, **21**-UCo_2-BPPA and **22**-UNi_2-BPPA, the χT product reachs a maximum, unambiguous for the Mn(II) and Fe(II) complexes and more subtle for the others, after which it drops. This behaviour is consistent with the presence of a magnetic exchange coupling between uranium and d metals.

The χT of **19**-UMn_2-BPPA revealed a field-dependent maximum, which may indicate the presence of intermolecular interactions. Unfortunately, no crystal structure was determined for this complex and consequently intermetallic distances cannot be discussed. Due to this result repeated on several independent samples, the magnetic properties have to be interpreted cautiously for this complex.

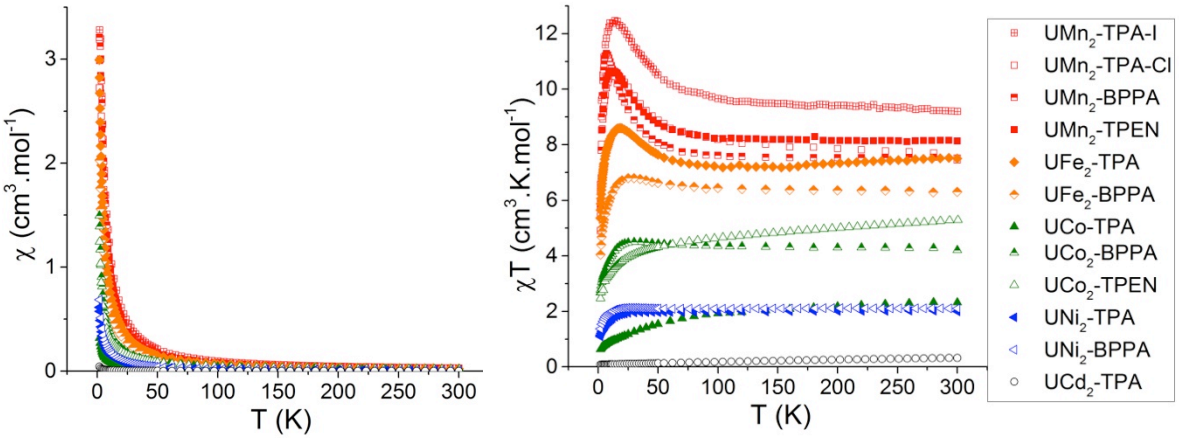

Figure III- 32 Plots of χ and χT versus T for a polycrystalline sample of all the discrete polynuclear d-5f[1] assemblies measured at 0.5 T applied field.

Table III- 5 χT (cm^3 K mol^{-1}) and T (K) and expected values (g=2):

	S_M	$\chi T_{th(M)}$ (T=300 K)	χT_{meas} (T=300 K)	χT_{max} (T_{max})	χT_{min} (T_{min})
13-UMn_2-TPA-I	5/2	4.375	9.2	12.5 (12)	6.0 (1.8)
15-UMn_2-TPA-Cl	5/2	4.375	7.5	10.6 (14)	4.9 (1.8)
19-UMn_2-BPPA	5/2	4.375	7.5	0.5T: 11.3 (7) 0.1T: 14.5 (4)	5.8
25-UMn_2-TPEN	5/2	4.375	8.1	10.6 (14)	6.0 (2)
16-UFe_2-TPA-Cl	2	3	7.5	8.6 (18)	5.3 (1.8)
20-UFe_2-BPPA	2	3	6.3	6.8 (30)	4.0 (1.8)
17-UCo-TPA	3/2	1.875	2.3	-	0.6 (2)
21-UCo_2-BPPA	3/2	1.875	4.2	4.5 (30)	2.7 (2)
26-UCo_2-TPEN	3/2	1.875	5.3	-	2.5 (2)
18-UNi_2-TPA-I	1	1	2	-	1.1 (1.8)
22-UNi_2-BPPA	1	1	2.11	2.13 (26)	1.4 (2)
14-UCd_2-TPA	0	0	0.32	-	0.09 (2)

III.2.2.1.7.2) Magnetic U-Mn coupling in UMn_2-TPA-I

The evaluation of the magnetic exchange coupling between uranium and manganese ions (J) in **13**-UMn_2-TPA-I was carried out by our collaborator Dr. F. Tuna (Univ. of Manchester). A similar procedure to that reported by Long and coworkers in modelling the exchange coupling within the trimetallic clusters (cyclam)M[(μ-Cl)U(IV)($Me_2Pz)_4]_2$ and (M=Co(II),Ni(II),Cu(II)) was used.[7,262,263] **14**-UCd_2-TPA is isostructural with **13**-UMn_2-TPA-I with diamagnetic Cd(II) centres instead of the two S = 5/2 Mn(II) centres, and it can be seen as a simpler model to account for the contribution resulting from spin-orbit and ligand-field effects of the U(V) centre. Therefore, if the experimental χT data of **13**-UMn_2-TPA-I are subtratcted from the experimental χT data of **14**-UCd_2-TPA, the contribution of the U(V) ion to the overall magnetism is removed, leaving only the magnetic contribution of the two Mn(II) ions and of the magnetic exchange coupling. In order to use the isotropic spin Hamiltonian ($H = -2J(S_{Mn1}S_U+S_US_{Mn2})$) to model the Mn-U interaction in **13**-UMn_2-TPA-I, a temperature-independent value of 0.094 cm^3 K mol^{-1}, accounting for the spin-only (S = ½) contribution of the U(V) centre, assuming g_U = 1, was added to the subtracted data. The experimental data above 30 K were fitted, using isotropic spin Hamiltonian in MAGPACK.[367]

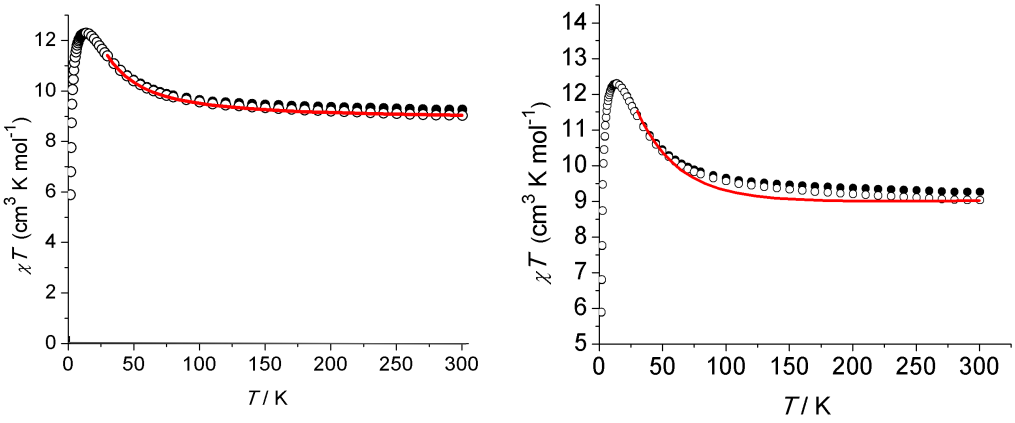

Figure III- 33 Plots of χT *versus* T for polycrystalline samples of **13**-UMn_2-TPA-I measured in 0.5 T dc field (open circles: subtraction of the **14**-UCd_2-TPA data from the **13**-UMn_2-TPA-I data with addition of 0.094 $cm^3.K.mol^{-1}$; red line: best fit with J = +7.5 cm^{-1} (left) and J = -14.3 cm^{-1} (right)).

Two different fits were performed. The first fit without any restriction on the sign of J gave the parameters J = +7.5 cm^{-1} for a ferromagnetic coupling, g_{Mn} = 2 and g_U = 1 (Figure III-33, left). A second fit restricting the sign of J to be negative, meaning that an antiferromagnetic coupling between Mn and U occured, yielded J = -14.3 cm^{-1}, g_{Mn} = 2.04 and g_U = 1; however, we can observe in Figure III- 33 right, that the quality of the fit is lower in the case of the antiferromagnetic coupling. Consequently, we assume that the magnetic exchange coupling U-Mn is ferromagnetic with J = +7.5 cm^{-1}. This value lies in the range of the values of exchange constants calculated with this method for the few other reported complexes $Co^{II}U_2^{IV}$ and $Ni^{II}U_2^{IV}$ (2.8-49 cm^{-1})[262,263] which also present ferromagnetic 3d-5f coupling. This calculation's method requires a certain number of assumptions and as such gives only an approximate estimation of the exchange coupling constant rather than an accurate value.

III.2.2.1.7.3) Characterisation of SMM properties

III.2.2.1.7.3.1) ZFC-FC measurements and hysteresis

The zero-field (ZFC) and field cooled (FC) experiments and the measurements of hysteresis cycles were performed to probe the presence of magnetic anisotropy and slow relaxation of the magnetisation under static field. Only the UMn_2 and **16**-UFe_2-TPA species revealed a divergence between ZFC and FC at low temperature, suggesting the presence of strong magnetic anisotropy (Figure III- 34).

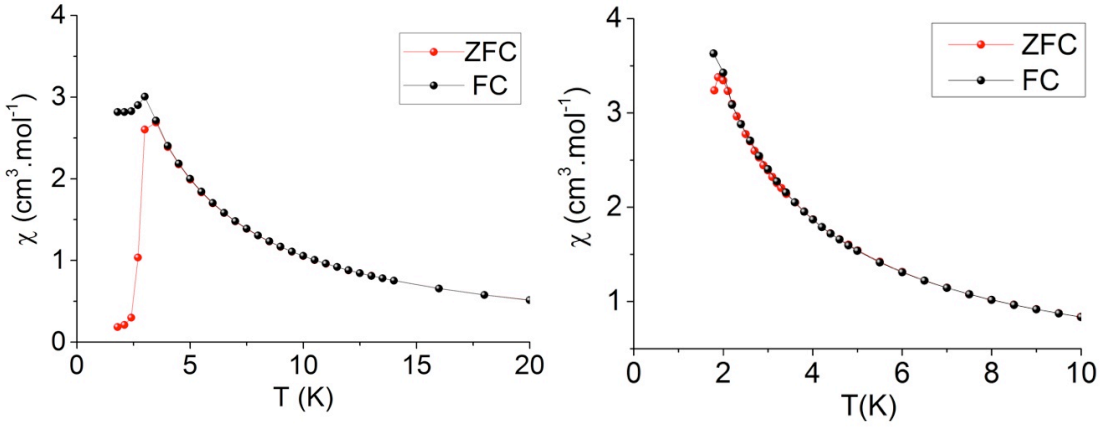

Figure III- 34 Temperature dependence of the susceptibility χ for **15**-UMn_2-TPA-Cl (left) and **16**-UFe_2-TPA (right) recorded at magnetic fields of 0.1T in field cooled (FC) and zero field cooled (ZFC).

16-UFe_2-TPA exhibits a weak hysteresis at 1.8 K with a collapse of the width at 0T (Figure III- 35 left). Contrary to this butterfly hysteresis shape, all UMn_2 assemblies present well-opened hysteresis loops. The width of the hysteresis decreases with increasing temperature, and vanishes around 3 K for each complex (Figure III- 35, Figure III- 36 and Table III- 6).

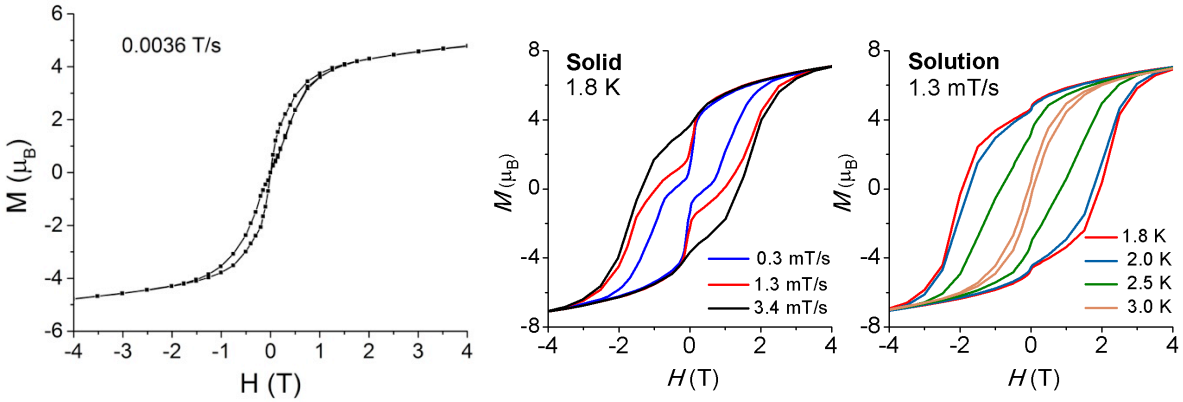

Figure III- 35 Magnetic hysteresis loops for polycrystalline sample of **16**-UFe_2-TPA (left) and for polycrystalline sample (middle) and pyridine solution (right) of **13**-UMn_2-TPA-I.

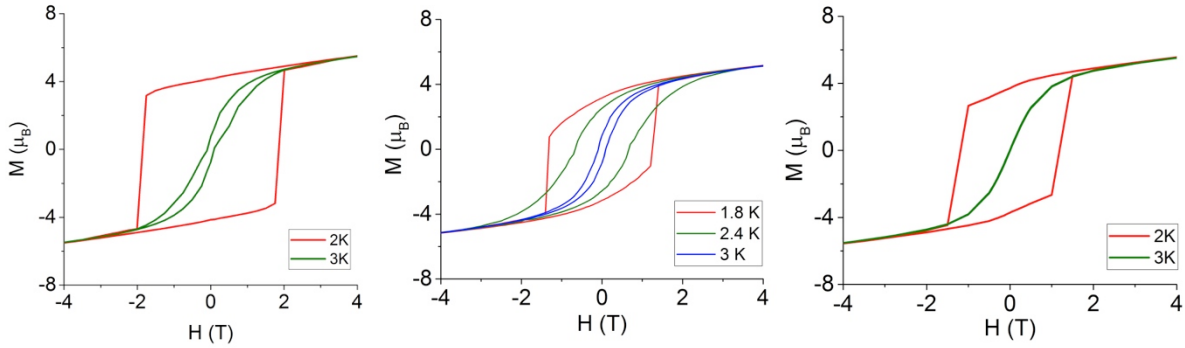

Figure III- 36 Hysteresis loops for polycrystalline samples of **15**-UMn_2-TPA-Cl (left) (0.0034 T/s field sweep rate), **19**-UMn_2-BPPA (middle) (0.0027 T/s field sweep rate) and (right) **25**-UMn_2-TPEN (0.0022 T/s field sweep rate).

Clear, open hysteresis cycles are observed in the M(H) data, for both solid-state and solution samples (21.4 mM in pyridine) of **13**-UMn_2-TPA-I (Figure III- 35). The larger coercive field in solution is probably due to the presence of weaker dipolar interactions than in the solid state. Quantum tunnelling at 0T provoked a step in the hysteresis curve and consequently a loss of the magnetisation. **15**-UMn_2-TPA-Cl, **19**-UMn_2-BPPA and **25**-UMn_2-TPEN present a rapid drop of the magnetisation at 1.8 and 2 K, in contrast to the well-defined quantum steps of **13**-UMn_2-TPA-I. This phenomenon is not yet very well understood.

The observation of divergence in ZFC/FC measurements and opened hysteresis loops for the UMn_2 and **16**-UFe_2-TPA clusters are indicative of single molecule magnet behaviour. None of these observations were seen with the other polynuclear assemblies, meaning that if they are single molecule magnets, their properties are much weaker.

Table III- 6 Sweep rate, coercive field and remanent magnetisation obtained at 1.8 K for UMn_2 assemblies

	13-UMn_2-TPA-I solid state	**13-UMn_2-TPA-I** frozen solution	**15-UMn_2-TPA-Cl**	**19-UMn_2-BPPA**	**25-UMn_2-TPEN**
Sweep rate (mT/s)	1.3	1.3	3.4	2.7	2.2
Coercive field (T)	1.9	1.9	1.9	1.3	1.2

III.2.2.1.7.3.2) In oscillating field

The magnetisation dynamics were investigated for each polymetallic complex. Both measurements versus frequency and temperature were performed; leading to the Argand plots (versus frequency) and to the ac plots (versus temperature). Peaks with strong frequency and temperature dependence were obtained both for the in-phase (χ') and out-of-phase (χ'') components of the ac susceptibility for the UMn_2-TPA-X, **19**-UMn_2-BPPA, **16**-UFe_2-TPA and **22**-UNi_2-BPPA complexes (Figure III- 37).

The application of a static magnetic field for the **21**-UCo_2-BPPA, **26**-UCo_2-TPEN, **18**-UNi_2-TPA and **14**-UCd_2-TPA complexes was necessary to observe maxima in the out-of-phase magnetic susceptibility. This phenomenon is known for molecules presenting quantum tunnelling of the magnetisation under zero-field.[8,165] Several measurements with various H_{dc} field were carried out to determine which static magnetic field to apply.

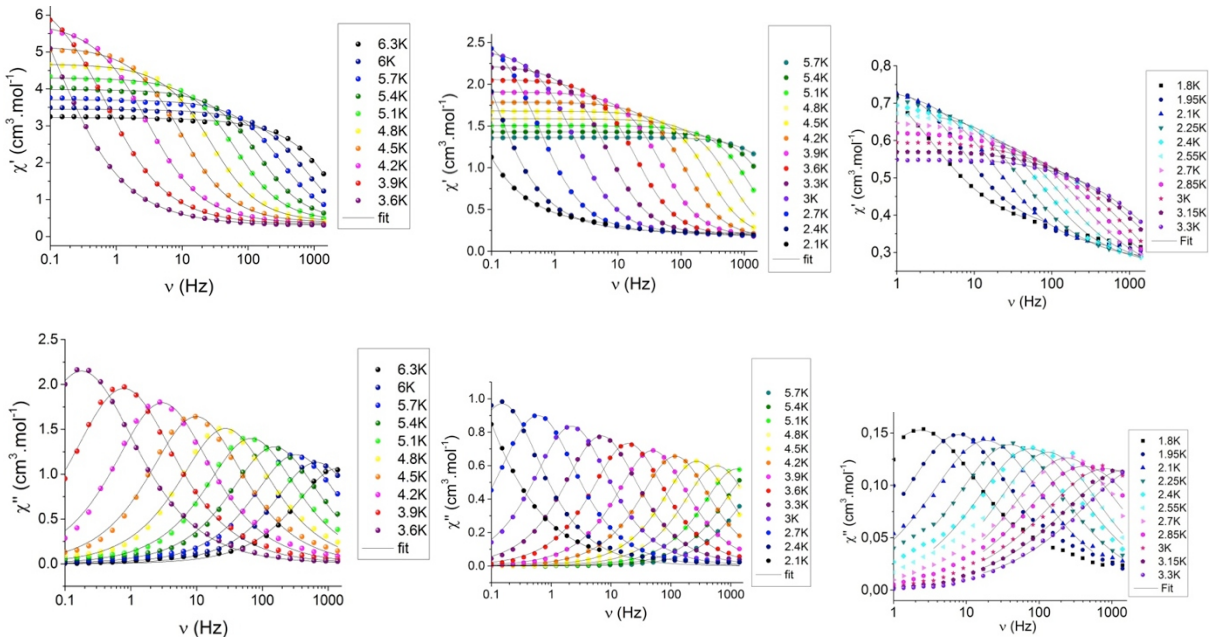

Figure III- 37 Frequency dependence of the (top) in-phase and (bottom) out-of-phase ac susceptibility components measured at 1.55G ac field of **15**-UMn_2-TPA-Cl (left), **16**-UFe_2-TPA (middle) and **22**-UNi_2-BPPA (right) under zero dc field.

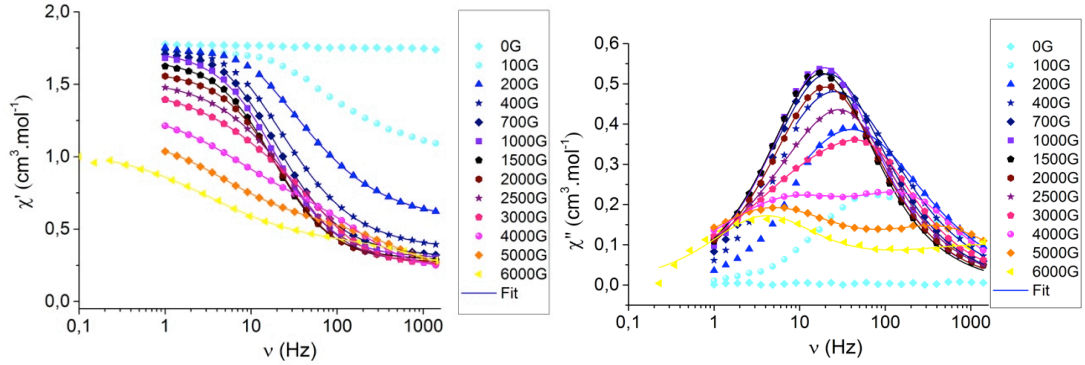

Figure III- 38 dc field dependence at 1.8 K of the in-phase (χ') (left) and out-phase (χ'') (right) ac susceptibility plotted vs. υ of **21**-UCo_2-BPPA recorded at 1.55 Oe ac field.

In Figure III- 38, the dc field dependence from 0 to 6000G at 1.8 K of the two magnetic ac susceptibilities versus frequency for **21**-UCo_2-BPPA is represented. The H_{dc} field at 1500G is the best compromise between the highest relaxation time and only one observed relaxation process. This field of 1500G was also found as the most effective one for **26**-UCo_2-TPEN and **14**-UCd_2-TPA (Figure III- 39). However, no applied field from 0 to 9000G was found to reveal slow relaxation of the magnetisation for **17**-UCo-TPA. The parameters used for the ac magnetic measurements are reported in Table III- 7.

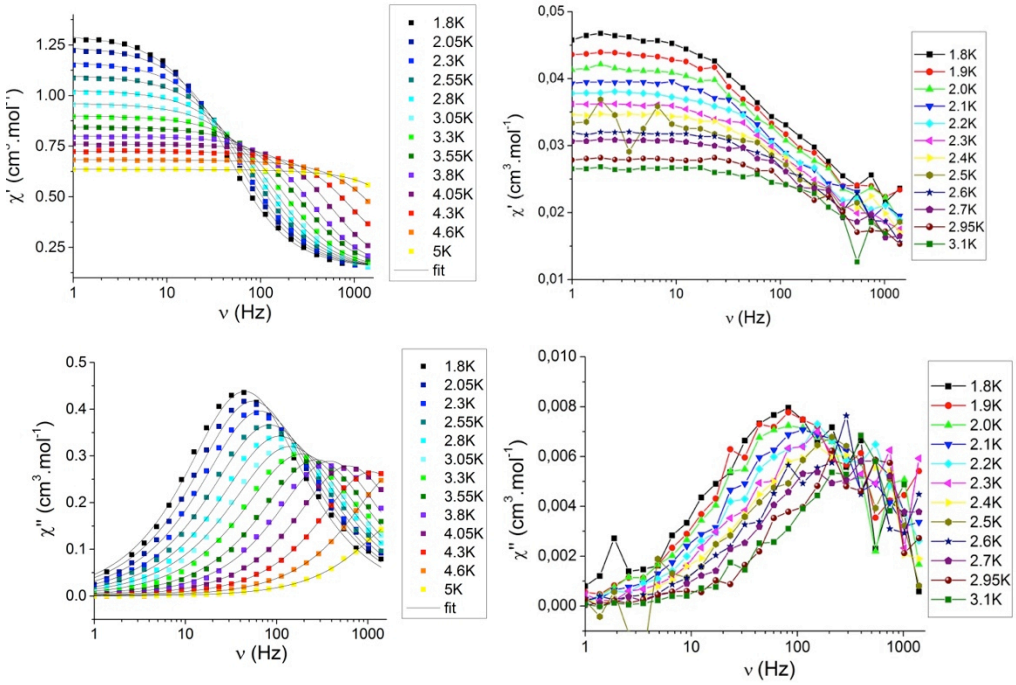

Figure III- 39 Frequency dependence of the (top) in-phase and (bottom) out-of-phase ac susceptibility components measured at 1.55G ac field of **26**-UCo_2-TPEN and **14**-UCd_2-TPA (right) under 0.15T dc field.

Table III- 7 Parameters used for ac measurements, fits with Debye model and results of Arrhenius fits

	H_{dc} (G)	ν (Hz)	$T_{meas\ ac}$ (K)	T_{fit} (K)	α	$T_{Arrhenius}$ (K)	ΔE (K)	τ_0 (s)
13-UMn_2-TPA-I	0	0.1-1400	1.8-10	3.9 - 6.3	0.01-0.15	3.6-6.7	81.0 ± 0.5	5.02×10^{-10}
15-UMn_2-TPA-Cl	0	0.1-1400	1.8-10	3.9-6.0	0.08-0.11	3.6-6.4	79.1 ± 0.2	4.86×10^{-10}
19-UMn_2-BPPA	0	0.1-1400	1.8-10	3.9-5.7	0.23-0.43	3.6-6.1	85.1 ± 0.7	1.03×10^{-10}
25-UMn_2-TPEN	0	0.1-1400	1.8-10	3.0-5.4	0.11-0.23	2.9-5.5	59.0 ± 0.4	3.09×10^{-9}
16-UFe_2-TPA	0	0.1-1400	1.8-8	2.7- 4.8	0.12-0.20	3.7-5.2	53.9 ± 0.9	3.40×10^{-9}
20-UFe_2-BPPA	0	1-1400	1.8-5	1.8-2.55	0.24-0.32	2.4-2.7	9.0 ± 1.1	7.82×10^{-6}
	400	1-1400	1.8-5	2.1-3	0.28-0.43	2.1-3	35.6 ± 0.6	3.14×10^{-9}
17-UCo-TPA	0-9000	1-1400	-	-	-	-	-	-
21-UCo_2-BPPA	1500	1-1400	1.8-5	1.9- 2.7	0.13-0.2	2.3-2.9	30.5 ± 0.9	2.90×10^{-9}
26-UCo_2-TPEN	1500	1-1400	1.8-5	1.8-4.05	0.09-0.19	3.3-4.0	20.4 ± 2.2	1.84×10^{-6}
18-UNi_2-TPA	1000	1-1400	1.8-7	-	-	2.1-2.7	32.4 ± 4.1	2.78×10^{-9}
22-UNi_2-BPPA	0	1-1400	1.8-5	1.8 - 2.9	0.26-0.40	2.4-3.2	27.4 ± 0.5	2.40×10^{-8}
14-UCd_2-TPA	1500	1-1400	1.85 - 3.1	-	-	-	≤ 5	

The Argand plots were fitted thanks to a Debye model for one relaxation process.[356] The α parameters are reported in Table III- 7 and reveal narrow distributions of relaxation time. The analysis of the Argand curves and of the measurement versus temperature

allowed for the determination of the relaxation time associated with a temperature. However, the signal was too noisy for **14**-UCd_2-TPA and in a very small temperature range (1.85 to 3.1 K) to precisely fit the curves; the energy barrier was estimated to less than 5 K. Each pair (τ, T) was used to plot ln(τ) versus T^{-1} and was fitted with an Arrhenius law $\tau = \tau_0 \exp(\Delta E/k_B T)$ (Table III- 7 and Figure III- 40). It is apparent that the energy barriers possess a wide range of values from 81 K to 5 K.

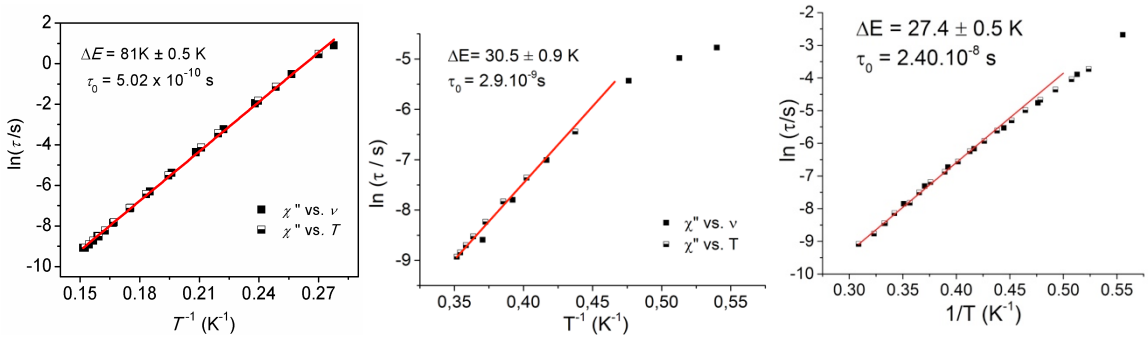

Figure III- 40 Arrhenius plots displaying T-dependence of the relaxation times for **13**-UMn_2-TPA-I (left), **21**-UCo_2-BPPA (middle) and **22**-UNi_2-BPPA (right).

III.2.2.1.7.3.3) Discussion

The results presented above show slow relaxation of the molecular magnetisation, indicative of single molecule magnet (SMM) behaviour for all trimetallic complexes. The energy barriers are reported in Table III- 7.

- **Cd:** The trimetallic complex **14**-UCd_2-TPA exhibits slow relaxation of the magnetisation under applied field, resulting from single ion behaviour due to the anisotropy of the uranyl(V) unit since Cd(II) is diamagnetic. However, the anisotropy is not high enough to allow high relaxation barriers, and an estimation of ≤ 5 K was made. This energy barrier is in the same order of magnitude as the **9**-$\{UO_2(salen)Cd\}_n$ polymer (ΔE = 7.5 K, 0.1T). In the literature, the only other example of a monometallic terminal mono-oxo U(V) complex (ΔE = 21 K, 0.1T)[72] does not have the uranyl entity. The coordination environment of uranium(V) is thus very different, showing the strong influence of the geometry.

- **Mn:** All Mn(II)-U(V) trimetallic complexes have energy barriers in the short range 59-85 K. The influence of the intermolecular interactions does not increase the energy barrier for **19**-UMn_2-BPPA very much compared to the other systems. We can also notice that apart from **25**-UMn_2-TPEN, the nature of the ligand coordinated to Mn(II) does not drastically affect

the relaxation of the magnetisation (ranging from 79 to 85 K). The lower anisotropy barrier found for the **25**-UMn_2-TPEN complex may be due to a weaker U-Mn interaction shown by the longer Mn-O_{yl} bond distances compared to the other UMn_2 assemblies. The blocking temperature is similar for all of these systems (2.6-3.2 K) and each one presents open hysteresis loops with high coercive fields. The energy barriers for the "UMn_2" units are the highest reported for a mono-uranyl(V) complex, and show the efficiency of the magnetic communication between U(V) and Mn(II), leading to improved SMMs. Furthermore, despite the presence of only three metal ions, this value remains high compared to the barrier found in the $U_{12}Mn_6$ wheel (ΔE = 142 K).[180] No SIM based only on Mn(II) have been reported so far and very few examples of field-induced SIM of monometallic Mn(III) are described with very small energy barriers (7.7-19.4 K, 0.1-0.5 T)[146,368-371] compared to our UMn_2 systems. To our knowledge, the highest energy barrier measured so far for single molecule magnets based on Mn(III) is around 86.4 K (the cluster in question contains six Mn(III) ions)[150,186,372] which is comparable to our UMn_2 complexes.

- **Fe:** The UFe_2 assemblies represent the first examples of magnetic coupling between one uranyl(V) and Fe(II). No evidence of such an interaction was found in the previously reported heterometallic uranyl(V)–$Fe(II)_2$ complex,[58] suggesting that the [Fe–O=U=O–Fe] arrangement is the key to the magnetic coupling. However, the two "UFe_2" complexes behave very differently. The energy barrier of **20**-UFe_2-BPPA (ΔE = 9.0 K) is significantly lower than in **16**-UFe_2-TPA (ΔE = 53.9 K). Detailed measurements revealed that the application of 400G static field results in a significant increase of the relaxation barrier (ΔE = 35.6 K, 0.04 T) for **20**-UFe_2-BPPA. The difference between these two UFe_2 complexes may arise from the difference in the coordination environment of the two Fe(II) cations in **20**-UFe_2-BPPA. In contrast to Mn(II), monometallic-Fe(II) single ion magnets have been reported.[146,147,149] The anisotropy barrier greatly depends on the coordination environment around the metal, with large anisotropy barriers for two-coordinate Fe(II) complexes in a linear geometry (258.6 K, 0.05 T)[145] or for trigonal pyramidal iron(II) complexes (93 K, 0.15 T).[373] Fe(II) can also be associated to radical ligand (radical-bridged bis-iron(II): 71 K)[374] or lanthanide ions such as dysprosium (Fe_2Dy : 459 K),[153] leading to high spin reversal energies, significantly higher than for **16**-UFe_2-TPA. However, the anisotropy barrier of **16**-UFe_2-TPA remains large compared to monometallic iron(II) in octahedron environment (22 K, 0.2 T)[375] as well as to large homometallic Fe(II) clusters (10-44 K).[376,377]

• **Co:** The bimetallic UCo does not exhibit SMM behaviour whereas the trimetallic assemblies under 1500G dc field show SMM behaviour with energy barriers ranging between 20 and 30 K (0.15T). The effective energy barriers of the two trimetallic assemblies differ by 10 K. The two cobalt cations are in an octahedral environment in **26**-UCo_2-TPEN while in the **21**-UCo_2-BPPA complex one Co(II) is in an octahedral environment and the second Co(II) is in a trigonal bipyramidal environment, and this may influence the value of the energy barrier. A large number of cobalt(II) based SIMs or SMMs have been reported so far, with a very broad range of activation energies (4-217 K for SIMs,[146,147,149,378] and 14-96 K for SMMs[124,379-381]). Other examples of SMMs can involve cobalt(II) associated to a radical bridge[382] or to 4f elements.[383,384] The UCo_2 systems are in the range of the lower reported values of cobalt(II) SMMs.

• **Ni:** The two UNi_2 assemblies revealed energy barriers of 32.4 K (0.1 T) and 27 K (0 T) for **18**-UNi_2-TPA and **22**-UNi_2-BPPA respectively. The difference between these two complexes may arise from the difference of the coordination environment between the two Ni(II) atoms in **18**-UNi_2-TPA and the presence of two different isomers. Compared to Fe(II) or Co(II), Ni(II) SMMs and SIMs are much less developed, even if some Ni(II) complexes display very large anisotropy values.[385] To our knowledge, only two examples of Ni(II) based SIMs (octahedral: 21 K (0.2T)[386] and trigonal bipyramidal: 28 K)[387] have been reported in the litterature. The anisotropy barrier of **22**-UNi_2-BPPA (27.4 K, 0T) is higher than for the octahedral nickel(II) SIM.[386] Moreover, it is significantly higher than the barriers reported so far for Ni(II) SMMs (4-28 K, 0.2T).[388-390]

To conclude, we can observe that the differences between the Mn, Fe, Ni and Cd series probably arise from the differences in spin states. The energy barrier is indeed proportional to the spin state and to the anisotropy. Consequently, if the energy barrier comes from the magnetic coupling between the uranyl(V) and the M(II) transition metals, we can expect a decrease of the energy barrier along with a decrease in the spin. It is effectively the tendency that we observe: Mn(II), with the highest number of spin, has the highest energy barrier under zero-applied field. The energy barrier decreases in the series Mn>Fe>Ni>Cd (Figure III- 41).

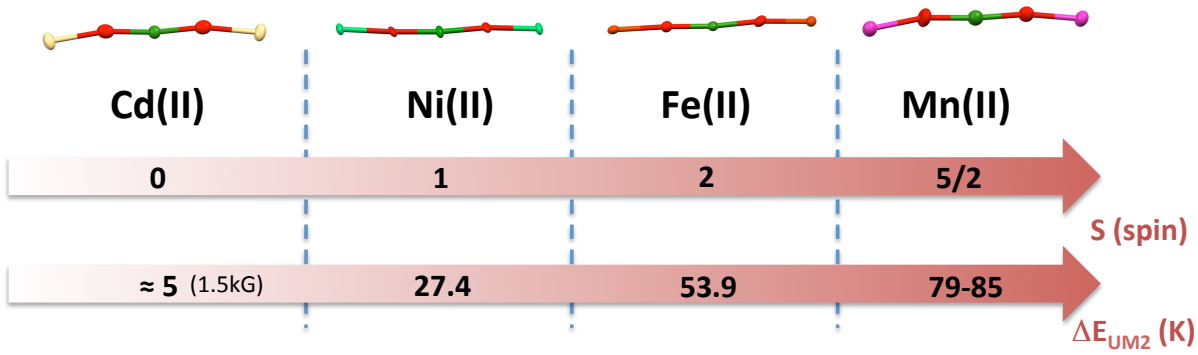

Figure III- 41 Evolution of the spin of the transition metal and the energy barriers obtained for UM_2 assemblies

The case of the cobalt is more unusual. A recent study of Chibotaru and coworkers showed that the association of two anisotropic cations may lead to a lower anisotropy barrier than the association of an anisotropic cation and an isotropic cation.[391] In the case of the association of two anisotropic cations in the **17**-UCo-TPA complex, no SMM behaviour was observed. It is plausible that the two anisotropies cancel each other out, whereas in the case of the trimetallic assemblies, the association of three anisotropies lead to a non-complete cancelation and a weak slow relaxation of the magnetisation remains. Theoretical calculations are currently being by Dr N. Chilton and Prof. L. Maron to understand these uranyl(V)-cobalt(II) systems.

III.2.2.2) Uranyl(V) and f-block metals

The magneto-structural study presented in the previous section highlights the importance of the overall spin of the transition metal and of its anisotropy in determining the behaviour of exchange coupled SMMs based on the uranium ion.

In order to obtain uranyl(V) based SMMs with improved properties we have investigated the possibility of synthesing polymetallic complexes associating uranyl(V) and lanthanide ions with high spin values. Strong magnetic exchanges between UO_2^+ and 4f ions have been indeed reported by Arnold and coworkers.[241,366] The lanthanides are mainly found in the +III oxidation state. We planned syntheses using the uranyl(V) Mesaldien complex and the Gd(III), Eu(III), Nd(III) and Dy(III) ions. Gd(III) and Eu(III) are isotropic with high-spin numbers, while the Dy(III) ion is highly anisotropic and Nd(III) is intermediate between a high spin number and high magnetic anisotropy.[143]

III.2.2.2.1) Synthesis of U_2Nd_3-TPA

As for the transition metals, we performed the reaction of $[UO_2(Mesaldien)K]_n$ with two equivalents of Ln(III) (Ln = Gd, Eu, Nd, Dy) ions coordinated to a chelating ligand to form discrete polymetallic assemblies. We perform syntheses with the TPA, BPPA and TPEN ligands as chelating ligands. However, the reaction with Eu(III) yielded the oxidation of the uranyl(V) unit into uranyl(VI), as revealed in proton NMR spectrum. The reactions of uranyl(V) with Gd(III) or Dy(III) led only to the isolation of the $\{[UO_2(Py)_5][KI_2(Py)_2]\}_n$ polymer. The polymer formation arises from ligand scrambling, occurring between the oxophilic Ln(III) ions and uranyl(V). Based on these results, we formed the bis-ligand $[Ln(BPPA)_2I]$ (Ln = Gd(III), Dy(III)) complex, hoping that this complex would be sufficiently stabilised by the two phenolate arms of the two BPPA ligands. The reaction of $[UO_2(Mesaldien)K]_n$ and two equivalents of $[Ln(BPPA)_2I]$ did not lead to ligand scrambling. Unfortunately, multiple attempts to grow X-ray quality crystals from this solution failed, preventing the characterisation of the resulting complex.

From the Ln(III) investigated, only the Nd(III) ion led to the isolation of a Nd-UO_2^+ assembly. The reaction between one equivalent of $[UO_2(Mesaldien)K]_n$ and two equivalents of $[Nd(TPA)I_3]$ did not yield a trinuclear U(V)-Nd(III)$_2$ assembly as observed with transition metals, but an unexpected pentanuclear assembly. Slow diffusion of hexane into a solution of the reaction mixture gave the $\{[Nd(TPA)(Py)I_2][UO_2(Mesaldien)][Nd(Mesaldien)][UO_2(Mesaldien)][Nd(TPA)(Py)I_2]\}I$, **27**-$U_2Nd_3$-TPA species (Figure III- 42). The difference between Nd(III) and Gd(III) or Dy(III) may arise from a smaller charge density for Nd(III), leading to lower oxophilicity.

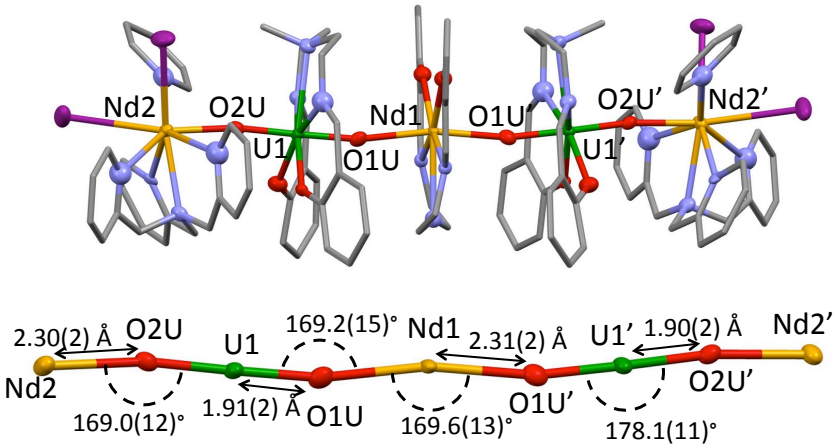

Figure III- 42 Molecular structure of **27**-U_2Nd_3-TPA (Solvent molecules, hydrogen, disorder and iodide counter-anion removed for clarity, ellipsoids: 30% probability, ligands drawn in capped sticks; Atoms: C (gray), N (light blue), O (red), I (purple), Nd (yellow), U (green))

The structure of **27**-U_2Nd_3-TPA consists of a cation-cation assembly where each oxo of the two uranyl(V) moieties are coordinated to Nd(III), forming an almost linear pentametallic core. The central $[Nd(Mesaldien)]^+$ cation bridges two $[UO_2(Mesaldien)]^-$ anions through a linear cation-cation interaction. The second oxygen of each uranyl(V) is coordinated to two $[Nd(TPA)(Py)I_2]^+$ external cations, forming a discrete pentametallic assembly. The two external Nd(III) metals in $[Nd(TPA)(Py)I_2]^+$ are eight coordinate, and each one is bound to the four nitrogen atoms of the TPA, two iodide ligands, one nitrogen atom of a pyridine and one oxygen atom of the uranyl(V), whereas the central Nd(III) in $[Nd(Mesaldien)]^+$ is seven coordinate and is bound to the two oxygen atoms of the two uranyl(V) moieties and the five donor atoms of the Mesaldien ligand. The uranium ion in $[UO_2(Mesaldien)]^-$ is also coordinated to the five donor atoms of the Mesaldien ligand coordinated in the equatorial plane while two oxygen atoms are present in the axial positions. The asymmetric unit contains only half of the pentametallic assembly as a 2-fold axis passes through the central Nd(1). The U=O bond distances lie in the range of the values observed for uranyl(V) complexes, but is slightly longer due to the CCI (U(1)-O(1U) = 1.91(2) Å, U(1)-O(2U) = 1.90(2) Å). The Nd-O_{yl} bond distances (Nd(1)-O(1U) = 2.31(2) Å and Nd(2)-O(2U) = 2.30(2) Å) are significantly shorter than in the reported uranyl(VI)–Nd(III) complex $(UO_2)_2^{Nd}(OH)(H_2O)_3(mel)$ (2.792(6) Å).[226] The Nd-N distances (mean value 2.57(3) Å) are closed in length to the ones in $[Nd(TPA)_2]I_3$ (mean value 2.59(2) Å).[392] The mean U-O-Nd and Nd-U-Nd angles are 169.12(13)° and 174.59(1)°, respectively. The mean intramolecular U-Nd distance is 4.19(2) Å whereas the intramolecular Nd-Nd distance is 8.37(1) Å.

From the 1:2 reaction of $[UO_2(Mesaldien)K]_n$ and $[Nd(TPA)I_3]$, only the **27**-U_2Nd_3-TPA product was characterised. The structure of **27**-U_2Nd_3-TPA revealed that the stoichiometry used in the reaction mixture is not correct. A partial ligand scrambling indeed occurred, as some $[Nd(Mesaldien)]^+$ is present in the structure.

Scheme III- 15 Synthesis of **27**-U_2Nd_3-TPA

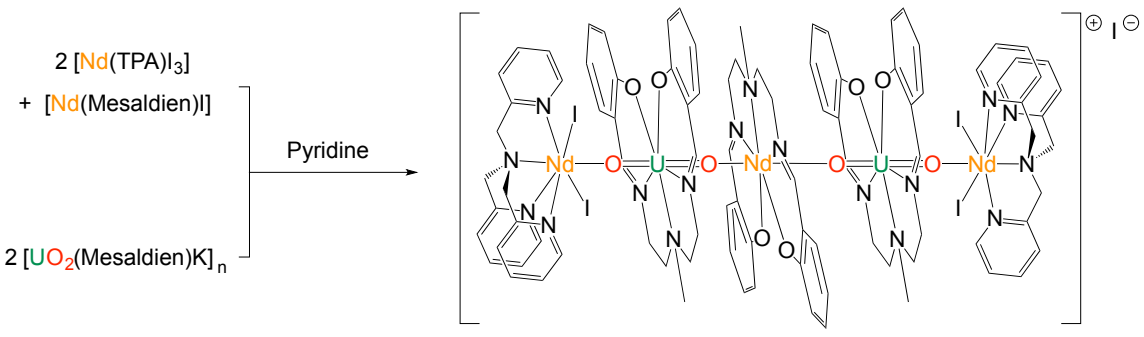

{[Nd(TPA)(Py)I_2][UO_2(Mesaldien)][Nd(Mesaldien)][UO_2(Mesaldien)][Nd(TPA)(Py)I_2]}I

The clean and reproducible synthesis of **27**-U_2Nd_3-TPA was then carried out, using the right 2/1/2 stoichiometry of $[UO_2(Mesaldien)K]_n$/[Nd(Mesaldien)I]/$[Nd(TPA)I_3]$, with the complexes of Nd(III) formed in situ in pyridine (Scheme III- 15). These two Nd(III) complexes were mixed together before being added to the uranyl(V) complex. **27**-U_2Nd_3-TPA was isolated in 84% yield thanks to the crystallisation of the reaction mixture with the right stoichiometry. ESI/MS studies revealed a complicated spectrum due to the complexity of the assembly; however, a weak peak at m/z = 3030.6 was observed, corresponding to the molecular cation $\{[Nd(TPA)I_2][UO_2(Mesaldien)][Nd(Mesaldien)][UO_2(Mesaldien)][Nd(TPA)I_2]\}^+$, demonstrating its existence in the gas phase.

III.2.2.2.2) Synthesis of UEu_2-TPEN

The strong charge of the Ln(III) ions led to ligand scrambling in the reaction mixture, making the stabilisation and isolation of a Ln(III)-uranyl(V) Mesaldien assembly particularly difficult. We then decided to investigate the reaction of $[UO_2(Mesaldien)K]_n$ with divalent lanthanide ions. The +II oxidation state of the europium is generally quite stable and it has a high spin number with a similar electronic configuration to Gd(III). We performed the reaction of $[UO_2(Mesaldien)K]_n$ with two equivalents of $[Eu(TPA)I_2]$ or [Eu(BPPA)I] or $[Eu(TPEN)I_2]$. From these three reactions, only the TPEN ligand allowed for the isolation of a polymetallic assembly.

The reaction between $[UO_2(Mesaldien)K]_n$ and two equivalents of $[Eu(TPEN)I_2]$ generated a trimetallic {[Eu(TPEN)I][UO_2(Mesaldien)][Eu(TPEN)I]}I, **28**-UEu_2-TPEN species, isolated in 91% yield (Scheme III- 16).

Scheme III- 16 Synthesis of **28**-UEu_2-TPEN

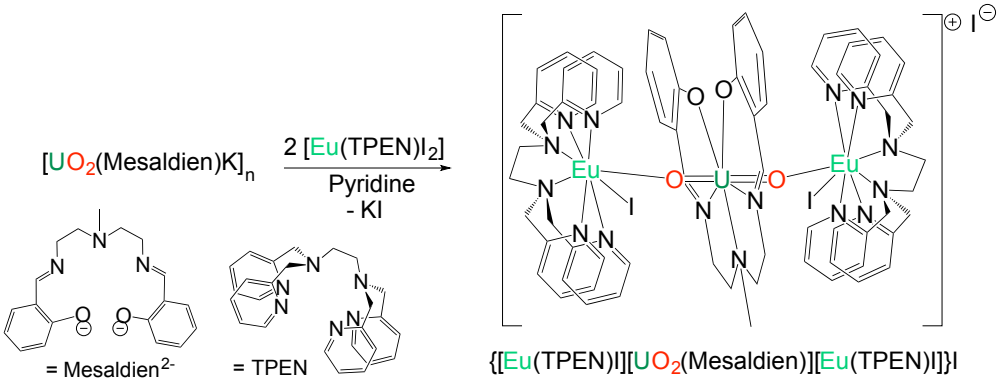

Slow diffusion of hexane into a pyridine solution containing **28**-UEu_2-TPEN afforded single crystals. The solid-state structure detrmined by X-ray diffraction studies shows a trimetallic core where each oxo group of the uranyl(V) in $[UO_2(Mesaldien)]^-$ is connected to a $[Eu(TPEN)I]^+$ cation (Figure III- 43 left). The coordination environment of Eu(II) is comprised of six nitrogen atoms of the TPEN ligand, one iodide ligand and one oxygen atom of the uranyl moiety. The mean U=O bond distance (1.905(1) Å) lies in the range of the values observed for uranyl(V) complexes but slightly longer due to the CCIs. The mean $Eu\text{-}O_{yl}$ distance (2.490(13) Å) lies in the range of Eu(II)-O bonds,[393-397] and are significantly longer than in the reported uranyl(V)–Eu(III) Pacman complex (2.200(2) Å)[244] probably due to the difference in ionic radii (0.2 Å) between Eu(II) and Eu(III). The mean $Eu\text{-}N_{amine}$ and $Eu\text{-}N_{Pyridyl}$ distances are 2.728(60) Å and 2.775(33) Å, respectively, in the range of Eu(II) complexes with tetradentate N,O-donor tripodal ligands.[397] The mean U-O-Eu and Eu-U-Eu angles are 168(1)° and 174.81(1)°, respectively. The mean intramolecular U-Eu distance is 4.37(2) Å whereas the intramolecular Eu-Eu distance is 8.730(1) Å. This assembly represents the first example of an assembly between a divalent lanthanide and uranyl(V).

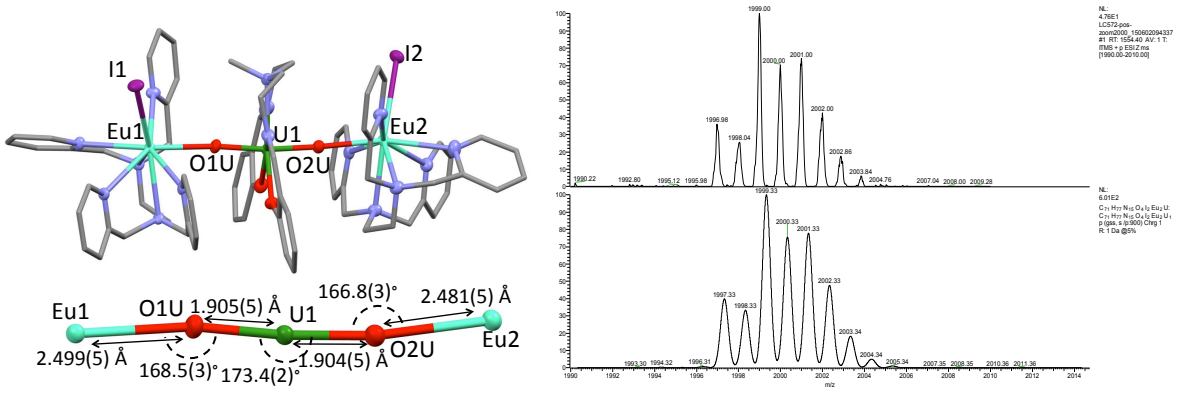

Figure III- 43 Structure of **28**-UEu_2-TPEN (left) (Solvent molecules, hydrogen and iodide counter-anion removed for clarity, ellipsoids: 30% probability, ligands drawn in capped sticks; Atoms: C (gray), N (light blue), O (red), I (purple), Eu (turquoise), U (green)) and zoom on the molecular peak (top right) compared with the theoretical isotopic (bottom right) profile calculated for $\{[Eu(TPEN)I][UO_2(Mesald)][Eu(TPEN)I]\}^+$.

ESI/MS studies revealed a peak at m/z = 1999.3 which corresponds to the molecular cation $\{[Eu(TPEN)I][UO_2(Mesaldien)][Eu(TPEN)I]\}^+$, proving its existence in the gas phase and the retention of the cation-cation interaction between uranyl(V) and Eu(II) (Figure III- 43 right).

III.2.2.2.3) Magnetic properties

Magnetic susceptibility measurements between 2-300 K in a static field were performed on polycrystalline samples of the **28**-UEu_2-TPEN and **27**-U_2Nd_3-TPA complexes (Figure III- 44). A χT value of 16.5 $cm^3.K.mol^{-1}$ and 4.4 $cm^3.K.mol^{-1}$ were obtained at 300 K for **28**-UEu_2-TPEN and **27**-U_2Nd_3-TPA, respectively. For one Eu(II) $4f^7$ ($^8S_{7/2}$, g = 2), the χT value at room temperature is expected to be 7.88 $cm^3.K.mol^{-1}$ according to the spin-orbit coupling theory.[398] The room temperature χT value of **28**-UEu_2-TPEN is then in agreement with two $4f^7$ Eu(II) ions and one uranyl(V) ion (experimental value of 0.32 cm^3 K mol^{-1} for **14**-UCd_2-TPA). Nd(III) ($^4I_{9/2}$, g_J = 8/11) has a theoretical χT value of 1.64 $cm^3.K.mol^{-1}$.[398] The room temperature value of **27**-U_2Nd_3-TPA is then smaller compared to the theoretical one expected for three Nd(III) and two U(V) but still in the range of experimental values reported.[103,398] The χT product decreases monotonically from 300 K to 2 K for **27**-U_2Nd_3-TPA, similar to Nd(III) magnetic curves due to the thermal depopulation of the excited doublets.[399] [400] [177] The χT product of **28**-UEu_2-TPEN decreases smoothly from 300 K to 20 K, after which it drops.

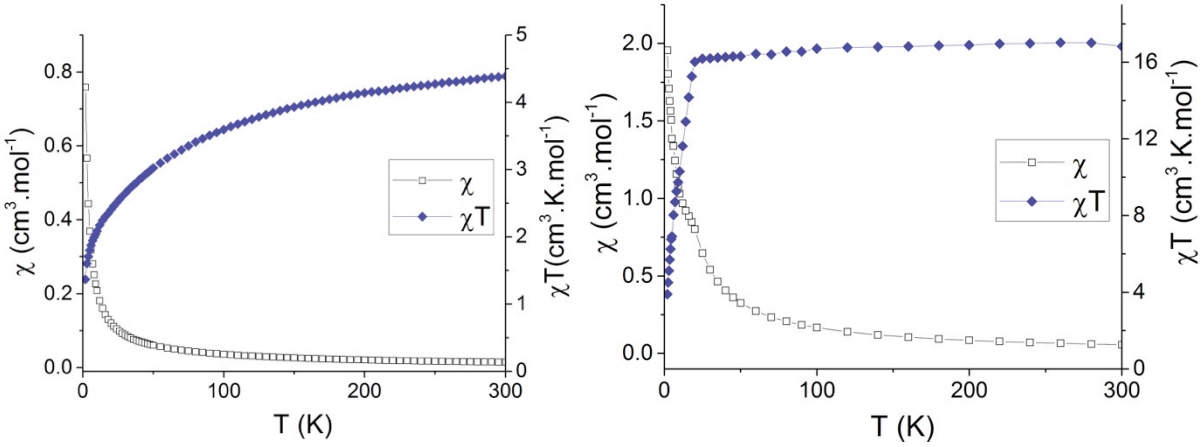

Figure III- 44 Magnetic susceptibilities **27**-U_2Nd_3-TPA (left) and **28**-UEu_2-TPEN (right) measured in field-cooled regime at magnetic fields of 0.5 T.

An ac field was then applied to investigate the dynamic magnetic properties. Unfortunately, even with the application of a dc field (Figure III- 45), no frequency dependent out-of-phase susceptibility was observed. Associated with the absence of difference in field cooled and zero field cooled or open hysteresis loops, the presence of SMM behaviour was ruled out for these two 4f-5f complexes.

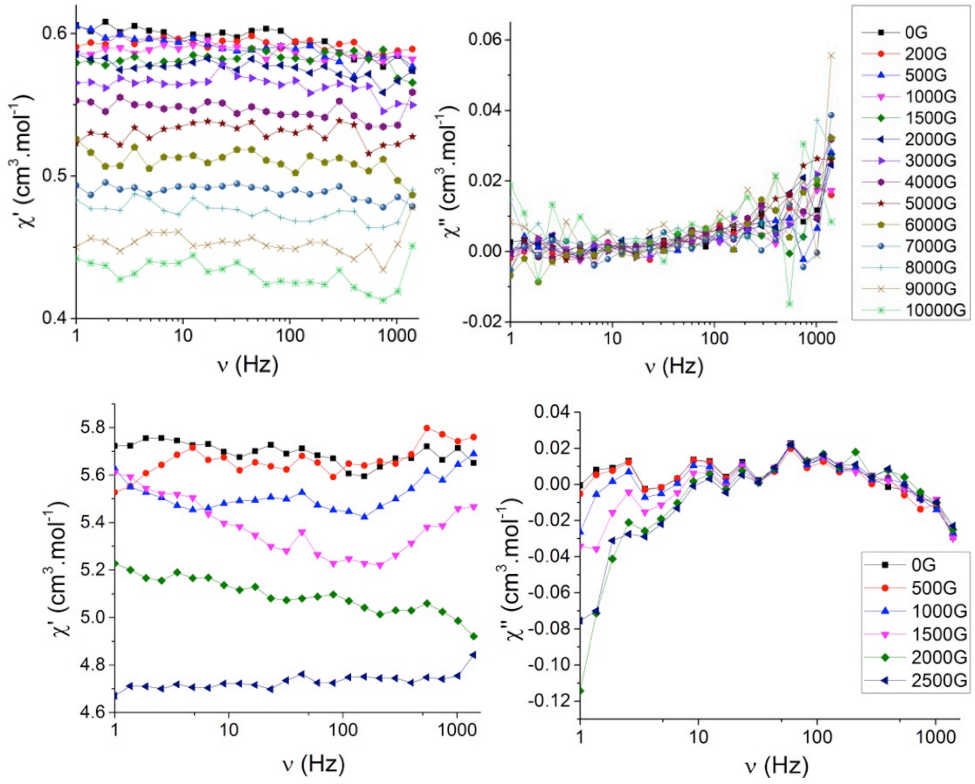

Figure III- 45 Frequency dependence of the (left) in-phase and (right) out-of-phase ac susceptibility components of **27**-U_2Nd_3-TPA (top) and **28**-UEu_2-TPEN (bottom) recorded at 1.8 K and 1.55 Oe ac field oscillating at frequencies between 1 and 1400 Hz under several static dc fields.

No unambiguous magnetic coupling between U(V) and Nd(III) or Eu(II) was observed in **27**-U_2Nd_3-TPA or **28**-UEu_2-TPEN. This result is surprising since the group of Arnold reported a possible magnetic exchange between U(V) and 4f ions through a CCI.[241,244] The Sm-O_{yl} bond distance in $[UO_2Sm(Py)_2(Pcm)]_2$ is 2.238(5) Å,[241] shorter than in **27**-U_2Nd_3-TPA (mean Nd-O_{yl} 2.305(7) Å) or **28**-UEu_2-TPEN (mean Eu-O_{yl} 2.490(13) Å). This difference could correspond to the difference in ionic radii between Nd(III) and Sm(III) but does not reveal a significantly stronger interaction. We can however notice that the 4f-5f interaction reported in $[UO_2Sm(Py)_2(Pcm)]_2$ is the only unambiguous example of an entire isostructural series with other Ln(III) ions. This observation reveals the complexity of the Ln(III) magnetic interactions with other metallic centres.

III.2.3) Stability of uranyl(V) with the salfen ligand: preliminary studies

In order to extend our work on heterometallic assemblies based on uranyl(V), we decide to explore the use of a new ligand to coordinate to the equatorial plane of the uranyl(V). We have indeed observed previously that the use of Mesaldien ligand induced structural changes in the formation of Mn(II)-uranyl(V) polymeric complexes compared to the salen ligand. In order to promote the formation of polymetallic assemblies with different geometries, we investigated the use of another Schiff base ligand with a different geometry.

The stabilisation of the uranyl(V) is very affected by the nature of the coordinated ligand in the equatorial plane. In our group, work with ONNO tetradentate dianionic diimine bis(tertbutyl-phenolate) ligands has shown that uranyl(V) can be stabilised with respect to disproportionation.[52,53] The use of non-bulky Schiff base ligands leads to different behaviours, depending on the presence of cations and the nature of the bridge. In the absence of cations, the uranyl(V) complexes with salen, containing a very flexible bridge, or salophen, containing a rigid bridge, are stable.[48] However, in the presence of cations (alkali, alkali-earth, Mn(II), Cd(II) metals), the uranyl(V) salen complex is stable and forms stable CC assemblies with various geometries,[48,180,231] while the uranyl(V) salophen complex disproportionates.[48] Only the presence of 18c6 to coordinate potassium cations has allowed for the isolation of a stable CC intermediate with salophen ligand.

We decide to investigate the coordination of Schiff base ligands containing a 1,1'-ferrocenyl bridge to the uranyl(V) group. The two ligands that we used are represented in Figure III- 46, and are called "salfen". The 1,1'-ferrocenyl fragment will lead to a different geometry than the ethyl or phenyl bridges respectively found in the salen and salophen ligands. These ligands have been poorly studied. Only four publications describe coordination chemistry studies of these ligands with Mg(II), Ti(IV), Zr(IV),[401], Y(III), Ce(III), Ce(IV),[402,403] and In(III).[404] The designed ONNO cavity is flexible and big enough to bind a uranium atom and should provide a different electronic and steric environment compared to salen and salophen.

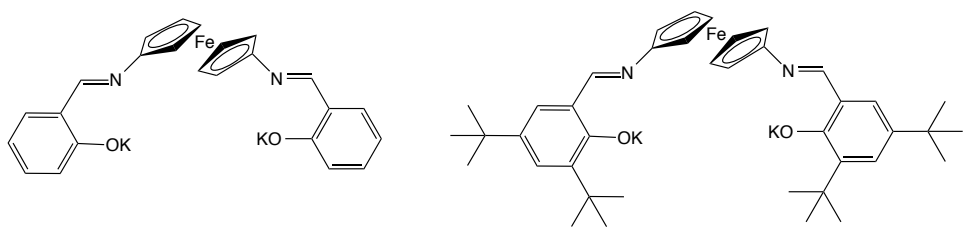

Figure III- 46 K_2salfen (left) and K_2salfen-^{t}Bu (right) ligands

Preliminary studies of salfen ligands with uranyl(V), the formation of heterometallic assemblies based on uranyl(V) with these ligands have not been explored yet.

III.2.3.1) Syntheses

The reaction of the pentavalent uranyl precursor $\{[UO_2(Py)_5][KI_2(Py)_2]\}_n$ with K_2salfen in pyridine led to complete disproportionation after 12 hours (Scheme III- 17). In the final reaction mixture, we identified the presence of the $[U^{IV}(salfen)_2]$ and $[U^{VI}O_2(salfen)]$ complexes after formation of a transient uranyl(V) species. This uranyl(V) complex has not been isolated. This behaviour is similar to the reactivity found for the reaction between $\{[UO_2(Py)_5][KI_2(Py)_2]\}_n$ and K_2salophen.[48] However, with the salophen ligand, a CC intermediate was successfully isolated with the presence of 18c6 in the reaction mixture. Similar experiments were carried out with the salfen ligand. 3.2 equivalents of 18c6 were mixed with K_2salfen in pyridine before addition to the uranyl(V) precursor, but the uranyl(V) salfen complex still disproportionated. However, the disproportionation was slower in the presence of 18c6 and complete in 24 h (Figure III- 47).

Scheme III- 17 Reaction of uranyl(V) polymer and salfen ligand yielding disproportionation products

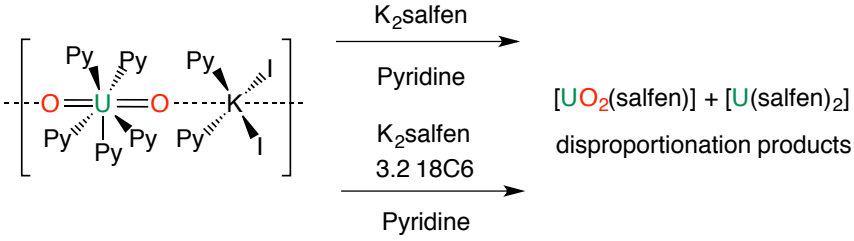

ESI/MS studies of a fresh solution containing "$[UO_2(salfen)](K18c6)$" were performed. No signal with a high m/z ratio corresponding to a polymetallic species was observed. However, a peak at m/z = 732 could correspond to a monometallic complex of U(V) $[U^{V}O_2(salfen)K]H^+$ (Figure III- 48).

Despite numerous crystallisation trials and the addition of 18c6 to stabilise the uranyl(V) complex, no intermediate product of the disproportionation was crystallised. Further investigations will be carried out to study the influence of the nature of the cation and the presence of [2.2.2]-cryptand on the stability of the uranyl(V) salfen complex.

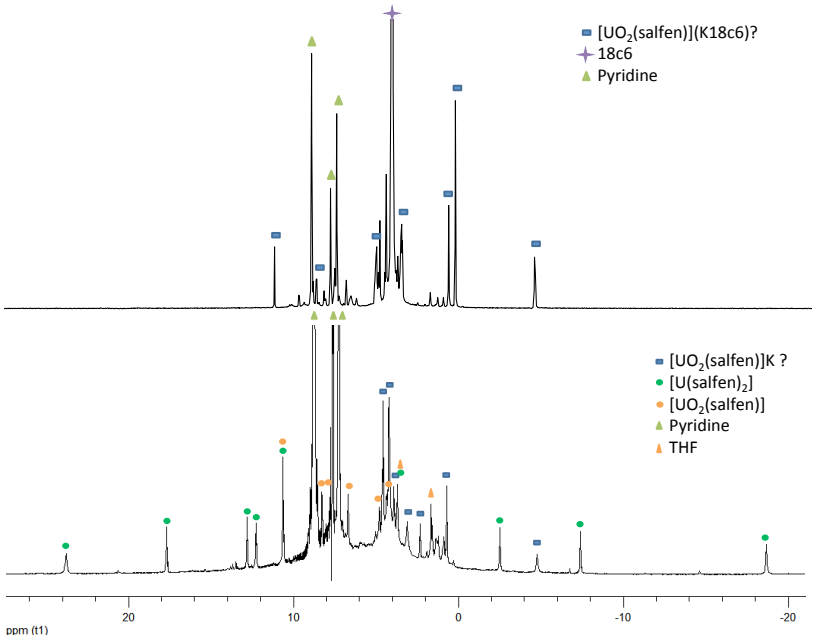

Figure III- 47 ^{1}H NMR spectra (200 MHz, Py-d_5, 298 K) of the crude reaction mixture of $\{[UO_2(Py)_5][KI_2(Py)_2]\}_n$ with one equivalent of K_2salfen after 15 minutes (bottom) and in presence of 3.2 equivalents of 18c6 after 15minutes (top).

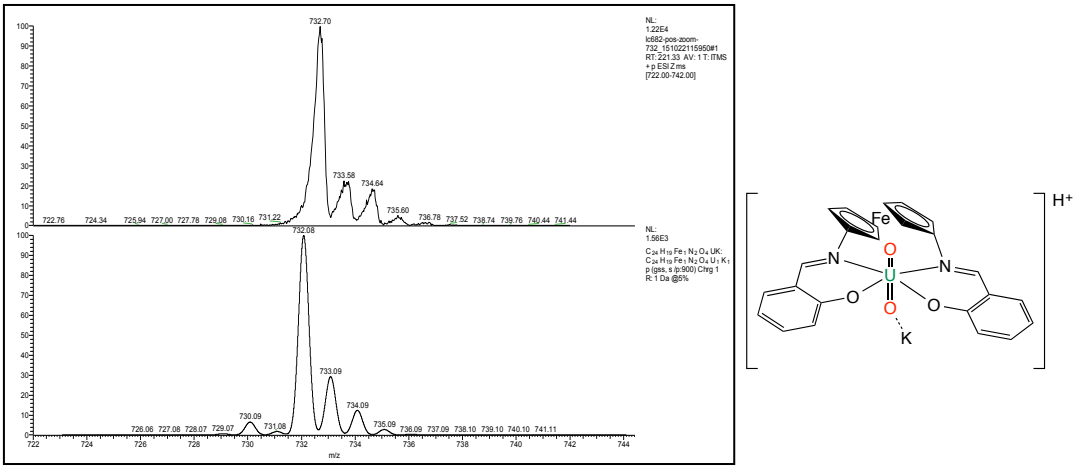

Figure III- 48 Zoom of the peak at m/z=732 (top) and the fit with the formula of the cation $[U^{V}O_2(salfen)K]H^{+}$ (bottom).

As discussed in the introduction chapter, bulky substituents on a polydentate Schiff base ligand can be used to stabilise uranyl(V) with respect to the disproportionation reaction, preventing the formation of CC complexes.[48,53] Therefore the reaction between the uranyl(V) precursor and the bulkier K_2salfen-$^{t}Bu_2$ ligand was carried out.

In contrast to the reaction with K_2salfen, the reaction of the bulky K_2salfen-$^{t}Bu_2$ ligand and $\{[UO_2(Py)_5][KI_2(Py)_2]\}_n$ in pyridine yielded a stable uranyl(V) complex (Scheme III- 18). Attempts to obtain single crystals of the $[UO_2$(salfen-$^{t}Bu_2)K]$ complex from pyridine/hexane failed due to the low stability of the complex in hexane (similar instability has been observed

for salophen-^{t}Bu). Slow diffusion of hexane into a pyridine solution of [UO_2(salfen-$^{t}Bu_2$)K] generated crystals of [$U^{VI}O_2$(salfen-$^{t}Bu_2$)], **29** (Figure III- 49). X-ray quality crystals of the uranyl(V) complex [UO_2(salfen-$^{t}Bu_2$)(K18c6)], **30** were obtained from toluene (Figure III- 50). The uranyl(VI) [$U^{VI}O_2$(salfen-$^{t}Bu_2$)], **29** complex was also independently synthesised by a salt metathesis reaction between K_2salfen-$^{t}Bu_2$ and [$UO_2I_2(Py)_3$] in pyridine.

Scheme III- 18 Reaction of uranyl(V) polymer and salfen-^{t}Bu ligand yielding a stable uranyl(V) complex

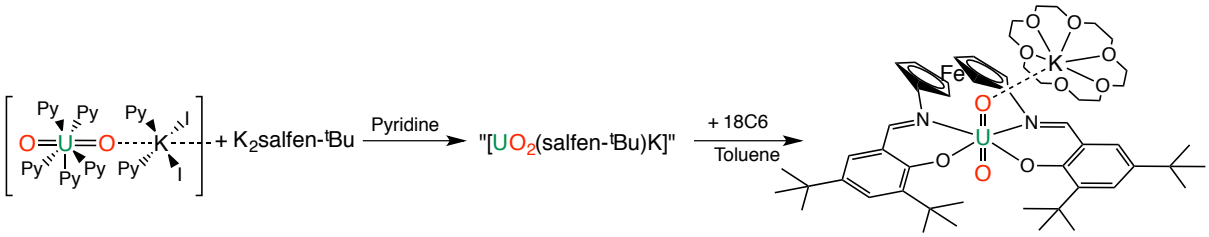

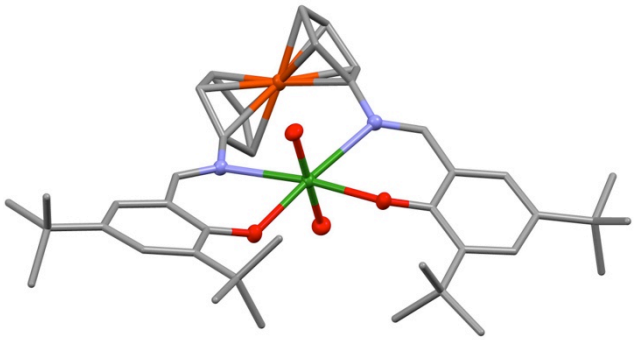

Figure III- 49 Molecular structure of [UO_2(salfen-$^{t}Bu_2$)], **29** (Hydrogen and solvent are omitted for clarity; Atoms: carbon grey, nitrogen light blue, oxygen red, iron orange, uranium green).

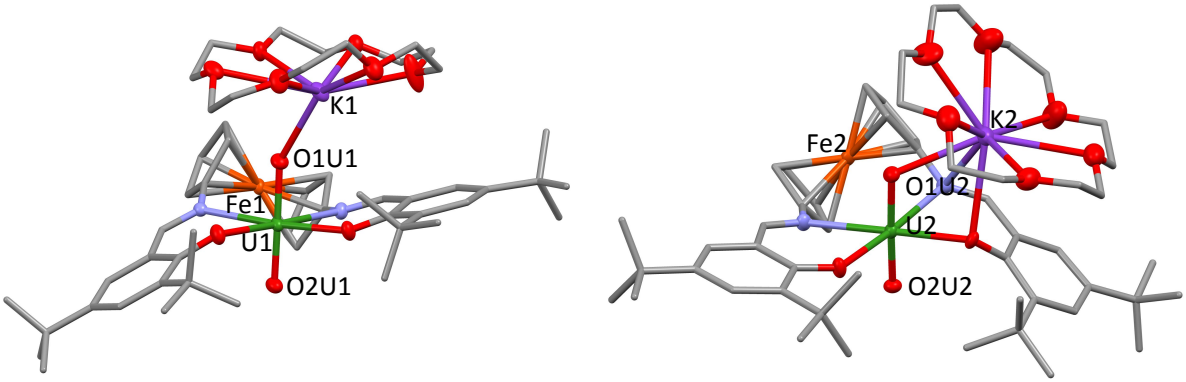

Figure III- 50 Molecular structures of the two complexes U1 and U2 present in the asymmetric unit of [UO_2(salfen-$^{t}Bu_2$)(K18c6)], **30** (Hydrogen and solvent are omitted for clarity; Atoms: carbon grey, nitrogen light blue, oxygen red, potassium purple, iron orange, uranium green).

The uranium centres in [UO_2(salfen-^{t}Bu_2)(K18c6)], **30** and in [UO_2(salfen-^{t}Bu_2)], **29** are hexacoordinated in a square bipyramidal coordination geometry with two oxygen and two nitrogen atoms of the salfen-^{t}Bu_2 ligand in the equatorial plane and two oxygen atoms in axial positions. The U(V)=O distances range between 1.831(4) and 1.864(4) Å, and these are significantly longer than those found in the uranyl(VI) complex (1.778(3) Å). These distances are in the range of those found in previously reported complexes of uranyl(V).[27,53,55,231,242] The solid-state crystal structures of **30** revealed two complexes in the asymmetric unit (Figure III-50). In both complexes of **30**, the $[K(18c6)]^+$ counter cation binds one oxo group of the uranyl group through a cation-cation interaction. In the U2 complex, the potassium ion also interacts with a phenolate oxygen (K-O =2.941(4) Å) and an imino nitrogen (3.327(5) Å) from the Schiff base, probably explaining the weaker K-O(1U2) interaction (K–O(1U1) : 2.568(4) Å, 0.2 Å smaller than K-O(1U2) : 2.792(4) Å). The presence of a stronger interaction of the ligand with the UO_2^{2+} cation resulted in metal-ligand distances that are 0.1 Å shorter than in the uranyl(V) complex (mean distances: U-O 2.221(3) Å, U-N 2.460(3) Å in **29** and U-O 2.31(1) Å, U-N 2.54(1) Å in **30**). Consequently, the value of the distance between the uranium and iron atoms in complex **30** (mean value 3.876(1) Å) is longer than the one in the hexavalent complex (3.708(1) Å). The Fe-U distances (mean U^V-Fe: 3.8755(1) Å and U^{VI}-Fe: 3.708(1) Å) are much longer than the one in the diamide U(IV) complexes [fc(NSi^t$BuMe_2$)$_2$U(CH_2Ph)$_2$] and [fc($NSiMe_2Ph$)$_2$U(CH_2Ph)$_2$] (3.1878(5) Å and 3.1874(4) Å, respectively) in which DFT calculations postulated a weak interaction between Fe(II) and U(IV).[405,406]

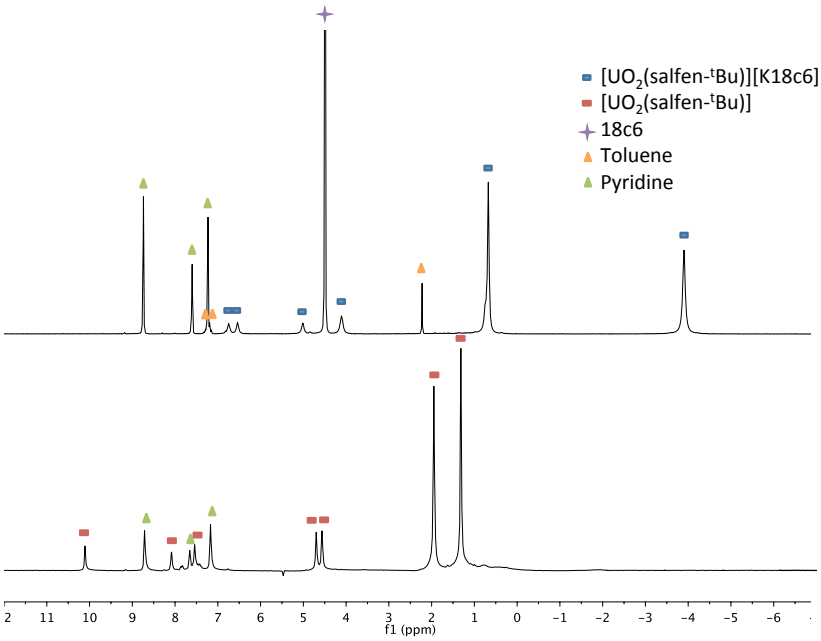

Figure III- 51 ^{1}H NMR spectra (200 MHz, Py-d_5, 298 K) of [UO_2(salfen-^{t}Bu_2)], **29** (bottom) and [UO_2(salfen-^{t}Bu_2)(K18c6)], **30** (top).

Mass spectrometry studies of solutions of [UO_2(salfen-^{t}Bu$_2$)], **29** and [UO_2(salfen-^{t}Bu$_2$)(K18c6)], **30** show peaks at m/z = 955.3 and m/z = 1522.2, attributed to [UO_2(salfen-^{t}Bu$_2$)]K^+ and [UO_2(salfen-^{t}Bu$_2$)(K18c6)](K18c6)$^+$, respectively. Bands at 891 cm^{-1} and 768 cm^{-1} in the infrared spectra of the respective solids **29** and **30** were assigned to the asymmetric UO_2^{2+} or UO_2^+ stretching modes. The shift to higher wavenumber for the hexavalent species is in agreement with a stronger U=O bond.

The ^{1}H NMR spectrum recorded for a pyridine solution of [UO_2(salfen-^{t}Bu$_2$)], **29** features 7 resonances in the diamagnetic region (Figure III- 51). This observation is in agreement with the presence of a f^0 uranyl(VI) complex and one low-spin Fe(II) centre. In comparison, the ^{1}H NMR spectrum of [UO_2(salfen-^{t}Bu$_2$)(K18c6)], **30** shows the presence of 7 paramagnetically shifted signals, between 6.83 ppm and -3.87 ppm in pyridine, in agreement with the presence of uranyl(V) C_{2v} symmetric solution species (Figure III- 51).

III.2.3.2) Electronic and magnetic properties

To further characterise the uranyl complexes, variable-temperature (2-300 K) dc magnetic susceptibility measurements were collected in the temperature range of 2-300 K on solid samples of [UO_2(salfen-^{t}Bu$_2$)(K18c6)], **30** and [UO_2(salfen-^{t}Bu$_2$)], **29**. A negative magnetic susceptibility (χ = -4.62.10^{-3} $cm^3.mol^{-1}$ at 300 K) was measured for **29**, in agreement with the presence of a low-spin Fe(II) and a diamagnetic UO_2^{2+}. At 300 K, **30** displays an effective magnetic moment per uranium of 2.09 μ_B (χT(300 K)= 0.55 $cm^3.mol^{-1}$) (Figure III- 52 left). This value is significantly reduced with respect to the theoretical one calculated for the free-ion value in the L-S coupling scheme (μ_{eff} = 2.54 μ_B), probably as a result of by the combined effect of ligand field and spin-orbit coupling,[53,407] but is still within the range of values reported for U^V compounds (1.42-2.57 μ_B).[103]

Cyclovoltammetric studies of salfen-^{t}Bu complexes were carried out to gain more insights into the redox properties of these heterometallic complexes, as they possess three different types of redox-active centres: the uranium cation, the Fe(II) centre of the ferrocene units and the imino moieties of the supporting ligand. The compound [UO_2(salfen-^{t}Bu$_2$)(K18c6)], **30** exhibits a reversible event at $E_{1/2}$ = -1.61 V (Figure III- 52 right). The [UO_2(salfen-^{t}Bu$_2$)], **29** complex displays the same reversible wave in the same conditions. This redox event was attributed to the U(VI)/U(V) couple, and is very similar to that reported for [UO_2(salophen-^{t}Bu$_2$)(Py)K].[53] This indicates that the degree of stabilisation of the uranyl(V) cation is similar in both systems. An irreversible oxidation wave is additionally

observed around 0.57 V with a shoulder at 0.34 V that can reasonably be assigned to the oxidation of the ligand ferrocene moiety.

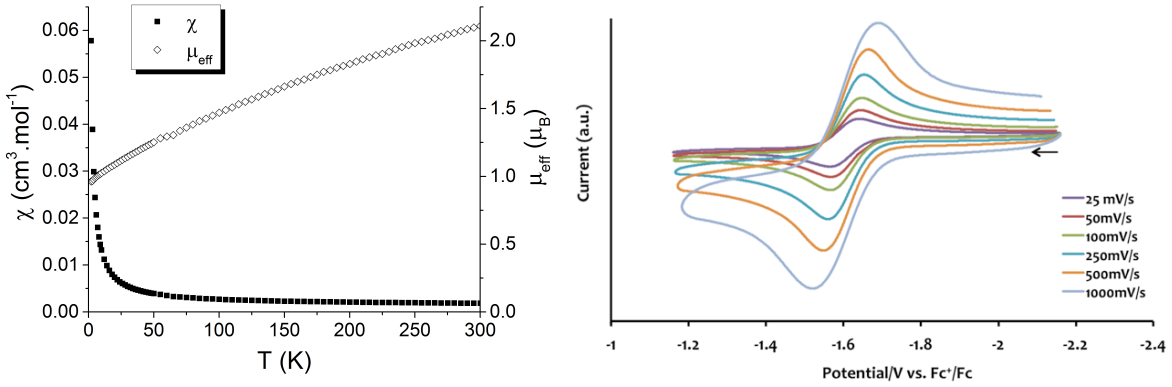

Figure III- 52 Temperature-dependent effective magnetic moment recorded for $[UO_2(salfen\text{-}^tBu_2)(K18c6)]$, **30** recorded in the range 2–300 K (left) and room temperature cyclic voltammogram for a 2 mM solution of $[UO_2(salfen\text{-}^tBu_2)(K18c6)]$, **30** recorded in 0.1 M $[Bu_4N][PF_6]$ pyridine solution at various scan rates (25 to 1000 mV/s) (redox potential are versu $[(C_5H_5)_2Fe]^{+/0}$)(right).

A stable uranyl(V) complex was synthesised using salfen-^{t}Bu, a ligand containing a 1,1'-ferrocenyl fragment, while uranyl(V) salfen disproportionates even in the presence of 18c6. Further studies will be performed with the non-bulky salfen ligand to explore the stability of the uranyl(V) complex in absence of cation or in presence of different cation than potassium. The stable uranyl(V) salfen-^{t}Bu complex will be used in the future as a building block for CC assemblies with transition metals.

III.3) Polymetallic complexes of neptunyl(V)

I spent two months at the CEA Marcoule in the LN1 laboratory of Atalante. This laboratory has all the facilities to handle highly radioactive actinides in low-pressure gloveboxes. One Schlenk line was installed inside one of the gloveboxes, allowing for the handling of transuranic elements under inert atmosphere.

Work with pentavalent neptunyl was carried out in order to probe similarities between the UO_2^+ and the NpO_2^+ moieties. Firstly, studies with transition metals and neptunyl(V) were performed in order to synthesise heteropolymetallic assemblies based on cation-cation interactions. In an attempt to synthesise an analogous neptunyl(V) polymer of **10**-$\{UO_2(salen)Mn\}_n$, we added $Mn^{II}(NO_3)_2$ to the neptunyl(V) salen complex formed from the

reaction of the NpO_2^+ precursor $\{[NpO_2(Py)_5][KI_2(Py)_2]\}_n$ with salenK_2 in pyridine. However, from this reaction mixture, X-ray quality crystals of the manganese(III) $[Mn(salen)(Py)_2]I$ complex were isolated. Surprisingly, during this reaction, ligand scrambling and a redox reaction occurred. Based on the redox potential in aqueous solution of the Mn^{3+}/Mn^{2+} couple (1.51 V vs. SHE) and the NpO_2^+/Np^{4+} couple (0.604 V vs. SHE),[9] the reaction of Mn(II) with neptunyl(V) should not lead to the reduction of neptunyl(V) in aqueous solution. However a recent study performed under environmental conditions showed that microbially-mediated Mn reduction can lead to reductive immobilisation of Np(V) to Np(IV) under anaerobic conditions.[408] Based on this result, we investigated the reaction of neptunyl(V) Mesaldien complexes with Mn(III) or Fe(III) TPA complexes to form analogous UM_2-TPA assemblies. Electronic absorption spectroscopy revealed that the neptunyl(V) was not reduced, however, every crystallisation attempt failed.

In parallel, the synthesis of homometallic assemblies using the monoanionic tetradentate aza β-diketiminate ligand, LK (L=2-(4-Tolyl)-1,3- bis(quinolyl)malondiiminate) was carried out.

III.3.1) Synthesis of homo-trimetallic neptunyl(V) complex

The reaction of the NpO_2^+ precursor $\{[NpO_2(Py)_5][KI_2(Py)_2]\}_n$,[51] with the potassium salt of LK in pyridine did not lead to the immediate formation of an insoluble complex as for the pentavalent uranyl $[UO_2L]_3$,[242] but to a red solution from which a red solid of $[NpO_2L]_3$, **31** precipitates overnight (Scheme III- 19). Recrystallisation of the red solid from acetonitrile led to single crystals, which were analysed by X-ray diffraction.

Scheme III- 19 Synthesis of $[NpO_2L]_3$, **31**

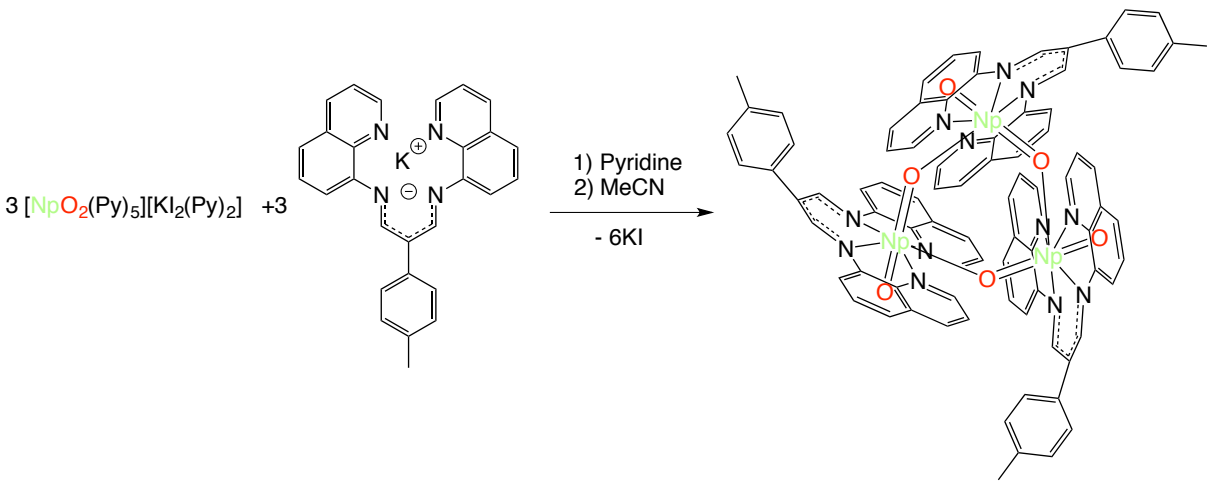

The crystal structure of $[NpO_2L]_3$, **31** is presented in Figure III- 53. It consists of a trimeric unit containing three neptunyl moieties coordinated to each other through CCI to form an equilateral triangle. A six-fold inversion axis is located in the centre of the equilateral triangle and a mirror plane passes through the three O=Np=O entities in the plane defined by the neptunyl(V) moieties. Consequently, the asymmetric unit contains half of a $[NpO_2L]$ unit. This trimeric structure is equivalent to the one of uranyl(V) with the same ligand $[UO_2L]_3$ presented in section III.1.3).[242] Similar triangular geometries have been reported, but in extended neptunyl(V) networks: $\{Cs[NpO_2(C_2O_4)_2]\}_3$,[409] $\{NH_4[(NpO_2)_3(C_2H_5COO)_4(H_2O)]\}$,[409] $(NH_4)_3[(NpO_2)_5\{C_6H_2(COO)_4\}_2]$ [410] and $[La(H_2O)_6][(NpO_2)_3(NO_3)_6]$ in which the ligands act as bridging ligands between two Np ions of different triangles.[211]

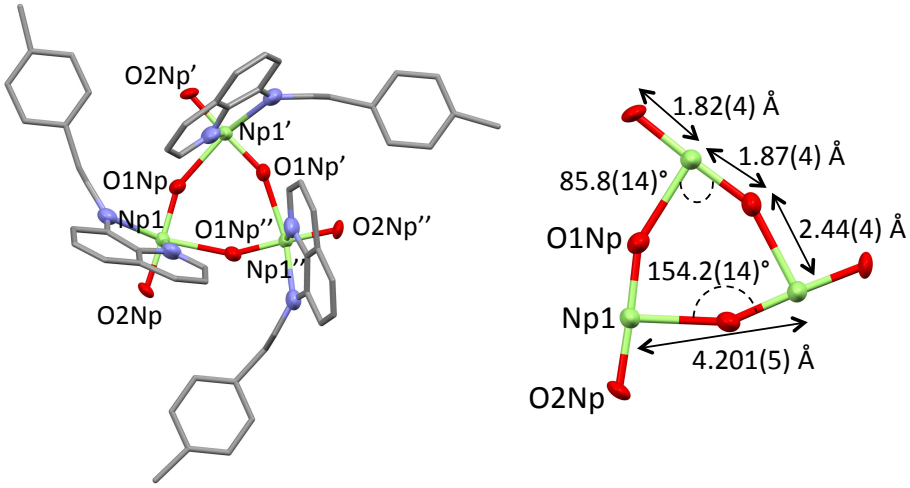

Figure III- 53 Molecular structure of $[NpO_2L]_3$, **31** (left) and its core with structural parameters (right). Ligand represented in pipes and hydrogen atom removed for clarity. Atoms: C grey, N blue, O red, Np light green.

The neptunium atom in $[NpO_2L]$ unit has a pentagonal bipyramidal coordination geometry with the four nitrogen atoms from the aza β-diketiminate ligand (Np-$N_{diketiminate}$=2.65(5) Å; Np-$N_{quinoline}$=2.57(4) Å) and the two oxygen atoms of the neptunyl. The neptunyl group remains nearly linear (O-Np-O angle 177.6(13)°) with terminal neptunyl bond distances (Np-O(2Np) distance 1.82(4) Å) shorter than the bridging neptunyl bonds (Np-O(1Np)=1.87(4) Å). These Np=O bond distances are in the range of the Np=O bonds involved in the CCI (1.832-1.877 Å) and to the unbound oxygen (1.804-1.8343 Å) found in the previous CC complexes.[211,239,409-411] A mean difference of 0.05 Å is found between the bound and unbound oxygen of the neptunyl(V) unit. This desymmetrisation of the neptunyl(V) moiety is common in CC complexes and is in the range of previous reported NpO_2^+

CCI.[181,211,239] A desymmetrisation of 0.08 Å of the uranyl(V) moieties was found in $[UO_2L]_3$, suggesting the presence of a weaker CCI in **31**.[242] The Np-(O=Np) bond distance of **31** (2.44(3) Å) is in the range of values reported in other triangular units (2.369(12)-2.485(13) Å).[409-411] Np-O-Np angle is 154.2(14)° in the **31** triangle, considerably larger than the Np-O-Np angles found in the other triangular units contained in extendred networks (range 136.5(7)-148.5(1)°). As a result of the larger Np-O-Np angle in **31**, the Np-Np sides are 4.201(5) Å long, longer than the Np-Np distances found in $\{Cs[NpO_2(C_2O_4)_2]\}_3$ (4.093(1)-4.102(1) Å),[409] $\{NH_4[(NpO_2)_3(C_2H_5COO)_4(H_2O)]\}$ (4.019(1)-4.154(2) Å)[411] and $(NH_4)_3[(NpO_2)_5\{C_6H_2(COO)_4\}_2]$ (4.080(53)Å).[410] The mean Np-Np distance (4.201(5) Å) in the **31** triangle is intermediate between the one found in the diamond-shaped $(NpO_2)_2$ cores found in the dinuclear $[(NpO_2)_2(C_6H_4F(COO))_2(bipy)_2]$ complex (3.438(3) Å)[236] and the one in the T-shaped cores of the $[\{NpO_2(salen)\}_4(\mu_8\text{-}K)_2][K(18c6)(Py)]_2$ complex (4.336 Å).[239]

The presence of the potassium counterion in $[\{NpO_2(salen)\}_4(\mu_8\text{-}K)_2][K(18c6)(Py)]_2$ results in the formation of a CC assemblies in a square shape with potassium cations linked to the oxo groups of the neptunyl(V) while the absence of potassium leads to the triangular structure $[NpO_2L]_3$, **31**. In these two systems, the geometries of the structures obtained with neptunyl(V) are analogous to the complexes with uranyl(V).

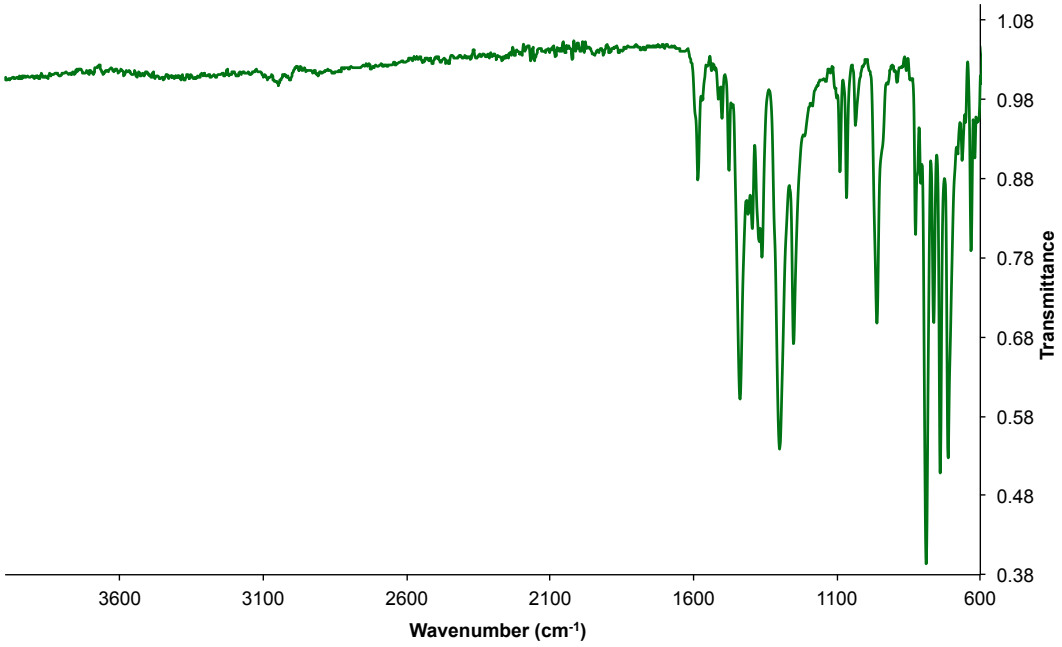

Figure III- 54 IR spectrum of the crystals of $[NpO_2L]_3$, **31** obtained from MeCN solution

The FTIR spectrum performed on a solid sample of recrystallised $[NpO_2L]_3$, **31** in anhydrous acetonitrile does not show the characteristic band of the O-H bond, demonstrating the absence of water in the solid state (Figure III- 54). It reveals the distinctive features of neptunyl compounds containing cation-cation interactions, with a broad vibrational band at 788 cm^{-1} assigned to the asymmetric vibrations of the neptunyl moiety in the trimeric core. This value is closed to the one reported at 775 cm^{-1} for the asymmetric vibrations of the neptunyl(V) in $[\{NpO_2(salen)\}_4(\mu_8\text{-}K)_2][K(18c6)(Py)]_2$.[239] It is however lower than the unique and intense band at 806 cm^{-1} found in $\{[NpO_2(Py)_5][KI_2(Py)_2]\}_n$.[51] This indicates a weakening of the neptunyl bond in the trimer compared to the pentapyridine neptunyl(V) precursor, as a result of the NpO_2^+---NpO_2^+ interaction. However, the Np=O bond remains stronger than in the tetrameric $[\{NpO_2(salen)\}_4(\mu_8\text{-}K)_2][K(18c6)(Py)]_2$ species, suggesting a weaker NpO_2^+---NpO_2^+ CCI interaction in the trimeric complex compared to the tetrameric one. This result could not be anticipated with respect to the structural parameters, as a similar desymmetrisation of 0.05 Å was observed for neptunyl(V) in both $[NpO_2L]_3$ and $[\{NpO_2(salen)\}_4(\mu_8\text{-}K)_2][K(18c6)(Py)]_2$ structures.

III.3.2) Magnetic properties of $[NpO_2L]_3$ and of $[\{NpO_2(salen)\}_4(\mu_8\text{-}K)_2][K(18c6)(Py)]_2$

dc magnetic susceptibility measurements between 2-300 K were performed on polycrystalline samples of $[NpO_2L]_3$, **31** and of $[\{NpO_2(salen)\}_4(\mu_8\text{-}K)_2][K(18c6)(Py)]_2$ [239] in ITU Karlsruhe (Figure III- 55).

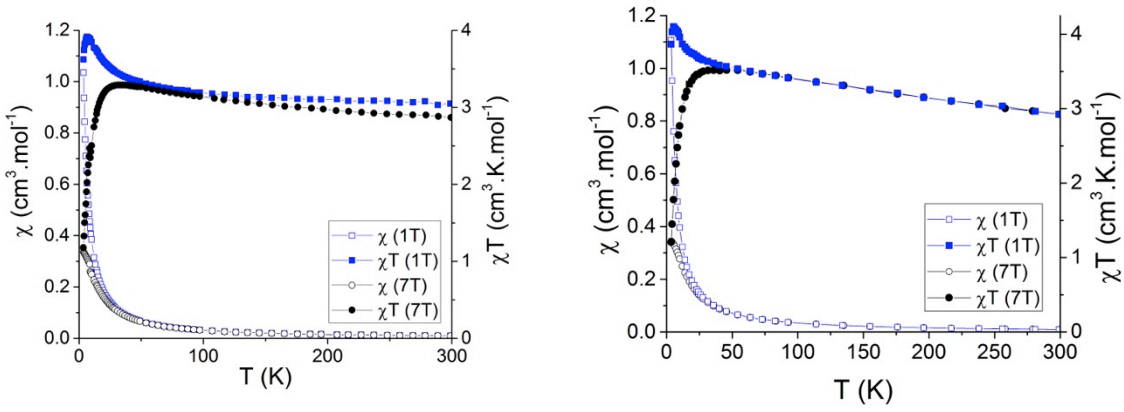

Figure III- 55 Magnetic susceptibilities of trimer $[NpO_2L]_3$, **31** (left) and tetramer $[\{NpO_2(salen)\}_4(\mu_8\text{-}K)_2][K(18c6)(Py)]_2$ (right) measured in field-cooled regime at magnetic fields of 1 and 7 T.

The χT value at room temperature in the spin-orbit coupling scheme of Np(V) $5f^2$ ($^3H_4$, g=4/5), is expected to be 1.60 $cm^3.K.mol^{-1}$, associated with a magnetic moment of 3.58 μ_B. However, the room temperature χT products of $[NpO_2L]_3$, **31** and $[\{NpO_2(salen)\}_4(\mu_8\text{-}K)_2][K(18c6)(Py)]_2$ are 3 $cm^3.K.mol^{-1}$ (2.83 μ_B per Np centre) and 2.9 $cm^3.K.mol^{-1}$ (2.45 μ_B per Np centre), respectively, much lower than the theoretical values, although these magnetic moments still lie in the range of values reported so far for neptunyl(V) molecular complexes or materials.[113,114,412] In both cases, the χT product at 1 T increases smoothly from 300 K before reaching a maximum around 6 K and then drops, whereas the maxima are not present at 7 T and a downturn occurs after 28 K. The 1/ χ versus T data are linear in the range 50-300 K for both complexes. This allows a Curie-Weiss fitting (χ = C/(T-T_c)). Parameters per neptunium obtained from the linear fit of 1/ χ versus T are C = 1.0 $cm^3.K.mol^{-1}$, T_c =5.6 K for **31** and C = 0.71 $cm^3.K.mol^{-1}$, T_c =15.5 K for $[\{NpO_2(salen)\}_4(\mu_8\text{-}K)_2][K(18c6)(Py)]_2$. These positive temperatures obtained from the Curie-Weiss fits suggest a ferromagnetic interaction between neptunium ions quite often encountered in neptunyl(V) CC complexes or materials.[114,412] However, non-open hysteresis cycles were measured for both complexes.

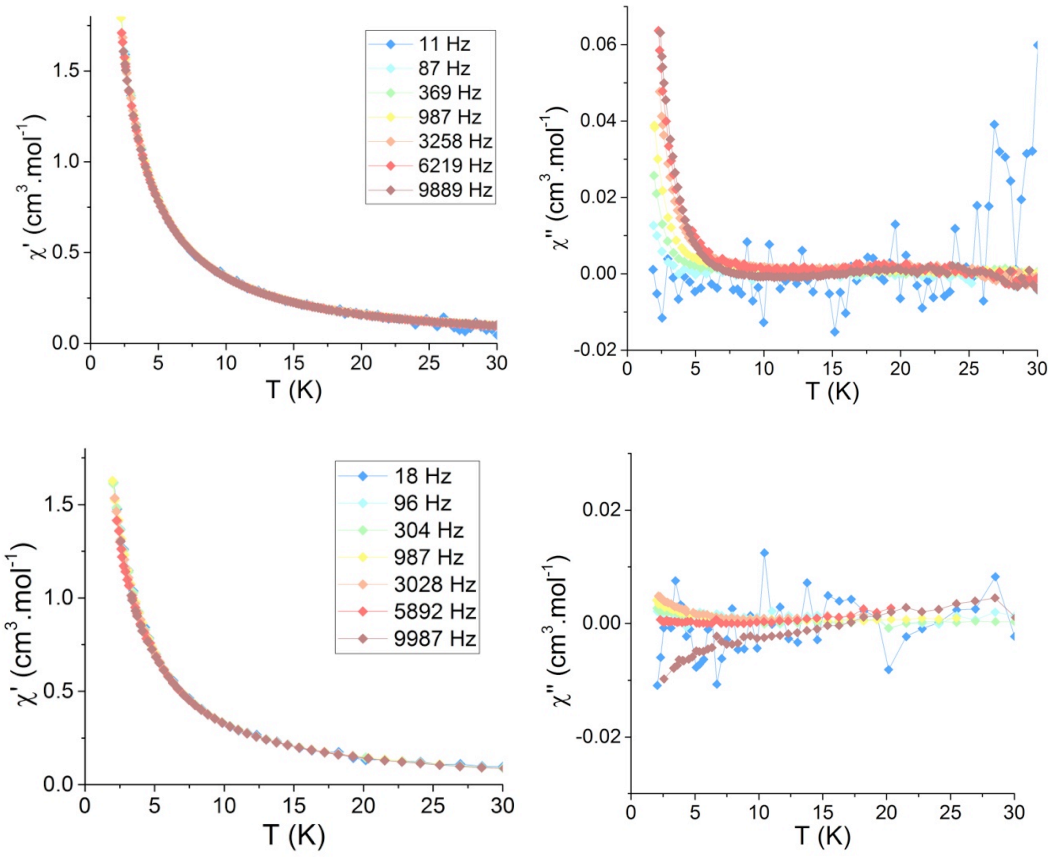

Figure III- 56 Temperature dependence of the (left) in-phase and (right) out-of-phase ac susceptibility components of $[NpO_2L]_3$, **31** (top) and $[\{NpO_2(salen)\}_4(\mu_8\text{-}K)_2][K(18c6)(Py)]_2$ (bottom) recorded between 2 and 30 K with ac field of 15.5 Oe oscillating between 18 and 9987 Hz under zero static dc fields.

To investigate the dynamic magnetic properties, an oscillating field was applied to these two neptunyl(V) complexes. The in-phase (χ') and out-of-phase (χ'') components of the ac susceptibility of $[NpO_2L]_3$, **31** show frequency dependence below 7.0 K in the frequency range of 87 and 9987Hz in a zero dc field without the presence of any maxima (Figure III- 56 top). Complex **31** exhibits slow magnetic relaxation phenomena, but temperatures lower than 2 K could not be measured. Various dc fields until 1T were applied, however, none of them revealed better results. In the case of $[\{NpO_2(salen)\}_4(\mu_8\text{-}K)_2][K(18c6)(Py)]_2$ no frequency dependence was observed, ruling out the presence of retention of the magnetisation (Figure III- 56 bottom). In contrast to the mixed-valent trinuclear $[\{Np^{VI}O_2Cl_2\}\{Np^{V}O_2Cl(THF)_3\}_2]$ complex displaying clear SMM poperties,[112,181] the neptunyl(V) assemblies investigated here do not reveal unambiguous SMM behaviour. The difference may come from a stronger interaction between the neptunyl(VI)-neptunyl(V) units in $[\{Np^{VI}O_2Cl_2\}\{Np^{V}O_2Cl(THF)_3\}_2]$ than between the neptunyl(V) groups in our sytems due to the higher charge of the Np(VI) centre. Notably, the desymmetrisation of the $O{=}Np^{V}{=}O^{+}$ unit due to the CCI is 0.12 Å in this complex, larger than the 0.05 Å found in the $[NpO_2L]_3$, **31** and $[\{NpO_2(salen)\}_4(\mu_8\text{-}K)_2][K(18c6)(Py)]_2$ complexes. This suggests the presence of a stronger CCI in $[\{Np^{VI}O_2Cl_2\}\{Np^{V}O_2Cl(THF)_3\}_2]$, promoting a strong magnetic exchange and SMM properties.

III.4) Conclusion and perspectives

In this chapter, it is demonstrated that stable uranyl(V) complexes can act as building blocks in the formation of cation-cation assemblies with 3d and 4f metals. Various uranyl(V) polynuclear assemblies have been assembled through CCI. The fine-tuning of the supporting ligands leads to the formation of polymeric structures or discrete complexes. In the absence of chelating ligands coordinated to the d-block transition metal, two different $U(V)O_2^{+}$-Mn(II) polymeric structures have been synthesised; while in the presence of a chelating ligand such as TPA or BPPA or TPEN bound to the transition metal or lanthanide ions, di-, tri- and pentanuclear discrete molecules have been obtained with Mn(II), Fe(II), Co(II), Ni(II), Cd(II), Eu(II) and Nd(III). However, we have observed that the use of Cu(II) and Eu(III) induced the oxidation of uranyl(V) Mesaldien, while Cr(II) was able to reduce it into uranium(IV). Moreover, the use of Gd(III) or Dy(III) led to ligand scrambling. With these examples, we have shown that the synthesis of polynuclear assemblies based on CCI between uranyl(V) and other metallic centre was not straightforward and could lead to complicated reaction mixtures. In the future, polydentate dianionic ligands based on triazacyclononane will be

investigated to stabilise Ln(III) ions and to allow the formation of CC assemblies with uranyl(V).

In the polynuclear assemblies containing uranyl(V) and d-block metals, the presence of magnetic communication between the uranyl(V) and the various d block metallic centres through the CC linkage has been identified. The combination of the magnetic anisotropy of uranium with the high spin number of a transition metal has led to improved exchange coupled single chain and single molecule magnets. The two synthesised polymeric chains represent the first examples of actinide-based Single Chain Magnets with high energy barriers and particularly large coercive fields. The synthesis of the large family of trinuclear complexes highlighted the influence of the nature of the transition metal on the magnetic properties. Notably, every trinuclear UMn_2 complexes display improved SMM properties compared to pure manganese clusters. A correlation between the height of the energy barrier and the spin of the transition metal has been observed. According to theory, the relaxation barrier decreases with the reduction of the spin number of the metal, highlighting the presence of the magnetic exchange coupling between the uranyl(V) and the transition metal. These results show that the properties of 3d-5f SMMs can be modulated by the nature of the transition metal. In the future, a systematic magneto-structural study will be carried out, using theoretical calculations to understand the role of uranyl(V) into determining the observed magnetic properties.

In the second part of this chapter, we have studied the stability of uranyl(V) with two Schiff base ligands containing a 1,1'-ferrocenyl bridge. The interaction of the salfen ligand with uranyl(V) led to the disproportionation of uranyl(V). Future work will be directed towards exploring the stability of uranyl(V) salfen in the absence of cations. A bulkier ligand, salfen-^{t}Bu, yielded a stable complex of uranyl(V), and could be used in the future with d-block metals to form heterometallic assemblies with new geometries. To study the direct interaction of one U(V) with a metallic centre, future work will also focus on tripodal heptadentate ligand such as H_3trensal (2,2',2''-tris(salicylideneimino)triethylamine, which may selectively lead to dinuclear assemblies by the direct coordination of one uranyl(V) with two arms, which should have a similar stability than the Mesaldien ligand, and a transition metal with the third arm. Furthermore, synthesis of larger assemblies using the trinuclear UM_2-TPA complexes as building unit could be considered. The presence of the chloride or iodide coordinated to the metallic centre could indeed be exchanged by bidentate ligands that are able to bridge different trinuclear assemblies and lead to complexes with novel geometries.

Finally, we have shown that uranyl(V) could act as a structural model of the more radioactive neptunium. Particularly, we have been able to reproduce the trimeric uranyl(V) cluster supported by β-diketiminate ligands with neptunyl(V) entities. The magnetic data of

this trimeric structure as well as those of the tetranuclear salen neptunyl(V) complex show probable ferromagnetic interactions. Moreover, in-depth measurements on $[NpO_2L]_3$ revealed the presence of slow relaxation of the magnetisation, which has never been observed in pure neptunyl(V) complexes.

CHAPTER IV. NITRIDE-BRIDGED URANIUM CLUSTERS

IV.1) Context

In recent years, there has been increased interest in molecular compounds containing actinide-nitrogen multiple-bonds.[71,109,273,413] The quest for more controlled and mild syntheses of uranium nitride complexes has been in part motivated by their potential use as precursors for uranium nitride, which has been envisaged as an alternative and more efficient nuclear fuel. These studies have recently led to the synthesis of several polynuclear uranium complexes.[414] Moreover, molecular uranium nitrides are also attractive synthetic targets due to their potential as efficient molecular catalysts in dinitrogen reduction to ammonia.[415,416] Molecular nitride complexes are also important models to better understand of f orbital participation in multiple bonding and covalency in actinide-ligand bonds.[5,71,417] Finally, nitride ligands are suitable bridging ligands to form polymetallic assemblies that should favour strong magnetic communication between metallic centres required in the design of SMMs.[418]

The synthesis of nitride and imido complexes is well established for transition metals but is much less developed for the 5f block elements.[419] Polynuclear molecules of uranium(V) and uranium(VI) containing bridging imido ligands from the reaction of uranium(III) complexes with organic azides are described in Chapter I.[62,69,278] In this chapter, the focus is on the description of polymetallic actinide assemblies containing bridging N_3^- azide or N^{3-} nitride ligands. Depending on the reaction conditions, N_3^- can indeed act as bridging ligand or be reduced, releasing N_2 and a nitrido ligand via the equation: $N_3^- + 2e^- \rightarrow N^{3-} + N_2$.

IV.1.1) Polymetallic azides complexes

The formation of polymetallic assemblies with azides as bridging ligands has been achieved under inert atmosphere from salt metathesis reactions between uranium(IV) and inorganic azides. The bimetallic complex $\{[U(C_5H_4(SiMe_3))_3]_2(\mu_2\text{-}N_3)\}[BPh_4]$ was isolated from the reaction of $[U(C_5H_4(SiMe_3))_3][BPh_4]$ with 0.5 equiv of NaN_3 by Ephrithikhine and coworkers. The two uranium atoms of this complex are bridged by an end-to-end azide ligand.[420] More recently, the Evans group described a trimetallic uranium(IV) complex $[U(C_5Me_5)_2N_3(\mu_2\text{-}N_3)]_3$ obtained from the reaction between $[U(C_5Me_5)_2Cl_2]$ and sodium azide.

The three uranium ions of this complex are localised on the vertices of a triangle end-to-end bridged by azide ligands (Figure IV- 1 left).[421]

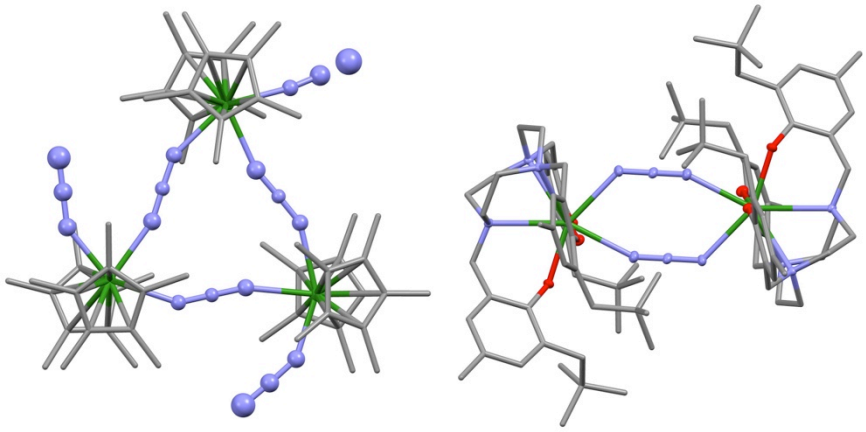

Figure IV- 1 Molecular structures of the uranium assemblies $[U(C_5Me_5)_2N_3(\mu_2\text{-}N_3)]_3$ (left) and $[\{U((^{nP,Me}ArO)_3tacn)\}_2(\mu_2\text{-}N_3)_2]$ (right). (H atoms, disorder and solvent molecules were omitted for clarity. Ligands are represented as pipes, C are represented in grey, N in blue, O in red and U in green.) [421,422]

In comparison to tetravalent uranium, the reaction of trivalent uranium with inorganic azides affords a diverse variety of products, depending on the steric hindrance around the uranium(III) ion. The reaction of azides with sterically hindered uranium(III) complexes led to polymetallic assemblies with bridging end-to-end azido ligands.[195,420] For example, the reaction of the sterically crowded $[U((^{nP,Me}ArO)_3tacn)]$ uranium(III) complex with trimethylstannyl azide was shown to lead to a dinuclear bis-μ-azido $[\{U((^{nP,Me}ArO)_3tacn)\}_2(\mu_2\text{-}N_3)_2]$ complex (Figure IV- 1 right).[422] Magnetic measurements on this complex were reported but do not reveal magnetic coupling between the two uranium(IV) atoms.

However, in other cases, and in particular when the uranium(III) precursor is not too sterically crowded, the reduction of the azide moiety can occur, leading to nitride ligands. Notably, an octanuclear U(IV) complex[423] and a tetranuclear uranium(IV)[83] complex containing both N_3^- and N^{3-} ligands were reported by Evans and co-workers in 2005, and by our group in 2008, respectively.

IV.1.2) Polymetallic nitride complexes

The nitride ion, N^{3-}, is an excellent π-donor ligand which is known to act as a bridging ligand in μ_2, μ_3 or μ_4 coordination modes, resulting in the formation of polynuclear complexes. The geometry of the resulting nitride complexes is therefore strongly impacted by the steric pressure exerted by the ancillary ligands, as illustrated below. With the exception of two examples from dinitrogen reduction, all the syntheses of nitride uranium clusters used the reduction of azide precursors.

Previous work in our team showed that the reaction between $[UI_3(THF)_4]$ and the uranium(IV) azide complex $[U(N_3)_7Cs_3]$ allowed for the formation of the unique polynuclear uranium μ_4-nitride complex $([U_4(\mu_4\text{-}N)(\mu\text{-}1,1\text{-}N_3)_8(CH_3CN)_8I_6][(Cs(CH_3CN)_3])_n$.[83] The μ_4-N^{3-} moiety bridges four U(IV) centres placed at the edges of a tetrahedron. Along the vertices of the tetrahedron, eight bridging end-on azide moieties hold the structure together (Figure IV- 2 left). The formation of a μ_4-nitride is most probably due to the absence of bulky ancillary ligands in the reaction media.

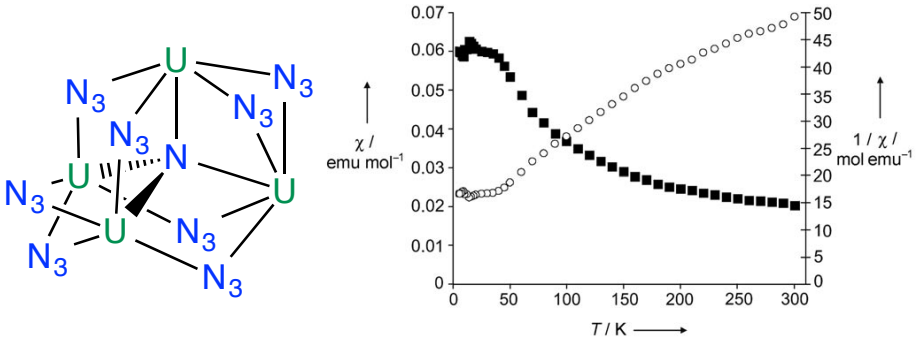

Figure IV- 2 (left) Schematic representation of the core of $[U_4(\mu_4\text{-}N)(\mu\text{-}1,1\text{-}N_3)_8(CH_3CN)_8I_6]^-$; (right) Temperature-dependent magnetic susceptibility data for $([U_4(\mu_4\text{-}N)(\mu\text{-}1,1\text{-}N_3)_8(CH_3CN)_8I_6][(Cs(CH_3CN)_3])_n$ from 6 to 300 K.[83]

The magnetic susceptibility of the $([U_4(\mu_4\text{-}N)(\mu\text{-}1,1\text{-}N_3)_8(CH_3CN)_8I_6][(Cs(CH_3CN)_3])_n$ cluster revealed temperature-independent paramagnetism between 6 and 45 K. This observation is a typical magnetic response of molecular U(IV) compound together (Figure IV-2 right) however no magnetic coupling between the uranium(IV) centres was observed.

In 2005, the Evans group isolated the octanuclear ring-shaped $[(Cp^*)_2U(\mu\text{-}N)U(\mu\text{-}N_3)(Cp^*)_2]_4$ (Cp^*: C_5Me_4R with R: Me, H) complex from the reaction of sodium azide and the U(III) complex $[U(Cp^*)_2(BPh_4)]$ (Scheme IV- 1).[423] This complex is comprised of eight uranium(IV) centres alternatively bridged by nearly linear U=N=U linkages and by bidentate end-to-end azido ligands. This cluster resulted from the reduction of 0.5 equiv of azide and the concomitant oxidation of U(III) into U(IV). Interestingly, the use of the uranium(III) $[U(C_5Me_5)I_2(THF)_3]$ complex, in which the uranium(III) ion is linked to only one $(C_5Me_5)^-$ ligand, led to a μ_3-nitride trinuclear uranium $[\{U(C_5Me_5)(\mu_2\text{-}I)_2\}_3(\mu_3\text{-}N)]$ complex.[421]

Scheme IV- 1 Synthesis of $[(Cp^*)_2U(\mu\text{-}N)U(\mu\text{-}N_3)(Cp^*)_2]_4$

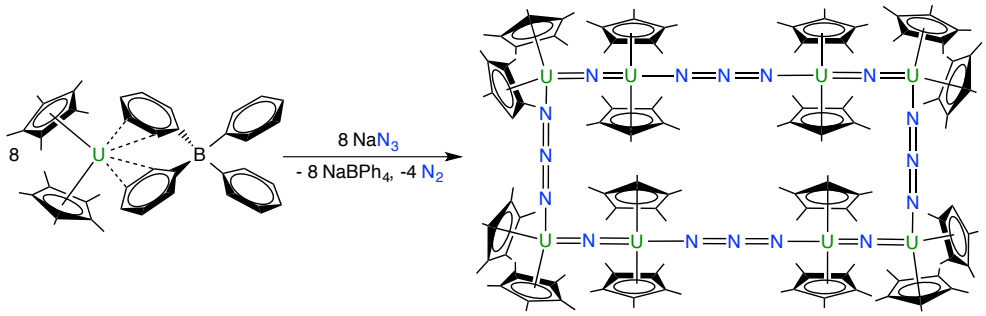

From these three examples, it is apparent that the presence of zero, one or two bulky Cp* ligands in the coordination sphere of the uranium(III) precursors resulted in the formation of μ_4-, μ_3- or μ_2-nitride ligands respectively. The structure of nitride complexes resulting from the reduction of azides by U(III) is thus affected by the number of bulky ancillary ligands and their steric properties.

Subsequent to these three examples, a few other polymetallic uranium(IV) nitride complexes formed from the reduction of azide have been reported. All of them consist of bridging μ_2-nitride ligands between two uranium(IV) ions in a linear or bent fashion. Some studies have revealed the possible selective oxidation of the uranium(IV) ions to form rare examples of nitride uranium(V) and uranium(VI) complexes.

In 2010, Cummins and coworkers first reported the reaction between sodium or tetrabutylammonium azide with the U(III) complex $[U(N^tBuAr)_3(THF)]$ (Ar = 3,5-$Me_2C_6H_3$). This reaction led to the linear nitride-bridged uranium(IV) ion pair $Na\{[U(N^tBuAr)_3]_2(\mu_2\text{-}N)\}$. This complex was quantitatively oxidised to form the corresponding U(V)-U(IV) and U(V)-U(V) nitride-bridged dimers (Scheme IV- 2).[424] The cyclic voltammetry measurements of $\{[U(N^tBuAr)_3]_2(\mu_2\text{-}N)\}$ in THF between 0.7 and -2.3V (vs $[Cp_2Fe]^{0/+}$) revealed two reversible electrochemical events at -1.69 and -0.64 V (vs $[Cp_2Fe]^{0/+}$) assigned to the U(V)-U(IV)/U(IV)-U(IV) and U(V)-U(V)/U(V)-U(IV) couples, respectively (Figure IV- 3). The magnetic properties of these complexes were not reported.

Scheme IV- 2 Synthesis and controlled oxidations of $Na\{[U(N^tBuAr)_3]_2(\mu_2\text{-}N)\}$

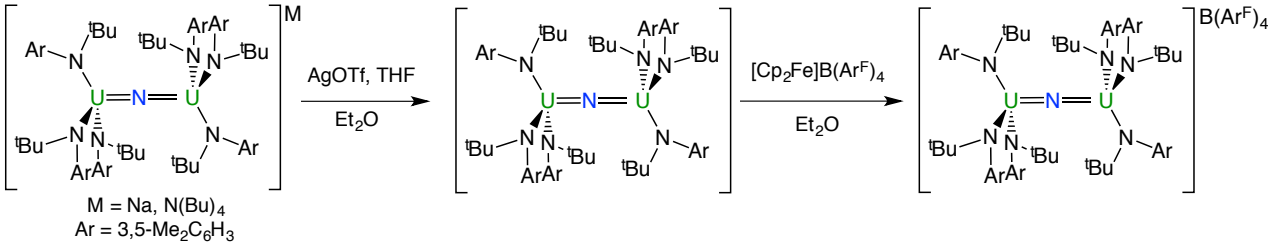

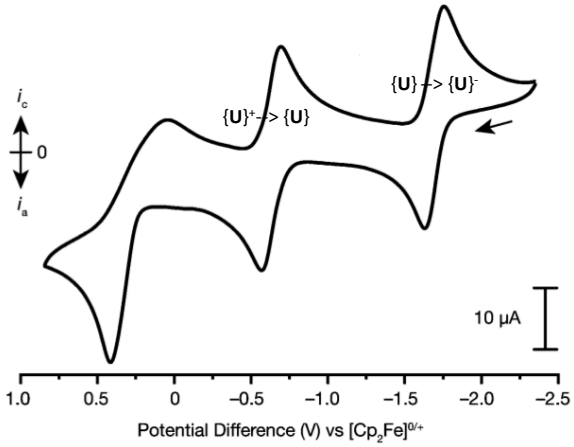

Figure IV- 3 Cyclic voltammogram of {[U(N^{t}BuAr)$_3$]$_2$(µ$_2$-N)} {**U**} in THF (200mV.s^{-1} sweep rate, 0.1M [N(n-Bu)$_4$][B(C$_6$F$_5$)$_4$] supporting electrolyte) showing the two one-electron redox couples that interconvert {**U**}^{n} (n=-1, 0, +1).[424]

In 2010, Hayton and coworkers also reported the reaction between sodium azide and the trivalent uranium complex [U(N(Si(Me)$_3$)$_2$)$_3$] (Scheme IV- 3) leading to nitride formation. The resulting complex [Na(DME)$_2$(TMEDA)][(NR$_2$)$_2$U(µ-N)(CH$_2$SiMe$_2$NR)U(NR$_2$)$_2$] (R: Si(Me)$_3$) features a bent UNU moiety due to the presence of a bridging CH$_2$SiMe$_2$NR ligand formed during the reaction.[425] This uranium(IV) dimer can be oxidised with 1 equivalent of Me$_3$NO to afford a trans oxo-nitrido [O=U^{VI}=N]$^+$ moiety or with 0.5 equiv of I$_2$ to yield a mixed-valent U(IV)/U(V) nitride complex (Scheme IV- 3).

Scheme IV- 3 Synthesis and reactivity of [Na(DME)$_2$(TMEDA)][(NR$_2$)$_2$U(µ-N)(CH$_2$SiMe$_2$NR)U(NR$_2$)$_2$]

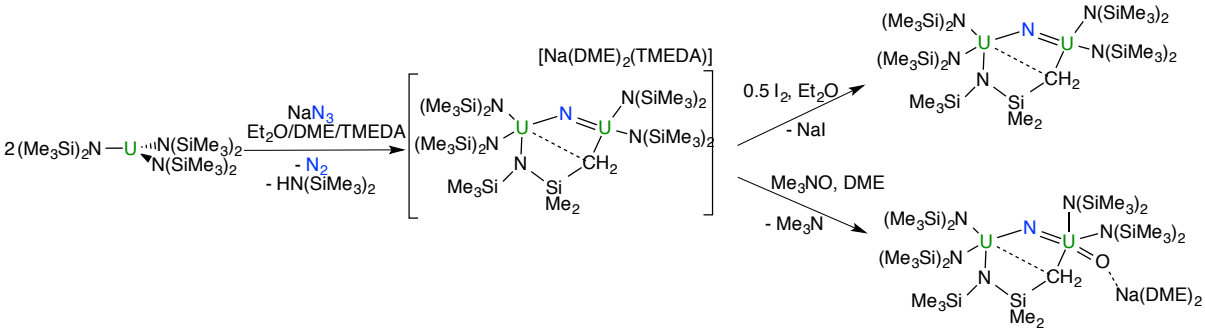

The χ versus T plots for either [Na(DME)$_2$(TMEDA)][(NR$_2$)$_2$U^{IV}(µ-N)(CH$_2$SiMe$_2$NR)U^{IV}(NR$_2$)$_2$] or [(NR$_2$)$_2$U^{IV}(µ-N)(CH$_2$SiMe$_2$NR)U^{V}(NR$_2$)$_2$] do not reveal obvious magnetic communication between the uranium centres. Interestingly, a sudden change in the magnetic moment plot of [(NR$_2$)$_2$U^{IV}(µ-N)(CH$_2$SiMe$_2$NR)U^{V}(NR$_2$)$_2$] is observed below 105 K. The authors rationalised this field independent transition by the presence of a

crystallographic phase change, confirmed by measurement of the unit cell parameters for a single crystal from 150 to 80 K (Figure IV- 4).

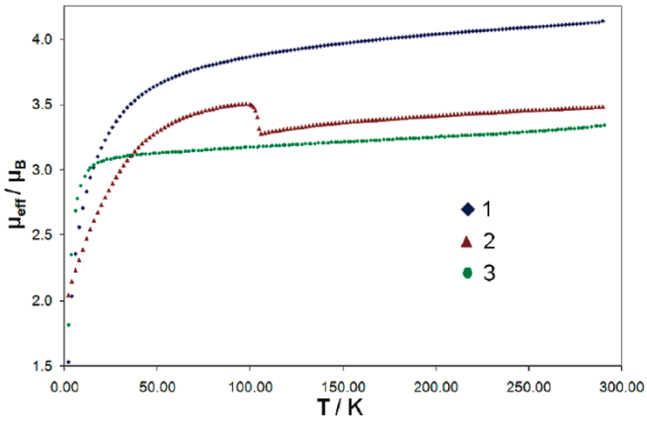

Figure IV- 4 Temperature-dependent SQUID magnetisation data for $[Na(DME)_2(TMEDA)][(NR_2)_2U(\mu\text{-}N)(CH_2SiMe_2NR)U(NR_2)_2]$ (1, blue diamond), $[(NR_2)_2U(\mu\text{-}N)(CH_2SiMe_2NR)U(NR_2)_2]$ (2, purple triangle) and $[Na(DME)_2][(NR_2)_2(O)U(\mu\text{-}N)(CH_2SiMe_2NR)U(NR_2)_2]$ (3, green dot)[425]

A dinuclear nitride-bridged uranium(IV) complex $[Cs\{U(OSi(O^tBu)_3)_3\}_2(\mu\text{-}N)]$ was recently prepared in our group from the reaction of the uranium(III) complex $[U(OSi(O^tBu)_3)_2(\mu\text{-}OSi(O^tBu)_3]_2$ and cesium azide (Scheme IV- 4).[69] $[Cs\{U(OSi(O^tBu)_3)_3\}_2(\mu\text{-}N)]$ features a linear U(IV)-N-U(IV) motif as found in the closely related dinuclear anionic U(IV)-N-U(IV) complex $Na\{[U(N^tBuAr)_3]_2(\mu_2\text{-}N)\}$ reported by Cummins group in 2010.[424] The main difference between the two structures is the neutral charge of $[Cs\{U(OSi(O^tBu)_3)_3\}_2(\mu\text{-}N)]$ and its heterometallic structure. Notably, a cesium cation is held in the structure by coordination to three siloxy ligands, which act as bridging bidentate ligands. Magnetic data of this complex were collected from 2 to 300 K, and an inflexion point was observed at low temperature in the magnetic susceptibility plot (Figure IV- 5). This behaviour could be either due to the temperature independent paramagnetism often seen for U(IV) ions, or to a magnetic interaction between the uranium ions.

Scheme IV- 4 Synthesis of $[Cs\{U(OSi(O^tBu)_3)_3\}_2(\mu\text{-}N)]$

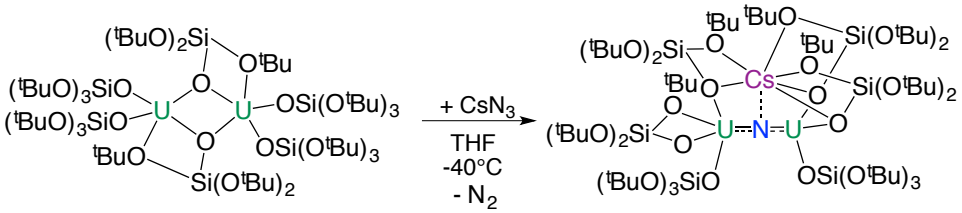

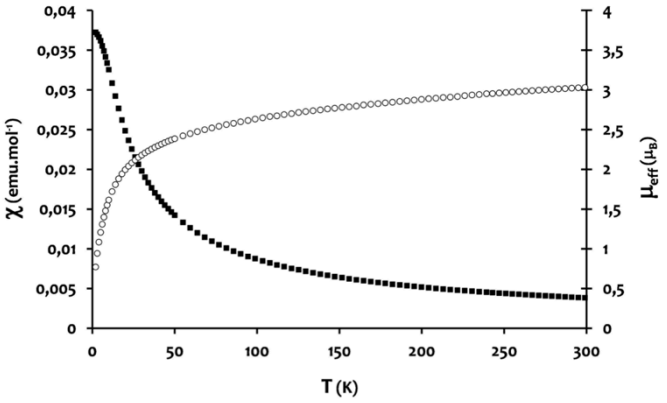

Figure IV- 5 Temperature-dependent SQUID magnetisation data (0.5 T) for complex $[Cs\{U(OSi(O^tBu)_3)_3\}_2(\mu\text{-}N)]$ (data per U center) plotted as χ (open circles) and μ_{eff} (black squares) versus temperature.[69]

Finally, crystals of a neutral dinuclear uranium(IV) nitride-bridged complex $[(\{(^{tBu2}ArO)_2Me_2\text{-cyclam}\})(N_3)U(\mu\text{-}N)U(\{(^{tBu2}ArO)_2Me_2\text{-cyclam}\})]$ were also isolated from the reaction of the uranium(III) complex $[U\{(^{tBu2}ArO)_2Me_2\text{-cyclam}\}I]$ with cesium azide. However, a reproducible synthetic route to this complex could not be identified.[426]

These examples demonstrate that the nitride ligand resulting from the activation of an azide by an uranium(III) complex can bridge 2, 3 and even 4 uranium metallic centres depending on the steric hindrance in the coordination sphere of the uranium atom. It should be noted that mononuclear terminal U(V) and U(VI) nitrides have also recently been prepared by Liddle et al. from the reaction of NaN_3 with a U(III) complex supported by a bulky polydentate ligand,[108,427] and by Cloke et al. from the reaction of NaN_3 with a U(III) mixed sandwich $C_8H_6\text{-}(1,4\text{-}Si^iPr_3)_2/Cp^*$ complex.[428]

Polymetallic nitride complexes can also be obtained from the reduction of dinitrogen by low-valent metal complexes. To date, only two examples of uranium nitrides have been obtained from dinitrogen reduction. In 2002, Gambarotta and coworkers reported the mixed-valent U(IV)/U(V) $[\{K(dme)U(calix[4]tetrapyrrole)\}_2(\mu\text{-}NK)_2][K(dme)_4]$ dinitride complex, which was obtained from the reduction of a calixarene uranium(III) complex under a nitrogen atmosphere (Scheme IV- 5). The complex features two bridging nitride ligands arranged in a diamond-shaped fashion.[429] The magnetic data collected for this $[\{K(dme)U(calix[4]tetrapyrrole)\}_2(\mu\text{-}NK)_2][K(dme)_4]$ dinitride complex do not reveal clear magnetic communication between uranium centres.

Scheme IV- 5 Synthesis of $[\{K(dme)U(calix[4]tetrapyrrole)\}_2(\mu\text{-}NK)_2][K(dme)_4]$

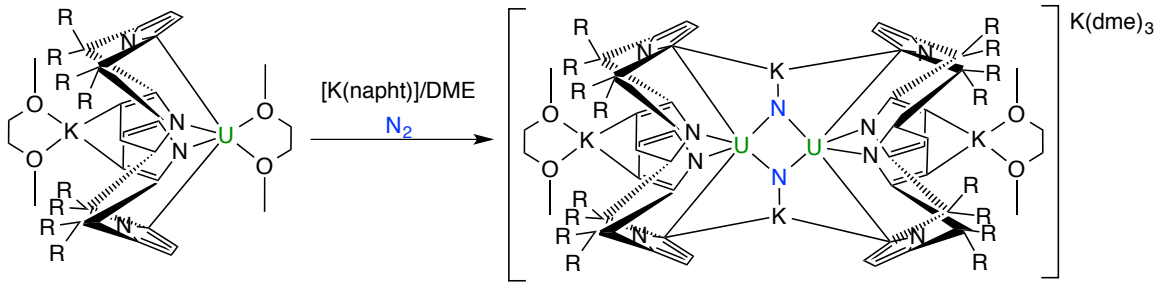

Evans also reported the octanuclear nitride complex $[U(C_5Me_5)(\mu_3\text{-}N)]_8$, which was obtained from the reduction of the uranium(III) $[U(C_5Me_5)_2][(\mu\text{-}Ph)_2BPh_2]$ complex with potassium graphite, under a nitrogen atmosphere (Scheme IV- 6). However, confirmation of the presence of nitride ligands was not possible experimentally and was only proposed according to DFT calculations.[430] These two examples demonstrate that further reduction of uranium(III) complexes may result in highly reactive "U(II)" species that are able to cleave the strong dinitrogen bond to afford nitride species N^{3-}.

Scheme IV- 6 Synthesis of $[U(C_5Me_5)(\mu_3\text{-}N)]_8$

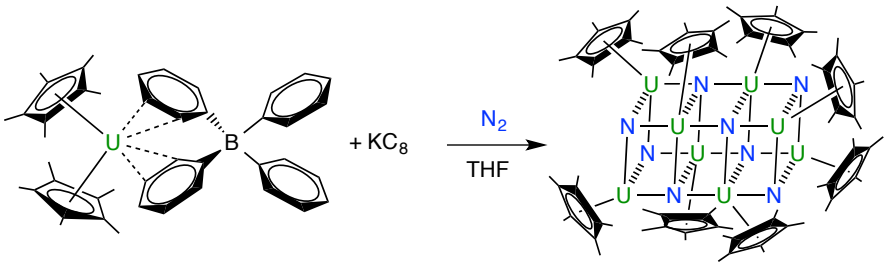

IV.1.3) Objectives

As outlined in the previous section, the formation of bridging nitride from azide or dinitrogen cleavage provides an attractive route to polymetallic uranium complexes. Most of the nitride complexes reported so far in the literature contain uranium in its +IV oxidation state, with a few systems containing U(V) and U(VI). In spite of their relevance in materials science and catalysis, and of the anticipated attractive reactivity of U(III) nitrides, no molecular uranium(III) nitride complex has been isolated in solution or in the solid state. Moreover, the magnetic properties of nitride-bridged polymetallic uranium compounds remain practically unexplored. The strong multiple bond formed by nitride bridging groups should

promote magnetic interaction between the metal centres and therefore provide a good tool for the design of uranium-based single molecule magnets. In order to design SMMs, we have explored the possibility of synthesising polynuclear uranium nitride complexes containing uranium in the +III or +V oxidation states.

In previous work from our group, crystals of the bis(nitride) U(V)-U(V) complex $[K\{U(OSi(OtBu)_3)_3\}(\mu_2\text{-}N)]_2$ were isolated from the reaction of the uranium(III) complex $(K18c6)[U(OSi(O^tBu)_3)_4]$ and cesium azide. This features two bridging nitrides arranged in a diamond-shaped U_2N_2 core. The reaction represented in Scheme IV- 7 afforded multiple products and a way to produce the bis(nitride) analytically pure was not identified prior to this work.[69]

Scheme IV- 7 Reaction of $(K18c6)[U(OSi(O^tBu)_3)_4]$ with CsN_3

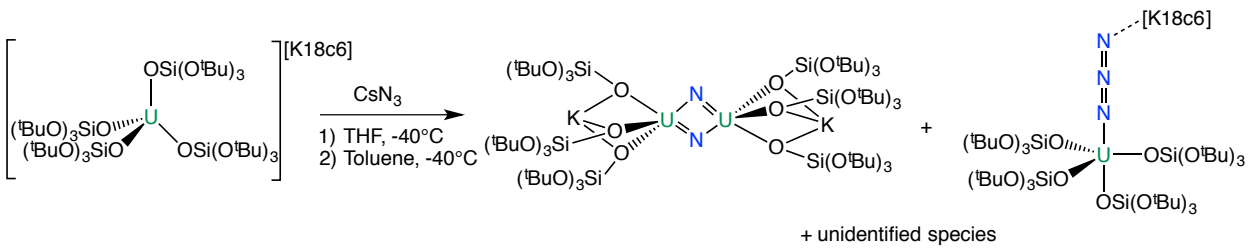

During my PhD, I have explored new synthetic routes to produce this U(V)-U(V) complex in order to investigate its magnetic properties. I have also investigated the reductive chemistry of the U(IV)-U(IV) complex $[Cs\{U(OSi(O^tBu)_3)_3\}_2(\mu\text{-}N)]$ (Scheme IV- 4)[69] reported previously in our group with the aim of obtaining linear nitride-bridged complexes containing uranium in a lower oxidation state. In the complex $[Cs\{U(OSi(O^tBu)_3)_3\}_2(\mu\text{-}N)]$, the Cs cation binds the bridging nitride and six oxygen atoms from the siloxide ligands, affording a unique heterometallic structure. The ability of the $OSi(O^tBu)_3$ ligand to bind to Cs^+, thus stabilising highly charged species, anticipates the possibility of stabilising the U---N---U fragment in highly reduced uranium species.

IV.2) Synthesis of nitride bridged di-uranium(III) complexes

The addition of one equivalent of 18c6 to a solution of $[Cs\{U(OSi(O^tBu)_3)_3\}_2(\mu\text{-}N)]$ in THF induces a shift of the ^1H NMR signal from -0.8 to -0.4ppm, indicating that crown ether removes the Cs^+ from the core.

Cyclic voltammetry measurements were carried out both in the presence or in the absence of 18c6, respectively, to investigate if reduced species were accessible and to assess the influence of the bound Cs^+ cation. Differences between the two electrochemical measurements were indeed observed (Figure IV- 6).

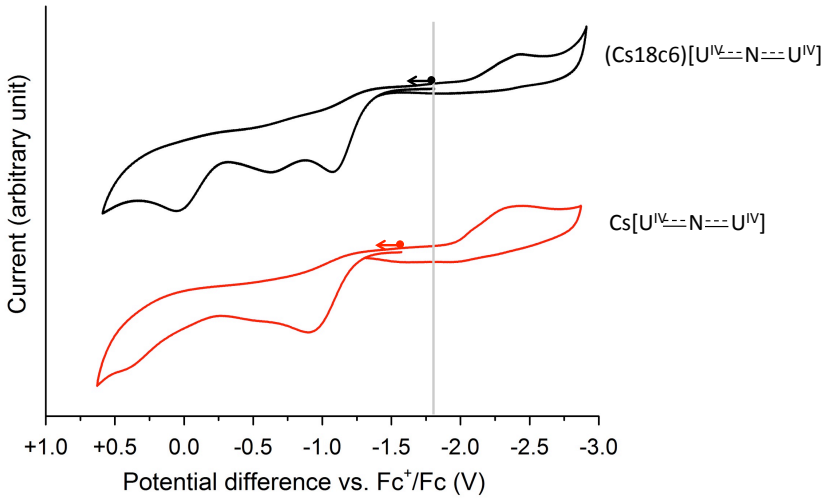

Figure IV- 6 Cp_2Fe^+/Cp_2Fe corrected cyclic voltammograms of a 2 mM THF solution of $[Cs\{U(OSi(O^tBu)_3)_3\}_2(\mu\text{-}N)]$ with or without added 18c6 in 0.1M $[Bu_4N][BArF_4]$ at 100 mV/s scan rate and 298 K. The red trace corresponds to the complex $[Cs\{U(OSi(O^tBu)_3)_3\}_2(\mu\text{-}N)]$ (E_{OCV} = -1.57 V) and the black trace corresponds to the complex $(Cs18c6)[\{U(OSi(O^tBu)_3)_3\}_2(\mu\text{-}N)]$ (E_{OCV} = -1.81 V).

The cyclic voltammogram of $[Cs\{U(OSi(O^tBu)_3)_3\}_2(\mu\text{-}N)]$ shows two irreversible electrochemical events at -2.34 and -0.92 V (vs $[Cp_2Fe]^{0/+}$) that correspond to the reduction and the oxidation of the uranium metal in the complex respectively. The irreversibility of these redox events may be due to an important rearrangement of the siloxide coordination sphere during the redox processes. After removal of Cs^+ with 18c6, the reduction wave is shifted to lower potential (E_{pc} = -2.43 V) indicating that the reduction of $[Cs\{U(OSi(O^tBu)_3)_3\}_2(\mu\text{-}N)]$ is more difficult in the absence of coordinated Cs^+, as the uranium centres are more electron-rich. We compared this behaviour with the cyclic voltammetry of the U(IV)-U(IV) $\{[U(N^tBuAr)_3]_2(\mu_2\text{-}N)\}^-$ complex reported by Cummins and coworkers (Figure IV- 3). This complex is supported by bulky unidentate amide ligands. Consequently, the counter-cation is not coordinated to the complex. $\{[U(N^tBuAr)_3]_2(\mu_2\text{-}N)\}^-$ is stabilised at lower

potentials (oxidation at -1.69V (vs $[Cp_2Fe]^{0/+}$)[424] than $[Cs\{U(OSi(O^tBu)_3)_3\}_2(\mu\text{-}N)]$ (oxidation at -0.92V (vs $[Cp_2Fe]^{0/+}$). The $\{[U(N^tBuAr)_3]_2(\mu_2\text{-}N)\}^-$ complex is thus more difficult to reduce as a result of the electron-rich uranium(IV) centres. In $[Cs\{U(OSi(O^tBu)_3)_3\}_2(\mu\text{-}N)]$, the presence of the multidentate siloxide groups capable of binding the Cs^+ cation seems to be the key to the possible isolation of highly charged reduced complexes. Chemical reduction of the uranium(IV) $[Cs\{U(OSi(O^tBu)_3)_3\}_2(\mu\text{-}N)]$ complex was then performed in the absence of 18c6. The effect of the nature of the counter ion was also explored using both Cs and K metal as reducing agents.

IV.2.2) Cesium as counter-cation

The reduction of $[Cs\{U(OSi(O^tBu)_3)_3\}_2(\mu\text{-}N)]$ carried out with 1 equivalent of Cs^0 in THF at -40°C afforded a mixed-valent U(III)/U(IV) nitride complex $[Cs_2\{U(OSi(O^tBu)_3)_3\}_2(\mu\text{-}N)]$ (**32**-$Cs_2[U^{III}\cdots N\cdots U^{IV}]$) in 67% yield (Scheme IV- 8). The reduction of $[Cs\{U(OSi(O^tBu)_3)_3\}_2(\mu\text{-}N)]$ with a large excess of reductant (5 equivalents of cesium), led to the $[Cs_3\{U(OSi(O^tBu)_3)_3\}_2(\mu\text{-}N)]$ complex (**33**-$Cs_3[U^{III}\cdots N\cdots U^{III}]$) in 77% yield (Scheme IV- 8).

Scheme IV- 8 Synthesis of **32**-$Cs_2[U^{III}\cdots N\cdots U^{IV}]$ and **33**-$Cs_3[U^{III}\cdots N\cdots U^{III}]$.

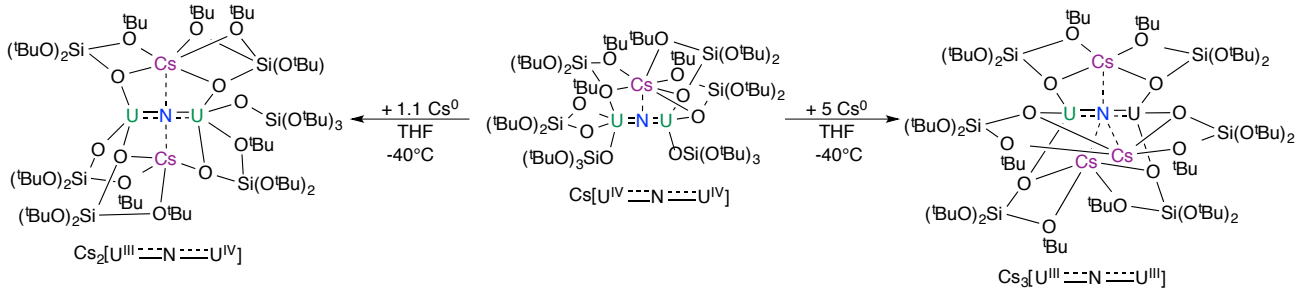

Both species were crystallised from concentrated solutions in THF at -40°C. Their solid-state molecular structures were determined by single-crystal X-ray diffraction and are represented in Figure IV- 7

Each uranium ion of both the **32**-$Cs_2[U^{III}\cdots N\cdots U^{IV}]$ and **33**-$Cs_3[U^{III}\cdots N\cdots U^{III}]$ complexes are coordinated to a nitride group and three siloxide oxygens, affording a pseudo-tetrahedral coordination geometry. The Cs^+ cations are bound to the bridging nitride and to the siloxide oxygens. In **32**-$Cs_2[U^{III}\cdots N\cdots U^{IV}]$, two Cs^+ cations bind the nitride in an almost linear fashion (Cs-N-Cs = 161.8(4)°) with the Cs-N-Cs and the U···N···U fragments located in the same plane and perpendicular to each other. In **33**-$Cs_3[U^{III}\cdots N\cdots U^{III}]$, three Cs^+ cations bind the nitride, forming an irregular triangle located in a plane perpendicular to the U···N···U

fragment (Cs-N-Cs angles: 119.1(4), 108.9(3) and 132.0(7)°). Bond distances are compared in section IV.2.4).

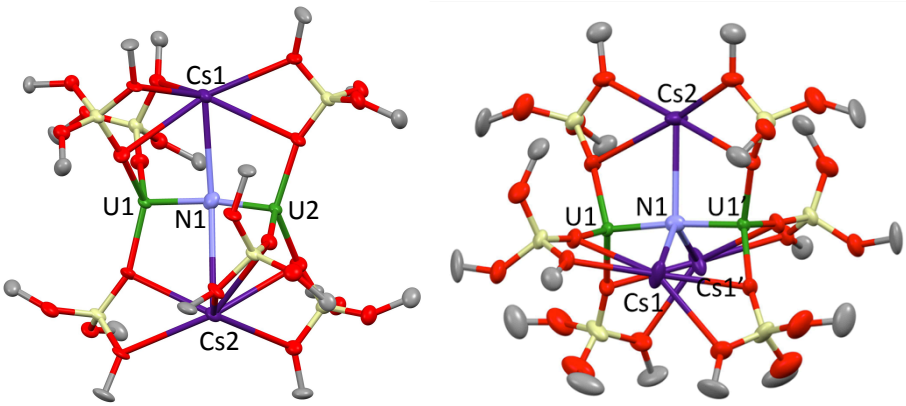

Figure IV- 7 Crystallographic structure of $[Cs_2\{U(OSi(O^tBu)_3)_3\}_2(\mu\text{-}N)]$ (left) and $[Cs_3\{U(OSi(O^tBu)_3)_3\}_2(\mu\text{-}N)]$ (right) crystallised from a saturated THF solution; ellipsoid probability 50%, with hydrogen atoms, methyl groups and disorder on Cs2 omitted for clarity on $[Cs_3\{U(OSi(O^tBu)_3)_3\}_2(\mu\text{-}N)]$. Atoms: C (grey), O (red), Si (light yellow), N (light blue), Cs (violet) and U (green).

The ^{1}H NMR spectra of both complexes in THF solution show the presence of only one signal for the six siloxide ligands, in agreement with the presence of symmetry-related siloxides and fluxionality of the bound Cs cation (Figure IV- 8).

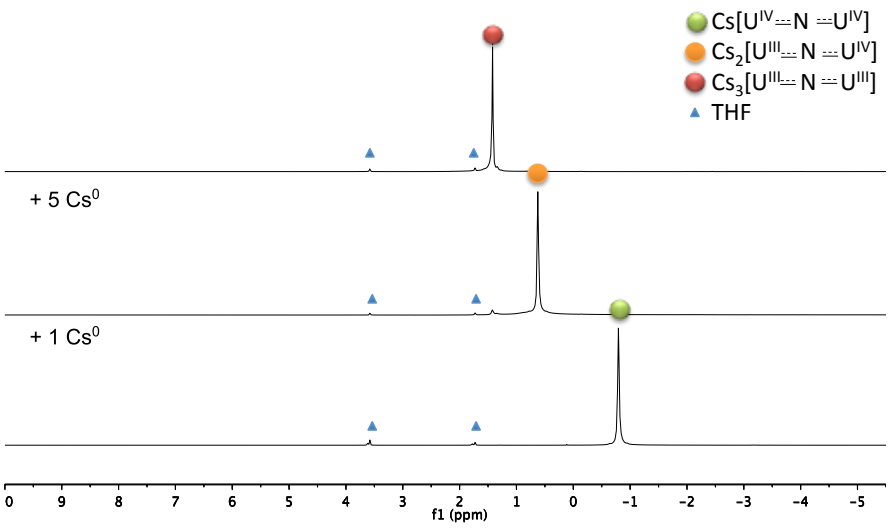

Figure IV- 8 ^{1}H NMR (400MHz, THF-d_8, 233 K) spectrum of $Cs[U^{IV}\text{---}N\text{---}U^{IV}]$ and the results of successive addition of metallic cesium.

32-$Cs_2[U^{III}\text{---}N\text{---}U^{IV}]$ can be prepared analytically pure and stored in the solid state under argon at -40 °C for several weeks. In solution, it is stable at -40°C for a long period of time (up to one month), while at room temperature this complex starts to decompose after 24 hours (after 48 hours at least 42% is decomposed).

Due to the high reactivity of **33**-$Cs_3[U^{III}{-}N{-}U^{III}]$, the synthesis of this complex required several adjustments. To get complete conversion of $Cs[U^{IV}{-}N{-}U^{IV}]$ into **33**-$Cs_3[U^{III}{-}N{-}U^{III}]$, a large excess of reductant was required or else a mixture of **33**-$Cs_3[U^{III}{-}N{-}U^{III}]$ and **32**-$Cs_2[U^{III}{-}N{-}U^{IV}]$ was obtained, regardless of the reaction time. However, the final complex **33**-$Cs_3[U^{III}{-}N{-}U^{III}]$ slowly decomposed in the presence of the excess Cs^0. The best compromise to get clean **33**-$Cs_3[U^{III}{-}N{-}U^{III}]$ was obtained using vigorous stirring of the reaction mixture in THF for 3 hours in the presence of a large excess of cesium at -40°C. Under these conditions, **33**-$Cs_3[U^{III}{-}N{-}U^{III}]$ can be obtained analytically pure, but it decomposes very quickly, even at -40°C, both in the solid state and in THF solution (decomposition products are observed after 1 hour in a solution stored at -40°C), yielding mixtures containing **32**-$Cs_2[U^{III}{-}N{-}U^{IV}]$ and free siloxide ligand as the only known decomposition products detectable by proton NMR spectroscopy (Figure IV- 9).

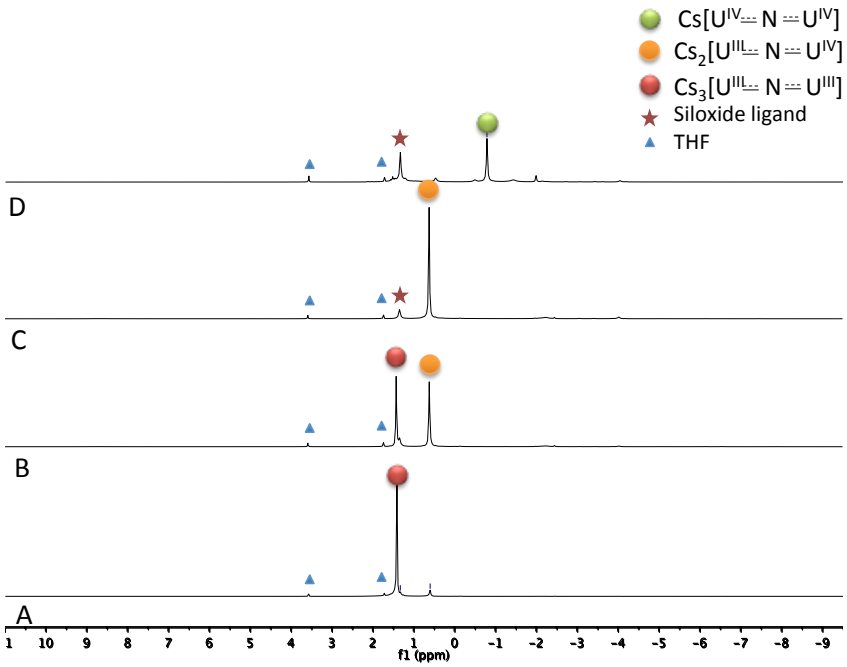

Figure IV- 9 Evolution over time of the ^1H NMR spectrum (400 MHz, THF-d_8, 233 K) at -40°C of the crude reaction mixture after reacting $Cs[U^{IV}{-}N{-}U^{IV}]$ with 5 equiv. of Cs^0 for 3 hours and removing the excess of Cs^0 to yield **33**-$Cs_3[U^{III}{-}N{-}U^{III}]$ (A), after 20h (B), after 40h (C) and after 60h (D).

The extremely high reactivity of these complexes is in agreement with the absence in the literature of any molecular nitride compounds containing uranium in the +III oxidation state. In order to compare the stability of this highly reduced species in the presence of different cations, we have also prepared the complex $[K\{U(OSi(O^tBu)_3)_3\}_2(\mu\text{-}N)]$ and investigated its reduction using KC_8.

IV.2.3) Potassium as counter-cation

IV.2.3.1) Synthesis of K[{U(OSi(O^{t}Bu)$_3$)$_3$}$_2$(μ-N)]

In order to synthesise [K{U(OSi(O^{t}Bu)$_3$)$_3$}$_2$(μ-N)], the U(III) complex [U(OSi(O^{t}Bu)$_3$)$_2$(μ-OSi(O^{t}Bu)$_3$)]$_2$ was reacted with potassium azide in THF at -40°C. However, this reaction led to a mixture of products (Scheme IV- 9).

Scheme IV- 9 Synthesis of **34**-K[U^{IV}---N---U^{IV}] and [K$_2${U(OSi(O^{t}Bu)$_3$)$_3$}$_2$(μ-N)(μ-N$_3$)], **35**.

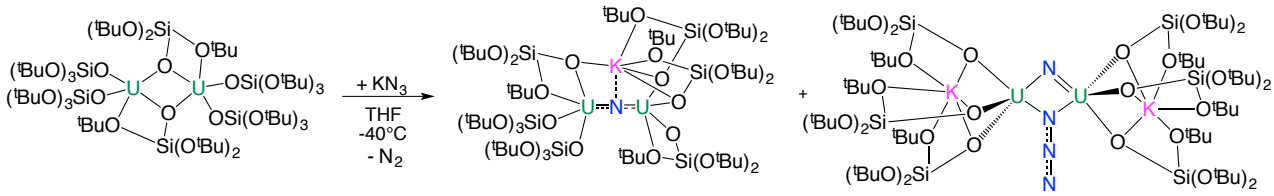

After 5 days of stirring at -40°C, a combination of starting material and two new species in an approximate 1:1 ratio was present in the reaction mixture, as revealed by ^{1}H NMR spectroscopy studies (Figure IV- 10 right). The two different species were identified by X-ray diffraction studies as the desired [K{U(OSi(O^{t}Bu)$_3$)$_3$}$_2$(μ-N)] complex (**34**-K[U^{IV}---N---U^{IV}]) (represented in Figure IV- 10 left) and as the [K$_2${U(OSi(O^{t}Bu)$_3$)$_3$}$_2$(μ-N)(μ-N$_3$)], **35** complex (see IV.3)). Successive recrystallisations of the reaction mixture in THF at -40°C gave pure [K{U(OSi(O^{t}Bu)$_3$)$_3$}$_2$(μ-N)] in 21% yield.

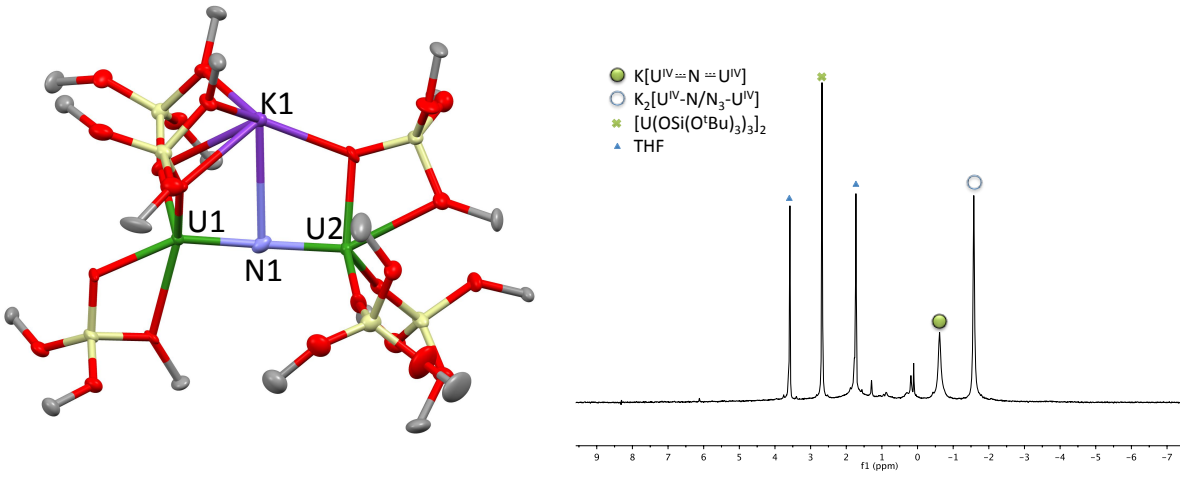

Figure IV- 10 (left) Crystallographic structure of **34**-K[U^{IV}---N---U^{IV}] crystallised from a saturated toluene solution; ellipsoid probability 50%, with hydrogen atoms, methyl groups and disorder omitted for clarity. Atoms: C (grey), O (red), Si (light yellow), N (light blue), K (purple) and U (green). (right) ^{1}H NMR spectrum (400 MHz, THF-d$_8$, 298 K) of the crude reaction mixture of [U(OSi(O^{t}Bu)$_3$)$_2$(μ-OSi(O^{t}Bu)$_3$)]$_2$ and potassium azide after 5 days at -40°C.

The structural arrangement of the metallic centres in **34**-K[U^{IV}---N---U^{IV}] is close to the one in Cs[U^{IV}---N---U^{IV}],[69] with the cesium cation replaced by a potassium (Figure IV- 10 left, selected bond distances and angles are reported in Table IV- 1). Two uranium(IV) cations are held together by a bridging nitrido N^{3-} ligand in a nearly linear fashion (U-N-U angle: 170.3(5)°). The short U-N nitride bond distances (mean U-N: 2.083(13) Å) are in agreement with the presence of a multiple U-N bond and are close to those observed for the other linear μ_2-N^{3-} uranium complexes (U-N distances ranging from 2.012(16)-2.090(8) Å and U-N-U angle ranging from 160 to 175°).[69,423,424,426] A potassium cation is held in the structure by coordination to three siloxy ligands (U1-N1-K1 angle: 82.1(1)°). The main differences between the two M[U^{IV}---N---U^{IV}] (M: K, Cs) structures arise from the different coordination environments of the uranium and alkali metals by the siloxide ligands. In **34**-K[U^{IV}---N---U^{IV}], the five-coordinate U1 centre is in a distorted square pyramidal coordination environment, featuring one bidentate O^-/O^tBu siloxide ligand and two siloxides bridging the U and K centres, while the five-coordinate U2 centre features a distorded trigonal bipyramidal geometry and is coordinated by two terminal siloxide ligands and a bidentate O^-/O^tBu siloxide ligand bridging the U and K centres.

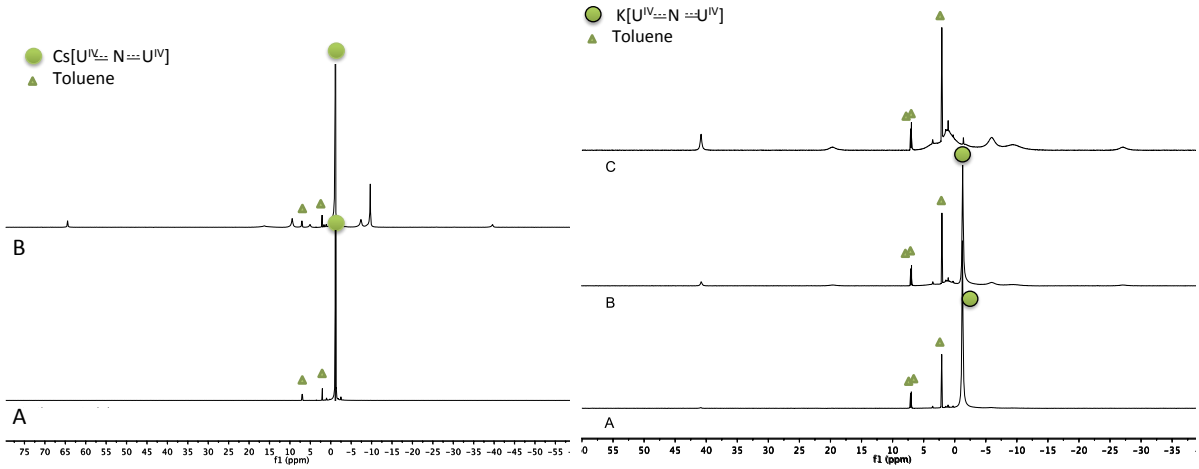

Figure IV- 11 Evolution over time of the ^{1}H NMR spectra (400 MHz, Toluene-d_8, 298 K) of (left) (A) Cs[U^{IV}---N---U^{IV}] and (B) after 5 days at room temperature, (right) (A) **34**-K[U^{IV}---N---U^{IV}], (B) after one hour and (C) after 24hours at room temperature.

34-K[U^{IV}---N---U^{IV}] shows reduced stability compared to the Cs analogue. Notably, **34**-K[U^{IV}---N---U^{IV}] decomposed fully over 24 hours at room temperature in toluene solution whereas the decomposition of the cesium analogue is complete only after one week (Figure IV- 11).

IV.2.3.2) Reduction with KC_8

Following the isolation of the $[K\{U(OSi(O^tBu)_3)_3\}_2(\mu\text{-}N)]$ complex, we investigated its possible reduction with KC_8. The reduction of $[K\{U(OSi(O^tBu)_3)_3\}_2(\mu\text{-}N)]$ with 10 equivalents of KC_8 in THF at -40°C afforded the bis-U(III) nitride complex $[K_3\{U(OSi(O^tBu)_3)_3\}_2(\mu\text{-}N)]$, **36**-$K_3[U^{III}{-}N{-}U^{IV}]$ (Scheme IV- 10).

However, we realised that when the reduction of $[Cs\{U(OSi(O^tBu)_3)_3\}_2(\mu\text{-}N)]$ with 10 equivalents of KC_8 in THF at -40°C also afforded the bis-U(III) nitride complex $[K_3\{U(OSi(O^tBu)_3)_3\}_2(\mu\text{-}N)]$, **36**-$K_3[U^{III}{-}N{-}U^{IV}]$, which was obtained analytically pure in 70% yield after recrystallisation from hexane at -70°C (Scheme IV- 10).

Scheme IV- 10 Synthesis of **36**-$K_3[U^{III}{-}N{-}U^{III}]$ and **37**-$K_3[U^{III}{-}N{-}U^{IV}]$.

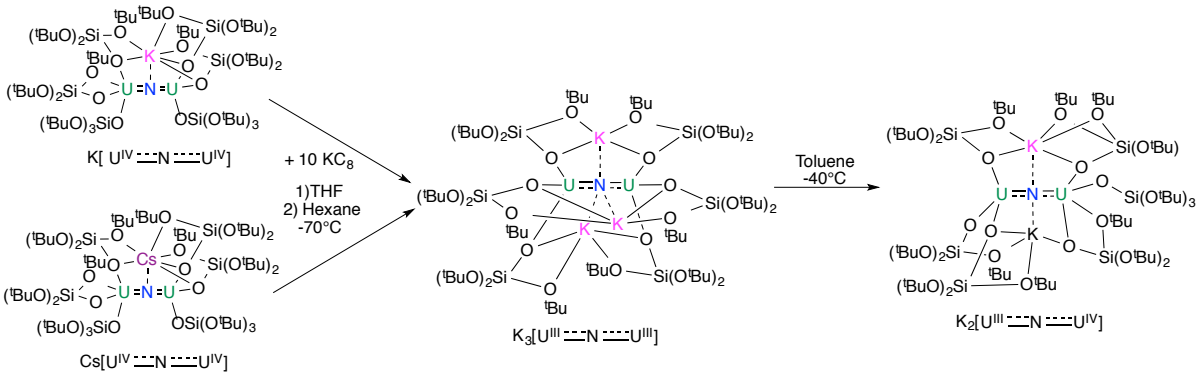

Based on the difficulty to prepare clean **34**-$K[U^{IV}{-}N{-}U^{IV}]$ from the reaction of the U(III) complex with KN_3, we decided to prepare $[K_3\{U(OSi(O^tBu)_3)_3\}_2(\mu\text{-}N)]$, **36**-$K_3[U^{III}{-}N{-}U^{III}]$ from the reduction of $[Cs\{U(OSi(O^tBu)_3)_3\}_2(\mu\text{-}N)]$, $Cs[U^{IV}{-}N{-}U^{IV}]$.

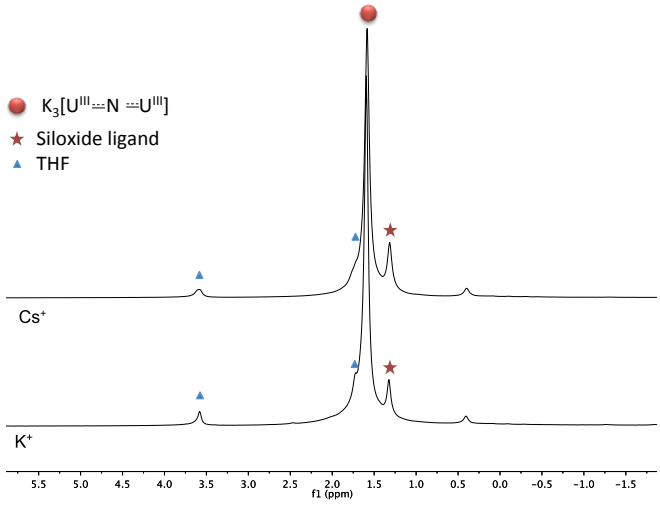

Figure IV- 12 ^{1}H NMR spectra (400 MHz, THF-d_8, 233 K) of the crude reaction mixture of $M[U^{IV}{-}N{-}U^{IV}]$ (M: Cs or K) with 10 equivalents of KC_8.

X-ray quality crystals of $[K_3\{U(OSi(O^tBu)_3)_3\}_2(\mu\text{-}N)]$, **36**-$K_3[U^{III}{-}N{-}U^{III}]$ were grown both from THF or hexane at -40°C over the course of two days. When a solution of **36**-$K_3[U^{III}{-}N{-}U^{III}]$ in toluene is left at -40°C, crystals of the decomposed mixed-valent product $[K_2\{U(OSi(O^tBu)_3)_3\}_2(\mu\text{-}N)]$, **37**-$K_2[U^{III}{-}N{-}U^{IV}]$ formed after one week.

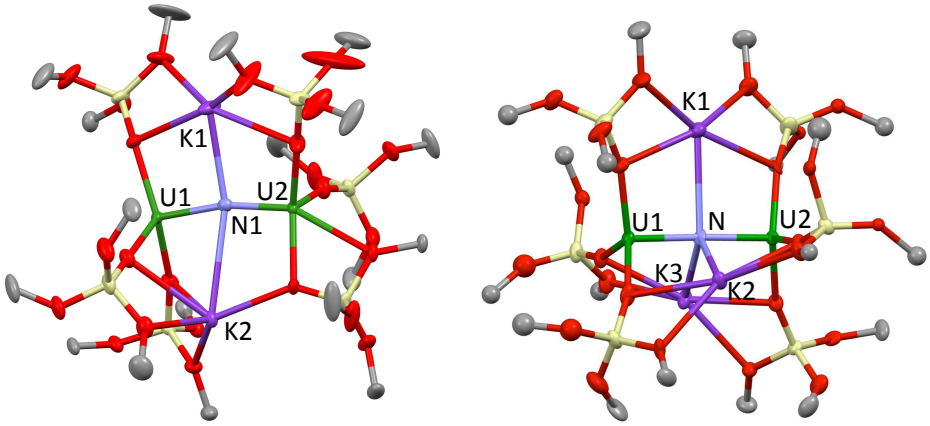

Figure IV- 13 Crystallographic structure of $[K_2\{U(OSi(O^tBu)_3)_3\}_2(\mu\text{-}N)]$, **37**-$K_3[U^{III}{-}N{-}U^{IV}]$ (left) and $[K_3\{U(OSi(O^tBu)_3)_3\}_2(\mu\text{-}N)]$, **36**-$K_3[U^{III}{-}N{-}U^{III}]$ (right) crystallised from a saturated THF solution; ellipsoid probability 50%, with hydrogen atoms, methyl groups and disorder. Atoms: C (grey), O (red), Si (light yellow), N (light blue), K (purple) and U (green).

The solid-state molecular structures of $[K_2\{U(OSi(O^tBu)_3)_3\}_2(\mu\text{-}N)]$ and $[K_3\{U(OSi(O^tBu)_3)_3\}_2(\mu\text{-}N)]$ were determined by single-crystal X-ray diffraction, and are represented in Figure IV- 13. Both structures are closely related to **32**-$Cs_2[U^{III}{-}N{-}U^{IV}]$ and **33**-$Cs_3[U^{III}{-}N{-}U^{III}]$ and feature two uranium atoms connected linearly via a nitride group. In complex **37**-$K_2[U^{III}{-}N{-}U^{IV}]$, the K^+ cations are bound to the bridging nitride in an almost linear way (K-N-K = 159.58(14)°) and to the siloxide oxygen. The K-N-K and the U-N-U fragments are located in the same plane and perpendicular each other. U1 is coordinated by a nitride group and three siloxide oxygen atoms with a pseudo-tetrahedral coordination geometry while the five-coordinate U2 has a distorded trigonal bipyramidal coordination geometry and is coordinated by two terminal siloxide ligands and a bidentate O^-/O^tBu siloxide ligand. In **36**-$K_3[U^{III}{-}N{-}U^{III}]$, a nitride group and three siloxide oxygen atoms give rise to a pseudo-tetrahedral coordination geometry around each uranium ion. Three K^+ cations bind the nitride, forming an irregular triangle located in a plane perpendicular to the U-N-U fragment (K-N-K angles: 115.7(5), 122.5(5) and 121.7(5)°). Bond distances are compared in section IV.2.4.

The ^{1}H NMR spectrum of **36**-$K_3[U^{III}{=}N{=}U^{III}]$ in THF solution shows the presence of only one signal for the six siloxide ligands, in agreement with the presence of symmetry-related siloxides and fluxionality of the bound potassium cation (Figure IV- 12).

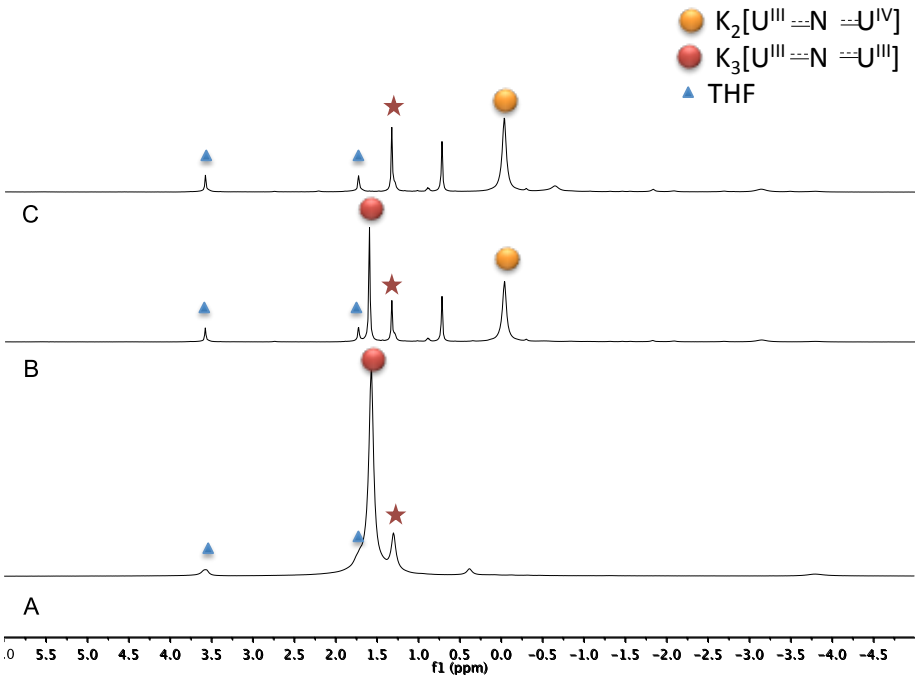

Figure IV- 14 Evolution over time of the ^{1}H NMR spectrum (400 MHz, THF-d_8, 233 K) of (A) **36**-$K_3[U^{III}{=}N{=}U^{III}]$, (B) after 7 days and (C) after 12 days at -40°C.

Similarly to **33**-$Cs_3[U^{III}{=}N{=}U^{III}]$, **36**-$K_3[U^{III}{=}N{=}U^{III}]$ is highly reactive and must be handled only at very low temperatures. The reduction of $Cs[U^{IV}{=}N{=}U^{IV}]$ was performed in THF, as in hexane (or toluene) a mixture of unknown products was obtained. The reduction of $Cs[U^{IV}{=}N{=}U^{IV}]$ in THF with 2 equivalents of KC_8 led to a mixture of **36**-$K_3[U^{III}{=}N{=}U^{III}]$ and **37**-$K_2[U^{III}{=}N{=}U^{IV}]$, while the use of an excess of KC_8 only gave **36**-$K_3[U^{III}{=}N{=}U^{III}]$. The reduction time is much more faster with KC_8 (2 minutes) than with cesium (3 hours), however the filtration of the graphite and the excess of KC_8 leads to a longer manipulation time, leading to a partial oxidation of **36**-$K_3[U^{III}{=}N{=}U^{III}]$. The best way to limit the decomposition of **36**-$K_3[U^{III}{=}N{=}U^{III}]$ was to perform the filtration in a cold well at -70°C. The **36**-$K_3[U^{III}{=}N{=}U^{III}]$ complex is much more stable than the **33**-$Cs_3[U^{III}{=}N{=}U^{III}]$ analogue. As opposed to **33**-$Cs_3[U^{III}{=}N{=}U^{III}]$, which decomposed too quickly in solution, **36**-$K_3[U^{III}{=}N{=}U^{III}]$ could be recrystallised from hexane at -70°C to afford an analytically pure complex. Recrystallised **36**-$K_3[U^{III}{=}N{=}U^{III}]$ can be stored in the solid state under argon at -40 °C for several months, while **33**-$Cs_3[U^{III}{=}N{=}U^{III}]$ decomposed even in the solid state at -40°C. A solution (THF or

toluene) stored at -40°C takes more than 7 days to fully decompose into free ligand and the mixed-valent U(III)/U(IV) nitride complex (Figure IV- 14), whereas the **33**-$Cs_3[U^{III}{-}N{-}U^{III}]$ analogue decomposes in only 40 hours. The highly charged structure is better stabilised by several smaller cations such as K^+ than Cs^+.

IV.2.4) Structural comparison

Bond distances and angles are reported in Table IV- 1. Complexes $M_2[U^{III}{-}N{-}U^{IV}]$ and $M_3[U^{III}{-}N{-}U^{III}]$ (M: Cs, K) display a linear U-N-U motif with U-N-U angles comparable to those found in the bis-U(IV) precursor. In complex **32**-$Cs_2[U^{III}{-}N{-}U^{IV}]$, the two U-N distances are similar, suggesting the presence of non-localised charge, whereas in complex **37**-$K_2[U^{III}{-}N{-}U^{IV}]$ the distances differ by 0.2 Å, suggesting the presence of localised U(III) and U(IV). The two U-N distances in complex **33**-$Cs_3[U^{III}{-}N{-}U^{III}]$ are equivalent (2.1495(12) Å) as a result of the two-fold crystallographic axis passing through one Cs atom and the nitride ion. The values of these distances are similar to the mean value of the U-N distances in **36**-$K_3[U^{III}{-}N{-}U^{III}]$ (2.120(13) Å). The mean U-N distances for reduced complexes $M_2[U^{III}{-}N{-}U^{IV}]$ and $M_3[U^{III}{-}N{-}U^{III}]$ (M = Cs, K) are longer than those found in the U(IV) dimer $Cs[U^{IV}{-}N{-}U^{IV}]$,[69] **34**-$K[U^{IV}{-}N{-}U^{IV}]$ and in the previously reported U(IV)/U(IV) nitrides containing a similar linear UNU motif (2.012(16)–2.090(8) Å).[423,424,426]

Table IV- 1 Comparative structural parameters of nitride complexes (bond lengths in Å and angles in °)

	$Cs[U^{IV}{-}N{-}U^{IV}]$ [69]	**34-$K[U^{IV}{-}N{-}U^{IV}]$**	**32-$Cs_2[U^{III}{-}N{-}U^{IV}]$**	**37-$K_2[U^{III}{-}N{-}U^{IV}]$**	**33-$Cs_3[U^{III}{-}N{-}U^{III}]$**	**36-$K_3[U^{III}{-}N{-}U^{III}]$**
U1-N	2.058(5)	2.092(9)	2.099(12)	2.209(4)	2.1495(12)	2.129(14)
U2-N	2.079(5)	2.073(9)	2.081(12)	2.003(4)		2.111(14)
U-O_{avg}	2.19(3)	2.21(2)	2.243(25)	2.272(51)	2.282(24)	2.288(26)
M1-N	3.393(4)	3.246(9)	3.276(12)	3.344(4)	3.348(8)	3.115(17)
M2-N	-	-	3.635(12)	2.879(4)	3.22(2)	3.017(16)
K3-N	-	-	-	-	-	3.243(15)
U-N-U	170.2(3)	170.3(5)	169.1(7)	162.17(19)	174.2(11)	173.7 (7)

The U(III)-N bond distances are 0.04-0.09 Å longer than those of the U(IV) precursor, in agreement with the larger size of U(III). This increase is similar to the one on the average U-O bond length (0.07-0.09 Å). Smaller variation in the U-N bond distances (0.03 Å) was observed by Cummins and coworkers in the successive oxidation of a linear U(IV)=N=U(IV) fragment supported by amide ligands to U(V)=N=U(V).[424] The larger variation in the U-N bond distances (0.04-0.09 Å) observed in the successive reduction of the $Cs[U^{IV}{-}N{-}U^{IV}]$ complex is, at least partly, due to the presence of an increasing number of Cs^+/K^+ cations

binding the nitride group and thus polarising and reducing the electron density on the U---N---U fragment. The lengthening of the U-N bonds upon alkali ion coordination to the imido group has been also observed in bimetallic U(IV) complexes.[431]

The U(III)-N bond distances in $M_2[U^{III}---N---U^{IV}]$ and $M_3[U^{III}---N---U^{III}]$ (M: Cs, K) remain much shorter than U(III)-N single bond distances (for example: $U\text{-}N_{cyanate}$ = 2.456(7) Å in $[U(Tren^{TIPS})(NCO)][K(B15C5)_2]$,[432] $U\text{-}N_{dinitrogen}$ = 2.401(8)-2.423(8) Å in $\{[U(Cp^*)(C_8H_4\{Si^iPr\text{-}1,4\}]_2(\mu\text{-}\eta^2\text{:}\eta^2\text{-}N_2)\}$,[258] or $U\text{-}N_{amide}$ = 2.320(4) Å in $U[N(SiMe_3)_2]_3$.[433] Longer U-N distances were also found in a U(IV) cluster with a $U_4(\mu_4\text{-}N)$ core (2.271(3)-2.399(5) Å).[83] This points to the presence of U^{III}-N multiple bonding in the reduced complexes $M_2[U^{III}---N---U^{IV}]$ and $M_3[U^{III}---N---U^{III}]$ (M: Cs, K).

IV.3) Synthesis of diuranium(V) complexes

As mentioned in section (IV.2.3.1)), the reaction of the dinuclear uranium(III) $[U(OSi(O^tBu)_3)_2(\mu\text{-}OSi(O^tBu)_3)]_2$ complex with one equivalent of potassium azide (Scheme IV- 9) yields a mixture of the nitride-bridged diuranium(IV) complex $[K\{U(OSi(O^tBu)_3)_3\}_2(\mu\text{-}N)]$ and of the nitrido/azido diuranium(IV) compound $[K_2\{U(OSi(O^tBu)_3)_3\}_2(\mu\text{-}N)(\mu\text{-}N_3)]$, **35**.

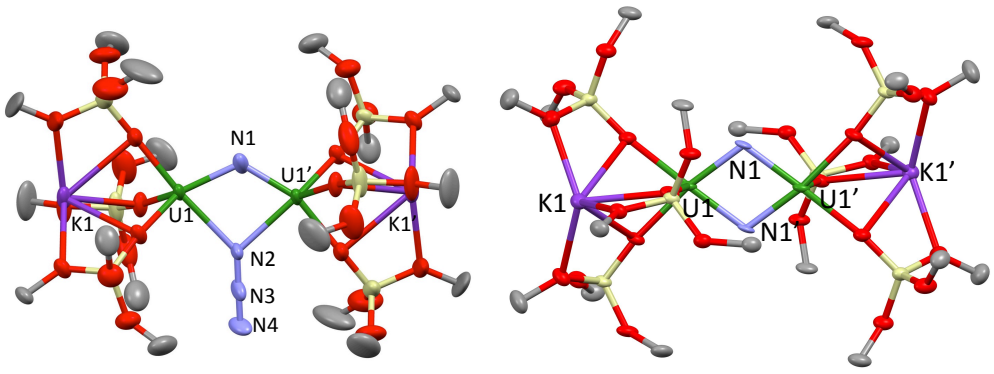

Figure IV- 15 Crystallographic structure of $[K_2\{U(OSi(O^tBu)_3)_3\}_2(\mu\text{-}N)(\mu\text{-}N_3)]$, **35** (left) and $[K\{U(OSi(O^tBu)_3)_3\}(\mu\text{-}N)]_2$, **38** [69] (right) crystallised from a saturated Toluene solution; ellipsoid probability 50%, with hydrogen atoms, methyl groups omitted for clarity. Atoms: C (grey), O (red), Si (light yellow), N (light blue), K (purple) and U (green). Selected bond lengths [Å] and angles [°] of **35** : U1-N1=2.018(12), U1'-N1=2.085(11), U1-N2=2.494(11), U1'-N2=2.575(12), $U\text{-}O_{avg}$=2.224(5), N2-N3=1.238(17), N3-N4=1.143(16), U1-N1-U1'=124.6(6), U1-N2-U1'=91.5(4); **38**: U1−N1=2.022(5);,U1−N1'=2.101(6), $U1\text{−}O_{avg}$=2.23(3), U1−U1'=3.2960(6), U1−N1−U1'=106.1(2).

The crystal structure of $[K_2\{U(OSi(O^tBu)_3)_3\}_2(\mu\text{-}N)(\mu\text{-}N_3)]$, **35** is represented in Figure IV- 15 (left). The two uranium cations in this complex are held together by a bridging nitrido ligand (U1−N1−U1': 124.6(6)°) and a 1,1-end-on bridging azido ligand (U1-N2-U1': 91.5(4)°). The coordination sphere of the uranium centres is completed by three siloxide ligands, giving a distorted square pyramidal coordination environment. The siloxide ligands bridge both the

U1 and the K1 centres, providing O_6 coordination pockets suitable for K^+ (K1-U1 3.564(1) Å). An inversion centre is found between the two uranium ions in **35**, thus the asymmetric unit contains only one uranium atom and one potassium ion. The mean uranium-nitride bond distance (2.05(5) Å) is in the range of those found in the previously reported U(IV) nitrides.[69,423-426] The U1-N2 bond distance (2.494(11) Å) lies in the range of those reported for 1,1-end-on coordinated azide to uranium(IV) (2.441(4)-2.511(4) Å).[83]

Scheme IV- 11 Controlled synthesis of $[K_2\{U(OSi(O^tBu)_3)_3\}_2(\mu\text{-}N)(\mu\text{-}N_3)]$, **35** and $[K\{U(OSi(O^tBu)_3)_3\}(\mu\text{-}N)]_2$, **38**

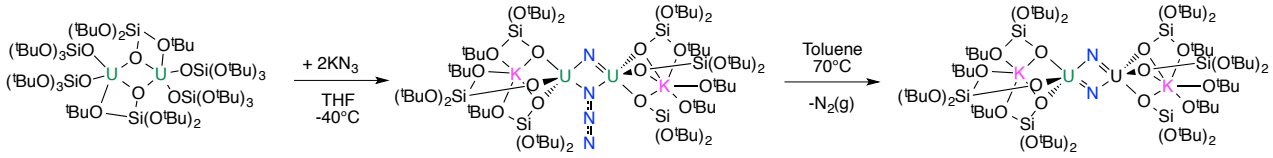

We anticipated that the nitride/azide complex $[K_2\{U(OSi(O^tBu)_3)_3\}_2(\mu\text{-}N)(\mu\text{-}N_3)]$, **35** could be an ideal precursor for the synthesis of a bis(nitride) U(V)-U(V) species. That is why we decided to perform the reaction of the U(III) complex $[U(OSi(O^tBu)_3)_2(\mu\text{-}OSi(O^tBu)_3)]_2$ with two equivalents of potassium azide in THF at -40°C, and this afforded pure **35** in good yield (72%) (Scheme IV- 11). This complex is stable in toluene solution at -40°C but decomposes over few days at room temperature (Figure IV- 16).

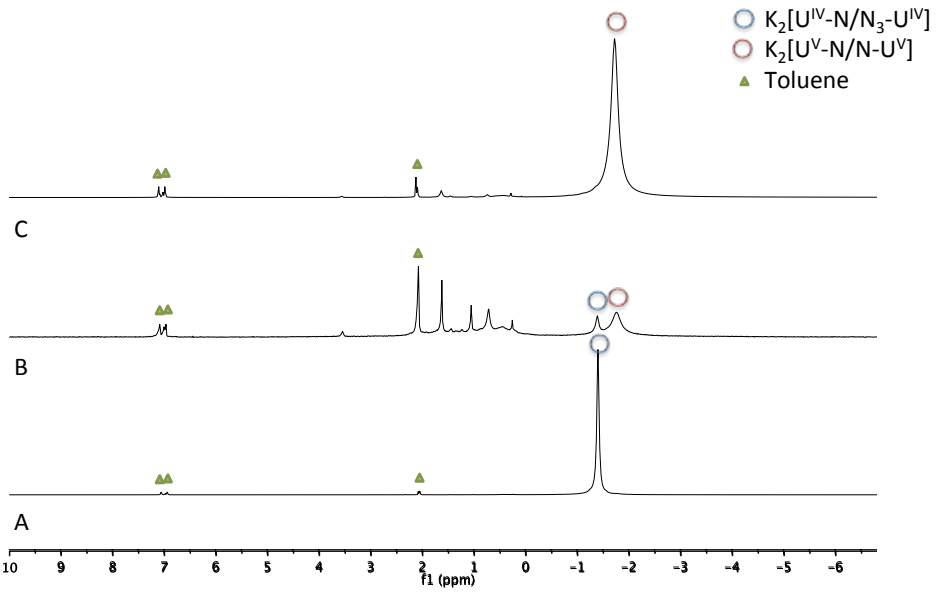

Figure IV- 16 ^{1}H NMR spectra (400 MHz, Toluene-d_8, 298 K) of $[K_2\{U(OSi(O^tBu)_3)_3\}_2(\mu\text{-}N)(\mu\text{-}N_3)]$, **35** (A), after 4.5days at room temperature (B) and after 12hours at 70°C (C).

One decomposition product was identified as the di-μ-nitrido diuranium(V) complex $[K\{U(OSi(O^tBu)_3)_3\}(\mu\text{-}N)]_2$, **38**.[69] The decomposition of the azide ligand in **35** to form a nitride ligand with release of nitrogen ($N_3^- + 2e^- = N^{3-} + N_2$), is associated with a two-electron transfer affording the diuranium(V) complex **38**. **35** is cleanly converted into $[K\{U(OSi(O^tBu)_3)_3\}(\mu\text{-}N)]_2$, **38** upon heating a toluene solution of **35** at 70°C for 12 hours (Figure IV- 16). Release of N_2(g) is clearly observed and the nature of the compound **38** was confirmed by performing a unit cell check of X-ray quality crystals. The crystal structure of **38** is represented in Figure IV- 15 right (taken from ref [69]). With this synthetic procedure, $[K\{U(OSi(O^tBu)_3)_3\}(\mu\text{-}N)]_2$, **38** was synthesised in 87% yield, enabling magnetic characterisation of this complex.

IV.4) Magnetic properties

Temperature-dependent magnetic susceptibility data were collected for **36**-$K_3[U^{III}\text{---}N\text{---}U^{III}]$, $[K\{U(OSi(O^tBu)_3)_3\}(\mu\text{-}N)]_2$ **38**, **34**-$K[U^{IV}\text{---}N\text{---}U^{IV}]$ and $[K_2\{U(OSi(O^tBu)_3)_3\}_2(\mu\text{-}N)(\mu\text{-}N_3)]$, **35** under an applied field of 0.5T (Figure IV- 17 and Figure IV- 18). Due to the high thermal sensitivity of **36**-$K_3[U^{III}\text{---}N\text{---}U^{III}]$, data were not collected above 200 K whereas magnetic susceptibility data were collected from 2 to 300 K for the three other complexes, which are more stable.

Above 100 K, **36**-$K_3[U^{III}\text{---}N\text{---}U^{III}]$ displays Curie-Weiss behaviour ($\chi = C/(T-T_C)$; C = 2.36 $cm^3.K.mol^{-1}$; T_C = -187 K), as expressed by the linearity of the $1/\chi$ curve. From these data, the effective magnetic moment at room temperature was extrapolated to 3.41 μ_B per uranium. This value is slightly lower than the theoretical value (3.62μ_B) calculated for a $5f^3$ ion with full spin-orbit coupling. This is commonly observed in trivalent uranium complexes due to the crystal-field splitting of the Russel-Saunders $^4I_{9/2}$ ground term and this value remains in the range of the other U(III) coordination compounds.[103]

A magnetic moment of 1.81μ_B per uranium was calculated for $[K\{U(OSi(O^tBu)_3)_3\}(\mu\text{-}N)]_2$, **38** ($\chi T$(300 K) = 0.82 $cm^3.K.mol^{-1}$), which is lower than the theoretical value (2.54μ_B) calculated for a $5f^1$ ion with full spin-orbit coupling ($^2F_{5/2}$, g = 6/7) but remains in the range of U(V) complexes.[103]

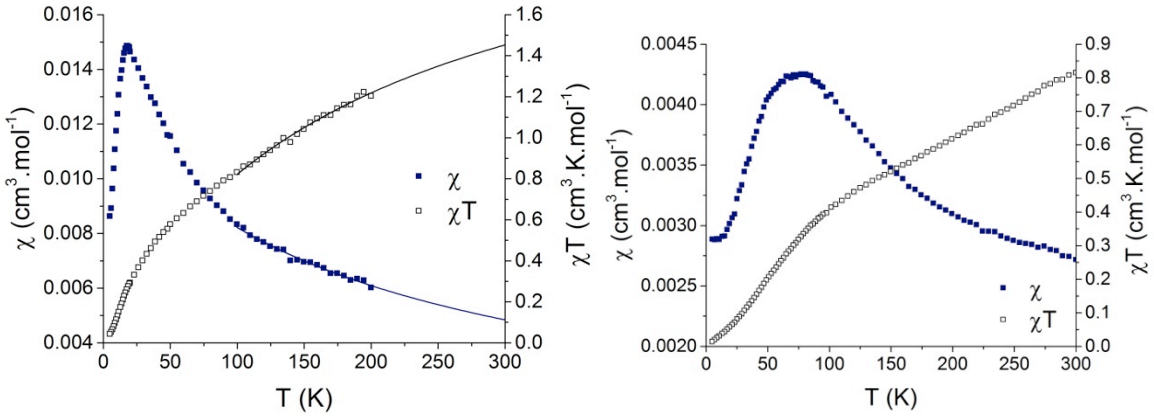

Figure IV- 17 Temperature-dependent magnetic susceptibility data (0.5 T) for complex **36**-$K_3[U^{III}\underline{\text{---}}N\underline{\text{---}}U^{III}]$ per uranium ion (left) and for $[K\{U(OSi(O^tBu)_3)_3\}(\mu\text{-}N)]_2$, **38** per uranium ion (right). Curie-Weiss linear fits are represented as linear curves in the 100-300 K section.

The magnetic susceptibility data of $[K\{U(OSi(O^tBu)_3)_3\}(\mu\text{-}N)]_2$, **38** plotted as a function of temperature present a clear maximum at 76.9 K (Figure IV- 17 right), suggesting the presence of antiferromagnetic coupling between the two uranium(V) ions. Unambiguous magnetic coupling in polymetallic complexes of U(V) are rare. In 1990, Andersen and coworkers presented the first antiferromagnetically coupled U(V)/U(V) complex $[\{(MeC_5H_4)_3U\}_2(\mu\text{-}1,4\text{-}N_2C_6H_4)]$.[62] In this case, the U centres are bridged by 1,4-diimidobenzene, which yields a T_N of 20 K. Our group reported cation-cation dimeric, trimeric and tetrameric uranyl(V) complexes displaying antiferromagnetic coupling with Neel temperatures ranging from 5 to 12 K. In these examples, uranyl(V) oxo groups act as bridging ligands via the cation-cation interaction.[47,48,231,242] In 2009, Boncella and co-workers reported exchange coupling in a bis(imido) analogue of uranyl(V) $[\{U(N^tBu)_2(I)(^tBu_2bpy)\}_2]$, assembled via diamond-shaped cation-cation interaction, in which T_N = 13 K.[276] In 2012, Arnold and co-workers studied the dinuclear complex $[(Me_3SiOUO)_2(Pcm)]$ (Pcm = polypyrrolic macrocycle Pacman) and reported relatively strong antiferromagnetic coupling, with an ordering temperature of 17 K.[204] Until recently, all Neel temperatures of $5f^1$-$5f^1$ coupled systems ranged from 5 to 20 K, significantly lower than that observed for the dinitride complex $[K\{U(OSi(O^tBu)_3)_3\}(\mu\text{-}N)]_2$, **38** ($T_N$ = 76.9 K). In 2014, a much higher value of Neel temperature (T_N = 70 K) comparable to that found in our dinitride complex was reported by Meyer for the bis(oxo) diuranium(V) complex $[\{((^{nP,Me}ArO)_3tacn)U\}_2(\mu\text{-}O)_2]$.[199] The U-U distance in $[K\{U(OSi(O^tBu)_3)_3\}(\mu\text{-}N)]_2$, **38** (3.2960(6) Å) is significantly smaller than in the bis(oxo) $[\{((^{nP,Me}ArO)_3tacn)U\}_2(\mu\text{-}O)_2]$ (3.4222(3) Å) but does not have much impact on the strength of the magnetic coupling (Table IV- 2). In comparison, the bis(oxo) U(V) complex $[(Me_3SiOUO)_2(Pcm)]$ reported by Arnold and coworkers presents similar structural

parameters to the $[KU(OSi(O^tBu)_3)_3(\mu\text{-}N)]_2$ complex (Table IV- 2) but weaker antiferromagnetic coupling at 17 K.[204] The two diamond-shaped cation-cation complexes, $[UO_2(dbm)_2K(18c6)]_2$ [47] and $[U(N^tBu)_2(I)(^tBu_2bpy)]_2$ [276] display much longer U-U distances and lower Neel temperatures than in **38** (Table IV- 2). With these examples, we can see that the nature of both the ligand and structural arrangements have a huge influence on the magnetic communication between the U(V) centres, leading to a large range of Neel temperatures (Table IV- 2). To our knowledge, the antiferromagnetic coupling of **38** is the highest value for two coupled U(V) ions.

Table IV- 2 Selected bond distances (Å) and angles (°) associated to the Neel temperature (K) of antiferromagnetically coupled uranium(V) complexes.

	$U_1\text{-}E_{1,2}$	$U_2\text{-}E_{1,2}$	$U_1\text{-}E_{1,2}\text{-}U_2$	U-U	T_N (K)
$[K\{U^V(OSi(O^tBu)_3)_3\}(\mu\text{-}N)]_2$ 38 [69]	2.022(5), 2.101(6)	2.022(5), 2.101(6)	106.1(2)	3.2960(6)	76.9
$[\{((^{nP,Me}ArO)_3tacn)U^V\}_2(\mu\text{-}O)_2]$ [199]	2.035(1), 2.182(1)	2.035(1), 2.182(1)	108.45(5)	3.4222(3)	70
$[(Me_3SiOU^VO)_2(Pcm)]$ [204]	2.099(4), 2.098(4)	2.085(4), 2.095(4)	106.5(2)	3.3557	17
$[\{U^V(N^tBu)_2(I)(^tBu_2bpy)\}_2]$ [276]	2.067(5), 2.380(5)	2.387(5), 2.078(5)	106.7(2)	3.577(1)	13
$[U^VO_2(dbm)_2K(18c6)]_2$ [47]	1.941(4), 2.384(4)	1.941(4), 2.384(4)	105.8(2)	3.462(4)	5

A clear maximum occurs in the plot of χ versus T at 18.5 K for the **36**-$K_3[U^{III}\text{---}N\text{---}U^{III}]$ complex (Figure IV- 17 left). This feature suggests the presence of antiferromagnetic coupling between the two uranium(III) centres. The presence of magnetic communication between two U(III) complexes has rarely been proposed.[179,434,435] To our knowledge, only two unambiguous examples of antiferromagnetic coupling for U(III) molecular compounds have been observed so far in the siloxide bridged diuranium(III) complex $[U(OSi(O^tBu)_3)_2(\mu\text{-}OSi(O^tBu)_3)]_2$ [69] and in an arene-bridged U(III) dimer reported by Cummins[283] that present a cusp in the plot of χ versus T at respectively 16 K and 110 K, respectively. The latter example represents the highest Neel temperature (T_N) reported for antiferromagnetically coupled uranium complexes. Despite the different coordination environments and U-U distances found in the nitride **36**-$K_3[U^{III}\text{---}N\text{---}U^{III}]$ complex (four-coordinate uranium, U-U distance of 4.232(1) Å, U-N1-U angle of 173.7(7)°) and the $[U(OSi(O^tBu)_3)_2(\mu\text{-}OSi(O^tBu)_3)]_2$ complex (five-coordinate uranium, U-U distance of 3.9862(2) Å, U-O1-U angle of 107.42(1)°), the Neel temperatures of the antiferromagnetic coupling are similar.

The antiferromagnetic couplings observed for **36**-$K_3[U^{III}\text{---}N\text{---}U^{III}]$ and $[K\{U(OSi(O^tBu)_3)_3\}(\mu\text{-}N)]_2$, **38** rule out the presence of a magnetic ground state and possible SMM properties.

The room temperature effective moments per uranium(IV) ions in **34**-$K[U^{IV}\text{---}N\text{---}U^{IV}]$ and $[K_2\{U(OSi(O^tBu)_3)_3\}_2(\mu\text{-}N)(\mu\text{-}N_3)]$, **35** are 2.9 μ_B and 2.7 μ_B respectively. These values are

lower than the theoretical value (3.58 μ_B) calculated for a $5f^2$ ion with full spin-orbit coupling ($^3H_4$) but falls in the range of other U(IV) coordination compounds[103] and are similar to the magnetic moment found for the Cs[U^{IV}---N---U^{IV}] complex (3.0 μ_B).[69] An inflexion point is observed at low temperature in the χ vs T plot of the complex **35**, and this could be due to temperature independent paramagnetism often seen for U(IV) ions or to a magnetic interaction between the uranium ions.

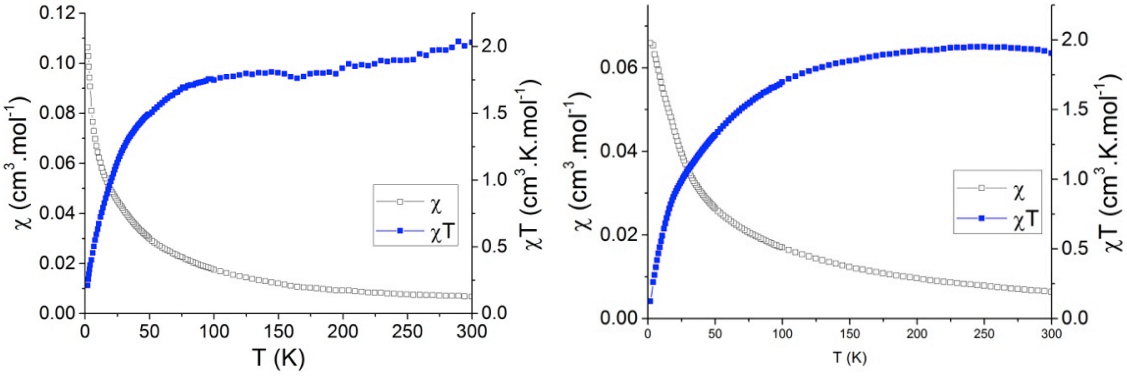

Figure IV- 18 Temperature-dependent magnetic susceptibility data (0.5T) for complex **34**-K[U^{IV}---N---U^{IV}] (left) and for [K_2{U(OSi(O^{t}Bu)$_3$)$_3$}$_2$(μ-N)(μ-N$_3$)], **35** (right).

Table IV- 3 Selected bond distances (Å) and angles (°) associated to the Neel temperature (K) of antiferromagnetically (AF) coupled uranium(IV) complexes.

	U_1-E	U_2-E	U_1-E-U_2	U-U	T_N
Cs[U^{IV}---N---U^{IV}] [69]	2.058(5)	2.079(5)	170.2(3)	4.1214(4)	-
34-K[U^{IV}---N---U^{IV}]	2.092(9)	2.073(9)	170.3(5)	4.1507(5)	-
[{((^{tBu}**ArO)$_3$tacn)U^{IV}}$_2$(μ-O)]** [187]	2.110(4)	2.110(4)	180	4.219(1)	20
[{U(Tren^{DMSB})}(μ-O){U(Tren$^{DMSB-C2O2}$)}] [200]	2.116(3)	2.138(3)	160.87(16)	4.195(1)	3

No unambiguous magnetic coupling is observed for the two measured dinuclear uranium(IV) complexes, **34**-K[U^{IV}---N---U^{IV}] and [K_2{U(OSi(O^{t}Bu)$_3$)$_3$}$_2$(μ-N)(μ-N$_3$)], **35** (Figure IV- 18). Unambiguous magnetic coupling has very rarely been observed between uranium(IV) atoms. To the best of our knowledge, only four examples of antiferromagnetic exchange coupling for U(IV) have been observed with Neel temperatures ranging from 3 to 20 K.[187,200] Despite the presence of a similar arrangement of the two uranium(IV) ions in the M[U^{IV}---N---U^{IV}] (M: Cs, K), [{((tBu)ArO)$_3$tacn)U^{IV}}$_2$(μ-O)] and [{U(Tren^{DMSB})}(μ-O){U(Tren$^{DMSB-C2O2}$)}] complexes (Table IV- 3), the magnetic measurements reveal strong differences. The two U(IV) ions connected with oxo bridge revealed antiferromagnetic couplings, while the two μ-nitride U(IV) complexes do not display unambiguous antiferromagnetic interactions.

In contrast to the [U{HC(SiMe$_2$Ar)$_2$(SiMe$_2$-μ-N)}(μ-η^1:η^1-Ar)U-(Ts^{Xy})] complex,[282] the compound **35** does not exhibit ferromagnetic interactions, despite the presence of a similar distorted diamond cores (Figure IV- 19).

The observation of magnetic coupling between uranium(IV) remains unusual. The magnetic properties of U(IV) ions are strongly influenced by their coordination environment.

[U{HC(SiMe$_2$Ar)$_2$(SiMe$_2$-μ-N)}(μ-η^1:η^1-Ar)U-(Ts^{Xy})][282]	**[K$_2${U(OSi(O^{t}Bu)$_3$)$_3$}$_2$(μ-N)(μ-N$_3$)], 35**
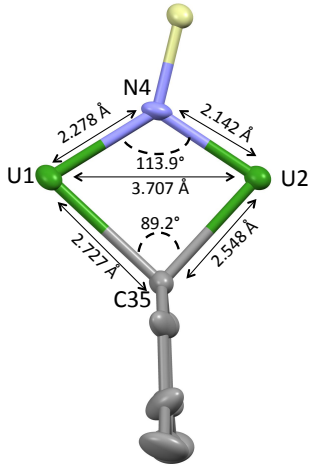	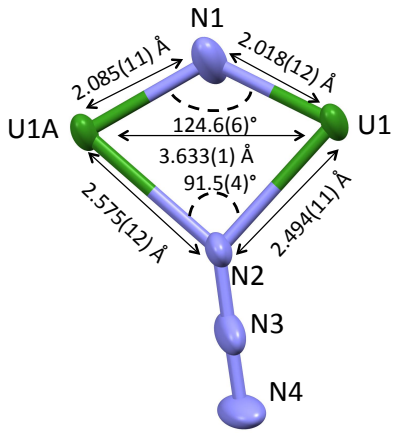
Ferro, J = + 20cm^{-1}	No coupling

Figure IV- 19 Diamond cores and structural parameters of [U{HC(SiMe$_2$Ar)$_2$(SiMe$_2$-μ-N)}(μ-η^1:η^1-Ar)U-(Ts^{Xy})] and [K$_2${U(OSi(O^{t}Bu)$_3$)$_3$}$_2$(μ-N)(μ-N$_3$)], **35**

IV.5) Conclusion

In conclusion, we have expanded the family of molecular uranium nitride complexes to the +III oxidation state. Unprecedented molecular uranium(III) nitride complexes have been synthesised by reducing the U(IV) nitride analogue with an excess of strong reducing agent. Structural studies demonstrate the presence of U(III)-N multiple bonding. Meanwhile, a bis-U(V) nitrido complex has been reproducibly synthesised from the activation of an azide ligand. Both nitride-bridged systems revealed antiferromagnetic coupling, with the highest value reported for a 5f^1-5f^1 coupled complex. We observed that the nitride ligand promotes magnetic interaction between actinide centres, however only antiferromagnetic coupling was observed.

In order to promote ferromagnetic interactions between uranium through nitride ligands and possibly reach uranium nitride SMMs, further studies will be directed towards

changing the coordination environment of the uranium, particularly to induce shorter U-N-U angles and U-U distances. Moreover, these multiply bonded uranium-nitride systems are expected to show high reactivity with a wide range of substrates and future studies will be directed to investigate the reactivity of such compounds towards small molecules such as CO_2, CO and N_2.

CHAPTER V. GENERAL CONCLUSION

The global objective of this thesis work was the development of rational methods for the synthesis of polynuclear actinide architectures with SMM properties. In order to reach this goal we were faced with two important challenges the underdeveloped supramolecular chemistry of actinides and the lack of fundamental knowledge on pathways leading to magnetic exchange in actinide compounds. In this thesis we designed and synthesised several polynuclear uranium(III, IV and V) and neptunyl(V) complexes and we explored the possibility of magnetic exchange between the metallic centres. This work contributed to the elaboration of controlled synthetic strategies to afford original polynuclear uranium clusters which in several cases displayed unambiguous magnetic exchange.

Firstly, we have investigated the synthetic method developed in the team for the synthesis of oxo/hydroxo uranium clusters. This method consists in the controlled hydrolysis of low valent precursors with a stoichiometric amount of water in presence of an organic ligand. Employing this synthetic method with tetravalent uranium precursors and a benzoate ligand, a new family of high nuclearity uranium(IV) oxo/hydroxo clusters was characterised. The study of the different reaction parameters such as the nature of the tetravalent uranium precursor, the solvent, the stoichiometry of benzoate and the temperature allows the synthesis of uranium oxo clusters with novel topologies. Notably, the variation of these experimental conditions leads to the isolation of clusters containing 6, 10, 13, 16 and even 38 uranium atoms. Investigation of the magnetic properties of mixed-valent U(IV)/U(V) clusters previously synthesised in the group did not reveal the presence of slow relaxation of the magnetisation. The presence of unsuitable coordination ligand for promoting a magnetic ground state for uranium(IV) or the absence of strong intermetallic interactions through the μ_3/μ_4-oxo ligands could lead to these observations.

Therefore we decided to focus on the $5f^1$ uranyl(V) cation which always displays a magnetic ground state and can lead to heterometallic assemblies through the cation-cation interaction. The coordination of the oxo group of the uranyl(V) to another metallic centre leads to the formation of a multiply bound bridging oxo group that provides a pathway for magnetic communication. However the stabilisation of uranyl(V) assemblies is extremely challenging due to the tendency of uranyl(V) to disproportionate through a cation-cation intermediate. During my Master project I had developed the first example of an exchange-coupled uranium based single molecule magnet with a high relaxation barrier which

consisted of a large $U_{12}Mn_6$ wheel built from the cation-cation interaction between uranyl(V) and manganese. In the thesis work uranyl(V) species fully stable towards disproportionation, in which the uranium ion is coordinated to Schiff base ligand, were used as building block for the formation of polymetallic cation-cation assemblies with 3d or 4f metals. A careful tuning of the reaction parameters allow us to design polymeric or discrete compounds. Two stable urany(V) complexes of salen and Mesaldien ligands were used in the presence of one equivalent of Mn(II) ions to afford polymeric structures. These two 1D coordination polymers displayed Single Chain Magnet (SCM) properties arising from strong intrachain U-Mn coupling and represent the first examples of actinide based SCMs. The association of a chelating ligand coordinated to the Mn(II) prevents the formation of polymeric structures and leads to the formation of a discrete UMn_2 trinuclear assemblies. This complex shows SMM behaviour with open hysteresis both in solution and in the solid state and the highest relaxation barrier ever observed for a compound containing only one uranium atom. We also identify synthetic routes to prepare analogous assemblies containing different metal cations. By changing the nature of the transition metal ion and of the chelating ligand, a large family of trinuclear assemblies with d-block metals (Mn, Fe, Co, Ni, Cd) was prepared and investigated. The use of CCI is an efficient strategy to design heterometallic assemblies and allowed the formation of molecules with SMM properties. We observe that the energy barriers decreases along the series Mn > Fe > Ni > Cd as well as the spin, which is the expected behaviour in presence of U-M magnetic coupling. The case of cobalt is however more complicated. More in depth magneto-structural studies will be performed to understand these differences. The synthesis of controlled 4f-5f assemblies faces more synthetic challenges due to the high charge density of Ln(III) cations leading to ligand scrambling, only a pentanuclear complex with Nd(III) was isolated. The use of the less charged Eu(II) ions leads to the formation of a trinuclear complex of structure analogous to the transition metals assemblies. However, these two molecules do not show clear 4f-5f magnetic interactions. Future studies will be directed to design novel chelating ligands for Ln(III) ions in order to prevent ligand scrambling and stabilise well-defined 4f-5f assemblies. Moreover, in the future other Schiff base ligands with different symmetries will be used with uranyl(V) cation to induce the synthesis of CC assemblies with novel topologies and different magnetic properties.

In parallel to these studies with uranyl(V), we explored the potential use of this moiety as a structural model for the coordination chemistry of the neptunyl(V) analogue. Notably, the use of a single charged tetradentate ligand afforded a homometallic tris-neptunyl(V) CC assembly which revealed to be isostructural of the uranyl(V) trimeric complex obtained with the same ligand. This trinuclear assembly represent a rare example of discrete neptunyl(V)

CC complex. The magnetic study reveals the presence of weak SMM behaviour and ferromagnetic coupling between neptunyl(V) centres.

In parallel we began to investigate the possibility of using bridging nitride groups to promote magnetic communication between metallic centres, via the multiple uranium-nitride bond. The reduction of uranium(IV) nitride complexes supported by siloxides ligands previously reported in our group allowed the isolation of unprecedented uranium(III) nitride complexes. The ability of the siloxide ligands to bind the alkali counterion is crucial for the isolation of these highly reactive uranium(III) complexes. Evidence of an antiferromagnetic coupling between two U(III) centres through the bridging nitride ligand was obtained. Furthermore, a new synthetic route towards the synthesis of a bis-nitride bis-uranium(V) complex with a large antiferromagnetic coupling was developed. These uranium nitride complexes featured uranium-nitrogen multiple bonds promoting antiferromagnetic exchange between U(III) and U(V) ions. Future studies will be directed to the design of new nitride bridged complexes leading to ferromagnetic communication rather than antiferromagnetic interactions.

Overall in this work, we developed several synthetic approaches which led to the isolation of well-defined polynuclear assemblies of uranium and neptunyl(V). These novel molecules contribute to the fundamental understanding of the actinide coordination chemistry, specifically providing simple models of the much more difficult actinide behaviour in the environment and reprocessing conditions. The variety of polynuclear complexes developed in this study not only afforded the first examples of uranium-based exchange coupled SMMs and SCMs but also provide significant insight of the parameters affecting magnetic exchange in actinide compounds. The newly developed nitride compounds are very promising for the design of exchange-coupled SMMs based on uranium(III), but also for the development of the redox reactivity of these species.

CHAPTER VI. EXPERIMENTAL SECTION

VI. 1) General considerations

Caution: Depleted uranium (primary isotope ^{238}U) is a weak α-emitter (4.197 MeV) with a half-life of 4.47×10^9 years and a specific activity of $1.8.10^4 Bq.g^{-1}$. Manipulations and reactions should be carried out in monitored fume hoods or in an inert atmosphere glovebox in a radiation laboratory equipped with α- and β-counting equipment.

Caution: ^{237}Np (half-life 2.144 x 10^6 years, $2.6.10^7 Bq.g^{-1}$) is a highly radioactive alpha emitting radionuclide (4.959MeV), research with this isotope is restricted to specialised laboratories and handled under appropriate regulatory controls and safe working practices.

All manipulations with uranium were carried out under an inert argon atmosphere using Schlenk techniques and an MBraun glovebox equipped with a purifier unit. The water and oxygen level were always kept at less than 0.1 ppm. Glassware was dried overnight at 130°C followed by 3 vacuum/argon cycles before use. Experiments using ^{237}Np were performed under an argon atmosphere using a Schlenk line contained within a regular atmosphere negative pressure radiological containment glovebox.

Starting materials Unless otherwise noted, reagents were purchased from commercial suppliers and used without further purification. Molecular sieves were heated at 200°C under high vacuum. The solvents were purchased from Aldrich in their anhydrous form conditioned under argon and were vacuum distilled from K/benzophenone (pyridine, THF, diisopropylether and toluene), sodium dispersion (hexane, eicosane) or CaH_2 (acetonitrile and dmso) and degassed by three freeze-pump-thaw cycles. dmso was stored over activated 3Å molecular sieves. Deuterated solvent purchased from Eurisotop or Cortecnet were prepared identically, except pyridine-d_5 and dmso-d_6 both obtained by drying commercial, degassed three time and further dried over 3Å activated molecular sieves. Water solutions were prepared from distilled and degassed MilliQ water and anhydrous solvents. Unless otherwise specified, all the reagent and ligands were dried under high vacuum (10^{-7} mBar) for minimum 5 days prior to use. $[Mn(NO_3)_2(Py)_3]$ and $Cd(NO_3)_2$ were obtained by extraction of the hydrated salts in hot pyridine followed by high vacuum drying at 40°C for 7 days. Pyridine N-oxide, 18-crown-6, I_2, benzoic acid and $HOSi(O^tBu)_3$ ligand were purchased from Aldrich and sublimated prior to use. Cp^*_2Co was purchased from Aldrich and extracted in

hexane prior to use. The H_2salen (N,N'-ethylene-bis(salicylideneimine)),[436] H_2salfen-^{t}Bu, H_2salfen,[401] H_2Mesaldien (N,N'-(2-aminomethyl)diethylenebis(salicylidene imine)),[208] HL (2-(4-tolyl)-1,3-bis(quinolyl)malondiiminate),[242] TPA (tris(2-pyridylmethyl)amine),[437] HBPPA (bis(2-picolyl)(2-hydroxybenzyl)amine),[438] and TPEN (N,N,N',N'-tetrakis(2-pyridylmethyl)ethylenediamine)[437] ligands were prepared according to the literature procedures and dried under high vacuum for a week prior to use. The $[Bu_4N][PF_6]$ electrolyte was recrystallised from warm toluene, conditioned under argon and dried under high vacuum (10^{-7} mbar) prior to use.

Depleted uranium turnings were purchased from the "Société Industrielle du Combustible Nucléaire" of Annecy (France). The starting materials $\{[UO_2(Py)_5][KI_2(Py)_2]\}_n$,[27] $[UO_2I_2(Py)_3]$,[27] $[UI_4(OEt_2)_2]$,[81] $[UCl_4]$,[76] $[U(N(SiMe_3)_2)_3]$,[439] $[U(OSi(O^tBu)_3)_2(\mu\text{-}OSi(O^tBu)_3)]_2$,[54] $[Cs[\{U(OSi(O^tBu)_3)_3\}_2(\mu\text{-}N)]$,[69] $[UO_2(salen)(Py)]$,[48] $\{[K(MeCN)]_2[U_{16}O_{22}(OH)_2(PhCOO)_{24}]\}$,[341] and $[UO_2(Mesaldien)K]_n$ [54] were prepared according to literature procedures. $[UI_3(THF)_4]$ was prepared by hot extraction of $[UI_3(1,4\text{-dioxane})_{1.5}]$ with THF.[82] The $[UO_2(Mesaldien)]$ complex was prepared from $UO_2(NO_3)_3$ and the H_2Mesaldien ligand according to the procedures used for other uranyl(VI) complexes.[52 53 54 440] $\{[NpO_2(Py)_5][KI_2(Py)_2]\}_n$ was prepared from a purified stock solution obtained from CEA Marcoule legacy stocks according to published procedure.[51] $[\{NpO_2(salen)\}_4(\mu_8\text{-}K)_2][K(18C6)(Py)]_2$ was prepared from $\{[NpO_2(Py)_5][KI_2(Py)_2]\}_n$ accordingly to reported synthesis.[239]

VI. 2) Characterisations

Electrochemistry Cyclic voltammetry experiments were performed using a Biologic SP-300 potentiostat in an argon-filled glovebox. The working electrode consisted of a platinum disk (1 mm diameter), a platinum counter electrode and an AgCl/Ag reference electrode. Solutions employed were typically 2-10 mM in complex with 0.1 M for $[Bu_4N][PF_6]$ as electrolyte. Reproducibility of the measurements was assessed on independent samples. Potential calibration was performed at the end of each data collection using $[Cp_2Fe]^{+/0}$ couple as an internal standard.

Elemental analyses were performed under argon by Analytische Laboratorien GMBH at Lindlar, Germany or with a Thermo Scientific Flash 2000 Organic Elemental Analyzer by EPFL, Switzerland.

^{1}H NMR experiments were carried out using NMR tubes adapted with J. Young valves. ^{1}H NMR spectra were recorded on Bruker 200 MHz and 500 MHz, Varian MERCURY 400 MHz and Agilent DD2 400MHz spectrometers at 298 K. NMR chemical shifts are reported in ppm with solvent as internal reference. Abbreviations used for describing multiplicity of the NMR signals are: s (singlet), d (doublet), dd (doublet of doublet), t (triplet), dt (doublet of triplet), q (quadruplet) and m (multiplet) and br (broad).

Diffusion coefficients measurements were performed using a Pulsed-Field Gradient STimulated Echo (PFGSTE) sequence, using bipolar Gradients, at 298 K and no spinning was applied to the NMR tube.[441] [442] The following BPP-LED (Bipolar Pulse Pair – Longitudinal Eddy-current Delay) pulse sequence was applied:[443]

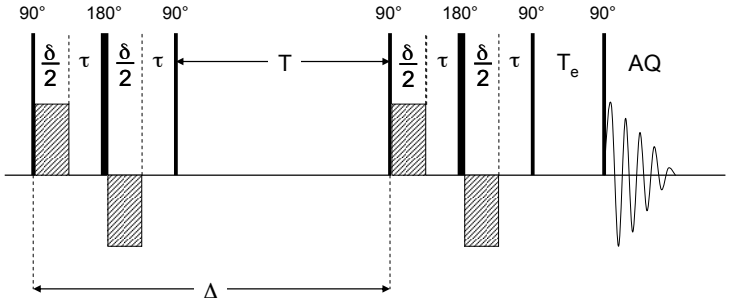

δ= 2 ms. τ = 0.5 ms.

The diffusion times T were optimised for each complex/solvent couple, with values ranking in the range 80-180 ms. The evolution of the pulsed-field gradient during the NMR diffusion experiments was established in 10 steps, applied linearly between 5.4 and 29.7 G.cm^{-1}. In the present sequence the intensity of the signal is given by the following equation:[443] $I(q) = I(0).\exp\left[-D.q^2.\left(\Delta - \frac{\delta}{3} - \frac{\tau}{2}\right)\right]$ with q = γ.δ.g

and D : diffusion coefficient (m².s^{-1}), Δ: time between the two gradient pulse sequences (s), δ : bipolar gradient duration (s), τ : pulse separation delay (s), γ : magnetogyric ratio of the observed nucleus (s^{-1}.T^{-1}) and finally g : gradient strength (T.m^{-1}). The diffusion coefficient is then the slope of the line obtained by plotting ln(I/I$_0$) against $q^2.\left(\Delta - \frac{\delta}{3} - \frac{\tau}{2}\right)$

The spherical hydrodynamic radius (called Stokes radius) of the molecule was calculated from the Stokes-Einstein equation and compared to a similar reference compound in the same solvent:

r_{sph} ($r_{sph} = \frac{k_B.T}{6\pi.\eta.D}$)

η (Pa.s) = viscosity of the medium; k_B (m².kg.s^{-2}.K^{-1}) = Boltzmann constant.

T: absolute temperature (K); D: diffusion coefficient (m².s^{-1})

The hydrodynamic radii calculated from the measured coefficient diffusion values were compared with the spherical radii evaluated from the crystal structure by considering the volume of the ellipsoid determined by the three main dimensions and calculating the radius of a sphere of the same volume.

IR spectra were recorded with a Perkin Elmer Spectrum 100 Series FTIR spectrophotometer or on a Bruker Equinox Spectrometer in KBr pellets or with a Varian Inc. Scimitar 800 FT-IR spectrophotometer with an adapter to keep the sample under argon atmosphere and were routinely corrected for baseline.

Magnetic measurements. Static magnetic properties were measured using a Quantum Design SQUID MPMS-XL 5.0 susceptometer with Ultra-Low Field Capability ±0.05 G for the 5 T magnets in the temperature range 2 to 300 K. Continuous Low Temperature Control/Temperature Sweep Mode (CLTC) - Sweep rate: 0.001 - 10 K/min. Dynamic magnetic properties were measured using a Quantum Design PPMS-14T platform using the mutual-inductance technique and a MPMS XL7 SQUID magnetometer as a function of temperature and frequency. The samples were crushed in an agate mortar, introduced in a 5mm Suprasil-Quartz tube, covered with eicosane to prevent sample torqueing and sealed under vacuum. Heat sensitive compounds were measured without eicosane and no torqueing was observed. Contribution to the magnetisation from quartz tube was measured independently and subtracted from the total measured signal to be corrected. Diamagnetic corrections were made using Pascal's constants.[444] For each compound, the measurements were performed at several fields. Reproducibility of the magnetic measurement was checked for each compound by the measurement of independently synthesised samples. The purity of each sample was checked by elemental analysis and ^{1}H NMR spectroscopy.

The real and imaginary components, χ' and χ", of the complex ac magnetic susceptibility were fitted to determine the energy barrier and the relaxation rate of SMMs.

• For the data obtained from fixed temperature T measurements, the χ' and χ'' components are plotted versus the frequency υ (Argand plot) and are fitted with one relaxation process Debye model using Origin:

$$\chi''(\omega)=\chi_S+\frac{(\chi_T-\chi_S)(1+\omega\tau)^{1-\alpha}\sin(1/2\alpha\pi)}{1+2(\omega\tau)^{1-\alpha}\sin(1/2\alpha\pi)+(\omega\tau)^{2(1-\alpha)}}$$

$$\chi''(\omega)=\frac{(\chi_T-\chi_S)(\omega\tau)^{1-\alpha}\cos(1/2\alpha\pi)}{1+2(\omega\tau)^{1-\alpha}\sin(1/2\alpha\pi)+(\omega\tau)^{2(1-\alpha)}}$$

with $\omega = 2\pi\upsilon$ the angular frequency, χ_T isothermal susceptibility χ $(\omega \to 0)$, χ_S adiabatic susceptibility χ $(\omega \to \infty)$, τ the relaxation time and α the distribution of relaxation time. So from these calculated curves, we obtain the relaxation time corresponding to each fixed temperature.

• For the data obtained from fixed frequency υ measurements, the χ' and χ'' components are plotted versus the temperature T. The fit using a Lorentzien function of the χ'' susceptibility gives the temperature of each maximum and the relaxation time is calculated using: $\omega\tau = 1$ valable at the maximum (with $\omega = 2\pi\upsilon$).

• Finally, each pair of (τ, T) values extracted from the previous analysis, are used to plot $\ln(\tau)$ versus 1/T as the relaxation behaviour follow an Arrhenius relation, $\tau = \tau_0 \exp\left({}^{\Delta E}/_{k_B T}\right)$ in the thermally activated regime. A linear regression of the experimental data provides the pre-exponential factor τ_0 and the energy barrier ΔE.

Mass spectra were acquired on a LXQ-linear ion trap (Thermo Scientific, San Jose, CA,USA), equipped with an electrospray source in a pyridine/acetonitrile mixture (1:1 to 1:5) which was prepared and filtered on microporous filters in the glove-box and maintained under argon until injection in the spectrometer. Electrospray full scan spectra, in the range of *m/z* 50 –3000 amu, were obtained by infusion through fused silica tubing at 2 – 10 μL min^{-1}. The LXQ calibration (*m/z* 50-2000) was achieved according to the standard calibration procedure from the manufacturer (mixture of caffeine/MRFA and Ultramark 1621). The LXQ calibration (*m/z* 2000-4000) was performed with ES tuning mix (Agilent). The temperature of the heated capillary of the LXQ was set to the range of 180-220 °C, the ion spray voltage was in the range of 1-3 kV with an injection time of 5-100 ms. The experimental isotopic profile was compared in each case to the theoretical one.

UV-Visible measurements were carried out in quartz cells (optical path lengths: 1 mm and 1cm) adapted with J. Young valves with a Varian Cary 50 Probe spectrophotometer while Visible-NIR spectra were recorded a Lambda 9 Perkin Elmer spectrophotometer.

X-Ray crystallography diffraction data were taken using three different diffractometers: a Bruker APEX II CCD diffractometer equipped with a kappa geometry goniometer using Mo-Kα radiation, a Oxford-Diffraction XCallibur S kappa geometry diffractometer (Mo-Kα radiation, graphite monochromator, λ = 0.71073 Å), and on an Agilent Technologies SuperNova dual system in combination with an Atlas CCD detector using Cu-Kα radiation. The data sets obtained with the APEX II diffractometer were reduced by EvalCCD[445] and

then corrected for absorption using SADABS Bruker software.[446] and with the XCallibur or SuperNova systems by Crysalis PRO then corrected for absorption using ABSPACK Oxford-diffraction program.[447] To prevent evaporation of co-crystallised solvent molecules the crystals were coated with light hydrocarbon oil and the data were collected at 100 or 150 K, only $[NpO_2L]_3$ was measured at 293 K due to a problem of ice formation. The cell parameters were obtained with intensities detected on three batches of 5 frames with the XCallibur apparatus and the number of settings and frames has been thus established taking in consideration the Laue symmetry of the cell by CrysAlisPro CCD Oxford-diffraction software; whereas in the case of the two other apparatus, the data collection were performed assuming a triclinic space group for every crystals. Then for each, space groups were determined from systematic absences, and they were confirmed by the successful solution of the structure. The structures were solved by direct methods using the SHELXTL 6.14 package[448] or Superflip software[449] and refined using SHELXTL 6.14 in OLEX2.[450] Figure Graphics were generated using MERCURY 3.6 supplied with Cambridge Structural Database; CCDC: Cambridge, U.K., 2004-2009. All non-hydrogen atoms were found by difference Fourier synthesis and anisotropically refined using full-matrix least squares based on F^2 whereas hydrogen atoms were fixed in ideal position. Details of the data collections and crystal parameters are given in appendix.

VI.3) Syntheses

VI.3.1) Potassium salts of the ligands

General synthesis of the potassium salts of the H_2salen, H_2Mesaldien and H_2salfen ligands

Solid KH (1.8 equiv.) was added to a solution of protonated ligand (1 equiv.) in THF (3 mL). The mixture was stirred more than 24h during which time gas evolution ended. The precipitate formed (cream for K_2salen and K_2Mesaldien; red for K_2salfen) was washed 3 times with 3 mL of THF and dried under vacuum.

SalenK_2: (salen)H_2 (215.0 mg, 0.80 mmol, 1 equiv.), KH (60.5 mg, 1.51 mmol, 1.88 equiv.) Yield (salen)K_2: (192.1 mg, 73.9 %) ^{1}H NMR: (dmso-d_6, 298 K, 200MHz): 3.53 (s, 2H); 5.75 (m, 1H); 6.03 (m, 1H); 6.70 (t, 1H); 7.27 (d, 1H); 8.55 (s, 1H).

K_2Mesaldien: H_2Mesaldien (1.202 g, 3.7 mmol, 1 equiv.), KH (267 mg, 6.6 mmol, 1.8 equiv.) Yield K_2Mesaldien: (1.374 g, 92 %) ^{1}H NMR: (dmso-d_6, 298 K, 200MHz): 8.25 (s, 2H); 7.30 (dd, 2H); 7.17 (dd, 2H); 6.91 (dd, 2H); 6.83 (td, 2H); 3.75 (m, 4H); 2.79 (m, 4H); 2.43 (s, 3H).

K_2salfen: H_2salfen (504 mg, 1.19 mmol, 1 equiv.), KH (85.8 mg, 2.14 mmol, 1.8 equiv.) Yield K_2salfen: (535 mg, 90 %) ^{1}H NMR: (THF-d_8, 298 K, 200MHz): 8.90 (s, 2H); 7.50 (d, 2H); 7.20 (t, 2H); 7.00 (d, 2H); 6.50 (t, 2H); 4.50 (s, 4H); 4.20 (s, 4H).

Synthesis of K_2salfen-^{t}Bu

Solid KH (44.6mg, 1.11mmol, 2.2 equiv.) was added to a solution of H_2salfen-^{t}Bu (328mg, 0.51mmol, 1 equiv.) in THF (4 mL). After 24hours of stirring, the excess of KH was removed by filtration and the red filtrate was taking to dryness. The resulting red powder was collected and dried for 3 hours to give K_2salfen-^{t}Bu (351mg, 96% yield). ^{1}H NMR: (Py-d_5, 298 K, 400MHz): 8.99 (s, 2H); 7.37 (s, 2H); 4.55 (s, 4H); 4.20 (s, 4H); 1.75 (s, 18H); 1.47 (s, 18H).

General synthesis of the potassium salts of the benzoic acid (BzH), 2-(4-tolyl)-1,3-bis(quinolyl)malondiiminate (HL) and the HBPPA ligands

Solid KH (0.9 equiv.) was added to a solution of protonated ligand (1 equiv.) in THF (3 mL). The mixture was stirred 24h until the gaseous clearing was complete. The precipitate formed (white for BzK and BPPAK; dark violet for KL) was washed 3 times with 3 mL of THF and dried under vacuum.

BzK: BzH (1.345g, 11.0 mol, 1 equiv.), KH (398 mg, 9.91 mmol, 0.9 equiv.) Yield BzK: (1.472 g , 83 %) ^{1}H NMR (400MHz, dmso-d_6, 298 K): δ=7.82 (t, 2H); 7.22 (t, 3H).

KL: HL (62 mg, 0.15 mmol, 1 equiv.), KH (5.4 mg, 0.14 mmol, 0.9 equiv.) Yield KL: (54 mg, 80 %) ^{1}H NMR (200MHz, CD_3CN, 298 K): δ=8.74 (s, 4H); 8.16 (d, 2H); 7.95 (s, 2H); 7.39 (t, 4H); 7.26 (d, 2H); 7.02 (d, 4H); 2.28 (s, 3H, -CH_3).

BPPAK: BPPAH (544 mg, 1.78 mmol, 1 equiv.), KH (64 mg, 1.60 mmol, 0.9 equiv.) Yield BPPAK: (283 mg, 48 %) ^{1}H NMR (200MHz, Py-d_5, 298 K): δ= 8.25 (d, 2 H), 7.38 (m, 4H), 7.12 (m, 3H), 6.86 (dd, 2H), 6.55 (td, 1H), 3.66 ppm (m, 6H).

VI.3.2) Oxo/hydroxo uranium complexes

Synthesis of $[U_6O_4(OH)_4(PhCOO)_{12}(Py)_4]$ 1

421 μL of a 0.5M solution of water (0.211 mmol, 2 equiv.) in pyridine were added dropwise under vigorous stirring to a blue solution of [UCl_4] (40.0 mg, 0.105 mmol, 1 equiv.) in 2 mL of pyridine, resulting in a colour change to green after 5 minutes stirring. A suspension of potassium benzoate (33.7 mg, 0.211 mmol, 2 equiv.) in pyridine (1.5 mL) was then added to the solution. The green resulting solution was stirred at room temperature over 48 h and then filtered to remove potassium chloride. The green solution was layered with diisopropylether

yielding X-ray quality crystals of 1 over 2weeks in 65 % yield (40mg, 0.012mmol). ^{1}H NMR (200MHz, Py-d_5, 298 K): δ= 17.76 (s, 2H), 9.96 (t, 2H), 9.69 (t, 1H).

Synthesis of $[U_{16}O_{15}(OH)_8(PhCOO)_{26}(Py)_2]$, 2

536 µL of a 0.5M solution of water (0.268 mmol, 1.7 equiv.) in acetonitrile were added dropwise under vigorous stirring to a green suspension of [UCl_4] (60.0 mg, 0.160 mmol, 1 equiv.) in 1 mL of acetonitrile. A suspension of potassium benzoate (43.0 mg, 0.268 mmol, 1.7 equiv.) in acetonitrile (0.5 mL) was then added to the solution. The green resulting solution was stirred at room temperature overnight and then filtered to remove potassium chloride. 50 µL of pyridine were added (0.630 mmol, 4 equiv.) resulting in a darker green solution. After 3 days, 37mg of crystals of 2 were recovered followed by 15mg collected after 1 week (total yield: 39%). Elemental analysis calcd (%) for $[U_{16}O_{15}(OH)_8(PhCOO)_{26}(Py)_2].4(H_2O).3MeCN.4KCl$ ($C_{198}H_{165}Cl_4K_4N_5O_{79}U_{16}$ MW=7985.12) C 29.78, H 2.08 and N 0.88; found C 29.54, H 2.05 and N 0.84. X-ray quality crystals of $2.4H_2O.4MeCN$ grew in a concentrated acetonitrile solution containing 2.

Isolation of $[U_{10}O_8(OH)_6(PhCOO)_{12.82}I_{3.18}](H_2O)_4(MeCN)_3]I_2$, 3

X-ray quality of green crystals of 3 were obtained in the reaction of 158 µL of a 0.5 M solution of water (0.078 mmol, 2 equiv.) in acetonitrile and a vigorously stirred dark red solution of [$UI_4(OEt_2)_4$] (14.8 mg, 0.039 mmol, 1 equiv.) in 3 mL of MeCN. A suspension of potassium benzoate (12.5 mg, 0.078 mmol, 2 equiv.) in MeCN (1 mL) was then added to the solution. The light green resulting solution was stirred over 48hours and then filtered to remove potassium iodide. Slow evaporation of the resulting solution yields green X-ray quality crystals of 3 after 1 week. Compound 3 was characterised by a cell check of the crystals from ref [341].

Synthesis of $[U_{13}K_4O_{12}(OH)_4(PhCOO)_{12}Cl_{14}]Cl_2$, 4 and $[U_{13}K_2O_{12}(OH)_7(PhCOO)_{12}Cl_{16}]Cl$, 5

1.05 mL of a 0.5M solution of water (0.527 mmol, 2 equiv.) in acetonitrile were added dropwise under vigorous stirring to a green suspension of [UCl_4] (100.0 mg, 0.263 mmol, 1 equiv.) in 0.5 mL of acetonitrile. A suspension of potassium benzoate (169.2 mg, 0.527 mmol, 2 equiv.) in acetonitrile (2.0 mL) was then added to the solution. The green resulting solution was stirred at room temperature over 48 h and then filtered to remove potassium chloride. The green solution was layered with diisopropylether yielding 17mg (15%) of a mixture of 4 and 5. X-ray quality crystals of both 4.6MeCN and 5 compounds were obtained independently by slow diffusion of diisopropylether into the acetonitrile solution or in concentrated acetonitrile solution. ^{1}H NMR (200 MHz, CD_3CN, 298 K): δ= 28.33 (s, 1H),

25.72(s, 1H), 18.90(s, 1H), 15.72(s, 1.5H), 12.06(s, 1.5H), 12.05(s, 1.5H), 11.79(s, 1H), 11.19(s, 3.5H), 10.30(s, 1.5H), 10.04(s, 3.5H), 9.03(s, 2H), 8.52(s, 2H), 7.91(s, 2H), 7.19 (s, 2.5H).

Synthesis of $[U_6O_4(PhCOO)_{16}(Py)_4]$, 6

526 µL of a 0.5M solution of water (0.263 mmol, 2 equiv.) in acetonitrile were added dropwise under vigorous stirring to a green suspension of $[UCl_4]$ (50.0 mg, 0.132 mmol, 1 equiv.) in 0.5 mL of acetonitrile. A suspension of potassium benzoate (26.5 mg, 0.789 mmol, 6 equiv.) in acetonitrile (1.5 mL) was then added to the solution resulting to resulting a light green solution and the formation of white-green powder. After 1 day stirring at room temperature the precipitate was filtered. This solid was partially solubilised in pyridine resulting to a green solution and a white solid removed by filtration. The green solution was layered with diisopropylether and after a week, the $[U_6O_4(PhCOO)_{16}(Py)_4]$.1.8Pyridine compound was recovered (53.8 mg, 63 %). Elemental analysis calcd (%) for $[U_6O_4(PhCOO)_{16}(Py)_4]$.1.8Pyridine ($C_{141}H_{109}N_{5.8}O_{36}U_6$ MW=3888.62) C 43.55, H 2.83, N 2.09; found C 43.50, H 2.98, N 2.16. ^{1}H NMR (200MHz, Py-d_5, 298 K): δ= 17.78 (s, 2H), 9.97 (t, 2H), 9.71 (t, 1H). X-ray quality crystals of 6.3Pyridine.1DIPE were obtained by slow diffusion of diisopropylether into the pyridine solution containing the cluster.

Reaction at high temperature: Isolation of $[U_{38}O_{56}Cl_{18}(PhCOO)_{22}(CH_3CONH_2)_{10}]$ 7

A Schlenck round bottom flask was charged with $[UCl_4]$ (100.0 mg, 0.263 mmol, 1 equiv.) in 10mL of acetonitrile and 1.05mL of a 0.5M water solution in acetonitrile (0.523 mmol, 2equiv.). A white suspension of potassium benzoate (84.3 mg, 0.523 mmol, 2 equiv.) was then added. The light green mixture was refluxed for 32hours under argon outside of the glove box and overtime the color became darker. A brownish-green solid was removed by centrifugation from the dark green solution which was layered with DIPE. X-ray quality crystals of $[U_{38}O_{56}Cl_{18}(PhCOO)_{22}(CH_3CONH_2)_{10}]$ 7 were obtained by slow diffusion of diisopropylether into the acetonitrile solution concomitant to the formation of a green precipitate.

Serendipitous traces of oxygen leads to the crystallisation of 7 and $[UO_2K_2Cl_4(MeCN)_2]$ 8 as characterised by X-ray diffraction.

VI.3.3) Cation-cation complexes

Synthesis of $\{[UO_2(salen)(Py)][Cd(Py)_4]NO_3\}_n$, 9-$\{UO_2(salen)Cd\}_n$

To a stirred orange suspension of $[UO_2(salen)(Py)]$ (100mg, 0.16mmol, 1 equiv.) in 1mL of pyridine is added a dark brown suspension of Cp^*_2Co (53.5mg, 0.16mmol, 1equiv.) in 1mL of pyridine. The dark green solution of $[UO_2(salen)(Py)][Cp^*_2Co]$ is then stirred for half an hour. A colorless solution of $Cd(NO_3)_2$ (38.4mg, 0.16mmol, 1equiv.) in 3mL pyridine is added, resulting immediately to a dark violet solution. After ten minutes of stirring, the solution is filtrated on a microfilter and let stand at room temperature. The violet microcrystalline powder formed overnight is isolated of the brown solution on frits (porosity n°4) and washed by 10*1mL pyridine until all traces of $Cp^*_2CoNO_3$ are removed and dry rapidly under vacuum (141 mg, 65 %). Elemental analysis calcd (%) for $\{[UO_2(salen)(Py)][Cd(Py)_4]NO_3\}_n$3.2(Py) ($C_{57}H_{55}N_{11.2}O_7CdU$, MW=1359.05) C 50.38, H 4.08, N 11.54; found C 50.34, H 4.17, N 11.55. X-ray quality crystals of $\{[UO_2(salen)(Py)][Cd(Py)_4]NO_3\}_n$ were obtained by slow diffusion in an H tube, where two solutions of $[UO_2(salen)(Py)][Cp_2^*Co]$ (0.10 mmol, 1 equiv) in pyridine (4 mL) and $Cd(NO_3)_2(Py)_3$ (0.10 mmol, 1 equiv) in pyridine (4 mL) were introduced in the two sections of the H tube connected by a layer of pyridine (10 mL). After two weeks diffusion; pink cubic crystals of $\{[UO_2(salen)(Py)][Cd(Py)_4]NO_3.2(Py)\}_n$, suitable for X ray crystallised at the interface. The pink crystals were collected by filtration and washed with pyridine (3 x 1.5 mL) and dried under vacuum to yield 68 mg of pink crystals of $\{[UO_2(salen)(Py)][Cd(Py)_4]NO_3\}_n$ (0.056 mmol, 56 %)

Synthesis of $\{[UO_2(salen)(Py)][Mn(Py)_4]NO_3\}_n$, 10-$\{UO_2(salen)Mn\}_n$

To a stirred orange solution of $[UO_2(salen)(Py)]$ (100mg, 0.16mmol, 1 equiv.) in 1mL of pyridine is added a dark brown suspension of Cp^*_2Co (53.5mg, 0.16mmol, 1 equiv.) in 1mL of pyridine. The dark green solution of $[UO_2(salen)(Py)][Cp^*_2Co]$ is then stirred for half an hour. A white suspension of $Mn(NO_3)_2(Py)_4$ (67.6mg, 0.16mmol, 1 equiv.) in 4mL of pyridine is added to the resulting solution affording a red solution. After ten minutes the resulting solution is filtered and then left standing at room temperature overnight. A purple microcrystalline powder forms which is collected by filtration and washed with 10*1mL pyridine until all traces of $Cp^*_2CoNO_3$ are removed yielding complex $\{[UO_2(salen)(Py)][Mn(Py)_4](NO_3)\}_n$.0.5Pyridine (114.1mg, 66% yield). Elemental analysis calcd (%) for $\{[UO_2(salen)(Py)][Mn(Py)_4](NO_3)\}_n$.0.5Pyridine ($C_{43.5}H_{41.5}N_{8.5}O_7MnU$, MW=1088.28) C 48.01, H 3.84, N 10.94; found C 47.92, H 3.88, N 10.81.

Synthesis of {[UO_2(Mesaldien)][Cp^*_2Co]} 11

To a stirred orange suspension of [UO_2(Mesaldien)] (35.5mg, 0.06mmol, 1 equiv.) in 1mL of pyridine, a dark brown suspension of Cp^*_2Co (19.7mg, 0.06mmol, 1 equiv.) in 2mL of pyridine is added. The resulting dark green solution of [UO_2(Mesaldien)][Cp^*_2Co] is then stirred for two hours and the solution is filtrated. This solution is then layered with 10mL of hexane to afford affording after 3 days, dark green X-ray quality crystals of {[UO_2(Mesaldien)][Cp^*_2Co]}.0.6Pyridine (52.4 mg, 90 %). Elemental analysis calcd (%) for {[UO_2(Mesaldien)][Cp^*_2Co]}.0.6Pyridine ($C_{42}H_{54}Co\ N_{3.6}O_4U$, MW=970.21) C 51.99, H 5.61, N 5.20; found C 51.85, H 5.45, N 5.54. ^{1}H NMR (200 MHz, Py-d_5, 298 K): δ = 6.86 (br s, 30H, Cp^*), 5.27 (tr, 2H), 4.37 (tr, 2H), 3.96 (d 2H), 3.68 (s, 2H), 1.14 (tr, 2H), -2.08 (d, 2H), -5.09 (d, 2H), -7.75 (s, 3H), -9.19 (d, 2H), -9.72 (tr, 3H).

Synthesis of {{[UO_2(Mesaldien)][$Mn(NO_3)(Py)_2$]}.2(Py)}$_n$, 12-{UO_2(Mesaldien)Mn}$_n$

A white suspension of $Mn(NO_3)_2(Py)_3$ (67.2mg, 0.16mmol, 1 equiv.) in 5mL of pyridine is added to a dark green solution of [UO_2(Mesaldien)][Cp^*_2Co] (147.4mg, 0.16mmol, 1 equiv.) in 5 mL of pyridine to yield a red solution. Dark pink crystals form overnight and are collected by filtration and washed with 10*1mL pyridine until all traces of $Cp^*_2CoNO_3$ are removed yielding complex {[UO_2(Mesaldien)][$Mn(NO_3)(Py)_2$]}.1.6Pyridine (106.2mg, 66% yield). Elemental analysis calcd (%) for {[UO_2(Mesaldien)][$Mn(NO_3)(Py)_2$]}.1.6Pyridine ($C_{37}H_{39}MnN_{7.6}O_7U$, MW=994.97) C 44.67, H 3.95, N 10.70; found C 44.57, H 4.10, N 11.07. X-ray quality single crystals of {[UO_2(Mesaldien)][$Mn(NO_3)(Py)_2$]}.2Pyridine were obtained from a diluted pyridine solution (5.4mM).

Synthesis of {[Mn(TPA)I][UO_2(Mesaldien)][Mn(TPA)I]}I, 13-UMn_2-TPA-I

A white suspension of [Mn(TPA)I_2], prepared *in situ* from the reaction of MnI_2 (60.7 mg, 0.197 mmol, 2 equiv.) with TPA (57.1 mg, 0.197 mmol, 2 equiv.) in 1 mL of pyridine, is added to a stirred dark blue solution of [UO_2(Mesaldien)K]$_n$ (62.2 mg, 0.098 mmol, 1 equiv.) in 2 mL of pyridine. Immediately the resulting solution becomes red. After 3 hours of stirring, KI is removed by filtration and the solution is layered with hexane. Red X-ray quality crystals were formed after one week of diffusion. Crystals were collected by filtration and washed with hexane (2 x 0.5 mL) and dried under vacuum to yield 109.4 mg of {[Mn(TPA)I][UO_2(Mesaldien)][Mn(TPA)I]}I.2.6Pyridine (0.058 mmol, 60%). Elemental analysis calcd (%) for {[Mn(TPA)I][UO_2(Mesaldien)][Mn(TPA)I]}I.2.6Pyridine ($C_{68}H_{70}N_{13.6}O_4I_3Mn_2U$, MW=1870.15) C 43.67, H 3.77 and N 10.18; found C 43.57, H 4.00 and N 10.37. ^{1}H NMR (400 MHz, CD_3CN, 298 K): δ = 94.52 (br, 4H), 63.88/54.57/52.09/51.36/48.65/47.38 (br m, 21H), 10.03 (br, 6H), 6.97 (s, 2H), 5.64 (s, 2H), 5.21 (br, 2H), 4.70 (br, 2H), 4.08 (br, 2H),

3.69 (s, 2H), 3.05 (s, 2H), 2.72 (s, 3H), -11.24/-11.54 (br d, 7H), -14.44 (br, 2H). ESI-MS: m/z=1536.8 ({[Mn(TPA)I][UO_2(Mesaldien)][Mn(TPA)I]}$^+$).

Synthesis of {[Cd(TPA)I][UO_2(Mesaldien)][Cd(TPA)I]}I, 14-UCd_2-TPA

A colorless solution of [Cd(TPA)I_2], prepared *in situ* from the reaction of CdI_2 (52.1 mg, 0.14 mmol, 2 equiv.) and TPA (41.3 mg, 0.14 mmol, 2 equiv.) in 1 mL of pyridine is added to a stirred dark blue solution of [UO_2(Mesaldien)K]$_n$ (45.5 mg, 0.07 mmol, 1 equiv.) in 2 mL of pyridine. Immediately the resulting solution turned a darker violet. After 3 hours of stirring, KI is removed by filtration and the solution is layered with hexane. The violet powder formed was then filtrated and washed with hexane (2 x 0.5 mL) and dried under vacuum to yield 86 mg of {[Cd(TPA)I][UO_2(Mesald)][Cd(TPA)I]}I.4.2Pyridine (0.042 mmol, 60%). Elemental analysis calcd (%) for {[Cd(TPA)I][UO_2(Mesaldien)][Cd(TPA)I]}I.4.2Pyridine ($C_{76}H_{78}N_{15.2}O_4I_3Cd_2U$, MW=2032.39) C 41.96, H 3.62 and N 9.79; found C 41.98, H 3.63 and N 9.78. ^{1}H NMR (400 MHz, CD_3CN, 298 K): δ = 11.26 (br, 2H), 10.04 (br, 6H, H_{aroTPA}), 7.62 (t, 6H, H_{aroTPA}), 7.42 (t, 6H, H_{aroTPA}), 7.14 (d, 6H, H_{aroTPA}), 6.45 (t, 2H), 5.47 (d, 2H), 5.27 (t, 2H), 5.23 (br, 12H, CH_{2TPA}), 1.26 (br, 2H), 0.64 (d, 2H), -2.00 (br, 2H), -3.09 (br, 2H), -4.98 (br, 3H). ESI-MS: m/z=1652.6 ({[Cd(TPA)I][UO_2(Mesaldien)][Cd(TPA)I]}$^+$). Light violet X-ray quality crystals were obtained after three week of diffusion of hexane in a very diluted pyridine solution of {[Cd(TPA)I][UO_2(Mesald)][Cd(TPA)I]}I.

Synthesis of {[Mn(TPA)Cl][UO_2(Mesaldien)][Mn(TPA)Cl]}I, 15-UMn_2-TPA-Cl

A white suspension of [Mn(TPA)Cl_2] prepared *in situ* from the reaction of $MnCl_2$ (11.8 mg, 0.094 mmol, 2 equiv.) with TPA (27.2 mg, 0.094 mmol, 2 equiv.) in 1 mL of pyridine is added to a stirred dark blue solution of [UO_2(Mesaldien)K]$_n$ (29.7 mg, 0.047 mmol, 1 equiv.) in 2 mL of pyridine. Immediately the resulting solution becomes red and was stirred overnight. KI (7.8mg, 0.047mmol, 1 equiv.) was added to the solution allowing the crystallisation of {[Mn(TPA)Cl][UO_2(Mesaldien)][Mn(TPA)Cl]}I.1.2Pyridine (60.8 mg, 0.038 mmol, 80%) by slow diffusion of hexane. Elemental analysis calcd (%) for {[Mn(TPA)Cl][UO_2(Mesald)][Mn(TPA)Cl]}I.1.2Pyridine ($C_{61}H_{63}N_{12.2}O_4Cl_2IMn_2U$, MW=1576.65) C 46.47, H 4.03 and N 10.84; found C 46.81, H 3.86 and N 10.75. ^{1}H NMR (400 MHz, CD_3CN, 298 K): δ = 93.16/87.89 (br, 6H), 50.79/49.94/48.79 (br m, 17H), 6.90 (s, 6H), 5.58 (s, 4H), 4.75 (br, 6H), 3.19 (br, 5H), 1.27 (br, 3H), -11.43/-11.70 (br d, 10H). ESI-MS: m/z=1353.1 ({[Mn(TPA)Cl][UO_2(Mesald)][Mn(TPA)Cl]}$^+$). X-ray quality crystals of {[Mn(TPA)Cl][UO_2(Mesaldien)][Mn(TPA)Cl]} grew in pyridine solution containing this complex and KI by slow diffusion of hexane.

Synthesis of {[Fe(TPA)Cl][UO_2(Mesaldien)][Fe(TPA)Cl]}I, 16-UFe_2-TPA

An orange suspension of [Fe(TPA)Cl_2] prepared *in situ* from the reaction of $FeCl_2$ (21.2 mg, 0.167 mmol, 2 equiv.) with TPA (48.6 mg, 0.167 mmol, 2 equiv.) in 1 mL of pyridine is added to a stirred dark blue solution of [UO_2(Mesaldien)K]$_n$ (53.1 mg, 0.084 mmol, 1 equiv.) in 2 mL of pyridine. Immediately the resulting solution becomes dark red and was stirred overnight. KI (13.9mg, 0.084mmol, 1 equiv.) was added to the solution allowing the crystallisation of X-ray quality crystals of {[Fe(TPA)Cl][UO_2(Mesaldien)][Fe(TPA)Cl]}I (53.5 mg, 0.036 mmol, 43%) by slow diffusion of hexane. Elemental analysis calcd (%) for. {[Fe(TPA)Cl][UO_2(Mesaldien)][Fe(TPA)Cl]}I ($C_{55}H_{57}N_{11}O_4Cl_2IFe_2U$, MW=1483.67) C 44.53, H 3.87 and N 10.38; found C 44.74, H 3.64 and N 10.55. ^{1}H NMR (200 MHz, Py-d_5, 298 K): δ = 112.18 (br, 2H), 54.36/52.32 (br m, 7H), 45.91 (br s, 7H), 38.13 (br, 1H), 26.78 (br s, 7H), 8.98 (br, 3H), 6.99 (s, 2H), 6.32 (br s, 2H), 4.05 (s, 1H), 3.17 (br s, 3H), 2.00 (s, 2H), -1.58/-6.32/-11.05 (br m, 7H), -39.92 (br, 1H). ESI-MS: m/z=1355.1 ({[Fe(TPA)Cl][UO_2(Mesaldien)][Fe(TPA)Cl]}$^+$).

Synthesis of {[UO_2(Mesaldien)][Co(TPA)]}I, 17-UCo-TPA

To a dark blue solution of [UO_2(Mesaldien)K]$_n$ (87.1 mg, 0.138 mmol, 1 equiv.) in 2 mL of pyridine is added a blue solution of [Co(TPA)I]I prepared *in situ* from the reaction of CoI_2 (41.5 mg, 0.138 mmol, 1 equiv.) and TPA (38.6 mg, 0.138 mmol, 1 equiv.) in 1 mL of pyridine. Immediately the color change to dark violet and a violet solid is precipitating. This suspension is stirred at room temperature for 3 hours before filtration of the violet solid, washed with 2*0.5mL of pyridine and dried under reduced pressure yielding 82.9 mg of {[UO_2(Mesaldien)][Co(TPA)]}I.0.1Pyridine. Another portion of the complex is obtained by slow diffusion of hexane in the violet filtrate yielding 25.6 mg more (0.100 mmol, 73%). Elemental analysis (%) calculated for {[UO_2(Mesaldien)][Co(TPA)]}I.0.1Pyridine ($C_{37.5}H_{39.5}N_{7.1}O_4CoIU$, MW=1077.53) C 41.80, H 3.70 and N 9.23 found C 41.79, H 3.70 and N 9.30. ^{1}H NMR (400 MHz, CD_3CN, 298 K): δ = 138.39 (br, 4H), 97.45 (br, 6H), 50.89 (s, 2H), 46.64 (s, 2H), 17.36 (s, 2H), 12.91 (s, 2H), 9.74 (s, 2H), 8.12 (s, 2H), 6.39 (s, 2H), 5.62 (s, 2H), 4.66 (s, 2H), 3.98 (s, 2H), 3.64 (s, 2H), 0.30 (s, 2H), -0.84 (s, 2H), -1.22 (br, 3H). ESI-MS: m/z=942.1 ({[Co(TPA)][UO_2(Mesaldien)]}$^+$). Dark violet X-ray quality crystals of {[UO_2(Mesaldien)][Co(TPA)]}I.Pyridine were formed after two weeks into a solution layered with hexane.

Synthesis of {[Ni(TPA)][UO_2(Mesaldien)][Ni(TPA)]}.3I, 18-UNi_2-TPA

A light blue solution of [Ni(TPA)I_2] prepared *in situ* from the reaction of NiI_2 (29.3 mg, 0.094 mmol, 2 equiv.) with TPA (27.2 mg, 0.094 mmol, 2 equiv.) in 1 mL of pyridine is added to a

stirred dark blue solution of $[UO_2(Mesaldien)K]_n$ (29.6 mg, 0.046 mmol, 1 equiv.) in 2 mL of pyridine. Volatiles are removed under reduce pressure. Dark violet residue is dissolved into 3mL of MeCN, and KI is removed by filtration. Slow evaporation of the volatiles lead to microcrystalline violet solid, collected by filtration and dried quickly under vacuum to yield 83.3 mg of {[Ni(TPA)][UO_2(Mesald)][Ni(TPA)]}.3I.3MeCN (0.044 mmol, 94%). Elemental analysis calcd (%) for {[Ni(TPA)][UO_2(Mesaldien)][Ni(TPA)]}.3I.3MeCN ($C_{61}H_{66}N_{14}O_4I_{3.7}K_{0.7}Ni_2U$, MW=1911.62) C 38.33, H 3.48 and N 10.26; found C 38.66, H 3.56 and N 9.86. ^{1}H NMR (400 MHz, Py-d_5, 298 K): δ = 50.18/47.90/46.45/44.62/44.04/41.96/40.04 (br m, 10H), 13.13/11.70 (br m, 9H), 6.72 (br d, 3H), 5.91 (br s, 4H), 5.38 (br d, 3H), 3.65 (br s, 2H), 2.02 (br s, 2H), 0.34/-0.27 (br m, 5H), -1.67/-2.12 (br m, 4H), -5.81/-5.95 (br d, 2H), -10.97/-12.87 (br m, 2H). ESI-MS: m/z=1545.18 ({[Ni(TPA)][UO_2(Mesaldien)][Ni(TPA)].2I}$^+$). X-ray quality crystals of {[{[Ni(TPA)(MeCN)][UO_2(Mesaldien)][Ni(TPA)I]}I_2/{[Ni(TPA)(MeCN)][UO_2(Mesaldien)][Ni(TPA)(MeCN)]}I_3]}.4.5MeCN were formed in acetonitrile solution by slow evaporation of the volatiles.

Synthesis of {[Mn(BPPA)(Py)][UO_2(Mesald)][Mn(BPPA)(Py)]}I, 19-UMn_2-BPPA

A light yellow suspension of [Mn(BPPA)I] prepared *in situ* from the reaction of MnI_2 (44.8 mg, 0.145 mmol, 2 equiv.) and BPPAK (49.8 mg, 0.145 mmol, 2 equiv.) in 1 mL of pyridine is added to a stirred dark blue solution of $[UO_2(Mesaldien)K]_n$ (45.8 mg, 0.072 mmol, 1 equiv.) in 2 mL of pyridine. Immediately the resulting solution becomes red. After 6 hours of stirring, a white precipitate of KI was removed by filtration and the solution is layered with hexane. Microcrystalline violet solid was collected by filtration and washed with hexane (2 x 0.5 mL) and dried under vacuum to yield 95.6 mg of {[Mn(BPPA)(Py)][UO_2(Mesald)][Mn(BPPA)(Py)]}I.KI (0.054 mmol, 75%). Elemental analysis calcd (%) for {[Mn(BPPA)(Py)][UO_2(Mesald)][Mn(BPPA)(Py)]}I.KI ($C_{67}H_{67}N_{13}O_6KI_2Mn_2U$, MW=1762.95) C 45.65, H 3.83 and N 8.74; found C 45.63, H 4.10 and N 8.51. ^{1}H NMR (200 MHz, Py-d_5, 298 K): δ = 84.24 (br, 1H), 50.51/49.06/48.08 (br m, 10H), 21.45 (s, 2H), 16.71 (br s, 2H), 6.15/5.83/5.17/3.76/2.97 (br m, 18H), -9.76 (br, 2H), -15.47/-16.02/-16.85/-17.09 (br m, 7H). ESI-MS: m/z=1311.3 ({[Mn(BPPA)][UO_2(Mesald)][Mn(BPPA)]}$^+$). This complex is almost unsoluble in MeCN and poorly soluble in pyridine, only small needles were obtained and were not suitable for X-ray diffraction.

Synthesis of {[Fe(BPPA)(Py)][UO_2(Mesaldien)][Fe(BPPA)]}I, 20-UFe_2-BPPA

A light orange suspension of [Fe(BPPA)I] prepared *in situ* from the reaction of FeI_2 (36.7 mg, 0.12 mmol, 2 equiv.) with BPPAK (40.7 mg, 0.12 mmol, 2 equiv.) in 1 mL of pyridine is added

to a stirred dark blue solution of $[UO_2(Mesaldien)K]_n$ (37.5 mg, 0.06 mmol, 1 equiv.) in 2 mL of pyridine. Immediately the resulting solution becomes dark red and was stirred overnight. KI is removed by filtration and volatiles are removed under vacuum. The resulting red solid is washed with hexane yielding {[Fe(BPPA)(Py)][UO_2(Mesaldien)][Fe(BPPA)]}I.3.3Pyridine (74.7 mg, 0.042 mmol, 70%). Elemental analysis calcd (%) for. {[Fe(BPPA)(Py)][UO_2(Mesaldien)][Fe(BPPA)]}I.3.3Pyridine ($C_{78.5}H_{78.5}N_{13.3}O_6IFe_2U$, MW=1780.67) C 52.95, H 4.44 and N 10.46; found C 52.87, H 4.35 and N 10.42. ^{1}H NMR (200 MHz, Py-d_5, 298 K): δ = 130.10 (br, 4H), 50.72 (s, 7H), 42.41/38.57 (br m, 6H), 31.47 (br s, 1H), 27.42 (s, 2H), 22.44 (s, 3H), 12.83 (s, 2H), 10.43 (s, 2H), 9.19 (s, 3H), 7.87 (s, 3H), 4.13 (br, 6H), -7.88 (br, 3H), -15.04/-15.99 (br d, 7H), -23.75/-24.42 (br d, 4H), -32.59 (br, 4H). ESI-MS: m/z=1313.3 ({[Fe(BPPA)][UO_2(Mesaldien)][Fe(BPPA)]}$^+$). Slow diffusion of DIPE into a pyridine solution containing a 2:1 mixture of [Fe(BPPA)I] and $[UO_2(Mesaldien)K]_n$ yields X-ray quality crystals of {[Fe(BPPA)(Py)][UO_2(Mesaldien)][Fe(BPPA)]}I.3Pyridine.

Synthesis of {[Co(BPPA)(Py)][UO_2(Mesaldien)][Co(BPPA)]}I, 21-UCo_2-BPPA

A brown suspension of [Co(BPPA)I] prepared *in situ* from the reaction of CoI_2 (52.4 mg, 0.167 mmol, 2 equiv.) and BPPAK (57.5 mg, 0.167 mmol, 2 equiv.) in 1 mL of pyridine is added to a stirred dark blue solution of $[UO_2(Mesaldien)K]_n$ (53.1 mg, 0.084 mmol, 1 equiv.) in 2 mL of pyridine. Immediately the resulting solution turned dark red. After 3 hours of stirring, KI was filtrated off and the solution was layered with hexane. Dark X-ray quality crystals were formed after two weeks of diffusion. Crystals were collected by filtration and washed with hexane (2 x 0.5 mL) and dried under vacuum to yield 130.1 mg of UO_2Co_2 {[Co(BPPA)][UO_2(Mesaldien)][Co(BPPA)(Py)]}I.2Pyridine (0.077 mmol, 92%). Elemental analysis calcd (%) for {[Co(BPPA)(Py)][UO_2(Mesaldien)][Co(BPPA)]}I.2Pyridine ($C_{72}H_{72}N_{12}O_6ICo_2U$, MW=1684.04) C 51.35, H 4.31 and N 9.98; found C 51.33, H 4.16 and N 10.33. ^{1}H NMR (200 MHz, CD_3CN, 298 K): δ = 145.49 (br, 3H), 134.36 (br, 4H), 101.733 (br, 2H), 70.03 (br, 3H), 60.39 (br, 1H), 51.44 (s, 4H), 40.4 (d, 4H), 35.00 (br, 2H), 25.34/24.47 (br m, 2H), 13.30 (br, 2H), 7.94 (d, 4H), 6.24 (s, 2H), 5.39 (s, 2H).4.65 (s, 2H), 4.39 (s, 2H), 4.11 (s, 2H), 3.63 (s, 2H), 1.43 (br, 2H), -0.16/-0.69 (br m, 5H), -15.35 (br, 2H), -19.39 (br, 2H). ESI-MS: m/z=1321.2 ({[Co(BPPA)][UO_2(Mesaldien)][Co(BPPA)]}$^+$).

Synthesis of {[Ni(BPPA)(Py)][UO_2(Mesaldien)][Ni(BPPA)(Py)]}I, 22-UNi_2-BPPA

A light green solution of [Ni(BPPA)I] prepared *in situ* from the reaction of NiI_2 (51.9 mg, 0.17 mmol, 2 equiv.) with BPPAK (57 mg, 0.17 mmol, 2 equiv.) in 1 mL of pyridine is added to a stirred dark blue solution of $[UO_2(Mesaldien)K]_n$ (52.5 mg, 0.08 mmol, 1 equiv.) in 2 mL of pyridine. Immediately the resulting solution becomes dark violet. After 3 hours of stirring, KI

is removed by filtration and the solution is layered with hexane. Microcrystalline solid is collected by filtration and washed with hexane (2 x 0.5 mL) and dried under vacuum to yield 127.2 mg of {[Ni(BPPA)(Py)][UO_2(Mesaldien)][Ni(BPPA)(Py)]}I.1.5Pyridine.0.5KI (0.070 mmol, 84%). Elemental analysis calcd (%) for {[Ni(BPPA)(Py)][UO_2(Mesaldien)][Ni(BPPA)(Py)]}I.1.5Pyridine.0.5KI ($C_{74.5}H_{74.5}N_{12.5}O_6I_{1.5}K_{0.5}Ni_2U$, MW=1805.95) C 49.55, H 4.16 and N 9.69; found C 49.34, H 4.14 and N 10.08. ^{1}H NMR (200 MHz, Py-d_5, 298 K): δ = 186.79 (br s, 1H), 147.31/132.98/127.15/120.21/105.99 (br m, 8H), 46.14/43.93/41.10 (br m, 11H), 30.14 (br s, 1H), 25.56 (s, 1H), 22.84 (s, 2H), 12.29/11.32/10.27/9.18 (br m, 8H), 6.93/6.73 (br d, 3H), 5.56/5.23 (br m, 2H), 3.41 (br s, 2H), 1.35/-0.55/-1.03 (br m, 5H), -2.41 (br s, 3H), -4.17 (br s, 3H), -5.31/-5.59 (br m ,5H), -8.38/-11.06 (br m, 2H). ESI-MS: m/z=1317.2 ({[Ni(BPPA)][UO_2(Mesaldien)][Ni(BPPA)]}$^+$). Slow diffusion of hexane into a pyridine solution containing a 2:1 mixture of [Ni(BPPA)I] and [UO_2(Mesaldien)K]$_n$ yields X-ray quality crystals of {[Ni(BPPA)(Py)][UO_2(Mesaldien)][Ni(BPPA)(Py)]}I.5.5Pyridine.

Isolation of [{Cr(BPPA)(μ-O)}4Cr]2I, 23

A brown solution of [Cr(BPPA)Cl] prepared *in situ* from the reaction of $CrCl_2$ (1.9 mg, 15.8 μmol, 2 equiv.) with BPPAK (5.4 mg, 15.8 μmol, 2 equiv.) in 1 mL of pyridine is added to a stirred dark blue solution of [UO_2(Mesaldien)K]$_n$ (5.0 mg, 7.9 μmol, 1 equiv.) in 0.5 mL of pyridine. ^{1}H NMR recorded in Py-d_5 of the resulting brown solution revealed a complicated mixture of species notably with sharp shifted peaks looking like an uranium(IV) complex. Slow diffusion of DIPE into an acetonitrile solution of this reaction mixture affords X-ray quality crystals of the mixed-valent Cr(II)/Cr(III) species [{Cr(BPPA)(μ-O)}$_4$Cr].2I.4MeCN.

Isolation of {[UO_2(Mesaldien)][Zn(BPPA)]}, 24

A colourless solution of [Zn(BPPA)I] prepared *in situ* from the reaction of ZnI_2 (2.5 mg, 15.8 μmol, 2 equiv.) with BPPAK (5.4 mg, 15.8 μmol, 2 equiv.) in 1 mL of pyridine is added to a stirred dark blue solution of [UO_2(Mesaldien)K]$_n$ (5.0 mg, 7.9 μmol, 1 equiv.) in 0.5 mL of pyridine. Slow diffusion of hexane into the resulting blue solution affords X-ray quality crystals of the dinuclear species {[UO_2(Mesaldien)][Zn(BPPA)]}.1.6Pyridine.

Synthesis of {[Mn(TPEN)][UO_2(Mesaldien)][Mn(TPEN)]}I_3, 25-UMn_2-TPEN

A colorless solution of [Mn(TPEN)]I_2 prepared *in situ* from the reaction of MnI_2 (49.7 mg, 0.161 mmol, 2 equiv.) with TPEN (68.4 mg, 0.161 mmol, 2 equiv.) in 2 mL of pyridine is added to a stirred dark blue solution of [UO_2(Mesaldien)K]$_n$ (51.2 mg, 0.081 mmol, 1 equiv.) in 2 mL of pyridine. Immediately the resulting solution becomes red. After 6 hours of stirring,

a white precipitate was removed by filtration. The volatiles were removed under reduced pressure and the pink residue was dissolved into 2mL of MeCN. The pink solution was layered with DIPE (8mL) and after 3 days of slow diffusion, pink crystals formed were filtrated and rapidly dried under vacuum to yield 100.9mg (total yield 63%) of {[Mn(TPEN)][UO_2(Mesaldien)][Mn(TPEN)]}I_3.MeCN.2.8KI. Elemental analysis calcd (%) for {[Mn(TPEN)][UO_2(Mesaldien)][Mn(TPEN)]}I_3.2.8KI ($C_{71}H_{77}N_{15}O_4K_{2.8}I_{5.8}Mn_2U$, MW=2397.93) C 35.56, H 3.24 and N 8.76; found C 35.51, H 3.11 and N 8.57.^{1}H NMR (400 MHz, CD_3CN, 298 K): δ = 69.02 (br, 7H), 57.75 (br, 5H), 39.24 (br, 14H), 7.50 (s, 2H), 7.14 (s, 2H), 6.93 (br, 2H), 5.47 (s, 2H), 4.78 (br s, 2H), 3.68 (br s, 4H), 2.99 (br, 4H), 1.10 (s, 3H), -8.65 (br, 8H). ESI-MS: m/z=1804.9 ({[Mn(TPEN)][UO_2(Mesaldien)][Mn(TPEN)I_2}$^+$). X-ray quality crystals of {[Mn(TPEN)][UO_2(Mesaldien)][Mn(TPEN)]}I_3.MeCN grew by slow diffusion of DIPE into an acetonitrile solution containing the trinuclear complex.

Synthesis of {[Co(TPEN)][UO_2(Mesaldien)][Co(TPEN)]}I_3, 26-UCo_2-TPEN

A pink solution of [Co(TPEN)]I_2 prepared *in situ* from the reaction of CoI_2 (49.6 mg, 0.159 mmol, 2 equiv.) with TPEN (67.1 mg, 0.159 mmol, 2 equiv.) in 2 mL of pyridine is added to a stirred dark blue solution of [UO_2(Mesaldien)K]$_n$ (50 mg, 0.079 mmol, 1 equiv.) in 2 mL of pyridine. Immediately the resulting solution becomes brown. After 6 hours of stirring, a white precipitate was removed by filtration. All volatiles removed under reduced pressure. Residue dissolved into a mixture 2/3 Pyridine/MeCN (2mL) and the resulted dark red solution layered with DIPE (8mL) for slow diffusion. After a week of slow diffusion, dark red crystals formed were filtrated and rapidly dried under vacuum to yield 82.5mg of {[Co(TPEN)][UO_2(Mesaldien)][Co(TPEN)]}I_3.0.5MeCN.2Pyridine (0.039mmol, 49%). Elemental analysis calcd (%) for {[Co(TPEN)][UO_2(Mesaldien)][Co(TPEN)]}I_3.0.5MeCN.2Pyridine ($C_{82}H_{88.5}N_{17.5}O_4I_3Co_2U$, MW=2119.63) C 46.67, H 4.21 and N 11.56; found C 46.85, H 4.12 and N 11.31.^{1}H NMR (400 MHz, CD_3CN, 298 K): δ = 73.88 (br, 4H), 58.44 (br, 2H), 40.64 (br, 6H), 17.33/13.81 (br m, 13H), 6.34 (br s, 4H), 2.24 (s, 2H), 1.08 (s, 2H), -9.62 (br, 2H). ESI-MS : m/z=1812.8 ({[Co(TPEN)][UO_2(Mesaldien)][Co(TPEN)I_2}$^+$). X-ray quality crystals of {[Co(TPEN)][UO_2(Mesaldien)][Co(TPEN)]}I_3.3.5MeCN.2Pyridine grew by slow diffusion of DIPE into a 2/3 Pyridine/MeCN solution containing the trinuclear complex.

Synthesis of {[Nd(TPA)(Py)I_2][UO_2(Mesaldien)][Nd(Mesaldien)][UO_2(Mesaldien)] [Nd(TPA)(Py)I_2]}I 27-U_2Nd_3-TPA

A light yellow solution of [Nd(Mesaldien)I] prepared *in situ* from the reaction of $NdI_3(THF)_{3.5}$ (31.1 mg, 0.04mmol, 1 equiv.) with K_2Mesaldien (15.9mg, 0.04mmol, 1 equiv.) in 1 mL of

pyridine is added to a stirred colourless solution of [NdI_3(TPA)] prepared from the reaction of $NdI_3(THF)_{3.5}$ (62.2 mg, 0.08mmol, 2 equiv.) with TPA (22.9 mg, 0.08mmol, 2 equiv.) in 1 mL of pyridine. This solution is then added to a stirred dark blue solution of $[UO_2(Mesaldien)K]_n$ (50 mg, 0.08mmol, 2 equiv.) in 1.5 mL of pyridine. Immediately the colour changes to orange. This solution is stirred at room temperature for 2 hours before layered with DIPE, yielding orange needles (113.3mg, 0.034mmol, 84%). Elemental analysis calcd (%) for {[Nd(TPA)(Py)I_2][UO_2(Mesald)][Nd(Mesald)][UO_2(Mesald)][Nd(TPA)(Py)I_2]}I.0.7Pyridine ($C_{106.5}H_{112.5}N_{19.7}O_{10}I_5Nd_3U_2$, MW=3371.73) C 37.94, H 3.36 and N 8.18; found C 37.86, H 3.42 and N 8.35. ^{1}H NMR (200 MHz, Py-d_5, 298 K): δ = 45.65 (s, 2H), 22.55 (br s, 3H), 20.63/20.31 (br m, 4H), 18.55 (br s, 2H), 16.44 (br s, 2H), 15.14/14.68/14.25 (br m, 5H), 12.98/12.32 (br d, 11H), 10.17/9.27 (br m, 6H), 6.58/6.21/5.39 (br m, 21H), 4.05/3.76 (br m, 7H), 1.22/0.75/0.40/-0.12/-0.84 (br m, 18H), -2.08/-2.49/-3.022 (br m, 8H), -5.37 (br s, 3H), -7.42 (br s, 2H), -9.31 (br s, 2H), -12.43/-13.08 (br m, 3H). ESI-MS: m/z=3030.6 ({[Nd(TPA)I_2][UO_2(Mesald)][Nd(Mesald)][UO_2(Mesald)][Nd(TPA)I_2]}$^+$). X-ray quality crystals of {[Nd(TPA)(Py)I_2][UO_2(Mesald)][Nd(Mesald)][UO_2(Mesald)][Nd(TPA)(Py)I_2]}I.Pyridine grew by slow diffusion of DIPE into a pyridine solution containing the 2/1/2 stoichiometry of $[UO_2(Mesaldien)K]_n$/[Nd(Mesaldien)I]/[Nd(TPA)I_3].

Synthesis of {[Eu(TPEN)I][UO_2(Mesaldien)][Eu(TPEN)I]}I, 28-UEu_2-TPEN

A red solution of [Eu(TPEN)I_2], prepared *in situ* from the reaction of EuI_2 (60 mg, 0.148 mmol, 2 equiv.) with TPEN (62.8 mg, 0.148 mmol, 2 equiv.) in 2 mL of pyridine, is added to a stirred dark blue solution of $[UO_2(Mesaldien)K]_n$ (46.8 mg, 0.074 mmol, 1 equiv.) in 2 mL of pyridine. Immediately the resulting solution becomes brown. After 2 hours of stirring, KI is removed by filtration and the solution is layered with hexane. Brown crystals were collected by filtration, washed with hexane (2 x 0.5 mL) and dried under vacuum to yield 148 mg of UEu_2-TPEN {[Eu(TPEN)I][UO_2(Mesaldien)][Eu(TPEN)I]}I.0.8Pyridine (0.067 mmol, 91%). Elemental analysis calcd (%) for {[Eu(TPEN)I][UO_2(Mesaldien)][Eu(TPEN)I]}I.0.8Pyridine ($C_{75}H_{81}N_{15.8}O_4I_3Eu_2U$, MW=2190.36) C 41.13, H 3.73 and N 10.10; found C 41.15, H 3.78 and N 9.95. Due to the presence of Eu(II), no signal in ^{1}H NMR were observed. ESI-MS: m/z=1999.3 ({[Eu(TPEN)I][UO_2(Mesaldien)][Eu(TPEN)I]}$^+$). Slow diffusion of hexane into a pyridine solution of UEu_2-TPEN yields to X-ray quality crystals of {[Eu(TPEN)I][UO_2(Mesaldien)][Eu(TPEN)I]}I.3.5Pyridine.

Reaction of K_2salfen with {[$UO_2(Py)_5$][$KI_2(Py)_2$]}$_n$

A solution of K_2salfen (10.0 mg, 0.018 mmol, 1 equiv.) in pyridine (1 mL) was added to an orange suspension of {[$UO_2(Py)_5$][$KI_2(Py)_2$]}$_n$ (20.2mg, 0.018 mmol, 1 equiv.) in pyridine (1

mL), resulting in a dark red solution. The solution was stirred over 15 min. The ^{1}H NMR of the solution revealed the presence of paramagnetic signals that resemble of the [U(salfen)$_2$] and [UO$_2$(salfen)] complexes. Complete disproportionation was achieved in 12 hours.

Reaction of K$_2$salfen with {[UO$_2$(Py)$_5$][KI$_2$(Py)$_2$]}$_n$ in presence of 18c6

A solution of SalfenK$_2$ (4.5mg, 0.0089 mmol, 1 equiv.) in pyridine (0.3 mL) was added to a colorless solution of 18C6 (7.6mg, 0.0280 mmol, 3.2 equiv.) in pyridine (0.2mL). Then an orange suspension of {[UO$_2$(Py)$_5$][KI$_2$(Py)$_2$]}$_n$ (10mg, 0.0089 mmol, 1 equiv.) in pyridine (0.5 mL) was added, resulting in a dark red solution. The solution was stirred over 5 min. The ^{1}H NMR of the solution revealed the presence of slightly shifted paramagnetic signals that resemble to a uranyl(V) species but disproportionate after 24h into the [U(salfen)$_2$] and [UO$_2$(salfen)] complexes.

Reaction of K$_2$salfen with [UO$_2$I$_2$(Py)$_3$] : [UO$_2$(salfen)]

A solution of K$_2$salfen (18.5 mg, 0.037 mmol, 1 equiv.) in pyridine (1 mL) was added to a dark red solution of [UO$_2$I$_2$(Py)$_3$] (27.9 mg, 0.037 mmol, 1 equiv.) in pyridine (1 mL), resulting in a dark red solution. The solution was stirred over 2 hours, and then a ^{1}H NMR spectrum was acquired. ^{1}H NMR (200 MHz, Py-d$_5$, 298 K) : δ = 10.13 (s, 2H), 8.11 (s, 2H), 7.70 (s, 2H), 4.76 (s, 4H), 4.63 (s, 4H), 2.03 (s, 18H), 1.41 (s, 18H).

Reaction of K$_2$salfen with [UI$_4$(OEt$_2$)$_2$] : [U(salfen)$_2$]

A solution of K$_2$salfen (50.0 mg, 0.099 mmol, 2 equiv.) in THF (4 mL) was added to a red solution of [UI$_4$(OEt$_2$)$_2$] (44.1 mg, 0.049 mmol, 1 equiv.) in THF (4 mL). The resulting red suspension was stirred for 12 h at room temperature before filtration. The resulting red filtrate was evaporated to dryness to give [U(salfen)$_2$].0.2 KI as a red powder (40.8 mg, 0.037 mmol, 75% yield). Elemental analysis calcd (%) for [U(salfen)$_2$].0.2(KI) ($C_{48}H_{36}Fe_2N_4O_4UK_{0.2}I_{0.2}$, MW=1115.76) C 51.67, H 3.25, N 5.02; found: C 51.70, H 3.48, N 4.96. ^{1}H NMR (200 MHz, Py-d$_5$, 298 K): δ = 23.9 (s, 4H), 17.8 (t, 4H), 12.9 (d, 4H), 12.3 (t, 4H), 10.7 (s, 4H), 4.1 (s, 4H), −2.6 (s, 4H), -7.6 (s, 4H), -19.0 (s, 4H). Single crystals suitable for X-ray diffraction were obtained by slow diffusion of diisopropyl ether into a THF solution of [U(salfen)$_2$].

Synthesis of [UO$_2$(salfen-^{t}Bu$_2$)], 29

A red solution of [UO$_2$I$_2$(Py)$_3$] (10.0 mg, 0.013 mmol, 1 equiv.) in pyridine (0.5 mL) was added to a light red solution of K$_2$salfen-^{t}Bu$_2$ (9.9 mg, 0.013 mmol, 1 equiv.) in pyridine (0.5 mL), yielding after 30 minutes stirring a dark red solution with an off-white precipitate. The off white precipitate was removed by filtration. Slow diffusion of hexane (one week) into this

solution afforded the desired compound as a red crystalline solid (11 mg, 0.011 mmol, 90 % yield). Elemental analysis calcd (%) for $[UO_2(salfen\text{-}^tBu_2)].0.15(KI)$ ($C_{40}H_{50}FeN_2O_4UK_{0.15}I_{0.15}$, MW=941.62) C 51.02, H 5.35, N 2.98; found: C 50.99, H 5.75, N 3.09. ^{1}H NMR (200 MHz, Py-d_5, 298 K): δ = 10.12 (s, 2H), 8.10 (d, 2H), 7.70 (d, 2H), 4.76 (t, 4H), 4.63 (t, 4H), 2.03 (s, 18H), 1.41 (s, 18H). ESI-MS: m/z=955.3 ($[UO_2(salfen\text{-}^tBu_2)]K^+$). FTIR : ν 2946(w), 2899(w), 2863(w), 1606(s), 1554(m), 1534(s), 1472(m), 1457(m), 1419(s), 1381(m), 1369(s), 1358(s), 1300(s), 1254(m), 1196(w), 1165(w), 1037(m), 976(s), 930(s), 911(s), 891(s, asymmetric stretching of uranyl(VI)), 835(s), 816(s), 780(s), 744(s), 695(s), 662(s), 640(s), 625(s) cm^{-1}.

Synthesis of $[UO_2(salfen\text{-}^tBu_2)(K18c6)]$, 30

A solution of $K_2salfen\text{-}^tBu_2$ (69.4 mg, 0.096 mmol, 1 equiv.) in pyridine (2 mL) was added to an orange suspension of $\{[UO_2(Py)_5][KI_2(Py)_2]\}_n$ (106.9 mg, 0.096 mmol, 1 equiv.) in pyridine (0.5 mL). A colorless solution of 18c6 (75.9 mg, 0.290 mmol, 3 equiv.) in pyridine (2 mL) was then added to the reaction mixture resulting in a dark red solution. The solution was stirred 30 min at room temperature and concentrated to 1 mL. This solution was filtered and hexane (6 mL) was added to the filtrate, resulting in the formation of a brown precipitate. The solid was recovered by filtration, washed with hexane (1 mL) and dried under vacuum to afford $[UO_2(salfen\text{-}^tBu)(K18c6)].0.8hex$. (52.9 mg , 45% yield). Elemental analysis calcd (%) for $[UO_2(salfen\text{-}^tBu)(K18c6)].0.8hex$ ($C_{56.8}H_{85.2}KFeN_2O_{10}U$, MW=1289.08) C 52.92, H 6.66, N 2.17; found: C 52.89, H 6.93, N 2.34. ^{1}H NMR of 2 (500 MHz, Py-d_5 , 323 K): d = 6.89 (s, 2H), 6.64 (s, 2H), 5.23 (s, 2H), 4.65 (s, 24H, 18c6), 4.27 (s, 4H), 1.09 (s, 4H), 0.77 (s, 18H), -3.41 (s, 18H). ESI-MS: m/z = 1522.2 ($[UO_2(salfen\text{-}^tBu_2)(K18c6)](K18c6)^+$). FTIR : ν 2944(w), 2939(m), 1592(w), 1539(s), 1521(m), 1457(m), 1421(m), 1380(w), 1351(m), 1319(w), 1270(w), 1251(m), 1220(w), 1194(w), 1157(s), 1103(w), 957(w), 931(s), 911(s), 871(s), 834(s), 809(s), 789(s), 768(s, asymmetric stretching of uranyl(V)), 739(s), 663(s), 634(m) cm^{-1}. Orange single crystals of 2 suitable for X-ray diffraction were obtained after 2 weeks by recrystallisation from toluene at room temperature.

Reaction of $K_2salfen\text{-}^tBu$ with $\{[UO_2(Py)_5][KI_2(Py)_2]\}_n$: $[UO_2(salfen\text{-}^tBu_2)K]$

A solution of $K_2salfen\text{-}^tBu_2$ (65.0 mg, 0.09 mmol, 1 equiv.) in pyridine (1 mL) was added to an orange suspension of $\{[UO_2(Py)_5][KI_2(Py)_2]\}_n$ (100 mg, 0.09 mmol, 1 equiv.) in pyridine (1 mL) resulting in a dark red solution. The solution was stirred for 4 hours and concentrated to 1 mL. This solution was filtered, and then hexane (6 mL) was added. The brown powder was filtered and washed with hexane (1 mL) before dried under vacuum to yield 76.1 mg of $[UO_2(salfen\text{-}^tBu_2)K]$ (yield 87%). Attempts to fit elemental analysis of the brown solid failed.

^{1}H NMR (200 MHz, Py-d_5, 298 K) : δ = 6.83 (s, 2H), 5.71 (s, 2H), 4.79 (s, 4H), 3.72 (s, 2H), 1.25 (s, 4H), 0.107 (s, 18H), -3.87 (s, 18H). Analysis by ^{1}H NMR shows that [UO_2(salfen-^{t}Bu$_2$)K] is stable over a one month period in pyridine solution. Attempts to grow single crystals of [UO_2(salfen-^{t}Bu$_2$)K] failed.

Synthesis of [$NpO_2L]_3$, 31

KL (12.3 mg, 27.2 µmol, 1 equiv.) in pyridine (2mL) was added to {[$NpO_2(Py)_5$][$KI_2(Py)_2$]}$_n$ (30.4 mg, 27.2 µmol, 1 equiv.) in suspension in pyridine (1mL) and the resulting red solution was stirred for 2 hours. Residual solid (KI) was removed by centrifugation and the red solution was concentrated under reduced pressure to 2mL. The red solid formed overnight was collected by centrifugation and washed twice with pyridine (2 × 0.5mL) and dried under vacuum (17.2 mg). This solid was recrystallised in MeCN (1.5mL) at room temperature yielding X-ray quality crystals. Red crystals were collected by centrifugation and washed twice with MeCN (2 × 0.25mL) and dried under vacuum (12.1 mg, 65%). ^{1}H NMR (400MHz, Py-d_5, 298 K): δ= 27.66 (br, 1H), -9.06 (br d, 3H), -15.04 (br, 1H), -28.37 (br, 1H), -39.87 (br, 1H). FTIR : ν 3064(m), 3033(m), 1585(m), 1502(m), 1477(s), 1438(w), 1396(m), 1373(m), 1301(w), 1251(s), 1089(s), 1066(s), 1035(s), 960(w), 825(s), 788(s, asymmetric stretching of neptunyl(V)), 763(s), 740(s), 713(s), 663(m), 632(s), 626(s) cm^{-1}.

VI.3.3) Nitride uranium complexes

Synthesis of [Cs_2{U(OSi(O^{t}Bu)$_3$)$_3$}$_2$(µ-N)], 32-$Cs_2[U^{III}$---N---U^{IV}]

A cold solution of [Cs{U(OSi(O^{t}Bu)$_3$)$_3$}$_2$(µ-N)] (65mg, 0.029mmol, 1 equiv.) in THF (3mL) was added to metallic cesium (3.9mg, 0.029mmol, 1 equiv.). The reaction mixture was stirred for 5 hours at -40°C with a glass coated stir bar. The resulting dark brown solution was filtrated and volatiles were removed under reduced pressure, yielding 70.1mg of brown solid. This solid was recrystallised at -40°C into 3mL of cold THF to give 50.4 mg of crystals of [Cs_2{U(OSi(O^{t}Bu)$_3$)$_3$}$_2$(µ-N)].2.9 THF (yield : 67%). Elemental analysis calcd (%) for [Cs_2{U(OSi(O^{t}Bu)$_3$)$_3$}$_2$(µ-N)].2.9THF ($C_{72}H_{162}Cs_2NO_{24}Si_6U_2$.2.9($C_4H_8O$), MW=2545.56): C 39.45, H 7.33, N 0.55; found: C 39.28, H 7.65, N 0.49. ^{1}H NMR (400 MHz, THF-d_8, 298 K): δ = 0.62 (s, 162H, CH_3), (400 MHz, Toluene-d_8, 298 K): δ = 0.81 (s, 162H, CH_3). X-ray quality crystals of [Cs_2{U(OSi(O^{t}Bu)$_3$)$_3$}$_2$(µ-N)].2THF, were obtained after 2days, from a solution of [Cs_2{U(OSi(O^{t}Bu)$_3$)$_3$}$_2$(µ-N)] (0.031 M) in THF at -40°C.

Synthesis of $[Cs_3\{U(OSi(O^tBu)_3)_3\}_2(\mu\text{-}N)]$, 33-$Cs_3[U^{III}\text{---}N\text{---}U^{III}]$

A cold solution of $[Cs\{U(OSi(O^tBu)_3)_3\}_2(\mu\text{-}N)]$ (90.3mg, 0.041mmol, equiv.) in 5mL of THF was added to metallic cesium (27.3mg, 0.205mmol, 5 equiv.). The reaction mixture was stirred for 3 hours at -40 °C with a glass coated stir bar. The stirring time should be kept as close as possible to 3 hours to avoid decomposition of the final complex $[Cs_3\{U(OSi(O^tBu)_3)_3\}_2(\mu\text{-}N)]$ by the excess Cs^0. The dark purple solution was quickly decanted or filtered at -40 to remove the excess of Cs^0 and the volatiles were removed under reduced pressure, yielding $[Cs_3\{U(OSi(O^tBu)_3)_3\}_2(\mu\text{-}N)].2THF$ as dark purple solid (83.1mg, 81%). Elemental analysis calcd (%) for $[Cs_3\{U(OSi(O^tBu)_3)_3\}_2(\mu\text{-}N)].2THF$ ($C_{72}H_{162}Cs_2NO_{24}Si_6U_2.2(C_4H_8O)$, MW=2480.66): C 36.76, H 6.87, N 0.54; found: C 36.77, H 7.13, N 0.55. ^1H NMR (400 MHz, THF-d_8, 233 K): δ = 1.42 (s, 162H, CH_3), (400 MHz, Toluene-d_8, 233 K): δ = 1.52 (s, 162H, CH_3). X-ray quality crystals of $[Cs_3\{U(OSi(O^tBu)_3)_3\}_2(\mu\text{-}N)]$ were obtained in a concentrated solution containing $[Cs_3\{U(OSi(O^tBu)_3)_3\}_2(\mu\text{-}N)]$ in THF at -40°C. The complex decomposes quickly in THF solution in the absence of Cs° at -40°C (decomposition products are observed after 1 hour). At room temperature $[Cs_3\{U(OSi(O^tBu)_3)_3\}_2(\mu\text{-}N)]$ decomposes immediately to give a mixture of complex $[Cs_2\{U(OSi(O^tBu)_3)_3\}_2(\mu\text{-}N)]$ and free siloxide as the only known decomposition products detectable by proton NMR.

Synthesis of $[K\{U(OSi(O^tBu)_3)_3\}_2(\mu\text{-}N)]$, 34-$K[U^{IV}\text{---}N\text{---}U^{IV}]$

A vial was charged with $[U(OSi(O^tBu)_3)_2(\mu\text{-}OSi(O^tBu)_3)]_2$ (182.9 mg, 0.089 mmol, 1 equiv.) and the compound was dissolved in 3 mL of THF and cooled to -40 °C. This cold solution was added onto cold KN_3 (7.2 mg, 0.089 mmol, 1 equiv.), and the reaction mixture was vigorously stirred with a glass-coated stir bar for 3days at −40 °C to give a mixture of starting material, $[K\{U(OSi(O^tBu)_3)_3\}_2(\mu\text{-}N)]$ **34-$K[U^{IV}\text{---}N\text{---}U^{IV}]$** and $[K_2\{U(OSi(O^tBu)_3)_3\}_2(\mu\text{-}N)(\mu\text{-}N_3)]$ **35**. Successive recrystallisations in THF at -40°C yield to a pure $[K\{U(OSi(O^tBu)_3)_3\}_2(\mu\text{-}N)]$ in 21% yield (40mg, 0.019mmol). Elemental analysis calcd (%) for $[K\{U(OSi(O^tBu)_3)_3\}_2(\mu\text{-}N)].2THF$ ($C_{72}H_{162}KNO_{24}Si_6U_2$, MW=2109.74): C 40.99, H 7.74, N 0.66; found: C 41.03, H 8.05, N 0.78. ^1H NMR (400 MHz, THF-d_8, 298 K): δ = −0.67 (s, 162H, CH_3). X-ray quality crystals of $[K\{U(OSi(O^tBu)_3)_3\}_2(\mu\text{-}N)]$.Toluene were obtained in a concentrated solution containing $[K\{U(OSi(O^tBu)_3)_3\}_2(\mu\text{-}N)]$ in toluene at -40°C.

Synthesis of $[K_2\{U(OSi(O^tBu)_3)_3\}_2(\mu\text{-}N)(\mu\text{-}N_3)]$, 35

A vial was charged with $[U(OSi(O^tBu)_3)_2(\mu\text{-}OSi(O^tBu)_3)]_2$ (99.2 mg, 0.048 mmol, 1 equiv.) and the compound was dissolved in 3 mL of THF and cooled to -40 °C. This cold solution was added onto cold KN_3 (7.8 mg, 0.097 mmol, 2 equiv.), and the reaction mixture was vigorously

stirred with a glass-coated stir bar for 3days at -40 °C. The resulting brown solution was filtrated on microfilter, and volatiles were removed under vaccum. The residue was dissolved in 1mL of toluene and stored at -40°C. Crystals were grown in three days from this solution. The crystals were collected, washed with 0.3mL of cold toluene and dried in vacuo to afford $[K_2\{U(OSi(O^tBu)_3)_3\}_2(\mu\text{-}N)(\mu\text{-}N_3)]$.1.5Toluene (81.8 mg, 0.035mmol, 72%). Elemental analysis calcd (%) for $[K_2\{U(OSi(O^tBu)_3)_3\}_2(\mu\text{-}N)(\mu\text{-}N_3)]$.1.5Toluene ($C_{72}H_{162}K_2N_4O_{24}Si_6U_2$.1.5($C_7H_8$), MW=2329.07): C 42.55, H 7.53, N 2.41; found: C 42.38, H 7.94, N 2.01. ^{1}H NMR (400 MHz, THF-d_8, 298 K): δ = −1.59 (s, 162H, CH_3), 400 MHz, Toluene-d_8, 298 K): δ = -1.39 (s, 162H, CH_3). X-ray quality crystals of $[K_2\{U(OSi(O^tBu)_3)_3\}_2(\mu\text{-}N)(\mu\text{-}N_3)]$.1Toluene were obtained from a concentrated toluene solution of this complex at -40°C.

Reduction of $[K\{U(OSi(O^tBu)_3)_3\}_2(\mu\text{-}N)]$ with KC_8

A cold solution (-40°C) of $[K\{U(OSi(O^tBu)_3)_3\}_2(\mu\text{-}N)]$ (6.0 mg, 0.0028 mmol, 1 equiv.) in 0.5 mL of THF-d_8 was added onto cold KC_8 (3.8 mg, 0.028 mmol, 10 equiv.). After 5minutes of stirring at -40 °C, the dark purple suspension was transferred into a sealed NMR tube. ^{1}H NMR spectrum of the supernatant (400 MHz, THF-d_8, 298 K) revealed the characteristic peak of $[K_3\{U(OSi(O^tBu)_3)_3\}_2(\mu\text{-}N)]$ at 1.56ppm (s, 162H, CH_3).

Synthesis of $[K_3\{U(OSi(O^tBu)_3)_3\}_2(\mu\text{-}N)]$, 36-$K_3[U^{III}\text{---}N\text{---}U^{III}]$

A vial was charged with $[Cs\{U(OSi(O^tBu)_3)_3\}_2(\mu\text{-}N)]$ (223.2 mg, 0.101 mmol, 1 equiv.) and the compound was dissolved in 2.0 mL of THF and cooled to -70 °C in the cold well. This cold brown red solution was added onto cold KC_8 (136.8 mg, 1.01 mmol, 10 equiv.). After 5minutes of stirring at −70 °C, the dark purple suspension was taken to dryness and the residue was extracted with 1mL of cold hexane. The resulting suspension was passed through a frits at -70°C to remove the excess of KC_8 and graphite, which were then washed with 10*1mL of cold hexane. The filtrate was concentrated to 1mL. After 4 hours at -70°C, The dark purple solid was filtrated on a cold frits, yielding 156.8mg of $[K_3\{U(OSi(O^tBu)_3)_3\}_2(\mu\text{-}N)]$.0.2Hexane (75%). Elemental analysis calcd (%) for $[K_3\{U(OSi(O^tBu)_3)_3\}_2(\mu\text{-}N)]$.0.2Hexane ($C_{73.2}H_{2.8}K_3NO_{24}Si_6U_2$, MW=2041.87): C 39.87, H 7.53, N 0.64; found: C 39.92, H 7.77, N 0.52. ^{1}H NMR of $[K_3\{U(OSi(O^tBu)_3)_3\}_2(\mu\text{-}N)]$ (400 MHz, THF-d_8, 298 K): δ = 1.56 (s, 162H, CH_3), (400 MHz, Toluene-d_8, 298 K): δ = 1.74 (s, 162H, CH_3). X-ray quality crystals of $[K_3\{U(OSi(O^tBu)_3)_3\}_2(\mu\text{-}N)]$ **36-$K_3[U^{III}\text{---}N\text{---}U^{III}]$** were obtained in a concentrated solution containing $[K_3\{U(OSi(O^tBu)_3)_3\}_2(\mu\text{-}N)]$ in hexane or THF in 2days at -40°C, whereas X-ray quality crystals of $[K_2\{U(OSi(O^tBu)_3)_3\}_2(\mu\text{-}N)]$ **37-$K_2[U^{III}\text{---}N\text{---}U^{IV}]$**were grown in toluene at -40°C in 2weeks.

Synthesis of $[K\{U(OSi(O^tBu)_3)_3\}(\mu\text{-}N)]_2$, 38

50.5mg of $[K_2\{U(OSi(O^tBu)_3)_3\}_2(\mu\text{-}N)(\mu\text{-}N_3)]$ (0.022mmol) were placed into 0.5mL of toluene in a NMR tube. After removal of the headspace, the brown solution was heated at 50°C in an oil bath for 12hours. Bubbles of N_2 are observed during the heating. Storage of dark brown resulted solution at -40°C leads to the formation of brown crystals of $[K\{U(OSi(O^tBu)_3)_3\}(\mu\text{-}N)]_2$.0.3Toluene which were collected (43.8 mg, 0.020 mmol, 91%). Elemental analysis calcd (%) for $[K\{U(OSi(O^tBu)_3)_3\}(\mu\text{-}N)]_2$.0.3Toluene ($C_{72}H_{162}K_2N_2O_{24}Si_6U_2$.0.3($C_7H_8$), MW=2190.48): C 40.63, H 7.57, N 1.28; found: C 40.60, H 7.40, N 1.08. ^{1}H NMR (400 MHz, Toluene-d_8, 298 K): δ = -1.76 (s, 162H, CH_3). The nature of the compound was also confirmed with cell check of X-ray quality crystals from ref [69].

BIBLIOGRAPHY

(1) Dam, H. H.; Reinhoudt, D. N.; Verboom, W. *Chem. Soc. Rev.* **2007**, *36*, 367-377.
(2) Kaltsoyannis, N.; Scott, P. *The f elements*; Oxford University Press: Oxford, 1999.
(3) Cotton, A. F.; Wilkinson, G. *Advanced inorganic chemistry*; fifth edition ed.; Wiley-Interscience, 1988.
(4) Burns, C. J.; Neu, M. P.; Boukhalfa, H.; Gutowski, K. E.; Bridges, N. J.; Rogers, R. D. *Comprehensive Coordination Chemistry II*; Elsevier ltd: Oxford, UK, 2004; Vol. 3.
(5) Neidig, M. L.; Clark, D. L.; Martin, R. L. *Coord. Chem. Rev.* **2013**, *257*, 394-406.
(6) Cotton, S. *Lanthanides and Actinides*; MacMillan Education: London, 1991.
(7) Rinehart, J. D.; Harris, T. D.; Kozimor, S. A.; Bartlett, B. M.; Long, J. R. *Inorg. Chem.* **2009**, *48*, 3382-3395.
(8) Long, J. R.; Meihaus, K. R. *Dalton Trans.* **2015**, *44*, 2517-2528.
(9) Edelstein, N. M.; Lander, G. H. *The Chemistry of the Actinide and Transactinide Elements*; Springer: Dordrecht, 2006.
(10) Choppin, G. R. *Radiochim. Acta* **1983**, *32*, 43-53.
(11) Den Auwer, C.; Charbonnel, M. C.; Drew, M. G. B.; Grigoriev, M.; Hudson, M. J.; Iveson, P. B.; Madic, C.; Nierlich, M.; Presson, M. T.; Revel, R.; Russell, M. L.; Thuery, P. *Inorg. Chem.* **2000**, *39*, 1487-1495.
(12) Karmazin, L.; Mazzanti, M.; Gateau, C.; Hill, C.; Pecaut, J. *Chem. Commun.* **2002**, 2892-2893.
(13) Mazzanti, M.; Wietzke, R.; Pécaut, J.; Latour, J.-M.; Maldivi, P.; Remy, M. *Inorg. Chem.* **2002**, *41*, 2389-2399.
(14) Nyman, M.; Burns, P. C. *Chem. Soc. Rev.* **2012**, *41*, 7354-7367.
(15) Qiu, J.; Burns, P. C. *Chem. Rev.* **2013**, *113*, 1097-1120.
(16) Ephritikhine, M. *Dalton Trans.* **2006**, 2501-2516.
(17) Fortier, S.; Hayton, T. W. *Coord. Chem. Rev.* **2010**, *254*, 197-214.
(18) Jones, M. B.; Gaunt, A. J. *Chem. Rev.* **2013**, *113*, 1137-1198.
(19) Sessler, J. L.; Melfi, P. J.; Pantos, G. D. *Coord. Chem. Rev.* **2006**, *250*, 816-843.
(20) Vigato, P. A.; Peruzzo, V.; Tamburini, S. *Coord. Chem. Rev.* **2012**, *256*, 953-1114.
(21) Clark, D. L.; Hobart, D. E.; Neu, M. P. *Chem. Rev.* **1995**, *95*, 25-48.
(22) Loiseau, T.; Mihalcea, I.; Henry, N.; Volkringer, C. *Coord. Chem. Rev.* **2014**, *266*, 69-109.
(23) Albrecht-Schmitt, T. E. *Angew. Chem. Int. Edit.* **2005**, *44*, 4836-4838.
(24) Krivovichev, S. V. *Eur. J. Inorg. Chem.* **2010**, 2594-2603.
(25) Liddle, S. T. *Angew. Chem. Int. Ed.* **2015**, *54*, 8604-8641.
(26) Wilkerson, M. P.; Burns, C. J.; Paine, R. T.; Scott, B. L. *Inorg. Chem.* **1999**, *38*, 4156-+.
(27) Natrajan, L.; Burdet, F.; Pecaut, J.; Mazzanti, M. *J. Am. Chem. Soc.* **2006**, *128*, 7152-7153.
(28) Altmaier, M.; Gaona, X.; Fanghaenel, T. *Chem. Rev.* **2013**, *113*, 901-943.
(29) Docrat, T. I.; Mosselmans, J. F. W.; Charnock, J. M.; Whiteley, M. W.; Collison, D.; Livens, F. R.; Jones, C.; Edmiston, M. J. *Inorg. Chem.* **1999**, *38*, 1879-1882.
(30) Ikeda, A.; Hennig, C.; Tsushima, S.; Takao, K.; Ikeda, Y.; Scheinost, A. C.; Bernhard, G. *Inorg. Chem.* **2007**, *46*, 4212-4219.
(31) Ilton, E. S.; Haiduc, A.; Cahill, C. L.; Felmy, A. R. *Inorg. Chem.* **2005**, *44*, 2986-2988.
(32) Ilton, E. S.; Boily, J.-F.; Buck, E. C.; Skomurski, F. N.; Rosso, K. M.; Cahill, C. L.; Bargar, J. R.; Felmy, A. R. *Environ. Sci. Technol.* **2010**, *44*, 170-176.
(33) Yuan, K.; Renock, D.; Ewing, R. C.; Becker, U. *Geochim. Cosmochim. Acta* **2015**, *156*, 194-206.
(34) Ekstrom, A. *Inorg. Chem.* **1974**, *13*, 2237-2241.
(35) Steele, H.; Taylor, R. J. *Inorg. Chem.* **2007**, *46*, 6311-6318.
(36) Sundararajan, M.; Campbell, A. J.; Hillier, I. H. *Journal of Physical Chemistry A* **2008**, *112*, 4451-4457.
(37) Sundararajan, M.; Assary, R. S.; Hillier, I. H.; Vaughan, D. J. *Dalton Trans.* **2011**, *40*, 11156-11163.
(38) Mizuguchi, K.; Park, Y. Y.; Tomiyasu, H.; Ikeda, Y. *J. Nucl. Sci. Technol.* **1993**, *30*, 542-548.

(39) Kim, S. Y.; Tomiyasu, H.; Ikeda, Y. *J. Nucl. Sci. Technol.* **2002**, *39*, 160-165.
(40) Mizuoka, K.; Kim, S. Y.; Hasegawa, M.; Hoshi, T.; Uchiyama, G.; Ikeda, Y. *Inorg. Chem.* **2003**, *42*, 1031-1038.
(41) Mizuoka, K.; Ikeda, Y. *Inorg. Chem.* **2003**, *42*, 3396-3398.
(42) Kim, S. Y.; Asakura, T.; Morita, Y.; Uchiyama, G.; Ikeda, Y. *Radiochim. Acta* **2005**, *93*, 75-81.
(43) Mizuoka, K.; Tsushima, S.; Hasegawa, M.; Hoshi, T.; Ikeda, Y. *Inorg. Chem.* **2005**, *44*, 6211-6218.
(44) Kim, S. Y.; Asakura, T.; Morita, Y.; Ikeda, Y. *J. Alloys Compd.* **2006**, *408*, 1291-1295.
(45) Takao, K.; Tsushima, S.; Takao, S.; Scheinost, A. C.; Bernhard, G.; Ikeda, Y.; Hennig, C. *Inorg. Chem.* **2009**, *48*, 9602-9604.
(46) Takao, K.; Kato, M.; Takao, S.; Nagasawa, A.; Bernhard, G.; Hennig, C.; Ikeda, Y. *Inorg. Chem.* **2010**, *49*, 2349-2359.
(47) Nocton, G.; Horeglad, P.; Pécaut, J.; Mazzanti, M. *J. Am. Chem. Soc.* **2008**, *130*, 16633–16645.
(48) Mougel, V.; Horeglad, P.; Nocton, G.; Pecaut, J.; Mazzanti, M. *Chem. Eur. J.* **2010**, *16*, 14365-14377.
(49) Berthet, J. C.; Nierlich, M.; Ephritikhine, M. *Angew. Chem. Int. Ed.* **2003**, *42*, 1952-1954.
(50) Berthet, J. C.; Siffredi, G.; Thuery, P.; Ephritikhine, M. *Chem. Commun.* **2006**, 3184-3186.
(51) Copping, R.; Mougel, V.; Petit, S.; Den Auwer, C.; Moisy, P.; Mazzanti, M. *Chem. Commun.* **2011**, *47*, 5497-5499.
(52) Horeglad, P.; Nocton, G.; Filinchuk, Y.; Pecaut, J.; Mazzanti, M. *Chem. Commun.* **2009**, 1843-1845.
(53) Nocton, G.; Horeglad, P.; Vetere, V.; Pecaut, J.; Dubois, L.; Maldivi, P.; Edelstein, N. M.; Mazzanti, M. *J. Am. Chem. Soc.* **2010**, *132*, 495-508.
(54) Mougel, V.; Pecaut, J.; Mazzanti, M. *Chem. Commun.* **2012**, *48*, 868-870.
(55) Hayton, T. W.; Wu, G. *J. Am. Chem. Soc.* **2008**, *130*, 2005-2014.
(56) Hayton, T. W.; Wu, G. *Inorg. Chem.* **2008**, *47*, 7415-7423.
(57) Schettini, M. F.; Wu, G.; Hayton, T. W. *Inorg. Chem.* **2009**, *48*, 11799-11808.
(58) Arnold, P. L.; Patel, D.; Wilson, C.; Love, J. B. *Nature* **2008**, *451*, 315-318.
(59) Arnold, P. L.; Love, J. B.; Patel, D. *Coord. Chem. Rev.* **2009**, *253*, 1973-1978.
(60) Selbin, J.; Ortego, J. D. *Chem. Rev.* **1969**, *69*, 657-671.
(61) Brennan, J. G.; Andersen, R. A. *J. Am. Chem. Soc.* **1985**, *107*, 514-516.
(62) Rosen, R. K.; Andersen, R. A.; Edelstein, N. M. *J. Am. Chem. Soc.* **1990**, *112*, 4588-4590.
(63) Castro-Rodriguez, I.; Nakai, H.; Meyer, K. *Angew. Chem. Int. Ed.* **2006**, *45*, 2389-2392.
(64) Graves, C. R.; Scott, B. L.; Morris, D. E.; Kiplinger, J. L. *J. Am. Chem. Soc.* **2007**, *129*, 11914-11915.
(65) Graves, C. R.; Yang, P.; Kozimor, S. A.; Vaughn, A. E.; Clark, D. L.; Conradson, S. D.; Schelter, E. J.; Scott, B. L.; Thompson, J. D.; Hay, P. J.; Morris, D. E.; Kiplinger, J. L. *J. Am. Chem. Soc.* **2008**, *130*, 5272-5285.
(66) Bart, S. C.; Anthon, C.; Heinemann, F. W.; Bill, E.; Edelstein, N. M.; Meyer, K. *J. Am. Chem. Soc.* **2008**, *130*, 12536-12546.
(67) Jilek, R. E.; Spencer, L. P.; Lewis, R. A.; Scott, B. L.; Hayton, T. W.; Boncella, J. M. *J. Am. Chem. Soc.* **2012**, *134*, 9876-9878.
(68) Lam, O. P.; Franke, S. M.; Nakai, H.; Heinemann, F. W.; Hieringer, W.; Meyer, K. *Inorg. Chem.* **2012**, *51*, 6190-6199.
(69) Camp, C.; Pecaut, J.; Mazzanti, M. *J. Am. Chem. Soc.* **2013**, *135*, 12101-12111.
(70) Fortier, S.; Brown, J. L.; Kaltsoyannis, N.; Wu, G.; Hayton, T. W. *Inorg. Chem.* **2012**, *51*, 1625-1633.
(71) Hayton, T. W. *Chem. Commun.* **2013**, *49*, 2956-2973.
(72) King, D. M.; Tuna, F.; McMaster, J.; Lewis, W.; Blake, A. J.; McInnes, E. J. L.; Liddle, S. T. *Angew. Chem. Int. Ed.* **2013**, *52*, 4921-4924.
(73) Graves, C. R.; Kiplinger, J. L. *Chem. Commun.* **2009**, 3831-3853.
(74) Hermann, J. A.; Suttle, J. F. *Inorg. Synth.* **1957**, *5*, 143-145.
(75) Khan, I. A.; Ahuja, H. S. *Inorg. Synth.* **1982**, *21*, 187-190.
(76) Kiplinger, J. L.; Morris, D. E.; Scott, B. L.; Burns, C. J. *Organometallics* **2002**, *21*, 5978-5982.
(77) Patel, D.; Wooles, A. J.; Hashem, E.; Omorodion, H.; Baker, R. J.; Liddle, S. T. *New. J. Chem.* **2015**, *39*, 7559-7562.
(78) Bagnall, K. W.; Brown, D.; Jones, P. J.; Dupreez, J. G. H. *J. Chem. Soc.* **1965**, 350-&.
(79) Berthet, J. C.; Thuery, P.; Ephritikhine, M. *Inorg. Chem.* **2005**, *44*, 1142-1146.

(80) Enriquez, A. E.; Scott, B. L.; Neu, M. P. *Inorg. Chem.* **2005**, *44*, 7403-7413.
(81) Carmichael, C. D.; Jones, N. A.; Arnold, P. L. *Inorg. Chem.* **2008**, *47*, 8577-8579.
(82) Monreal, M. J.; Thomson, R. K.; Cantat, T.; Travia, N. E.; Scott, B. L.; Kiplinger, J. L. *Organometallics* **2011**, *30*, 2031-2038.
(83) Nocton, G.; Pecaut, J.; Mazzanti, M. *Angew. Chem. Int. Ed.* **2008**, *47*, 3040-3042.
(84) Berthet, J. C.; Ephritikhine, M. *Coord. Chem. Rev.* **1998**, *180*, 83-116.
(85) Berthet, J.-C.; Thuery, P.; Ephritikhine, M. *Dalton Trans.* **2015**, *44*, 7727-7742.
(86) Ephritikhine, M. *Organometallics* **2013**, *32*, 2464-2488.
(87) Knope, K. E.; Soderholm, L. *Chem. Rev.* **2013**, *113*, 944-994.
(88) Camp, C.; Mougel, V.; Horeglad, P.; Pecaut, J.; Mazzanti, M. *J. Am. Chem. Soc.* **2010**, *132*, 17374-17377.
(89) Baker, R. J. *Coord. Chem. Rev.* **2012**, *256*, 2843-2871.
(90) Clark, D. L.; Sattelberger, A. P.; Bott, S. G.; Vrtis, R. N. *Inorg. Chem.* **1989**, *28*, 1771-1773.
(91) Avens, L. R.; Bott, S. G.; Clark, D. L.; Sattelberger, A. P.; Watkin, J. G.; Zwick, B. D. *Inorg. Chem.* **1994**, *33*, 2248-2256.
(92) Vandersluys, W. G.; Burns, C. J.; Huffman, J. C.; Sattelberger, A. P. *J. Am. Chem. Soc.* **1988**, *110*, 5924-5925.
(93) Odom, A. L.; Arnold, P. L.; Cummins, C. C. *J. Am. Chem. Soc.* **1998**, *120*, 5836-5837.
(94) Andersen, R. A. *Inorg. Chem.* **1979**, *18*, 1507-1509.
(95) Castro-Rodriguez, I.; Olsen, K.; Gantzel, P.; Meyer, K. *J. Am. Chem. Soc.* **2003**, *125*, 4565-4571.
(96) Karmazin, L.; Mazzanti, M.; Pecaut, J. *Inorg. Chem.* **2003**, *42*, 5900-5908.
(97) Gardner, B. M.; Liddle, S. T. *Chem. Commun.* **2015**, *51*, 10589-10607.
(98) Mougel, V.; Camp, C.; Pecaut, J.; Coperet, C.; Maron, L.; Kefalidis, C. E.; Mazzanti, M. *Angew. Chem. Int. Ed.* **2012**, *51*, 12280-12284.
(99) Cooper, O.; Camp, C.; Pecaut, J.; Kefalidis, C. E.; Maron, L.; Gambarelli, S.; Mazzanti, M. *J. Am. Chem. Soc.* **2014**, *136*, 6716-6723.
(100) MacDonald, M. R.; Fieser, M. E.; Bates, J. E.; Ziller, J. W.; Furche, F.; Evans, W. J. *J. Am. Chem. Soc.* **2013**, *135*, 13310-13313.
(101) La Pierre, H. S.; Scheurer, A.; Heinemann, F. W.; Hieringer, W.; Meyer, K. *Angew. Chem. Int. Edit.* **2014**, *53*, 7158-7162.
(102) Windorff, C. J.; MacDonald, M. R.; Meihaus, K. R.; Ziller, J. W.; Long, J. R.; Evans, W. J. *Chem. Eur. J.* **2016**, *22*, 772-782.
(103) Kindra, D. R.; Evans, W. J. *Chem. Rev.* **2014**, *114*, 8865-8882.
(104) Autillo, M.; Guerin, L.; Bolvin, H.; Moisy, P.; Berthon, C. *Physical Chemistry Chemical Physics* **2016**, *18*, 6515-6525.
(105) Autillo, M.; Kaden, P.; Geist, A.; Guerin, L.; Moisy, P.; Berthon, C. *Physical Chemistry Chemical Physics* **2014**, *16*, 8608-8614.
(106) Wall, T. F.; Jan, S.; Autillo, M.; Nash, K. L.; Guerin, L.; Le Naour, C.; Moisy, P.; Berthon, C. *Inorg. Chem.* **2014**, *53*, 2450-2459.
(107) Castro-Rodriguez, I.; Meyer, K. *Chem. Commun.* **2006**, 1353-1368.
(108) King, D. M.; Tuna, F.; McInnes, E. J. L.; McMaster, J.; Lewis, W.; Blake, A. J.; Liddle, S. T. *Science* **2012**, *337*, 717-720.
(109) Gardner, B. M.; Liddle, S. T. *Eur. J. Inorg. Chem.* **2013**, *2013*, 3753-3770.
110) Schelter, E. J.; Yang, P.; Scott, B. L.; Thompson, J. D.; Martin, R. L.; Hay, P. J.; Morris, D. E.; Kiplinger, J. L. *Inorg. Chem.* **2007**, *46*, 7477-7488.
(111) Magnani, N.; Apostolidis, C.; Morgenstern, A.; Colineau, E.; Griveau, J. C.; Bolvin, H.; Walter, O.; Caciuffo, R. *Angew. Chem. Int. Ed.* **2011**, *50*, 1696-1698.
(112) Magnani, N.; Colineau, E.; Eloirdi, R.; Griveau, J. C.; Caciuffo, R.; Cornet, S. M.; May, I.; Sharrad, C. A.; Collison, D.; Winpenny, R. E. P. *Physical Review Letters* **2010**, *104*, 197202(197204).
(113) Forbes, T. Z.; Burns, P. C.; Skanthakumar, S.; Soderholm, L. *J. Am. Chem. Soc.* **2007**, *129*, 2760-2761.
(114) Jin, G. B.; Skanthakumar, S.; Soderholm, L. *Inorg. Chem.* **2012**, *51*, 3220-3230.
(115) Sessoli, R.; Gatteschi, D.; Caneschi, A.; Novak, M. A. *Nature* **1993**, *365*, 141-143.
(116) Sessoli, R.; Tsai, H. L.; Schake, A. R.; Wang, S. Y.; Vincent, J. B.; Folting, K.; Gatteschi, D.; Christou, G.; Hendrickson, D. N. *J. Am. Chem. Soc.* **1993**, *115*, 1804-1816.
(117) Ishikawa, N.; Sugita, M.; Ishikawa, T.; Koshihara, S.; Kaizu, Y. *J. Am. Chem. Soc.* **2003**, *125*, 8694-8695.

(118) Bogani, L.; Wernsdorfer, W. *Nature Mater.* **2008**, *7*, 179-186.
(119) Mannini, M.; Pineider, F.; Sainctavit, P.; Danieli, C.; Otero, E.; Sciancalepore, C.; Talarico, A. M.; Arrio, M.-A.; Cornia, A.; Gatteschi, D.; Sessoli, R. *Nature Mater.* **2009**, *8*, 194-197.
(120) F. Donati, S. R., S. Stepanow, C. Wäckerlin, A. Singha, L. Persichetti, R. Baltic, K. Diller, F. Patthey, E. Fernandes, J. Dreiser, Ž. Šljivančanin, K. Kummer, C. Nistor, P. Gambardella, H. Brune *Science* **2016**, *352*, 318-321.
(121) Neese, F.; Pantazis, D. A. *Faraday Discussions* **2011**, *148*, 229-238.
(122) Gatteschi, D.; Sessoli, R.; Villain, J. *Molecular Nanomagnets*; Oxford University Press: Oxford, UK, 2006.
(123) Sessoli, R.; Powell, A. K. *Coord. Chem. Rev.* **2009**, *253*, 2328-2341.
(124) Murrie, M. *Chem. Soc. Rev.* **2010**, *39*, 1986-1995.
(125) Blagg, R. J.; Ungur, L.; Tuna, F.; Speak, J.; Comar, P.; Collison, D.; Wernsdorfer, W.; McInnes, E. J. L.; Chibotaru, L. F.; Winpenny, R. E. P. *Nature Chem.* **2013**, *5*, 673-678.
(126) Woodruff, D. N.; Winpenny, R. E. P.; Layfield, R. A. *Chem. Rev.* **2013**, *113*, 5110-5148.
(127) Yang, C. I.; Zhang, Z. Z.; Lin, S. B. *Coord. Chem. Rev.* **2015**, *289*, 289-314.
(128) Zhang, P.; Zhang, L.; Tang, J. K. *Dalton Trans.* **2015**, *44*, 3923-3929.
(129) Ako, A. M.; Hewitt, I. J.; Mereacre, V.; Clerac, R.; Wernsdorfer, W.; Anson, C. E.; Powell, A. K. *Angew. Chem. Int. Edit.* **2006**, *45*, 4926-4929.
(130) Manoli, M.; Alexandrou, S.; Pham, L.; Lorusso, G.; Wernsdorfer, W.; Evangelisti, M.; Christou, G.; Tasiopoulos, A. J. *Angew. Chem. Int. Edit.* **2016**, *55*, 679-684.
(131) Blagg, R. J.; Tuna, F.; McInnes, E. J. L.; Winpenny, R. E. P. *Chem. Commun.* **2011**, *47*, 10587-10589.
(132) Blagg, R. J.; Muryn, C. A.; McInnes, E. J. L.; Tuna, F.; Winpenny, R. E. P. *Angew. Chem. Int. Edit.* **2011**, *50*, 6530-6533.
(133) Feltham, H. L. C.; Brooker, S. *Coord. Chem. Rev.* **2014**, *276*, 1-33.
(134) Rosado Piquer, L.; Carolina Sanudo, E. *Dalton Trans.* **2015**, *44*, 8771-8780.
(135) Rinehart, J. D.; Fang, M.; Evans, W. J.; Long, J. R. *Nature Chem.* **2011**, *3*, 538-542.
(136) Rinehart, J. D.; Fang, M.; Evans, W. J.; Long, J. R. *J. Am. Chem. Soc.* **2011**, *133*, 14236-14239.
(137) Demir, S.; Zadrozny, J. M.; Nippe, M.; Long, J. R. *J. Am. Chem. Soc.* **2012**, *134*, 18546-18549.
(138) Le Roy, J. J.; Ungur, L.; Korobkov, I.; Chibotaru, L. F.; Murugesu, M. *J. Am. Chem. Soc.* **2014**, *136*, 8003-8010.
(139) Pointillart, F.; Bernot, K.; Golhen, S.; Le Guennic, B.; Guizouarn, T.; Ouahab, L.; Cador, O. *Angew. Chem. Int. Edit.* **2015**, *54*, 1504-1507.
(140) Gregson, M.; Chilton, N. F.; Ariciu, A. M.; Tuna, F.; Crowe, I. F.; Lewis, W.; Blake, A. J.; Collison, D.; McInnes, E. J. L.; Winpenny, R. E. P.; Liddle, S. T. *Chem. Sci.* **2016**, *7*, 155-165.
(141) Chen, Y. C.; Liu, J. L.; Ungur, L.; Liu, J.; Li, Q. W.; Wang, L. F.; Ni, Z. P.; Chibotaru, L. F.; Chen, X. M.; Tong, M. L. *J. Am. Chem. Soc.* **2016**, *138*, 2829-2837.
(142) Liu, J. C., Y.; Liu, J.; Vieru, V.; Ungur, L.; Jia, J.; Chibotaru, L.; Lan, Y.; Wernsdorfer, W.; Gao, S.; Chen, X.; Tong, M. *J. Am. Chem. Soc.* **2016**.
(143) Rinehart, J. D.; Long, J. R. *Chem. Sci.* **2011**, *2*, 2078-2085.
(144) Chilton, N. F. *Inorg. Chem.* **2015**, *54*, 2097-2099.
(145) Zadrozny, J. M.; Atanasov, M.; Bryan, A. M.; Lin, C. Y.; Rekken, B. D.; Power, P. P.; Neese, F.; Long, J. R. *Chem. Sci.* **2013**, *4*, 125-138.
(146) Craig, G. A.; Marbey, J. J.; Hill, S.; Roubeau, O.; Parsons, S.; Murrie, M. *Inorg. Chem.* **2015**, *54*, 13-15.
(147) Gomez-Coca, S.; Aravena, D.; Morales, R.; Ruiz, E. *Coord. Chem. Rev.* **2015**, *289*, 379-392.
(148) Frost, J. M.; Harriman, K. L. M.; Murugesu, M. *Chem. Sci.* **2016**, *7*, 2470-2491.
(149) Bar, A. K.; Pichon, C.; Sutter, J. P. *Coord. Chem. Rev.* **2016**, *308*, 346-380.
(150) Milios, C. J.; Vinslava, A.; Wernsdorfer, W.; Moggach, S.; Parsons, S.; Perlepes, S. P.; Christou, G.; Brechin, E. K. *J. Am. Chem. Soc.* **2007**, *129*, 2754-2755.
(151) Pugh, T.; Tuna, F.; Ungur, L.; Collison, D.; McInnes, E. J. L.; Chibotaru, L. F.; Layfield, R. A. *Nat. Commun.* **2015**, *6*.
(152) Langley, S. K.; Wielechowski, D. P.; Vieru, V.; Chilton, N. F.; Moubaraki, B.; Abrahams, B. F.; Chibotaru, L. F.; Murray, K. S. *Angew. Chem. Int. Edit.* **2013**, *52*, 12014-12019.
(153) Liu, J.-L.; Wu, J.-Y.; Chen, Y.-C.; Mereacre, V.; Powell, A. K.; Ungur, L.; Chibotaru, L. F.; Chen, X.-M.; Tong, M.-L. *Angew. Chem. Int. Ed.* **2014**, *53*, 12966-12970.

(154) Caneschi, A.; Gatteschi, D.; Lalioti, N.; Sangregorio, C.; Sessoli, R.; Venturi, G.; Vindigni, A.; Rettori, A.; Pini, M. G.; Novak, M. A. *Angew. Chem. Int. Ed.* **2001**, *40*, 1760-1763.
(155) Bogani, L.; Vindigni, A.; Sessoli, R.; Gatteschi, D. *Journal of Materials Chemistry* **2008**, *18*, 4750-4758.
(156) Miyasaka, H.; Julve, M.; Yamashita, M.; Clerac, R. *Inorg. Chem.* **2009**, *48*, 3420-3437.
(157) Sun, H. L.; Wang, Z. M.; Gao, S. *Coord. Chem. Rev.* **2010**, *254*, 1081-1100.
(158) Zhang, W. X.; Ishikawa, R.; Breedlove, B.; Yamashita, M. *Rsc Advances* **2013**, *3*, 3772-3798.
(159) Pedersen, K. S.; Bendix, J.; Clerac, R. *Chem. Commun.* **2014**, *50*, 4396-4415.
(160) Dhers, S.; Feltham, H. L. C.; Brooker, S. *Coord. Chem. Rev.* **2015**, *296*, 24-44.
(161) Vaz, M. G. F.; Allao Cassaro, R. A.; Akpinar, H.; Schlueter, J. A.; Lahti, P. M.; Novak, M. A. *Chem. Eur. J.* **2014**, *20*, 5460-5467.
(162) Allao Cassaro, R. A.; Reis, S. G.; Araujo, T. S.; Lahti, P. M.; Novak, M. A.; Vaz, M. G. F. *Inorg. Chem.* **2015**, *54*, 9381-9383.
(163) Clerac, R.; Miyasaka, H.; Yamashita, M.; Coulon, C. *J. Am. Chem. Soc.* **2002**, *124*, 12837-12844.
(164) Bogani, L.; Sangregorio, C.; Sessoli, R.; Gatteschi, D. *Angew. Chem. Int. Edit.* **2005**, *44*, 5817-5821.
(165) Rinehart, J. D.; Long, J. R. *J. Am. Chem. Soc.* **2009**, *131*, 12558-12559.
(166) Magnani, N. *International Journal of Quantum Chemistry* **2014**, *114*, 755-759.
(167) Antunes, M. A.; Coutinho, J. T.; Santos, I. C.; Marcalo, J.; Almeida, M.; Baldovi, J. J.; Pereira, L. C. J.; Gaita-Arino, A.; Coronado, E. *Chem. Eur. J.* **2015**, *21*, 17817-17826.
(168) Rinehart, J. D.; Meihaus, K. R.; Long, J. R. *J. Am. Chem. Soc.* **2010**, *132*, 7572-7573.
(169) Meihaus, K. R.; Rinehart, J. D.; Long, J. R. *Inorg. Chem.* **2011**, *50*, 8484-8489.
(170) Rinehart, J. D.; Long, J. R. *Dalton Trans.* **2012**, *41*, 13572-13574.
(171) Meihaus, K. R.; Minasian, S. G.; Lukens, W. W., Jr.; Kozimor, S. A.; Shuh, D. K.; Tyliszczak, T.; Long, J. R. *J. Am. Chem. Soc.* **2014**, *136*, 6056-6068.
(172) Coutinho, J. T.; Antunes, M. A.; Pereira, L. C. J.; Bolvin, H.; Marcalo, J.; Mazzanti, M.; Almeida, M. *Dalton Trans.* **2012**, *41*, 13568-13571.
(173) Antunes, M. A.; Pereira, L. C. J.; Santos, I. C.; Mazzanti, M.; Marcalo, J.; Almeida, M. *Inorg. Chem.* **2011**, *50*, 9915-9917.
(174) Pereira, L. C. J.; Camp, C.; Coutinho, J. T.; Chatelain, L.; Maldivi, P.; Almeida, M.; Mazzanti, M. *Inorg. Chem.* **2014**, *53*, 11809-11811.
(175) Moro, F.; Mills, D. P.; Liddle, S. T.; Slangeren, J. *Angew. Chem. Int. Ed. Engl.* **2013**, *52*, 1-5.
(176) Goodwin, C. A. P.; Tuna, F.; McInnes, E. J. L.; Liddle, S. T.; McMaster, J.; Vitorica-Yrezabal, I. J.; Mills, D. P. *Chem. Eur. J.* **2014**, *20*, 14579-14583.
(177) Le Roy, J. J.; Gorelsky, S. I.; Korobkov, I.; Murugesu, M. *Organometallics* **2015**, *34*, 1415-1418.
(178) Magnani, N.; Colineau, E.; Griveau, J. C.; Apostolidis, C.; Walter, O.; Caciuffo, R. *Chem. Commun.* **2014**, *50*, 8171-8173.
(179) Mills, D. P.; Moro, F.; McMaster, J.; van Slageren, J.; Lewis, W.; Blake, A. J.; Liddle, S. T. *Nature Chem.* **2011**, *3*, 454-460.
(180) Mougel, V.; Chatelain, L.; Pécaut, J.; Caciuffo, R.; Colineau, E.; Griveau, J.-C.; Mazzanti, M. *Nat Chem* **2012**, *4*, 1011-1017.
(181) Cornet, S. M.; Haller, L. J. L.; Sarsfield, M. J.; Collison, D.; Helliwell, M.; May, I.; Kaltsoyannis, N. *Chem. Commun.* **2009**, 917-919.
(182) Gardner, B. M.; Tuna, F.; McInnes, E. J. L.; McMaster, J.; Lewis, W.; Blake, A. J.; Liddle, S. T. *Angew. Chem. Int. Edit.* **2015**, *54*, 7068-7072.
(183) Clark, D. L.; Hobart, D. E.; Neu, M. P. *Chem. Rev.* **1995**, *95*, 25-48.
(184) Yang, W.; Parker, T. G.; Sun, Z.-M. *Coord. Chem. Rev.* **2015**, *303*, 86-109.
(185) Van Der Sluys, W. G.; Sattelberger, A. P. *Chem. Rev.* **1990**, *90*, 1027-1040.
(186) Milios, C. J.; Inglis, R.; Vinslava, A.; Bagai, R.; Wernsdorfer, W.; Parsons, S.; Perlepes, S. P.; Christou, G.; Brechin, E. K. *J. Am. Chem. Soc.* **2007**, *129*, 12505-12511.
(187) Lam, O. P.; Heinemann, F. W.; Meyer, K. *Chem. Sci.* **2011**, *2*, 1538-1547.
(188) Salmon, L.; Thuery, P.; Ephritikhine, M. *Polyhedron* **2006**, *25*, 1537-1542.
(189) Duval, P. B.; Burns, C. J.; Clark, D. L.; Morris, D. E.; Scott, B. L.; Thompson, J. D.; Werkema, E. L.; Jia, L.; Andersen, R. A. *Angew. Chem. Int. Ed.* **2001**, *40*, 3357-3361.
(190) Korobkov, I.; Gambarotta, S.; Yap, G. P. A. *Organometallics* **2001**, *20*, 2552-2559.
(191) Larch, C. P.; Cloke, F. G. N.; Hitchcock, P. B. *Chem. Commun.* **2008**, 82-84.
(192) Salmon, L.; Thuery, P.; Ephritikhine, M. *Polyhedron* **2004**, *23*, 623-627.

(193) Berthet, J. C.; Nierlich, M.; Miquel, Y.; Madic, C.; Ephritikhine, M. *Dalton Trans.* **2005**, 369-379.
(194) Travia, N. E.; Scott, B. L.; Kiplinger, J. L. *Chem. Eur. J.* **2014**, *20*, 16846-16852.
(195) Castro-Rodriguez, I.; Meyer, K. *J. Am. Chem. Soc.* **2005**, *127*, 11242-11243.
(196) Evans, W. J.; Kozimor, S. A. *Coord. Chem. Rev.* **2006**, *250*, 911-935.
(197) Lam, O. P.; Bart, S. C.; Kameo, H.; Heinemann, F. W.; Meyer, K. *Chem. Commun.* **2010**, *46*, 3137-3139.
(198) Mansell, S. M.; Kaltsoyannis, N.; Arnold, P. L. *J. Am. Chem. Soc.* **2011**, *133*, 9036-9051.
(199) Schmidt, A.-C.; Heinemann, F. W.; Lukens, W. W., Jr.; Meyer, K. *J. Am. Chem. Soc.* **2014**, *136*, 11980-11993.
(200) Gardner, B. M.; Stewart, J. C.; Davis, A. L.; McMaster, J.; Lewis, W.; Blake, A. J.; Liddle, S. T. *Proc. Nat. Acad. Sci. U.S.A.* **2012**, *109*, 9265-9270.
(201) Berthet, J. C.; Thuery, P.; Ephritikhine, M. *Chem. Commun.* **2005**, 3415-3417.
(202) Berthet, J. C.; Thuery, P.; Ephritikhine, M. *Inorg. Chem.* **2010**, *49*, 8173-8177.
(203) Mokry, L. M.; Dean, N. S.; Carrano, C. J. *Angew. Chem. Int. Ed.* **1996**, *35*, 1497-1498.
(204) Arnold, P. L.; Jones, G. M.; Odoh, S. O.; Schreckenbach, G.; Magnani, N.; Love, J. B. *Nature Chem.* **2012**, *4*, 221-227.
(205) Jones, G. M.; Arnold, P. L.; Love, J. B. *Angew. Chem. Int. Ed.* **2012**, *51*, 12584-12587.
(206) Jones, G. M.; Arnold, P. L.; Love, J. B. *Chem. Eur. J.* **2013**, *19*, 10287-10294.
(207) Mougel, V.; Biswas, B.; Pecaut, J.; Mazzanti, M. *Chem. Commun.* **2010**, *46*, 8648-8650.
(208) Mougel, V., Université Joseph Fourier Grenoble, 2012.
(209) Guillaume, B.; Begun, G. M.; Hahn, R. L. *Inorg. Chem.* **1982**, *21*, 1159-1166.
(210) Stoyer, N. J.; Hoffman, D. C.; Silva, R. J. *Radiochim. Acta* **2000**, *88*, 279-282.
(211) Krot, N. N.; Grigoriev, M. S. *Russ. Chem. Rev.* **2004**, *73*, 89-100.
(212) Newton, T. W.; Baker, F. B. *Inorg. Chem.* **1962**, *1*, 368-377.
(213) Cousson, A.; Dabos, S.; Abazli, H.; Nectoux, F.; Pages, M.; Choppin, G. *J. Less-Common Met.* **1984**, *99*, 233-240.
(214) Andreev, G.; Budantseva, N.; Tananaev, I.; Myasoedov, B. *Inorg. Chem. Commun.* **2010**, *13*, 679-682.
(215) Jin, G. B. *Inorg. Chem.* **2013**, *52*, 12317-12319.
(216) Wang, S.; Diwu, J.; Alekseev, E. V.; Jouffret, L. J.; Depmeier, W.; Albrecht-Schmitt, T. E. *Inorg. Chem.* **2012**, *51*, 7016-7018.
(217) Sullens, T. A.; Jensen, R. A.; Shvareva, T. Y.; Albrecht-Schmitt, T. E. *J. Am. Chem. Soc.* **2004**, *126*, 2676-2677.
(218) Alekseev, E. V.; Krivovichev, S. V.; Depmeier, W.; Siidra, O. I.; Knorr, K.; Suleimanov, E. V.; Chuprunov, E. V. *Angew. Chem. Int. Edit.* **2006**, *45*, 7233-7235.
(219) Thuery, P. *Inorg. Chem. Commun.* **2009**, *12*, 800-803.
(220) Lhoste, J.; Henry, N.; Roussel, P.; Loiseau, T.; Abraham, F. *Dalton Trans.* **2011**, *40*, 2422-2424.
(221) Morrison, J. M.; Moore-Shay, L. J.; Burns, P. C. *Inorg. Chem.* **2011**, *50*, 2272-2277.
(222) Mihalcea, I.; Henry, N.; Clavier, N.; Dacheux, N.; Loiseau, T. *Inorg. Chem.* **2011**, *50*, 6243-6249.
(223) Severance, R. C.; Smith, M. D.; zur Loye, H.-C. *Inorg. Chem.* **2011**, *50*, 7931-7933.
(224) Adelani, P. O.; Burns, P. C. *Inorg. Chem.* **2012**, *51*, 11177-11183.
(225) Tian, T.; Yang, W.; Pan, Q.-J.; Sun, Z.-M. *Inorg. Chem.* **2012**, *51*, 11150-11154.
(226) Volkringer, C.; Henry, N.; Grandjean, S.; Loiseau, T. *J. Am. Chem. Soc.* **2012**, *134*, 1275-1283.
(227) Andrews, M. B.; Cahill, C. L. *Chem. Rev.* **2013**, *113*, 1121-1136.
(228) Cantos, P. M.; Jouffret, L. J.; Wilson, R. E.; Burns, P. C.; Cahill, C. L. *Inorg. Chem.* **2013**, *52*, 9487-9495.
(229) Thuery, P. *CrystEngComm* **2013**, *15*, 6533-6545.
(230) Balboni, E.; Burns, P. C. *J. Solid State Chem.* **2014**, *213*, 1-8.
(231) Mougel, V.; Horeglad, P.; Nocton, G.; Pecaut, J.; Mazzanti, M. *Angew. Chem. Int. Ed.* **2009**, *48*, 8477-8480.
(232) Taylor, J. C.; Ekstrom, A.; Randall, C. H. *Inorg. Chem.* **1978**, *17*, 3285-3289.
(233) Wilkerson, M. P.; Burns, C. J.; Dewey, H. J.; Martin, J. M.; Morris, D. E.; Paine, R. T.; Scott, B. L. *Inorg. Chem.* **2000**, *39*, 5277-5285.
(234) Arnold, P. L.; Patel, D.; Blake, A. J.; Wilson, C.; Love, J. B. *J. Am. Chem. Soc.* **2006**, *128*, 9610-9611.

(235) Thuery, P.; Nierlich, M.; Souley, B.; Asfari, Z.; Vicens, J. *Journal of the Chemical Society, Dalton Transactions: Inorganic Chemistry* **1999**, 2589-2594.
(236) Grigoriev, M. S.; Krot, N. N.; Bessonov, A. A.; Suponitsky, K. Y. *Acta Crystallographica Section E-Structure Reports Online* **2007**, *63*, M561-M562.
(237) Charushnikova, I. A.; Krot, N. N.; Starikova, Z. A. *Radiochim. Acta* **2007**, *95*, 495-499.
(238) Charushnikova, I.; Bosse, E.; Guillaumont, D.; Moisy, P. *Inorg. Chem.* **2010**, *49*, 2077-2082.
(239) Copping, R.; Mougel, V.; Den Auwer, C.; Berthon, C.; Moisy, P.; Mazzanti, M. *Dalton Trans.* **2012**, *41*, 10900-10902.
(240) Burdet, F.; Pecaut, J.; Mazzanti, M. *J. Am. Chem. Soc.* **2006**, *128*, 16512-16513.
(241) Arnold, P. L.; Hollis, E.; White, F. J.; Magnani, N.; Caciuffo, R.; Love, J. B. *Angew. Chem. Int. Ed.* **2011**, *50*, 887-890.
(242) Chatelain, L.; Mougel, V.; Pecaut, J.; Mazzanti, M. *Chem. Sci.* **2012**, *3*, 1075-1079.
(243) Mills, D. P.; Cooper, O. J.; Tuna, F.; McInnes, E. J. L.; Davies, E. S.; McMaster, J.; Moro, F.; Lewis, W.; Blake, A. J.; Liddle, S. T. *J. Am. Chem. Soc.* **2012**, *134*, 10047-10054.
(244) Arnold, P. L.; Hollis, E.; Nichol, G. S.; Love, J. B.; Griveau, J.-C.; Caciuffo, R.; Magnani, N.; Maron, L.; Castro, L.; Yahia, A.; Odoh, S. O.; Schreckenbach, G. *J. Am. Chem. Soc.* **2013**, *135*, 3841-3854.
(245) Le Borgne, T.; Riviere, E.; Marrot, J.; Girerd, J. J.; Ephritikhine, M. *Angew. Chem. Int. Ed.* **2000**, *39*, 1647-1649.
(246) Le Borgne, T.; Riviere, E.; Marrot, J.; Thuery, P.; Girerd, J. J.; Ephritikhine, M. *Chem. Eur. J.* **2002**, *8*, 774-783.
(247) Salmon, L.; Thuery, P.; Riviere, E.; Girerd, J. J.; Ephritikhine, M. *Dalton Trans.* **2003**, 2872-2880.
(248) Salmon, L.; Thuery, P.; Riviere, E.; Girerd, J. J.; Ephritikhine, M. *Chem. Commun.* **2003**, 762-763.
(249) Salmon, L.; Thuery, P.; Ephritikhine, M. *Polyhedron* **2007**, *26*, 631-636.
(250) Andrez, J.; Pecaut, J.; Bayle, P.-A.; Mazzanti, M. *Angew. Chem. Int. Ed.* **2014**, *53*, 10448-10452.
(251) Lapadula, G.; Conley, M. P.; Coperet, C.; Andersen, R. A. *Organometallics* **2015**, *34*, 2271-2277.
(252) Camp, C.; Cooper, O.; Andrez, J.; Pecaut, J.; Mazzanti, M. *Dalton Trans.* **2015**, *44*, 2650-2656.
(253) Camp, C.; Kefalidis, C. E.; Pecaut, J.; Maron, L.; Mazzanti, M. *Angew. Chem. Int. Ed.* **2013**, *52*, 12646-12650.
(254) Mansell, S. M.; Farnaby, J. H.; Germeroth, A. I.; Arnold, P. L. *Organometallics* **2013**, *32*, 4214-4222.
(255) Camp, C.; Mougel, V.; Pecaut, J.; Maron, L.; Mazzanti, M. *Chem. Eur. J.* **2013**, *19*, 17528-17540.
(256) Roussel, P.; Scott, P. *J. Am. Chem. Soc.* **1998**, *120*, 1070-1071.
(257) Roussel, P.; Errington, W.; Kaltsoyannis, N.; Scott, P. *J. Organomet. Chem.* **2001**, *635*, 69-74.
(258) Cloke, G., F. N.; Hitchcock, P. B. *J. Am. Chem. Soc.* **2002**, *124*, 9352-9353.
(259) Reynolds, J. G.; Zalkin, A.; Templeton, D. H.; Edelstein, N. M.; Templeton, L. K. *Inorg. Chem.* **1976**, *15*, 2498-2502.
(260) Reynolds, J. G.; Zalkin, A.; Templeton, D. H.; Edelstein, N. M. *Inorg. Chem.* **1977**, *16*, 599-603.
(261) Reynolds, J. G.; Zalkin, A.; Templeton, D. H.; Edelstein, N. M. *Inorg. Chem.* **1977**, *16*, 1858-1861.
(262) Kozimor, S. A.; Bartlett, B. M.; Rinehart, J. D.; Long, J. R. *J. Am. Chem. Soc.* **2007**, *129*, 10672-10673.
(263) Rinehart, J. D.; Bartlett, B. M.; Kozimor, S. A.; Long, J. R. *Inorg.Chim. Acta* **2008**, *361*, 3534-3538.
(264) Schelter, E. J.; Veauthier, J. M.; Thompson, J. D.; Scott, B. L.; John, K. D.; Morris, D. E.; Kiplinger, J. L. *J. Am. Chem. Soc.* **2006**, *128*, 2198-2199.
(265) Schelter, E. J.; Wu, R. L.; Scott, B. L.; Thompson, J. D.; Morris, D. E.; Kiplinger, J. L. *Angew. Chem. Int. Ed.* **2008**, *47*, 2993-2996.
(266) Kiplinger, J. L.; Pool, J. A.; Schelter, E. J.; Thompson, J. D.; Scott, B. L.; Morris, D. E. *Angew. Chem. Int. Ed.* **2006**, *45*, 2036-2041.
(267) Schelter, E. J.; Veauthier, J. M.; Graves, C. R.; John, K. D.; Scott, B. L.; Thompson, J. D.; Pool-Davis-Tournear, J. A.; Morris, D. E.; Kiplinger, J. L. *Chem. Eur. J.* **2008**, *14*, 7782-7790.

(268) Rinehart, J. D.; Kozimor, S. A.; Long, J. R. *Angew. Chem. Int. Edit.* **2010**, *49*, 2560-2564.
(269) Broderick, E. M.; Gutzwiller, N. P.; Diaconescu, P. L. *Organometallics* **2010**, *29*, 3242-3251.
(270) Lu, E.; Cooper, O. J.; McMaster, J.; Tuna, F.; McInnes, E. J. L.; Lewis, W.; Blake, A. J.; Liddle, S. T. *Angew. Chem. Int. Edit.* **2014**, *53*, 6696-6700.
(271) Jilek, R. E.; Spencer, L. P.; Kuiper, D. L.; Scott, B. L.; Williams, U. J.; Kikkawa, J. M.; Schelter, E. J.; Boncella, J. M. *Inorg. Chem.* **2011**, *50*, 4235-4237.
(272) Diaconescu, P. L.; Arnold, P. L.; Baker, T. A.; Mindiola, D. J.; Cummins, C. C. *J. Am. Chem. Soc.* **2000**, *122*, 6108-6109.
(273) Hayton, T. W. *Dalton Trans* **2010**, *39*, 1145-1158.
(274) Hayton, T. W.; Boncella, J. M.; Scott, B. L.; Palmer, P. D.; Batista, E. R.; Hay, P. J. *Science* **2005**, *310*, 1941-1943.
(275) Hayton, T. W.; Boncella, J. M.; Scott, B. L.; Batista, E. R.; Hay, P. J. *J. Am. Chem. Soc.* **2006**, *128*, 10549-10559.
(276) Spencer, L. P.; Schelter, E. J.; Yang, P.; Gdula, R. L.; Scott, B. L.; Thompson, J. D.; Kiplinger, J. L.; Batista, E. R.; Boncella, J. M. *Angew. Chem. Int. Ed.* **2009**, *48*, 3795-3798.
(277) Anderson, N. H.; Odoh, S. O.; Yao, Y.; Williams, U. J.; Schaefer, B. A.; Kiernicki, J. J.; Lewis, A. J.; Goshert, M. D.; Fanwick, P. E.; Schelter, E. J.; Walensky, J. R.; Gagliardi, L.; Bart, S. C. *Nature Chem.* **2014**, *6*, 919-926.
(278) Anderson, N. H.; Yin, H.; Kiernicki, J. J.; Fanwick, P. E.; Schelter, E. J.; Bart, S. C. *Angew. Chem. Int. Edit.* **2015**, *54*, 9386-9389.
(279) Brennan, J. G.; Andersen, R. A.; Zalkin, A. *J. Am. Chem. Soc.* **1988**, *110*, 4554-4558.
(280) Newell, B. S.; Rappe, A. K.; Shores, M. P. *Inorg. Chem.* **2010**, *49*, 1595-1606.
(281) Paul, F.; Bondon, A.; da Costa, G.; Malvolti, F.; Sinbandhit, S.; Cador, O.; Costuas, K.; Toupet, L.; Boillot, M.-L. *Inorg. Chem.* **2009**, *48*, 10608-10624.
(282) Patel, D.; Moro, F.; McMaster, J.; Lewis, W.; Blake, A. J.; Liddle, S. T. *Angew. Chem. Int. Ed.* **2011**, *50*, 10388-10392.
(283) Vlaisavljevich, B.; Diaconescu, P. L.; Lukens, W. L., Jr.; Gagliardi, L.; Cummins, C. C. *Organometallics* **2013**, *32*, 1341-1352.
(284) Cotton, F. A.; Schwotzer, W. *Organometallics* **1985**, *4*, 942-943.
(285) Cotton, F. A.; Schwotzer, W.; Simpson, C. Q. *Angew. Chem. Int. Ed.* **1986**, *25*, 637-639.
(286) Lukens, W. W.; Beshouri, S. M.; Stuart, A. L.; Andersen, R. A. *Organometallics* **1999**, *18*, 1247-1252.
(287) Newell, B. S.; Schwaab, T. C.; Shores, M. P. *Inorg. Chem.* **2011**, *50*, 12108-12115.
(288) Ephritikhine, M. *Chem. Rev.* **1997**, *97*, 2193-2242.
(289) Evans, W. J.; Miller, K. A.; DiPasquale, A. G.; Rheingold, A. L.; Stewart, T. J.; Bau, R. *Angew. Chem. Int. Edit.* **2008**, *47*, 5075-5078.
(290) Patel, D.; Tuna, F.; McInnes, E. J. L.; Lewis, W.; Blake, A. J.; Liddle, S. T. *Angew. Chem. Int. Edit.* **2013**, *52*, 13334-13337.
(291) Gardner, B. M.; Balazs, G.; Scheer, M.; Wooles, A. J.; Tuna, F.; McInnes, E. J. L.; McMaster, J.; Lewis, W.; Blake, A. J.; Liddle, S. T. *Angew. Chem. Int. Edit.* **2015**, *54*, 15250-15254.
(292) Abraham, F.; Arab-Chapelet, B.; Rivenet, M.; Tamain, C.; Grandjean, S. *Coord. Chem. Rev.* **2014**, *266*, 28-68.
(293) Stamatatos, T. C.; Teat, S. J.; Wernsdorfer, W.; Christou, G. *Angew. Chem. Int. Edit.* **2009**, *48*, 521-524.
(294) Lin, P.-H.; Burchell, T. J.; Ungur, L.; Chibotaru, L. F.; Wernsdorfer, W.; Murugesu, M. *Angew. Chem. Int. Edit.* **2009**, *48*, 9489-9492.
(295) Burns, P. C.; Ewing, R. C.; Navrotsky, A. *Science* **2012**, *335*, 1184-1188.
(296) Walther, C.; Denecke, M. A. *Chem. Rev.* **2013**, *113*, 995-1015.
(297) Maher, K.; Bargar, J. R.; Brown, G. E., Jr. *Inorg. Chem.* **2013**, *52*, 3510-3532.
(298) Kersting, A. B. *Inorg. Chem.* **2013**, *52*, 3533-3546.
(299) Natrajan, L. S.; Swinburne, A. N.; Andrews, M. B.; Randall, S.; Heath, S. L. *Coord. Chem. Rev.* **2014**, *266*, 171-193.
(300) Ilton, E. S.; Heald, S. M.; Smith, S. C.; Elbert, D.; Liu, C. *Environ. Sci. Technol.* **2006**, *40*, 5003-5009.
(301) Regenspurg, S.; Schild, D.; Schaefer, T.; Huber, F.; Malmstrom, M. E. *Appl. Geochem.* **2009**, *24*, 1617-1625.
(302) Chakraborty, S.; Favre, F.; Banerjee, D.; Scheinost, A. C.; Mullet, M.; Ehrhardt, J.-J.; Brendle, J.; Vidal, L.; Charlet, L. *Environ. Sci. Technol.* **2010**, *44*, 3779-3785.

(303) Kirsch, R.; Fellhauer, D.; Altmaier, M.; Neck, V.; Rossberg, A.; Fanghaenel, T.; Charlet, L.; Scheinost, A. C. *Environ. Sci. Technol.* **2011**, *45*, 7267-7274.
(304) Honeyman, B. D. *Nature* **1999**, *397*, 23-24.
(305) Runde, W.; Goff, G. S. *Radionucleides in the Environment*; John Wiley & Sons: Chichester, West Sussex, 2010.
(306) Wang, Y.; Frutschi, M.; Suvorova, E.; Phrommavanh, V.; Descostes, M.; Osman, A. A. A.; Geipel, G.; Bernier-Latmani, R. *Nat. Commun.* **2013**, *4*.
(307) Zhang, Y. J.; Bryan, N. D.; Livens, F. R.; Jones, M. N. *Environmental Pollution* **1997**, *96*, 361-367.
(308) Kubatko, K. A. H.; Helean, K. B.; Navrotsky, A.; Burns, P. C. *Science* **2003**, *302*, 1191-1193.
(309) Burns, P. C.; Kubatko, K. A.; Sigmon, G.; Fryer, B. J.; Gagnon, J. E.; Antonio, M. R.; Soderholm, L. *Angew. Chem. Int. Edit.* **2005**, *44*, 2135-2139.
(310) Sachs, S.; Bernhard, G. *J. Radioanal. Nucl. Chem.* **2011**, *290*, 17-29.
(311) Armstrong, C. R.; Nyman, M.; Shvareva, T.; Sigmon, G. E.; Burns, P. C.; Navrotsky, A. *Proc. Nat. Acad. Sci. U.S.A.* **2012**, *109*, 1874-1877.
(312) Lovley, D. R.; Phillips, E. J. P.; Gorby, Y. A.; Landa, E. R. *Nature* **1991**, *350*, 413-416.
(313) Lloyd, J. R. *FEMS microbiology reviews* **2003**, *27*, 411-425.
(314) Simonoff, M.; Sergeant, C.; Poulain, S.; Pravikoff, M. S. *C. R. Chimie* **2007**, *10*, 1092-1107.
(315) Williams, K. H.; Bargar, J. R.; Lloyd, J. R.; Lovley, D. R. *Current Opinion in Biotechnology* **2013**, *24*, 489-497.
(316) Suzuki, Y.; Kelly, S. D.; Kemner, K. M.; Banfield, J. F. *Nature* **2002**, *419*, 134-134.
(317) Schofield, E. J.; Veeramani, H.; Sharp, J. O.; Suvorova, E.; Bernier-Latmani, R.; Mehta, A.; Stahlman, J.; Webb, S. M.; Clark, D. L.; Conradson, S. D.; Ilton, E. S.; Bargar, J. R. *Environ. Sci. Technol.* **2008**, *42*, 7898-7904.
(318) Bargar, J. R.; Bernier-Latmani, R.; Giammar, D. E.; Tebo, B. M. *Elements* **2008**, *4*, 407-412.
(319) Sharp, J. O.; Schofield, E. J.; Veeramani, H.; Suvorova, E. I.; Kennedy, D. W.; Marshall, M. J.; Mehta, A.; Bargar, J. R.; Bernier-Latmani, R. *Environ. Sci. Technol.* **2009**, *43*, 8295-8301.
(320) Renshaw, J. C.; Butchins, L. J. C.; Livens, F. R.; May, I.; Charnock, J. M.; Lloyd, J. R. *Environ. Sci. Technol.* **2005**, *39*, 5657-5660.
(321) Grossmann, K.; Arnold, T.; Krawczyk-Barsch, E.; Diessner, S.; Wobus, A.; Bernhard, G.; Krawietz, R. *Environ. Sci. Technol.* **2007**, *41*, 6498-6504.
(322) Jones, D. L.; Andrews, M. B.; Swinburne, A. N.; Botchway, S. W.; Ward, A. D.; Lloyd, J. R.; Natrajan, L. S. *Chem. Sci.* **2015**, *6*, 5133-5138.
(323) Bernier-Latmani, R.; Veeramani, H.; Dalla Vecchia, E.; Junier, P.; Lezama-Pacheco, J. S.; Suvorova, E. I.; Sharp, J. O.; Wigginton, N. S.; Bargar, J. R. *Environmental science and technology* **2010**, *44*, 9456-9462.
(324) Fletcher, K. E.; Boyanov, M. I.; Thomas, S. H.; Wu, Q.; Kemner, K. M.; Loeffler, F. E. *Environ. Sci. Technol.* **2010**, *44*, 4705-4709.
(325) Veeramani, H.; Alessi, D. S.; Suvorova, E. I.; Lezama-Pacheco, J. S.; Stubbs, J. E.; Sharp, J. O.; Dippon, U.; Kappler, A.; Bargar, J. R.; Bernier-Latmani, R. *Geochim. Cosmochim. Acta* **2011**, *75*, 2512-2528.
(326) Boyanov, M. I.; Fletcher, K. E.; Kwon, M. J.; Rui, X.; O'Loughlin, E. J.; Loeffler, F. E.; Kemner, K. M. *Environ. Sci. Technol.* **2011**, *45*, 8336-8344.
(327) Bargar, J. R.; Williams, K. H.; Campbell, K. M.; Long, P. E.; Stubbs, J. E.; Suvorova, E. I.; Lezama-Pacheco, J. S.; Alessi, D. S.; Stylo, M.; Webb, S. M.; Davis, J. A.; Giammar, D. E.; Blue, L. Y.; Bernier-Latmani, R. *Proc. Nat. Acad. Sci. U.S.A.* **2013**, *110*, 4506-4511.
(328) Lundgren, G. *Arkiv. Kemi.* **1952**, *5*, 349.
(329) Takao, S.; Takao, K.; Kraus, W.; Ernmerling, F.; Scheinost, A. C.; Bernhard, G.; Hennig, C. *Eur. J. Inorg. Chem.* **2009**, 4771-4775.
(330) Hennig, C.; Takao, S.; Takao, K.; Weiss, S.; Kraus, W.; Emmerling, F.; Meyer, M.; Scheinost, A. C. In *15th International Conference on X-Ray Absorption Fine Structure*; Wu, Z. Y., Ed. 2013; Vol. 430.
(331) Knope, K. E.; Wilson, R. E.; Vasiliu, M.; Dixon, D. A.; Soderholm, L. *Inorg. Chem.* **2011**, *50*, 9696-9704.
(332) Takao, K.; Takao, S.; Scheinost, A. C.; Bernhard, G.; Hennig, C. *Inorg. Chem.* **2012**, *51*, 1336-1344.
(333) Knope, K. E.; Soderholm, L. *Inorg. Chem.* **2013**, *52*, 6770-6772.
(334) Soderholm, L.; Almond, P. M.; Skanthakumar, S.; Wilson, R. E.; Burns, P. C. *Angew. Chem. Int. Edit.* **2008**, *47*, 298-302.

(335) Wilson, R. E.; Skanthakumar, S.; Soderholm, L. *Angew. Chem. Int. Edit.* **2011**, *50*, 11234-11237.
(336) Berthet, J.-C.; Nierlich, M.; Miquel, Y.; Madic, C.; Ephritikhine, M. *Dalton Transaction* **2005**, 369-379.
(337) Lukens, W. W.; Beshouri, S. M.; Blosch, L. L.; Andersen, R. A. *J. Am. Chem. Soc.* **1996**, *118*, 901-902.
(338) Nocton, G.; Burdet, F.; Pecaut, J.; Mazzanti, M. *Angew. Chem. Int. Ed.* **2007**, *46*, 7574-7578.
(339) Nocton, G., Université Joseph-Fourier Grenoble 2009.
(340) Nocton, G.; Pecaut, J.; Filinchuk, Y.; Mazzanti, M. *Chem. Commun.* **2010**, *46*, 2757-2759.
(341) Biswas, B.; Mougel, V.; Pecaut, J.; Mazzanti, M. *Angew. Chem. Int. Ed.* **2011**, *50*, 5744-5747.
(342) Edward, J. T. J. *Chem. Ed.* **1970**, *47*, 261-269.
(343) Falaise, C.; Volkringer, C.; Vigier, J.-F.; Beaurain, A.; Roussel, P.; Rabu, P.; Loiseau, T. *J. Am. Chem. Soc.* **2013**, *135*, 15678-15681.
(344) Falaise, C.; Volkringer, C.; Hennig, C.; Loiseau, T. *Chem. Eur. J.* **2015**, *21*, 16654-16664.
(345) Rogers, R. D.; Kurihara, L. K.; Benning, M. M. *Inorg. Chem.* **1987**, *26*, 4346-4352.
(346) Danis, J. A.; Lin, M. R.; Scott, B. L.; Eichhorn, B. W.; Runde, W. H. *Inorg. Chem.* **2001**, *40*, 3389-3394.
(347) Servaes, K.; Hennig, C.; Van Deun, R.; Gorller-Walrand, C. *Inorg. Chem.* **2005**, *44*, 7705-7707.
(348) Schnaars, D. D.; Wilson, R. E. *Inorg. Chem.* **2013**, *52*, 14138-14147.
(349) Zegke, M.; Nichol, G. S.; Arnold, P. L.; Love, J. B. *Chem. Commun.* **2015**, *51*, 5876-5879.
(350) Arnold, P. L.; Pecharman, A.-F.; Lord, R. M.; Jones, G. M.; Hollis, E.; Nichol, G. S.; Maron, L.; Fang, J.; Davin, T.; Love, J. B. *Inorg. Chem.* **2015**, *54*, 3702-3710.
(351) Carretta, S.; Amoretti, G.; Santini, P.; Mougel, V.; Mazzanti, M.; Gambarelli, S.; Colineau, E.; Caciuffo, R. *J. Phys.: Condens. Matter* **2013**, *25*, 486001.
(352) Burns, P. C.; Finch, R. J. *American Mineralogist* **1999**, *84*, 1456-1460.
(353) Alsobrook, A. N.; Hauser, B. G.; Hupp, J. T.; Alekseev, E. V.; Depmeier, W.; Albrecht-Schmitt, T. E. *Chem. Commun.* **2010**, *46*, 9167-9169.
(354) Coulon, C.; Clerac, R.; Lecren, L.; Wernsdorfer, W.; Miyasaka, H. *Physical Review B* **2004**, *69*.
(355) Zheng, Y. Z.; Lan, Y. H.; Wernsdorfer, W.; Anson, C. E.; Powell, A. K. *Chem. Eur. J.* **2009**, *15*, 12566-12570.
(356) Cole, K. S.; Cole, R. H. *J. Chem. Phys.* **1941**, *9*, 341-351.
(357) Huser, D.; Vanduyneveldt, A. J.; Nieuwenhuys, G. J.; Mydosh, J. A. *Journal of Physics C-Solid State Physics* **1986**, *19*, 3697-3717.
(358) Przybylak, S. W.; Tuna, F.; Teat, S. J.; Winpenny, R. E. P. *Chem. Commun.* **2008**, 1983-1985.
(359) Lescouezec, R.; Toma, L. M.; Vaissermann, J.; Verdaguer, M.; Delgado, F. S.; Ruiz-Perez, C.; Lloret, F.; Julve, M. *Coord. Chem. Rev.* **2005**, *249*, 2691-2729.
(360) Thielemann, D. T.; Klinger, M.; Wolf, T. J. A.; Lan, Y.; Wernsdorfer, W.; Busse, M.; Roesky, P. W.; Unterreiner, A. N.; Powell, A. K.; Junk, P. C.; Deacon, G. B. *Inorg. Chem.* **2011**, *50*, 11990-12000.
(361) Nagao, H.; Komeda, N.; Mukaida, M.; Suzuki, M.; Tanaka, K. *Inorg. Chem.* **1996**, *35*, 6809-6815.
(362) Mukhopadhyay, U.; Bernal, I.; Massoud, S. S.; Mautner, F. A. *Inorg.Chim. Acta* **2004**, *357*, 3673-3682.
(363) Schnaars, D. D.; Wu, G.; Hayton, T. W. *J. Am. Chem. Soc.* **2009**, *131*, 17532-17533.
(364) Schnaars, D. D.; Wu, G.; Hayton, T. W. *Inorg. Chem.* **2011**, *50*, 4695-4697.
(365) DeGayner, J. A.; Jeon, I. R.; Harris, T. D. *Chem. Sci.* **2015**, *6*, 6639-6648.
(366) Arnold, P. L.; Hollis, E.; Nichol, G. S.; Love, J. B.; Griveau, J. C.; Caciuffo, R.; Magnani, N.; Maron, L.; Castro, L.; Yahia, A.; Odoh, S. O.; Schreckenbach, G. *J. Am. Chem. Soc.* **2013**, *135*, 3841-3854.
(367) Borras-Almenar, J. J.; Clemente-Juan, J. M.; Coronado, E.; Tsukerblat, B. S. *J. Comput. Chem.* **2001**, *22*, 985-991.
(368) Vallejo, J.; Pascual-Alvarez, A.; Cano, J.; Castro, I.; Julve, M.; Lloret, F.; Krzystek, J.; De Munno, G.; Armentano, D.; Wernsdorfer, W.; Ruiz-Garcia, R.; Pardo, E. *Angew. Chem. Int. Edit.* **2013**, *52*, 14075-14079.
(369) Grigoropoulos, A.; Pissas, M.; Papatolis, P.; Psycharis, V.; Kyritsis, P.; Sanakis, Y. *Inorg. Chem.* **2013**, *52*, 12869-12871.

(370) Ishikawa, R.; Miyamoto, R.; Nojiri, H.; Breedlove, B. K.; Yamashita, M. *Inorg. Chem.* **2013**, *52*, 8300-8302.
(371) Pascual-Alvarez, A.; Vallejo, J.; Pardo, E.; Julve, M.; Lloret, F.; Krzystek, J.; Armentano, D.; Wernsdorfer, W.; Cano, J. *Chem. Eur. J.* **2015**, *21*, 17299-17307.
(372) Tomsa, A. R.; Martinez-Lillo, J.; Li, Y. L.; Chamoreau, L. M.; Boubekeur, K.; Farias, F.; Novak, M. A.; Cremades, E.; Ruiz, E.; Proust, A.; Verdaguer, M.; Gouzerh, P. *Chem. Commun.* **2010**, *46*, 5106-5108.
(373) Harman, W. H.; Harris, T. D.; Freedman, D. E.; Fong, H.; Chang, A.; Rinehart, J. D.; Ozarowski, A.; Sougrati, M. T.; Grandjean, F.; Long, G. J.; Long, J. R.; Chang, C. J. *J. Am. Chem. Soc.* **2010**, *132*, 18115-18126.
(374) Jeon, I.-R.; Park, J. G.; Xiao, D. J.; Harris, T. D. *J. Am. Chem. Soc.* **2013**, *135*, 16845-16848
(375) Feng, X.; Mathoniere, C.; Jeon, I.-R.; Rouzieres, M.; Ozarowski, A.; Aubrey, M. L.; Gonzalez, M. I.; Clerac, R.; Long, J. R. *J. Am. Chem. Soc.* **2013**, *135*, 15880-15884.
(376) Oshio, H.; Hoshino, N.; Ito, T. *J. Am. Chem. Soc.* **2000**, *122*, 12602-12603.
(377) Boudalis, A. K.; Sanakis, Y.; Clemente-Juan, J. M.; Donnadieu, B.; Nastopoulos, V.; Mari, A.; Coppel, Y.; Tuchagues, J.-P.; Perlepes, S. P. *Chem. Eur. J.* **2008**, *14*, 2514-2526.
(378) Novikov, V. V.; Pavlov, A. A.; Nelyubina, Y. V.; Boulon, M.-E.; Varzatski, O. A.; Voloshin, Y. Z.; Winpenny, R. E. P. *J. Am. Chem. Soc.* **2015**, *137*, 9792-9795.
(379) Yoshihara, D.; Karasawa, S.; Koga, N. *J. Am. Chem. Soc.* **2008**, *130*, 10460-+.
(380) Fortier, S.; Le Roy, J. J.; Chen, C.-H.; Vieru, V.; Murugesu, M.; Chibotaru, L. F.; Mindiola, D. J.; Caulton, K. G. *J. Am. Chem. Soc.* **2013**, *135*, 14670-14678.
(381) Zhang, Y.-Z.; Brown, A. J.; Meng, Y.-S.; Sun, H.-L.; Gao, S. *Dalton Trans.* **2015**, *44*, 2865-2870.
(382) Woods, T. J.; Ballesteros-Rivas, M. F.; Ostrovsky, S. M.; Palii, A. V.; Reu, O. S.; Klokishner, S. I.; Dunbar, K. R. *Chem. Eur. J.* **2015**, *21*, 10302-10305.
(383) Yamaguchi, T.; Costes, J.-P.; Kishima, Y.; Kojima, M.; Sunatsuki, Y.; Brefuel, N.; Tuchagues, J.-P.; Vendier, L.; Wernsdorfer, W. *Inorg. Chem.* **2010**, *49*, 9125-9135.
(384) Goura, J.; Brambleby, J.; Goddard, P.; Chandrasekhar, V. *Chem. Eur. J.* **2015**, *21*, 4926-4930.
(385) Rogez, G.; Rebilly, J. N.; Barra, A. L.; Sorace, L.; Blondin, G.; Kirchner, N.; Duran, M.; van Slageren, J.; Parsons, S.; Ricard, L.; Marvilliers, A.; Mallah, T. *Angew. Chem. Int. Edit.* **2005**, *44*, 1876-1879.
(386) Miklovic, J.; Valigura, D.; Boca, R.; Titis, J. *Dalton Trans.* **2015**, *44*, 12484-12487.
(387) Marriott, K. E. R.; Bhaskaran, L.; Wilson, C.; Medarde, M.; Ochsenbein, S. T.; Hill, S.; Murrie, M. *Chem. Sci.* **2015**, *6*, 6823-6828.
(388) Bell, A.; Aromi, G.; Teat, S. J.; Wernsdorfer, W.; Winpenny, R. E. P. *Chem. Commun.* **2005**, 2808-2810.
(389) Biswas, R.; Ida, Y.; Baker, M. L.; Biswas, S.; Kar, P.; Nojiri, H.; Ishida, T.; Ghosh, A. *Chem. Eur. J.* **2013**, *19*, 3943-3953.
(390) Aromi, G.; Parsons, S.; Wernsdorfer, W.; Brechin, E. K.; McInnes, E. J. L. *Chem. Commun.* **2005**, 5038-5040.
(391) Ungur, L.; Thewissen, M.; Costes, J.-P.; Wernsdorfer, W.; Chibotaru, L. F. *Inorg. Chem.* **2013**, *52*, 6328-6337.
(392) Natrajan, L.; Pécaut, J.; Mazzanti, M.; LeBrun, C. *Inorg. Chem.* **2005**, *44*, 4756-4765.
(393) Evans, W. J.; Greci, M. A.; Ziller, J. W. *Chem. Commun.* **1998**, 2367-2368.
(394) Deacon, G. B.; Forsyth, C. M.; Junk, P. C.; Skelton, B. W.; White, A. H. *Chem. Eur. J.* **1999**, *5*, 1452-1459.
(395) Moustiakimov, M.; Kritikos, M.; Westin, G. *Inorg. Chem.* **2005**, *44*, 1499-1504.
(396) Guo, H.; Zhou, H.; Yao, Y.; Zhang, Y.; Shen, Q. *Dalton Trans.* **2007**, 3555-3561.
(397) Andrez, J.; Bozoklu, G.; Nocton, G.; Pecaut, J.; Scopelliti, R.; Dubois, L.; Mazzanti, M. *Chem. Eur. J.* **2015**, *21*, 15188-15200.
(398) Meihaus, K. R.; Fieser, M. E.; Corbey, J. F.; Evans, W. J.; Long, J. R. *J. Am. Chem. Soc.* **2015**, *137*, 9855-9860.
(399) Arauzo, A.; Lazarescu, A.; Shova, S.; Bartolome, E.; Cases, R.; Luzon, J.; Bartolome, J.; Turta, C. *Dalton Trans.* **2014**, *43*, 12342-12356.
(400) Jassal, A. K.; Aliaga-Alcalde, N.; Corbella, M.; Aravena, D.; Ruiz, E.; Hundal, G. *Dalton Trans.* **2015**, *44*, 15774-15778.
(401) Shafir, A.; Fiedler, D.; Arnold, J. *Dalton Trans.* **2002**, 555-560.
(402) Broderick, E. M.; Diaconescu, P. L. *Inorg. Chem.* **2009**, *48*, 4701-4706.

(403) Broderick, E. M.; Thuy-Boun, P. S.; Guo, N.; Vogel, C. S.; Sutter, J.; Miller, J. T.; Meyer, K.; Diaconescu, P. L. *Inorg. Chem.* **2011**, *50*, 2870-2877.
(404) Quan, S. M.; Diaconescu, P. L. *Chem. Commun.* **2015**, *51*, 9643-9646.
(405) Monreal, M. J.; Diaconescu, P. L. *Organometallics* **2008**, *27*, 1702-1706.
(406) Duhovic, S.; Oria, J. V.; Odoh, S. O.; Schreckenbach, G.; Batista, E. R.; Diaconescu, P. L. *Organometallics* **2013**, *32*, 6012-6021.
(407) Lukens, W. W.; Edelstein, N. M.; Magnani, N.; Hayton, T. W.; Fortier, S.; Seaman, L. A. *J. Am. Chem. Soc.* **2013**, *135*, 10742-10754.
(408) Thorpe, C. L.; Morris, K.; Lloyd, J. R.; Denecke, M. A.; Law, K. A.; Dardenne, K.; Boothman, C.; Bots, P.; Law, G. T. W. *Appl. Geochem.* **2015**, *63*, 303-309.
(409) Charushnikova, I. A. K., N. N.; Polyakova, I. N. *Radiochemistry* **2006**, *48*, 223-226.
(410) Cousson, A. *Acta Crystallogr. C* **1985**, *41*, 1758-1761.
(411) Grigoriev, M. S. A., M. Yu.; Krot, N. N. *Radiochemistry* **2006**, *48*, 6-10.
(412) Nakamura, A.; Nakada, M.; Nakamoto, T.; Kitazawa, T.; Takeda, M. *J. Alloys Compd.* **2007**, *444*, 621-633.
(413) King, D. M.; Liddle, S. T. *Coord. Chem. Rev.* **2014**, *266*, 2-15.
(414) Streit, M.; Ingold, F. *J. Eur. Ceram. Soc.* **2005**, *25*, 2687-2692.
(415) Haber, F. Haber, F Ammonia German patent DE 229126, 1909; Vol. DE 229126.
(416) Fox, A. R.; Bart, S. C.; Meyer, K.; Cummins, C. C. *Nature* **2008**, *455*, 341-349.
(417) Kaltsoyannis, N. *Inorg. Chem.* **2013**, *52*, 3407-3413.
(418) Ding, M.; Rouzieres, M.; Losovyj, Y.; Pink, M.; Clerac, R.; Smith, J. M. *Inorg. Chem.* **2015**, *54*, 9075-9080.
(419) Eikey, R. A.; Abu-Omar, M. M. *Coord. Chem. Rev.* **2003**, *243*, 83-124.
(420) Berthet, J. C.; Lance, M.; Nierlich, M.; Vigner, J.; Ephritikhine, M. *J. Organomet. Chem.* **1991**, *420*, C9-C11.
(421) Evans, W. J.; Miller, K. A.; Ziller, J. W.; Greaves, J. *Inorg. Chem.* **2007**, *46*, 8008-8018.
(422) Schmidt, A.-C.; Heinemann, F. W.; Maron, L.; Meyer, K. *Inorg. Chem.* **2014**, *53*, 13142-13153.
(423) Evans, W. J.; Kozimor, S. A.; Ziller, J. W. *Science* **2005**, *309*, 1835-1838.
(424) Fox, A. R.; Arnold, P. L.; Cummins, C. C. *J. Am. Chem. Soc.* **2010**, *132*, 3250-3251.
(425) Fortier, S.; Wu, G.; Hayton, T. W. *J. Am. Chem. Soc.* **2010**, *132*, 6888-6889.
(426) Maria, L.; Santos, I. C.; Sousa, V. R.; Marcalo, J. *Inorg. Chem.* **2015**, *54*, 9115-9126.
(427) King, D. M.; Tuna, F.; McInnes, E. J. L.; McMaster, J.; Lewis, W.; Blake, A. J.; Liddle, S. T. *Nature Chem.* **2013**, *15*, 482-488.
(428) Cloke, N. T. A. F. R. K. C. J. I. F. G. N. *Chem. Sci.* **2016**.
(429) Korobkov, I.; Gambarotta, S.; Yap, G. P. A. *Angew. Chem. Int. Ed.* **2002**, *41*, 3433-3436.
(430) Todorova, T. K.; Gagliardi, L.; Walensky, J. R.; Miller, K. A.; Evans, W. J. *J. Am. Chem. Soc.* **2010**, *132*, 12397-12403.
(431) King, D. M.; McMaster, J.; Tuna, F.; McInnes, E. J. L.; Lewis, W.; Blake, A. J.; Liddle, S. T. *J. Am. Chem. Soc.* **2014**, *136*, 5619-5622.
(432) Cleaves, P. A.; King, D. M.; Kefalidis, C. E.; Maron, L.; Tuna, F.; McInnes, E. J. L.; McMaster, J.; Lewis, W.; Blake, A. J.; Liddle, S. T. *Angew. Chem. Int. Ed.* **2014**, *53*, 10412-10415.
(433) Stewart, J. L.; Andersen, R. A. *Polyhedron* **1998**, *17*, 953-958.
(434) Korobkov, I.; Gambarotta, S.; Yap, G. P. A.; Thompson, L.; Hay, P. J. *Organometallics* **2001**, *20*, 5440-5445.
(435) Arnold, P. L.; Potter, N. A.; Magnani, N.; Apostolidis, C.; Griveau, J. C.; Colineau, E.; Morgenstern, A.; Caciuffo, R.; Love, J. B. *Inorg. Chem.* **2010**, *49*, 5341-5343.
(436) Appleton, T. G. *J. Chem. Educ.* **1977**, *54*, 443-444.
(437) Anderegg, G.; Wenk, F. *Helv. Chim. Acta* **1967**, *50*, 2330-2332.
(438) Thapper, A.; Behrens, A.; Fryxelius, J.; Johansson, M. H.; Prestopino, F.; Czaun, M.; Rehder, D.; Nordlander, E. *Dalton Trans.* **2005**, 3566-3571.
(439) Avens, L. R.; Bott, S. G.; Clark, D. L.; Sattelberger, A. P.; Watkin, J. G.; Zwick, B. D. *Inorg. Chem.* **1994**, *33*, 2248-2256.
(440) Bharara, M. S.; Tonks, S. A.; Gorden, A. E. V. *Chem. Commun.* **2007**, 4006-4008.
(441) Tanner, J. E. *J. Chem. Phys.* **1970**, *52*, 2523-&.
(442) Johnson, C. S. *Progress in Nuclear Magnetic Resonance Spectroscopy* **1999**, *34*, 203-256.
(443) Wu, D. H.; Chen, A. D.; Johnson, C. S. *Journal of Magnetic Resonance, Series A* **1995**, *115*, 260-264.
(444) Bain, G. A.; Berry, J. F. *J. Chem. Educ.* **2008**, *85*, 532-536.

(445) Duisenberg, A. J. M.; Kroon-Batenburg, L. M. J.; Schreurs, A. M. M. *J. Appl. Cryst.* **2003**, *36*, 220-229.
(446) Blessing, R. H. *Acta Crystallogr., Sect. A* **1995**, *51*, 33-38.
(447) Agilent In *CrysAlis PRO.*; technologies, A., Ed. Yarnton, England, 2010.
(448) Sheldrick, G. M.; 6.14 ed.; University of Göttingen, Germany: Germany, 2006.
(449) Palatinus, L.; Chapuis, G. *J. Appl. Cryst.* **2007**, *40*, 786-790.
(450) Dolomanov, O. V.; Bourhis, L. J.; Gildea, R. J.; Howard, J. A. K.; Puschmann, H. *J. Appl. Cryst.* **2009**, *42*, 339-341.

APPENDIX

Crystallographic data

Table 1 X-ray crystallographic data.

Compound	**[2].4H2O.4MeCN**	**[4].6MeCN**	**[5]**	**[6].3Py.1DIPE**
Formula	$C_{200}H_{168}N_6O_{79}U_{16}$	$C_{96}H_{82}Cl_{16}K_4N_6O_{40}U_{13}$	$C_{84}H_{64}Cl_{17}K_2O_{40}U_{13}$	$C_{153}H_{129}N_7O_{37}U_6$
Formula weight	7727.87	5777.67	5488.59	4085.80
Temperature (K)	150.0(2)	150.0(2)	150.0(2)	150.0(2)
Crystal system	Monoclinic	Monoclinic	Monoclinic	Triclinic
Space group	$P2_1/n$	I2/m	I2/m	P-1
a (Å)	20.8156(5)	15.1988(5)	15.2373(17)	14.7314(6)
b (Å)	32.9274(9)	20.6495(8)	20.511(4)	15.4129(5)
c (Å)	33.6580(9)	25.1583(12)	25.029(9)	17.1466(6)
α (°)	90	90	90	70.709(3)
β (°)	94.474(2)	96.627(4)	96.99(2)	79.131(3)
γ (°)	90	90	90	81.968(3)
Volume ($Å^3$)	22999.0(10)	7843.1(5)	7764(3)	3596.1(2)
Z	4	2	2	1
Density (calc.) ($g.cm^{-3}$)	2.232	2.446	2.348	1.887
Absorption correction	Semi-empirical from equivalents	Semi-empirical from equivalents	Semi-empirical from equivalents	Semi-empirical from equivalents
Absorption coefficient (mm^{-1})	11.303	13.809	13.905	6.812
F(000)	14056	5128	4822	1944
Crystal size (mm)	0.151 x 0.107 x 0.071	0.20 x 0.14 x 0.05	0.23 x 0.11 x 0.08	0.5822 x 0.4662 x 0.4062
Theta range for data collection (°)	3.268 to 26.373	3.31 to 28.30	6.56 to 65.082	3.455 to 26.372
Limiting indices	-26<=h<=20 -35<=k<=41 -41<=l<=42	-15<=h<=20 -27<=k<=27 -33<=l<=33	-22 ≤ h ≤ 22 -30 ≤ k ≤ 30 -35 ≤ l ≤ 37	-18<=h<=18 -19<=k<=19 -21<=l<=20
Total no. reflexions	128014	29333	44710	32879
Unique reflexions [R(int)]	46910 [R(int) = 0.1131]	9884 [R(int) = 0.0971]	13419 [R(int) = 0.0490]	14701 [R(int) = 0.0465]
Data / restraints / parameters	46910 / 1645 / 2039	9884 / 201 / 505	13419/414/435	14701 / 222 / 1017
Final R indices [I>2s(I)]	R1 = 0.1108, wR2 = 0.2777	R1 = 0.0582, wR2 = 0.1058	R1 = 0.0763, wR2 = 0.1974	R1 = 0.0381, wR2 = 0.0786
R indices (all data)	R1 = 0.1773, wR2 = 0.3252	R1 = 0.1419, wR2 = 0.1357	R_1 = 0.1259, wR_2 = 0.2238	R1 = 0.0591, wR2 = 0.0887
Largest diff. peak and hole ($e.Å^{-3}$)	4.642 and -6.418	2.268 and -1.678	4.68 and-1.87	3.297 and -1.635
GOF	0.979	0.988	0.852	1.039

Table 2 X-ray crystallographic data.

Compound	**[7]**	**[8].2MeCN**	**9-{UO_2(salen)Cd}.2Py**	**[11].Pyridine**
Formula	$C_{174}H_{160}Cl_{18}N_{10}O_{10}U_{38}$	$C_8H_{12}Cl_8K_4N_4O_4U_2$	$C_{51}H_{49}CdN_{10}O_7U$	$C_{44}H_{56}CoN_4O_4U$
Formula weight	13834.35	11144.28	1264.43	1001.89
Temperature (K)	150.0(2)	150.0(2)	150(2)	150(2)
Crystal system	Tetragonal	Triclinic	Monoclinic	4106.56(18)
Space group	I4/m	P-1	$P2_1/c$	$P4_2$
a (Å)	21.7282(8)	7.4888(6)	20.6165(13)	15.8348(3)
b (Å)	21.7282(8)	11.6251(8)	21.7877(12)	15.8348(3)
c (Å)	29.7370(14)	18.1835(11)	33.9309(17)	16.3777(5)
α (°)	90	75.012(6)	90	90
β (°)	90	83.574(6)	98.215(6)	90
γ (°)	90	73.050(7)	90	90
Volume ($Å^3$)	14039.3(12)	1461.59(19)	15084.9(15)	4106.56(18)
Z	2	2	12	4
Density (calc.) ($g.cm^{-3}$)	3.273	2.600	1.670	1.621
Absorption correction	Semi-empirical from equivalents	Semi-empirical from equivalents	Analytical	Semi-empirical from equivalents
Absorption coefficient (mm^{-1})	22.073	12.388	3.701	4.389
F(000)	11912	1032	7452	1996
Crystal size (mm)	0.055 x 0.044 x 0.028	1.536 x 0.913 x 0.691	0.23 x 0.14 x 0.04	0.85 x 0.48 x 0.47
Theta range for data collection (°)	3.266 to 30.504	3.544 to 30.508	3.28 to 24.71	3.5722 to 32.3379
Limiting indices	-31<=h<=26 -22<=k<=26 -42<=l<=36	-10<=h<=10 -16<=k<=16 -25<=l<=25	-24<=h<=20 -25<=k<=25 -35<=l<=39	-22<=h<=15 -17<=k<=22 -23<=l<=20
Total no. reflexions	35509	17438	54830	54830
Unique reflexions [R(int)]	10896 [R(int) = 0.1206]	8879 [R(int) = 0.1606]	25648 [R(int) = 0.1159]	14109 [R(int) = 0.0331]
Data / restraints / parameters	10896 / 612 / 536	8879 / 0 / 278	25648 / 132 / 1928	10601 / 439 / 594
Final R indices [I>2s(I)]	R1 = 0.0675 wR2 = 0.0724	R1 = 0.0997 wR2 = 0.2297	R1 = 0.0985 wR2 = 0.1845	R1 = 0.0526 wR2 = 0.0823
R indices (all data)	R1 = 0.2075 wR2 = 0.1018	R1 = 0.1289 wR2 = 0.2550	R1 = 0.1966 wR2 = 0.2277	R1 = 0.0822 wR2 = 0.1316
Largest diff. peak and hole ($e.Å^{-3}$)	2.734 and -2.245	7.690 and -4.673	2.730 and -2.160	3.443 and -1.185
GOF	0.955	0.995	1.067	1.021

Table 3 X-ray crystallographic data.

Compound	**12-{UO_2(Mesaldien)Mn}.2Py**	**13-UMn2-TPA-I.3Pyridine**	**14-UCd2-TPA-I.1Pyridine**	**15-UMn_2-TPA-Cl**
Formula	$C_{39}H_{41}MnN_8O_7U$	$C_{70}H_{72}I_3Mn_2N_{14}O_4U$	$C_{60}H_{62}Cd_2I_3N_{12}O_4U$	$C_{55}H_{57}N_{11}O_4Cl_2Mn_2IU$
Formula weight	1026.77	1902.03	1858.74	1481.82
Temperature (K)	150.0(2)	150.0(2)	150.0(2)	100(2)
Crystal system	Monoclinic	Monoclinic	Monoclinic	Monoclinic
Space group	C2/c	$P2_1$	$P2_1/m$	$P2_1/n$
a (Å)	38.007(4)	13.3812(5)	13.5808(11)	15.191(2)
b (Å)	13.2053(3)	15.4665(9)	15.5533(10)	24.823(3)
c (Å)	23.759(2)	17.7709(10)	17.6965(14)	15.4656(10)
α (°)	90	90	90	90
β (°)	137.802(19)	102.328(5)	102.239(8)	98.488(8)
γ (°)	90	90	90	90
Volume ($Å^3$)	8010(2)	3593.0(3)	3653.0(5)	5768.2(11)
Z	8	2	2	4
Density (calc.) ($g.cm^{-3}$)	1.703	1.758	1.690	1.706
Absorption correction	Analytical	Analytical	Analytical	Empirical
Absorption coefficient (mm^{-1})	4.413	3.940	4.103	3.914
F(000)	4032	1846	1770	2900
Crystal size (mm)	0.378 x 0.052x 0.013	0.29 x 0.20 x 0.08	0.1772 x 0.1126 x 0.0300	0.39 × 0.266 × 0.26
Theta range for data collection (°)	3.339 to 30.505	3.36 to 26.43	3.372 to 20.815	3.128 to 60.0
Limiting indices	-36<=h<=32 -18<=k<=18 -33<=l<=30	-16<=h<=16, -19<=k<=19, -21<=l<=22	-13<=h<=13, -15<=k<=15, -17<=l<=17	-21 ≤ h ≤ 20 -34 ≤ k ≤ 34 -21 ≤ l ≤ 21
Total no. reflexions	24224	36753	24407	92223
Unique reflexions [R(int)]	12081 [R(int) = 0.0654]	14556 [R(int) = 0.1042]	3991 [R(int) = 0.1328]	16670 [R(int) = 0.0554]
Data / restraints / parameters	12079 / 236 / 607	14556 / 165 / 806	3991 / 1122 / 645	16670/24/725
Final R indices [I>2s(I)]	R1 = 0.0487 wR2 = 0.0665	R1 = 0.0714 wR2 = 0.1540	R1 = 0.0696 wR2 = 0.1823	R1 = 0.0455 wR2 = 0.1021
R indices (all data)	R1 = 0.1141 wR2 = 0.0853	R1 = 0.1212 wR2 = 0.1815	R1 = 0.1085 wR2 = 0.2163	R1 = 0.0748 wR2 = 0.1289
Largest diff. peak and hole ($e.Å^{-3}$)	2.727 and -1.640	2.903 and -0.938	1.994 and -1.225	2.06/-1.24
GOF	0.954	1.059	1.068	1.211

Table 4 X-ray crystallographic data.

Compound	**16-UFe_2-TPA**	**17-UCo-TPA.1Pyridine**	**18-UNi2-TPA.4.5MeCN**	**20-UFe_2-BPPA.2.5Pyridine**
Formula	$C_{55}H_{57}Cl_2Fe_2IN_{11}O_4U$	$C_{42}H_{44}CoIN_8O_4U$	$C_{62.50}H_{68.25}I_3N_{14.75}Ni_2O_4U$	$C_{77}H_{77}Fe_2IN_{13}O_6U$
Formula weight	1483.64	1148.71	1826.21	1757.14
Temperature (K)	150.0(2)	150.0(2)	150.0(2)	150.0(2)
Crystal system	Monoclinic	Trigonal	Triclinic	Monoclinic
Space group	$P2_1/n$	R-3	P-1	I2/c
a (Å)	14.9915(5)	43.0624(8)	16.5628(4)	27.3106(11)
b (Å)	24.8777(5)	43.0624(8)	20.7120(6)	19.4831(7)
c (Å)	15.4086(5)	12.2847(2)	21.2881(6)	32.3421(13)
α (°)	90	90	106.064(3)	90
β (°)	99.407(3)	90	100.575(2)	113.798(5)
γ (°)	90	120	92.873(2)	90
Volume ($Å^3$)	5669.4(3)	19728.4(6)	6859.0(3)	15745.8(12)
Z	4	18	4	8
Density (calc.) ($g.cm^{-3}$)	1.738	1.740	1.768	1.482
Absorption correction	Analytical	Analytical	Analytical	Semi-empirical from equivalents
Absorption coefficient (mm^{-1})	4.048	4.821	4.304	2.865
F(000)	2908	10008	3542	7000
Crystal size (mm)	0.315 x 0.062 x 0.016	0.92 x 0.12 x 0.09	0.460 x 0.148 x 0.028	0.150 x 0.080 x 0.080
Theta range for data collection (°)	3.310 to 30.507	3.36 to 30.51	2.960 to 30.508	3.037 to 26.371
Limiting indices	-21<=h<=20 -35<=k<=33 -22<=l<=22	-61<=h<=61 -61<=k<=60 -17<=l<=17	-23<=h<=23 -29<=k<=29 -30<=l<=30	-34<=h<=27 -24<=k<=23 -40<=l<=40
Total no. reflexions	34430	81984	84082	37030
Unique reflexions [R(int)]	17193 [R(int) = 0.0708]	13354 [R(int) = 0.0347]	41423 [R(int) = 0.0743]	16078 [R(int) = 0.0560]
Data / restraints / parameters	17193 / 0 / 686	13354 / 0 / 573	41423 / 198 / 1650	16078 / 156 / 991
Final R indices [I>2s(I)]	R1 = 0.0597 wR2 = 0.0855	R1 = 0.0428 wR2 = 0.1007	R1 = 0.0638 wR2 = 0.1095	R1 = 0.0516 wR2 = 0.1238
R indices (all data)	R1 = 0.1256 wR2 = 0.1043	R1 = 0.0586 wR2 = 0.1077	R1 = 0.1438 wR2 = 0.1367	R1 = 0.0849 wR2 = 0.1391
Largest diff. peak and hole ($e.Å^{-3}$)	2.511 and -1.201	4.798 and -2.425	3.314 and -2.900	1.137 and -0.824
GOF	1.000	1.080	1.019	1.053

Table 5 X-ray crystallographic data.

Compound	**21-UCo_2-BPPA.2.5Pyridine**	**22-UNi_2-BPPA.5.5Pyridine**	**[23].4MeCN**	**[24].1.6Py**
Formula	$C_{74.50}H_{74.50}Co_2IN_{12.50}O_6U$	$C_{94.50}H_{94.50}IN_{16.50}Ni_2O_6U$	$C_{84}H_{84}Cr_5I_2N_{16}O_8$	$C_{46.12}H_{47.12}N_{7.62}O_5UZn$
Formula weight	1723.75	2039.71	1959.47	1091.69
Temperature (K)	150.0(2)	150.0(2)	150.0(2)	150.0(2)
Crystal system	Monoclinic	Triclinic	Triclinic	Triclinic
Space group	I2/a	P-1	P-1	P-1
a (Å)	31.576(2)	14.4080(10)	11.9294(10)	15.4896(6)
b (Å)	19.4882(11)	16.7833(13)	12.1442(10)	16.7485(7)
c (Å)	27.130(2)	19.9789(14)	15.4655(11)	18.6147(10)
α (°)	90	97.559(6)	92.785(6)	75.939(4)
β (°)	112.290(9)	105.950(6)	112.386(7)	70.751(4)
γ (°)	90	103.412(6)	99.976(7)	72.994(4)
Volume ($Å^3$)	15447(2)	4418.9(6)	2024.1(3)	4302.0(4)
Z	8	2	1	4
Density (calc.) ($g.cm^{-3}$)	1.482	1.533	1.607	1.686
Absorption correction	Semi-empirical from equivalents	Semi-empirical from equivalents	Analytical	Analytical
Absorption coefficient (mm^{-1})	2.972	2.663	1.480	4.373
F(000)	6848	2052	990	2157
Crystal size (mm)	0.373 x 0.316 x 0.197	0.700 x 0.500 x 0.500	0.167 x 0.087 x 0.028	0.622 x 0.135 x 0.073
Theta range for data collection (°)	3.369 to 30.508	2.984 to 28.282	2.958 to 26.371	2.864 to 30.508
Limiting indices	-45<=h<=44 -27<=k<=27 -38<=l<=38	-19<=h<=19 -22<=k<=20 -26<=l<=26	-14<=h<=14 -15<=k<=15 -14<=l<=19	-22<=h<=21 -23<=k<=23 -26<=l<=26
Total no. reflexions	48922	45425	18262	50766
Unique reflexions [R(int)]	23483 [R(int) = 0.0964]	21835 [R(int) = 0.1002]	8260 [R(int) = 0.1149]	25893 [R(int) = 0.0749]
Data / restraints / parameters	23483 / 150 / 983	21835 / 90 / 1123	8260 / 23 / 532	25893 / 144 / 1125
Final R indices [I>2s(I)]	R1 = 0.0864 wR2 = 0.1943	R1 = 0.0837 wR2 = 0.1856	R1 = 0.0769 wR2 = 0.0941	R1 = 0.0927 wR2 = 0.2148
R indices (all data)	R1 = 0.1838 wR2 = 0.2495	R1 = 0.1316 wR2 = 0.2200	R1 = 0.1583 wR2 = 0.1176	R1 = 0.1462 wR2 = 0.2472
Largest diff. peak and hole ($e.Å^{-3}$)	2.260 and -1.356	4.707 and -3.061	0.778 and -0.705	8.477 and -3.195
GOF	1.011	1.055	0.974	1.128

Table 6 X-ray crystallographic data.

Compound	**25-UMn_2-TPEN.1MeCN**	**26-UCo_2-TPEN.2Pyridine.3.5MeCN**	**27-U_2Nd_3-TPA.1Pyridine**	**28-UEu_2-TPEN.3.5Pyridine**
Formula	$C_{73}H_{80}I_3Mn_2N_{16}O_4U$	$C_{88}H_{97.50}Co_2I_3N_{20.5}O_4U$	$C_{108}H_{114}I_5N_{20}Nd_3O_{10}U_2$	$C_{88.5}H_{94.5}Eu_2I_3N_{18.5}O_4U$
Formula weight	1974.14	2242.95	3395.47	2403.97
Temperature (K)	150.0(2)	150.0(2)	150.0(2)	100(2)
Crystal system	Triclinic	Monoclinic	Tetragonal	Monoclinic
Space group	P-1	C2/c	P-4	$P2_1/c$
a (Å)	13.2818(5)	23.2625(11)	29.054(3)	9.8624(6)
b (Å)	13.4962(6)	31.2135(17)	29.054(3)	32.524(4)
c (Å)	43.6831(18)	14.3038(6)	9.7559(16)	28.504(5)
α (°)	97.534(3)	90	90	90
β (°)	91.108(3)	96.507(4)	90	94.505(8)
γ (°)	94.989(3)	90	90	90
Volume ($Å^3$)	7729.6(5)	10319.1(8)	8235.6(18)	9115(2)
Z	4	4	2	4
Density (calc.) ($g.cm^{-3}$)	1.696	1.444	1.369	1.752
Absorption correction	Analytical	Analytical	Semi-empirical from equivalents	Semi-empirical from equivalents
Absorption coefficient (mm^{-1})	3.667	2.834	3.871	4.207
F(000)	3852	4424	3222	4656
Crystal size (mm)	0.203 x 0.162 x 0.144	0.7641 x 0.3657 x 0.1803	0.35 x 0.04 x 0.03	0.408 × 0.199 × 0.167
Theta range for data collection (°)	3.031 to 23.256	2.975 to 30.507	3.50 to 20.99	1.252 to 30.028
Limiting indices	-14<=h<=14 -14<=k<=14 -48<=l<=48	-33<=h<=32 -44<=k<=44 -20<=l<=20	-29<=h<=20 -28<=k<=29 -9<=l<=5	-13 ≤ h ≤ 13 -44 ≤ k ≤ 45 -39 ≤ l ≤ 40
Total no. reflexions	50412	61656	11590	145792
Unique reflexions [R(int)]	22144 [R(int) = 0.0865]	15749 [R(int) = 0.0554]	7960 [R(int) = 0.1014]	26529 [R(int) = 0.0642]
Data / restraints / parameters	22144 / 1006 / 1940	15749 / 117 / 620	7960 / 637 / 669	26529/103/1169
Final R indices [I>2s(I)]	R1 = 0.1235 wR2 = 0.2406	R1 = 0.0573 wR2 = 0.1551	R1 = 0.0976 wR2 = 0.2103	R1 = 0.0663 wR2 = 0.1465
R indices (all data)	R1 = 0.1550 wR2 = 0.2565	R1 = 0.0862 wR2 = 0.1752	R1 = 0.1642 wR2 = 0.2465	R1 = 0.0873 wR2 = 0.1602
Largest diff. peak and hole ($e.Å^{-3}$)	2.802 and -3.165	2.181 and -3.196	1.513 and -1.267	6.04/-1.53
GOF	1.198	1.087	0.962	1.297

Table 7 X-ray crystallographic data.

Compound	**[29]**	**[30].1.5Toluene**	**[31].1Pyridine**
Formula	$C_{40}H_{25}FeN_2O_4U$	$C_{114.50}H_{160}Fe_2K_2N_4O_{20}U_2$	$C_{89}H_{68}N_{13}Np_3O_6$
Formula weight	891.50	2578.42	2126.56
Temperature (K)	150(2)	150(2)	293(2)
Crystal system	Orthorhombic	Triclinic	Hexagonal
Space group	C m m a	P-1	P 6_3/m
a (Å)	12.0997(2)	13.4971(3)	17.161(2)
b (Å)	22.9943(5)	21.8515(5)	17.161(2)
c (Å)	13.6876(3)	22.1835(4)	16.615(3)
α (°)	90	106.2941(18)	90
β (°)	90	106.6784(18)	90
γ (°)	90	92.5543(19)	120
Volume (Å^3)	3808.22(14)	5959.7(2)	4237.6(15)
Z	4	2	2
Density (calc.) (g.cm^{-3})	1.555	1.437	1.667
Absorption correction	Semi-empirical from equivalents	Analytical	Semi-empirical from equivalents
Absorption coefficient (mm^{-1})	4.667	3.082	3.710
F(000)	1716	2618	2040
Crystal size (mm)	0.24 x 0.02 x 0.01	0.202x0.073x0.060	0.172x0.103x0.060
Theta range for data collection (°)	3.37 to 28.28	3.232 to 30.507	1.370 to 18.614
Limiting indices	-16<=h<=12 -29<=k<=30 -18<=l<=17	-19<=h<=18 -31<=k<=31 -31<=l<=31	-15<=h<=15 -15<=k<=14 -11<=l<=14
Total no. reflexions	8989	72214	11602
Unique reflexions [R(int)]	2537 [R(int) = 0.0390]	35987 [R(int) = 0.0657]	1129 [R(int) = 0.2253]
Data / restraints / parameters	2537 / 18 / 207	35987 / 257 / 1338	1129 / 243 / 221
Final R indices [I>2s(I)]	R1 = 0.0386 wR2 = 0.0910	R1 = 0.0569 wR2 = 0.1071	R1 = 0.0829 wR2 = 0.2243
R indices (all data)	R1 = 0.0474 wR2 = 0.0922	R1 = 0.1234 wR2 = 0.1290	R1 = 0.1689 wR2 = 0.3067
Largest diff. peak and hole (e.Å^{-3})	2.331 and -0.767	2.019 and -1.088	2.243 and -2.713
GOF	0.981	1.000	1.139

Table 8 X-ray crystallographic data.

Compound	**32-$Cs_2[U^{III}$---N---U^{IV}].2THF**	**33-$Cs_3[U^{III}$---N---U^{III}]**	**34-$K[U^{IV}$---N---U^{IV}] .Toluene**
Formula	$C_{80}H_{178}Cs_2NO_{26}Si_6U_2$	$C_{72}H_{162}Cs_3NO_{24}Si_6U_2$	$C_{79}H_{170}KNO_{24}Si_6U_2$
Formula weight	2480.65	2469.35	2201.85
Temperature (K)	120(2)	100(2)	100(2)
Crystal system	Monoclinic	Orthorhombic	Monoclinic
Space group	$P2_1/n$	Pnn2	$P2_1/c$
a (Å)	14.155(3)	14.215(2)	14.210(3)
b (Å)	29.331(7)	17.0473(14)	28.1537(19)
c (Å)	27.558(5)	24.193(3)	27.910(3)
α (°)	90	90	90
β (°)	91.061(16)	90	104.632(8)
γ (°)	90	90	90
Volume ($Å^3$)	11440(4)	5862.6(13)	10803(2)
Z	4	2	4
Density (calc.) ($g.cm^{-3}$)	1.440	1.399	1.354
Absorption correction	Semi-empirical from equivalents	Semi-empirical from equivalents	Semi-empirical from equivalents
Absorption coefficient (mm^{-1})	3.577	3.791	3.159
F(000)	5004	2452	4252
Crystal size (mm)	0.45 x 0.18 x 0.13	0.383 x 0.220 x 0.214	0.642 × 0.503 × 0.419
Theta range for data collection (°)	1.01 to 27.50	2.047 to 29.999°	2.09 to 55.058
Limiting indices	-18 ≤ h ≤ 18 -38 ≤ k ≤ 38 -35 ≤ l ≤ 35	-20 ≤ h ≤ 20 -23 ≤ k ≤ 23 -34 ≤ l ≤ 34	-18 ≤ h ≤ 18 -36 ≤ k ≤ 36 -36 ≤ l ≤ 36
Total no. reflexions	140023	82819	115467
Unique reflexions [R(int)]	26201 [R(int) = 0.0938]	16936 [R(int) = 0.0885]	24316 [R(int) = 0.1089]
Data / restraints / parameters	26201 / 60 / 1109	16936 / 43 / 493	24316/287/1174
Final R indices [I>2s(I)]	R1 = 0.0788 wR2 = 0.1712	R1 = 0.0613 wR2 = 0.1540	R1 = 0.0677 wR2 = 0.1499
R indices (all data)	R1 = 0.1196 wR2 = 0.1999	R1 = 0.0840 wR2 = 0.1756	R1 = 0.1368 wR2 = 0.1965
Largest diff. peak and hole ($e.Å^{-3}$)	3.333 and -2.808	5.369 and -3.666	2.19/-2.89
GOF	1.136	1.054	1.220

Table 9 X-ray crystallographic data.

Compound	**[35].Toluene**	**36-$K_3[U^{III}{=}{=}{=}N{=}{=}{=}U^{III}]$**	**37-$K_2[U^{III}{=}{=}{=}N{=}{=}{=}U^{IV}]$. 1Toluene**
Formula	$C_{79}H_{170}K_2N_4O_{24}Si_6U_2$	$C_{72}H_{162}K_3NO_{24}Si_6U$	$C_{79}H_{170}K_2NO_{24}Si_6U_2$
Formula weight	2282.99	2187.92	2240.96
Temperature (K)	100(2)	100(2)	100(2)
Crystal system	Monoclinic	Monoclinic	Monoclinic
Space group	$P2_1/n$	C2/c	$P2_1/c$
a (Å)	14.382(2)	56.507(9)	15.316(2)
b (Å)	17.661(3)	14.4927(15)	25.990(5)
c (Å)	21.819(4)	29.069(3)	28.321(5)
α (°)	90	90	90
β (°)	92.012(9)	93.331(10)	100.230(14)
γ (°)	90	90	90
Volume ($Å^3$)	5538.4(16)	23766(5)	11094(3)
Z	2	8	4
Density (calc.) ($g.cm^{-3}$)	1.369	1.223	1.342
Absorption correction	Semi-empirical from equivalents	Semi-empirical from equivalents	Semi-empirical from equivalents
Absorption coefficient (mm^{-1})	3.121	2.940	3.114
F(000)	2340	8944	4596
Crystal size (mm)	0.48 x 0.31 x 0.26	0.402 x 0.111 x 0.046	0.49 x 0.28 x 0.23
Theta range for data collection (°)	2.71 to 32.00	1.403 to 25.400	1.07 to 30.03
Limiting indices	$-20 \le h \le 21$ $-26 \le k \le 26$ $-32 \le l \le 32$	$-68 \le h \le 68$ $-17 \le k \le 17$ $-35 \le l \le 35$	$-21 \le h \le 21$ $-36 \le k \le 36$ $-39 \le l \le 39$
Total no. reflexions	97664	124838	158932
Unique reflexions [R(int)]	19104 [R(int) = 0.0447]	21850 [R(int) = 0.0946]	31958 [R(int) = 0.0450]
Data / restraints / parameters	19104 / 206 / 565	21850 / 432 / 1001	31958 / 0 / 1027
Final R indices [I>2s(I)]	R1 = 0.0548, wR2 = 0.1031	R1 = 0.1066, wR2 = 0.2327	R1 = 0.0471, wR2 = 0.0846
R indices (all data)	R1 = 0.1170, wR2 = 0.1445	R1 = 0.1395, wR2 = 0.2477	R1 = 0.0801, wR2 = 0.0997
Largest diff. peak and hole ($e.Å^{-3}$)	4.554 and -2.815	2.638 and -2.276	2.026 and -2.285
GOF	1.190	1.150	1.217

Bond valence sum calculations

Table 10 Bond valence sum for compounds **2**, **4**, **5**, **6** and **7**. Numbers in brackets refer to the numbering of the crystallographic structure.

Compound	U(1)	U(2)	U(3)	U(4)	U(5)	U(6)	U(7)	U(8)
2	4.14	3.96	3.91	4.25	3.98	4.24	4.08	4.20
4	3.91	4.06	4.36	3.57	3.72	-	-	-
5	3.91	4.05	4.35	3.74	4.24	-	-	-
6	4.15	4.10	4.12	-	-	-	-	-
7	4.19	4.34	4.18	4.23	4.24	3.91	4.10	-

Compound	U(9)	U(10)	U(11)	U(12)	U(13)	U(14)	U(15)	U(16)
2	3.97	4.11	4.00	4.16	4.37	4.07	3.86	4.09

Electrochemistry

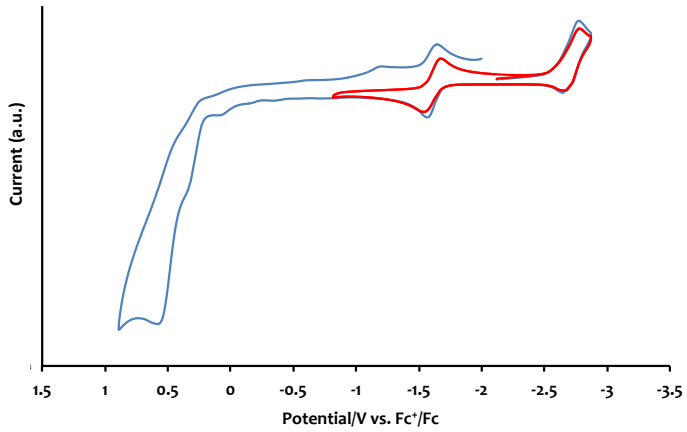

Figure 1 Room temperature cyclic voltammogram for a 2 mM solution of [UO_2(salfen-^{t}Bu_2)(K18c6)] **30** recorded in 0.1 M [Bu_4N][PF_6] pyridine solution at 100 mV.s-1 scan rate.

Electronic absorption spectra

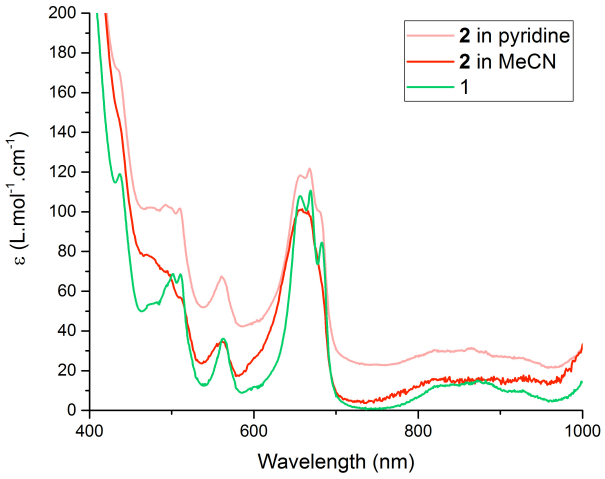

Figure 2 Electronic absorption spectra of complexes **1** and **2** in pyridine and in acetonitrile

^{1}H NMR

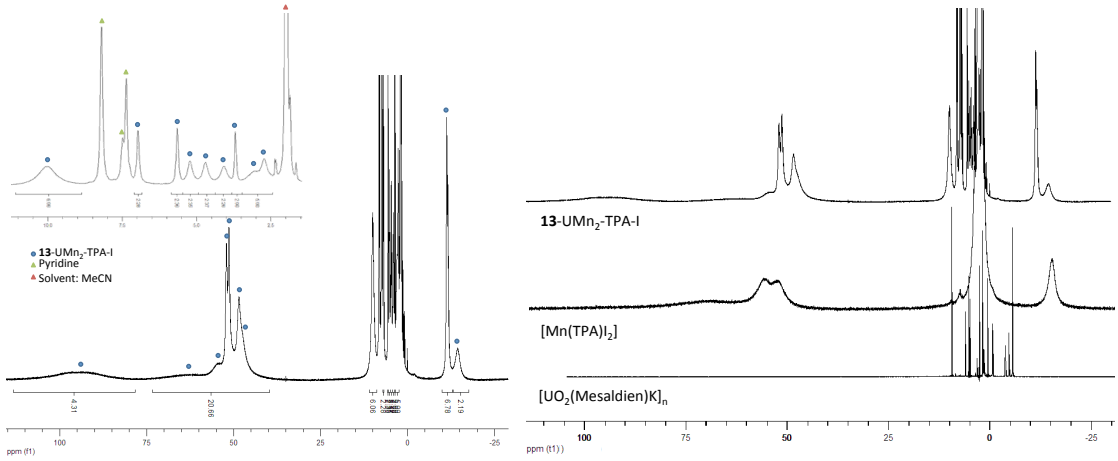

Figure 3 ^{1}H NMR spectrum (200MHz, CD_3CN, 298 K) of complex **13**-UMn_2-TPA-I (left) and compared to the proton NMR spectra of the $[Mn(TPA)I_2]$ and $[UO_2(Mesaldien)K]_n$ complexes (right).

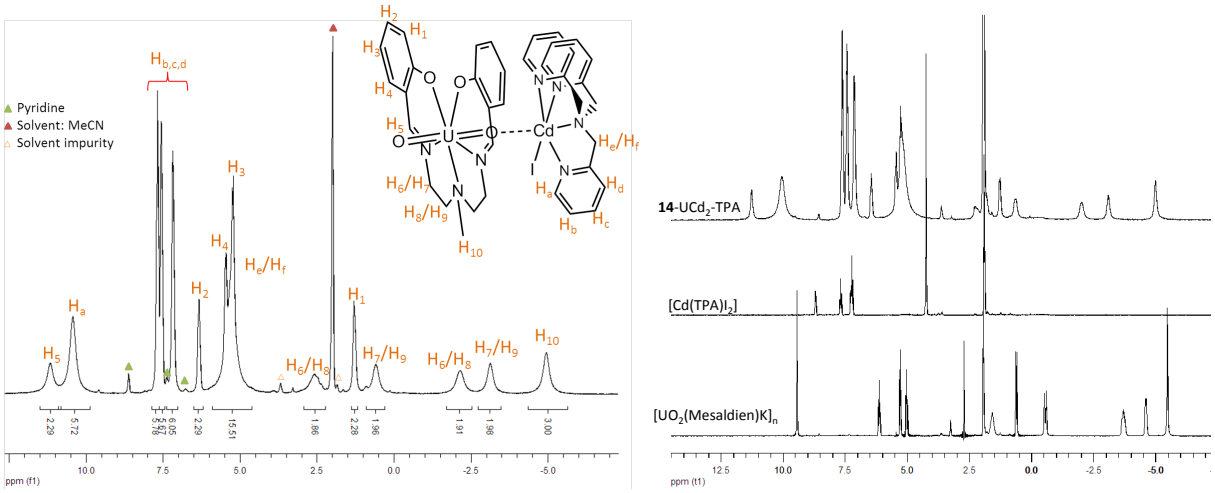

Figure 4 ^{1}H NMR spectrum (200 MHz, CD_3CN, 298 K) of complex **14**-UCd_2-TPA (left) and compared to the proton NMR spectra of the $[Cd(TPA)I_2]$ and $[UO_2(Mesaldien)K]_n$ complexes (right).

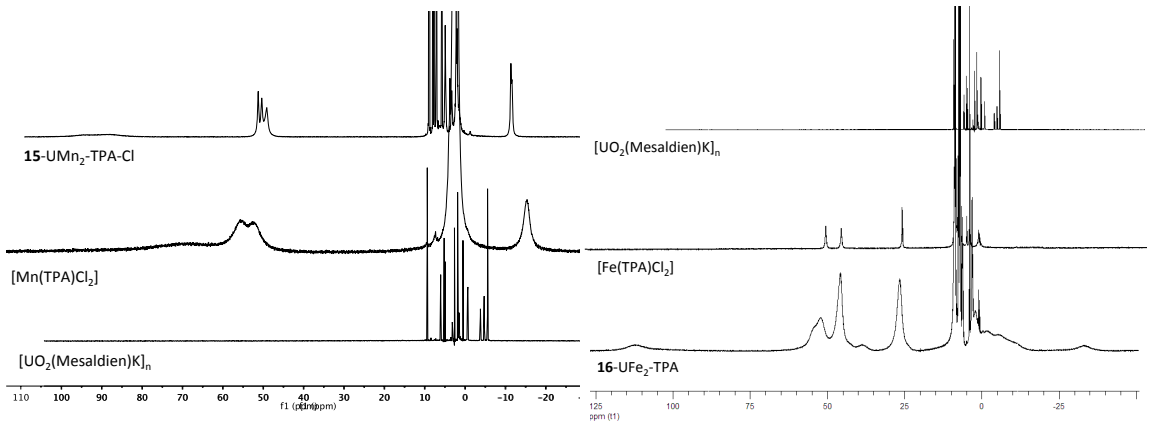

Figure 5 ^{1}H NMR spectra (200MHz, CD_3CN, 298 K) of **15**-UMn_2-TPA compared to $[Mn(TPA)Cl_2]$ and $[UO_2(Mesaldien)K]_n$ complexes (left) and **16**-UFe_2-TPA compared to $[Fe(TPA)Cl_2]$ and $[UO_2(Mesaldien)K]_n$ complexes (right).

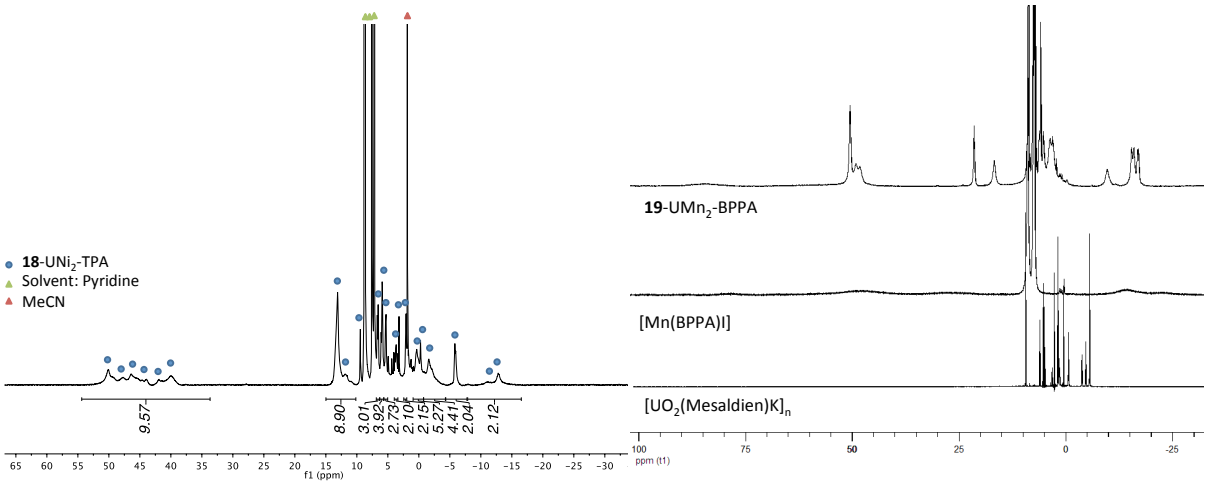

Figure 6 ^{1}H NMR spectrum (200 MHz, Py-D_5, 298 K) of complex **18**-UNi_2-TPA (left) and ^{1}H NMR spectra (200MHz, Py-D_5, 298 K) of complex **19**-UMn_2-BPPA compared to [Mn(BPPA)I] and $[UO_2(Mesaldien)K]_n$ complexes.

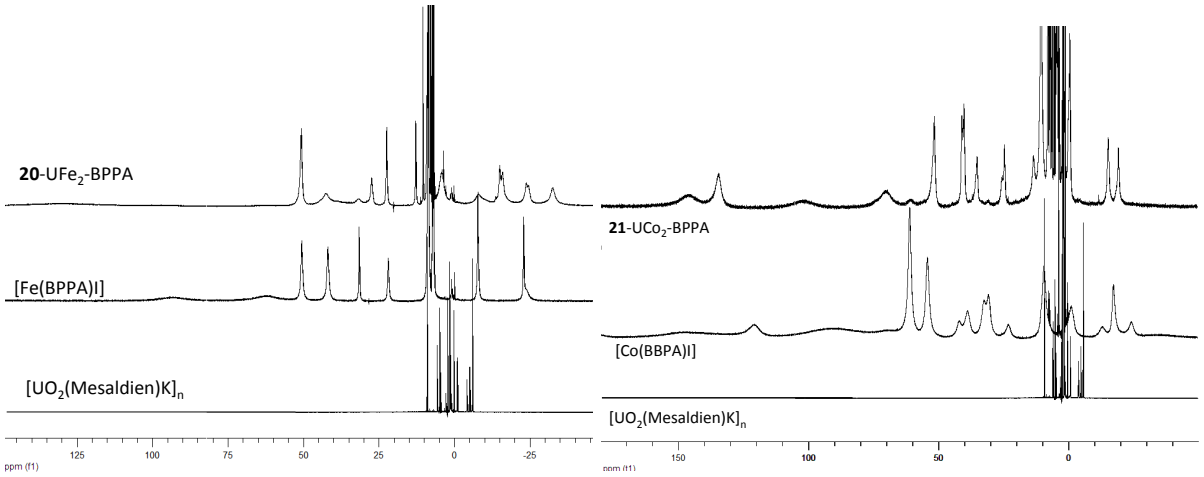

Figure 7 ^{1}H NMR spectra (200MHz, Py-D_5, 298 K) of **20**-UFe_2-BPPA compared to [Fe(BPPA)I] and $[UO_2(Mesaldien)K]_n$ complexes (left) and of **21**-UCo_2-BPPA compared to [Co(BPPA)I] and $[UO_2(Mesaldien)K]_n$ complexes (right).

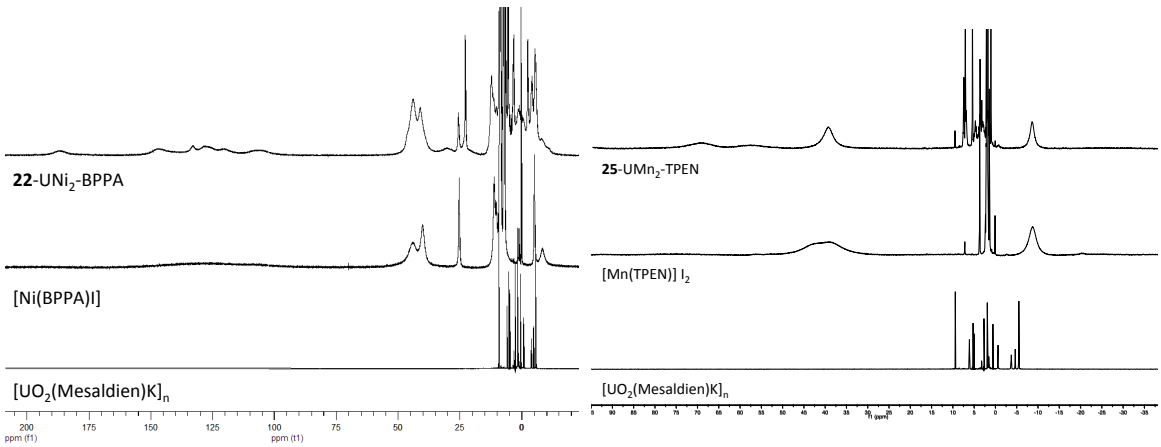

Figure 8 ^{1}H NMR spectra (200MHz, Py-D_5, 298 K) of **22**-UNi_2-BPPA compared to [Ni(BPPA)I] and $[UO_2(Mesaldien)K]_n$ complexes (left) and (400MHz, CD_3CN, 298 K) of **25**-UMn_2-TPEN compared to $[Mn(TPEN)]I_2$ and $[UO_2(Mesaldien)K]_n$ complexes (right).

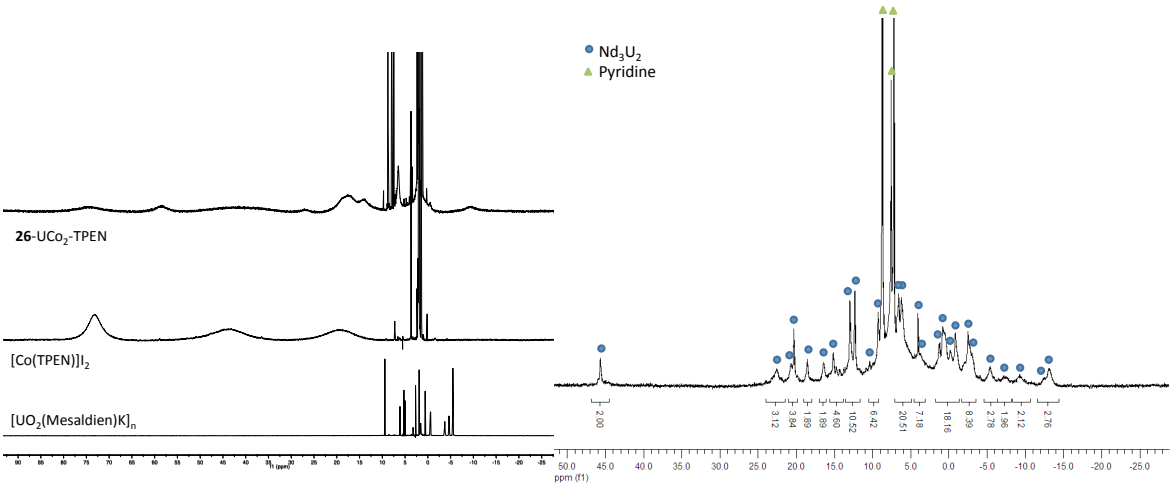

Figure 9 (left) ^{1}H NMR spectra (400 MHz, CD_3CN, 298 K) of **26**-UCo_2-TPEN compared to $[Co(TPEN)]I_2$ and $[UO_2(Mesaldien)K]_n$ complexes. (right) ^{1}H NMR spectrum (200MHz, Py-D_5, 298 K) of complex **27**-U_2Nd_3-TPA.

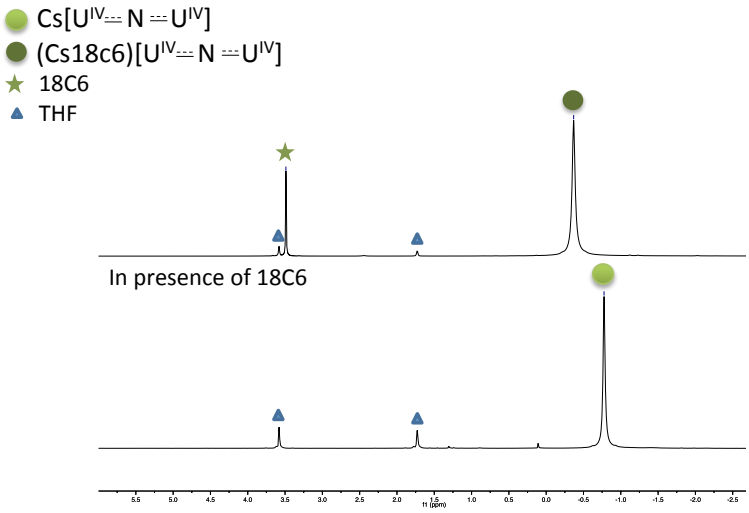

Figure 10 ^{1}H NMR (400MHz, THF-D_8, 298 K) of complex $[Cs\{U(OSi(O^tBu)_3)_3\}_2(\mu\text{-}N)]$ in presence of 18C6.

Diffusion coefficient data

Table 11 Diffusion coefficient values and estimated spherical radii of a mixture of **4** and **5**

MeCN η= 0.343 mPa.s (298 K)	Diffusion coefficient ($m^2.s^{-1}$)	Hydrodynamic radii (Å)	Radii evaluated from crystal structure (Å)
4 and **5**	$9.04\ 10^{-10}$	7.1	8.3

Table 12 Diffusion coefficient values and estimated spherical radii in pyridine

Pyridine η= 0.879 mPa.s (298 K)	Diffusion coefficient ($m^2.s^{-1}$)	Hydrodynamic radii (Å)	Radii evaluated from crystal structure (Å)
1	$3.29\ 10^{-10}$	7.5	8.5
6	$3.09\ 10^{-10}$	8.0	9.2
[UO_2(Mesaldien)]	$6.29\ 10^{-10}$	3.9	3.59
13-UMn_2-TPA-I	$3.33\ 10^{-10}$	7.4	5.71
14-UCd_2-TPA	$3.20\ 10^{-10}$	7.7	5.74

IR spectra

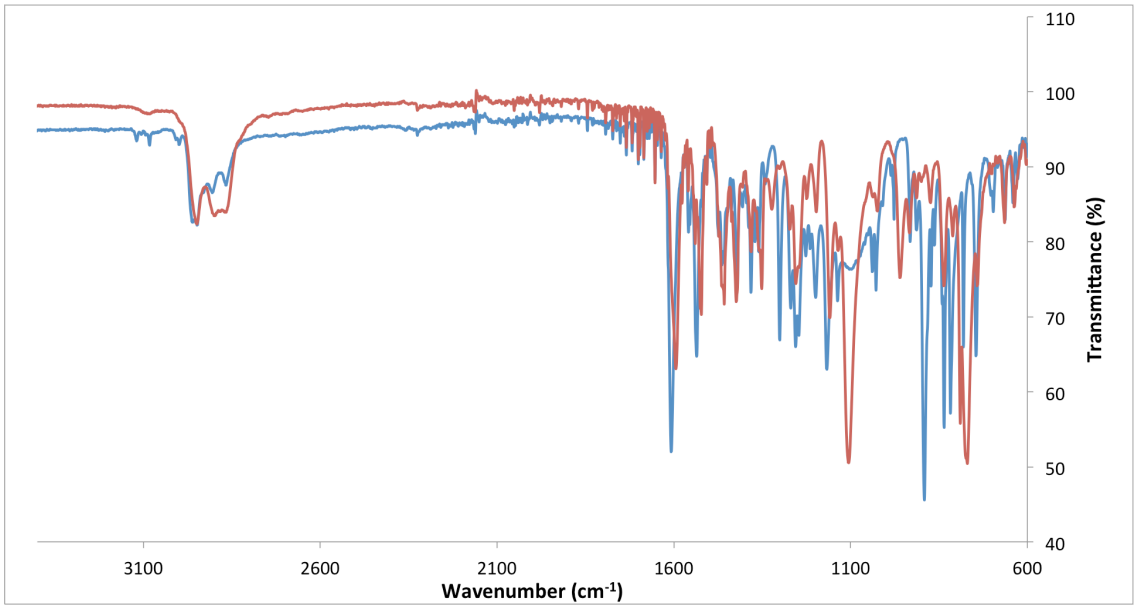

Figure 11 IR Spectra of complexes 29 (blue trace) and 30 (red trace).

Magnetic data

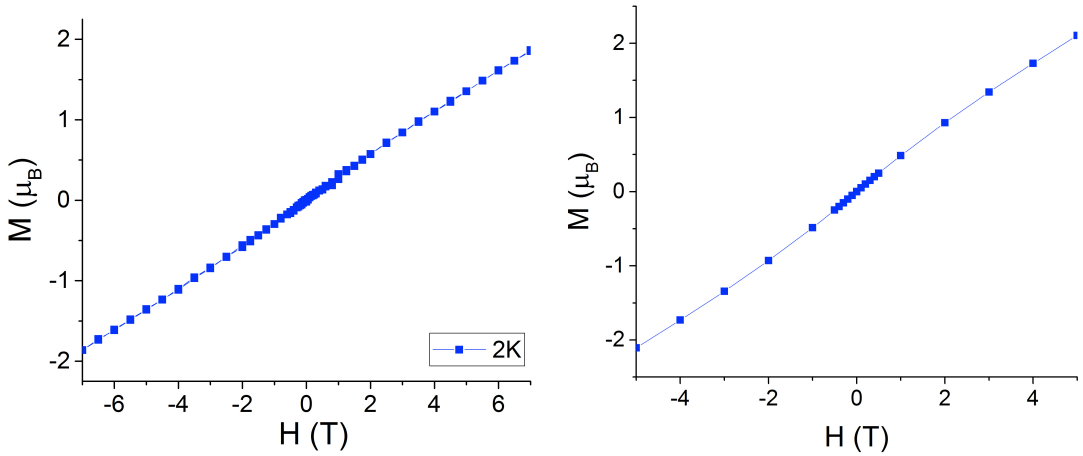

Figure 12 Hysteresis cycles of $[U_{12}(\mu_3\text{-}OH)_8(\mu_3\text{-}O)_{12}I_2(\mu_2\text{-}OTf)_{16}(CH_3CN)_8]$ (left) and of $\{[K(MeCN)]_2[U_{16}O_{22}(OH)_2(PhCOO)_{24}]\}$ (right) recorded at 2 K

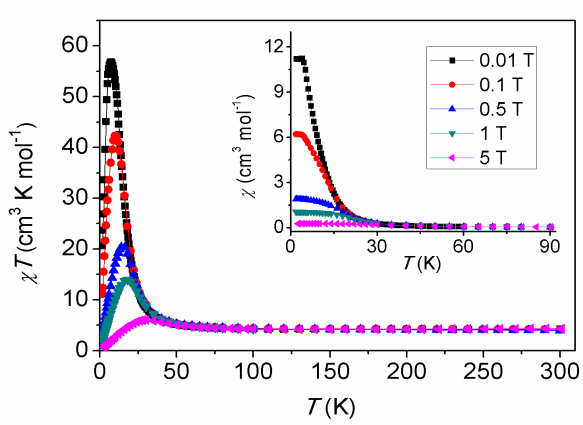

Figure 13 Temperature dependence of χT for **10**-$\{UO_2(salen)Mn\}_n$ measured at five different fields between 0.01 and 5 T. Inset: Temperature dependence of χ for the same fields.

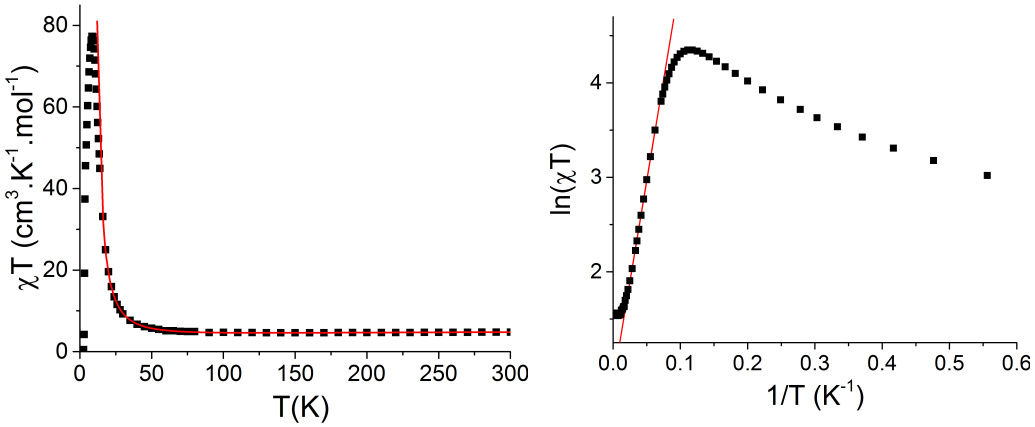

Figure 14 Left: Plots of χT *versus* T and (right) $\ln(\chi T)$ *versus* $1/T$ for a polycrystalline sample of **12**-$\{UO_2(Mesaldien)Mn\}_n$ measured at 0.1 T applied field.

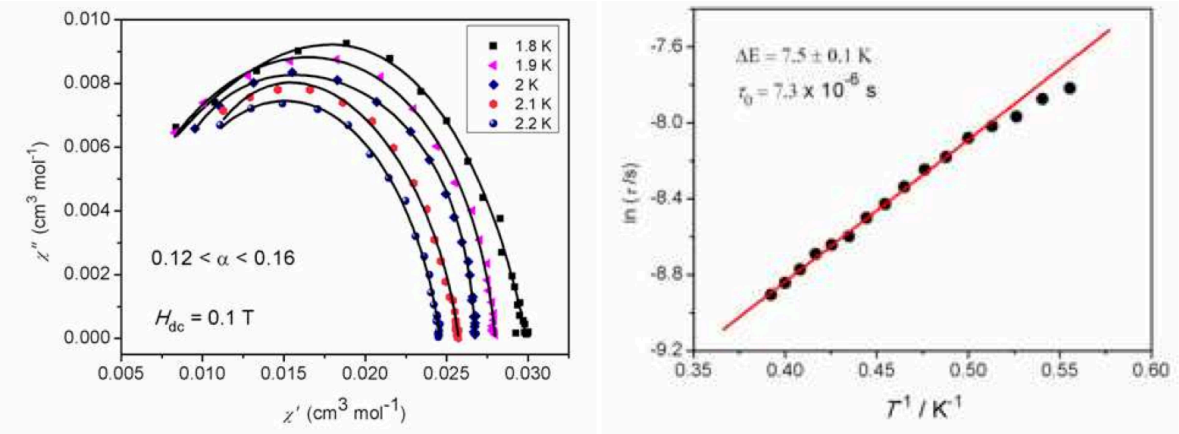

Figure 15 (left) Cole Cole plots for **9**-{UO_2(salen)Cd}$_n$ at temperatures between 1.8 and 2.2 K; (right) Arrhenius plot displaying T-dependence of the relaxation time for **9**-{UO_2(salen)Cd}$_n$

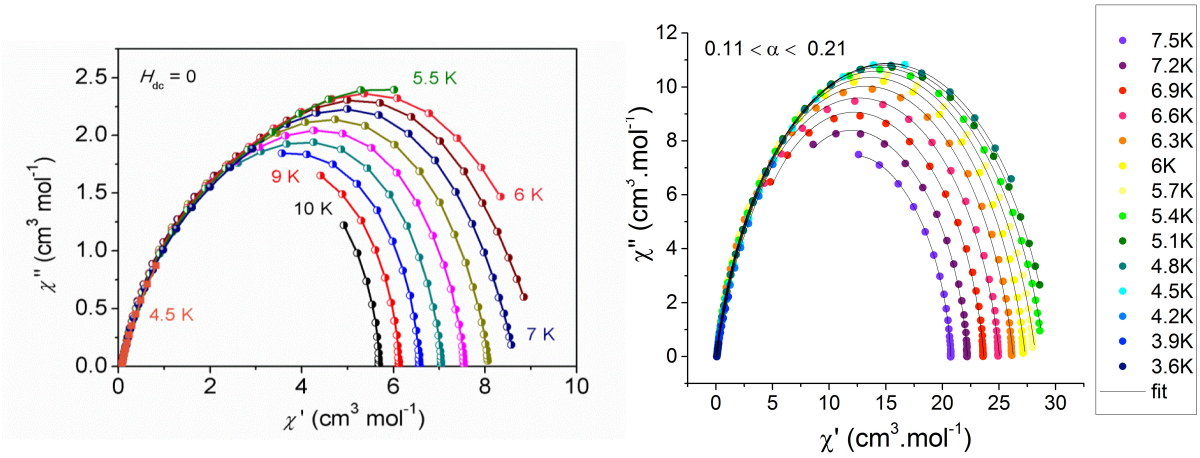

Figure 16 Cole-Cole plots measured at zero-dc field and an ac field of 1.55 G oscillating at frequencies between 0.1 and 1400 Hz for **10**-{UO_2(salen)Mn}$_n$ (left) and for **12**-{UO_2(Mesaldien)Mn}$_n$ (Debye fits represented in straight lines) (right).

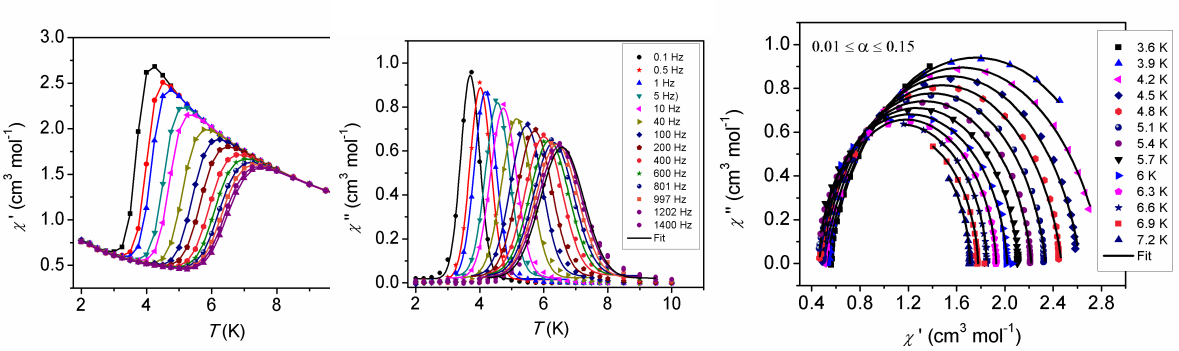

Figure 17 Temperature dependence at zero dc field of the in-phase ac susceptibility (χ') (left), of the out-of-phase ac susceptibility (χ'') (middle) and Cole Cole plots (right) of **13**-UMn_2-TPA-I, recorded with an ac field of 1.55 Oe oscillating at the indicated frequencies. The straight lines represent the Gaussian fits to the experimental data.

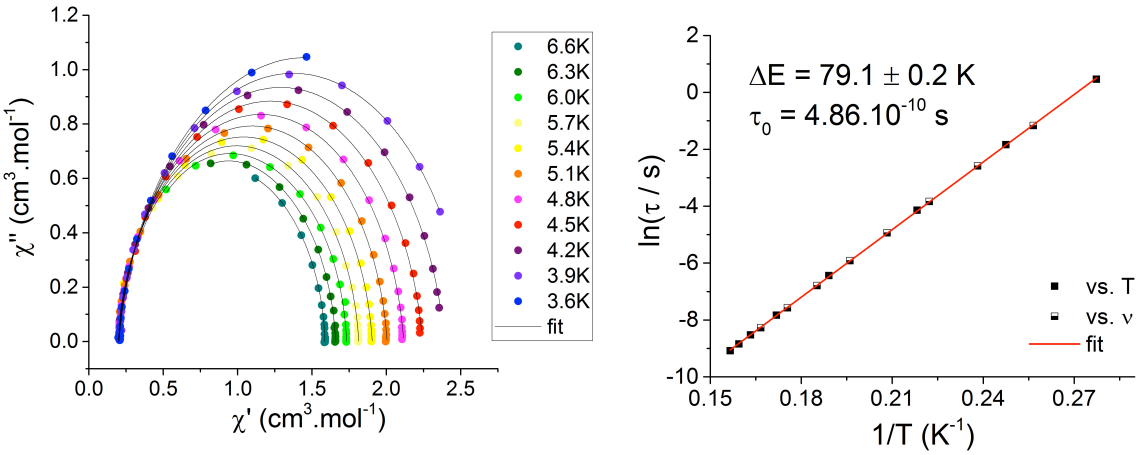

Figure 18 (left) Cole-Cole plots and Debye fits (straight lines) for **15**-UMn_2-TPA-Cl at several temperatures between 3.6 and 6.6 K; (right) Arrhenius plot displaying T-dependence of the relaxation times for **15**-UMn_2-TPA-Cl.

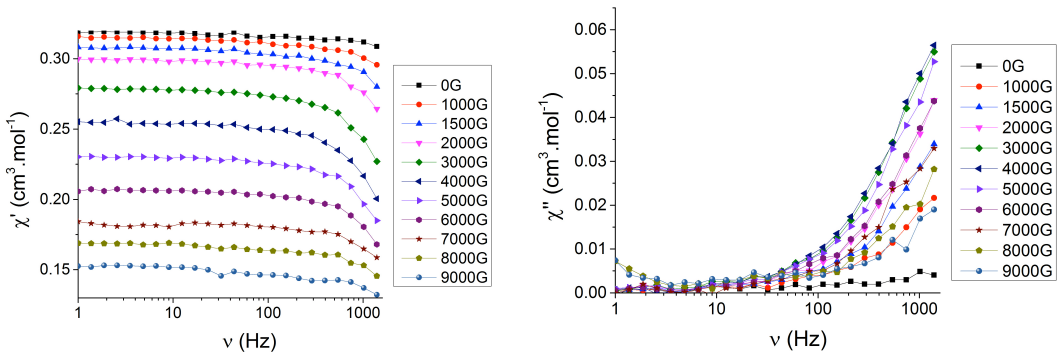

Figure 19 dc field dependence at 1.8 K of the in-phase ac susceptibility (χ') of **17**-UCo-TPA, plotted vs. n (left) and the out-of-phase ac susceptibility of **17**-UCo-TPA plotted vs. n (right) recorded with an ac field of 1.55 Oe oscillating between 0.1 and 1400Hz.

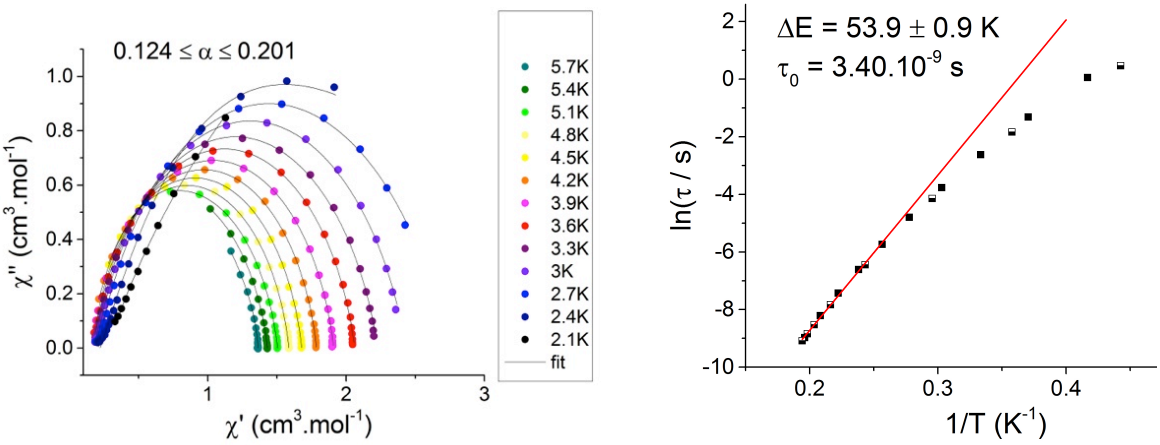

Figure 20 (left) Cole-Cole plots and Debye fits (straight lines) for **16**-UFe_2-TPA at several temperatures between 2.1 and 5.7 K; (right) Arrhenius plot displaying T-dependence of the relaxation times for **16**-UFe_2-TPA.

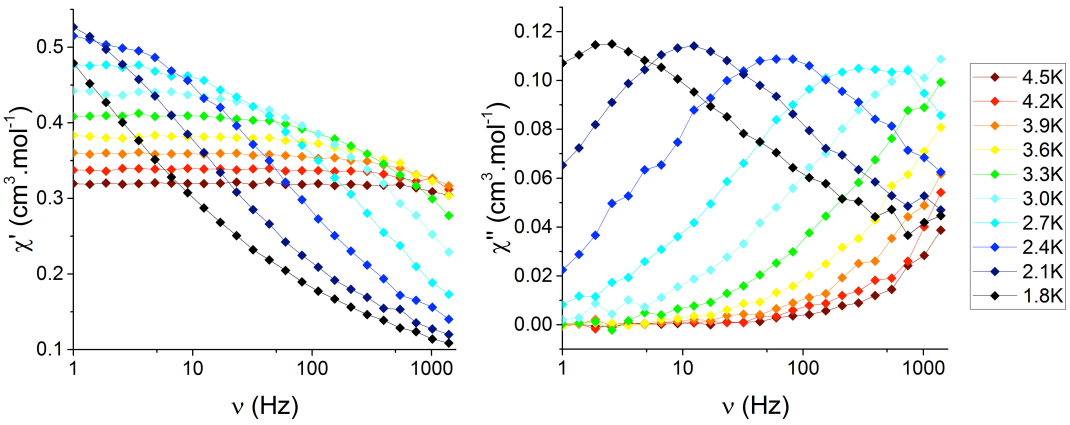

Figure 21 Frequency dependence at 1000G dc field of the (left) in-phase and (right) out-of-phase ac susceptibility components of **18**-UNi$_2$-TPA recorded at several temperatures between 1.8 and 4.5 K with an ac field of 1.55 Oe oscillating at frequencies between 1 and 1400 Hz.

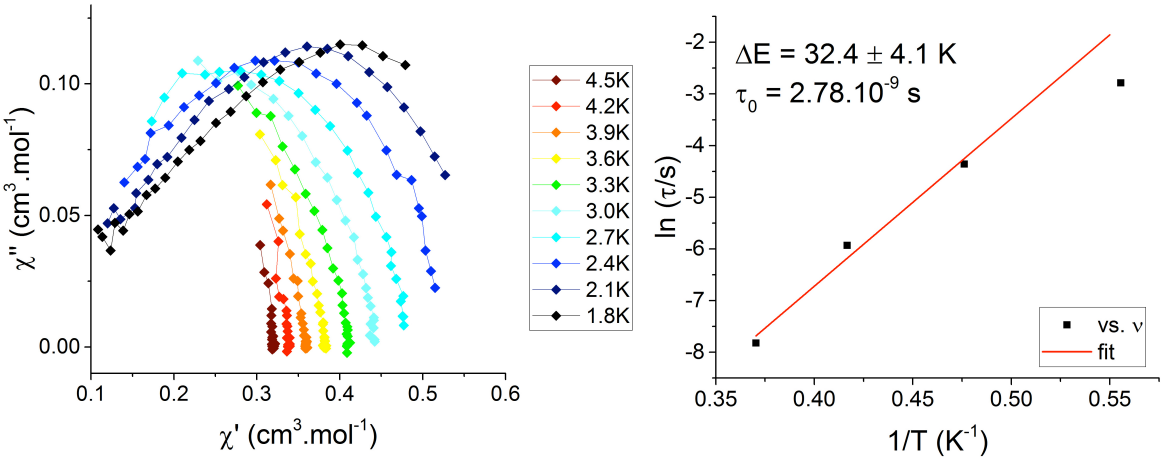

Figure 22 (left) Cole-Cole plots for **18**-UNi$_2$-TPA recorded at several temperatures between 1.8 and 4.5 K under 1000G dc field with an ac field of 1.55 Oe oscillating at frequencies between 1 and 1400 Hz; (right) Arrhenius plot displaying T-dependence of the relaxation times for **18**-UNi$_2$-TPA.

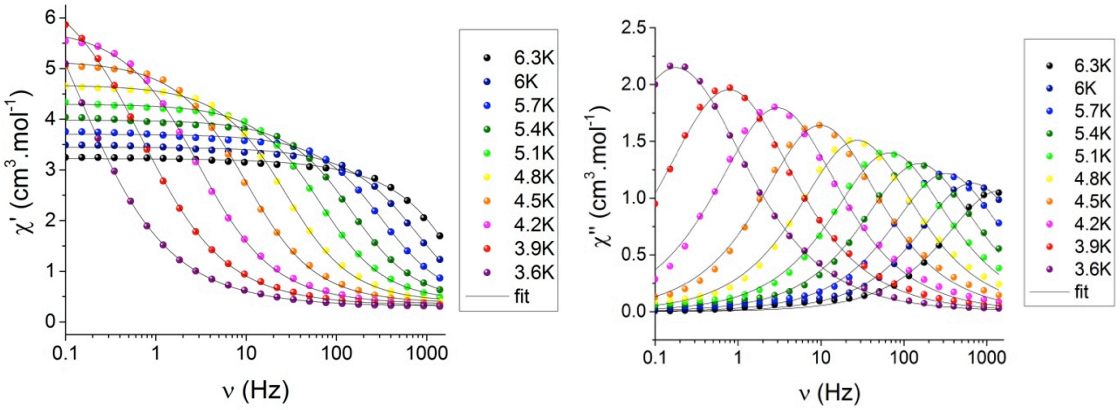

Figure 23 Frequency dependence at zero dc field of the (left) in-phase and (right) out-of-phase ac susceptibility components of **19**-UMn$_2$-BPPA recorded at several temperatures between 3.6 and 6.3 K with and ac field of 1.55 Oe oscillating at frequencies between 0.1 and 1400 Hz. The straight lines represent the Debye fits to the experimental data.

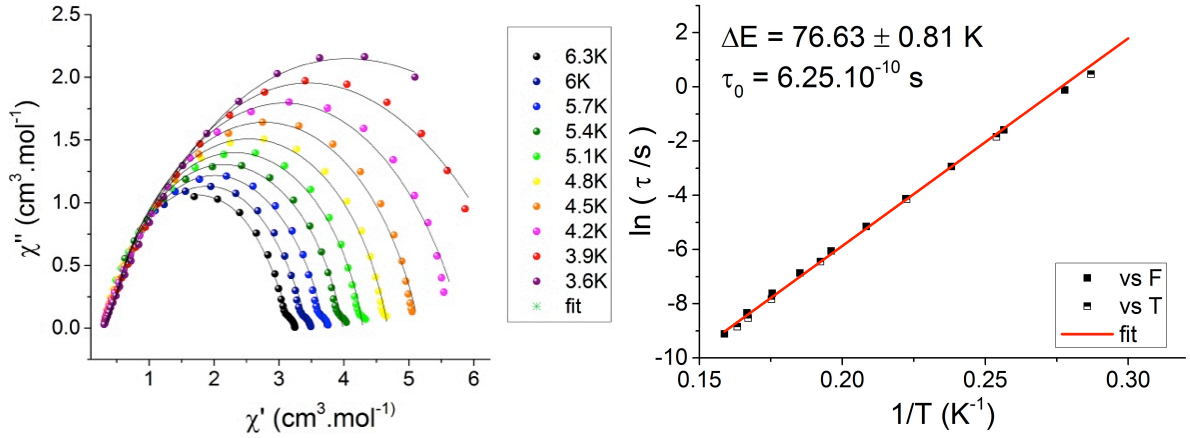

Figure 24 (left) Cole-Cole plots and Debye fits (straight lines) for **19**-UMn_2-BPPA at several temperatures between 3.6 and 6.3 K; (right) Arrhenius plot displaying T-dependence of the relaxation times for **19**-UMn_2-BPPA.

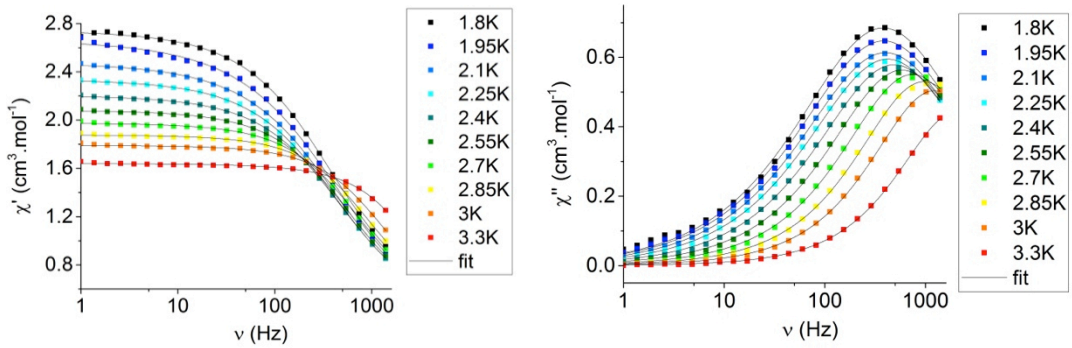

Figure 25 Frequency dependence at zero dc field of the (left) in-phase and (right) out-of-phase ac susceptibility components of **20**-UFe_2-BPPA recorded at several temperatures between 1.8 and 3.3 K with and ac field of 1.55 Oe oscillating at frequencies between 1 and 1400 Hz.

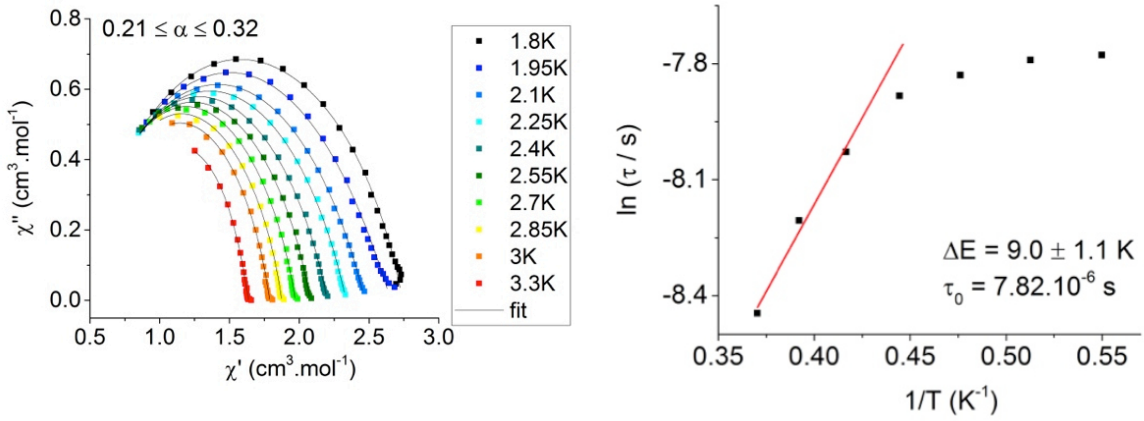

Figure 26 Cole-Cole plots for **20**-UFe_2-BPPA recorded at zero dc field at several temperatures between 1.8 and 3.3 K under zero dc field (left). Arrhenius plot displaying T-dependence of the relaxation times for **20**-UFe_2-BPPA under zero dc field (right).

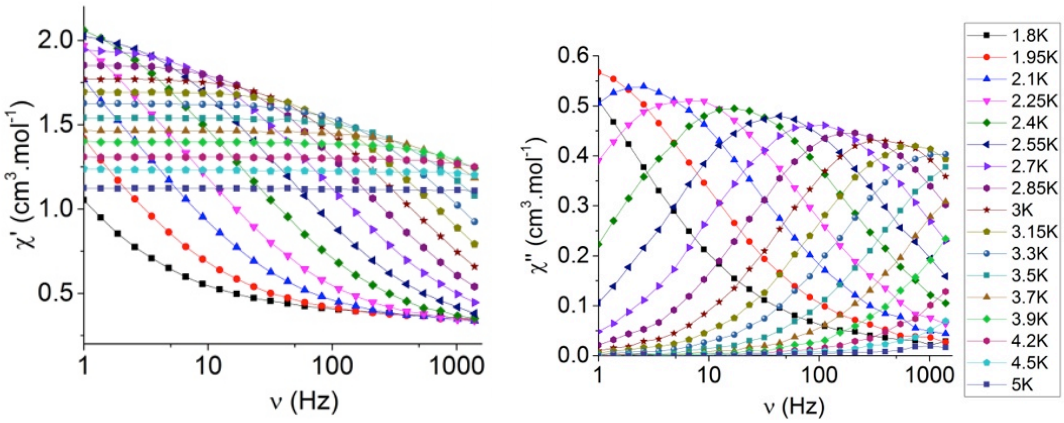

Figure 27 Frequency dependence of the (left) in-phase and (right) out-of-phase ac susceptibility components of **20**-UFe_2-BPPA recorded at several temperatures between 1.8 and 5 K with and ac field of 1.55 Oe oscillating at frequencies between 1 and 1400 Hz under 400G dc field.

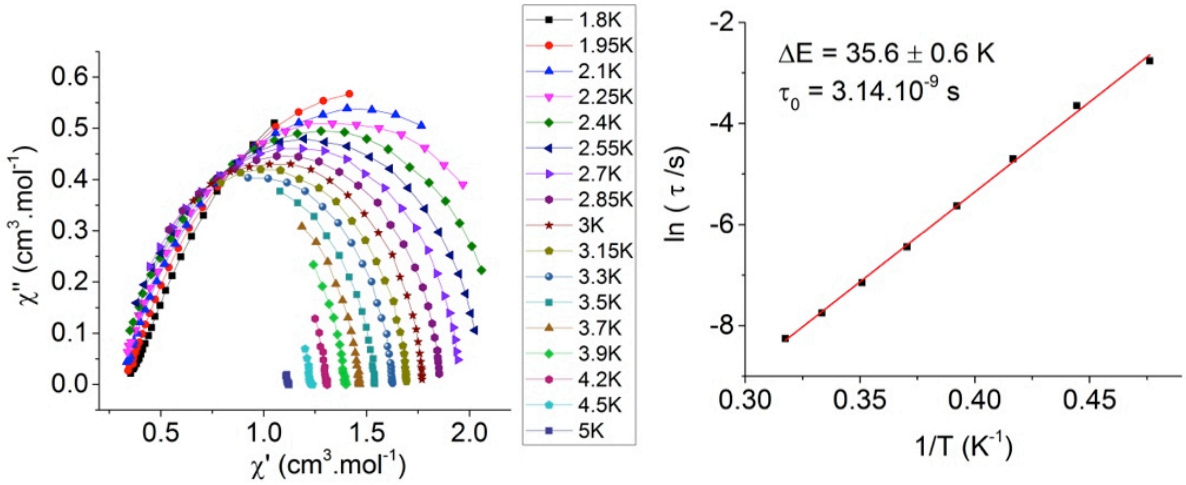

Figure 28 (left) Cole-Cole plots for **20**-UFe_2-BPPA recorded at several temperatures between 1.8 and 5 K under 400G dc field; (right) Arrhenius plot displaying T-dependence of the relaxation times for **20**-UFe_2-BPPA.

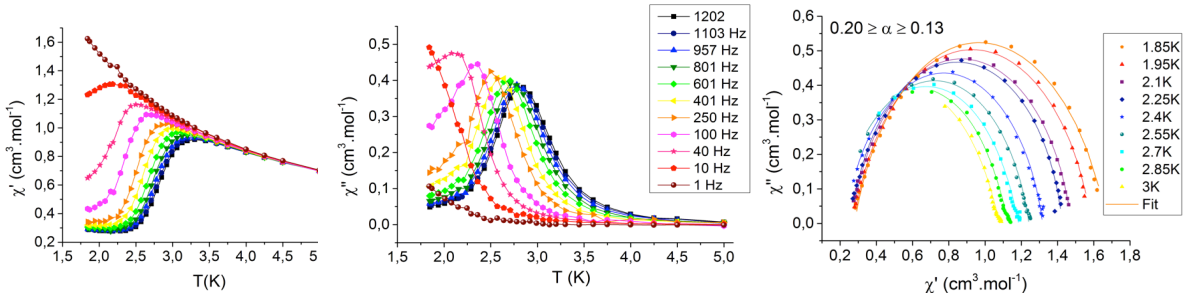

Figure 29 Temperature dependence of the (left) real (χ') and (middle) imaginary (χ'') ac. susceptibility for **21**-UCo_2-BPPA measured under 1500G dc field and 1.55 G ac field. Cole Cole plots of **21**-UCo_2-BPPA recorded at several temperatures between 1.85 and 3 K under 1500G dc field (right).

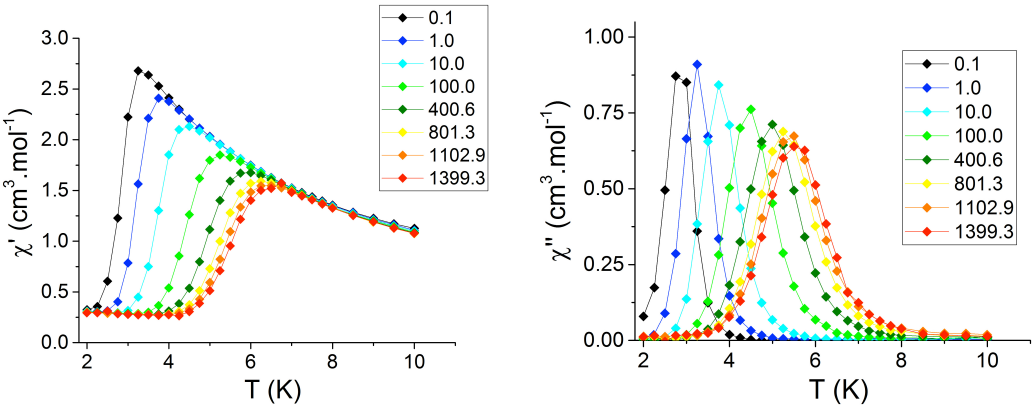

Figure 30 Temperature dependence of the (left) real (χ') and (right) imaginary (χ'') ac. susceptibility for **25**-UMn_2-TPEN measured at zero dc field and 1.55 G ac field.

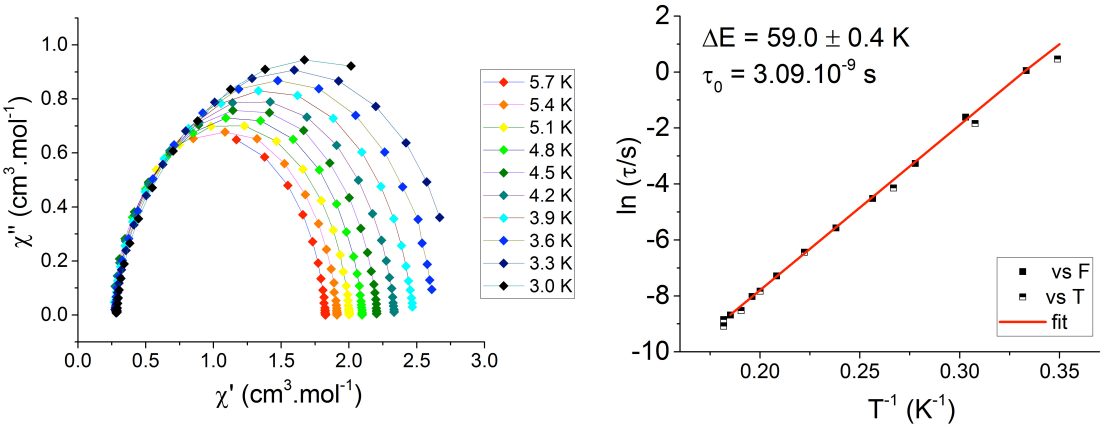

Figure 31 (left) Cole-Cole plots and Debye fits (straight lines) for **25**-UMn_2-TPEN at several temperatures between 3.0 and 5.7 K; (right) Arrhenius plot displaying T-dependence of the relaxation times for **25**-UMn_2-TPEN under zero dc field

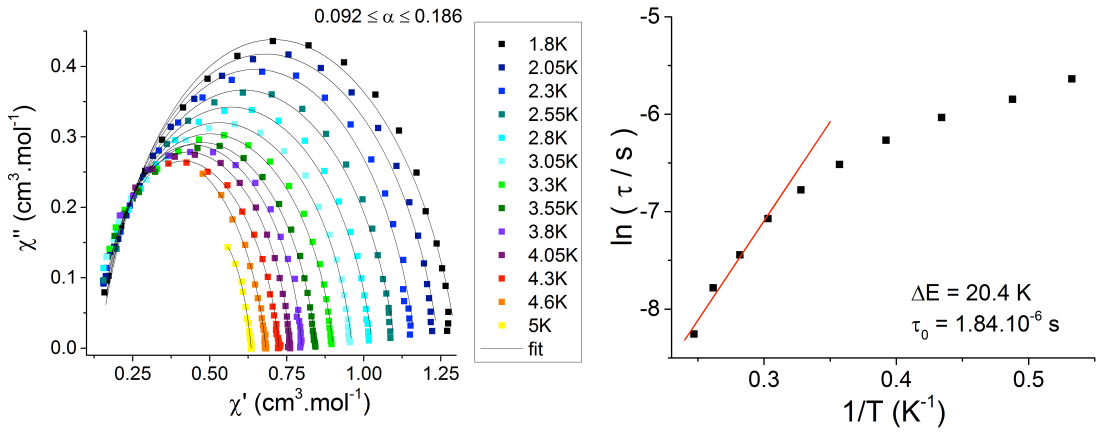

Figure 32 (left) Cole-Cole plots and Debye fits (straight lines) for **26**-UCo_2-TPEN at several temperatures between 1.8 and 5 K; (right) Arrhenius plot displaying T-dependence of the relaxation times for **26**-UCo_2-TPEN under 1500G dc field

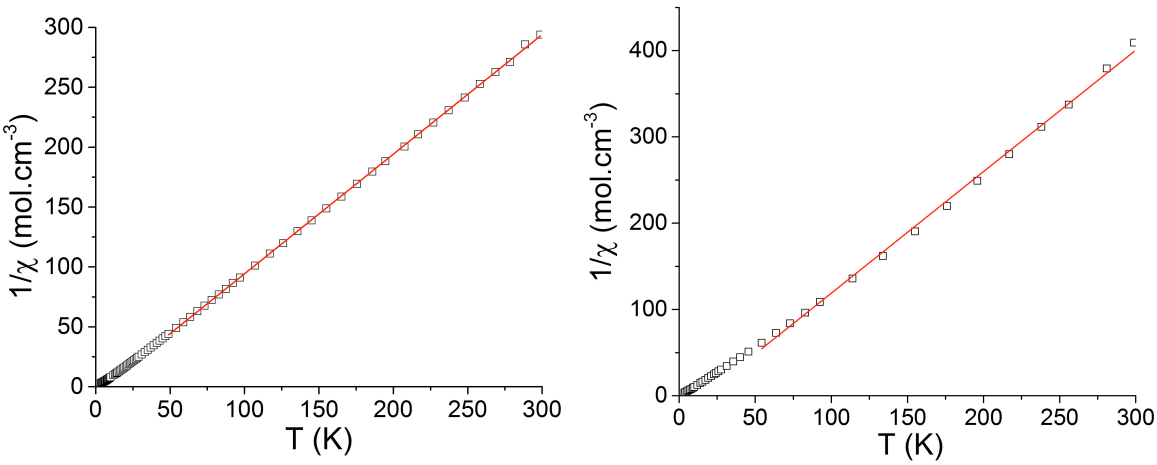

Figure 33 1/χ versus T data under 1T for $[NpO_2L]_3$ **31** (left) and tetramer $[\{NpO_2(salen)\}_4(\mu_8\text{-}K)_2][K(18C6)Py]_2$ (right) plotted per neptunium ion and linear Curie-Weiss fit of the 50-300 K range.

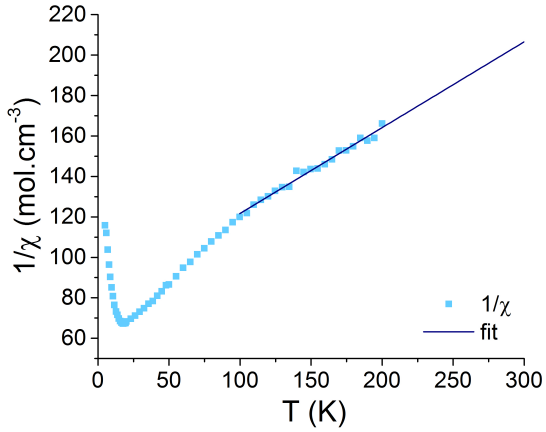

Figure 34 1/χ versus T data under 1T for **36**-$K_3[U^{III}\text{---}N\text{---}U^{III}]$ plotted per uranium ion and linear Curie-Weiss fit of the 100-300 K range.

Mass spectrometry

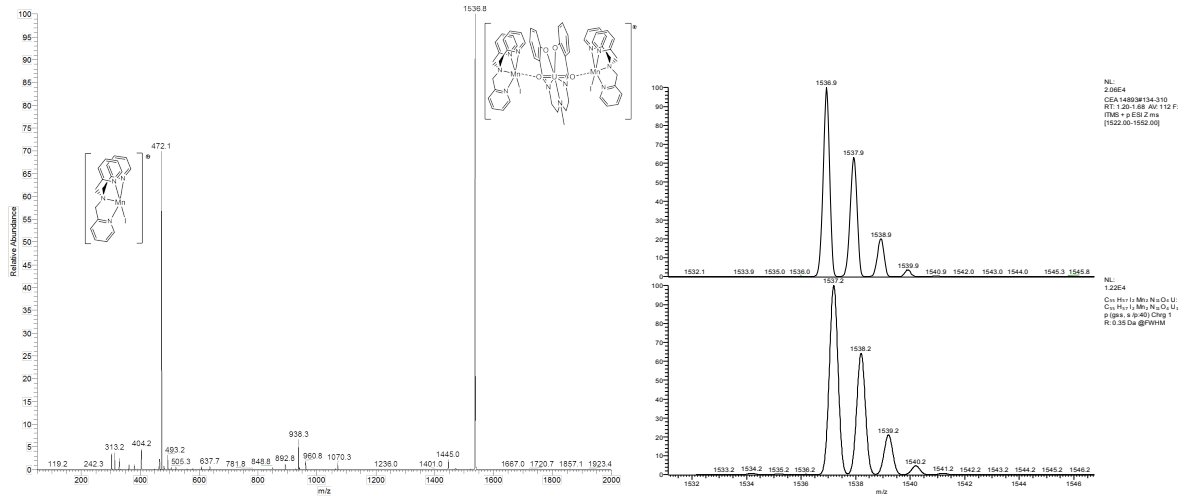

Figure 35 ESI/MS spectra of **13**-UMn_2-TPA-I in acetonitrile (left) and zoom on the molecular peak (top) compared with the theoretical isotopic (bottom) profile calculated for {[Mn(TPA)I][UO_2(Mesaldien)][Mn(TPA)I]}$^+$(right).

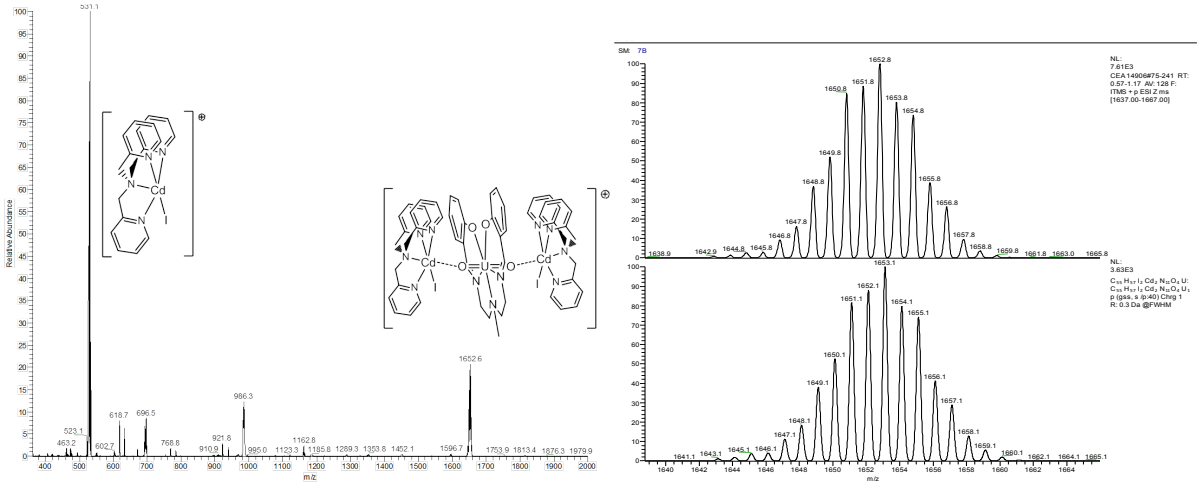

Figure 36 ESI/MS spectra of **14**-UCd_2-TPA in acetonitrile (left) and zoom on the molecular peak (top) compared with the theoretical isotopic (bottom) profile calculated for {[Cd(TPA)I][UO_2(Mesaldien)][Cd(TPA)I]}$^+$ (right).

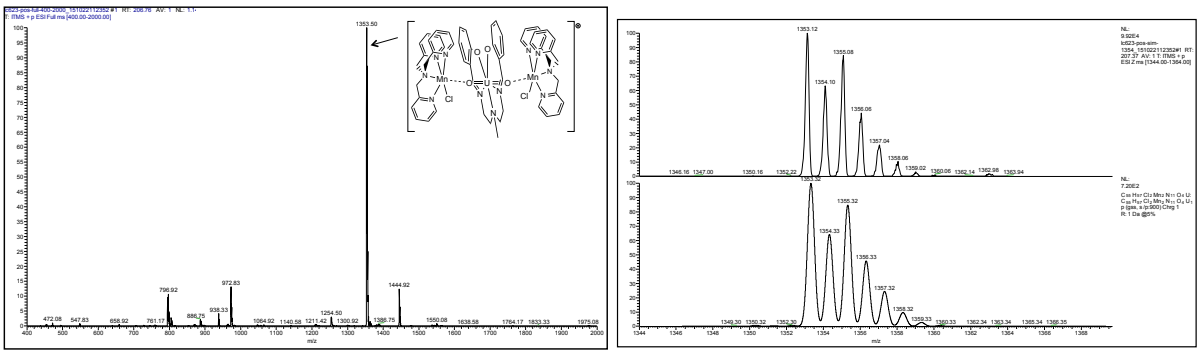

Figure 37 ESI/MS spectra of **15**-UMn_2-TPA-Cl in acetonitrile (top) and zoom on the molecular peak (middle) compared with the theoretical isotopic (bottom) profile calculated for {[Mn(TPA)Cl][UO_2(Mesaldien)][Mn(TPA)Cl]}$^+$.

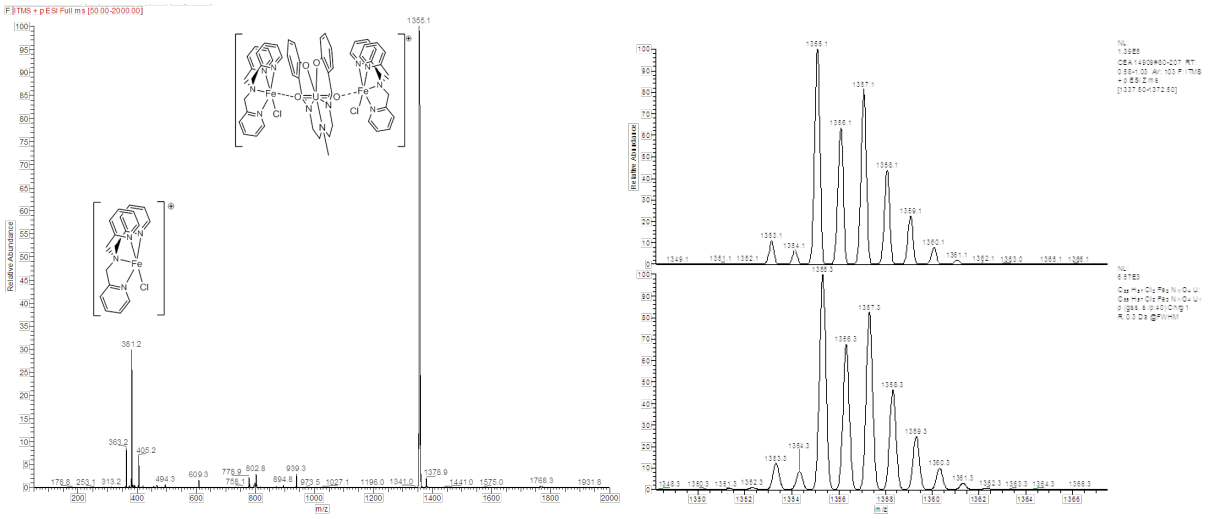

Figure 38 ESI/MS spectra of **16**-UFe_2-TPA in acetonitrile (left) and zoom on the molecular peak (top) compared with the theoretical isotopic (bottom) profile calculated for {[Fe(TPA)Cl][UO_2(Mesaldien)][Fe(TPA)Cl]}$^+$(right).

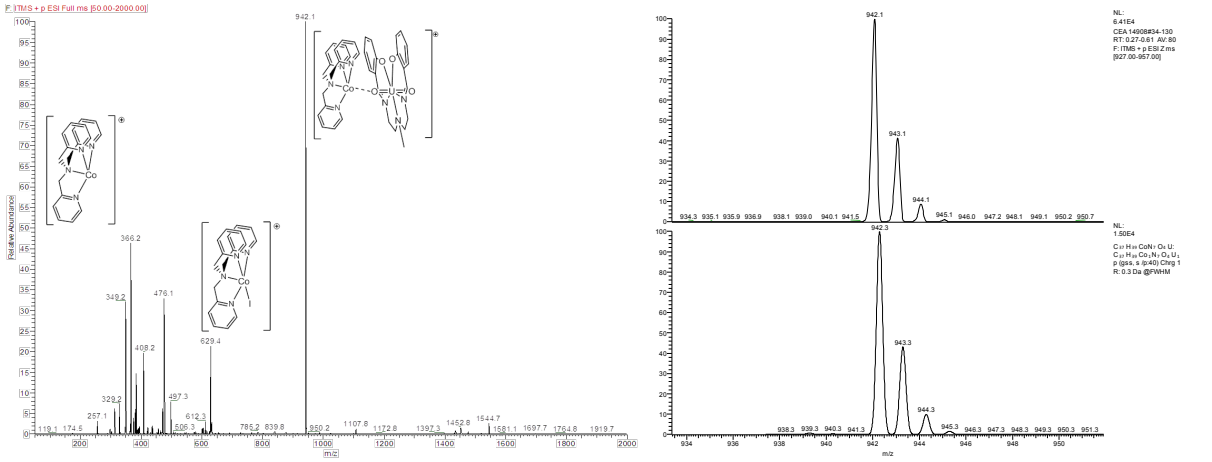

Figure 39 ESI/MS spectra of **17**-UCo-TPA in acetonitrile (top) and zoom on the molecular peak (middle) compared with the theoretical isotopic (bottom) profile calculated for {[Co(TPA)I][UO_2(Mesaldien)]}$^+$.

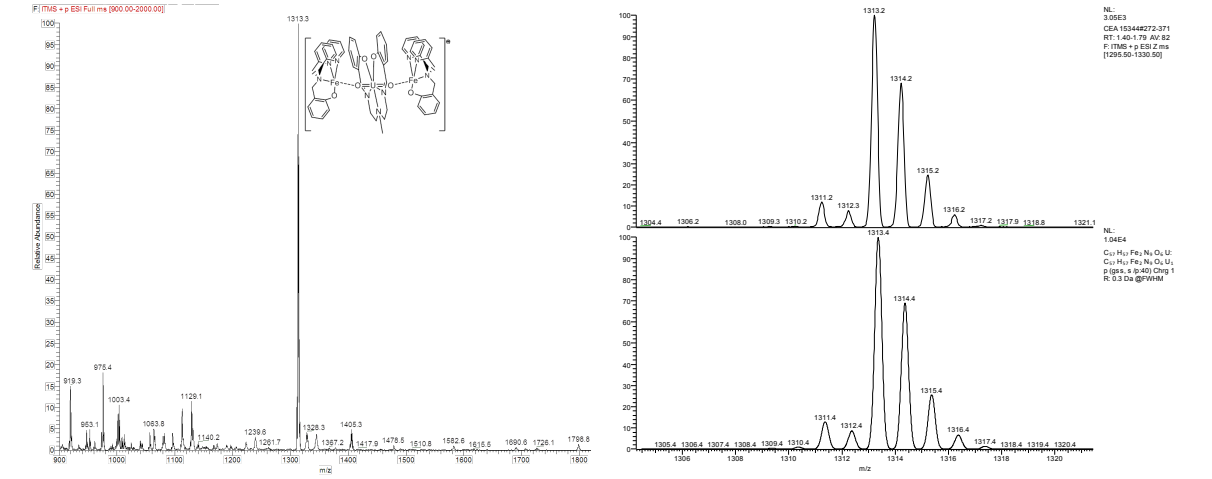

Figure 40 ESI/MS spectra of **20**-UFe_2-BPPA in acetonitrile (left) and zoom on the molecular peak (top) compared with the theoretical isotopic (bottom) profile calculated for {[Fe(BPPA)][UO_2(Mesaldien)][Fe(BPPA)]}$^+$ (right).

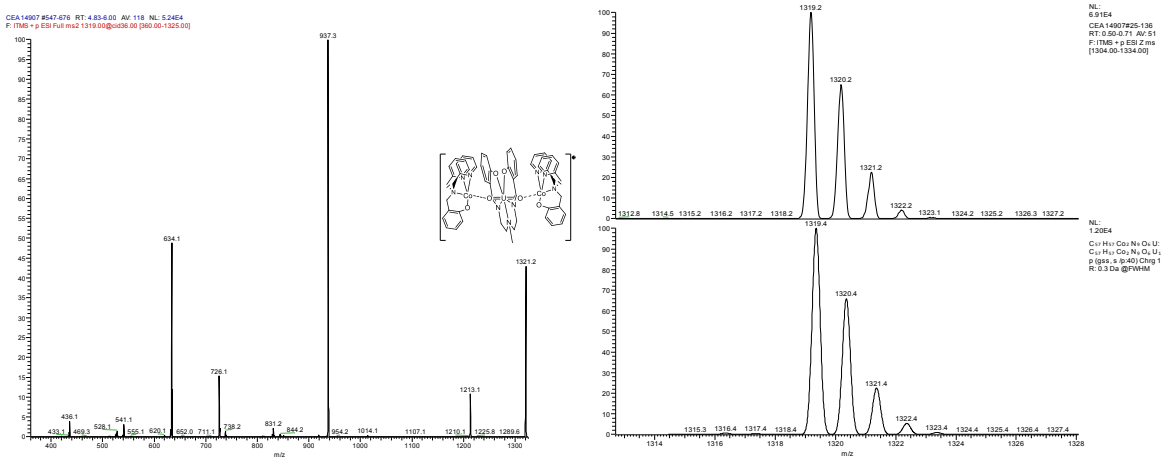

Figure 41 ESI/MS spectra of **21**-UCo_2-BPPA in acetonitrile (left) and zoom on the molecular peak (top) compared with the theoretical isotopic (bottom) profile calculated for $\{[Co(BBPA)][UO_2(Mesaldien)][Co(BBPA)]\}^+$ (right)

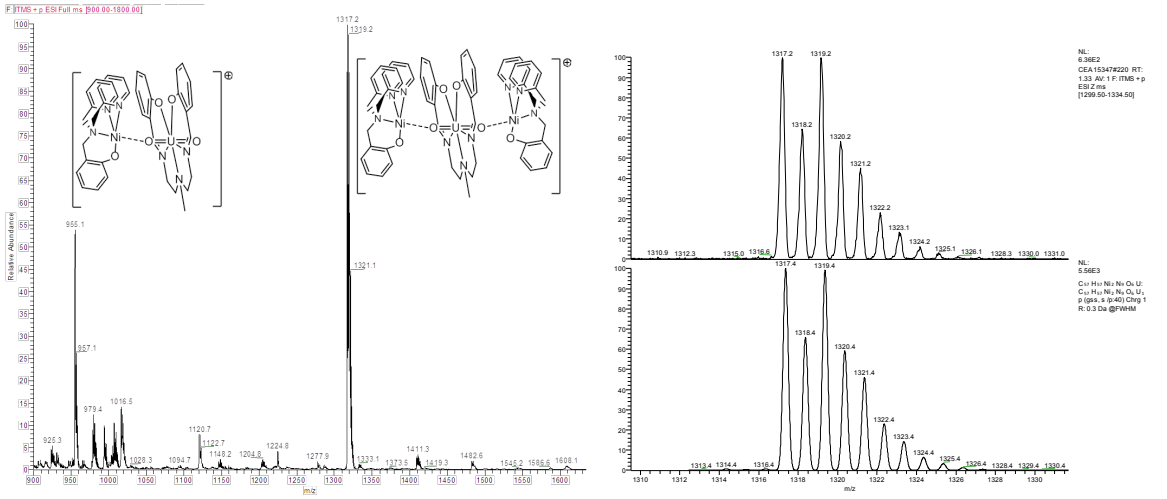

Figure 42 ESI/MS spectra of **22**-UNi_2-BPPA in acetonitrile (left) and zoom on the molecular peak (top) compared with the theoretical isotopic (bottom) profile calculated for $\{[Ni(BPPA)][UO_2(Mesaldien)][Ni\ (BPPA)]\}^+$ (right)

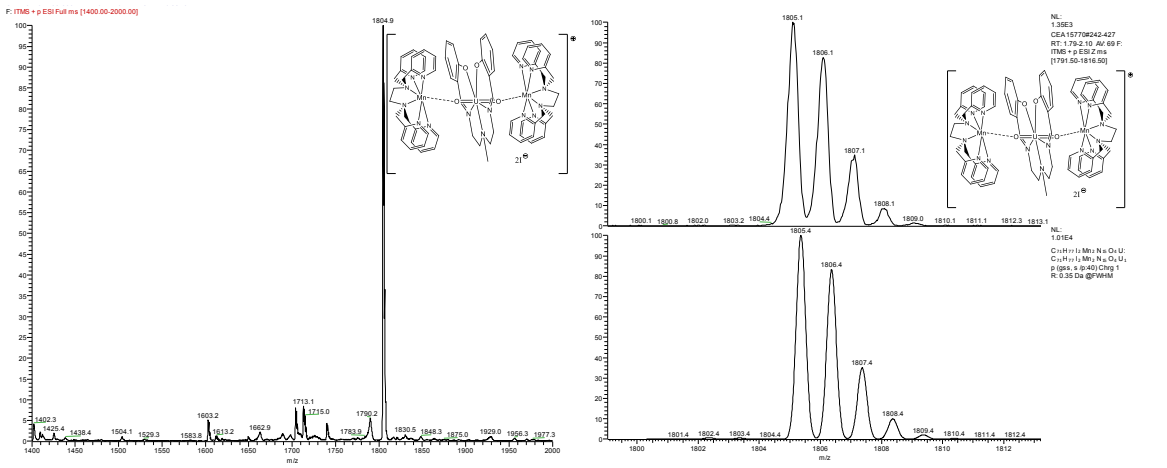

Figure 43 ESI/MS spectra of **25**-UMn_2-TPEN in acetonitrile (left) and zoom on the molecular peak (top) compared with the theoretical isotopic (bottom) profile calculated for $\{[Mn(TPEN)][UO_2(Mesaldien)][Mn(TPEN)]I_2\}^+$ (right).

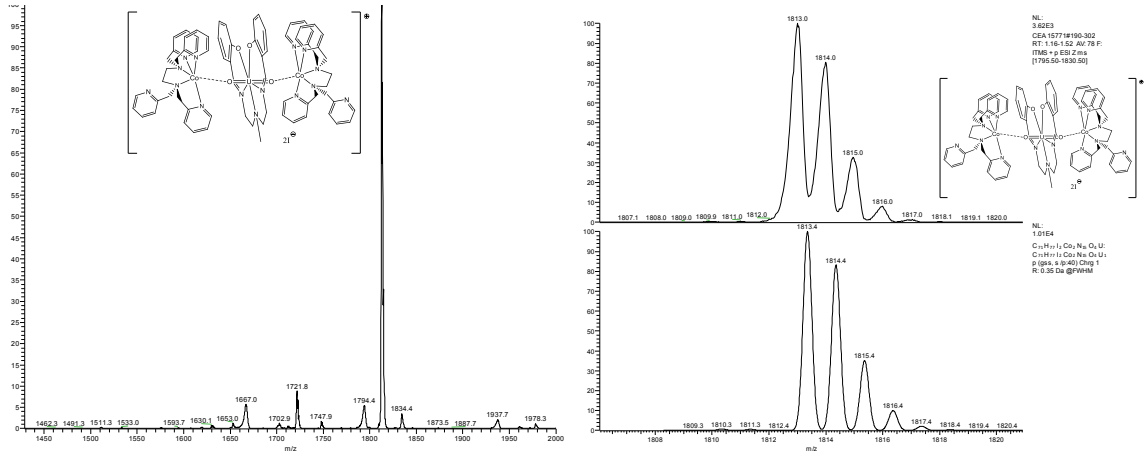

Figure 44 ESI/MS spectra of **26**-UCo_2-TPEN in acetonitrile (left) and zoom on the molecular peak (top) compared with the theoretical isotopic (bottom) profile calculated for $\{[Co(TPEN)][UO_2(Mesaldien)][Co(TPEN)]I_2\}^+$ (right).

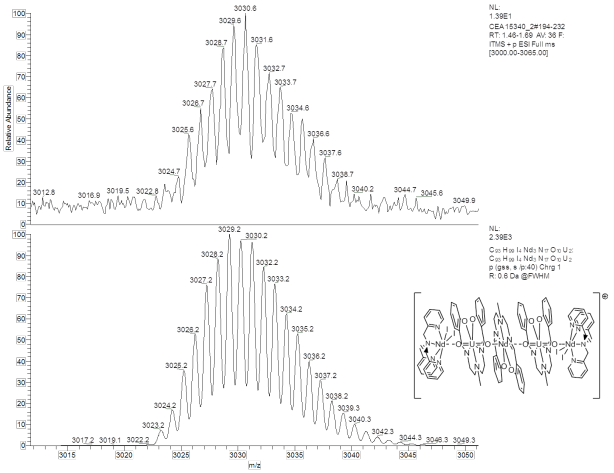

Figure 45 ESI/MS spectra of **27**-U_2Nd_3-TPA in acetonitrile : zoom on the molecular peak (top) compared with the theoretical isotopic (bottom) profile calculated for $\{[Nd(TPA)I_2][UO_2(Mesaldien)][Nd(Mesaldien)][UO_2(Mesaldien)][Nd(TPA)I_2]\}^+$.

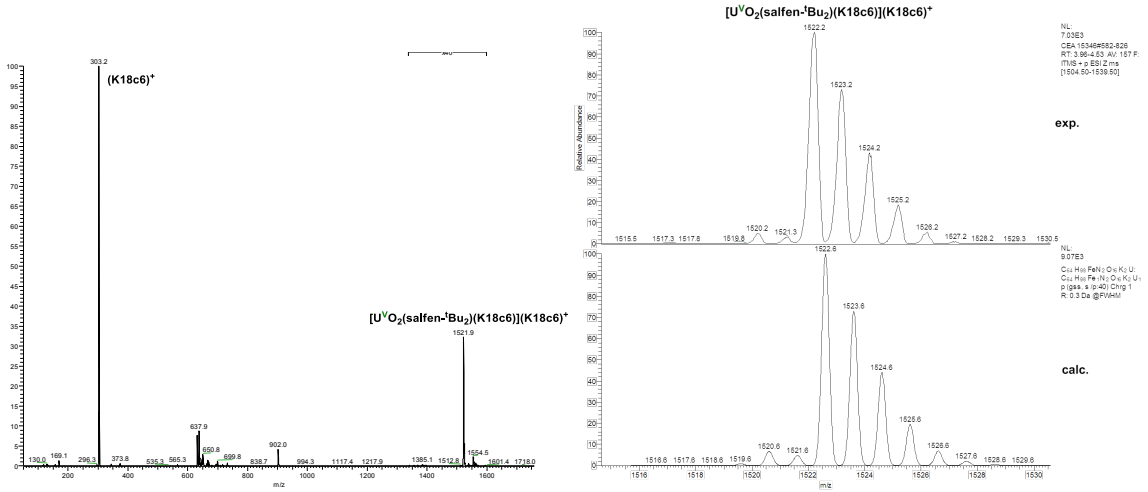

Figure 46 ESI/MS spectra of **30** in acetonitrile/pyridine (90/10) (left) and zoom on the molecular peak (top) compared with the theoretical isotopic (bottom) profile calculated for $[UO_2(salfen\text{-}^tBu_2)(K18c6)](K18c6)^+$.

List of compounds

$[U_6O_4(OH)_4(PhCOO)_{12}(Py)_3]$	**1**
$[U_{16}O_{15}(OH)_8(PhCOO)_{26}(Py)_2]$	**2**
$[U_{10}O_8(OH)_6(PhCOO)_{12.82}I_{3.18}(H_2O)_4(MeCN)_3]I_2$	**3**
$[U_{13}K_4O_{12}(OH)_4(PhCOO)_{12}Cl_{14}]Cl_2$	**4**
$[U_{13}K_2O_9(OH)_7(PhCOO)_{12}Cl_{16}]Cl$	**5**
$[U_6O_4(PhCOO)_{16}(Py)_4]$	**6**
$[U_{38}O_{56}Cl_{18}(PhCOO)_{22}(CH_3CONH_2)_{10}]$	**7**
$[UO_2K_2Cl_4(MeCN)_2]$	**8**
$\{[UO_2(salen)(Py)][Cd(Py)_4](NO_3)\}_n$	**9**-$\{UO_2(salen)Cd\}_n$
$\{[UO_2(salen)(Py)][Mn(Py)_4](NO_3)\}_n$	**10**-$\{UO_2(salen)Mn\}_n$
$[UO_2(Mesaldien)][Cp^*_2Co]$	**11**
$\{[UO_2(Mesaldien)][Mn(NO_3)(Py)_2]\}_n$	**12**-$\{UO_2(Mesaldien)Mn\}_n$
$[\{[Mn(TPA)I][UO_2(Mesaldien)][Mn(TPA)I]\}I]$	**13**-UMn_2-TPA-I
$[\{[Cd(TPA)I][UO_2(Mesaldien)][Cd(TPA)I]\}I]$	**14**-UCd_2-TPA
$[\{[Mn(TPA)Cl][UO_2(Mesaldien)][Mn(TPA)Cl]\}I]$	**15**-UMn_2-TPA-Cl
$[\{[Fe(TPA)Cl][UO_2(Mesaldien)][Fe(TPA)Cl]\}I]$	**16**-UFe_2-TPA
$[\{[Co(TPA)][UO_2(Mesaldien)]\}I]$	**17**-UCo-TPA
$[\{[Ni(TPA)(MeCN)][UO_2(Mesaldien)][Ni(TPA)(MeCN)]\}I_2]$	**18**-UNi_2-TPA
$[\{[Ni(TPA)(MeCN)][UO_2(Mesaldien)][Ni(TPA)(MeCN)]\}I_3]$	
$[\{[Mn(BPPA)(Py)][UO_2(Mesaldien)][Mn(BPPA)(Py)]\}I]$	**19**-UMn_2-BPPA
$[\{[Fe(BPPA)(Py)][UO_2(Mesaldien)][Fe(BPPA)]\}I]$	**20**-UFe_2-BPPA
$[\{[Co(BPPA)(Py)][UO_2(Mesaldien)][Co(BPPA)]\}I]$	**21**-UCo_2-BPPA
$[\{[Ni(BPPA)(Py)][UO_2(Mesaldien)][Ni(BPPA)(Py)]\}I]$	**22**-UNi_2-BPPA
$[\{Cr(BPPA)(\mu\text{-}O)\}_4Cr].2I$	**23**
$\{[UO_2(Mesaldien)][Zn(BPPA)]\}$	**24**
$[\{[Mn(TPEN)][UO_2(Mesaldien)][Mn(TPEN)]\}I_3]$	**25**-UMn_2-TPEN
$[\{[Co(TPEN)][UO_2(Mesaldien)][Co(TPEN)]\}I_3]$	**26**-UCo_2-TPEN
$\{[Nd(TPA)(Py)I_2][UO_2(Mesaldien)][Nd(Mesaldien)]$	**27**-U_2Nd_3-TPA
$[UO_2(Mesaldien)][Nd(TPA)(Py)I_2]\}I$	
$\{[Eu(TPEN)I][UO_2(Mesaldien)][Eu(TPEN)I]\}I$	**28**-UEu_2-TPEN
$[UO_2(salfen\text{-}^tBu_2)]$	**29**
$[UO_2(salfen\text{-}^tBu_2)(K18c6)]$	**30**
$[NpO_2L]_3$	**31**
$[Cs_2\{U(OSi(O^tBu)_3)_3\}_2(\mu\text{-}N)]$	**32**-$Cs_2[U^{III}\text{---}N\text{---}U^{IV}]$
$[Cs_3\{U(OSi(O^tBu)_3)_3\}_2(\mu\text{-}N)]$	**33**-$Cs_3[U^{III}\text{---}N\text{---}U^{III}]$
$[K\{U(OSi(O^tBu)_3)_3\}_2(\mu\text{-}N)]$	**34**-$K[U^{IV}\text{---}N\text{---}U^{IV}]$
$[K_2\{U(OSi(O^tBu)_3)_3\}_2(\mu\text{-}N)(\mu\text{-}N_3)]$	**35**
$[K_3\{U(OSi(O^tBu)_3)_3\}_2(\mu\text{-}N)]$	**36**-$K_3[U^{III}\text{---}N\text{---}U^{III}]$
$[K_2\{U(OSi(O^tBu)_3)_3\}_2(\mu\text{-}N)]$	**37**-$K_2[U^{III}\text{---}N\text{---}U^{IV}]$
$[K\{U(OSi(O^tBu)_3)_3\}(\mu\text{-}N)]_2$	**38**

List of abbreviations

ac	alternating current
acac	acetylacetonate
acacen	N,N'-ethylene-bis(acetylacetoneimine)
Ad	adamantly
An	actinide
bipy	bipyridine
Bu	butyl
Bz	CH_2Ph
CC	cation-cation
Cp	cyclopentadienyl
Cp*	pentamethylcyclopentadienyl
d	doublet
dc	direct current
DFT	density functional theory
DIPE	diisopropylether
DME	dimetoxyethane
dmf	dimethylformamide
dmso	dimethylsulfoxide
equiv	equivalents
ESI-MS	electro-spray ionization mass spectrometry
Et	ethyl
Fc	ferrocene
hfac	1,1,1,5,5,5-Hexafluoro-2,4-pentanedione
Hz	hertz
IR	infrared
^{i}Pr	isopropyl
Ln	lanthanide
m	multiplet
Me	methyl
Mes	mesityl (1,3,5-trimethylbenzyl)
$MesaldienH_2$	N,N'-(2-aminomethyl)diethylenebis(salicylideneimine)
NMR	nuclear magnetic resonance
OTf	triflate : $CF_3SO_3^-$
Ph	phenyl
ppm	parts per million
Py	pyridine
RT	room temperature
s	singlet
saldien	N,N'-disalicylidenediethylenetriaminate
salen	N,N'-bis(salicyldiene)-ethylenediamine
salophen	N,N'-bis(salicyldiene)-*o*-phenylenediamine
salophen-$^{t}Bu_2H_2$	N,N'-phenylene-bis-(3,5-di-tert-butylsalicylideneimine
SCM	single chain magnet
SIM	single ion magnet
SMM	single molecule magnet
SQUID	superconducting quantum interference device
t	triplet
tacn	triazacyclononane
^{t}Bu	tertiobutyl
THF	tetrahydrofuran
TIP	temperature independent paramagnetism
TMEDA	tetramethylethylenediamine
TMS	trimethylsilyl
UV	ultra-violet
Vis	visible
vs	versus

List of publications

11/ M. Falcone, L. Chatelain, M. Mazzanti « Nucleophilic Reactivity of a Nitride-Bridged Diuranium(IV) Complex : CO_2 and CS_2 Functionalization » *Angew. Chem. Int. Ed.* **2016**, *55*, 4074-4078 + front cover

10/ L. Chatelain, R. Scopelliti, M. Mazzanti « Synthesis and Structure of Nitride-Bridged Uranium(III) Complexes » *J. Am. Chem. Soc.* **2016**, *138*, 1784-1787.

9/ L. Chatelain, J. Pécaut, F. Tuna, M. Mazzanti « Heterometallic Fe_2^{II}–U^{V} and Ni_2^{II}–U^{V} Exchange-coupled Single-Molecule Magnets: Effect of the 3d Ion on the Magnetic Properties » *Chem. .Eur. J.* **2015**, *21*, 18038-18042.

8/ C. Camp, L. Chatelain, V. Mougel, J. Pécaut, M. Mazzanti « Ferrocene-Based Tetradentate Schiff Bases as Supporting Ligands in Uranium Chemistry » *Inorg. Chem.* **2015**, *54*, 5774-5783.

7/ C. Camp, L. Chatelain, C. Kefalidis, J. Pécaut, L. Maron, M. Mazzanti « CO_2 conversion to isocyanate *via* multiple N–Si bond cleavage at a bulky uranium (III) complex » *Chem. Commun.* **2015**, *51*, 15454-15457.

6/ L. Chatelain, F. Tuna, J. Pécaut, M. Mazzanti « A zig-zag uranyl(V)–Mn(II) single chain magnet with a high relaxation barrier » *Chem. Commun.* **2015**, *51*, 11309-11312.

5/ L. Chatelain, J. Walsh, J. Pécaut, F. Tuna, M. Mazzanti « Self-Assembly of a 3d–5f Trinuclear Single-Molecule Magnet from a Pentavalent Uranyl Complex » *Angew. Chem. Int. Ed.* **2014**, *53*, 13434-13438 + inside back cover

4/ L. Pereira, C. Camp, J. Coutinho, L. Chatelain, P. Maldivi, M. Almeida, M. Mazzanti « Single-Molecule-Magnet Behavior in Mononuclear Homoleptic Tetrahedral Uranium (III) Complexes » *Inorg. Chem.* **2014**, *53*, 11809−11811; 13258-13258.

3/ V. Mougel, L. Chatelain, J. Hermle, R. Caciuffo, E. Colineau, F. Tuna, N. Magnani, A. Degeyer, J. Pécaut, M. Mazzanti « Uranium Based UO_2^{+}-Mn^{2+} Single Chain Magnet Assembled through Cation-Cation Interaction » *Angew. Chem. Int. Ed.* **2014**, *53*, 819-823.

2/ V. Mougel, L. Chatelain, J. Pécaut, R. Caciuffo, E. Colineau, J-C. Griveau, and M. Mazzanti « Uranium and manganese assembled in a wheel-shaped nanoscale single-molecule magnet with high spin-reversal barrier » *Nature Chem.* **2012**, *4*, 1011-1017.

1/ L. Chatelain, V. Mougel, J. Pécaut and M. Mazzanti « Magnetic communication and reactivity of a stable homometallic cation-cation trimer of pentavalent uranyl » *Chem. Sci.* **2012,** *3*, 1075-1079.

Chemical Science

Cite this: *Chem. Sci.*, 2012, **3**, 1075

www.rsc.org/chemicalscience

EDGE ARTICLE

Magnetic communication and reactivity of a stable homometallic cation–cation trimer of pentavalent uranyl†

Lucile Chatelain, Victor Mougel, Jacques Pécaut and Marinella Mazzanti*

Received 10th October 2011, Accepted 13th December 2011
DOI: 10.1039/c2sc00782g

The reaction of the UO_2^+ precursor $[(UO_2Py_5)(KI_2Py_2)]_n$, with the potassium salt of the tetradentate aza β-diketiminate ligand L (L = 2-(4-tolyl)-1,3-bis(quinolyl)malondiiminate) affords the first homometallic cation–cation complex of pentavalent uranyl. The complex $[UO_2L]_3$ has a new triangular geometry of the cation–cation interaction in the solid state, which gives rise to a clear magnetic interaction with a maximum in the plot of χ *versus* T at 12 K. It retains its solid state trinuclear structure in solution and is fully stable in organic anaerobic solvents, but reacts rapidly with molecular oxygen to form a rare dinuclear oxo complex of uranyl(VI), $([UO_2(L)]_2[\mu_2\text{-}O])$.

Introduction

Polynuclear complexes of uranium are attracting increasing interest for their relevance in materials science, nuclear reprocessing and in the environmental migration of uranium,[1–3] but also for their attractive magnetic properties, unusual reactivity and for the important fundamental information they can provide on the electronic structure of 5f elements.[4–12] The mutual coordination of actinyl ions through the oxo group, also known as cation–cation interaction (CCI), is an important feature in the chemistry of 5f elements, such as NpO_2^+(V) and to a lesser extent UO_2^{2+}(VI), leading spontaneously to the self-assembly of extended networks and to fewer examples of discrete polynuclear complexes.[13–18] Polynuclear complexes containing U(V) f^1 centers are particularly attractive for the investigation of magnetic communication in actinides due to the lack of inter-electronic repulsion, and have indeed yielded rare examples of unambiguous magnetic coupling between uranium centers.[6,8,19,20] However, cation–cation complexes of pentavalent uranyl are difficult to isolate because they are involved as reactive intermediates in the aqueous and non-aqueous disproportionation of UO_2^+ into U(IV) and UO_2^{2+}.[21,22,20,30] Accordingly, the recent advances in the chemistry of pentavalent uranyl in organic solution[23–26] have focused on the development of bulky diketiminate,[27] Schiff base,[26] or aminophenolate ligands[28] capable of preventing cation–cation interactions between UO_2^+ moieties that would inevitably lead to unstable polynuclear complexes.[20,29] Only a few examples of cation–cation complexes of pentavalent uranyl have been reported. Our group has isolated diamond-shaped dinuclear and T-shaped tetranuclear (Fig. 1) cation–cation complexes of pentavalent uranyl using the dianionic bidentate dibenzoylmethanate ligand[20,29] or tetradentate dianionic salen-type ligands.[6,30] A diamond-shaped cation–cation complex has also been isolated with a polypyrrolic macrocycle called "pacman" ligand.[10] While the cation–cation complexes based on bidentate diketonate ligands have limited solution stability and eventually lead to the disproportionation of UO_2^+, Schiff base ligands are the only identified family of ligands affording polynuclear assemblies with CCI's, which shows an exceptional stability both in the solid state and in solution.

The few reported CCI complexes of pentavalent uranyl are all heterobimetallic with the uranyl oxygens involved in cation–cation interactions with alkali,[6,29,30] lanthanide[10] or d-block metal cations,[31] which play an important role in determining the structure and the stability of the final complex. The cation can also significantly influence the magnetic exchange, rendering the

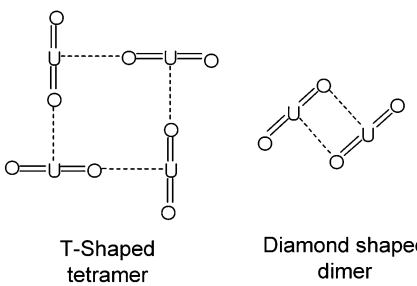

Fig. 1 The geometry of cation–cation interactions in previous pentavalent uranyl complexes.

Laboratoire de Reconnaissance Ionique et Chimie de Coordination, SCIB, UMR-E 3 CEA-UJF, INAC, CEA-Grenoble, 17 rue des Martyrs, 38054 Grenoble Cedex 09. E-mail: marinella.mazzanti@cea.fr; Fax: +33 4 38 78 5090; Tel: +33 4 3878 3955

† Electronic supplementary information (ESI) available: Synthetic and characterization details for the reported complexes, proton NMR spectra and ESI/MS spectra of complex **1** in different solvents. Additional ORTEP views and details of coefficient diffusion measurements. CCDC reference numbers 848286–848288. For ESI and crystallographic data in CIF or other electronic format see DOI: 10.1039/c2sc00782g

observation of a clear signature of magnetic communication between uranyl ions difficult.[10]

Here we report the first homometallic cation–cation complex of pentavalent uranyl. The tetradentate monoanionic aza β-diketiminate ligand 2-(4-Tolyl)-1,3-bis(quinolyl)malondiiminate (L) forms a new type of stable cation–cation complex of pentavalent uranyl. It presents only uranium ions, which are arranged in a new trigonal geometry and give rise to a clear antiferromagnetic interaction with the appearance of a maximum of the magnetic susceptibility at higher temperature (12 K) with respect to the previously reported uranyl CCI's complexes. These results show that stable cation–cation complexes of pentavalent uranyl can form in the absence of additional cations, if suitable supporting ligands are used, leading to a new geometry and stronger magnetic interaction. Thus, the CCI interaction provides a route to the expansion of UO_2^+ chemistry and to the identification of new compounds presenting magnetic coupling between uranium ions. Preliminary studies show that this uranyl(v) complex reacts with dioxygen leading to a rare uranyl(vi) μ-oxo dimer.

Results and discussion

The reaction of the UO_2^+ precursor $[(UO_2Py_5)(KI_2Py_2)]_n$,[32] with the potassium salt of the aza β-diketiminate ligand, LK (L = 2-(4-Tolyl)-1,3-bis(quinolyl)malondiiminate)[33] in pyridine leads to the immediate formation of the complex of pentavalent uranyl $[UO_2L]_3$, **1**, as a dark red powder (Scheme 1).‡ The analytically pure complex can be obtained after removal of coprecipitated KI with dibenzo-18-crown-6 ether. Crystals of **1** suitable for X-ray diffraction were obtained by slow diffusion of diisopropylether into a saturated solution (3.6×10^{-4} M) of **1** in acetonitrile.

The crystal structure of **1** was determined by single crystal X-ray diffraction. An ORTEP view of **1** is presented in Fig. 2. The crystal structure of **1** presents a trimeric unit consisting of uranyl moieties coordinated to each other to form an equilateral triangle of sides 4.19(2) Å long with a mean U–O–U angle of 156.1(11). Each uranium atom in the trimer has a pentagonal-bipyramidal coordination with the four nitrogen atoms from the aza β-diketiminate ligand (mean $U–N_{dikeiminate}$ 2.53(1) Å; mean $U–N_{quinoline}$ 2.62(1) Å) and the bridging uranyl oxygen from the adjacent uranyl group (mean U–O 2.37(1) Å) in the equatorial plane. The environments of the three uranium atoms are equivalent with a *pseudo* threefold axis located in the center of the equilateral triangle. This is the first example of a triangular geometry for cation–cation complexes of pentavalent uranyl. A similar triangular geometry has been previously reported only for the trimeric complex of uranyl(vi) $[UO_2(hfa)_2]_3$[14] and the neptunyl(v) oxalate complex $NH_4[NpO_2(C_2O_4)]$ both containing a cation–cation interaction.[34]

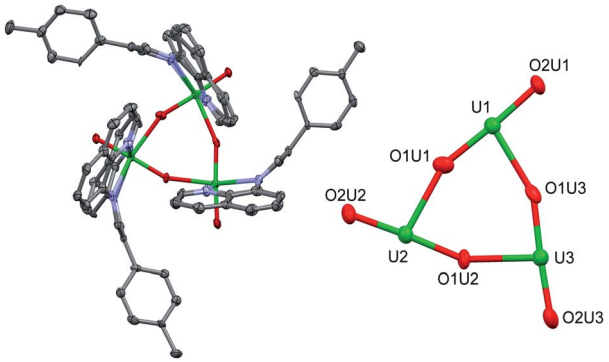

Fig. 2 Displacement ellipsoid plots of **1** (left) and of its uranyl core (right) with thermal ellipsoids at 30% probability. Hydrogen atoms and solvent molecules were omitted for clarity. Selected bonds lengths (Å) and angles (°): U(1)–O(1U1).1.842(10), U(1)–O(2U1) 1.905(10), U(1)–O(1U3) 2.374(8); O(1U1)–U(1)–O(2U1) 176.7(4);O(1U1)–U1–O(1U3) 84.2(3), O(2U1)–U1–O(1U3) 99.0(3); U(1)–O(1U1)–U(2) 157.1(5).

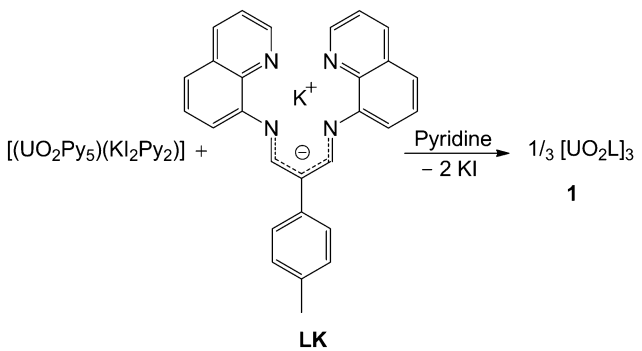

Scheme 1 The synthesis of the trinuclear cation–cation complex of pentavalent uranyl $[UO_2L]_3$ **1**.

The mean U–U distance in the triangle (4.19(1) Å) is shorter than the mean U–U distance found in the T-shaped cores of the dbm tetramer $[UO_2(dbm)_2]_4[K_4(CH_3CN)_4]$, (4.315(5) Å)[20] and of the salen tetramer $[\{UO_2(salen)\}_4(\mu_8\text{-}K)_2][\{K(18C6)Py)_2\}]$,[6] (4.31(3) Å), but is significantly longer than the U–U distances reported for the asymmetric diamond-shaped $(UO_2)_2$ cores found in the dinuclear $[UO_2(dbm)_2K(18C6)]_2$ (dbm^- = dibenzoylmethanate) and in the $[UO_2(pacman)_2Sm(Py)]_2$[10] complexes, which show similar geometrical parameters (U–U =3.462 Å for the dbm complex and 3.471 Å for the pacman complex).

Temperature-dependent magnetic susceptibility was measured for **1** in the temperature range 2–300 K. At 300 K, **1** displays an effective magnetic moment of 1.88 μ_B per uranium, which is lower then the theoretical value calculated for the free f^1 ion in the L–S coupling scheme (μ_{eff} = 2.54 μ_B) but within the range of the values reported for U(v) compounds.[35,36] The plot of χ *versus* T (Fig. 3) suggests the presence of an antiferromagnetic coupling between the f^1 ions with a maximum at 12 K. Unambiguous evidence of magnetic communication between uranium centers is limited to four examples of U(v) complexes, which include the imido-bridged $5f^1$–$5f^1$ complex $[(MeC_5H_4)_3U]_2$ [μ-1,4-$N_2C_6H_4$], the dimeric $[UO_2(dbm)_2K(18C6)]_2$ and tetrameric $[\{UO_2(salen)\}_4(\mu_8\text{-}K)_2][\{K(18C6)Py)_2\}]$ uranyl(v) CCI complexes[6,8,19,20] and three recently reported dimeric U(iv) complexes.[37] This is the first example of unambiguous magnetic coupling in a triangular

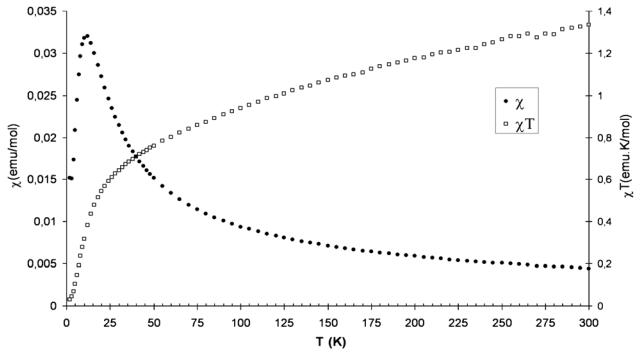

Fig. 3 Temperature-dependent magnetic susceptibility data for **1** in the range 2–300 K. A μ_{eff} of 1.88 μ_B per uranium at 300 K was calculated for **1** ($X_{dia} = -1.19 \times 10^{-3}$ emu mol^{-1}, $m = 6.8$ mg, $M = 2050$ g mol^{-1}).

oxo-bridged uranyl complex. Moreover, the maximum in the plot of χ *versus* T occurs at higher temperatures in **1** than in all other U(v) oxo-bridged complexes (the maximum χ was observed at 6 K for $[UO_2(dbm)_2K(18C6)]_2$ and $[\{UO_2(salen)\}_4(\mu_8\text{-}K)_2][\{K(18C6)Py)_2\}]$ complexes), suggesting a stronger coupling between the uranium ions and comparable to that found in an imido-bridged U(v) complex presenting a short U–U distance of 3.57 Å (maximum at 13 K).[8] However, a final conclusion on the strength of the magnetic coupling will require the modelling of the magnetic data. From these results, it appears that the strength of the coupling in CCI complexes (probably involving a superexchange through the uranyl oxo group) cannot be clearly correlated to the U–U distances since weaker coupling can be observed in complexes with shorter U–U distances (shorter U–U distances are found in the $[UO_2(dbm)_2K(18C6)]_2$ complex). A lack of correlation between the strength of magnetic coupling and U–U distances has been observed in a series of oxide and chalcogenide bridged U(IV) complexes recently reported by Meyer and coworkers, which was discussed in terms of the different geometry of the bridging ligand.[37] While the triangular geometry of the CCI could play a role in enhancing the magnetic coupling in **1** with respect to the previously reported dimeric and tetrameric CCI complexes, the increased negative charge localized on the terminal uranyl oxygen atoms in the absence of coordinated cations and the electronic structure of the ligand are likely to play an important role in the magnetic properties of **1**.

The absence of supporting cations, the new triangular topology and the strength of the magnetic coupling renders this complex particularly suitable for investigating the mechanism and origins of the magnetic coupling. Future work, including detailed EPR and DFT studies, will be directed to investigate the magnetic coupling in this and analogous systems.

ESI-MS spectrometry (m/z = 2051,0 corresponding to the protonated complex $[UO_2(L)]_3H^+$) is in agreement with the presence of a trinuclear complex in solution. Pulsed-Field Gradient STimulated Echo (PFGSTE) diffusion NMR was used to measure the diffusion coefficient (D) of **1** in pyridine solution using the mononuclear $[UO_2(L)Cl]$ complex in pyridine as an external reference.[38] The spherical hydrodynamic radii (called Stokes radii) calculated from the measured diffusion coefficient using the Stokes–Einstein equation (see supporting information†) indicate that complex **1** retains its trinuclear form in pyridine solution. This suggests that the coordinating pyridine solvent is not competing with the mutual coordination of the uranyl ions. It should be noted that our previous studies with diketonate or Schiff base ligands showed that CCIs leading to polymetallic compounds occurred only in the presence of alkali metal ions. In the absence of alkali metal ions only the formation of mononuclear complexes was observed. The neutral nature of the interacting $[UO_2L]$ fragments in **1** could be at the origin of the stronger cation–cation interaction observed for **1** with respect to the complexes $[UO_2(dbm)_2]_4[K_4(CH_3CN)_4]$ and $[\{UO_2(salen)\}_4(\mu_8\text{-}K)_2][\{K(18C6)Py)_2\}]$ where the interacting fragments (*e.g.* $[UO_2(dbm)_2]^-$), are anionic.

Proton NMR of **1** in deuterated dmso solution shows the presence of an additional solution species, suggesting that partial dissociation of the trinuclear structure occurs in the more coordinating dmso solvent. The dissociation process is reversible and the trinuclear structure is restored in pyridine solution after removal of dmso. Since complex **1** is highly stable with respect to the disproportionation process, it is particularly suited for reactivity studies. Preliminary studies show that complex **1** is highly reactive towards oxidizing agents.

Complex **1** reacts rapidly with CH_2Cl_2 to form the hexavalent complex $[UO_2LCl]$, **2** probably through chloride abstraction from the solvent. The crystal structure of complex **2** was determined by X-ray diffraction and an ORTEP view is shown in Fig. 4. It shows an uranium ion in a slightly distorted pentagonal bipyramidal geometry with the two uranyl groups in axial positions (U=O distances =1.757(9) and 1.785(8) Å) and the chloride and the four nitrogen atoms from the azadiketiminate ligand (mean $U\text{–}N_{dikeiminate}$ 2.47(1) Å; mean $U\text{–}N_{quinoline}$ 2.62(1) Å) in equatorial positions.

Complex **1** also reacts with dioxygen (Scheme 2) in acetonitrile solution to yield the dinuclear complex $\{[UO_2(L)]_2[\mu_2\text{-}O]\}$, **3**, presenting two oxo-bridged uranyl(VI) complexes arranged perpendicular to each other, probably to reduce steric interactions, resulting in a overall *pseudo* C_2 symmetry.

Fig. 5 shows an ORTEP view of **3**. Each U(VI) ion is found in a distorted pentagonal bipyramidal geometry, where the fifth equatorial position is occupied by a μ_2-O. The mean U–O bond distance of the two *trans* uranyl oxo groups (1.80(1) Å) is longer

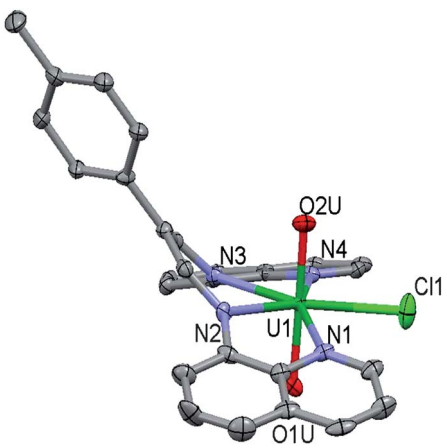

Fig. 4 Displacement ellipsoid plots of **2** with thermal ellipsoids at 30% probability. Hydrogen atoms and solvent molecules are omitted for clarity.

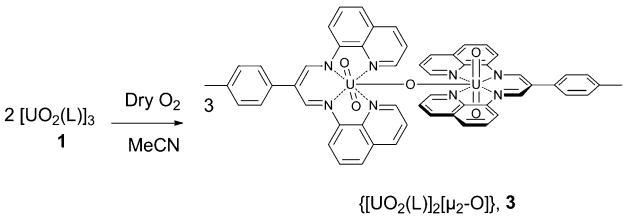

Scheme 2 Reaction of $[UO_2L]_3$ **1** with dry O_2 to yield **3**.

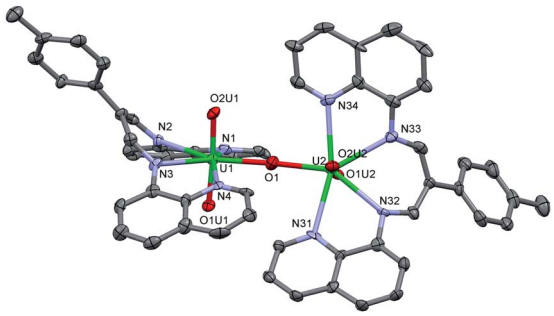

Fig. 5 Displacement ellipsoid plots of **3** with thermal ellipsoids at 30% probability. Hydrogen atoms and solvent molecules are omitted for clarity. Selected bond lengths (Å) and angles (°): U(1)–O(1) 2.19(1), U(1)–O(1U1) 1.79(1), U(1)–O(2U1) 1.79(1), U(2)–O(1) 2.19(1), U(2)–O(1U2) 1.80(1), U(1)–O(2U2) 1.82(1), U(1)–O(1)–U(2) 177.2(7); O(2U1)–U(1)–O(1U1) 176.2(5); O(2U1)–U(1)–O(1) 91.7(5).

than in the uranyl(v) complex 2 (1.77(1) Å), but is very similar to that reported for the oxo uranyl(vi) complex [Na(thf)$UO_2(NCN)_2$](μ-O) (1.81(1) Å. The U-(μ-O) distances (2.19(1) Å) are of length comparable to those found in the structurally analogous complexes [Na(thf)$UO_2(NCN)_2$](μ-O) (2.18(1) and 2.22(1) Å) and [{$UO_2(Py)_4$}](μ-O)][CF_3SO_3]$_2$ (2.105(5) and 2.085(5) Å).[39,40]

The proton NMR of **3** shows only one set of 20 signals in the diamagnetic region, suggesting the presence of a rigid C_2 symmetric species in solution in agreement with the solid state structure. The formation of complex **3** is also observed in moist air, but together with other products that remain to be identified. Only a few examples of uranyl oxo compounds containing μ_2-O bridging groups have been reported.[30,39,40] These complexes were obtained as minor products of uranyl(vi) hydrolysis or uranyl(v) disproportionation reactions. Several well-characterized examples of U(iv) μ-oxo complexes have also been reported, which were obtained from the reaction of U(iii) complexes with CO_2,[41] N_2O[37] or H_2O.[42,43] Interestingly, the reaction of **1** with oxygen provides a synthetic route to uranyl(vi) oxo-bridged species and shows a possible reaction pathway, which does not involve disproportionation, for the conversion of pentavalent uranyl into hexavalent uranyl in an aerobic environment. Future studies will be directed to investigate the formation and the reactivity of this oxo species.

Conclusion

A tetradentate monoanionic aza β-diketiminate ligand afforded the first homometallic cation–cation complex of pentavalent uranyl. The trimeric complex shows a new triangular geometry that results in an unambiguous magnetic coupling between the uranyl ions. The stability of this complex with respect to the disproportionation reaction suggests that the formation of stable cation–cation complexes could be a general trend in pentavalent uranyl chemistry in spite of their predicted implication as highly reactive intermediates in pentavalent uranyl disproportionation. More importantly, cation–cation interactions in pentavalent uranyl complexes provide an excellent tool for the design of supramolecular assemblies with magnetic communication and possibly to access polynuclear uranium complexes with single molecule magnet behaviour.[5,7] Finally, the polynuclear nature of this pentavalent uranyl complex is probably at the origin of the observed unusual reactivity with molecular oxygen leading to a rare uranyl(vi) oxo dimer.

Acknowledgements

We acknowledge support from the Commissariat à l'Energie Atomique, Direction de l'Energie Nucléaire, RBPCH program and the "Agence National de la Recherche", (ANR-10-BLAN-0729). We thank Lydia Plassais for help in ligand synthesis and Dr Lionel Dubois for his suggestions in magnetic measurements.

Notes and references

‡ Synthesis of $[UO_2(L)]_3$, **1**. A dark violet suspension of LK (64 mg, 0.14 mmol, 1 equiv.) in pyridine (2 mL) was added to a light orange suspension of $[UO_2(py)_5][KI_2(py)_2]$ (160 mg, 0.14 mmol, 1equiv.) in pyridine (2 mL). The reaction mixture was stirred over 12h, resulting in a dark red suspension. In order to remove the KI formed during the course of the reaction, dibenzo-18-crown-6 (100 mg, 0.28 mmol, 2 equiv.) was added to the reaction mixture, which was then stirred for an additional 2 h. The resulting suspension was centrifuged, and the dark reddish solid was collected, washed with pyridine (10 × 1.5 mL), rinsed with diisopropylether (2 × 1.5 mL) and dried under reduced pressure to yield 90.1 mg (0.043 mmol, 93%) of $[UO_2(L)]_3$ as a dark red solid. While the ligand is light sensitive, complex **1** is not sensitive to light over a period of a month. ^{1}H NMR (400MHz, CD_3CN, 298 K): $\delta = 9.17$ (d, 2H, $J^3_{H-H} = 7$ Hz); 6.20 (d, 2H, $J^3_{H-H} = 7$ Hz); 4.98 (t, 2H, $J^3_{H-H} = 7.7$ Hz); 4.86 (d, 2H, $J^3_{H-H} = 7.9$ Hz); 3.85 (s, 3H); 3.67 (d, 2H, $J^3_{H-H} = 8$ Hz); 0.98 (m, 2H); −2.23 (s, 2H); −6.50 (d, 2H, $J^3_{H-H} = 8$ Hz), −12.99 (br s, 2H).
Crystals of **1** suitable for X-ray diffraction were obtained by slow diffusion of diisopropylether into a saturated solution (3.6×10^{-4} M) of **1** in acetonitrile.
Elemental analysis (%) calculated for $[UO_2(L)]_3$ ($C_{84}H_{63}N_{12}O_6U_3$ 2050.56g mol^{-1}) C 49.20, H 3.10 and N 8.20, found C 49.39 H 3.27 N 8.46.
ESI-MS: 2051 ($M-H^+$). The absence of iodine and potassium was confirmed using silver nitrate and flame tests.
Synthesis of {$[UO_2(L)]_2[\mu_2$-O]}, **3**. Dry O_2 (1 atm.) was added to a dark red suspension of $[UO_2(L)]_3$ (24 mg 0.011 mmol, 1 eq) in MeCN (3 mL) resulting in a colour change of the solution to brown. After letting the solution stand at room temperature for 2 days, dark red crystals of {$[UO_2(L)]_2[\mu_2$-O]} suitable for single crystal X-ray diffraction formed. The crystals were filtered, washed with cold MeCN (2*2 mL) and dried under vacuum to yield 17.6 mg of the title compound (0.012 mmol, 72%). ^{1}H NMR (400MHz, Py, 298 K): $\delta = 11.93$ (d, 2H, $J = 4.9$ Hz); 11.37 (d, 2H, $J = 4.9$ Hz); 9.76 (s, 2H); 9.57 (s, 2H); 8.17 (d, 2H, $J = 8.6$ Hz); 8.08 (d, 2H, $J = 8.6$ Hz); 7.94 (d, 2H, $J = 8.6$ Hz); 7.86 (d, 2H, $J = 8.6$ Hz); 7.70 (m, 6H); 7.62 (m, 6H); 7.41 (d, 2H, $J = 7.9$ Hz); 7.37 (d, 2H, $J = 7.9$ Hz); 7.09 (dd, 2H, $J = 7.9$, 4.9 Hz); 6.98 (dd, 2H, $J = 7.9$, 4.9 Hz); 2.41 (s, 3H), 2.38 (s, 3H).
Elemental analysis (%) calculated for {$[UO_2(L)]_2[\mu_2$-O]}·2MeCN (($C_{60}H_{48}N_{10}O_5U_2$ 1465.17;g mol^{-1}) C 49.19, H 3.30 and N 9.56, found C 49.50, H 3.41 and N 9.68.
ESI-MS: 1384.1 ({$[UO_2(L)]_2[\mu_2$-O]}$-H^+$)

1 S. V. Krivovichev, V. Kahlenberg, R. Kaindl, E. Mersdorf, I. G. Tananaev and B. F. Myasoedov, *Angew. Chem., Int. Ed.*, 2005, **44**, 1134–1136.
2 L. R. Morss, N. M. Edelstein and J. Fuger, *The Chemistry of the Actinide and Transactinide Elements*, Springer, Dordrecht, 2006.
3 Y. Suzuki, S. D. Kelly, K. M. Kemner and J. F. Banfield, *Nature*, 2002, **419**, 134–134.
4 W. J. Evans, S. A. Kozimor and J. W. Ziller, *Science*, 2005, **309**, 1835–1838.
5 D. P. Mills, F. Moro, J. McMaster, J. van Slageren, W. Lewis, A. J. Blake and S. T. Liddle, *Nat. Chem.*, 2011, **3**, 454–460.
6 V. Mougel, P. Horeglad, G. Nocton, J. Pecaut and M. Mazzanti, *Angew. Chem., Int. Ed.*, 2009, **48**, 8477–8480.
7 J. D. Rinehart, T. D. Harris, S. A. Kozimor, B. M. Bartlett and J. R. Long, *Inorg. Chem.*, 2009, **48**, 3382–3395.
8 L. P. Spencer, E. J. Schelter, P. Yang, R. L. Gdula, B. L. Scott, J. D. Thompson, J. L. Kiplinger, E. R. Batista and J. M. Boncella, *Angew. Chem., Int. Ed.*, 2009, **48**, 3795–3798; E. J. Schelter, R. L. Wu, J. M. Veauthier, E. D. Bauer, C. H. Booth, R. K. Thomson, C. R. Graves, K. D. John, B. L. Scott, J. D. Thompson, D. E. Morris and J. L. Kiplinger, *Inorg. Chem.*, 2010, **49**, 1995–2007.
9 O. P. Lam, F. W. Heinemann and K. Meyer, *Angew. Chem., Int. Ed.*, 2011, **50**, 5965–5968.
10 P. L. Arnold, E. Hollis, F. J. White, N. Magnani, R. Caciuffo and J. B. Love, *Angew. Chem., Int. Ed.*, 2011, **50**, 887–890.
11 J. D. Rinehart and J. R. Long, *J. Am. Chem. Soc.*, 2009, **131**, 12558–12559.
12 S. G. Minasian, J. L. Krinsky, J. D. Rinehart, R. Copping, T. Tyliszczak, M. Janousch, D. K. Shuh and J. Arnold, *J. Am. Chem. Soc.*, 2009, **131**, 13767–13783.
13 N. N. Krot and M. S. Grigoriev, *Russ. Chem. Rev.*, 2004, **73**, 89–100.
14 J. C. Taylor, A. Ekstrom and C. H. Randall, *Inorg. Chem.*, 1978, **17**, 3285–3289.
15 I. Mihalcea, N. Henry, N. Clavier, N. Dacheux and T. Loiseau, *Inorg. Chem.*, 2011, **50**, 6243–6249.
16 J. M. Morrison, L. J. Moore-Shay and P. C. Burns, *Inorg. Chem.*, 2011, **50**, 2272–2277.
17 R. Copping, A. J. Gaunt, I. May, C. A. Sharrad, D. Collison, M. Helliwell, O. D. Fox and C. J. Jones, *Chem. Commun.*, 2006, 3788–3790.
18 N. Belai, M. Frisch, E. S. Ilton, B. Ravel and C. L. Cahill, *Inorg. Chem.*, 2008, **47**, 10135–10140.
19 R. K. Rosen, R. A. Andersen and N. M. Edelstein, *J. Am. Chem. Soc.*, 1990, **112**, 4588–4590.
20 G. Nocton, P. Horeglad, J. Pecaut and M. Mazzanti, *J. Am. Chem. Soc.*, 2008, **130**, 16633–16645.
21 H. Steele and R. J. Taylor, *Inorg. Chem.*, 2007, **46**, 6311–6318.
22 A. Ekstrom, *Inorg. Chem.*, 1974, **13**, 2237–2241.
23 T. W. Hayton, *Dalton Trans*, **39**, 1145–1158.
24 P. L. Arnold, J. B. Love and D. Patel, *Coord. Chem. Rev.*, 2009, **253**, 1973–1978; P. L. Arnold, A. Pécharman, E. Hollis, A. Yahia, L. Maron, S. Parsons and J. B. Love, *Nat. Chem.*, 2010, **2**, 1056–1061.
25 C. R. Graves and J. L. Kiplinger, *Chem. Commun.*, 2009, 3831–3853.
26 G. Nocton, P. Horeglad, V. Vetere, J. Pecaut, L. Dubois, P. Maldivi, N. M. Edelstein and M. Mazzanti, *J. Am. Chem. Soc.*, 2010, **132**, 495–508.
27 T. W. Hayton and G. Wu, *J. Am. Chem. Soc.*, 2008, **130**, 2005–2014.
28 P. Horeglad, G. Nocton, Y. Filinchuck, J. Pécaut and M. Mazzanti, *Chem. Commun.*, 2009, 1843–1845.
29 F. Burdet, J. Pecaut and M. Mazzanti, *J. Am. Chem. Soc.*, 2006, **128**, 16512–16513.
30 V. Mougel, P. Horeglad, G. Nocton, J. Pecaut and M. Mazzanti, *Chem.–Eur. J.*, 2010, **16**, 14365–14377.
31 P. L. Arnold, D. Patel, C. Wilson and J. B. Love, *Nature*, 2008, **451**, 315–318.
32 L. Natrajan, F. Burdet, J. Pecaut and M. Mazzanti, *J. Am. Chem. Soc.*, 2006, **128**, 7152–7153.
33 J. M. Fritsch, K. A. Thoreson and K. McNeill, *Dalton Trans.*, 2006, 4814–4820.
34 N. N. Krot and M. S. Grigoriev, *Russ. Chem. Rev.*, 2004, **73**, 89–100.
35 S. C. Bart, C. Anthon, F. W. Heinemann, E. Bill, N. M. Edelstein and K. Meyer, *J. Am. Chem. Soc.*, 2008, **130**, 12536–12546.
36 C. R. Graves, P. Yang, S. A. Kozimor, A. E. Vaughn, D. L. Clark, S. D. Conradson, E. J. Schelter, B. L. Scott, J. D. Thompson, P. J. Hay, D. E. Morris and J. L. Kiplinger, *J. Am. Chem. Soc.*, 2008, **130**, 5272–5285.
37 O. P. Lam, F. W. Heinemann and K. Meyer, *Chem. Sci.*, 2011, **2**, 1538–1547.
38 A. R. Waldeck, P. W. Kuchel, A. J. Lennon and B. E. Chapman, *Prog. Nucl. Magn. Reson. Spectrosc.*, 1997, **30**, 39–68.
39 J. C. Berthet, M. Lance, M. Nierlich and M. Ephritikhine, *Eur. J. Inorg. Chem.*, 2000, 1969–1973.
40 M. J. Sarsfield, M. Helliwell and J. Raftery, *Inorg. Chem.*, 2004, **43**, 3170–3179; M. P. Wilkerson, C. J. Burns, H. J. Dewey, J. M. Martin, D. E. Morris, R. T. Paine and B. L. Scott, *Inorg. Chem.*, 2000, **39**, 5277–5285.
41 I. Castro-Rodriguez and K. Meyer, *J. Am. Chem. Soc.*, 2005, **127**, 11242–11243.
42 L. Karmazin, M. Mazzanti and J. Pécaut, *Inorg. Chem.*, 2003, **42**, 5900–5908.
43 W. W. Lukens, S. M. Beshouri, L. L. Blosch and R. A. Andersen, *J. Am. Chem. Soc.*, 1996, **118**, 901–902.

nature chemistry

ARTICLES

PUBLISHED ONLINE: 11 NOVEMBER 2012 | DOI: 10.1038/NCHEM.1494

Uranium and manganese assembled in a wheel-shaped nanoscale single-molecule magnet with high spin-reversal barrier

Victor Mougel[1], Lucile Chatelain[1], Jacques Pécaut[1], Roberto Caciuffo[2], Eric Colineau[2], Jean-Christophe Griveau[2] and Marinella Mazzanti[1]*

Discrete molecular compounds that exhibit both magnetization hysteresis and slow magnetic relaxation below a characteristic 'blocking' temperature are known as single-molecule magnets. These are promising for applications including memory devices and quantum computing, but require higher spin-inversion barriers and hysteresis temperatures than currently achieved. After twenty years of research confined to the *d*- block transition metals, scientists are moving to the *f*-block to generate these properties. We have now prepared, by cation-promoted self-assembly, a large 5*f*–3*d* $U_{12}Mn_6$ cluster that adopts a wheel topology and exhibits single-molecule magnet behaviour. This uranium-based molecular wheel shows an open magnetic hysteresis loop at low temperature, with a non-zero coercive field (below 4 K) and quantum tunnelling steps (below 2.5 K), which suggests that uranium might indeed provide a route to magnetic storage devices. This molecule also represents an interesting model for actinide nanoparticles occurring in the environment and in spent fuel separation cycles.

In the quest for systems that can function as molecular nanomagnets, and find application in information storage, quantum information processing, spintronics and magnetocaloric refrigeration[1–5], a number of increasingly larger molecular clusters containing one or more types of *d*-block transition metals have been synthesized.

The development of single-molecule magnets (SMMs) requires the association of high-spin ground states (S) with a large magnetic anisotropy (D). Together, these properties create a barrier to magnetization reversal—and thus a magnetization hysteresis—below a 'blocking' temperature T_B that is specific to each system. Within the 3*d*-block, manganese(III) clusters are the most studied SMM compounds because of the high uniaxial anisotropy and spin ground state of the Mn(III) ion, and have provided the highest reported relaxation barriers ($U_{eff} = S^2|D|$ up to 86.4 K with $S = 12$) and blocking temperatures (~4.3 K)[4]. High-spin ground states up to $S = 83/2$ have been obtained by associating high-spin Mn(II) to Mn(III) in large clusters, but in these systems the presence of the isotropic Mn(II) ion and the geometry of the anisotropic Mn(III) ions result in a low magnetic relaxation barrier (a hysteresis below 0.5 K has been measured for the Mn_{19} $S = 83/2$)[6].

Although high spin states can be achieved with *d*-block ions, *f* elements have higher single-ion anisotropy, which makes them very attractive for the development of SMMs with improved properties. Notably, the molecular compounds showing the highest relaxation barriers reported to date are mono- or multimetallic lanthanide complexes, with a record barrier of 530 K having been achieved for a Dy_6 cluster[7–10]. However, only a few complexes have shown hysteresis in the magnetization: a bis-phthalocyaninato (Pc) rare earth(III)[7] compound, and two dinuclear complexes consisting of Dy(III)[8] or Tb(III)[11] ions linked by a N_2^{3-} radical, which showed blocking temperatures of 8.3 and 14 K, respectively.

SMMs based on actinide ions, such as uranium, have not been studied to such an extent, and the first examples, U(III) and Np(IV) mononuclear complexes[12–14], have only recently been reported. A dinuclear complex, for which the presence of magnetic coupling between the U(III) ions remain ambiguous, also shows SMM behaviour[15,16]. A combination of slow relaxation of the magnetization and effective superexchange interactions (that is, occurring between two magnetic centres through a non-magnetic bridge) between 5*f* ions has been observed only in a trinuclear heterovalent neptunyle trimer[17]. So far, however, magnetic memory effects in 5*f*-block clusters have been reported only in the form of butterfly-shaped hysteresis loops, with negligible remanent magnetization at zero applied field, even at the lowest observation temperature.

Actinides are particularly attractive for attaining higher relaxation barriers because, in contrast to lanthanide ions, they can establish partially covalent interactions and therefore be involved in magnetic communication[18–25], leading to concerted magnetic behaviour. As well as focusing on their potential applications, magnetic actinide complexes are of high fundamental interest in the investigation of the role of 5*f* orbitals in bonding and magnetic properties. However, the supramolecular chemistry of actinides is poorly developed[26], with only a few examples of large paramagnetic homometallic clusters described in the literature[27–29]. A lack of appropriate synthetic approaches means that heterometallic systems containing 5*f* and 3*d* metals are even rarer, being limited to a few dinuclear and trinuclear examples[20,30–32]. For some of them[20,30], clear evidence of 5*f*–3*d* magnetic coupling has been reported, but to date there are no examples of 5*f*–3*d* complexes showing SMM behaviour.

The development of synthetic strategies leading to large 5*f*–3*d* assembly is also of high relevance to nuclear technology and

[1]Laboratoire de Reconnaissance Ionique et Chimie de Coordination, SCIB, UMR-E 3 CEA-UJF, INAC, CEA-Grenoble, 17 rue des Martyrs, F-38054 Grenoble Cedex 09, France, [2]European Commission, Joint Research Centre, Institute for Transuranium Elements, PO Box 2340, D-76125 Karlsruhe, Germany.
*e-mail: marinella.mazzanti@cea.fr

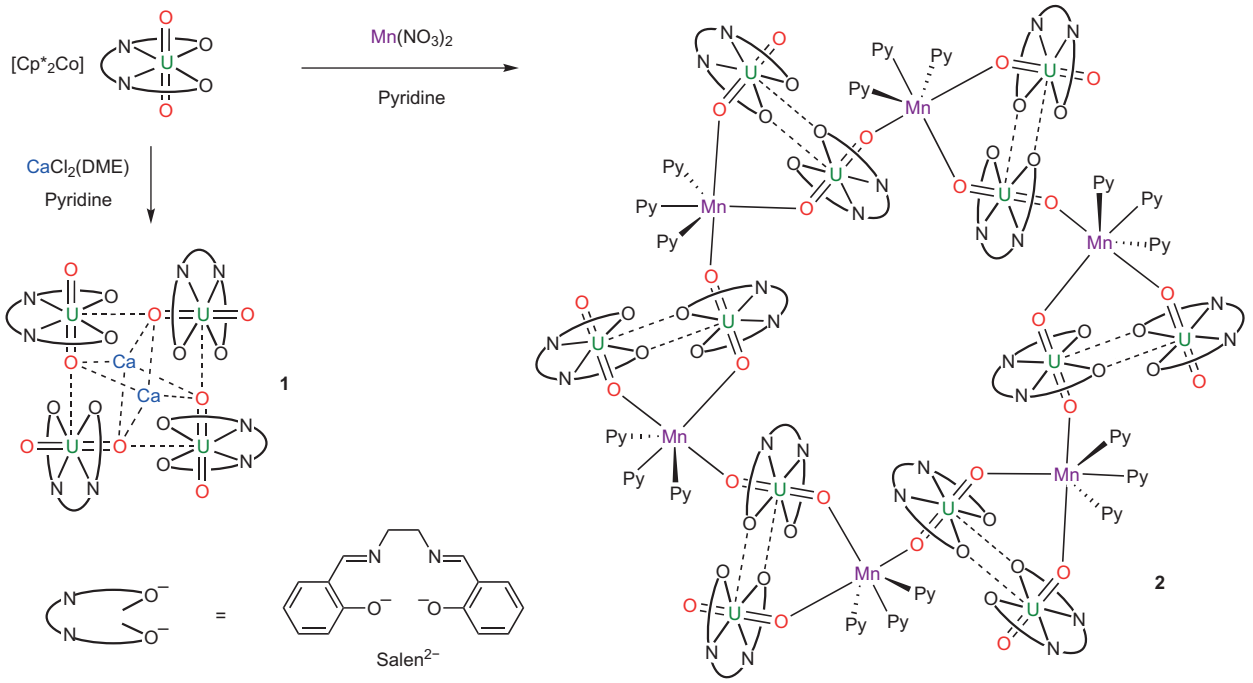

Figure 1 | Reaction scheme. The mononuclear pentavalent uranyl complex $[UO_2(salen)(Py)][Cp^*_2Co]$ reacts with $CaCl_2(DME)$ to produce tetrameric complex **1** and with $Mn(NO_3)_2$ to yield $[\{[UO_2(salen)]_2Mn(Py)_3\}_6]$ (**2**), a dodecanuclear uranyl(v) complex containing six manganese(ii) centres.

associated environmental clean-up strategies. 3*d* transition-metal ions are present in the environment and in spent nuclear fuel streams, and therefore nanosized clusters formed by actinides and 3*d* elements provide a good model of species involved in actinide migration and of colloidal species affecting the technology of nuclear fuel reprocessing.

Cation–cation interactions, a term used to describe the interaction of the actinyl oxo groups with the metal of another actinyl group, or with metal cations from the alkali, 4*f* or 3*d* series are a key feature of solid-state and molecular actinide chemistry, which provide an attractive route to supramolecular structures and magnetic communication[14,21,33,34]. Notably, we have recently isolated stable dinuclear[21], trinuclear[22] and tetranuclear[21,23,35] complexes of pentavalent uranyl, assembled via UO_2^+–UO_2^+ and UO_2^+–M (M = K, Rb) interactions, which present unambiguous magnetic communication, rarely found in actinide ions. These polynuclear complexes are noteworthy because of their stability with respect to the disproportionation reaction that is commonly observed for pentavalent uranyl. Only dinuclear complexes showing cation–cation interaction between UO_2^+ and Fe(ii), Zn(ii) or Ln(iii) cations have been reported to date. In the last case, the magnetic data were analysed in terms of UO_2^+–Ln(iii) antiferromagnetic interaction[31,34]. In contrast to these dinuclear systems, here we report the formation of a large cluster resulting from the interaction of UO_2^+ with Mn(ii) cations. We show that the ability of the Schiff base complexes of pentavalent uranyl to form cation–cation interactions with elements of the 3*d* block provides a versatile route to the assembly of a $U_{12}Mn_6$ wheel, which is the largest reported heterometallic 5*f*–3*d* complex. We also demonstrate that the topology of the polynuclear assembly is tuned by the nature of the cation (UO_2^+–Ca^{2+} interaction yields a tetramer). Whereas all the previously reported examples of actinides-based SMMs show butterfly-shaped hysteretic loops[14,15], the $U_{12}Mn_6$ wheel presents, below $T_B = 4$ K, an open staircase-like hysteresis with non-zero remanent magnetization, a necessary requirement for information storage. The coercive field H_c (the magnetic field required to switch the magnetization from saturation to zero) increases with decreasing temperature and reaches a value of ~1.4 T at 2.25 K. This behaviour does not originate from intermolecular cooperative interactions as in long-range magnetically ordered systems, but is of purely molecular origin and is related to the presence of the energy barrier hindering the relaxation of the magnetization towards equilibrium. Abrupt steps in the hysteresis loop, appearing below ~2.5 K at $\mu_0 H = 0$ and 1.65 T, reveal that at these fields the relaxation rate is strongly enhanced by quantum tunnelling of the magnetization through the relaxation barrier, providing evidence of quantum-mechanical properties on a macroscopic scale, as observed in several transition-metal and rare earth systems but never reported for an actinide complex[2].

Results and discussion

Synthesis and structural characterization. We have previously identified a convenient route to salen-based heterometallic tetranuclear uranyl(v)–uranyl(v)–M (M = K, Rb) cation–cation clusters that consists in reacting the monomeric $[UO_2(salen)(Py)][Cp^*_2Co]$ ($salenH_2$ = *N*,*N*′-ethylenebis(salicylimine); Cp^* = pentamethylcyclopentadienyl; Py = pyridine) complex with the desired MI salt (M = K, Rb)[35]. Here, we have used this strategy to prepare cation–cation clusters with divalent cations. At first, we studied the influence of the presence of a divalent alkaline-earth metal (which has no preferential coordination number or geometry) on the final structure. We then used paramagnetic divalent manganese to assemble a cation–cation cluster containing a UO_2^+–Mn interaction and to promote magnetic coupling between the isotropic Mn^{2+} ion and the anisotropic uranyl(v) ion. The most common geometry for manganese(ii) is octahedral (although it can be found in other geometries depending on the ligand set). The preference of Mn(ii) for an octahedral coordination geometry in the reaction conditions used in this work affords a cation–cation cluster with a new wheel structure. Thus, we demonstrate that the presence of a transition metal with a specific geometric preference can be used to control the final structure and to design new cluster topologies.

The reaction of 2 equiv. of monomeric uranyl(v) complex $[UO_2(salen)(Py)][Cp^*_2Co]$ with 1 equiv. of $CaCl_2(DME)$ (DME = dimethoxyethane) in pyridine results in the formation of the tetrameric complex $\{[UO_2(salen)]_4Ca_2\}$ (**1**) in 70% yield (Fig. 1).

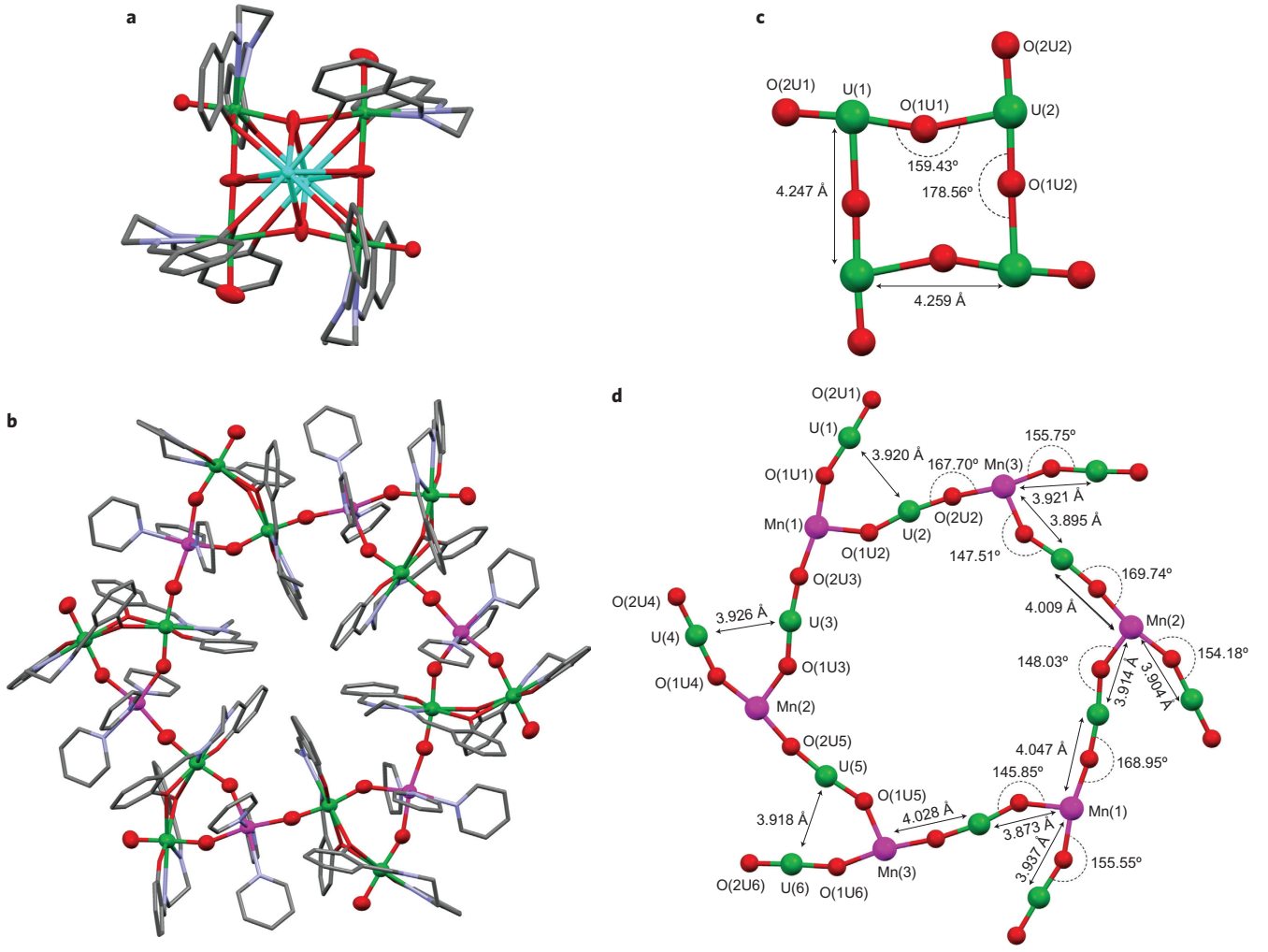

Figure 2 | Solid-state structure of {[UO_2(salen)]$_4$$Ca_2$} (1) and [{[$UO_2$(salen)]$_2$Mn(Py)$_3$}$_6$] (2). a–d, Ellipsoid plots at 50% probability of **1** (**a**) and **2** (**b**) and detail of the cores in ball-and-stick representations of **1** (**c**) and **2** (**d**). Co-crystallized solvent molecules and H are omitted and ligands are represented with pipes for clarity. C atoms are represented in grey, O atoms in red, N atoms in blue, Ca atoms in turquoise, Mn atoms in magenta and U atoms in green.

An X-ray diffraction study carried out on single crystals of **1** grown from a dichloromethane solution showed the presence of a square-shaped tetranuclear structure (Fig. 2a,c), similar to that found for the previously reported[23,35] tetranuclear uranyl(v) salen complexes {[UO_2(salen)]$_4$[μ_8-K]$_2$}·2[K(18C6)(Py)] and {[UO_2(salen)$_4$][μ_8-Rb]$_2$[Rb(18C6)]$_2$} (18C6 is 18-crown-6, or 1,4,7,10,13,16-hexaoxacyclooctadecane)[23,36].

Similar to the reactivity observed with calcium, the reaction of 2 equiv. of monomeric uranyl(v) complex [UO_2(salen)(Py)][Cp*$_2$Co] with 1 equiv. of $Mn(NO_3)_2$ in pyridine produced a highly insoluble dark violet microcrystalline powder. The presence of Mn(ii) results in a lower solubility and stability with respect to complex **1**; attempts to recrystallize it from dichloromethane resulted in partial decomposition, as indicated by the NMR spectrum showing the presence of uranyl(vi) salen in the resulting solution. However, crystals of reasonable quality were obtained by slow diffusion of a solution of 1 equiv. of $Mn(NO_3)_2$ in pyridine to a solution of 2 equiv. of [UO_2(salen)(Py)][Cp*$_2$Co] in pyridine. X-ray diffraction studies revealed the presence of a $U_{12}Mn_6$ cluster of uranyl(v) with a wheel topology (Fig. 2b,d).

Complex **2** provides a new example of a uranyl(v) cluster that is stable with respect to the disproportionation reaction and is the largest reported to date and the first containing UO_2^+–Mn cation–cation interactions. In contrast with the uranyl(v) clusters previously reported, **2** does not contain UO_2^+···UO_2^+ interactions; only the phenolate oxygens from the salen ligand bridge the uranium centres (Supplementary Fig. S13).

The structure of **2** is described as a centrosymmetric hexamer assembled from six triangles consisting of two salen-bound UO_2^+ cations, mutually coordinated through two salen–phenolate bridges, which are both involved through the uranyl oxygen in a cation–cation interaction with the same Mn^{2+} ion. This structure differs significantly from those of complex **1** and the few other characterized discrete polynuclear complexes of pentavalent uranyl. In all these systems, the oxo group of the uranyl moiety acts as a bridging group between two U atoms, producing different geometrical arrangement (T-shaped[21,35], diamond-shaped[21,34] and butterfly-shaped[37], as shown in Supplementary Fig. S13) with U–U distances ranging from 3.35 to 4.19 Å. In contrast, in the $U_{12}Mn_6$ wheel, two phenolate oxygens (each from a different salen ligand) bridge two uranyl(v) centres at 3.92(1) Å and one oxo group from each uranyl(v) complex binds a Mn(ii) ion to produce a triangle.

The six triangles are connected together to yield the final $U_{12}Mn_6$ wheel through the cation–cation interaction of the manganese ion from one triangle with the uranyl oxygen of an adjacent triangle. As a result, both oxygens of six uranyl(v) complexes are bound to a Mn(ii) ion; for the remaining six uranyl(v) complexes only one of the two oxygens is Mn-bound. Each Mn(ii) ion is six-coordinated by three pyridine nitrogens and by three uranyl(v) oxo groups from three different uranyl(v)–salen complexes, of which two belong to

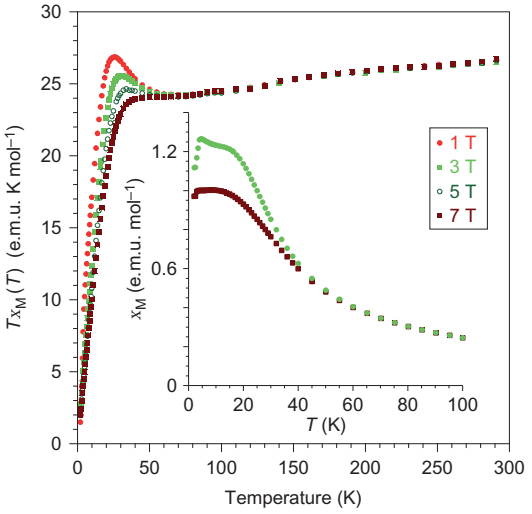

Figure 3 | Temperature dependence of the molar d.c. magnetic susceptibility $\chi_M(T)$ of complex 2. The $T\chi_M(T)$ data were collected after zero-field cooling in a magnetic field of 1 T (red circles), 3 T (green squares), 5 T (open olive circles) and 7 T (brown squares). Inset: $\chi_M(T)$ curve between 2 and 100 K in a field of 3 and 7 T. A contribution due to a ferromagnetic impurity has been subtracted, as discussed in the Supplementary Section S5.1.

the same triangle. The twelve U and six Mn ions are coplanar (mean deviation from the mean plane = 0.19(3) Å) and are arranged in a large circular array with a diameter of 2 nm (longest distance between two U ions). The 2:1 UO_2^+:Mn^{2+} ratio ensures the balance of charges and gives a neutral cluster. The mean value of the Mn–Mn distances (7.89(3) Å) is much longer than those reported for Mn_6 clusters presenting magnetic interaction between the Mn ions (3.2–3.4 Å)[38].

The mean Mn–O_{yl} bond distance (where O_{yl} is a uranyl oxygen)—2.15(2)Å—is similar to that found in a heterodinuclear uranyl(VI)–Mn(II) complex of a tetra-anionic pyrrole-imine macrocycle (often called 'pacman ligand') (Mn–O = 2.163(4) Å)[39]. The distance falls in the range of Mn–O_{Ph} (where O_{Ph} is a phenyl oxygen of the salen ligand) distances reported for Mn(II) ions in manganese clusters (2.135–2.500 Å)[6,40]. A similar distance (taking into account the difference of 0.128 Å between the Sm(III) and Mn(II) ionic radii) was also found for a uranyl(V)–Sm(III) complex (2.238(5) Å), showing strong magnetic coupling between uranium and samarium[39].

As observed in other UO_2^+ cation–cation clusters, the mean value of the U–O_{yl} distance is longer for the Mn-functionalized oxo group (U–O_{yl}(Mn) = 1.89(1) Å) than for the oxo group not involved in cation–cation interactions (U–O_{yl} = 1.83(3) Å). These U–O_{yl} distances are longer than those found in the uranyl(VI)–Mn(II) 'pacman' complex with the tetra-anionic pyrrole-imine macrocycle ligand (U–O_{yl} = 1.768(5) Å and U–O_{yl}(Mn) = 1.808(4) Å), in agreement with the presence of UO_2^+.

The new topology of the structure of **2** compared to the previously obtained dinuclear, trinuclear and tetranuclear cation–cation complexes is most probably the result of a combination of structure-directing parameters — the 2:1 UO_2^+:Mn^{2+} ratio used, the divalent charge of the Mn^{2+} ion, and the strong preference of divalent manganese for a octahedral geometry. Here, the UO_2^+–Mn^{2+} cation–cation interaction plays the structure-directing role.

Although several uranyl(V) mononuclear, polymeric and oligomeric complexes with different topologies have been reported that contain alkali ions[23,35,41], Fe(II)[42], Zn(II)[42], Sm(III)[38] or Y(III)[38], we are not aware of any other uranyl(V)–Mn(II) clusters. In contrast to previously reported uranyl(V) cluster compounds, **2** does not contain UO_2^+–UO_2^+ interactions but is exclusively built from the functionalization of the uranyl-oxo group by a Mn(II) ion. This provides further insight into the structure-directing parameters and should open the way to a rich variety of fascinating topologies. Moreover, **2** is the largest uranyl(V) cluster reported to date, with an original wheel topology that complements the previously reported diamond[21,34], square[23,35] and triangular structures[22].

Magnetic characterization. The temperature dependence of the d.c. magnetic susceptibility of the tetrameric U_4Ca_2 complex **1** (Supplementary Fig. S10) is very similar to that reported for the $[UO_2(salen)]_4[\mu_8\text{-}K]_2K_2$ analogue, showing a cusp at ~5 K, which initially suggested the presence of oxo-mediated antiferromagnetic coupling between the two uranyl ions. However, further magnetic characterization did not show features that would be consistent with a single-molecule magnet behaviour for **1**, as we had anticipated from the antiferromagnetic character of the U–U interaction.

Figure 3 shows the temperature-dependent d.c. magnetic susceptibility of the $U_{12}Mn_6$ wheel, $\chi_M(T)$, measured with a superconducting quantum interference device (SQUID) magnetometer and displayed as the product $T\chi_M(T)$. Below ~60 K, the $T\chi_M(T)$ curve shows a strong deviation from Curie behaviour. The increase with decreasing temperature observed between ~60 and ~30 K and the field variation of the magnetic response are very similar to those reported for the triangular-shaped $\{Np^{VI}O_2Cl_2\}\{Np^{V}O_2Cl(thf)_3\}_2$ complex (thf = tetrahydrofuran)[17]. In that case, the observed behaviour was understood as a combination of ligand field and superexchange interactions between the 5*f* centres. We suggest that a similar scenario is realized in **2**.

The ground-state degeneracy of the ions coupled by superexchange interactions is lifted by the magnetic field, leading to a higher energy state with parallel U and Mn magnetic moments and a lower energy state with antiparallel orientations. The susceptibility first increases with decreasing temperature because of the higher energy level contribution, then drops down when only the lower energy level is thermally populated.

The finite value of 1.5 e.m.u. K mol^{-1} for $T\chi_M(T)$, observed at ~2 K for B = 1 T, suggests a magnetic ground state for the wheel,

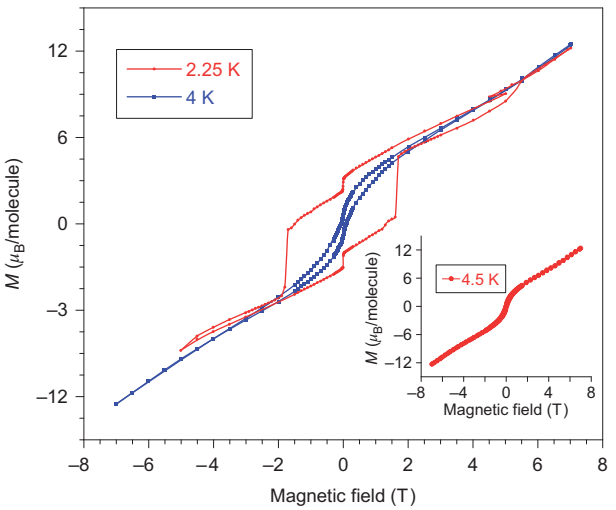

Figure 4 | Low-temperature magnetic hysteresis loops showing an open cycle. Magnetization versus applied d.c. field scan measured at 2.25 and 4 K while sweeping the field from 7 to −7 T and back, with a sweep rate of 0.004 T s^{-1}. Step-like changes at periodic field values are due to quantum tunnelling of the magnetization. Data collected at 4.5 K are shown in the inset.

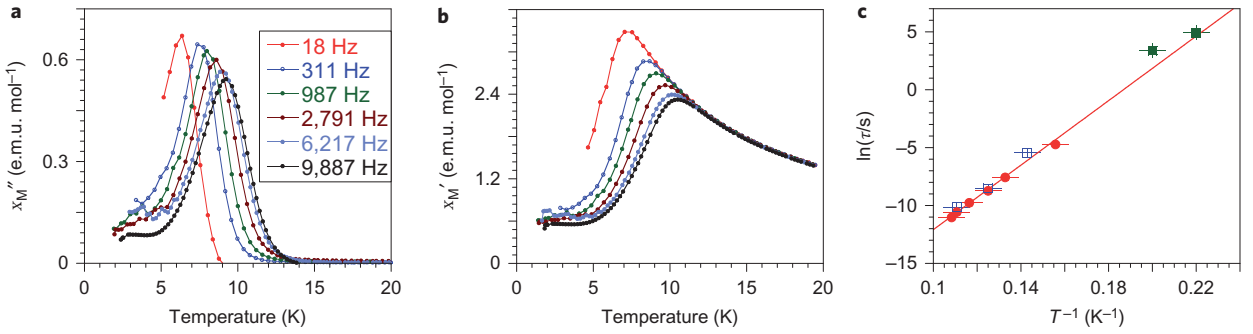

Figure 5 | Dynamic magnetic data and magnetization relaxation time data for compound 2. a,**b**, Temperature dependence of the out-of-phase (χ_M'', **a**) and in-phase (χ_M', **b**) components of the a.c. magnetic susceptibility measured in a 10 Oe a.c. field oscillating at the indicated frequencies, under zero d.c. field. **c**, Temperature dependence of the magnetic relaxation time τ under zero d.c. field is shown as ln(τ) versus T^{-1}, as obtained from data collected in temperature (filled circles) and frequency (open square) variation regimes. The values for the two lowest temperatures (filled squares) were obtained from time relaxation measurements of the d.c. magnetization assuming a monomodal distribution of the characteristic relaxation rate. The straight line is a fit to the Arrhenius relation, giving a thermal energy barrier for the relaxation of $\Delta = 142 \pm 7$ K and a pre-exponential factor $\tau_0 = (3 \pm 2) \times 10^{-12}$ s.

which is expected in the presence of strong antiferromagnetic interactions between the U^V and the Mn^{II} centres and a weaker antiferromagnetic interaction between the two U^V centres within a triangle. The former coupling is mediated by the uranyl O atoms, forming almost linear bonds with mean values of U–Mn distances of 3.92(1) and 3.89(2) Å within a given triangle, and of 4.03(1) Å between adjacent triangles. The interaction between two U(V) ions belonging to a given triangle is mediated by the salen–phenolate oxygens with mean U–U distance at 3.921 Å. Such an exchange topology would result in parallel coupling between the U moments, and antiparallel between the U and Mn moments. The difference between the magnetic moment of the Mn^{II} ions in the high-spin ($S = 5/2$) state and that of the $5f^1$ ions with a Γ_7 doublet stabilized by a strong axial ligand field means that the ground state of the wheel is magnetically uncompensated. A magnetic ground state would also be obtained in the case of low-spin Mn^{II} ions and a quasi-quartet ground state for the U ions.

Above 100 K, fitting $T\chi_M(T)$ as the sum of a Curie and a van Vleck term gives a T-independent contribution of ~0.01 e.m.u. mol^{-1} (due to the population of excited ligand-field states) and a paramagnetic moment $\mu_{eff} = 13.5 \pm 0.2\mu_B$, that is, $5.5\mu_B$ per each triangular unit. This value is about half that expected for a system formed by one Mn^{II} and two U^V free ions, suggesting that the overall exchange and ligand field splitting is much larger than 300 K. No attempts to quantify ligand field and exchange interactions have been put forth because the complexity of the system prevents a quantitative analysis in the absence of further information. The successful synthesis of an isostructural analogue with Mn replaced by a diamagnetic ion (such as Cd^{II}) and its magnetic characterization would allow the separate quantification of the U–U interactions in the complex and will be the subject of further studies.

The presence of a magnetic ground state is confirmed by the observation of magnetic hysteretic loops. As shown in Fig. 4, magnetic bistability is observed in the magnetization versus applied d.c. field scan taken at 4 K. With decreasing temperature the coercive field increases, reaching a value of ~1.5 T at 2.25 K. This behaviour is typical of a single-molecule magnet below its blocking temperature T_B (refs 43–45). Moreover, highly resolved step-like features are observed below 2.5 K, revealing the occurrence of quantum tunnelling of the magnetization increasing the relaxation rate[44,46,47]. These phenomena have been reported previously for several transition-metal complexes[48], in mononuclear lanthanide phthalocyanines[7] and in mixed 3*d*–4*f* complexes[49,50].

The in-phase component of the a.c. susceptibility, χ_M', shows a peak at a frequency-dependent temperature, reaching ~10 K at ~1 kHz, accompanied by a maximum in the out-of-phase component χ_M'' clearly indicating the occurrence of slow magnetic relaxation (Fig. 5). The overall behaviour of the peaks in χ_M'' closely resembles the data of Ishikawa *et al.* on diluted rare-earth bis-phthalocyanine samples rather than on pure ones[7], and together with the ratio between the peak amplitudes in the out-of-phase and in-phase susceptibility components[14] confirms that intermolecular interactions are extremely weak. The crystal structure of this complex clearly shows that there are no strong intermolecular contacts, with the shortest intermetallic distances being 8–10 Å, ruling out the presence of strong intermolecular magnetic interactions.

The relaxation behaviour can be fitted (see Methods and Supplementary Section S5.2) to an Arrhenius relation, $\tau = \tau_0 \exp(\Delta/k_BT)$, corresponding to a thermally activated regime, and a linear regression of the experimental data provides a pre-exponential factor of $\tau_0 = (3 \pm 2) \times 10^{-12}$ s and a barrier to relaxation of $\Delta = 142 \pm 7$ K (Fig, 5c), larger than for any previously reported manganese cluster[4]. The value of τ_0 is smaller than for typical small transition-metal SMMs (for instance, τ_0 is of the order of 1×10^{-10} s for the manganese compound $[Mn(III)_6O_2(Etsao)_6\{O_2CPh(Me)_2\}(EtOH)_6]$) (ref. 4), but similar values are commonly found in high-nuclearity SMMs[51]. Moreover, a much smaller value of τ_0 in 5*f*-block SMMs than in transition-metal SMMs can be expected because active orbital degrees of freedom can affect the magnetoelastic interaction.

Conclusions

Our results demonstrate that cation–cation interaction between actinyl complexes and 3*d* transition-metal cations provides an effective way to build large heterometallic 5*f*–3*d* assemblies. The $U_{12}Mn_6$ wheel is the largest heterometallic 5*f*–3*d* cluster reported to date. A rich variety of topologies can be anticipated by the reaction between actinyl complexes in different ligand environments and in the presence of different transition-metal cations. Future efforts will be directed in this direction for the development of new stable polymetallic clusters based on pentavalent uranyl and its NpO_2^+ analogues. The $U_{12}Mn_6$ wheel prepared in this work exhibit superparamagnetic behaviour with a relaxation barrier higher than that of any molecular wheel reported so far. In contrast with the few previous reports on 5*f*-block organo-metallic SMM complexes, which all present butterfly-shaped hysteresis with zero coercive field, this $U_{12}Mn_6$ cluster shows open staircase-like magnetization hysteretic loops with non-zero coercive field (below about 4 K) and clear evidence of quantum relaxation phenomena (below 2.25 K). The interesting magnetic properties of the $U_{12}Mn_6$ cluster suggest that the use of the highly

anisotropic uranium ions is a very promising route in the quest for better performing single-molecule magnets.

Methods

Synthesis of complex **1** is described in Supplementary Section S2.1.

The proton NMR spectrum of solutions of **1** in pyridine displays features similar to those observed for the K and Rb adducts, in agreement with the retention of the tetranuclear structure. The Fourier transform infrared (FTIR) spectrum of **1** in KBr pellets (Supplementary Fig. S1) contains a band at 756 cm^{-1} assigned to U–O stretches that are weakened with respect to the uranyl(VI) analogue $[UO_2(salen)(Py)]$ complex (asymmetric U–O stretch at 892 cm^{-1})[23]. These data support the pentavalent oxidation state of the isolated compound.

2. A dark brown solution of Cp^*_2Co (53.5 mg, 0.162 mmol, 1 equiv.) in pyridine (1 ml) was added under stirring to give a bright orange solution of $[UO_2(salen)(py)]$ (100 mg, 0.162 mmol, 1 equiv.) in pyridine (2 ml), resulting in a dark green solution, which was stirred for 1 h. The dark green solution was filtered, and a solution of $Mn(NO_3)_2$ (14.5 mg, 0.081 mmol, 0.5 equiv.) in pyridine (5 ml) was added dropwise to the filtrate under stirring, resulting in the precipitation of a dark violet powder. The suspension was stirred for 3 h at room temperature, and the dark violet precipitate was filtered out and washed with pyridine (10 × 1.5 ml) and dried thoroughly under vacuum to yield 82 mg of a violet powder of $[\{[UO_2(salen)]_2Mn(Py)_3\}_6]$ (0.010 mmol, 74%).

Elemental analysis (%) calculated for $[\{[UO_2(salen)]_2Mn(Py)_3\}_6]$ ($C_{282}H_{258}N_{42}Mn_6O_{48}U_{12}$ 8189.38 g mol^{-1}) C 41.36, H 3.18 and N 7.18, found C 41.02, H 3.18 and N 7.08.

Crystals suitable for X-ray diffraction were obtained using a slow diffusion method, as described in Supplementary Section S2.2.

The FTIR spectrum in KBr pellets of X-ray quality crystals of **2** prepared by the slow diffusion method is identical to that for the bulk dark violet microcrystalline powder. The spectrum shows similar features to **1** with a band at 752 cm^{-1} assigned to uranyl(V) U–O stretches (Supplementary Fig. S2). Elemental analysis and magnetic data (see below) also confirm the formula of the complex and that the same species is obtained using either method (slow diffusion and direct reaction).

Crystallographic data were collected using a Oxford Diffraction Xcalibur-S kappa geometry diffractometer (Mo-Kα radiation, graphite monochromator, λ = 0.71073 Å) and have been deposited in the Cambridge Structural Database as CCDC 871784 (**1**) and CCDC 871785 (**2**).

Temperature-dependent d.c. magnetic susceptibility data of the $U_{12}Mn_6$ wheel were collected from 2 to 300 K at different fields up to 7 T, after zero-field cooling from room temperature. The raw experimental data were corrected by subtracting the calculated diamagnetic contribution and a temperature-independent magnetization term, $M_{imp} = 6.7 \times 10^{-3}\mu_B$, as described in Supplementary Section S5. To characterize the relaxation of the magnetization at low temperature, a.c. magnetic susceptibility measurements were performed on polycrystalline samples in a 10 Oe a.c. field oscillating at a frequency f varying between 18 and 9,887 Hz. Data were collected either as a function of temperature T for a given f (Fig. 5) or by sweeping f at constant temperature (Supplementary Figs S7–S9).

The characteristic relaxation time $\tau(T)$ can be estimated from the inverse of the driving field angular frequency, $\omega = 2\pi f$, at the peak temperature of the χ_M'' curves. Alternatively, $\tau(T)$ can be determined by fitting a.c. susceptibility isotherms measured as a function of ω to a generalized Debye model providing the average relaxation time and a parameter α, determining the width of the distribution function of relaxation times (Supplementary Information). The values obtained for α suggest a more complex relaxation scenario than in transition-metal SMMs, with a wide distribution of relaxation times. The results obtained are shown in Fig. 5. The value corresponding to the lowest temperatures (T = 4.5 K and 5 K) were obtained by fitting to a single stretched-exponential behaviour the time dependence of the d.c. magnetization measured with the SQUID, giving τ = 140 s for T = 4.5 K and τ = 30 s for T = 5 K. Additional details on magnetic measurements are provided in the Supplementary Information.

Received 10 May 2012; accepted 4 October 2012; published online 11 November 2012

References

1. Wernsdorfer, W., Aliaga-Alcalde, N., Hendrickson, D. N. & Christou, G. Exchange-biased quantum tunnelling in a supramolecular dimer of single-molecule magnets. *Nature* **416,** 406–409 (2002).
2. Gatteschi, D., Sessoli, R. & Villain, J. *Molecular Nanomagnets* (Oxford Univ. Press, 2006).
3. Affronte, M. *et al.* Linking rings through diamines and clusters: exploring synthetic methods for making magnetic quantum gates. *Angew. Chem. Int. Ed.* **44,** 6496–6500 (2005).
4. Milios, C. *et al.* A record anisotropy barrier for a single-molecule magnet. *J. Am. Chem. Soc.* **129,** 2754–2755 (2007).
5. Bogani, L. & Wernsdorfer, W. Molecular spintronics using single-molecule magnets. *Nature Mater.* **7,** 179–186 (2008).
6. Ako, A. *et al.* A ferromagnetically coupled Mn-19 aggregate with a record S = 83/2 ground spin state. *Angew. Chem. Int. Ed.* **45,** 4926–4929 (2006).
7. Ishikawa, N., Sugita, M., Ishikawa, T., Koshihara, S. & Kaizu, Y. Lanthanide double-decker complexes functioning as magnets at the single-molecular level. *J. Am. Chem. Soc.* **125,** 8694–8695 (2003).
8. Rinehart, J. D., Fang, M., Evans, W. J. & Long, J. R. Strong exchange and magnetic blocking in $(N_2)^{3-}$-radical-bridged lanthanide complexes. *Nature Chem.* **3,** 538–542 (2011).
9. Blagg, R. J., Tuna, F., McInnes, E. J. L. & Winpenny, R. E. P. Pentametallic lanthanide-alkoxide square-based pyramids: high energy barrier for thermal relaxation in a holmium single molecule magnet. *Chem. Commun.* **47,** 10587–10589 (2011).
10. Blagg, R. J., Muryn, C. A., McInnes, E. J. L., Tuna, F. & Winpenny, R. E. P. Single pyramid magnets: Dy_5 pyramids with slow magnetic relaxation to 40 K. *Angew. Chem. Int. Ed.* **50,** 6530–6533 (2011).
11. Rinehart, J. D., Fang, M., Evans, W. J. & Long, J. R. A $(N_2)^{3-}$-radical-bridged terbium complex exhibiting magnetic hysteresis at 14 K. *J. Am. Chem. Soc.* **133,** 14236–14239 (2011).
12. Rinehart, J. D., Meihaus, K. R. & Long, J. R. Observation of a secondary slow relaxation process for the field-induced single-molecule magnet $U(H_2BPz_2)_3$. *J. Am. Chem. Soc.* **132,** 7572–7573 (2010).
13. Antunes, M. A. *et al.* $[U(Tp(Me_2))_2(bipy)]^+$: a cationic uranium(III) complex with single-molecule-magnet behavior. *Inorg. Chem.* **50,** 9915–9917 (2011).
14. Magnani, N. *et al.* Magnetic memory effect in a transuranic mononuclear complex. *Angew. Chem. Int. Ed.* **50,** 1696–1698 (2011).
15. Mills, D. *et al.* A delocalized arene-bridged diuranium single-molecule magnet. *Nature Chem.* **3,** 454–460 (2011).
16. Mazzanti, M. Uranium memory. *Nature Chem.* **3,** 426–427 (2011).
17. Magnani, N. Superexchange coupling and slow magnetic relaxation in a transuranium polymetallic complex. *Phys. Rev. Lett.* **104,** 197202 (2010).
18. Lam, O. P., Heinemann, F. W. & Meyer, K. Activation of elemental S, Se and Te with uranium(III): bridging U–E–U (E = S, Se) and diamond-core complexes $U–(E)_2–U$ (E=O, S, Se, Te). *Chem. Sci.* **2,** 1538–1547 (2011).
19. Spencer, L. P. *et al.* M. Cation–cation interactions, magnetic communication, and reactivity of the pentavalent uranium ion $[U(N^tBu)_2]^+$. *Angew. Chem. Int. Ed.* **48,** 3795–3798 (2009).
20. Kozimor, S. A., Bartlett, B. M., Rinehart, J. D. & Long, J. R. Magnetic exchange coupling in chloride-bridged 5*f*–3*d* heterometallic complexes generated via insertion into a uranium(IV) dimethylpyrazolate dimer. *J. Am. Chem. Soc.* **129,** 10672–10673 (2007).
21. Nocton, G., Horeglad, P., Pecaut, J. & Mazzanti, M. Polynuclear cation–cation complexes of pentavalent uranyl: relating stability and magnetic properties to structure. *J. Am. Chem. Soc.* **130,** 16633–16645 (2008).
22. Chatelain, L., Mougel, V., Pecaut, J. & Mazzanti, M. *Chem. Sci.* **3,** 1075–1079 (2012).
23. Mougel, V., Horeglad, P., Nocton, G., Pecaut, J. & Mazzanti, M. Stable pentavalent uranyl species and selective assembly of a polymetallic mixed-valent uranyl complex by cation–cation interactions. *Angew. Chem. Int. Ed.* **48,** 8477–8480 (2009).
24. Rosen, R. K., Andersen, R. A. & Edelstein, N. M. $[MeC_5H_4)_3U]_2$ [μ-1,4-$N_2C_6H_4$]—a bimetallic molecule with antiferromagnetic coupling between the uranium centers. *J. Am. Chem. Soc.* **112,** 4588–4590 (1990).
25. Kiplinger, J. L. *et al.* Actinide-mediated cyclization of 1,2,4,5-tetracyanobenzene: synthesis and characterization of self-assembled trinuclear thorium and uranium macrocycles. *Angew. Chem. Int. Ed.* **45,** 2036–2041 (2006).
26. Sigmon, G. E. & Burns, P. C. Rapid self-assembly of uranyl polyhedra into crown clusters. *J. Am. Chem. Soc.* **133,** 9137–9139 (2011).
27. Evans, W. J., Kozimor, S. A. & Ziller, J. W. Molecular octa-uranium rings with alternating nitride and azide bridges. *Science* **309,** 1835–1838 (2005).
28. Nocton, G., Pecaut, J. & Mazzanti, M. A nitrido-centered uranium azido cluster obtained from a uranium azide. *Angew. Chem. Int. Ed.* **47,** 3040–3042 (2008).
29. Biswas, B., Mougel, V., Pecaut, J. & Mazzanti, M. Base-driven assembly of large uranium oxo/hydroxo clusters. *Angew. Chem. Int. Ed.* **50,** 5744–5747 (2011).
30. Le Borgne, T., Riviere, E., Marrot, J., Girerd, J. J. & Ephritikhine, M. Synthesis, crystal structure, and magnetic behavior of linear M_2(II)–U(IV) complexes (M=Co, Ni, Cu, Zn). *Angew. Chem. Int. Ed.* **39,** 1647–1649 (2000).
31. Arnold, P. L., Patel, D., Wilson, C. & Love, J. B. Reduction and selective oxo group silylation of the uranyl dication. *Nature* **451,** 315–318 (2008).
32. Monreal, M. J., Carver, C. T. & Diaconescu, P. L. Redox processes in a uranium bis(1,1′-diamidoferrocene) complex. *Inorg. Chem.* **46,** 7226–7228 (2007).
33. Krot, N. N. & Grigoriev, M. S. Cation–cation interaction in crystalline actinide compounds. *Russ. Chem. Rev.* **73,** 89–100 (2004).
34. Arnold, P. *et al.* Single-electron uranyl reduction by a rare-earth cation. *Angew. Chem. Int. Ed.* **50,** 887–890 (2011).
35. Mougel, V., Horeglad, P., Nocton, G., Pecaut, J. & Mazzanti, M. Cation–cation complexes of pentavalent uranyl: from disproportionation intermediates to stable clusters. *Chem. Eur. J.* **16,** 14365–14377 (2010).

36. Mougel, V., Biswas, B., Pecaut, J. & Mazzanti, M. New insights into the acid mediated disproportionation of pentavalent uranyl. *Chem. Commun.* **46,** 8648–8650 (2010).
37. Arnold, P. L. *et al.* Strongly coupled binuclear uranium–oxo complexes from uranyl oxo rearrangement and reductive silylation. *Nature Chem.* **4,** 221–222 (2012).
38. Milios, C. J. *et al.* Toward a magnetostructural correlation for a family of Mn_6 SMMs. *J. Am. Chem. Soc.* **129,** 12505–12511 (2007).
39. Arnold, P. L., Patel, D., Blake, A. J., Wilson, C. & Love, J. B. Selective oxo functionalisation of the uranyl ion with 3*d* metal cations. *J. Am. Chem. Soc.* **128,** 9610–9611 (2006).
40. Boskovic, C. *et al.* Single-molecule magnets: novel Mn_8 and Mn_9 carboxylate clusters containing an unusual pentadentate ligand derived from pyridine-2,6-dimethanol. *Inorg. Chem.* **41,** 5107–5118 (2002).
41. Nocton, G. *et al.* Synthesis, structure, and bonding of stable complexes of pentavalent uranyl. *J. Am. Chem. Soc.* **132,** 495–508 (2010).
42. Arnold, P. L. *et al.* Uranyl oxo activation and functionalization by metal cation coordination. *Nature Chem.* **2,** 1056–1061 (2010).
43. Gatteschi, D. Molecular magnetism—a basis for new materials. *Adv. Mater.* **6,** 635–645 (1994).
44. Sessoli, R., Gatteschi, D., Caneschi, A. & Novak, M. A. Magnetic bistability in a metal-ion cluster. *Nature* **365,** 141–143 (1993).
45. Sessoli, R. *et al.* High-spin molecules—$[Mn_{12}O_{12}(O_2Cr)_{16}(H_2O)_4]$. *J. Am. Chem. Soc.* **115,** 1804–1816 (1993).
46. Thomas, L. *et al.* Macroscopic quantum tunnelling of magnetization in a single crystal of nanomagnets. *Nature* **383,** 145–147 (1996).
47. Gatteschi, D. & Sessoli, R. Quantum tunneling of magnetization and related phenomena in molecular materials. *Angew. Chem. Int. Ed.* **42,** 268–297 (2003).
48. Stamatatos, T. C. *et al.* 'Switching on' the properties of single-molecule magnetism in triangular manganese(III) complexes. *J. Am. Chem. Soc.* **129,** 9484–9499 (2007).
49. Stamatatos, T. C., Teat, S. J., Wernsdorfer, W. & Christou, G. Enhancing the quantum properties of manganese-lanthanide single-molecule magnets: observation of quantum tunneling steps in the hysteresis loops of a $\{Mn_{12}Gd\}$ cluster. *Angew. Chem. Int. Ed.* **48,** 521–524 (2009).
50. Rinck, J. *et al.* An octanuclear $[Cr_4(III)Dy_4(III)]$ 3*d*–4*f* single-molecule magnet. *Angew. Chem. Int. Ed.* **49,** 7583–7587 (2010).
51. Papatriantafyllopoulou, C., Wernsdorfer, W., Abboud, K. A. & Christou, G. $Mn_{21}Dy$ cluster with a record magnetization reversal barrier for a mixed 3*d*/4*f* single-molecule magnet. *Inorg. Chem.* **50,** 421–423 (2011).

Acknowledgements

The authors acknowledge support from the Commissariat à l'Energie Atomique, Direction de l'Energie Nucléaire, RBPCH programme and by the 'Agence Nationale de la Recherche', (ANR-10-BLAN-0729). The authors also thank F. Jacquot and L. Dubois for support and suggestions regarding the magnetic measurements, A. De Geyer for recording the PXRD diffractogram, N. Magnani, P. Santini and S. Carretta for useful discussions on the interpretation of the magnetic data.

Author contributions

V.M. carried out the synthesis experiments, measured the d.c. magnetic data and analysed the experimental data. L.C. performed the preliminary experiments. R.C., E.C. and J.C.G. collected and analysed the magnetic measurement data and created the magnetic model. J.P. and V.M. carried out X-ray single-crystal structure analyses. M.M. originated the central idea, coordinated the work and analysed the experimental data. M.M., V.M. and R.C. wrote the manuscript.

Additional information

Supplementary information and chemical compound information are available in the online version of the paper. Reprints and permission information is available online at http://www.nature.com/reprints. Correspondence and requests for materials should be addressed to M.M.

Competing financial interests

The authors declare no competing financial interests.

Molecular Magnets

DOI: 10.1002/anie.201307366

A Uranium-Based UO_2^+–Mn^{2+} Single-Chain Magnet Assembled trough Cation–Cation Interactions**

*Victor Mougel, Lucile Chatelain, Johannes Hermle, Roberto Caciuffo, Eric Colineau, Floriana Tuna, Nicola Magnani, Arnaud de Geyer, Jacques Pécaut, and Marinella Mazzanti**

Abstract: *Single-chain magnets (SCMs) are materials composed of magnetically isolated one-dimensional (1D) units exhibiting slow relaxation of magnetization. The occurrence of SCM behavior requires the fulfillment of stringent conditions for exchange and anisotropy interactions. Herein, we report the synthesis, the structure, and the magnetic characterization of the first actinide-containing SCM. The 5f–3d heterometallic 1D chains $[\{[UO_2(salen)(py)][M(py)_4](NO_3)\}]_n$ (M = Cd (**1**) and M = Mn (**2**); py = pyridine) are assembled trough cation–cation interaction from the reaction of the uranyl(V) complex $[UO_2(salen)py][Cp^*_2Co]$ (Cp^* = pentamethylcyclopentadienyl) with $Cd(NO_3)_2$ or $Mn(NO_3)_2$ in pyridine. The infinite UMn chain displays a high relaxation barrier of 134 ± 0.8 K (93 ± 0.5 cm^{-1}), probably as a result of strong intra-chain magnetic interactions combined with the high Ising anisotropy of the uranyl(V) dioxo group. It also exhibits an open magnetic hysteresis loop at T < 6 K, with an impressive coercive field of 3.4 T at 2 K.*

Single-chain magnets (SCMs) present an attractive alternative to discrete molecular clusters behaving as single molecule magnets (SMMs) in the design of molecular materials for magnetic information storage and processing.[1] SCMs[2] are one-dimensional coordination polymers that display slow relaxation of the magnetization and hysteresis effects as a result of the intra-chain exchange interactions that usually develop into 1D ferromagnetic spin–spin correlations at low temperature. In the design of improved SCMs required for application at practical temperatures, three strict requirements need to be fulfilled: a strong Ising anisotropy of the magnetic centers, strong intra-chain magnetic interactions, and weak interchain interactions. Since the first experimental evidence of the existence of a SCM was reported in 2001[3] (predicted earlier by Glauber[4]), efforts in the design of SCMs with higher reversal barriers have focused on the use of metal ions with strong anisotropy, such as Co^{2+}, Ni^{2+}, Mn^{3+}, Fe^{2+}, Re^{4+},[2c,5] and, more recently, lanthanide ions.[6]

Actinides, and uranium in particular, are currently attracting large attention in the field of molecular magnetism because of their large single-ion anisotropy and enhanced covalency, as compared to lanthanide ions, which should promote magnetic communication.[7] As such, uranium-based compounds are well suited for the design of molecular magnets with higher anisotropy barriers and hysteresis temperatures for practical applications. Several examples of mononuclear complexes of uranium showing slow relaxation of magnetization have been reported in the last few years.[8] The single-ion magnetic behavior of these compounds arises from the high anisotropy generated by the axial ligand environment. Fewer examples of polynuclear-actinide-based single-molecule magnets have also been reported.[9] However, to date there are no reported examples of actinide-based SCMs.

Cation–cation interactions[10] (CCI; a term used to describe the bonding interaction of an actinyl oxo or imido group with a metal cation) provide a versatile route for the assembly of homopolymetallic and heteropolymetallic discrete clusters[9c,11–13,17] or 1D chains[14] of pentavalent uranium, and a pathway for intermetallic magnetic exchange.[9c,12,13a,15] We have also recently reported the first 5f–3d cation–cation cluster, a large $U_{12}Mn_6$ wheel that exhibits SMM behavior,[9c] but CCI has not yet been used to promote the assembly of 1D

[*] Dr. V. Mougel, L. Chatelain, Dr. J. Hermle, Dr. J. Pécaut, Dr. M. Mazzanti
Laboratoire de Reconnaissance Ionique et Chimie de Coordination
SCIB, UMR-E3 CEA-UJF, INAC, CEA-Grenoble
17 rue des Martyrs, 38054 Grenoble Cedex 09 (France)
E-mail: marinella.mazzanti@cea.fr
Homepage: http://inac.cea.fr/Pisp/51/marinella.mazzanti.html
Dr. A. de Geyer
Service Général des Rayons X, SP2M, INAC, CEA-Grenoble
17 rue des Martyrs, 38054 Grenoble Cedex 09 (France)
Dr. F. Tuna
EPSRC UK EPR Facility, School of Chemistry and Photon Science Institute, The University of Manchester
Oxford Road, Manchester, M13 9PL (UK)
Dr. R. Caciuffo, Dr. E. Colineau
European Commission, Joint Research Centre
Institute for Transuranium Elements
P.O. Box 2340, 76125 Karlsruhe (Germany)
Dr. N. Magnani
Institute of Nanotechnology
Karlsruhe Institute of Technology
Hermann-von-Helmholtz Platz 1
76344 Eggenstein-Leopoldshafen (Germany)

[**] We thank François Jacquot for his support and suggestions in magnetic measurements. We acknowledge support from the Commissariat à l'Energie Atomique, Direction de l'Energie Nucléaire (RBPCH program), the "Agence Nationale de la Recherche" (ANR-10-BLAN-0729) and EPSRC UK.

Supporting information for this article is available on the WWW under http://dx.doi.org/10.1002/anie.201307366.

chains associating pentavalent uranyl and d-block transition metals.

Herein, we report the first example of a uranium-based SCM that is formed by CCI between the Mn^{II} ion and the two oxo groups of a uranyl(V) complex. This infinite chain displays a high relaxation barrier of 134 ± 0.8 K, probably as a result of strong intra-chain magnetic interactions combined with the high Ising anisotropy of the uranyl(V) dioxo group. It also exhibits an open magnetic hysteresis loop at $T < 6$ K, with an impressive coercive field of 3.4 T at 2 K.

The reaction of the monomeric uranyl(V) complex $[UO_2(salen)py][Cp^*_2Co]$ with $Cd(NO_3)_2$ in pyridine in a 1:1 ratio affords the coordination polymer $[\{[UO_2(salen)(py)][Cd(py)_4](NO_3)\}]_n$ (**1**), as a pink microcrystalline powder in 65% yield (Scheme 1). X-ray quality single crystals of **1**·2 py

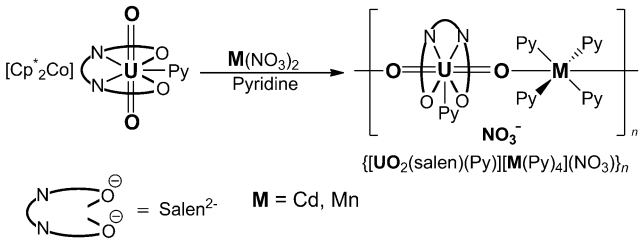

Scheme 1. Synthesis of the 1D chains **1** and **2**.

were obtained by slow diffusion of pyridine solutions of the two reactants. Using a similar procedure, the manganese analogue $[\{[UO_2(salen)(py)][Mn(py)_4](NO_3)\}]_n$ (**2**) was synthesized in 65% yield.

Both complexes are stable in the solid state for months under argon atmosphere. It is also quite remarkable that, in spite of the higher charge of the Mn^{2+} and Cd^{2+} ions compared to UO_2^+, scrambling of the salen ligand is not observed, which points to the presence of a very strong CCI interaction in **1** and **2**.

X-ray diffraction studies of **1** show the presence of alternating layers of NO_3^- anions and of cationic dimetallic chains $\{[UO_2(salen)(py)][Cd(py)_4]\}_n^{n+}$ (Figure 1; see also the Supporting Information, Figure S2). The asymmetric unit of **1** contains three uranium and three cadmium ions, which are crystallographically non-equivalent due to the non-linear arrangement of the UO_2^+ groups and Cd^{2+} ions along the chain (Figure 1, bottom). The cationic polymeric chain $\{[UO_2(salen)(py)][Cd(py)_4]\}_n^+$ is formed by the cation–cation interaction of each uranyl(V) oxo group of $[UO_2(salen)py]^-$ complexes with a Cd^{2+} ion. The U-O-Cd angle deviates slightly from linearity and ranges from 161.67° to 175.15°. The uranium atom is heptacoordinated with a slightly distorted pentagonal bipyramidal geometry, with the four donor atoms of the salen ligand situated in the equatorial plane and the two uranyl oxygens in the axial position; the seventh coordination position is occupied by a pyridine nitrogen. The cadmium ion is six coordinated in an octahedral geometry, with the two uranyl(V) oxo groups in apical positions and the four pyridine nitrogens in its equatorial plane. The mean Cd–O_{yl} distance of 2.28(2) Å, is in the range of those found in a heterobimetallic U^{VI}/Cd^{II} carboxyphosphonate networks with Cd^{2+} ions coordinated to the apical oxygens of the uranyl(VI) moieties[16] (Cd-O_{yl} = 2.252(4) Å). The U–O_{yl} distance in **1** (1.87(2) Å) is in the range of U–O_{yl} distances found for uranyl(V) oxo groups involved in cation–cation interactions leading to discrete clusters[9c,17] or 1D polymeric chains.[14,18]

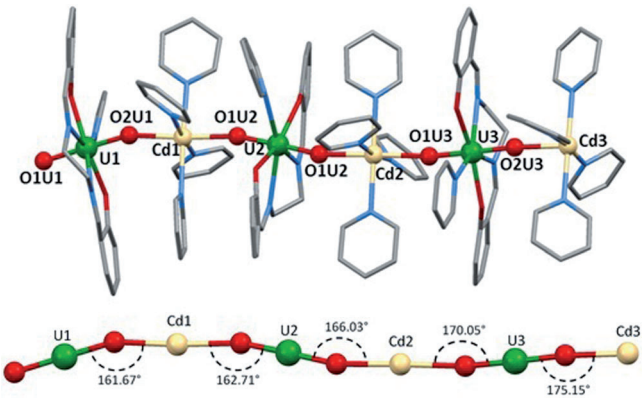

Figure 1. Mercury view of the structure of **1** (top) and a detail of the core with associated distances and angles (bottom). Hydrogen atoms and cocrystallized solvent molecules omitted for clarity. C grey, O red, Cd cream, N light blue, U green.

X-ray analysis was also performed on single crystals of **2** and shows the presence of a coordination polymer isostructural to complex **1** (see the Supporting Information). The poor quality of the crystals does not lead to a publishable structure, but the connectivity of the polymer is unambiguously determined. The difference in ionic radii of Mn^{2+} (0.67 Å) compared to Cd^{2+} (0.95 Å) results in shorter intra-chain separations between neighboring U^V ions (U–U = 8.0 and 8.1 Å in **2**, and 8.19 and 8.36 Å in **1**) and between neighboring M^{II} ions (Mn–Mn = 8.1 Å in **2**, and Cd–Cd = 8.32 and 8.25 Å in **1**).

X-ray powder diffraction patterns recorded for microcrystalline samples of **1** and **2** (see the Supporting Information) are consistent with those calculated from the X-ray single crystal data and show that both bulk samples contain homogeneous isostructural compounds.

There is no evidence of significant inter-chain hydrogen bonding or π-stacking interactions in the structure of **1**. Owing to the presence of the bulky salen ligand, the chains are well-separated, with the shortest inter-chain U–U and U–Cd distances at 11.99 and 11.69 Å, respectively, in **1**; the shortest inter-chain U–U, U–Mn and Mn–Mn distances are 11.4, 10.9 and 11.5 Å, respectively, in **2**. These features indicate the presence of magnetically isolated chains in the two isostructural complexes **1** and **2**.[2a,c]

Variable-temperature (2–300 K) magnetic susceptibility measurements were performed on polycrystalline samples of **1** and **2** in static magnetic fields ranging from 0.01 to 5 T (Figure 2 and the supplementary information). The measured χT value for **2** at room temperature is approximately 4.3 $cm^3 K mol^{-1}$; considering that the susceptibility curves for the Cd-based analogue **1** (see the Supporting Information) point towards a much smaller χT value (below 0.3 $cm^3 K mol^{-1}$) we can conclude that this value is in line

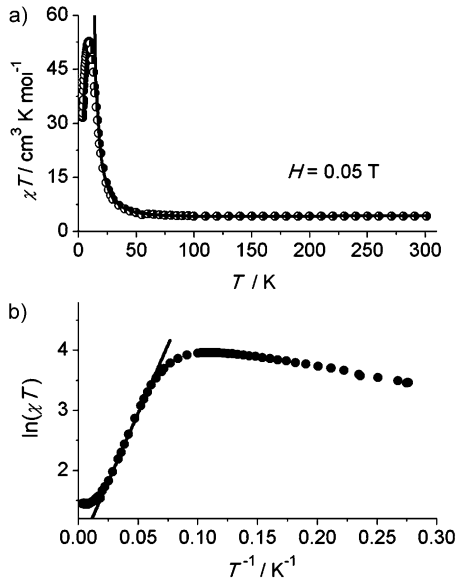

Figure 2. Plots of a) χT vs. T and b) ln (χT) vs. $1/T$ for a polycrystalline sample of **2** measured at 0.05 T applied field.

with what is expected for one spin-only divalent manganese (with $S = 5/2$ and g close to 2) and one pentavalent uranium ion, whose magnetic moment is significantly reduced with respect to the free-ion value by the combined effect of ligand field and covalent bonding.[19] The χT product decreases with decreasing temperature to 4.1–4.2 cm^3 K mol^{-1} at 150 K; the fact that the same quantitative behavior is observed for **1** and that the decrease is similar in absolute value for the two compounds, allows the attribution of this effect to the ligand-field state depopulation for the anisotropic uranium centers, whereas the contribution of the more isotropic manganese ions can be approximately regarded as constant within this temperature range. Below 150 K, the susceptibility of **2** increases to reach a field-dependent maximum, with values of 56.8 cm^3 K mol^{-1} at 0.01 T (Figure S9) and 52.7 cm^3 K mol^{-1} at 0.05 T (Figure 2), before dropping rapidly at very low temperatures owing to saturation effects, magnetic anisotropy, and possibly inter-chain antiferromagnetic interactions. The increase of χT below 150 K, as well as the strong deviation from the Curie–Weiss behavior of χ^{-1} vs. T (see the Supporting Information), suggests dominant ferromagnetic interactions leading to an aligned-spin ground state. None of this is observed for the Cd-based analogue **1**, where only an abrupt decrease of the χT product below 25 K is observed, which is most likely due to single-ion crystal field effects associated with U^V,[8a] quenching of the orbital angular momentum, and possibly weak next-nearest-neighbor antiferromagnetic exchange between uranium centers.

A scaling procedure of the χT data of **2** (Figure 2) clearly indicates the occurrence of a linear regime, which is characteristic of Ising 1D systems.[2a,20] The ln(χT) versus $1/T$ plot increases linearly between 45 and 16 K. Fitting the experimental data within this linear regime using the equation $\chi T = C_{eff} \exp(\Delta/k_B T)$, which describes a ferromagnetically coupled infinite chain, gives an energy gap (Δ/k_B) of 45.5 K and a pre-exponential factor (C_{eff}) of 1.98. Very similar results for the ferromagnetic exchange gap are obtained by fitting the magnetic susceptibility data of **2** at 16–300 K with the equation $\chi T = [C_1 \exp(\Delta_1/k_B T)] + [C_2 \exp(\Delta_2/k_B T)]$, where a second negative exponential that vanishes at 0 K is added to take into account the high-temperature crystal field effect or antiferromagnetic contribution.[6c] In this case, we obtained $\Delta_1/k_B = 45.5$ K, $\Delta_2/k_B = -90.2 \pm 9.4$ K, $C_1 = 1.98$, and $C_2 = 2.73$, which is in very good agreement with the previous considerations. As expected, the high-temperature extrapolated Curie constant, $C = C_1 + C_2 = 4.71$ cm^3 K mol^{-1}, is close to the expected value for one Mn^{II} ion and one U^V ion.

The existence of a magnetic ground state in **2** is further confirmed by the observation of magnetic hysteresis loops. As shown in Figure 3, magnetic bistability is observed in all

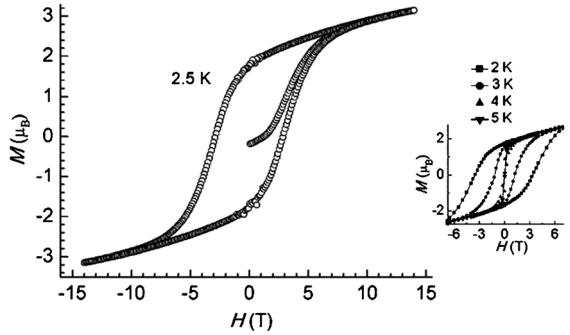

Figure 3. Field dependence of the magnetization of **2** measured at 2.5 K. Inset shows hysteresis loops recorded at four different temperatures.

magnetization versus field scans at 2–5 K. With decreasing temperature, the coercive field increases, reaching a value of 3.4 T at 2 K. At zero field, a remanent magnetization (REM) of 1.7 μ_B is preserved. This behavior is typical of a single-chain magnet below its blocking temperature (T_B). Indeed, below 6 K a divergence is observed between zero-field-cooled and field-cooled magnetizations as a function of temperature (see the Supporting Information). In addition, REM vanishes at ca. 5.8 K, which corresponds to the blocking temperature of the material.

To probe the magnetization relaxation in **2**, zero-field alternating current (AC) susceptibility measurements at 2–15 K were carried out at several frequencies: at 10–9887 Hz with a 10 G AC field (Figure 4; see also the Supporting Information), and at 0.1–1399 Hz with a 1.55 G AC field (see the Supporting Information). Below 12 K, both the in-phase (χ') and out-of-phase (χ'') components of the AC susceptibility are strongly frequency dependent, and $\chi'(T,f)$ and $\chi''(T,f)$ maxima are clearly observed (f is the AC frequency). This result precludes any tri-dimensional ordering; moreover, the relative variation of the temperature of the χ'' peak with respect to the frequency is measured by a parameter $\phi = (\Delta T_{max}/T_{max})/\Delta(\log f) =$ ca. 0.13, which is in the range of normal superparamagnets, and excludes the possible occurrence of a spin glass state.[15a,21]

Semicircular Cole–Cole plots (χ'' vs. χ') are obtained for temperatures below 10 K, which can be fitted to a generalized Debye model[22] with an α parameter of 0.20–0.43; this is

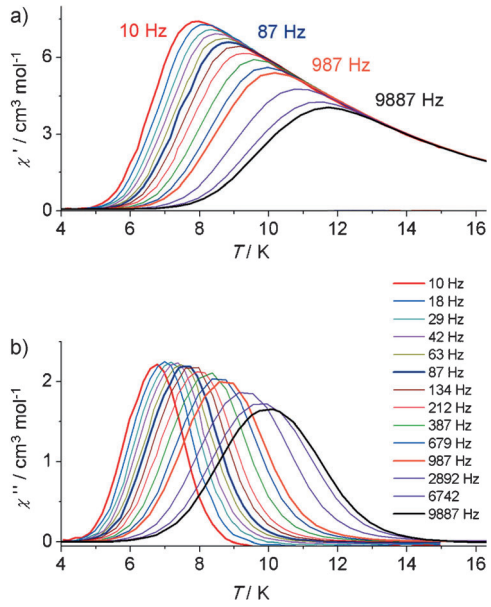

Figure 4. Temperature dependence of the a) real (χ') and b) imaginary (χ'') AC susceptibility for **2** measured at zero static field and 10 G AC field.

indicative of a moderately wide distribution of relaxation times (see the Supporting Information). The magnetization relaxation time obtained from the AC experiments as a function of temperature and frequency was fitted to the Arrhenius equation $\tau = \tau_0 \exp(\Delta E/k_B T)$, where τ is the relaxation time, ΔE is the energy barrier for the relaxation of magnetization, and τ_0 is the pre-exponential factor (Figure 5). From the least-squares fit, ΔE was found to be 134 ± 0.8 K (93 ± 0.5 cm^{-1}) and $\tau_0 = 3.1 \times 10^{-11}$ s. As expected, the ΔE barrier extracted from the AC data is larger than the energy gap deducted from susceptibility measurements, a situation that is often observed in SCMs, particularly those consisting of highly-anisotropic repeating units.[2a,5a] In such cases, the dynamics of the magnetization are governed

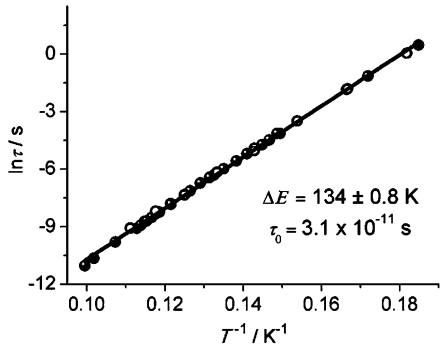

Figure 5. Arrhenius plot displaying T-dependence of the relaxation times for **2**. Open circles indicate that the corresponding relaxation time was extracted from fitting the frequency-dependent AC susceptibility curves with a modified Debye model (see the Supporting Information), whereas the dots indicate that the temperature corresponding to the peak maximum in AC curves was measured at constant frequency.

by both magnetic correlations and the relaxation barrier experienced by individual magnetic units.[20] The large anisotropy of **2** is explained by the strong Ising-type ligand field due to the close pair of linearly arranged oxygens characteristic of the uranyl group.[19b] A similar situation occurs in **1** and indeed slow relaxation of the magnetization due to anisotropic U^V units is observed at low temperatures, under applied field (see the Supporting Information). SMM behavior in a monometallic U^V terminal mono-oxo complex was recently reported by Liddle et al.[8a] The polymeric chain **2** is the first example of an actinide-based SCM. Its thermal relaxation barrier of 134 K (93 cm^{-1}) is slightly smaller than that of the previously reported $U_{12}Mn_6$ SMM (ΔE = ca. 142 K (99 cm^{-1})),[9c] but significantly larger than those reported for lanthanide-based single-chain magnets.[2,6] Lower values of the relaxation energy barrier were reported for SMMs based on mononuclear U^{III} and U^V (highest value: 30 K (21 cm^{-1})).[8] Moreover, compound **2** shows the largest blocking temperature ever reported for any actinide-based molecular magnet.

In conclusion, we have shown that 5f–3d heterometallic 1D chains can be conveniently built taking advantage of the strong cation–cation interaction occurring between the pentavalent uranyl oxo groups and Cd^{II} or Mn^{II}, which prevents scrambling of the salen ligand. The Mn-UO_2-Mn coordination polymer exhibits a slow relaxation of magnetization with a high relaxation barrier and shows an open hysteresis, thus providing the first example of an actinide-based SCM. The high magnetic anisotropy of the pentavalent uranyl complex and the high spin of Mn^{II} associated with significant intrachain magnetic communication and long interchain intermetallic distances are probably at the origin of the SCM behavior. The convenient route to uranium-based 1D heterodimetallic chains presented here, in association with the wide range of possible Schiff bases available, provides an entry to the development of actinide-based SCMs.

Received: August 21, 2013
Published online: December 6, 2013

Keywords: actinides · cations · polymetallic complexes · single-chain magnets · uranium

[1] a) D. Gatteschi, R. Sessoli, J. Villain, *Molecular Nanomagnets*, Oxford University Press, Oxford, UK, **2006**; b) C. Coulon, H. Miyasaka, R. Clerac, in *Structure and Bonding* (ed. R. Winpenny), Springer, **2006**, pp. 163–206.

[2] a) W. X. Zhang, R. Ishikawa, B. Breedlove, M. Yamashita, *RSC Adv.* **2013**, *3*, 3772–3798; b) H. Miyasaka, M. Julve, M. Yamashita, R. Clérac, *Inorg. Chem.* **2009**, *48*, 3420–3437; c) R. Clérac, H. Miyasaka, M. Yamashita, C. Coulon, *J. Am. Chem. Soc.* **2002**, *124*, 12837–12844; d) R. Lescouezec, L. M. Toma, J. Vaissermann, M. Verdaguer, F. S. Delgado, C. Ruiz-Perez, F. Lloret, M. Julve, *Coord. Chem. Rev.* **2005**, *249*, 2691–2729; e) H. L. Sun, Z. M. Wang, S. Gao, *Coord. Chem. Rev.* **2010**, *254*, 1081–1100.

[3] A. Caneschi, D. Gatteschi, N. Lalioti, C. Sangregorio, R. Sessoli, G. Venturi, A. Vindigni, A. Rettori, M. G. Pini, M. A. Novak, *Angew. Chem.* **2001**, *113*, 1810–1813; *Angew. Chem. Int. Ed.* **2001**, *40*, 1760–1763.

[4] R. J. Glauber, *J. Math. Phys.* **1963**, *4*, 294 – 307.
[5] a) S. W. Przybylak, F. Tuna, S. J. Teat, R. E. P. Winpenny, *Chem. Commun.* **2008**, 1983 – 1985; b) M. Ferbinteanu, H. Miyasaka, W. Wernsdorfer, K. Nakata, K. Sugiura, M. Yamashita, C. Coulon, R. Clerac, *J. Am. Chem. Soc.* **2005**, *127*, 3090 – 3099; c) T. D. Harris, C. Coulon, R. Clerac, J. R. Long, *J. Am. Chem. Soc.* **2011**, *133*, 123 – 130.
[6] a) D. T. Thielemann, M. Klinger, T. J. A. Wolf, Y. Lan, W. Wernsdorfer, M. Busse, P. W. Roesky, A. N. Unterreiner, A. K. Powell, P. C. Junk, G. B. Deacon, *Inorg. Chem.* **2011**, *50*, 11990 – 12000; b) L. Bogani, C. Sangregorio, R. Sessoli, D. Gatteschi, *Angew. Chem.* **2005**, *117*, 5967 – 5971; *Angew. Chem. Int. Ed.* **2005**, *44*, 5817 – 5821; c) Y. Z. Zheng, Y. H. Lan, W. Wernsdorfer, C. E. Anson, A. K. Powell, *Chem. Eur. J.* **2009**, *15*, 12566 – 12570.
[7] a) J. D. Rinehart, J. R. Long, *Chem. Sci.* **2011**, *2*, 2078 – 2085; b) J. J. Baldoví, S. Cardona-Serra, J. M. Clemente-Juan, E. Coronado, A. Gaita-Ariño, *Chem. Sci.* **2013**, *4*, 938 – 946.
[8] a) D. M. King, F. Tuna, J. McMaster, W. Lewis, A. J. Blake, E. J. L. McInnes, S. T. Liddle, *Angew. Chem.* **2013**, *125*, 5021 – 5024; *Angew. Chem. Int. Ed.* **2013**, *52*, 4921 – 4924; b) F. Moro, D. P. Mills, S. T. Liddle, J. van Slageren, *Angew. Chem.* **2013**, *125*, 3514 – 3517; *Angew. Chem. Int. Ed.* **2013**, *52*, 3430 – 3433; c) J. D. Rinehart, J. R. Long, *J. Am. Chem. Soc.* **2009**, *131*, 12558 – 12559; d) J. D. Rinehart, K. R. Meihaus, J. R. Long, *J. Am. Chem. Soc.* **2010**, *132*, 7572; e) M. A. Antunes, L. C. J. Pereira, I. C. Santos, M. Mazzanti, J. Marcalo, M. Almeida, *Inorg. Chem.* **2011**, *50*, 9915 – 9917; f) J. T. Coutinho, M. A. Antunes, L. C. J. Pereira, H. Bolvin, J. Marcalo, M. Mazzanti, M. Almeida, *Dalton Trans.* **2012**, *41*, 13568 – 13571.
[9] a) D. P. Mills, F. Moro, J. McMaster, J. van Slageren, W. Lewis, A. J. Blake, S. T. Liddle, *Nat. Chem.* **2011**, *3*, 454 – 460; b) N. Magnani, E. Colineau, R. Eloirdi, J. C. Griveau, R. Caciuffo, S. M. Cornet, I. May, C. A. Sharrad, D. Collison, R. E. P. Winpenny, *Phys. Rev. Lett.* **2010**, *104*, 197202; c) V. Mougel, L. Chatelain, J. Pecaut, R. Caciuffo, E. Colineau, J. C. Griveau, M. Mazzanti, *Nat. Chem.* **2012**, *4*, 1011 – 1017.
[10] N. N. Krot, M. S. Grigoriev, *Russ. Chem. Rev.* **2004**, *73*, 89 – 100.
[11] V. Mougel, P. Horeglad, G. Nocton, J. Pecaut, M. Mazzanti, *Angew. Chem.* **2009**, *121*, 8629 – 8632; *Angew. Chem. Int. Ed.* **2009**, *48*, 8477 – 8480.
[12] G. Nocton, P. Horeglad, J. Pecaut, M. Mazzanti, *J. Am. Chem. Soc.* **2008**, *130*, 16633 – 16645.
[13] a) L. Chatelain, V. Mougel, J. Pecaut, M. Mazzanti, *Chem. Sci.* **2012**, *3*, 1075 – 1079; b) P. L. Arnold, E. Hollis, G. S. Nichol, J. B. Love, J. C. Griveau, R. Caciuffo, N. Magnani, L. Maron, L. Castro, A. Yahia, S. O. Odoh, G. Schreckenbach, *Inorg. Chem.* **2013**, *52*, 135, 3841 – 3854.
[14] P. Horeglad, G. Nocton, Y. Filinchuk, J. Pecaut, M. Mazzanti, *Chem. Commun.* **2009**, 1843 – 1845.
[15] a) P. L. Arnold, E. Hollis, F. J. White, N. Magnani, R. Caciuffo, J. B. Love, *Angew. Chem.* **2011**, *123*, 917 – 920; *Angew. Chem. Int. Ed.* **2011**, *50*, 887 – 890; b) P. L. Arnold, *Nat. Chem.* **2012**, *4*, 967 – 969; c) L. P. Spencer, E. J. Schelter, P. Yang, R. L. Gdula, B. L. Scott, J. D. Thompson, J. L. Kiplinger, E. R. Batista, J. M. Boncella, *Angew. Chem.* **2009**, *121*, 3853 – 3856; *Angew. Chem. Int. Ed.* **2009**, *48*, 3795 – 3798.
[16] A. N. Alsobrook, B. G. Hauser, J. T. Hupp, E. V. Alekseev, W. Depmeier, T. E. Albrecht-Schmitt, *Chem. Commun.* **2010**, *46*, 9167 – 9169.
[17] V. Mougel, P. Horeglad, G. Nocton, J. Pecaut, M. Mazzanti, *Chem. Eur. J.* **2010**, *16*, 14365 – 14377.
[18] V. Mougel, J. Pecaut, M. Mazzanti, *Chem. Commun.* **2012**, *48*, 868 – 870.
[19] a) W. W. Lukens, N. M. Edelstein, N. Magnani, T. W. Hayton, S. L. A. Fortier, *J. Am. Chem. Soc.* **2013**, *135*, 10742 – 10754; b) G. Nocton, P. Horeglad, V. Vetere, J. Pecaut, L. Dubois, P. Maldivi, N. M. Edelstein, M. Mazzanti, *J. Am. Chem. Soc.* **2010**, *132*, 495 – 508.
[20] C. Coulon, R. Clerac, L. Lecren, W. Wernsdorfer, H. Miyasaka, *Phys. Rev. B* **2004**, *69*, 132408.
[21] $\phi = 0.01$ is a typical value for a spin glass; for details, see: J. A. Mydosh, *Spin Glasses: An Experimental Introduction*, Taylor & Francis, London, **1993**.
[22] K. S. Cole, R. H. Cole, *J. Chem. Phys.* **1941**, *9*, 341 – 351.

A Journal of the Gesellschaft Deutscher Chemiker

Angewandte International Edition Chemie

GDCh

www.angewandte.org

2014–53/49

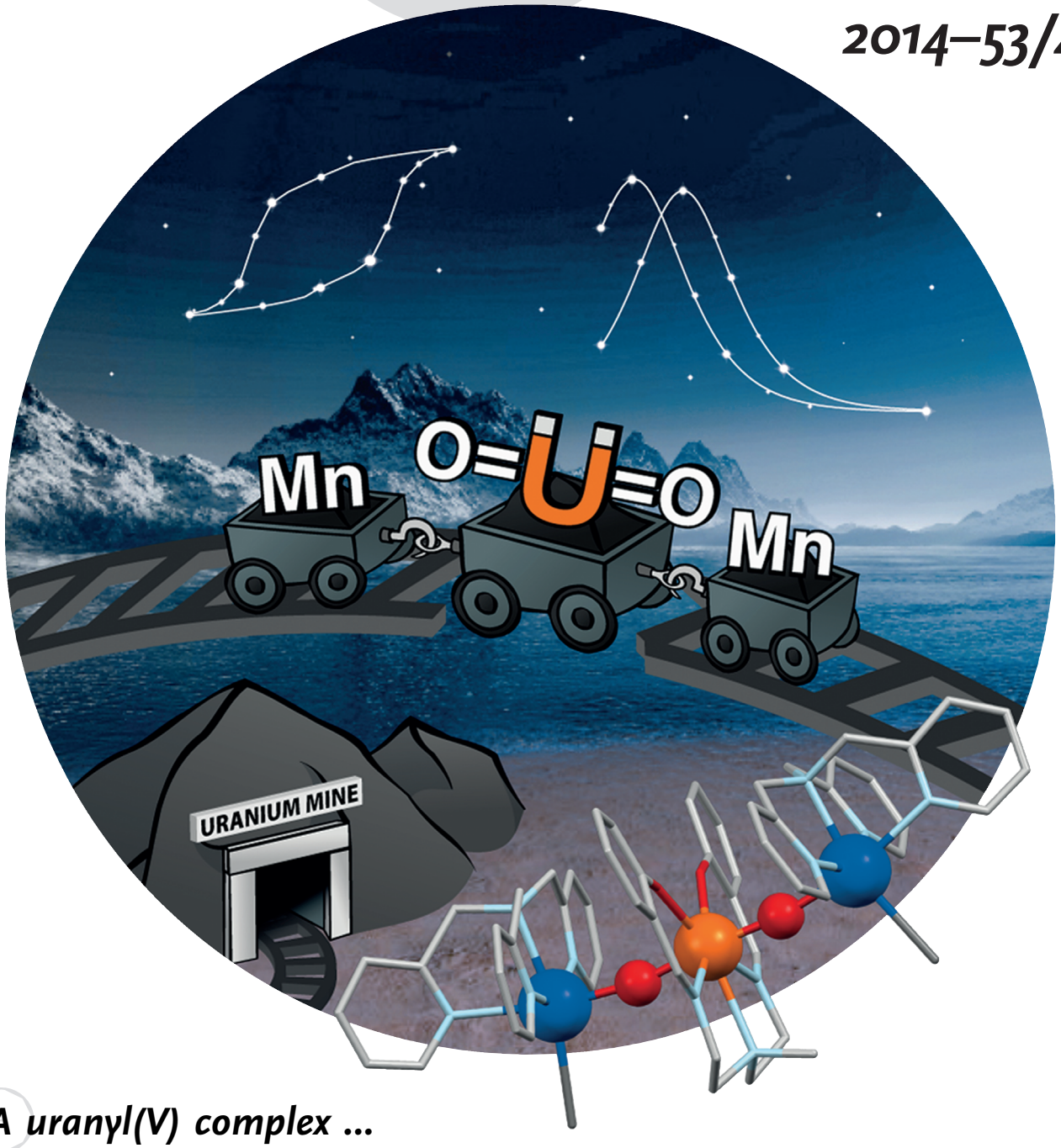

A uranyl(V) complex ...

… is used as a building block in the rational assembly of a trinuclear {Mn–O=U=O–Mn} complex. M. Mazzanti and co-workers demonstrate in their Communication on page 13434 ff. that the trinuclear system exhibits the behavior of a single-molecule magnet with the highest effective barrier to relaxation reported to date for a mono-uranium system ($\Delta E = (81 \pm 0.5)$ K), resulting from the large Ising anisotropy of the uranyl-based bridge and intramolecular Mn–U exchange interactions.

WILEY-VCH

Single-Molecule Magnets

DOI: 10.1002/anie.201407334

Self-Assembly of a 3d–5f Trinuclear Single-Molecule Magnet from a Pentavalent Uranyl Complex**

*Lucile Chatelain, James P. S. Walsh, Jacques Pécaut, Floriana Tuna, and Marinella Mazzanti**

Dedicated to Professor Marius Andruh on the occasion of his 60th birthday

Abstract: *Mixed-metal uranium compounds are very attractive candidates in the design of single-molecule magnets (SMMs), but only one 3d–5f hetero-polymetallic SMM containing a uranium center is known. Herein, we report two trimeric heterodimetallic 3d–5f complexes self-assembled by cation–cation interactions between a uranyl(V) complex and a TPA-capped M^{II} complex (M = Mn (**1**), Cd (**2**); TPA = tris(2-pyridylmethyl)amine). The metal centers were strategically chosen to promote the formation of discrete molecules rather than extended chains. Compound **1**, which contains an almost linear {Mn–O=U=O–Mn} core, exhibits SMM behavior with a relaxation barrier of 81 ± 0.5 K—the highest reported for a mono-uranium system—arising from intramolecular Mn–U exchange interactions combined with the high Ising anisotropy of the uranyl(V) moiety. Compound **1** also exhibits an open magnetic hysteresis loop at temperatures less than 3 K, with a significant coercive field of 1.9 T at 1.8 K.*

Uranium compounds have been identified as attractive candidates in the search for new molecules displaying slow magnetic relaxation of a purely molecular origin (i.e. single-molecule magnets, or SMMs).[1] The high magnetic anisotropy of the uranium ion over a range of oxidation states, combined with its ability to engage in strong magnetic exchange interactions with other metal centers, makes it particularly promising for the development of SMMs with barriers to spin reversal of a magnitude sufficient to observe hysteresis at workable temperatures—a crucial prerequisite for the use of SMMs in molecular devices.[2]

Over the last five years, SMM behavior has been observed in mono- and dinuclear compounds containing the highly anisotropic U^{III} ion.[3] Slow magnetic relaxation under applied fields and at low temperatures has been reported for compounds containing mono-oxo and dioxo U^{V} units.[4] These results suggest that the highly anisotropic $5f^1$ UO_2^+ uranyl cation could be used to build improved SMMs by incorporating it into exchange-coupled heterometallic 3d–5f assemblies with high ground-state spin values.

Unfortunately, the rational design of supramolecular multimetallic assemblies of uranium is extremely challenging because of its highly variable coordination number and geometry. As a result, the supramolecular chemistry of uranium is underdeveloped,[5] and there are relatively few polynuclear complexes exhibiting unambiguous magnetic exchange interactions.[6] In particular, strategies to generate polynuclear complexes containing 5f and 3d metal centers remain especially limited.[7]

However, uranyl(V) oxo groups have been shown to bind easily to other metal cations, leading to the formation of homo- and heterometallic supramolecular assemblies.[6e,f,8] Perhaps most importantly, this interaction, commonly referred to as a cation–cation interaction (CCI), has been shown to provide an efficient pathway for magnetic exchange.[6e,f,8a,d,e,9]

To date, only one discrete polymetallic 3d–5f cluster exhibiting exchange-coupled SMM behavior has been established.[8f] This large $\{U_{12}Mn_6\}$ wheel-shaped uranyl(V) cluster exhibits an open magnetic hysteresis loop at low temperatures (below 4 K), and has a non-zero coercive field.[8f] However, the large size and complicated nature of the assembly precludes a programmed modulation of the overall geometry and of the identity of the 3d ion, hampering further investigations into any magneto–structural relationships that might enable us to tune the SMM properties.

Herein, we present the self-assembly of a novel trinuclear 3d–5f $\{UO_2Mn_2\}$ complex that is only the second example of a uranium-based exchange-coupled SMM, and the first to contain only one uranyl ion. The $\{UO_2Mn_2\}$ complex exhibits a large barrier to relaxation of 81 ± 0.5 K, likely as a result of strong intramolecular U–Mn exchange interactions combined with the high Ising anisotropy of the uranyl(V) dioxo group. It

[*] L. Chatelain, Dr. J. Pécaut
Laboratoire de Reconnaissance Ionique
et Chimie de Coordination SCIB
UMR-E3 CEA-UJF, INAC, CEA-Grenoble
17 rue des Martyrs, F-38054 Grenoble Cedex 09 (France)
J. P. S. Walsh, Dr. F. Tuna
School of Chemistry and Photon Science Institute
The University of Manchester
Oxford Road, Manchester, M13 9PL (UK)
Dr. M. Mazzanti
Institut des Sciences et Ingénierie Chimiques
Ecole Polytechnique Fédérale de Lausanne (EPFL)
CH-1015 Lausanne (Switzerland)
E-mail: marinella.mazzanti@epfl.ch

[**] We thank François Jacquot for his support and suggestions in magnetic measurements, and Pierre-Alain Bayle and Colette Lebrun for their help in physico-chemical measurements. We thank L. Plassais for technical support. We acknowledge support from the Agence Nationale de la Recherche (ANR-10-BLAN-0729), and the EPSRC UK National EPR Facility. This work benefited from COST Action CM1006 - EUFEN: European F-Element Network. We thank Prof. David Collison for useful discussions during the preparation of the manuscript.

Supporting information for this article is available on the WWW under http://dx.doi.org/10.1002/anie.201407334.

also shows an open magnetic hysteresis loop at temperatures less than 3 K, with a coercive field of 1.9 T at 1.8 K.

Two trinuclear 3d–5f complexes were assembled using a salt metathesis reaction of the polymeric uranyl(V) complex, $[UO_2(Mesaldien)K]_n$[10] (Mesaldien = *N*,*N*′-(2-aminomethyl)diethylenebis(salicylidene imine)), with strategically chosen TPA-capped complexes (TPA = tris(2-pyridylmethyl)amine) of the d-block ions Mn^{II} (**1**) and Cd^{II} (**2**). We anticipated that the association of the high spin of the Mn^{II} ion to the high Ising anisotropy of the uranyl group[8c] would lead to SMM behavior with a high relaxation barrier.[8f] The {M–O=U=O–M} trimers, which maintain their structure in pyridine solution, are formed by the linear cation–cation interaction of the two uranyl(V) oxo groups with the two d-block cations.

The reaction of $[UO_2(Mesaldien)K]_n$[10] with two equivalents of $[M(TPA)I_2]$ (M = Mn,[11] Cd) in pyridine (Scheme 1) leads to the substitution of the oxo-bound potassium cation by

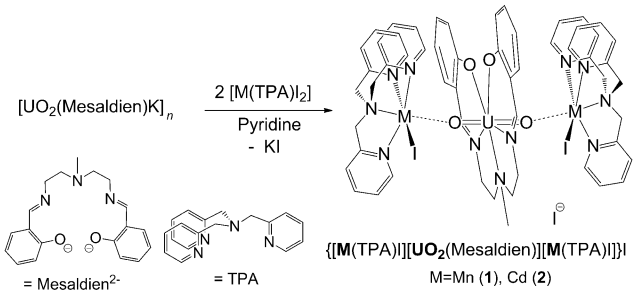

Scheme 1. The synthesis of 3d–5f trinuclear complexes **1** and **2**.

a TPA-bound manganese ion, and to the disruption of the polymeric structure of $[UO_2(Mesaldien)K]_n$. The reaction yields the stable trinuclear compounds [{[M(TPA)I]-[UO_2(Mesaldien)][M(TPA)I]}I] (M = Mn (**1**), Cd (**2**)) in 60–65% yield. Single crystals of **1**.3Py suitable for X-ray diffraction were obtained by slow diffusion of hexane into a pyridine solution of **1**. The two complexes are stable in the solid state and in pyridine or acetonitrile solution for months under an argon atmosphere. Moreover, ^{1}H and PFGSTE NMR spectroscopy and ESI mass spectrometry studies show that the two complexes retain their trimeric structure in solution (PFGSTE NMR = pulsed field-gradient stimulated echo NMR).

The neutral tripodal tetradentate ligand TPA was used to block the coordination sphere of the Mn^{2+} cations to prevent the formation of 1D coordination polymers.[4b] Indeed, the choice of the capping ligand is crucial to determine the metal nuclearity of the final structure.

The structures of complexes **1** and **2** consist of two $[M(TPA)I]^+$ cations bound to the two oxo groups of the $[UO_2(Mesaldien)]^-$ anion in a linear cation–cation interaction (Figure 1). In both compounds the uranium atoms are heptacoordinate with a slightly distorted pentagonal bipyramid geometry, with the uranium centers coordinated to two uranyl oxygen atoms and the five donor atoms of the $Mesaldien^{2-}$ ligand in the equatorial plane. The transition metal centers are hexacoordinate, with a slightly distorted

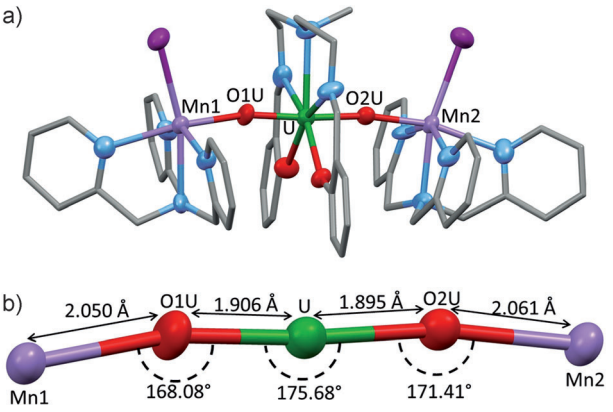

Figure 1. a) Molecular structure of $\{UO_2Mn_2\}$ with hydrogen atoms and cocrystallized solvent molecules omitted for clarity. b) View of the linear core with corresponding bond lengths and angles. Atom colors: C (gray), O (red), Mn (violet), N (light blue), I (purple), U (green.)

octahedral geometry defined by the four nitrogen atoms of the TPA ligand, one oxygen atoms from the uranyl(V) group, and a coordinated iodide anion.

In both complexes, the mean U=O bond lengths lie in the range of the values typically observed for uranyl(V) complexes, with the uranyl–metal interaction resulting in a slight lengthening of the bond (1.901 Å in **1**, 1.887 Å in **2**). The mean Mn–O_{yl} (where O_{yl} is the uranyl oxygen atom) bond length in **1** is 2.055(6) Å, significantly shorter than that found in the heteronuclear $\{U_{12}Mn_6\}$ wheel (2.15(2) Å)[8f] and in a heterodimetallic uranyl(VI)–manganese(II) complex (2.163(4) Å).[12] In compound **2**, the Cd–O_{yl} distance (2.201(16) Å) is slightly shorter than that found in a Cd–uranyl(V) polymer complex (2.28(2) Å),[13] and in a heterodimetallic U^{VI}/Cd^{II} system (2.252(4) Å).[13] The mean U-O-M angle measures 169.7(1.7)° in **1** and 168.7(8)° in **2**, whereas the M-U-M angle is 173.77(5)° in **1** and 174.86(6)° in **2**. The deviation from linearity arises from the presence of intramolecular hydrogen bonds between the protons on the TPA ligand and the oxygen atoms of the $Mesaldien^{2-}$ ligand. The mean intramolecular U–M bond lengths are 3.939(5) Å in **1** and 4.072(2) Å in **2**. The Mn–Mn intramolecular distance in **1** is 7.8666(4) Å and the intramolecular distance Cd–Cd in **2** is 8.1354(6) Å. The shortest intermolecular U–U, U–M, and M–M distances are 10.9469(4), 8.7589(4), and 7.6296(4) Å in **1** and 11.0107(7), 8.6904(7), and 7.4179(5) Å in **2**, respectively.

Direct current (dc) magnetic susceptibility measurements were performed on polycrystalline samples of **1** and **2** over the temperature range 1.8–300 K (Figure 2). The measured χT value (χ = molar magnetic susceptibility, T = temperature) of 0.32 $cm^3 K mol^{-1}$ for **2** at room temperature, equating to 1.55 μ_B per uranyl(V) ion (the Cd^{II} ion is diamagnetic), is significantly smaller than anticipated for an isolated $^2F_{5/2}$ uranium(V) ion (0.80 $cm^3 K mol^{-1}$, assuming $g_J = 6/7$ and a fully unquenched orbital momentum). This indicates that not all crystal field components of the ground multiplet state are fully occupied at 300 K, in agreement with previous reports.[8c,14] The χT value decreases on cooling to approximately 0.09 $cm^3 K mol^{-1}$ at 1.8 K (Figure 2) because of depopulation of the U^V excited Stark sublevels.[4b,8c]

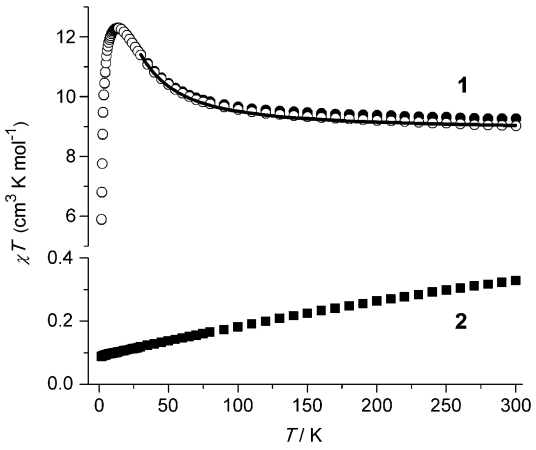

Figure 2. Plots of χT values versus temperature (T) for polycrystalline samples of **1** (●) and **2** (■), measured in a 0.5 T dc field. Open circles (○) correspond to the χT values after subtraction of the $\{UO_2Cd_2\}$ data from the $\{UO_2Mn_2\}$ data, to which a value of 0.094 $cm^3 K mol^{-1}$ has been added as the spin-only contribution of the U^V center. Solid line: the best fit of the data to Equation (1) with $J = +7.5$ cm^{-1}.

For **1**, the χT value is 9.2 $cm^3 K mol^{-1}$ at room temperature, close to the expected value of 9.05 $cm^3 K mol^{-1}$ for two noninteracting Mn^{II} ions ($S = 5/2$, $g_{iso} = 2$, $\chi T = 4.375$ $cm^3 K mol^{-1}$) and one uranium(V) ion. This χT value increases smoothly with decreasing temperature down to 100 K, and then more rapidly, reaching a maximum of 12.5 $cm^3 K mol^{-1}$ at 12 K, after which it decreases to a value of 6 $cm^3 K mol^{-1}$ at 1.8 K. The increase of χT values with decreasing temperature indicates the occurrence of magnetic exchange coupling between uranium and manganese ions in **1**. The presence of a Mn–Mn interaction is ruled out because the Mn···Mn separation is significantly larger (7.912(3) Å) than those reported for compounds presenting magnetic interaction between the Mn ions (3.2–3.4 Å).[15] The downturn in χT values below 12 K is the result of zero-field splitting (zfs) effects associated with the resulting high-spin ground state.

As the $\{UO_2Cd_2\}$ compound **2** is isostructural to **1**, but features two diamagnetic Cd^{II} centers instead of the two $S = 5/2$ Mn^{II} centers in **1**, it can be used as a reasonable model to establish the contribution arising from spin–orbit and ligand field effects associated with the U^V center. Thus, subtraction of the experimental χT values of **2** from the experimental χT values of **1** removes any contribution from the U^V ion to the overall magnetism of **1**, leaving only the magnetic contribution of the two Mn^{II} ions together with any remnants of magnetic exchange coupling. Subsequent addition to the $\Delta\chi T$ data of a temperature-independent value of 0.094 $cm^3 K mol^{-1}$, to account for the spin-only ($S = 1/2$) contribution of the U^V center (assuming $g_U = 1$), enables the use of the isotropic spin Hamiltonian Equation (1) to model the Mn–U interaction in **1**. A similar procedure was used by Long et al. when modelling the exchange coupling within the trimetallic clusters (cyclam)M[(μ-Cl)U^{IV}(Me$_2$Pz)$_4$]$_2$ (M=Co^{II}, Ni^{II}, Cu^{II}; cyclam = 1,4,8,11-tetraazacyclotetradecane).[2a,7c]

$$H = -2J(S_{Mn1}S_U + S_U S_{Mn2}) \quad (1)$$

The best fit of the experimental data above 30 K, using Equation (1) in MAGPACK,[16] yielded $J = +7.5$ cm^{-1}, $g_{Mn} = 2$, and $g_U = 1$ (see solid line in Figure 2), where J measures the exchange coupling between adjacent Mn^{II} and U^V centers. The positive sign of J indicates ferromagnetic coupling. This value falls in the range of the values of exchange constants calculated for the few other reported complexes $Co^{II}U_2^{IV}$ and $Ni^{II}U_2^{IV}$ (2.8–49 cm^{-1}) which also present ferromagnetic 3d–5f coupling.[7c,17]

The molar magnetization (M) curves as a function of magnetic field for **1** do not show signs of saturation under magnetic fields up to 7 T, and the $M(H/T)$ curves (where H is the magnetic field strength) cannot be superimposed (see the Supporting Information), indicative of significant magnetic anisotropy and/or low-lying excited states. The magnetization dynamics for **1** were investigated by alternating current (ac) magnetic susceptibility measurements as a function of temperature (1.8–10 K) and frequency ($\nu = 0.1$–1400 Hz), in a zero dc field (Figure 3 and the Supporting Information).

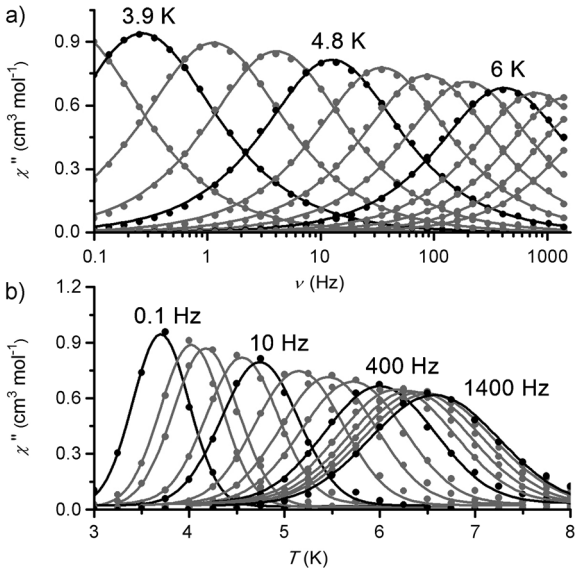

Figure 3. a) Frequency and b) temperature dependence of the out-of-phase ac susceptibility of **1** measured at zero dc field and 1.55 G ac field oscillating at frequencies in the range 0.1–1400 Hz. The solid lines correspond to fits to the Debye (a) and Gaussian (b) models.

Both the in-phase (χ') and out-of-phase (χ'') components of the ac susceptibility show strong frequency dependence below approximately 7.5 K, and maxima are observed in $\chi''(T)$. These observations are indicative of slow relaxation of the molecular magnetization, and thus of single-molecule-magnet (SMM) behavior.

The relaxation time (τ) was determined from both $\chi_M''(T)$ values and from Argand (χ_M'' versus χ_M') diagrams. For the Argand diagrams, semicircular Cole–Cole plots were obtained at fixed temperatures between 3.9 and 6.6 K. The plots could be fitted to a generalized Debye model[18] with an α parameter in the range of 0.01–0.15, consistent with a narrow distribution of relaxation times (see the Supporting Information). A plot of the derived relaxation time constants

(τ) as ln(τ) versus T^{-1} is linear in this temperature range, and hence can be fitted to the Arrhenius law $\tau = \tau_0 \exp(\Delta E/k_B T)$, giving an effective thermal energy barrier to magnetization relaxation $\Delta E = 81 \pm 0.5$ K with a pre-exponential factor of $\tau_0 = 5.02 \times 10^{-10}$ s (Figure S17 in the Supporting Information). This is the highest reported for trinuclear complexes containing 3d ions. Moreover this value remains high compared to the barrier found for the large 3d–5f $\{U_{12}Mn_6\}$ SMM (142 K) despite the presence of only three metal ions. Slow relaxation of the magnetization as a result of anisotropic U^V units is also observed for **2** at low temperatures, under an applied dc field (Supporting Information). SMM behavior arising from monometallic U^V complexes has been previously reported.[4a,14]

Below 3 K, clear hysteresis loops which are due to slow magnetic relaxation are observed in the $M(H)$ data, for both solid-state and solution samples of **1** (Figure 4). The observation of a hysteresis loop for solutions of **1** in pyridine where

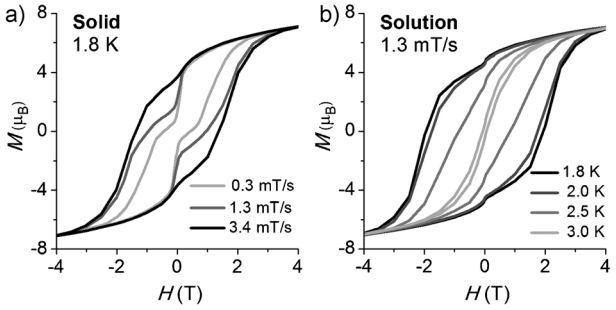

Figure 4. Hysteresis loops for a) the polycrystalline sample of **1** and b) the pyridine solution of **1**, at the indicated temperatures and field sweep rates.

the complex retains its trinuclear structure confirms the molecular origins of the SMM behavior. Within the same temperature range, a divergence between zero-field-cooled (ZFC) and field-cooled (FC) magnetizations as a function of temperature is observed (Figure S11). The width of the hysteresis increases with increasing the field sweep rate (Figure 4a) and with decreasing temperature (Supporting Information), as would be expected for a single molecule magnet. A remarkable coercive field of 1.9 T is obtained at 1.8 K, and a remnant magnetization of 4.6 μ_B is preserved at 0 T. The larger coercive field observed in solution is probably because of the presence of weaker dipolar interactions compared to the solid state. A partial loss of the magnetization because of quantum tunneling relaxation occurs at very low temperatures, and a sharp step at 0 T is indeed observed. These features are indicative of single-molecule magnetism. The remnant magnetization disappears at approximately 3.1 K, corresponding to the blocking temperature of the material.

In conclusion, we have identified a versatile route to the programmed assembly of 3d–5f trinuclear heterodimetallic complexes from the pentavalent uranyl ion. An appropriate choice of the ligand which binds to the 3d metal ion allows for a strong cation–cation interaction to take place between the two uranyl(V) oxo groups and the two 3d metal centers, affording the desired trinuclear complex and preventing further oligomerization. Compound **1** is only the second example of a uranium-based polymetallic complex exhibiting SMM behavior and open hysteresis. A comparative study of the magnetic properties of the isostructural cadmium analogue **2** unambiguously demonstrates that the SMM behavior of **1** is a property of the trinuclear entity. The SMM behavior of **1** is associated with its high-spin ground state resulting from ferromagnetic coupling between Mn^{II} and U^V ions, and a large Ising-type anisotropy defined by the O=U=O axis. The effective energy barrier to the reversal of magnetization of 81 ± 0.5 K is significantly larger than any reported for uranium-based SMMs, driving their behavior from single-ion effects. This highlights the importance of using anisotropic UO_2^+ as a bridging component for the construction of SMMs. The role of the 3d metal anisotropy, if any, is yet to be understood. More studies, including EPR measurements, will be necessary to clarify this aspect, and the investigation should be expanded to other mixed uranyl–transition metal complexes. The synthetic approach used in this work should be easily applicable to other metals through the careful tuning of the supporting ligand. We anticipate that a large library of trinuclear 3d–5f complexes will be afforded by this method, and that this will facilitate magneto-structural studies on uranium systems, which might ultimately lead to the design of uranium-based SMMs with vastly improved properties.

Received: July 17, 2014
Revised: August 26, 2014
Published online: October 3, 2014

Keywords: exchange interactions · magnetism · polymetallic complexes · single-molecule magnets · uranium

[1] D. Gatteschi, R. Sessoli, J. Villain, *Molecular Nanomagnets*, Oxford University Press, Oxford, UK, **2006**.
[2] a) J. D. Rinehart, T. D. Harris, S. A. Kozimor, B. M. Bartlett, J. R. Long, *Inorg. Chem.* **2009**, *48*, 3382 – 3395; b) R. A. Layfield, *Organometallics* **2014**, *33*, 1084 – 1099; c) D. N. Woodruff, R. E. P. Winpenny, R. A. Layfield, *Chem. Rev.* **2013**, *113*, 5110 – 5148.
[3] a) J. D. Rinehart, J. R. Long, *J. Am. Chem. Soc.* **2009**, *131*, 12558 – 12559; b) J. D. Rinehart, K. R. Meihaus, J. R. Long, *J. Am. Chem. Soc.* **2010**, *132*, 7572 – 7573; c) M. A. Antunes, L. C. J. Pereira, I. C. Santos, M. Mazzanti, J. Marcalo, M. Almeida, *Inorg. Chem.* **2011**, *50*, 9915 – 9917; d) J. T. Coutinho, M. A. Antunes, L. C. J. Pereira, H. Bolvin, J. Marcalo, M. Mazzanti, M. Almeida, *Dalton Trans.* **2012**, *41*, 13568 – 13571; e) D. P. Mills, F. Moro, J. McMaster, J. van Slageren, W. Lewis, A. J. Blake, S. T. Liddle, *Nat. Chem.* **2011**, *3*, 454 – 460; f) F. Moro, D. P. Mills, S. T. Liddle, J. Slangeren, *Angew. Chem. Int. Ed.* **2013**, *52*, 3430 – 3433; *Angew. Chem.* **2013**, *125*, 3514 – 3517; g) J. D. Rinehart, J. R. Long, *Dalton Trans.* **2012**, *41*, 13572 – 13574; h) K. R. Meihaus, J. D. Rinehart, J. R. Long, *Inorg. Chem.* **2011**, *50*, 8484 – 8489.
[4] a) D. M. King, F. Tuna, J. McMaster, W. Lewis, A. J. Blake, E. J. L. McInnes, S. T. Liddle, *Angew. Chem. Int. Ed.* **2013**, *52*, 4921 – 4924; *Angew. Chem.* **2013**, *125*, 5021 – 5024; b) V. Mougel, L. Chatelain, J. Hermle, R. Caciuffo, E. Colineau, F. Tuna, N. Magnani, A. Degeyer, J. Pécaut, M. Mazzanti, *Angew. Chem. Int. Ed.* **2014**, *53*, 819 – 823; *Angew. Chem.* **2014**, *126*, 838 – 842.

[5] a) J. L. Kiplinger, J. A. Pool, E. J. Schelter, J. D. Thompson, B. L. Scott, D. E. Morris, *Angew. Chem. Int. Ed.* **2006**, *45*, 2036 – 2041; *Angew. Chem.* **2006**, *118*, 2090 – 2095; b) E. J. Schelter, J. M. Veauthier, J. D. Thompson, B. L. Scott, K. D. John, D. E. Morris, J. L. Kiplinger, *J. Am. Chem. Soc.* **2006**, *128*, 2198 – 2199; c) W. J. Evans, S. A. Kozimor, J. W. Ziller, *Science* **2005**, *309*, 1835 – 1838.

[6] a) O. P. Lam, F. W. Heinemann, K. Meyer, *Chem. Sci.* **2011**, *2*, 1538 – 1547; b) L. P. Spencer, E. J. Schelter, P. Yang, R. L. Gdula, B. L. Scott, J. D. Thompson, J. L. Kiplinger, E. R. Batista, J. M. Boncella, *Angew. Chem. Int. Ed.* **2009**, *48*, 3795 – 3798; *Angew. Chem.* **2009**, *121*, 3853 – 3856; c) P. L. Arnold, G. M. Jones, S. O. Odoh, G. Schreckenbach, N. Magnani, J. B. Love, *Nat. Chem.* **2012**, *4*, 221 – 222; d) R. K. Rosen, R. A. Andersen, N. M. Edelstein, *J. Am. Chem. Soc.* **1990**, *112*, 4588 – 4590; e) L. Chatelain, V. Mougel, J. Pecaut, M. Mazzanti, *Chem. Sci.* **2012**, *3*, 1075 – 1079; f) V. Mougel, P. Horeglad, G. Nocton, J. Pecaut, M. Mazzanti, *Angew. Chem. Int. Ed.* **2009**, *48*, 8477 – 8480; *Angew. Chem.* **2009**, *121*, 8629 – 8632.

[7] a) T. Le Borgne, E. Riviere, J. Marrot, J. J. Girerd, M. Ephritikhine, *Angew. Chem. Int. Ed.* **2000**, *39*, 1647 – 1649; *Angew. Chem.* **2000**, *112*, 1713 – 1715; b) M. J. Monreal, C. T. Carver, P. L. Diaconescu, *Inorg. Chem.* **2007**, *46*, 7226 – 7228; c) S. A. Kozimor, B. M. Bartlett, J. D. Rinehart, J. R. Long, *J. Am. Chem. Soc.* **2007**, *129*, 10672 – 10673.

[8] a) G. Nocton, P. Horeglad, J. Pecaut, M. Mazzanti, *J. Am. Chem. Soc.* **2008**, *130*, 16633 – 16645; b) V. Mougel, P. Horeglad, G. Nocton, J. Pecaut, M. Mazzanti, *Chem. Eur. J.* **2010**, *16*, 14365 – 14377; c) G. Nocton, P. Horeglad, V. Vetere, J. Pecaut, L. Dubois, P. Maldivi, N. M. Edelstein, M. Mazzanti, *J. Am. Chem. Soc.* **2010**, *132*, 495 – 508; d) P. L. Arnold, E. Hollis, F. J. White, N. Magnani, R. Caciuffo, J. B. Love, *Angew. Chem. Int. Ed.* **2011**, *50*, 887 – 890; *Angew. Chem.* **2011**, *123*, 917 – 920; e) P. L. Arnold, E. Hollis, G. S. Nichol, J. B. Love, J. C. Griveau, R. Caciuffo, N. Magnani, L. Maron, L. Castro, A. Yahia, S. O. Odoh, G. Schreckenbach, *J. Am. Chem. Soc.* **2013**, *135*, 3841 – 3854; f) V. Mougel, L. Chatelain, J. Pecaut, R. Caciuffo, E. Colineau, J. C. Griveau, M. Mazzanti, *Nat. Chem.* **2012**, *4*, 1011 – 1017; g) P. L. Arnold, D. Patel, C. Wilson, J. B. Love, *Nature* **2008**, *451*, 315 – 318.

[9] a) N. Magnani, E. Colineau, R. Eloirdi, J. C. Griveau, R. Caciuffo, S. M. Cornet, I. May, C. A. Sharrad, D. Collison, R. E. P. Winpenny, *Phys. Rev. Lett.* **2010**, *104*, 4; b) P. L. Arnold, N. A. Potter, N. Magnani, C. Apostolidis, J. C. Griveau, E. Colineau, A. Morgenstern, R. Caciuffo, J. B. Love, *Inorg. Chem.* **2010**, *49*, 5341 – 5343.

[10] V. Mougel, J. Pecaut, M. Mazzanti, *Chem. Commun.* **2012**, *48*, 868 – 870.

[11] C. Duboc, T. Phoeung, S. Zein, J. Pecaut, M. N. Collomb, F. Neese, *Inorg. Chem.* **2007**, *46*, 4905 – 4916.

[12] P. L. Arnold, D. Patel, A. J. Blake, C. Wilson, J. B. Love, *J. Am. Chem. Soc.* **2006**, *128*, 9610 – 9611.

[13] A. N. Alsobrook, B. G. Hauser, J. T. Hupp, E. V. Alekseev, W. Depmeier, T. E. Albrecht-Schmitt, *Chem. Commun.* **2010**, *46*, 9167 – 9169.

[14] See Ref. [4b].

[15] C. J. Milios, R. Inglis, A. Vinslava, R. Bagai, W. Wernsdorfer, S. Parsons, S. P. Perlepes, G. Christou, E. K. Brechin, *J. Am. Chem. Soc.* **2007**, *129*, 12505 – 12511.

[16] J. J. Borrás-Almenar, J. M. Clemente-Juan, E. Coronado, B. S. Tsukerblat, *J. Comput. Chem.* **2001**, *22*, 985 – 991.

[17] J. D. Rinehart, B. M. Bartlett, S. A. Kozimor, J. R. Long, *Inorg. Chim. Acta* **2008**, *361*, 3534 – 3538.

[18] K. S. Cole, R. H. Cole, *J. Chem. Phys.* **1941**, *9*, 341 – 351.

Inorganic Chemistry

Communication

pubs.acs.org/IC

Single-Molecule-Magnet Behavior in Mononuclear Homoleptic Tetrahedral Uranium(III) Complexes

Laura C. J. Pereira,[†,‡] Clément Camp,[‡,§] Joana T. Coutinho,[†] Lucile Chatelain,[§,⊥] Pascale Maldivi,[§] Manuel Almeida,*[,†] and Marinella Mazzanti*[,⊥]

[†]C2TN, Instituto Superior Técnico, Universidade de Lisboa/CFMCUL, Estrada Nacional 10, 2695-066 Bobadela LRS, Portugal

[§]Univ. Grenoble Alpes, INAC-SCIB, RICC, and CEA, INAC-SCIB, , F-38000 Grenoble, France

[⊥]Institut des Sciences et Ingénierie Chimiques, Ecole Polytechnique Fédérale de Lausanne (EPFL), CH-1015 Lausanne, Switzerland

Supporting Information

ABSTRACT: The magnetic properties of the two uranium coordination compounds, $[K(18c6)][U(OSi(O^tBu)_3)_4]$ and $[K(18c6)][U(N(SiMe_3)_2)_4]$, both presenting the U^{III} ion in similar pseudotetrahedral coordination environments but with different O- or N-donor ligands, have been measured. The static magnetic susceptibility measurements and density functional theory studies suggest the presence of different ligand fields in the two compounds. Alternating-current susceptibility studies conducted at frequencies ranging from 95 to 9995 Hz and at temperatures in the 1.7−10 K range revealed for both compounds slow magnetic relaxation already at zero static magnetic field with similar energy barriers U ~24 K.

Actinide-based compounds are attracting increasing interest for the design of molecular magnets[1] with larger relaxation barriers and higher blocking temperatures because of the large single-ion anisotropy and the strong spin−orbit coupling of actinide ions.[2] The larger extension of 5f orbitals compared to that of 4f ones enables stronger metal−ligand interactions, rendering actinide ions attractive for the development of mononuclear[2f,3] and exchange-coupled polynuclear single-molecule magnets (SMMs).[4] Slow relaxation in mononuclear compounds arises from the intrinsic properties of the single ion subject to ligand field. As such, the coordination geometry is an important parameter in determining slow relaxation of magnetization. The nature of ligand donor atoms should also play an important role in determining the magnetic properties of uranium compounds as a result of differences in the ligand field strength and covalent contribution to uranium−ligand bonding. However, besides three structurally unrelated mononuclear uranium(III) SMMs reported by Liddle and co-workers,[5] most of the mononuclear uranium(III) complexes showing single-ion-magnet behavior present high coordination numbers (6−8) and are based on similar scorpionate-type ligands with heterocyclic pyrazolyl N-donor atoms in a trigonal-prismatic geometry.[2f,6,3,5] The first study investigating the effect of donor atoms on slow relaxation for uranium compounds in a similar geometry has just appeared in the literature.[6] The latter study elegantly shows that strongly donating N-heterocyclic carbene ligands lead to higher relaxation barriers compared to heterocyclic N donors as a result of the larger ligand field induced by the carbene atoms.[6]

Here we report two new rare examples of uranium(III)-based single-ion magnets, which are the first ones based on tetrahedral uranium compounds.[7] The two four-coordinated complexes, $[K(18c6)][U(OSi(O^tBu)_3)_4]$ (**1**) and $[K(18c6)][U(N(SiMe_3)_2)_4]$ (**2**), presenting the U^{III} ion in the same geometry but different ligand environments, both show slow relaxation of magnetization at low temperatures and SMM behavior even under zero magnetic field with similar energy barriers.

Complex **2** has been prepared in good yield from reduction of the tetrakis(silylamido) complex $[U\{N(SiMe_3)_2\}_4]$[8] with KC_8 in tetrahydrofuran (THF) in the presence of 18c6. As a result, complex **2** can be easily prepared in an analytically pure form for magnetic studies. X-ray-quality crystals of $[K(18c6)(THF)_2][U(N(SiMe_3)_2)_4]$ (**3**) were obtained from a THF solution at −40 °C. The crystal structure of complex **3** shows the presence of an isolated ion pair similar to the previously reported crystal structure of $\{U[N(SiMe_3)_2]_4\}\{K(THF)_6\}$.[9] The coordination polyhedra of the anion $[U(OSi(O^tBu)_3)_4]^-$ in **1**·toluene[7] and of the anion $[U(N(SiMe_3)_2)_4]^-$ in **3** are presented in Figure 1.

Both anions show distorted tetrahedral geometries, with a more irregular geometry observed for the $[U(N(SiMe_3)_2)_4]^-$ anion (N−U−N angles ranging from 100.4° to 114.9° in **3**

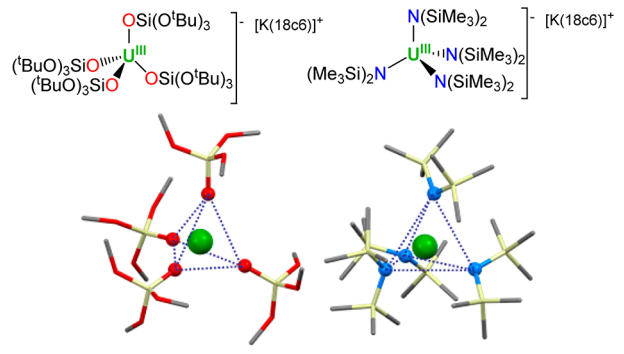

Figure 1. Structure of $[K(18c6)][UL_4]$ complexes (top) and Mercury diagrams (bottom) of the $[U(OSi(O^tBu)_3)_4]^-$ anion in **1**·toluene[7] (left) and of the $[U(N(SiMe_3)_2)_4]^-$ anion in **3** (right).

Received: June 30, 2014
Published: October 29, 2014

compared to O−U−O angles ranging from 108.4° to 111.3° in **1**) probably because of the presence of the bulkier amide ligands. The mean U−O siloxide bond distances in **1** at 2.228(17) Å are similar to those found in uranium(III) triphenoxide[10] or trisiloxide complexes,[11] while the mean U−N distance in **3** [2.434(13) Å] is very close to the one in $\{U[N(SiMe_3)_2]_4\}\{K(THF)_6\}$[9] (2.432 Å). In both cases, the mean U−N distance is significantly longer than that found in the neutral uranium(III) complex $[U(N(SiMe_3)_2)_3]$ [2.320(4) Å].[12] The shortest intermolecular U−U distances are at 12.4 Å for the tetrasiloxide complex **1**·toluene[7] and at 13.3 Å for the tetraamide complex **3**. These U−U distances are significantly longer than those found in the $\{U[N(SiMe_3)_2]_4\}\{K(THF)_6\}$[9] complex (10.1 Å), probably as a result of the presence of the crown ether.

The temperature dependence of the solid-state static magnetic susceptibility of complexes **1** and **2** was measured in the 2−300 K range using a SQUID magnetometer. Compound **2** presents paramagnetic behavior with a χT product dropping monotonically upon cooling, from 1.36 emu K mol^{-1} at 300 K to 0.35 emu K mol^{-1} at 2 K, as shown in Figure 2. Complex **1** shows a

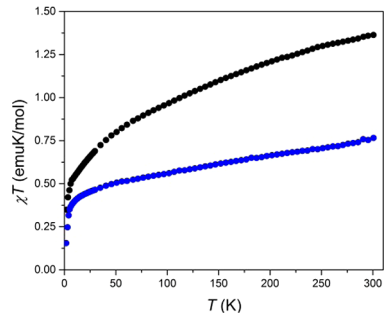

Figure 2. Temperature-dependent χT for **1** (blue) and **2** (black) measured under an applied field of 5000 Oe between 2 and 300 K after being zero-field-cooled.

significantly smaller temperature dependence of χT versus T at high temperature compared to **2** (Figure 1). The magnetic moment at 300 K for **2** (3.3 μ_B) is higher than that for **1** (2.48 μ_B; see Figures S2 and S3 in the Supporting Information, SI). The different temperature dependence of the χT product and the lower value of the room temperature magnetic moment could be interpreted in terms of a higher covalent contribution to bonding in complex **1** compared to complex **2**.[6,13] In order to elucidate potential differences in the electronic structures of these two complexes, we have performed density functional theory (DFT) calculations with two objectives: (i) gain insight in the ionic/covalent character of the U−ligand bond and (ii) estimate the ligand-field splitting for both ligands. Analysis of the Kohn−Sham orbital composition, of the charges, and of the spin densities on the uranium and ligands clearly shows that both the U^{III}−N and U^{III}−O bonds are mainly ionic in character with a negligible covalent contribution (see the SI for details). The difference observed in the χ_T curves could not therefore originate from covalency effects. Moreover, the computed value of the ligand-field splitting on f orbitals is clearly lower for **2** than for **1**, independent of the type of calculation. This leads to a lower temperature-independent paramagnetism for **1** than for **2**, which may account for the lower slope in χT versus T (Figure 2) for **1** compared to **2**.[9]

The field dependence of the magnetization M plotted versus B/T at different temperatures (Figure S8 in the SI) shows for both compounds curves not superimposed. This could be ascribed to the magnetic anisotropy or to the presence of low-lying magnetic states.[14] The magnetization cycling data (inset of Figure S8 in the SI) at several temperatures above 1.6 K, obtained with a sweeping rate of 90 Oe s^{-1}, do not show any coercivity, probably denoting efficient quantum tunneling of the magnetization occurring at zero field. This is probably caused by low-symmetry components of the crystal field, as was already observed in other mononuclear compounds of uranium[3a] and of lanthanides with SMM behavior (i.e., faster than the thermal-activated relaxation).[15]

The magnetization dynamics of both complexes were investigated by alternating-current (ac) susceptibility measurements as a function of the temperature (1.7−10 K) and frequency (ω = 33−9995 Hz), in zero and higher static magnetic fields. In the absence of a static magnetic field, there is already a significant frequency dependence, although more pronounced in complex **1**, with clear maxima in both the in-phase (χ') and out-of-phase (χ'') signals, denoting slow relaxation of magnetization (Figure S7 in the SI). This frequency dependence under zero dc field is in these cases more evident than that in other uranium(III) compounds already classified as SMMs such as the pyrazolyl derivatives $U(Ph_2BPz_2)_3$,[5] $U(H_2BPz_2)_3$,[3c] and $[U(TpMe_2)_2(bipy)]I$,[3a] where χ' was found to be almost frequency-independent. The application of a static field of 500 Oe still clearly slows the relaxation dynamics of **1** and **2** with the occurrence of strong frequency and temperature dependence with well-resolved peaks in both χ' and χ'', as shown in Figure3.

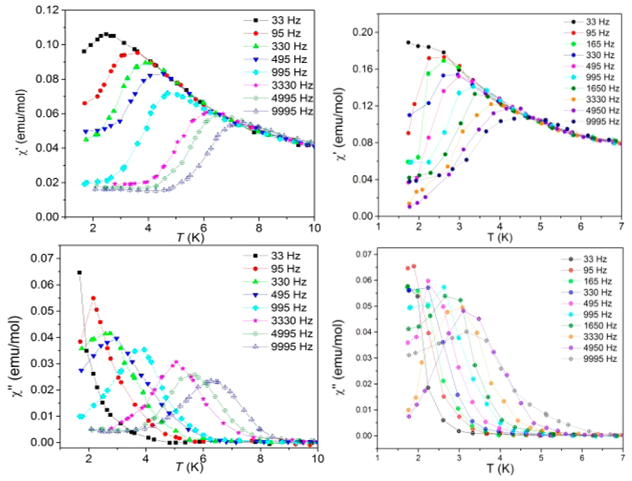

Figure 3. In-phase and out-of-phase components of ac susceptibility at different frequencies in the low-temperature range for **1** (left) and **2** (right) with H_{ac} = 5 Oe and H_{dc} = 500 Oe.

The magnetization relaxation rate was probed in the 1.8−10 K temperature range by measuring χ' and χ'' at fixed temperatures, while the frequency ω of the ac field was varied from 10 Hz to 10 kHz. The Cole−Cole plots at low temperatures (see Figures S9 and S11 in the SI) for both complexes show distorted semicircles and can be fitted to the generalized Debye model.[4a,16] For each complex, the single relaxation time τ extracted from the frequency-dependent ac susceptibility data taken for dc fields at 0 and 500 Oe were fitted to an Arrhenius law, $\tau = \tau_0 \exp(U/k_BT)$, where U is the effective energy barrier and k_B is the Boltzmann constant (Figure 4). The values of the energy barriers [U = 26 (±2) K for **1** and U = 23 (±3) K for **2** at H_{dc} = 0 Oe] and of the preexponential factors ($\tau_0 = 2.6 \times 10^{-7}$ s for **1** and $\tau_0 = 2.20 \times 10^{-8}$ s for **2** at H_{dc} = 0 Oe) are consistent with a slow magnetic

dx.doi.org/10.1021/ic501520c | Inorg. Chem. 2014, 53, 11809−11811

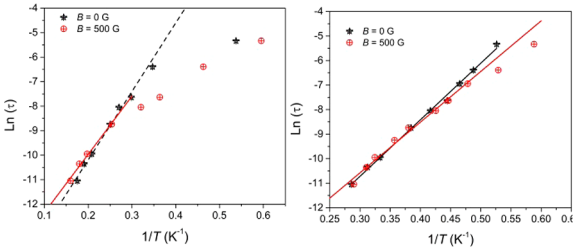

Figure 4. Plots of ln (τ) versus T^{-1} with a fitting to the Arrhenius law for complexes **1** (left) and **2** (right).

relaxation, with energy barriers falling in the high end of the range (5.5−31 K) reported so far for uranium(III) SMM complexes.[2f,3] For both static fields, the U barriers of complexes **1** and **2** are almost identical, slightly higher in the first compound. Also, by a comparison of both plots of ln(τ) versus T^{-1} (Figure 4), it is observable that in the case of **1** the Arrhenius law is only followed in the higher temperature range, although in the lower temperature range, a clear deviation from the activated regime is noticed in both fields, certainly because of the approach of a quantum tunneling regime expected to occur at lower temperatures, as was already observed in other uranium(III) compounds.

In conclusion, we have identified two new examples of uranium-based SMMs. Slow relaxation of magnetization has been reported for a small number of mononuclear complexes of uranium(III), but tetrasiloxide and tetrasilylamide are the first examples of a tetrahedral uranium(III)-based SMM. In spite of the different coordination environments provided by the siloxide ligands compared to the silylamide ligands, which lead to significantly different values of the high-temperature magnetic moment and of its temperature dependence, the two complexes show similar values of the relaxation barriers, which are among the highest reported to date. The difference in the ligand-field splitting shown by DFT studies for these complexes may lead to the very slightly larger value of the relaxation barrier found for the siloxide complex. A significantly higher relaxation barrier was found in isostructural trigonal-prismatic complexes presenting strongly donating carbene donors (U = 33 cm^{-1}) compared to N donors (U = 0 cm^{-1}).[9] Future studies will be directed to investigate tetrahedral complexes of stronger donating ligands.

■ ASSOCIATED CONTENT

Ⓢ Supporting Information

Synthetic details, ^{1}H NMR spectra, and XRD, magnetic, and computational data. This material is available free of charge via the Internet at http://pubs.acs.org.

■ AUTHOR INFORMATION

Corresponding Authors

*E-mail: malmeida@itn.pt.

*E-mail: marinella.mazzanti@epfl.ch.

Author Contributions

‡L.C.J.P. and C.C. contributed equally.

Notes

The authors declare no competing financial interest.

■ ACKNOWLEDGMENTS

We thank Jean-François Jacquot for his support in magnetic measurements and Eric J. Schelter for useful discussions. This work benefited from COST Action CM1006−EUFEN: European F-Element Network. J.T.C. thanks FCT (Portugal) for a doctoral grant (SFRH/BD/84628/2012). We acknowledge support from FCT (Portugal) under Contract PTDC/QEQ-SUP/1413/2012.

■ REFERENCES

(1) (a) Gatteschi, D.; Sessoli, R.; Villain, J. *Molecular Nanomagnets*; Oxford University Press: Oxford, U.K., 2006. (b) Sessoli, R.; Gatteschi, D.; Caneschi, A.; Novak, M. A. *Nature* **1993**, *365*, 141−143. (c) Milios, C. J.; Vinslava, A.; Wernsdorfer, W.; Moggach, S.; Parsons, S.; Perlepes, S. P.; Christou, G.; Brechin, E. K. *J. Am. Chem. Soc.* **2007**, *129*, 2754−2755. (d) Coulon, C.; Miyasaka, H.; Clerac, R. *Struct. Bonding (Berlin)* **2006**, *122*, 163−206. (e) Wang, X.-Y.; Avendano, C.; Dunbar, K. R. *Chem. Soc. Rev.* **2011**, *40*, 3213−3238.

(2) (a) Rinehart, J. D.; Harris, T. D.; Kozimor, S. A.; Bartlett, B. M.; Long, J. R. *Inorg. Chem.* **2009**, *48*, 3382−3395. (b) Layfield, R. A. *Organometallics* **2014**, *33*, 1084−1099. (c) Magnani, N.; Colineau, E.; Eloirdi, R.; Griveau, J. C.; Caciuffo, R.; Cornet, S. M.; May, I.; Sharrad, C. A.; Collison, D.; Winpenny, R. E. P. *Phys. Rev. Lett.* **2010**, *104*, 197202−197204. (d) Mills, D. P.; Moro, F.; McMaster, J.; van Slageren, J.; Lewis, W.; Blake, A. J.; Liddle, S. T. *Nat. Chem.* **2011**, *3*, 454−460. (e) Magnani, N.; Apostolidis, C.; Morgenstern, A.; Colineau, E.; Griveau, J. C.; Bolvin, H.; Walter, O.; Caciuffo, R. *Angew. Chem., Int. Ed.* **2011**, *50*, 1696−1698. (f) Rinehart, J. D.; Long, J. R. *Dalton Trans.* **2012**, *41*, 13572−13574. (g) Rinehart, J. D.; Long, J. R. *Chem. Sci.* **2011**, *2*, 2078−2085. (h) Mougel, V.; Chatelain, L.; Hermle, J.; Caciuffo, R.; Colineau, E.; Tuna, F.; Magnani, N.; de Geyer, A.; Pecaut, J.; Mazzanti, M. *Angew. Chem., Int. Ed.* **2014**, *53*, 819−823.

(3) (a) Antunes, M. A.; Pereira, L. C. J.; Santos, I. C.; Mazzanti, M.; Marcalo, J.; Almeida, M. *Inorg. Chem.* **2011**, *50*, 9915−9917. (b) Coutinho, J. T.; Antunes, M. A.; Pereira, L. C. J.; Bolvin, H.; Marcalo, J.; Mazzanti, M.; Almeida, M. *Dalton Trans.* **2012**, *41*, 13568−13571. (c) Coutinho, J. T.; Antunes, M. A.; Pereira, L. C. J.; Marçalo, J.; Almeida, M. *Chem. Commun.* **2014**, *50*, 10262−10264. (d) Rinehart, J. D.; Meihaus, K. R.; Long, J. R. *J. Am. Chem. Soc.* **2010**, *132*, 7572−7573.

(4) (a) Mougel, V.; Chatelain, L.; Pecaut, J.; Caciuffo, R.; Colineau, E.; Griveau, J. C.; Mazzanti, M. *Nat. Chem.* **2012**, *4*, 1011−1017. (b) Carretta, S.; Amoretti, G.; Santini, P.; Mougel, V.; Mazzanti, M.; Gambarelli, S.; Colineau, E.; Caciuffo, R. *J. Phys.: Condens. Matter* **2013**, *25*, 486001(6pp).

(5) Rinehart, J. D.; Long, J. R. *J. Am. Chem. Soc.* **2009**, *131*, 12558−12559.

(6) Meihaus, K. R.; Minasian, S. G.; Lukens, W. W., Jr.; Kozimor, S. A.; Shuh, D. K.; Tyliszczak, T.; Long, J. R. *J. Am. Chem. Soc.* **2014**, *136*, 6056−6068.

(7) Camp, C.; Pecaut, J.; Mazzanti, M. *J. Am. Chem. Soc.* **2013**, *135*, 12101−12111.

(8) Lewis, A. J.; Williams, U. J.; Carroll, P. J.; Schelter, E. J. *Inorg. Chem.* **2013**, *52*, 7326−7328.

(9) Evans, W. J.; Lee, D. S.; Rego, D. B.; Perotti, J. M.; Kozimor, S. A.; Moore, E. K.; Ziller, J. W. *J. Am. Chem. Soc.* **2004**, *126*, 14574−14582.

(10) Vandersluys, W. G.; Burns, C. J.; Huffman, J. C.; Sattelberger, A. P. *J. Am. Chem. Soc.* **1988**, *110*, 5924−5925.

(11) (a) Mougel, V.; Camp, C.; Pecaut, J.; Coperet, C.; Maron, L.; Kefalidis, C. E.; Mazzanti, M. *Angew. Chem., Int. Ed.* **2012**, *51*, 12280−12284. (b) Camp, C.; Kefalidis, C. E.; Pecaut, J.; Maron, L.; Mazzanti, M. *Angew. Chem., Int. Ed.* **2013**, *52*, 12646−12650.

(12) Stewart, J. L.; Andersen, R. A. *Polyhedron* **1998**, *17*, 953−958.

(13) Morss, L. R.; Edelstein, N. M.; Fuger, J. *The Chemistry of the Actinide and Transactinide Elements*; Springer: Dordrecht, The Netherlands, 2006.

(14) Abbas, G.; Lan, Y.; Kostakis, G. E.; Wernsdorfer, W.; Anson, C. E.; Powell, A. K. *Inorg. Chem.* **2010**, *49*, 8067−8072.

(15) (a) Silva, M. R.; Martin-Ramos, P.; Coutinho, J. T.; Pereira, L. C. J.; Martin-Gil, J. *Dalton Trans.* **2014**, *43*, 6752−6761. (b) Ishikawa, N.; Sugita, M.; Ishikawa, T.; Koshihara, S.; Kaizu, Y. *J. Phys. Chem. B* **2004**, *108*, 11265−11271.

(16) Cole, K. S.; Cole, R. H. *J. Chem. Phys.* **1941**, *9*, 341−351.

ChemComm

COMMUNICATION

View Article Online
View Journal | View Issue

Cite this: *Chem. Commun.*, 2015, 51, 11309

Received 9th April 2015,
Accepted 4th June 2015

DOI: 10.1039/c5cc02945g

www.rsc.org/chemcomm

A zig-zag uranyl(v)–Mn(ii) single chain magnet with a high relaxation barrier†

Lucile Chatelain,[abc] Floriana Tuna,[d] Jacques Pécaut[ab] and Marinella Mazzanti*[c]

The synthesis, structural characterization and magnetic properties of a 1D zig-zag coordination polymer based on a cation–cation $[(U^{V}O_2)Mn^{II}]$ repeated unit are reported; it shows single chain magnet (SCM) behaviour with a high energy barrier of 122 K.

Single chain magnets (SCMs) have been attracting increasing attention in the last decade[1] following the first report of slow relaxation of the magnetization in a 1 D coordination polymer.[2] Notably SCMs provide an attractive alternative to 0 D molecular magnets (SMMs) for the development of information storage devices.[1a,3] The requirements to observe the SCM behaviour first predicted by Glauber[4] are the presence of strong Ising anisotropy, high intra-chain magnetic coupling and weak inter-chain interactions. Notably, the high anisotropy of 5d and 4f ions has been successfully exploited to afford 1 D coordination polymers with SCM behaviour.[5,6]

Actinide ions have been recently attracting increasing attention for the design of SMMs due to their high anisotropy and their ability to engage in strong magnetic exchange.[7,8] However only one example of an actinide based single chain magnet has been reported so far.[9]

Our group and others have demonstrated that cation–cation interactions (described as the bonding of an actinyl imido or an oxo group with a metal cation) provide a convenient route to magnetic exchange[7j,m,8b,9,10] and to the assembly of exchange-coupled SMMs.[7j,m,8b,9] In particular, we have recently shown that, depending on the reaction stoichiometry, the cation–cation interaction between the uranyl(v) $[UO_2(salen)(Py)]^-$ building block and the $[Mn(II)(Py)_n]$ unit leads either to a $\{U_{12}Mn_6\}$ wheel-shaped uranyl(v) cluster with SMM behaviour[7m] or to a linear 1 D polymer with a SCM behaviour.[9]

Here we report the first actinide based 1D zig-zag coordination polymer $\{[UO_2(Mesaldien)][Mn(NO_3)(Py)_2]\}_n$, **2**, that is built from the cation–cation interaction of the uranyl(v) complex $[UO_2(saldien)]^-$ with $[Mn(II)(NO_3)(Py)_2]$. Polymer **2** shows slow relaxation of the magnetization with a high relaxation barrier of 122 K and an open magnetic hysteresis loop at $T < 3$ K, with a coercive field of 1.75 T at 2 K. Compound **2** is thus only the second example of an actinide based polymer showing SCM behaviour which most likely arises from a strong intra-chain coupling combined with the high Ising anisotropy of the uranyl(v) dioxo group.

The monomeric uranyl(v) complex $[UO_2(Mesaldien)][Cp^*_2Co]$, **1**, containing the pentadentate Schiff base Mesaldien was prepared in high yield (90%) by reduction of the analogous monomeric uranyl(vi) complex with one equivalent of Cp^*_2Co in pyridine (see the ESI†). Complex **1** is fully stable in the solid state and in a variety of organic solvents. The stability of complex **1** with respect to the disproportionation reaction is consistent with previously reported spectroscopic and synthetic studies showing that pentadentate Schiff bases stabilize pentavalent uranyl by saturating the equatorial coordination sites and therefore preventing the formation of dimeric disproportionation intermediates.[11a–c] As such complex **1** provides an excellent precursor for the controlled synthesis of heteropolymetallic cation–cation assemblies. Notably, the reaction of **1** with one equivalent of the $Mn(NO_3)_2$ salt affords the 1D polymer $\{[UO_2(Mesaldien)][Mn(NO_3)(Py)_2]\}_n$, **2**, as a pink microcrystalline powder in 66% yield (Scheme 1). The X-ray crystal structure of **2** is shown in Fig. 1.

In the structure of **2** the oxo groups of the uranyl(v), $[UO_2(Mesaldien)]^-$ units bridge through a linear cation–cation interaction between two $[Mn(NO_3)(Py)_2]^+$ cations to yield a zig-zag one-dimensional chain. The asymmetric unit of **2** contains only one uranium and one manganese atoms forming the neutral repeated entity $\{[UO_2(Mesaldien)][Mn(NO_3)(Py)_2]\}$. The uranium atom is heptacoordinated with a slightly distorted pentagonal

[a] *Univ. Grenoble Alpes, INAC-SCIB, F-38000 Grenoble, France*
[b] *CEA, INAC-SCIB, F-38000 Grenoble, France*
[c] *Institut des Sciences et Ingénierie Chimiques, Ecole Polytechnique Fédérale de Lausanne (EPFL), CH-1015 Lausanne, Switzerland. E-mail: marinella.mazzanti@epfl.ch*
[d] *School of Chemistry and Photon Science Institute, University of Manchester, Oxford Road, Manchester, M13 9PL, UK*

† Electronic supplementary information (ESI) available. CCDC 1058487 and 1058488. For ESI and crystallographic data in CIF or other electronic format see DOI: 10.1039/c5cc02945g

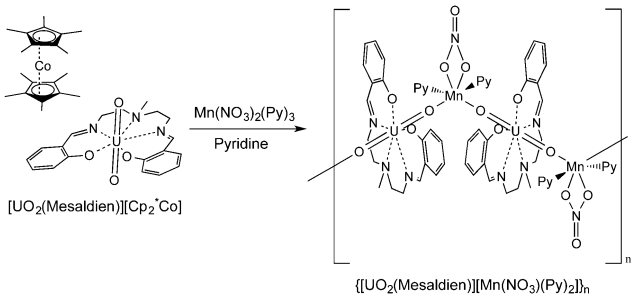

Scheme 1 Synthesis of **2**.

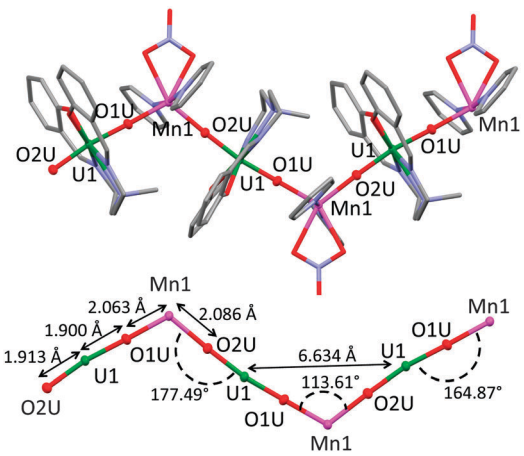

Fig. 1 Mercury view of the structure of **2** (top) and enhanced view of the zig-zag core with associated distances and angles. (bottom) (Ligands were represented in pipes, H and co-crystallised solvent molecules were omitted for clarity, C is represented in grey, O in red, N in light blue, Mn in pink and U in green.)

bipyramidal geometry by the five donor atoms of the Mesaldien ligand situated in the equatorial plane and by the two uranyl oxygens in the axial position. The manganese(II) ion is hexa-coordinated, by two uranyl oxygens from two different uranyl(V) units, two pyridines and the two oxygens of the bidentate nitrate ligand. Due to the U(V)O_2–Mn(II) cation–cation interactions, the U=O bond distances are lengthened (U1–O1U 1.900(3) Å and U1–O2U 1.913(3) Å) compared to those found in [UO_2(Mesaldien)][Cp^*_2Co] **1** (U1–O1U 1.847(6) Å and U1–O2U 1.846(6) Å). The mean Mn–O_{yl} (where O_{yl} is the uranyl oxygen) bond distance in **2** is 2.075(3) Å, significantly shorter than that found in the {$U_{12}Mn_6$} wheel-shaped uranyl(V) cluster[7m] (2.15(2) Å) but similar to that found in a trinuclear [U(V)O_2Mn(II)$_2$] complex (2.055(6) Å).[8b] The U–O–Mn angles deviate slightly from linearity and range from 164.87° to 177.49°. The asymmetric unit is repeated thanks to a 2-fold screw axis along the 0, *y*, 1/4 direction resulting in a zig-zag topology with a U–Mn–U angle of 113.61°. The observed geometry is very different from that observed for the only other reported uranium based SCM {[UO_2(salen)(Py)][Mn(Py)$_4$]NO_3}$_n$,[9] assembled from the uranyl(V) complex of the tetradentate Schiff base salen, where the mean U–M–U angle is practically linear (170.25°). The deviation from linearity probably results from the presence of a bidentate nitrate ligand bonded to the manganese cation.

An intra-chain separation between neighbouring U(V) ions of 6.634 Å and a separation between neighbouring Mn(II) ions of 7.897 Å are found in **2** whereas the mean intramolecular U–Mn distance is 3.96(3) Å. Each chain is separated from the nearest chain with a minimum intermetallic distance of 11.881, 10.336 and 9.019 Å, respectively, for U–U, U–Mn and Mn–Mn. No significant interchain π-stacking is observed in the structure of **2**.

Magnetic susceptibility measurements were performed first between 2 and 300 K on a polycrystalline sample of **2** at magnetic fields of 0.01, 0.1, 0.5 and 5 T (see the ESI†). The measured χT value for **2** at room temperature is approximately 4.8 cm^3 K mol^{-1} which is consistent with the values reported for heteropolymetallic Mn(II)–uranyl(V) assemblies containing one spin-only divalent manganese (with $S = 5/2$ and g close to 2) and one pentavalent uranium ion.[9] The χT product remains constant from 300 K to 80 K before reaching a field-dependent maximum (177.8 cm^3 K mol^{-1} at 0.01 T, 77.29 cm^3 K mol^{-1} at 0.1 T, 26.3 cm^3 K mol^{-1} at 0.5 T; 6.7 cm^3 K mol^{-1} at 5 T). At very low temperatures this product drops rapidly probably due to saturation effects, magnetic anisotropy and/or inter-chain anti-ferromagnetic interactions. The increase of χT below 80 K suggests the presence of a dominant ferromagnetic interaction leading to an aligned-spin ground state.

The scaling of the χT data of **2** (Fig. 2, left) clearly shows the occurrence of a linear regime characteristic of Ising 1D systems. The ln(χT) *versus* 1/T plot increases linearly between 45 and 16 K (1/T from 0.063 to 0.022 K^{-1}). The experimental data were fitted within this linear regime using the equation $\chi T = C_{eff}\exp(\Delta/k_BT)$ which describes a ferromagnetically coupled infinite chain. The fit gives an energy gap Δ/k_B of 43.4 K and a pre-exponential factor C_{eff} = 2.50. The magnetic susceptibility data of **2** between 16 and 300 K at 0.01 T were also fitted with the equation $\chi T = C_1\exp(\Delta_1/k_BT) + C_2\exp(\Delta_2/k_BT)$, where a second negative exponential is added to take into account the high-temperature crystal field effect and possible antiferromagnetic

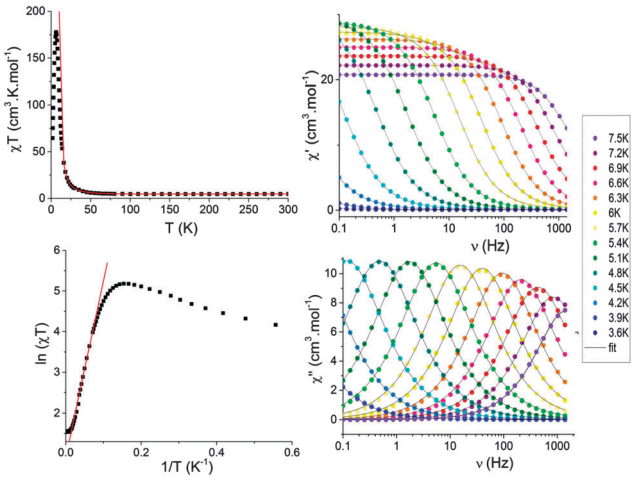

Fig. 2 Left: plots of (top) χT *versus* T and (bottom) ln(χT) *versus* 1/T for a polycrystalline sample of **2**, measured at 0.01 T applied field. Right: temperature dependence of the (top) real (χ') and (bottom) imaginary (χ'') ac susceptibilities for **2** measured at zero-dc field and 1.5 G ac field.

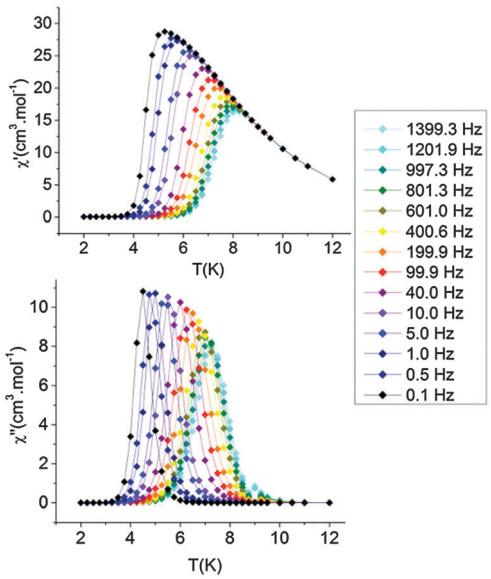

Fig. 3 Frequency dependence of the (top) real (χ') and (bottom) imaginary (χ'') ac susceptibilities for **2** measured at zero-dc field and an ac field of 1.5 oscillating at frequencies between 0.1 and 1400 Hz.

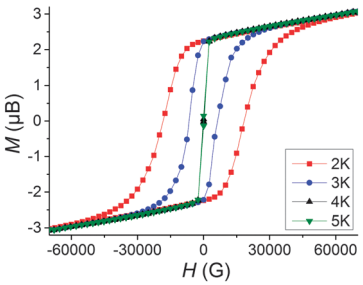

Fig. 4 Field dependence of the magnetisation of **2** measured at four different temperatures with a field sweep rate of 0.0061 T.s^{-1}.

contributions. In this case we obtained Δ_1/k_B = 44.1 K, Δ_2/k_B = −107.8 ± 10.5 K, C_1 = 2.43 cm^3 K mol^{-1}, and C_2 = 2.80 cm^3 K mol^{-1}, in very good agreement with the previous considerations. The high-temperature extrapolated Curie constant, $C = C_1 + C_2$ = 5.23 cm^3 K mol^{-1}, is close to the expected value for one Mn(II) and one U(V) ions.

Isothermal variable-field (−7 T to +7 T) magnetisation measurements were then performed at several temperatures between 2 and 5 K (Fig. 4). These measurements reveal an open hysteresis cycle below 3 K. This result confirms the existence of a magnetic ground state in **2** and the presence of a magnetic bistability. A significant coercive field of 1.75 T is obtained at 2 K, which decreases with increasing temperatures. A divergence between field cooled and zero field cooled magnetisations as a function of temperature is observed below 3 K and a remanent magnetisation (REM) of 2.2 μ_B is preserved at very low temperatures under zero field before vanishing after 3 K. These features suggest that this material behaves like a single chain magnet with a blocking temperature T_B = 3 K. The blocking temperature of **2** is significantly smaller than that reported for the linear chain $\{[UO_2(salen)(Py)][Mn(Py)_4]NO_3\}_n$[9] (5.8 K) highlighting the effect of the zig-zag geometry and of the ligand coordinated to the uranyl(V) on the magnetic properties.

The dynamic magnetisation was investigated to probe magnetic relaxation in **2**. Zero-field ac susceptibility measurements between 3.6 and 7.5 K were carried out at several frequencies between 0.1 and 1399 Hz with a 1.55 G ac field (Fig. 2 right). Both the in-phase (χ') and out-of-phase (χ'') components of the ac susceptibility show strong frequency dependence below *ca.* 7.5 K; maxima are observed in $\chi''(T)$ (Fig. 3). This result rules out the presence of any tridimensional ordering. Moreover, the value of the parameter $\phi = (\Delta T_{max}/T_{max})/\Delta(\log f) \approx 0.10$, measuring the relative variation of the temperature of the maximum of $\chi''(T)$ with respect to the frequency, is in the range of normal superparamagnets and excludes the possible occurrence of a spin glass state.[12]

The frequency dependence of the in-phase (χ') and out-of-phase (χ'') components of the ac susceptibility was fitted to a generalized Debye model for one relaxation process with the α parameter in the range of 0.11–0.20 revealing a narrow distribution of relaxation times. Semi-circular Cole–Cole plots (χ'' *vs.* χ') are obtained for temperatures below 7.2 K confirming that only one relaxation process occurs. Both ac experiments as a function of frequency or temperature allow the determination of relaxation times and they were fitted to the Arrhenius equation $\tau = \tau_0 \exp(U/k_BT)$, where τ is the relaxation time, U_1 = 122.1(14) K is the energy barrier for the relaxation of the magnetisation and $\tau_0^{(1)} = 6.2 \times 10^{-12}$ s is the pre-exponential factor (Fig. S9, ESI†). A crossing in the Arrhenius plot occurs, giving a second energy barrier of U_2 = 107.0(7) K associated with $\tau_0^{(2)} = 7.4 \times 10^{-11}$ s. This value must be regarded with caution because of the limited T-range over which the relaxation times were determined. Several SCM systems were reported to show two activated regions due to finite-size effects.[1] Thus, the energy barrier of the zig-zag chain is very high and only moderately smaller than for the previously reported U(V)Mn(II) linear chain (134.0(8) K).[9] The high relaxation barrier of the zig-zag chain is most likely the result of the ferromagnetic intra-chain coupling associated with the large anisotropy from the strong Ising-type ligand field of the uranyl group.[13]

In conclusion we have shown that the cation–cation assembly of the uranyl(V) complex of a pentadentate Schiff base ligand with the $[Mn(II)(NO_3)(Py)_2]$ unit affords a 5f–3d heterometallic 1D chain with a novel zig-zag topology. The presented results show that different chain topologies can be obtained just by changing the nature of the Schiff base ligand in the uranyl(V) building block. Variable-temperature dc magnetic susceptibility measurements demonstrate the presence of intrachain ferromagnetic exchange coupling within the chain. Moreover, this zig-zag 1D polymer shows SCM behaviour with a high relaxation barrier and an open magnetic hysteresis affording the second example of actinide based SCM so far isolated. The high stability of the $[UO_2(Mesaldien)]^-$ building block provides a versatile route to a wide variety of 3d–5f 1D chains that will be investigated in future studies.

Notes and references

1 (*a*) W. X. Zhang, R. Ishikawa, B. Breedlove and M. Yamashita, *RSC Adv.*, 2013, **3**, 3772–3798; (*b*) H. L. Sun, Z. M. Wang and S. Gao, *Coord. Chem. Rev.*, 2010, **254**, 1081–1100; (*c*) H. Miyasaka, M. Julve, M. Yamashita and R. Clerac, *Inorg. Chem.*, 2009, **48**, 3420–3437; (*d*) S. W. Przybylak, F. Tuna, S. J. Teat and R. E. P. Winpenny, *Chem. Commun.*, 2008, 1983–1985.

2 (*a*) A. Caneschi, D. Gatteschi, N. Lalioti, C. Sangregorio, R. Sessoli, G. Venturi, A. Vindigni, A. Rettori, M. G. Pini and M. A. Novak, *Angew. Chem., Int. Ed.*, 2001, **40**, 1760–1763; (*b*) R. Clerac, H. Miyasaka, M. Yamashita and C. Coulon, *J. Am. Chem. Soc.*, 2002, **124**, 12837–12844.

3 D. Gatteschi, R. Sessoli and J. Villain, *Molecular Nanomagnets*, Oxford University Press, Oxford, UK, 2006.

4 R. J. Glauber, *J. Math. Phys.*, 1963, **4**, 294–307.

5 (*a*) E. V. Peresypkina, A. M. Majcher, M. Rams and K. E. Vostrikova, *Chem. Commun.*, 2014, **50**, 7150–7153; (*b*) T. D. Harris, M. V. Bennett, R. Clerac and J. R. Long, *J. Am. Chem. Soc.*, 2010, **132**, 3980–3988.

6 (*a*) K. Bernot, L. Bogani, A. Caneschi, D. Gatteschi and R. Sessoli, *J. Am. Chem. Soc.*, 2006, **128**, 7947–7956; (*b*) R. Sessoli and A. K. Powell, *Coord. Chem. Rev.*, 2009, **253**, 2328–2341; (*c*) Y. Z. Zheng, Y. H. Lan, W. Wernsdorfer, C. E. Anson and A. K. Powell, *Chem. – Eur. J.*, 2009, **15**, 12566–12570.

7 (*a*) J. R. Long and K. R. Meihaus, *J. Chem. Soc., Dalton Trans.*, 2015, **44**, 2517–2528; (*b*) N. Magnani, *Int. J. Quantum Chem.*, 2014, **114**, 755–759; (*c*) K. R. Meihaus, S. G. Minasian, W. W. Lukens, Jr., S. A. Kozimor, D. K. Shuh, T. Tyliszczak and J. R. Long, *J. Am. Chem. Soc.*, 2014, **136**, 6056–6068; (*d*) J. D. Rinehart, K. R. Meihaus and J. R. Long, *J. Am. Chem. Soc.*, 2010, **132**, 7572–7573; (*e*) J. D. Rinehart and J. R. Long, *J. Am. Chem. Soc.*, 2009, **131**, 12558–12559; (*f*) M. A. Antunes, L. C. J. Pereira, I. C. Santos, M. Mazzanti, J. Marcalo and M. Almeida, *Inorg. Chem.*, 2011, **50**, 9915–9917; (*g*) J. T. Coutinho, M. A. Antunes, L. C. J. Pereira, H. Bolvin, J. Marcalo, M. Mazzanti and M. Almeida, *J. Chem. Soc., Dalton Trans.*, 2012, **41**, 13568–13571; (*h*) L. C. J. Pereira, C. Camp, J. T. Coutinho, L. Chatelain, P. Maldivi, M. Almeida and M. Mazzanti, *Inorg. Chem.*, 2014, **53**, 11809–11811; (*i*) N. Magnani, C. Apostolidis, A. Morgenstern, E. Colineau, J. C. Griveau, H. Bolvin, O. Walter and R. Caciuffo, *Angew. Chem., Int. Ed.*, 2011, **50**, 1696–1698; (*j*) N. Magnani, E. Colineau, R. Eloirdi, J. C. Griveau, R. Caciuffo, S. M. Cornet, I. May, C. A. Sharrad, D. Collison and R. E. P. Winpenny, *Phys. Rev. Lett.*, 2010, **104**, 197202; (*k*) N. Magnani, E. Colineau, J. C. Griveau, C. Apostolidis, O. Walter and R. Caciuffo, *Chem. Commun.*, 2014, **50**, 8171–8173; (*l*) S. Carretta, G. Amoretti, P. Santini, V. Mougel, M. Mazzanti, S. Gambarelli, E. Colineau and R. Caciuffo, *J. Phys.: Condens. Matter*, 2013, **25**, 486001; (*m*) V. Mougel, L. Chatelain, J. Pecaut, R. Caciuffo, E. Colineau, J. C. Griveau and M. Mazzanti, *Nat. Chem.*, 2012, **4**, 1011–1017; (*n*) D. P. Mills, F. Moro, J. McMaster, J. van Slageren, W. Lewis, A. J. Blake and S. T. Liddle, *Nat. Chem.*, 2011, **3**, 454–460; (*o*) D. M. King, F. Tuna, J. McMaster, W. Lewis, A. J. Blake, E. J. L. McInnes and S. T. Liddle, *Angew. Chem., Int. Ed.*, 2013, **52**, 4921–4924.

8 (*a*) F. Moro, D. P. Mills, S. T. Liddle and J. Slangeren, *Angew. Chem., Int. Ed.*, 2013, **52**, 1–5; (*b*) L. Chatelain, J. P. S. Walsh, J. Pecaut, F. Tuna and M. Mazzanti, *Angew. Chem., Int. Ed.*, 2014, **53**, 13434–13438.

9 V. Mougel, L. Chatelain, J. Hermle, R. Caciuffo, E. Colineau, F. Tuna, N. Magnani, A. de Geyer, J. Pecaut and M. Mazzanti, *Angew. Chem., Int. Ed.*, 2014, **53**, 819–823.

10 (*a*) P. L. Arnold, E. Hollis, G. S. Nichol, J. B. Love, J. C. Griveau, R. Caciuffo, N. Magnani, L. Maron, L. Castro, A. Yahia, S. O. Odoh and G. Schreckenbach, *J. Am. Chem. Soc.*, 2013, **135**, 3841–3854; (*b*) P. L. Arnold, E. Hollis, F. J. White, N. Magnani, R. Caciuffo and J. B. Love, *Angew. Chem., Int. Ed.*, 2011, **50**, 887–890; (*c*) L. Chatelain, V. Mougel, J. Pecaut and M. Mazzanti, *Chem. Sci.*, 2012, **3**, 1075–1079; (*d*) V. Mougel, P. Horeglad, G. Nocton, J. Pecaut and M. Mazzanti, *Angew. Chem., Int. Ed.*, 2009, **48**, 8477–8480; (*e*) G. Nocton, P. Horeglad, J. Pécaut and M. Mazzanti, *J. Am. Chem. Soc.*, 2008, **130**, 16633–16645; (*f*) L. P. Spencer, E. J. Schelter, P. Yang, R. L. Gdula, B. L. Scott, J. D. Thompson, J. L. Kiplinger, E. R. Batista and J. M. Boncella, *Angew. Chem., Int. Ed.*, 2009, **48**, 3795–3798.

11 (*a*) K. Takao, M. Kato, S. Takao, A. Nagasawa, G. Bernhard, C. Hennig and Y. Ikeda, *Inorg. Chem.*, 2010, **49**, 2349–2359; (*b*) K. Takao, S. Tsushima, S. Takao, A. C. Scheinost, G. Bernhard, Y. Ikeda and C. Hennig, *Inorg. Chem.*, 2009, **48**, 9602–9604; (*c*) V. Mougel, J. Pecaut and M. Mazzanti, *Chem. Commun.*, 2012, **48**, 868–870.

12 J. A. Mydosh, *Spin Glasses: An Experimental Introduction*, Taylor and Francis, London, 1993.

13 G. Nocton, P. Horeglad, V. Vetere, J. Pecaut, L. Dubois, P. Maldivi, N. M. Edelstein and M. Mazzanti, *J. Am. Chem. Soc.*, 2010, **132**, 495–508.

ChemComm

COMMUNICATION

View Article Online
View Journal | View Issue

Cite this: *Chem. Commun.*, 2015, 51, 15454

Received 10th August 2015,
Accepted 27th August 2015

DOI: 10.1039/c5cc06707c

www.rsc.org/chemcomm

CO_2 conversion to isocyanate *via* multiple N–Si bond cleavage at a bulky uranium(III) complex†

Clément Camp,[ab] Lucile Chatelain,[abc] Christos E. Kefalidis,[d] Jacques Pécaut,[ab] Laurent Maron*[d] and Marinella Mazzanti*[c]

The reaction of the sterically saturated uranium(III) tetrasilylamido complex [K(18c6)][U(N(SiMe$_3$)$_2$)$_4$] with CO_2 leads to CO_2 insertion into the U–N bond affording the stable U(IV) isocyanate complex [K(18c6)][U(N(SiMe$_3$)$_2$)$_3$(NCO)$_2$]$_n$ that was crystallographically characterized. DFT studies indicate that the reaction involves the [2+2] cycloaddition of a double bond of O=CO to the U–N(SiMe$_3$)$_2$ bond and proceeds to the final product through multiple silyl migration steps.

The reactivity of uranium(III) with small molecules such as CO_2, CO or N_2 has been attracting increasing interest in recent years due to the ability of uranium to promote unusual transformations.[1,2] Bulky amides have been successfully used in uranium chemistry, as innocent ancillary ligands, as alternatives to the ubiquitous cyclopentadienyl systems.[3] In particular the simple neutral [U(N(SiMe$_3$)$_2$)$_3$][4] complex has provided a versatile precursor and has demonstrated interesting reactivity[5] including arene reduction and functionalization,[6] CO activation,[7] and nitride formation.[8] In contrast, the ability of the U–N bonds to undergo insertion reactions has been much less explored compared to U–C σ-bonds.[1c] Only a few examples of insertion of CO_2 into U(III)–NR_2 and U(IV)–NR_2 bonds leading to the formation of U(III)[9] and U(IV) carbamates[10] have been reported. Examples of the insertion of CO_2 into metal–silylamide bonds have been reported[11] for main group, d-block and f-block metals[12] but are much rarer than the insertion of CO_2 into N-alkylamide bonds. In particular, [U^{III}(N(SiMe$_3$)$_2$)$_3$] was reported to react with CO_2 to give O=C=NSiMe$_3$ and a second product identified as the tetravalent uranium silanolate [U(OSiMe$_3$)$_4$].[12a]

Herein we show that the reaction of CO_2 with the sterically saturated uranium(III) tetrasilylamido complex [K(18c6)][U(N(SiMe$_3$)$_2$)$_4$], **1**, leads to CO_2 insertion into the U–N bond and to the formation of the stable U(IV) isocyanate complex [K(18c6)][U(N(SiMe$_3$)$_2$)$_3$(NCO)$_2$]$_n$ **2**. DFT studies were used in combination with reactivity studies to investigate the mechanism leading to the formation of complex **2**. Complex **2** provides a rare example of cyanate formation at a uranium center. To date there have been only three examples of uranium-mediated OCN^- formation and they involve the reaction of CO with a nitride,[13] imido[14] or nitrosyl complex.[15]

Complex **1** was prepared from [U(N(SiMe$_3$)$_2$)$_4$][16] according to the previously reported procedure.[17] The reaction of **1** with 2.5 equivalents of carbon dioxide proceeded slowly (completed after 48 hours) at room temperature affording after workup and recrystallization the U(IV) bis-cyanate complex [K(18c6)][U(N(SiMe$_3$)$_2$)$_3$(NCO)$_2$]$_n$, **2** as a pale pink microcrystalline solid in 48% yield (Scheme 1). The stoichiometry of this reaction requires the presence of additional uranium compounds and reduced by-products (U(III) has been oxidized to U(IV)) that have not been isolated. THF solutions of **2** are stable for at least 48h at room temperature. The ^{1}H NMR spectrum for **2** recorded from deuterated THF at room temperature displays a broad resonance at −10.9 ppm corresponding to the three equivalent {N(SiMe$_3$)$_2$} moieties together with a resonance at 4.7 ppm for the potassium crown ether counter cation.

The X-ray crystal structure of **2** shows the presence of a 1D coordination polymer (Fig. 1). The uranium environment is trigonal bipyramidal with three silylamido ligands at equatorial

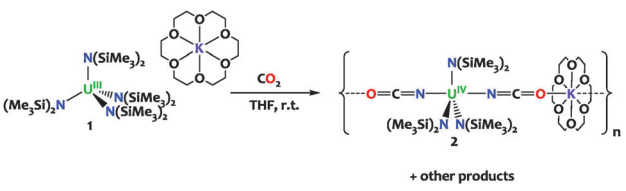

Scheme 1

[a] *Univ. Grenoble Alpes, INAC-SCIB, F-38000 Grenoble, France*
[b] *CEA, INAC-SCIB, Reconnaissance Ionique et Chimie de Coordination, 17 Rue des Martyrs, F-38000 Grenoble, France*
[c] *Institut des Sciences et Ingénierie Chimiques, Ecole Polytechnique Fédérale de Lausanne (EPFL), CH-1015 Lausanne, Switzerland. E-mail: marinella.mazzanti@epfl.ch*
[d] *LPCNO, CNRS & INSA, UPS, Université de Toulouse, 135 Avenue de Rangueil, F-31077 Toulouse, France*

† Electronic supplementary information (ESI) available: Synthetic details, full crystallographic data, ^{1}H and ^{13}C NMR spectra, ESI/MS spectra and computational data are included. CCDC 1417064. For ESI and crystallographic data in CIF or other electronic format see DOI: 10.1039/c5cc06707c

positions and two NCO^- anions at apical positions. A K(18c6) cation bridges two NCO ligands from two distinct uranium complexes. The U1–N_{amido} bond distances fall in the range of what was observed in the U(IV) silylamido species. Notably the structure of **2** is closely related to the isoelectronic azide species $[Na(THF)_4][U\{N(SiMe_3)_2\}_3(N_3)_2]$ reported by Hayton and coworkers[5e] featuring similar geometry and uranium-ligand bond distances. The three atoms X═C═X′ units are disordered across the mirror plane of the *P*21/*m* space group and refine equally well when N or O or a mixture of both are used at the X and X′ positions. Thus, the X-ray data do not allow us to discriminate between a cyanate (coordination through O) and an isocyanate (coordination through N) ligand. Similar disorder issues were observed in the $[\{Me_2Al(\mu\text{-}OSiMe_3)_2Mg(THF)_2(\mu\text{-}OCN)\}_3]$ complex[11c] and in the dimeric U(IV) complex $[U(\eta\text{-}C_8H_6\{Si^iPr_3\text{-}1,4\}_2)(\eta\text{-}Cp^*)(NCO)]_2$.[15] However, in most previously reported U(IV) complexes the NCO ligand is N-bound[18] and DFT calculations are in agreement with an N-bound coordination (see below and ref. 13). Therefore the structure was refined with N-bound OCN ligands (Fig. 1). The two U–N_{NCO} bond distances at 2.337(3) and 2.338(4) Å are in the range of those found in the few uranium isocyanate complexes reported (2.338(3),[13] 2.389(6)[18b] and 2.336(5) Å[19]).

The absorption band at 2201 cm^{-1} in the IR spectrum of **2** was assigned to the asymmetric stretching mode ν_{NCO}. This value is similar to those found in the few terminal[18] or bridging[15] U(IV) and U(III)[13] isocyanate complexes reported (2199–2122 cm^{-1}).

All the spectroscopic and analytical data (see ESI†) support the assignment of the three atoms in **2** as NCO ligands. Notably the quaternary carbon (after reaction with $^{13}CO_2$) resonance at δ = 492.4 ppm in the ^{13}C NMR spectrum, the microanalytical data, and the parent ion in the mass spectrum for the anion $[U(N(SiMe_3)_2)_3(NCO)_2]^-$ (m/z = 802.4) are in agreement with the assigned formula.

^1H and ^{13}C NMR studies of the reaction of **1** with $^{13}CO_2$ were performed. After addition of 1 equivalent of $^{13}CO_2$ the reaction leads to the slow disappearance of the ^1H signals assigned to complex **1** with completion after 48 hours. The ^{13}C NMR spectrum of the final reaction mixture shows the presence of a signal at 307 ppm that could be assigned to the quaternary carbon of a carbamate or an isocyanate intermediate. No evident color change was observed during the reaction. Additional ^{13}C NMR signals are also observed in the 5.6–1.8 ppm region. Further addition of 1 equivalent of $^{13}CO_2$ leads to a slow color change of the reaction mixture from dark purple to light pink. ^{13}C NMR monitoring of the reaction showed a slow evolution with time with the disappearance of the ^{13}C NMR signal at 307 ppm and the appearance of the ^{13}C NMR signal at 492.4 ppm assigned to the isocyanate complex **2**. All the ^{13}C NMR resonances in the 5.6–1.8 ppm region remained present in the final ^{13}C NMR spectrum but with increased intensity. In particular, two signals at 0.07 ppm in the ^1H NMR spectrum and at 1.84 ppm in the ^{13}C NMR spectrum were assigned to the hexamethyldisiloxane $(SiMe_3)_2O$ by-product. Signals for $SiMe_3NCO$ were not observed. The ^1H NMR spectrum of the final reaction mixture showed the resonances assigned to complex **2** and additional broad shifted resonances assigned to unidentified U(IV) products. Mass spectrometry studies showed the presence of $[U_2(OSiMe_3)_9]^-$ and $[U_2(NCO)(OSiMe_3)_8]^-$ species (see ESI†).

In order to shed light on the mechanistic aspects of this peculiar reactivity outcome, DFT investigations using the B3PW91 functional were performed. The system of choice is the full anionic system $[U(N(SiMe_3)_2)_4]^-$, where the counter-cation is not taken into account.[13] The anionic $[U(IV)\text{–}CO_2^{\bullet}]^-$ intermediate **Int1** is formed from the electronic reduction of CO_2 that occurs at the coordination to the initial U(III) complex (so-called coordination-induced reduction).[20] The first step of the mechanism involves the [2+2] cyclo-addition of a double bond from the O═CO$^{\bullet}$ radical anion to the U–$N(SiMe_3)_2$ bond, as it is shown in Fig. 2. The activation barrier for this process is found to be relatively small (14.8 kcal mol^{-1}). In particular, in the transition state the amide group that is involved in the insertion step is considerably far from the uranium center, at a non-bonding distance ($d_{U\text{–}N}$ = 3.63 Å). The nature of this late-transition state is most probably due to the directionality of the occupied molecular orbital of the nitrogen with respect to the electrophilic carbon of the carbon dioxide molecule. Moreover, the steric hindrance of the ligand environment may also play an important role in the non-bonding situation between the nitrogen and the uranium, providing a logical explanation for the outcome of this step. In particular, the IRC calculation did not converge into

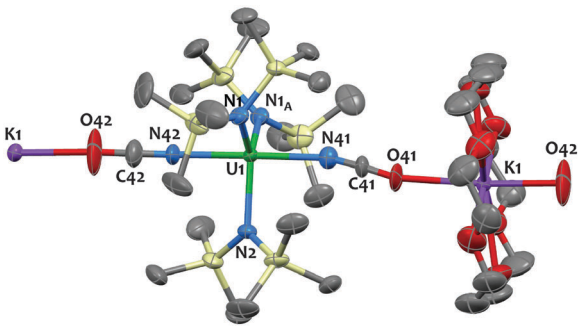

Fig. 1 Solid-state molecular structure of $[K(18c6)][U(N(SiMe_3)_2)_3(NCO)_2]_n$ **2** crystallized from THF/hexane. Hydrogen atoms and disorder are omitted for clarity. Uranium (green), potassium (purple), silicon (yellow), nitrogen (blue), oxygen (red) and carbon (grey) atoms are represented with 30% probability ellipsoids. Selected bond distances [Å] and angles [deg]: U1–N1 2.2679(2), U1–N2 2.2696(2), U1–O/N42 = 2.3358(1), U1–O/N41 = 2.3370(1), X42–C42–X′42 = 171.6(1), X41–C41–X′41 = 175.5(1).

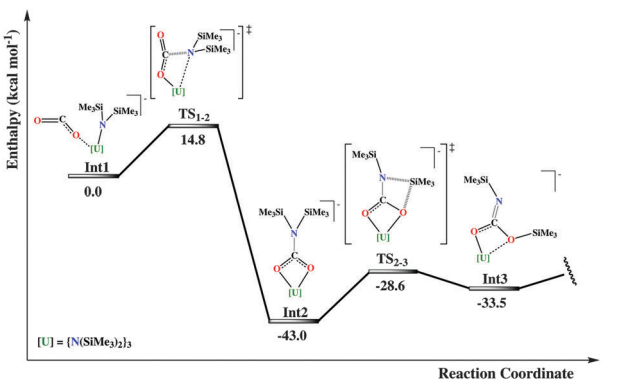

Fig. 2 Part of the energy profile that leads to the formation of the isocyanate complex **2**.

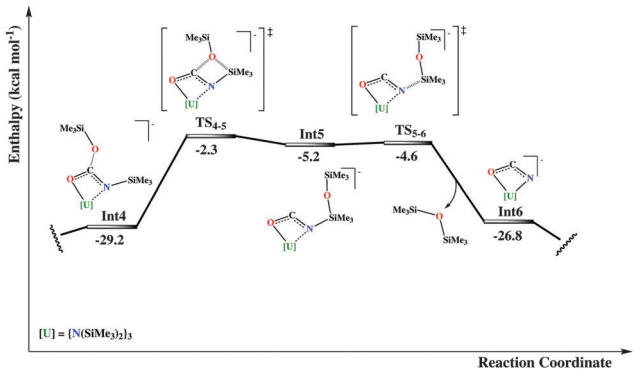

Fig. 3 Part of the energy profile that leads to the formation of the isocyanate complex **2**.

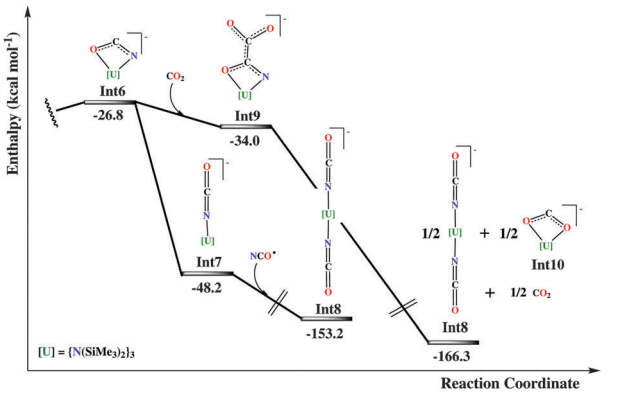

Fig. 4 Part of the energy profile that leads to the formation of the isocyanate complex **2**.

an O,N-bound carbamate intermediate, but instead into an O,O-bound one (**Int2**), with a subsequent significant drop in enthalpy energy (43.0 kcal mol^{-1} with respect to the CO_2 reduced adduct).

From the ligated dianionic O,O-bound carbamate the reaction can proceed through a sequence of two successive silyl migration steps (Fig. 2 and 3).

More specifically, the first step refers to the migration of the trimethylsilyl group from the nitrogen atom to one oxygen of the carbamate group, surmounting a moderate activation energy barrier of 14.4 kcal mol^{-1}. From the ensuing intermediate, **Int3**, rotation around the $O_{siloxide}$–C bond of the silyl group is required for the Si atom to approach the coordinated oxygen atom, for the second migration to occur. This isomerization is an almost thermo-neutral process, with enthalpy energy difference of only 4.3 kcal mol^{-1} in favor of **Int3**. The following migration of the silyl group is more energy demanding than the previous one, with an accessible activation energy barrier of 26.9 kcal mol^{-1} in terms of $\Delta H^{\ddagger}$.

In the following intermediate, **Int5**, a kind of cyanate fragment has been formed, now developing an η^2-N,O-type coordination with the uranium atom. This fragment can easily expel a siloxane molecule, which is observed experimentally, through an almost barrierless energy micro-step, *via* **TS$_{5-6}$**. The resulting intermediate, **Int6**, is formally described as an OCN^{2-} complex of U(IV). At this point, one can envision two different potential paths, the first corresponding to the isomerization of the cyanate group to give a terminal bonded isocyanate complex or to the nucleophilic attack by a second CO_2 molecule on the carbon atom of the OCN^{2-} moiety (Fig. 4). The first possibility results in an important stabilization energy of 21.4 kcal mol^{-1} with respect to the η^2-bound one. Then a putative free NCO radical (originating from a second uranium complex) can coordinate the vacant coordination site of **Int7**, on the axial position, *trans* to the other isocyanate, of the trigonal bipyramid. This can be done through two different coordination modes since OCN^- is an ambident ligand. Even though both correspond to highly exothermic processes (more than 100 kcal mol^{-1} stabilization energy), the N-bound intermediate, **Int8**, is more stable than the O-bound one, (see **Int8′** in the ESI†), by almost 10 kcal mol^{-1}. This observation suggests that most probably the two OCN groups in the X-ray structure of complex **2** are bound to the uranium through their nitrogen atoms while the oxygen atoms bind the potassium atoms of the K(18c6) cation.

Besides, since the experimental reactivity is found to be influenced by the number of CO_2 equivalents reacted with U(III), a second CO_2 molecule can undergo a nucleophilic attack at the carbon of the η^2-cyanate group in intermediate **Int6** (Fig. 4). This will result in the formation of an oxalate-like complex, **Int9**. Such reactivity is reminiscent of the oxalate formation in U(III) chemistry.[21] Two molecules of **Int9** can then disproportionate in order to give the bis-cyanate product **Int8** and a CO_2^{2-} complex (**Int10**). Also in this route, an important stabilization energy is found (almost 130 kcal mol^{-1}). Attempts to compute a reaction pathway involving the insertion of CO_2 into a U(III) species were not successful but showed that such a pathway is higher in energy.

In conclusion the bulky uranium(III) tetrasilylamido complex $[K(18c6)][U(N(SiMe_3)_2)_4]$ reacts with CO_2 to afford a rare example of a U(IV) isocyanate complex. DFT computational studies suggest that the reaction proceeds through carbon dioxide reduction followed by the [2+2] cyclo-addition of the carbonyl double bond of the reduced carbon dioxide to the U–$N(SiMe_3)_2$ bond and multiple silyl migration. The reactivity of this bulky "ate" complex differs from that reported for the neutral analogue $[U(N(SiMe_3)_2)_3]$[12a] highlighting the importance of the coordination environment for controlling the CO_2 conversion at the uranium center.

This work was supported by the CEA, the Swiss National Science Foundation, and by the EPFL. We thank O. Cooper for recording some analytical data. LM is member of the Institut Universitaire de France. Humboldt Foundation and Calmip are also acknowledged.

Notes and references

1 (*a*) P. L. Arnold, *Chem. Commun.*, 2011, **47**, 9005–9010; (*b*) O. P. Lam and K. Meyer, *Polyhedron*, 2012, **32**, 1–9; (*c*) H. S. La Pierre and K. Meyer, *Prog. Inorg. Chem.*, ed. K. D. Karlin, 2014, vol. 58, pp. 303–415; (*d*) S. T. Liddle, *Angew. Chem., Int. Ed.*, 2015, **54**, 8604–8641.
2 (*a*) A. R. Fox, S. C. Bart, K. Meyer and C. C. Cummins, *Nature*, 2008, **455**, 341–349; (*b*) M. S. Eisen, *C–X Bond Formation*, ed. A. Vigalok, 2010, vol. 31, pp. 157–184; (*c*) M. B. Jones and A. J. Gaunt, *Chem. Rev.*, 2013, **113**, 1137–1198.
3 (*a*) D. M. King and S. T. Liddle, *Coord. Chem. Rev.*, 2014, **266**, 2–15; (*b*) A. R. Fox, P. L. Arnold and C. C. Cummins, *J. Am. Chem. Soc.*, 2010, **132**, 3250–3251; (*c*) P. L. Diaconescu and C. C. Cummins,

J. Am. Chem. Soc., 2002, **124**, 7660–7661; (*d*) P. L. Diaconescu, *Acc. Chem. Res.*, 2010, **43**, 1352–1363; (*e*) B. M. Gardner and S. T. Liddle, *Chem. Commun.*, 2015, **51**, 10589–10607.

4 (*a*) R. A. Andersen, *Inorg. Chem.*, 1979, **18**, 1507–1509; (*b*) L. R. Avens, S. G. Bott, D. L. Clark, A. P. Sattelberger, J. G. Watkin and B. D. Zwick, *Inorg. Chem.*, 1994, **33**, 2248–2256.

5 (*a*) D. L. Clark, M. M. Miller and J. G. Watkin, *Inorg. Chem.*, 1993, **32**, 772–774; (*b*) C. J. Burns, D. L. Clark, R. J. Donohoe, P. B. Duval, B. L. Scott and C. D. Tait, *Inorg. Chem.*, 2000, **39**, 5464–5468; (*c*) H. Nakai, X. L. Hu, L. N. Zakharov, A. L. Rheingold and K. Meyer, *Inorg. Chem.*, 2004, **43**, 855–857; (*d*) S. Fortier, G. Wu and T. W. Hayton, *J. Am. Chem. Soc.*, 2010, **132**, 6888–6889; (*e*) S. Fortier, G. Wu and T. W. Hayton, *J. Chem. Soc., Dalton Trans.*, 2010, **39**, 352–354; (*f*) S. Fortier, N. Kaltsoyannis, G. Wu and T. W. Hayton, *J. Am. Chem. Soc.*, 2011, **133**, 14224–14227; (*g*) S. Fortier, J. R. Walensky, G. Wu and T. W. Hayton, *J. Am. Chem. Soc.*, 2011, **133**, 6894–6897; (*h*) S. Fortier, J. L. Brown, N. Kaltsoyannis, G. Wu and T. W. Hayton, *Inorg. Chem.*, 2012, **51**, 1625–1633; (*i*) A. J. Lewis, E. Nakamaru-Ogiso, J. M. Kikkawa, P. J. Carroll and E. J. Schelter, *Chem. Commun.*, 2012, **48**, 4977–4979; (*j*) A. J. Lewis, U. J. Williams, P. J. Carroll and E. J. Schelter, *Inorg. Chem.*, 2013, **52**, 7326–7328; (*k*) W. J. Evans, D. S. Lee, D. B. Rego, J. M. Perotti, S. A. Kozimor, E. K. Moore and J. W. Ziller, *J. Am. Chem. Soc.*, 2004, **126**, 14574–14582; (*l*) K. C. Mullane, A. J. Lewis, H. Yin, P. J. Carroll and E. J. Schelter, *Inorg. Chem.*, 2014, **53**, 9129–9139.

6 P. L. Arnold, S. M. Mansell, L. Maron and D. McKay, *Nat. Chem.*, 2012, **4**, 668–674.

7 P. L. Arnold, Z. R. Turner, R. M. Bellabarba and R. P. Tooze, *Chem. Sci.*, 2011, **2**, 77–79.

8 S. Fortier, G. Wu and T. W. Hayton, *J. Am. Chem. Soc.*, 2010, **132**, 6888–6889.

9 E. M. Matson, P. E. Fanwick and S. C. Bart, *Organometallics*, 2011, **30**, 5753–5762.

10 (*a*) K. W. Bagnall and E. Yanir, *J. Inorg. Nucl. Chem.*, 1974, **36**, 777–779; (*b*) P. J. Fagan, J. M. Manriquez, S. H. Vollmer, C. S. Day, V. W. Day and T. J. Marks, *J. Am. Chem. Soc.*, 1981, **103**, 2206–2220; (*c*) S. C. Bart, C. Anthon, F. W. Heinemann, E. Bill, N. M. Edelstein and K. Meyer, *J. Am. Chem. Soc.*, 2008, **130**, 12536–12546; (*d*) J. A. H. Frey, G. N. Cloke and S. M. Roe, *Organometallics*, 2015, **34**, 2102–2105.

11 (*a*) W. Sattler and G. Parkin, *J. Am. Chem. Soc.*, 2011, **133**, 9708–9711; (*b*) M. T. Whited, A. J. Kosanovich and D. E. Janzen, *Organometallics*, 2014, **33**, 1416–1422; (*c*) H. Phull, D. Alberti, I. Korobkov, S. Gambarotta and P. H. M. Budzelaar, *Angew. Chem., Int. Ed.*, 2006, **45**, 5331–5334; (*d*) L. R. Sita, J. R. Babcock and R. Xi, *J. Am. Chem. Soc.*, 1996, **118**, 10912–10913; (*e*) C. A. Stewart, D. A. Dickie, M. V. Parkes, J. A. Saria and R. A. Kemp, *Inorg. Chem.*, 2010, **49**, 11133–11141.

12 (*a*) S. M. Mansell, N. Kaltsoyannis and P. L. Arnold, *J. Am. Chem. Soc.*, 2011, **133**, 9036–9051; (*b*) P. L. Arnold, Z. R. Turner, A. I. Germeroth, I. J. Casely, G. S. Nichol, R. Bellabarba and R. P. Tooze, *J. Chem. Soc., Dalton Trans.*, 2013, **42**, 1333–1337.

13 P. A. Cleaves, D. M. King, C. E. Kefalidis, L. Maron, F. Tuna, E. J. L. McInnes, J. McMaster, W. Lewis, A. J. Blake and S. T. Liddle, *Angew. Chem., Int. Ed.*, 2014, **53**, 10412–10415.

14 I. Castro-Rodriguez and K. Meyer, *Chem. Commun.*, 2006, 1353–1368.

15 A. S. P. Frey, F. G. N. Cloke, M. P. Coles and P. B. Hitchcock, *Chem. – Eur. J.*, 2010, **16**, 9446–9448.

16 A. J. Lewis, U. J. Williams, P. J. Carroll and E. J. Schelter, *Inorg. Chem.*, 2013, **52**, 7326–7328.

17 L. C. J. Pereira, C. Camp, J. T. Coutinho, L. Chatelain, P. Maldivi, M. Almeida and M. Mazzanti, *Inorg. Chem.*, 2014, **53**, 11809–11811.

18 (*a*) M. J. Crawford, P. Mayer, H. Noth and M. Suter, *Inorg. Chem.*, 2004, **43**, 6860–6862; (*b*) I. Castro-Rodriguez, H. Nakai and K. Meyer, *Angew. Chem., Int. Ed.*, 2006, **45**, 2389–2392; (*c*) R. K. Thomson, B. L. Scott, D. E. Morris and J. L. Kiplinger, *C. R. Chim.*, 2010, **13**, 790–802; (*d*) C. Camp, N. Settineri, J. Lefevre, A. R. Jupp, J. M. Goicoechea, L. Maron and J. Arnold, *Chem. Sci.*, 2015, DOI: 10.1039/C5SC02150B.

19 I. Castro-Rodriguez, H. Nakai, L. N. Zakharov, A. L. Rheingold and K. Meyer, *Science*, 2004, **305**, 1757–1759.

20 (*a*) L. Castro, C. E. Kefalidis, D. McKay, S. Essafi, L. Perrin and L. Maron, *J. Chem. Soc., Dalton Trans.*, 2014, **43**, 12124–12134; (*b*) C. E. Kefalidis, L. Castro, A. Yahia, L. Perrin and L. Maron, *Computational Methods in Lanthanide and Actinide Chemistry*, John Wiley & Sons Ltd, Chichester, UK, 2015.

21 (*a*) A.-C. Schmidt, F. W. Heinemann, C. E. Kefalidis, L. Maron, P. W. Roesky and K. Meyer, *Chem. – Eur. J.*, 2014, **20**, 13501–13506; (*b*) N. Tsoureas, L. Castro, A. F. R. Kilpatrick, F. G. N. Cloke and L. Maron, *Chem. Sci.*, 2014, **5**, 3777–3788; (*c*) L. Castro, O. P. Lam, S. C. Bart, K. Meyer and L. Maron, *Organometallics*, 2010, **29**, 5504–5510.

Inorganic Chemistry

Article

pubs.acs.org/IC

Ferrocene-Based Tetradentate Schiff Bases as Supporting Ligands in Uranium Chemistry

Clément Camp,[†,§] Lucile Chatelain,[†,§,‡] Victor Mougel,[†,§] Jacques Pécaut,[†,§] and Marinella Mazzanti*[,‡]

[†]Univ. Grenoble Alpes, INAC-LCIB, RICC, and [§]CEA, INAC-LCIB F-38000 Grenoble, France

[‡]Institut des Sciences et Ingénierie Chimiques, Ecole Polytechnique Fédérale de Lausanne (EPFL), CH-1015 Lausanne, Switzerland

Supporting Information

ABSTRACT: Uranyl(VI), uranyl(V), and uranium(IV) complexes supported by ferrocene-based tetradentate Schiff-base ligands were synthesized, and their solid-state and solution structures were determined. The redox properties of all complexes were investigated by cyclic voltammetry. The bulky salfen-^{t}Bu$_2$ allows the preparation of a stable uranyl(V) complex, while a stable U(IV) bis-ligand complex is obtained from the salt metathesis reaction between $[UI_4(OEt_2)_2]$ and K_2salfen. The reduction of the $[U(salfen)_2]$ complex leads to an unprecedented intramolecular reductive coupling of the Schiff-base ligand resulting in a C−C bond between the two ferrocene-bound imino groups.

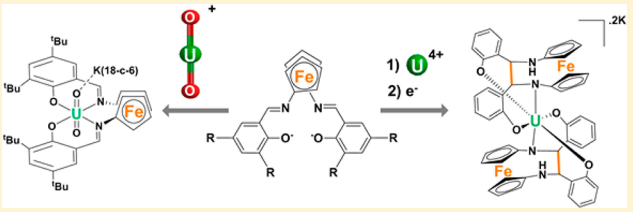

INTRODUCTION

Ligand design has played a crucial role in the recent advancements witnessed in uranium chemistry. Notably, the choice of the ancillary ligand is particularly crucial in the stabilization of highly reactive species and unusual oxidation states,[1,2] in promoting original reactivity[3,4] and implementing magnetic properties.[5,6]

Tetradentate ONNO Schiff-base ligands have extensively been used as supporting ligands in d-block chemistry because of their ability to stabilize metals in various oxidation states. Surprisingly, the use of Schiff bases as ancillary ligands in uranium chemistry remains limited for oxidation states lower than (VI).[7] Notably, only a very few examples of U(IV)[8] and U(III)[9,10] complexes of Schiff bases have been reported so far. Only in recent years, Schiff bases have been increasingly used as effective ligands for the stabilization of uranium in the elusive oxidation state of +V.[11] Our group has reported the synthesis of several stable mononuclear and polynuclear uranyl(V)[11c−g] complexes, which have proven to be attractive building blocks in the design of actinide-based molecular magnets.[6b,12] The structure and electronic properties of the Schiff-base ligand have proven crucial for the stabilization of uranyl(V) with respect to the disproportionation reaction to UO_2^{2+} and U(IV).[11b,d] In addition, our group has also shown that Schiff bases could be used to promote ligand-centered multielectron redox reactivity in U(IV) species.[8a,13] Notably the reduction of U(IV) salophen (salophen = *N*,*N*′-disalicylidene-*o*-phenylenediaminate) complexes promote C−C bond formation to afford dinuclear or mononuclear U(IV) amido complexes (Scheme 1) that can release up to four electrons to substrates through the oxidative cleavage of the C−C bond.

The redox properties of such ligand-centered redox-active U(IV) systems should be easily tuned by straightforward changes on the Schiff-base scaffold involving either the phenol substituents or the diimine bridging moiety.[14] In this context, ferrocene-based Schiff-base ligands such as salfen^{2-} (Figure 1) are an attractive class of redox-active ligands because they associate two different redox-active fragments on the same ligand (imino group and ferrocene). Notably, the capability of the ferrocene unit to participate in redox events might increase the reactivity possibilities of their complexes. Moreover, compared to the salophen platform, the length of the spacer fragment (1,1′-ferrocenyl vs 1,2-phenyl bridge) is increased, providing a larger ONNO cavity well-suited for uranium.

1,1′-disubstituted ferrocene-based ligands have proven versatile supporting ligands in the chemistry of group 3 elements and uranium due to the flexibility and redox-active

Scheme 1. Reductive Coupling of the Salophen Ligand in Uranium Chemistry

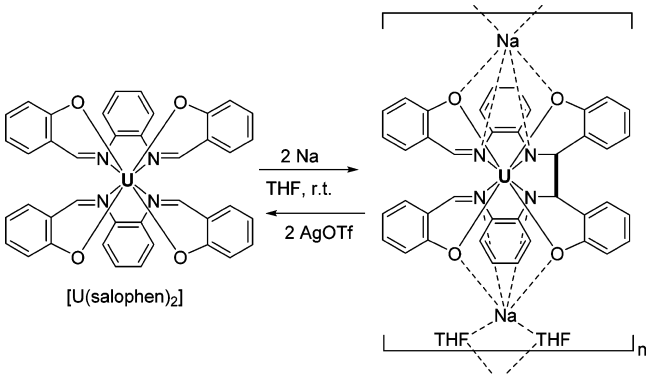

Received: February 27, 2015
Published: May 26, 2015

DOI: 10.1021/acs.inorgchem.5b00467
Inorg. Chem. 2015, 54, 5774−5783

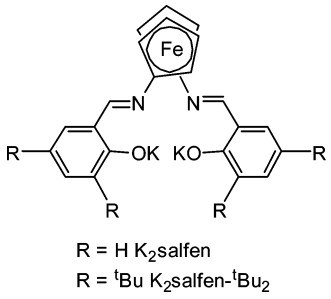

Figure 1. Representation of salfen ligands.

character of ferrocene, leading to effective catalysts, to novel reactivity, and to effective intermetallic electronic communication between iron and the metal center.[15,16] However, the coordination chemistry of the ferrocene-based Schiff-base salfen ligand remains practically unexplored with only three reports on the use of this Schiff-base ligand in combination with Mg(II),[17] Zr(IV),[17] Ti(IV),[17] Ce(III),[18] Ce(IV),[19] and Y-(III).[18,19] In view of the high steric and electronic flexibility of these ligands we set out to explore its ability to stabilize unusual uranium oxidation states and to support ligand-centered multielectron redox chemistry in uranium-containing compounds. Here we report the synthesis, characterization, and redox properties of salfen complexes of uranium in different oxidation states.

EXPERIMENTAL SECTION

General Considerations. Unless otherwise noted, all manipulations were performed at ambient temperature under an inert argon atmosphere using Schlenk techniques and an MBraun glovebox equipped with a purifier unit. The water and oxygen levels were always kept lower than 1 ppm. Glassware was dried overnight at 130 °C before use and dried in vacuo. ^{1}H NMR experiments were performed using NMR tubes adapted with J. Young valves. ^{1}H NMR spectra were recorded on Bruker 200 and 500 MHz and Varian Mercury 400 MHz spectrometers. NMR chemical shifts are reported in parts per million with solvent as internal reference. Elemental analyses were performed under argon by Analytische Laboratorien GMBH at Lindlar, Germany.

Starting Materials. Unless otherwise noted, reagents were purchased from commercial suppliers and used without further purification. The solvents were purchased from Aldrich or Eurisotop (deuterated solvents) in their anhydrous form, conditioned under argon and vacuum distilled from K/benzophenone (toluene, hexane, pyridine (Py), and tetrahydrofuran (THF)). All solid reagents were dried under high vacuum for 7 d prior to use. $[UO_2I_2(Py)_3]$,[1d] $\{[(UO_2(Py)_5)][(KI_2(Py)_2)]\}_n$,[1d11c] $[UI_4(OEt_2)_2]$,[20] and $[UI_3(THF)_4]$[21] were prepared according to the published procedures. The H_2salfen and H_2salfen-^{t}Bu$_2$ ligands and the K_2salfen and $[K(THF)]_2$(salfen-^{t}Bu$_2$) ligand salts were prepared according to the published procedures.[17,19]

Caution! *Depleted uranium (primary isotope ^{238}U) is a weak α-emitter (4.197 MeV) with a half-life of 4.47 × 10^9 years. Manipulations and reactions should be performed in monitored fume hoods or in an inert atmosphere glovebox in a radiation laboratory equipped with α-counting equipment.*

Synthesis of [UO$_2$(salfen-^{t}Bu$_2$)], 1. A red solution of $[UO_2I_2(Py)_3]$ (10.0 mg, 0.013 mmol, 1 equiv) in pyridine (0.5 mL) was added to a light red solution of K_2salfen-^{t}Bu$_2$.$(THF)_2$ (9.5 mg, 0.013 mmol, 1 equiv) in pyridine (0.5 mL), yielding, after 30 min of stirring, a dark red solution with an off-white precipitate. The off-white precipitate was removed by filtration. Slow diffusion of hexane (one week) into this solution afforded the desired compound as a red crystalline solid (11 mg, 0.011 mmol, 90% yield). ^{1}H NMR (200 MHz, Py-d_5, 298 K): δ = 10.12 (s, 2H), 8.10 (d, 2H), 7.70 (d, 2H), 4.76 (t, 4H), 4.63 (t, 4H), 2.03 (s, 18H), 1.41 (s, 18H). Electrospray ionization mass spectrometry (ESI-MS): m/z = 955.3 ($[UO_2$(salfen-^{t}Bu$_2$)]K$^+$). Anal. Calcd for $[UO_2$(salfen-^{t}Bu$_2$)]·0.15KI $C_{40}H_{50}FeN_2O_4UK_{0.15}I_{0.15}$: C, 51.02; H, 5.35; N, 2.98. Found: C, 50.99; H, 5.75; N, 3.09%.

Synthesis of [UO$_2$(salfen-^{t}Bu$_2$)(K18-c-6)], 2. A solution of K_2salfen-^{t}Bu$_2$·$(THF)_{0.31}$ (71.5 mg, 0.096 mmol, 1 equiv) in pyridine (2 mL) was added to an orange suspension of $\{[(UO_2(Py)_5)]$-$[KI_2(Py)_2]\}_n$ (106.9 mg, 0.096 mmol, 1 equiv) in pyridine (0.5 mL). A colorless solution of 18-c-6 (75.9 mg, 0.290 mmol, 3 equiv) in pyridine (2 mL) was then added to the reaction mixture resulting in a dark red solution. The solution was stirred 30 min at room temperature and concentrated to 1 mL. This solution was filtered, and hexane (6 mL) was added to the filtrate, resulting in the formation of a brown precipitate. The solid was recovered by filtration, washed with hexane (1 mL), and dried under vacuum to afford $[UO_2$(salfen-^{t}Bu)(K18-c-6)]·0.8hexane. (52.9 mg, 45% yield). Anal. Calcd for $[UO_2$(salfen-^{t}Bu)(K18-c-6)]·0.8hex $C_{56.8}H_{85.2}KFeN_2O_{10}U$: C, 52.92; H, 6.66; N, 2.17. Found: C, 52.89; H, 6.93; N, 2.34%. Orange single crystals of **2** suitable for X-ray diffraction were obtained after two weeks by recrystallization from toluene at room temperature. ^{1}H NMR of **2** (500 MHz, Py-d_5, 323 K): δ = 6.89 (s, 2H), 6.64 (s, 2H), 5.23 (s, 2H), 4.65 (s, 24H, 18-c-6), 4.27 (s, 4H), 1.09 (s, 4H), 0.77 (s, 18H), −3.41 (s, 18H). ESI-MS: m/z = 1522.2 ($[UO_2$(salfen-^{t}Bu$_2$)(K18-c-6)](K18-c-6)$^+$).

Reaction of K$_2$salfen with $\{[(UO_2(Py)_5)][KI_2(Py)_2]\}_n$. A solution of K_2salfen (10.0 mg, 0.018 mmol, 1 equiv) in pyridine (1 mL) was added to an orange suspension of $\{[(UO_2(Py)_5][KI_2(Py)_2]\}_n$ (20.2 mg, 0.018 mmol, 1 equiv) in pyridine (1 mL), resulting in a dark red solution. The solution was stirred over 15 min. Analysis of the crude reaction mixture by ^{1}H NMR revealed the presence of the signals of $[U(salfen)_2]$ and of $[UO_2(salfen)]$. Complete disproportionation was achieved in 12 h.

Synthesis of [U(salfen)$_2$], 3. A solution of K_2salfen (50.0 mg, 0.099 mmol, 2 equiv) in THF (4 mL) was added to a red solution of $[UI_4(OEt_2)_2]$ (44.1 mg, 0.049 mmol, 1 equiv) in THF (4 mL). The resulting red suspension was stirred for 12 h at room temperature before filtration. The resulting red filtrate was evaporated to dryness to give $[U(salfen)_2]$·0.2 KI as a red powder (40.8 mg, 0.037 mmol, 75% yield). Single crystals suitable for X-ray diffraction were obtained by slow diffusion of diisopropyl ether into a THF solution of $[U(salfen)_2]$. ^{1}H NMR (200 MHz, THF-d_8, 298 K): δ = 23.5 (s, 4H), 17.6 (t, 4H), 12.8 (d, 4H), 12.2 (t, 4H), 10.6 (s, 4H), 3.6 (s, 4H), −2.9 (s, 4H), −7.6 (s, 4H), −19.0 (s, 4H). ^{1}H NMR (200 MHz, py-d_5, 298 K): δ = 23.9 (s, 4H), 17.8 (t, 4H), 12.9 (d, 4H), 12.3 (t, 4H), 10.7 (s, 4H), 4.1 (s, 4H), −2.6 (s, 4H), −7.6 (s, 4H), −19.0 (s, 4H). Anal. Calcd for $[U(salfen)_2]$·0.2(KI) $C_{48}H_{36}Fe_2N_4O_4UK_{0.2}I_{0.2}$: C, 51.67; H, 3.25; N, 5.02. Found: C, 51.70; H, 3.48; N, 4.96%.

Reaction of K$_2$salfen with [UI$_3$(THF)$_4$]. A solution of K_2salfen (7.5 mg, 0.010 mmol, 1 equiv) in THF-d_8 (0.5 mL) was added to a blue solution of $[UI_3(THF)_4]$ (5.0 mg; 0.010 mmol, 1 equiv) in THF-d_8 (0.5 mL). The resulting brown suspension was stirred for 1 h at room temperature, and the solids were removed by filtration. The ^{1}H NMR spectrum of this solution shows that $[U(salfen)_2]$ is obtained as the unique salfen-containing species.

Reduction of [U(salfen)$_2$]. A solution of K_2salfen (50.0 mg, 0.099 mmol, 2 equiv) in THF (4 mL) was added to a red solution of $[UI_4(OEt_2)_2]$ (44.1 mg, 0.049 mmol, 1 equiv) in THF (4 mL). The resulting red suspension was stirred for 30 min at room temperature. To the resulting red-orange suspension was added KC_8 (26.5 mg, 0.196 mmol, 4.0 equiv), and the mixture was stirred at room temperature for 2 h. This afforded a dark brown suspension. The solid residues were removed by centrifugation. The ^{1}H NMR spectrum of the supernatant showed the formation of mixture of K_3[U(bis-salfen)(Hbis-salfen)] **4-H** and K_2[U(Hbis-salfen)$_2$] **4-H$_2$**. Attempts to separate the two species by crystallization were unsuccessful. While the reduction gives reproducibly a mixture of the **4-H** and **4-H$_2$**, the isolation of each of these species in analytically pure form was not possible.

A few single crystals of **4-H** suitable for X-ray diffraction were grown by slow diffusion of diisopropyl ether into this solution. While

DOI: 10.1021/acs.inorgchem.5b00467
Inorg. Chem. 2015, 54, 5774−5783

the quality of the structure is not sufficient for a discussion of the metrical parameters, the connectivity clearly shows the presence of a complex of formula K_3[U(bis-salfen)(Hbis-salfen)] ; space group $P2_1/a$; a = 20.5937(13) Å, b = 31.3962(15) Å, c = 25.6297(12) Å, $\alpha = \beta = 90°$, γ = 108.864(6)°.

Spectroscopic data performed on isolated crystals of K_3[U(bis-salfen)(Hbis-salfen)] **4-H**: ESI-MS: m/z = 1201.0 $[M + H]^+$. ^{1}H NMR (200 MHz, THF-d_8, 298 K): δ = 36.4 (d, 1H), 32.3 (d, 1H), 30.5 (d, 1H), 27.5 (d, 1H), 21.0 (t, 1H), 17.3 (d, 1H), 16.2 (d, 1H), 15.7 (d, 1H), 13.6 (d, 1H), 12.1 (s, 1H), 10.4 (s, 1H), 10.1 (s, 1H), 9.6 (t, 1H), 9.3 (t, 1H), 9.1 (t, 1H), 9.0 (t, 1H), 7.0 (t, 1H), 6.8 (t, 1H), 6.4 (t, 1H), 6.1 (t, 1H), 4.5 (s, 1H), 3.4 (s, 1H), 3.3 (s, 1H), 2.5 (s, 1H), 2.1 (s, 1H), 2.0 (d, 1H), 1.5 (s, 1H), 0.4 (s, 1H), 0.3 (d, 1H), −1.5 (d, 1H), −1.7 (s, 1H), −2.6 (s, 1H), −3.0 (s, 1H), −23.2 (s, 1H), −26.6 (s, 1H), −27.5 (s, 1H).

Spectroscopic data for K_2[(Hbis-salfen)$_2$] **4-H$_2$** obtained from a reaction mixture after partial separation: ^{1}H NMR (200 MHz, THF-d_8, 298 K): δ = 19.7 (d, 2H), 13.5 (t, 2H), 13.0 (d, 2H), 11.7 (t, 2H), 10.4 (t, 2H), 9.6 (t, 2H), 9.2 (d, 2H), 8.0 (d, 2H), −2.7 (s, 2H), −3.1 (s, 2H), −3.3 (s, 2H), −5.3 (s, 2H), −6.1 (s, 2H), −6.9 (s, 2H), −12.0 (s, 2H), −13.1 (s, 2H), −16.8 (s, 2H), −19.1 (brs, 2H).

Single crystals of [(K18-c-6)$_2$U(bis-salfen)(Hbis-salfen)]$_2$(K18-c-6)$_2$·7thf, **5**, suitable for X-ray diffraction were grown by slow diffusion of diisopropyl ether into the THF reaction mixture in the presence of 18-c-6.

Single crystals of [K(dibenzo18-c-6)(py)]$_2$[U(Hbis-salfen)$_2$]·py$_5$, **6** suitable for X-ray diffraction were grown by slow diffusion of hexane into a pyridine solution of the complex reaction mixture in the presence of excess dibenzo18-c-6.

Oxidation of 4H and 4H$_2$. A red solution of [U(salfen)$_2$] **3** (6.0 mg, 0.006 mmol, 1 equiv) in THF-d_8 (0.7 mL) was added to solid KC_8 (3 mg, 0.022 mmol, 4.0 equiv) at room temperature. To the resulting dark brown suspension of a mixture of K_3[U(bis-salfen)(Hbis-salfen)] **4-H** and K_2[U(Hbis-salfen)$_2$] **4-H$_2$** was added solid AgOTf (5.7 mg, 0.022 mmol, 4.0. equiv) affording a red solution and a black solid. ^{1}H NMR spectra were recorded at each step, and integrals were compared to an internal reference (toluene). The addition of 4 equiv of AgOTf allows a complete conversion of the mixture of reduced species into the initial [U(salfen)$_2$] complex.

Electrochemical Methods. Cyclic voltammetry experiments were performed at room temperature in an argon-filled glovebox described above. Data were collected using a Biologic SP-300 potentiostat. All samples were 2−6 mM in complex with 0.1 M $[Bu_4N][PF_6]$ supporting electrolyte in pyridine solution. The experiments were performed with a platinum disk (d = 5 mm) working electrode, a platinum wire counter electrode, and a Ag/AgCl reference electrode. The experiments were repeated on independently synthesized samples to assess the reproducibility of the measurement. Potential calibration was performed at the end of each data collection cycle using the ferrocene/ferrocenium $[(C_5H_5)_2Fe]^{+/0}$ couple as an internal standard.

Magnetic Methods. Static magnetic properties were measured using a Quantum Design SQUID MPMS-XL 5.0 susceptometer. Ultra-Low Field Capability (0.05 G for the 5 T magnets. Continuous Low Temperature Control/Temperature Sweep Mode (CLTC) − Sweep rate: 0.001−10 K/min. The samples were pressed under argon and blocked from torquing using eicosane into a 5 mm Suprasil-Quartz tube, which was then sealed under vacuum. Contribution to the magnetization from the empty Suprasil-Quartz tube was measured independently and subtracted from the total measured signal. Diamagnetic corrections were made using Pascal's constants.

X-ray Crystallography. Diffraction data were taken using an Oxford-Diffraction XCallibur S kappa geometry diffractometer (Mo Kα radiation, graphite monochromator, λ = 0.710 73 Å). To prevent evaporation of cocrystallized solvent molecules the crystals were coated with light hydrocarbon oil, and the data were collected at 150 K. The cell parameters were obtained with intensities detected on three batches of five frames. The crystal-detector distance was 4.5 cm. The number of settings and frames has been established taking in consideration the Laue symmetry of the cell by CrysAlisPro Oxford-diffraction software.[22] 225 for **1**, 491 for **2**, 964 for **3**, 500 for **5**, and 1009 for **6** narrow data were collected for 1° increments in ω with a 40 s exposure time for **1**, 180 s for **2**, 10 s for **3**, 1 s for **5**, and 4 s for **6**. Unique intensities detected on all frames using the Oxford-diffraction Red program were used to refine the values of the cell parameters. The substantial redundancy in data allows empirical absorption corrections to be applied using the ABSPACK Oxford-diffraction program[22] for **1** and **6**, and analytical absorption correction for **2**, **3**, and **5**. Space groups were determined from systematic absences, and they were confirmed by the successful solution of the structure. The structures were solved by direct methods using the SHELXTL 6.14 package or by charge flipping method using superflip. All non-hydrogen atoms were found by difference Fourier syntheses and refined on F^2. For **3** hydrogen atoms were found by Fourier syntheses except for interstitial solvent H atoms, which were fixed in ideal position. For **1**, **2**, **5**, and **6** hydrogen atoms were fixed in ideal position. Full crystallographic details are given in Supporting Information, Table S.1.

RESULTS AND DISCUSSION

Uranyl Complexes. The uranyl (VI) complex [UO_2(salfen-^{t}Bu$_2$)], **1**, was prepared from the salt metathesis reaction between K_2salfen-^{t}Bu$_2$ and [UO_2I_2(Py)$_3$][1d] in pyridine (Scheme 2). The ^{1}H NMR spectrum recorded for a pyridine

Scheme 2. Synthesis of the Uranyl Complexes [UO_2(salfen-^{t}Bu$_2$)] 1 and [UO_2(salfen-^{t}Bu$_2$)(K18-c-6)] 2

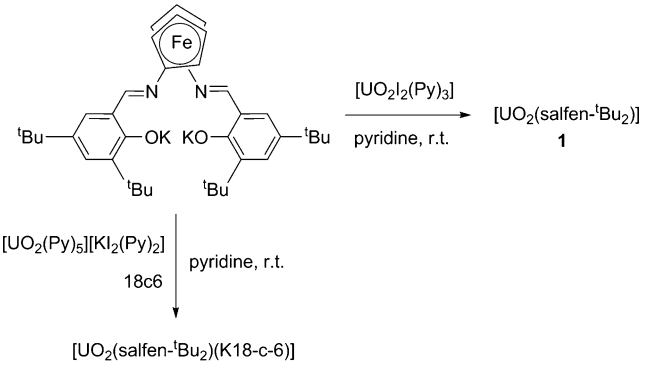

solution of **1** features seven resonances in the diamagnetic region, as expected for a symmetric f^0 uranyl(VI) compound with one low-spin Fe(II) center.

The reaction of the uranyl(V) precursor {[(UO_2(Py)$_5$)]-[KI_2(Py)$_2$]}$_n$[1d] with K_2salfen-^{t}Bu$_2$ in pyridine led to the formation of a stable uranyl(V) complex as suggested by the paramagnetically shifted ^{1}H NMR spectrum, which displays a single set of seven resonances between 6.83 ppm and −3.87 ppm in pyridine (Supporting Information, Figure S.5). The stable uranyl(V) complex [UO_2(salfen-^{t}Bu$_2$)(K18-c-6)], **2**, is isolated in the presence of 18-c-6 (Scheme 2). The proton NMR spectrum recorded for a pyridine solution of **2** (Supporting Information, Figure S.7) shows seven paramagnetically shifted signals for the salfen-^{t}Bu$_2$ ligand, in agreement with the presence of a uranyl(V) C_{2v} symmetric complex. ^{1}H NMR studies show that complex **2** is highly stable with respect to the disproportionation for at least 20 d in pyridine solution (see Supporting Information).

Note that the reaction of the uranyl(V) precursor {[(UO_2(Py)$_5$)][KI_2(Py)$_2$]}$_n$[1d] with K_2salfen in pyridine leads, after formation of a transient uranyl(V) species, to disproportionation of uranyl(V) resulting in the formation of a mixture of U(IV) and UO_2^{2+} species from which we identified the presence of the [U(salfen)$_2$] and [UO_2(salfen)] complexes

DOI: 10.1021/acs.inorgchem.5b00467
Inorg. Chem. 2015, 54, 5774−5783

(Supporting Information, Figure S.4). The disproportionation is complete after 12 h.

This highlights the important role of the steric hindrance provided by the bulky *tert*-butyl groups on the phenol arms in preventing the disproportionation of uranyl(V) in the $[UO_2(salfen\text{-}^tBu_2)(K18\text{-}c\text{-}6)]$ complex. The disproportionation of uranyl(V) is believed to occur through the formation of UO_2^+–UO_2^+ cation–cation dimeric species. The presence of bulky groups probably prevents the formation of such dimeric cation–cation intermediates by hindering the coordination to the uranium center of the uranyl(V) oxo group. Similar behavior was previously observed with tetradentate Schiff-base salophen and aminophenolate supporting ligands.[11c,23]

The solid-state crystal structures of complexes **1** and **2** were determined by X-ray diffraction studies and are presented in Figures 2 and 3, respectively. The crystal structure of **2** shows

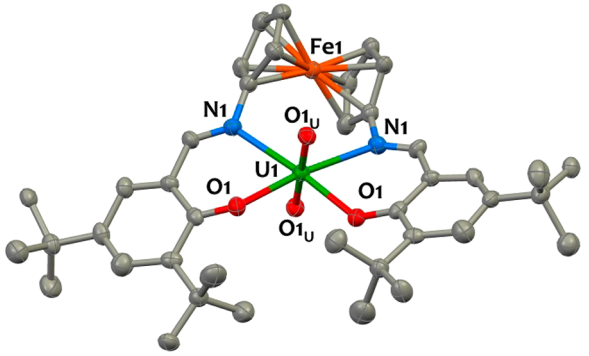

Figure 2. Solid-state molecular structure of $[UO_2(salfen\text{-}^tBu_2)]$ **1**. Hydrogen atoms and solvent molecules are omitted for clarity. Uranium (green), iron (orange), nitrogen (blue), oxygen (red), and carbon (gray) atoms are represented with 50% probability ellipsoids.

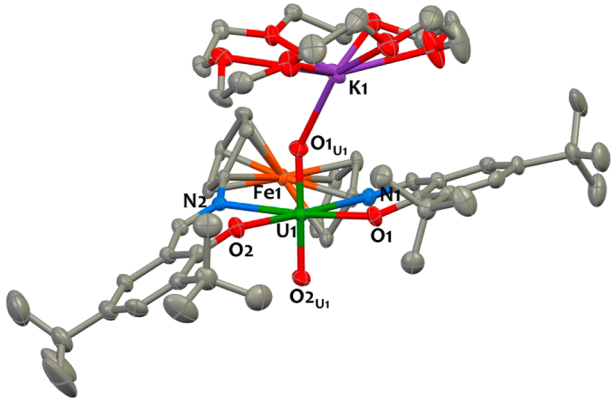

Figure 3. Solid-state molecular structure of the complex $[U_1O_2(salfen\text{-}^tBu_2)(K18\text{-}c\text{-}6)]$ in **2**. Hydrogen atoms and solvent molecules are omitted for clarity. Uranium (green), iron (orange), nitrogen (blue), potassium (purple), oxygen (red), and carbon (gray) atoms are represented with 50% probability ellipsoids.

the presence of two independent uranium complexes **U1** and **U2** in the asymmetric unit. Selected bond distances for **1** and **2** are given in Supporting Information, Table S.2. The coordination environment around the uranium center is similar in the two complexes. In compounds **1** and **2**, the uranium atoms are hexacoordinated in a tetragonal bipyramidal coordination geometry. The four donor atoms of the salfen-^{t}Bu$_2$ ligand (two oxygen and two nitrogen atoms) occupy the equatorial plane of the uranium ion (mean deviation from the plane of 0.04 Å in **1** and **U1**, of 0.06 Å in **U2**). The axial positions in **1** are occupied by two oxo ligands with U=O distances ranging between 1.831(4) and 1.864(4) Å and significantly longer than those found in the uranyl(VI) complex **1** (1.778(3) Å). These distances are in the range of those found in previously reported complexes of uranyl(V).[1d–f,11c,24] In the complexes **U1** and **U2** the $[K(18\text{-}c\text{-}6)]^+$ countercation binds one oxo group of the uranyl group through cation–cation interaction.[25] The K–O(1U1) distance (2.568(4) Å) is 0.2 Å smaller than K–O(1U2) (2.792(4) Å). This difference is probably because in **U2** the potassium ion interacts also with a phenolate oxygen (K–O = 2.941(4) Å) and an imino nitrogen (3.327(5) Å) from the Schiff base. The value of the distance between the uranium and iron atoms in complex **1** (3.708(1) Å) is smaller than the ones in **2** (mean distance 3.876(1) Å). This is the result of the presence of a stronger interaction of the ligand with the UO_2^{2+} cation resulting in shorter metal–ligand distances; notably, all the distances between the uranium ion and the ligand donor atoms in the equatorial plane are smaller by 0.1 Å in the uranyl(VI) complex compared to the uranyl(V) one (mean distances: U–O 2.221(3) Å, U–N 2.460(3) Å in **1** and U–O 2.31(1) Å, U–N 2.54(1) Å in **2**).

The above results show that the ferrocene-based salfen-^{t}Bu$_2$ ligand leads to stable complexes of uranyl(VI) and uranyl(V). We then become interested in studying the ability of these ligands to support uranium in lower oxidation states. In particular we have explored the possibility of obtaining homoleptic bis-ligand complexes of U(IV) with the objective of investigating the uranium-mediated communication between the two iron centers.[16b]

Tetravalent Uranium Salfen Complex. To favor the formation of a homoleptic bis-ligand complex of U(IV) the nonsubstituted salfen ligand was chosen to minimize steric hindrance. The salt metathesis reaction between $[UI_4(OEt_2)_2]$ and 2 equiv of the potassium salt of the tetradentate Schiff-base ligand K_2salfen in THF affords the homoleptic U(IV) complex $[U(salfen)_2]$ **3** in 75% yield (Scheme 3). The ^{1}H NMR spectra

Scheme 3. Synthesis of $[U(salfen)_2]$ 3

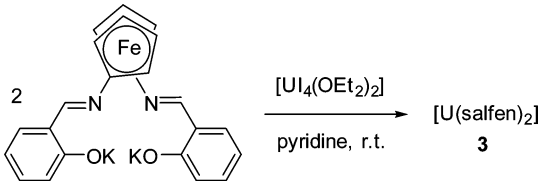

recorded for **3** in deuterated THF or pyridine show the presence of a single set of nine sharp resonances in agreement with the presence of a D_{2h} symmetric solution species.

Single crystals of **3** suitable for X-ray diffraction studies were grown by slow diffusion of diisopropyl ether into a THF solution of **3**. The solid-state structure of **3** is represented in Figure 4. The complex crystallizes in the monoclinic $P2_1/n$ space group. The uranium cation is encapsulated between two overlapping salfen ligands that provide a N_4O_4 coordination sphere around the metal. The resulting coordinating polyhedron around uranium is best described as a distorted square antiprism with N1–O1–N31–O31 and N2–O2–N32–O32 defining the square bases of the polyhedron. In the structures of the previously reported heteroleptic monoligand complexes $[Ce(salfen\text{-}^tBu_2)(O^tBu)_2]$[19] and $[Zr(salfen\text{-}^tBu_2)(CH_2Ph)_2]$,[17]

DOI: 10.1021/acs.inorgchem.5b00467
Inorg. Chem. 2015, 54, 5774–5783

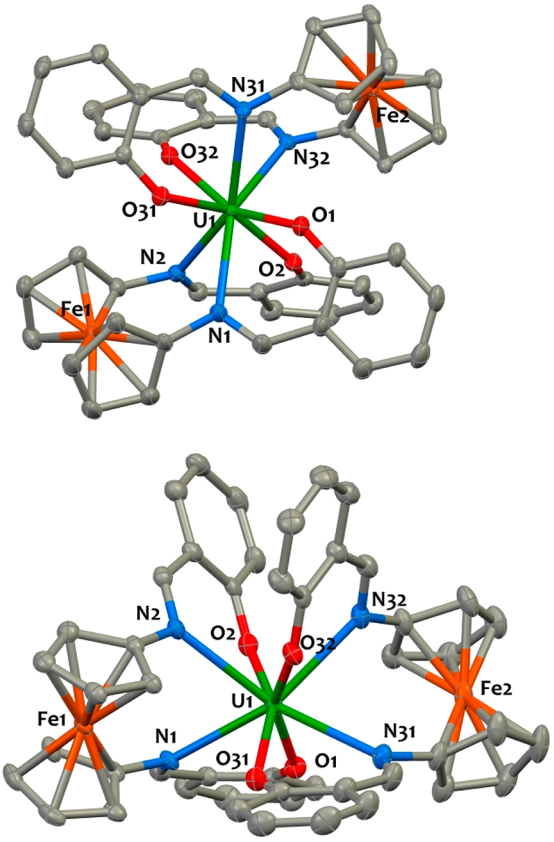

Figure 4. Two different views of the solid-state molecular structure of $[U(salfen)_2]$, **3**. Hydrogen atoms and solvent molecules are omitted for clarity. Uranium (green), iron (orange), nitrogen (blue), oxygen (red), and carbon (gray) atoms are represented with 50% probability ellipsoids. Selected metrical parameters are reported in Table 1.

as well as in **1** and **2**, the salfen ligand adopts a planar geometry. In contrast, in **3** the two N,O coordinating arms of the ligand are strongly twisted with respect to each other with an average angle of 73.7(7)° between the phenolate planes from the same ligand. This arrangement differs significantly from that found in the sandwich structure of the bis-ligand complex $[U(salophen)_2]$,[8a] highlighting the higher flexibility of the ferrocene Schiff base. The $U-O_{avg}$ 2.231(9) Å and $U-N_{avg}$ 2.664(7) Å bond distances are comparable to the ones in $[U(salophen)_2]$[8a] and fall in the range of those found in related uranium(IV) complexes.[13,26]

The two ferrocene units of the ligands are almost perpendicular, as indicated by the 71.3° value for the torsion angle between the Cp centroids and the irons in **3**. Both ferrocene moieties adopt roughly eclipsed conformations, with values of the N1−C1−C6−N2 and N31−C31−C36−N32 dihedral angles of 16.3(3)° and 15.7(2)°, respectively. The mean Fe−C distances 2.041(7) Å are close to those found in ferrocene.[27] The U···Fe separations (U1···Fe1 = 4.3087(5) Å ; U1···Fe2 = 4.3237(4) Å) have similar values for both ferrocene ligands. These values are longer than the ones (3.32 and 2.961 Å) respectively observed in the solid-state molecular structure of the related bis-diamidoferrocene complexes $[U(fc[NSiMe_3]_2)_2]$[28] and $[U(fc[NSi(t\text{-}Bu)Me_2]_2)_2][BPh_4]$.[16b] This is the result of the presence in the salfen ligand of imino groups with longer U−N distances, compared to the U−N distances in the diamidoferrocene complexes, which maintain the uranium further apart from the ferrocene.

Magnetic Data. The observed diamagnetism of compound **1** ($\chi = -4.62.10^{-3}$ emu·mol^{-1} at 300 K) is in agreement with the presence of a low-spin Fe(II) and a diamagnetic UO_2^{2+}. Temperature-dependent magnetic data for **2** and **3** were collected in the temperature range of 2−300 K. At 300 K, **2** displays an effective magnetic moment of 2.09 μ_B (Figure 5),

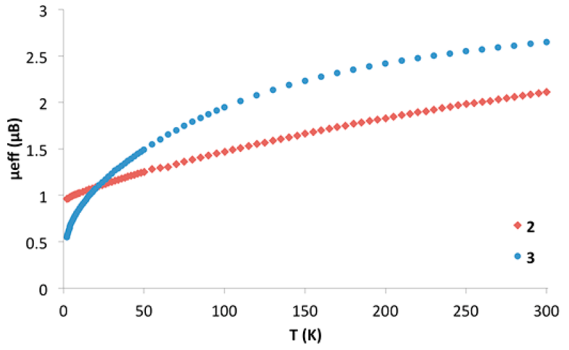

Figure 5. Temperature-dependent effective magnetic moment for **2** (red trace) and **3** (blue trace) recorded under 500 G in the range of 2−300 K. A μ_{eff} of 2.09 μ_B at 300 K was calculated for **2** ($\chi_{dia} = -7.44 \times 10^{-4}$ emu·mol^{-1}, m = 19.3 mg, Mw = 1291.4 g·mol^{-1}). A μ_{eff} of 2.64 μ_B at 300 K was calculated for **3** ($\chi_{dia} = -4.53 \times 10^{-4}$ emu·mol^{-1}, m = 24 mg, Mw = 1078.93 g·mol^{-1}).

which is in agreement with the presence of low-spin Fe(II) and U(V) ions. The magnetic moment of the U(V) ion is lower than the theoretical value calculated for the free $5f^1$ ion in the L−S coupling scheme (μ_{eff} = 2.54 μ_B), but within the range of values reported for U^V compounds (1.42−2.57 μ_B).[29] The magnetic moment for **2** decreases with decreasing temperature and reaches 0.96 μ_B at 2 K, a behavior typically found in mononuclear uranyl(V) complexes.[11c]

In comparison, complex **3** exhibits a magnetic moment at 300 K of 2.64 μ_B, which falls in the typical range of values recorded for U(IV) complexes.[29] At low temperatures, the magnetic moment for **3** decreases drastically and tends to zero at 0 K, a behavior consistent with a singlet ground state as typically found for the f^2 uranium(IV) ion. A similar behavior had been reported for the U(IV) bis(1,1′-diamidoferrocene) complex $[U(fc[NSi(t\text{-}Bu)Me_2]_2)_2]$.[16b]

Redox Properties of Complexes 2 and 3. Complexes **2** and **3** possess three different types of redox-active centers: the uranium cation, the Fe(II) centers of the ferrocene units, and the imino moieties of the supporting ligand. To get more insight into the redox properties of these heterometallic complexes, cyclovoltammetric studies were performed. The measurements were performed on 2 mM pyridine solutions of complexes using $[Bu_4N][PF_6]$ as supporting electrolyte. The pyridine was used as solvent because of the instability of the uranyl(V) complex in THF. All redox potentials are referenced against the $[(C_5H_5)_2Fe]^{+/0}$ redox couple. The cyclovoltammetric study of K_2salfen-^{t}Bu$_2$ ligand show the presence of a redox event at $E_{1/2}$ = 0.24 V assigned to the Fe(II)/Fe(III) couple in the ferrocene spacer. This value compares well with the value measured for the H_2salfen-^{t}Bu$_2$ ligand in thf (0.29 V).[18]

Compound **2** exhibits a reversible event at $E_{1/2}$ = −1.61 V (Figure 6), which corresponds to a U(VI)/U(V) couple. The same reversible wave is observed in the voltammogram of **1** recorded using the same conditions. The value of the measured redox potential is very similar to that reported for

DOI: 10.1021/acs.inorgchem.5b00467
Inorg. Chem. 2015, 54, 5774−5783

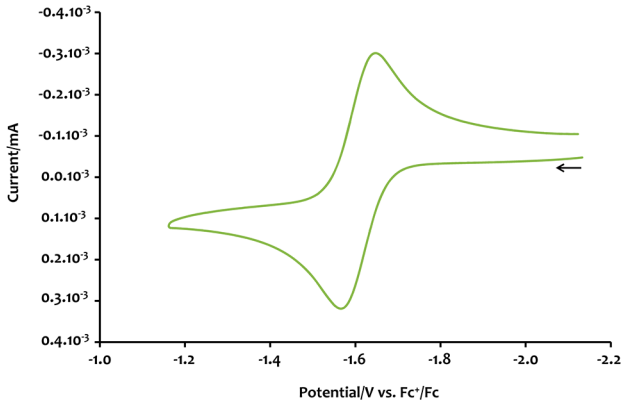

Figure 6. Room-temperature cyclic voltammogram for $[UO_2(salfen\text{-}^tBu_2)(K18\text{-}c\text{-}6)]$ **2** recorded in 0.1 M $[Bu_4N][PF_6]$ in 2 mM pyridine solution at 100 mV/s scan rate, Cp_2Fe/Cp_2Fe^+ corrected.

$[UO_2(salophen\text{-}^tBu_2)(Py)K]$,[11c] indicating that the degree of stabilization of the uranyl(V) cation is similar in both systems. Additionally, an irreversible oxidation wave is observed around 0.57 V with a shoulder at 0.34 V that can reasonably be assigned to the oxidation of the ligand ferrocene moiety. The high intensity of wave at 0.57 V suggests that further oxidation events might occur at this potential that might be assigned to the formation of ligand phenoxy radicals.

Complex **3** shows an irreversible reduction wave at E_{pc} = −2.49 V (Figure 7). This process is associated with several

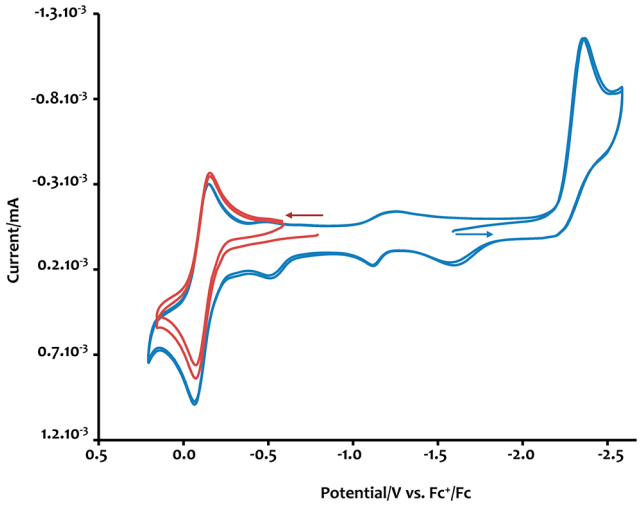

Figure 7. Room-temperature cyclic voltammograms for $[U(salfen)_2]$ **3** recorded in 0.1 M $[Bu_4N][PF_6]$ in 2 mM pyridine solution at 100 mV/s scan rate, Cp_2Fe/Cp_2Fe^+ corrected. The red trace corresponds to the voltammogram swept initially from −0.9 V to the positive direction, and the blue trace corresponds to the voltammogram swept initially from −1.5 V to the negative direction.

irreversible oxidation waves of lower intensity at E_{pa} = −1.54, −1.10, and −0.55 V, which are not observed when the voltammogram is swept initially from −2.0 V to the positive direction (Supporting Information, Figure S.23). On the basis of previous studies of the redox chemistry of f-elements bis-salophen complexes,[13,14b] this electrochemical signature is evocative of a reduction/oxidation feature involving the Schiff-base ligand, even if a U(IV)/U(III) process could also occur in this potential window.[16a] This process remains irreversible at higher scan-rate (5000 mV/s), suggesting that the electrochemically generated reduced species has a very short lifetime and undergoes rapid rearrangement/reaction. The multiple irreversible reoxidation waves indicate the formation of several products, which is in agreement with what is observed when the chemical reduction of **3** is performed (vide infra).

We also considered the electrochemical oxidation of $[U(salfen)_2]$, **3**. The cyclic voltammogram displays a reversible feature centered at $E_{1/2}$ = −0.14 V that is assigned to the Fe(II)/Fe(III) couple of the ferrocene moieties. Indeed, this potential is close to that of ferrocene and lies in between the values measured for the Fe^{2+}/Fe^{3+} oxidation in the monoligand complexes $[Ln(^{tBu}salfen)(O^tBu)(X)]$ ({Ln, X} = {Y, THF}: $E_{1/2}$ = 0.09 V; {Ln, X} = {Ce, O^{t}Bu}, $E_{1/2}$ = −0.28).[18] This indicates that the two chemically equivalent ferrocenes from the two Schiff-base ligands are oxidized at the same potential. Therefore, it is reasonable to assume that no iron−iron communication is occurring in **3**, which is consistent with the large U···Fe separation observed in the solid-state structure. Notably, systems in which an electronic communication occurs between two ferrocene units generally display two clearly distinct one-electron reversible waves.[16b,18,30]

Ligand-Centered Reduction. The ability of the salfen ligand to support uranium in a reduced form was also explored. The addition of 1 equiv of K_2salfen to a THF solution of $[UI_3(THF)_4]$ resulted in a rapid color change from deep blue to brown accompanied by the formation of KI precipitate. Analysis of the crude reaction mixture by ^{1}H NMR showed the formation of $[U(salfen)_2]$ **3** as the only salfen-containing species (Scheme 4).

Scheme 4. Reaction of $[UI_3(THF)_4]$ with K_2salfen

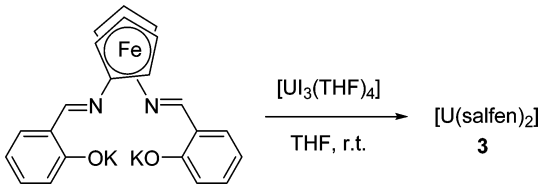

The uranium(IV) complex $[U(salfen)_2]$ is presumably formed by a disproportionation process yielding some form of U(0) that is removed by filtration. A similar behavior has been previously reported for various ligands when reacted with $[UI_3(THF)_4]$,[16c,26,31] including for the related bis(1,1′-diamidoferrocene) ligand $[K_2(OEt_2)_2]$fc[NSi-(*t*-Bu)Me$_2$]$_2$.[16b]

Overall, salt metathesis reactions of uranium iodides with salfen potassium salts underline that the salfen scaffold is able to stabilize and saturate the coordination sphere of a U(IV) ion but does not allow the synthesis of stable uranium(III) complexes.

Since previous studies on the related Schiff-base complex $[U(salophen)_2]$ have shown that further reduction of this complex was possible leading to the reduction of the imino group (Scheme 1), we decided to investigate the chemical reduction of compound **3**.

The reaction of **3** with 4 equiv of KC_8 per uranium atom in THF resulted in a color change of the solution from orange to dark brown. Analysis of the crude mixture by ^{1}H NMR revealed that a mixture of compounds was reproducibly obtained. The ^{1}H NMR spectrum recorded in deuterated THF for the crude reaction mixture displays a series of sharp resonances

DOI: 10.1021/acs.inorgchem.5b00467
Inorg. Chem. 2015, 54, 5774−5783

Scheme 5. Reduction of $[U(salfen)_2]$ 3

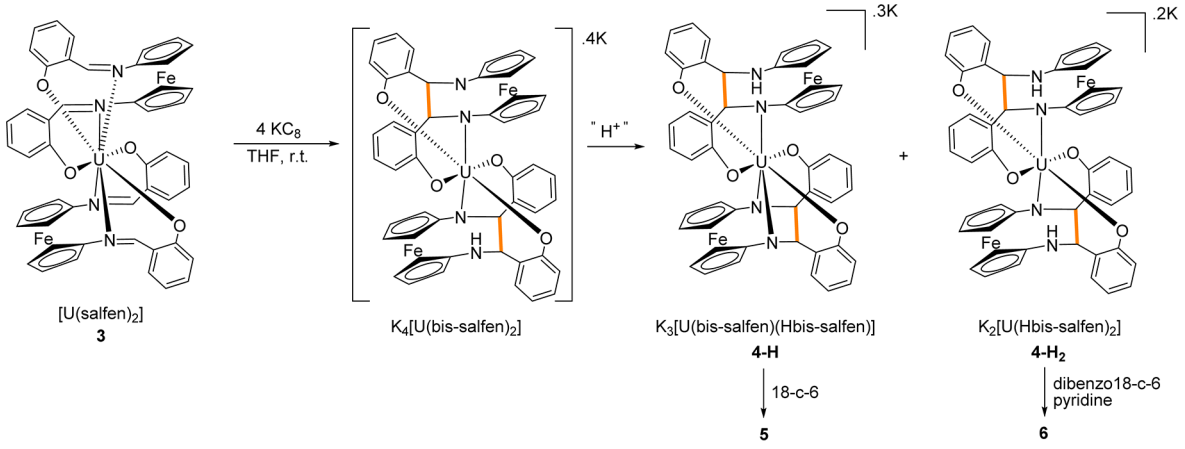

paramagnetically shifted in the +40 to −30 ppm range characteristic of U(IV) complexes.

A few crystals of the complex **4-H** (Scheme 5) could be grown by slow diffusion of diisopropylether in the crude mixture in THF. While the quality of the structure is not sufficient to allow for a detailed discussion of the metrical parameters of the structure, it is of reasonable quality to indicate atom connectivity. In the crystal structure of **4-H**, reported in Supporting Information, the uranium complexes $K_3[U(bis\text{-}salfen)(Hbis\text{-}salfen)]\cdot(THF)_n$ (Figure 8) are connected in a one-dimensional coordination polymer by bridging potassium counter cations with different coordination modes and geometries (see Supporting Information, Figures S.18 and S.19). The ^1H NMR spectrum of **4-H** in THF-d_8 at 298 K features 36 sharp resonances over the range from 36.4 to −27.5 ppm. This shows the presence of fully asymmetric uranium(IV) solution species in agreement with the solid-state structure of this heteroleptic species. ESI/MS studies further support the formulation of **4-H** as $K_3[U(bis\text{-}salfen)(Hbis\text{-}salfen)]$ in THF solution (m/z = 1201.0 corresponding to the $\{K_3[U(bis\text{-}salfen)(Hbis\text{-}salfen)]+H\}^+$ moiety).

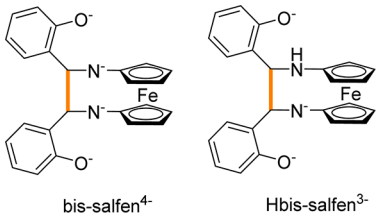

Figure 8. Drawing of the bis-salfen^{4-} and Hbis-salfen^{3-} ligands.

In presence of 18-c-6, the solid-state polymeric structure was disrupted, and single crystals of the dimer $[(K18\text{-}c\text{-}6)_2U(bis\text{-}salfen)(Hbis\text{-}salfen)]_2(K18\text{-}c\text{-}6)_2\cdot 7thf$, **5**, were obtained. X-ray diffraction studies show the presence of a centrosymmetric structure composed of two $[(K18\text{-}c\text{-}6)U(bis\text{-}salfen)(Hbis\text{-}salfen)]^{2-}$ moieties bridged by $2(K18\text{-}c\text{-}6)^+$ units, as shown in Figure 9. The charge is balanced by two $[K(18\text{-}c\text{-}6)]^+$ countercations.

Selected metrical parameters are reported in Table 1. The uranium ion is heptacoordinated in a distorted capped trigonal prismatic arrangement. Upon reduction two new intramolecular C−C bonds formed between the imino moieties of each salfen ligand. This results in the formation of a new

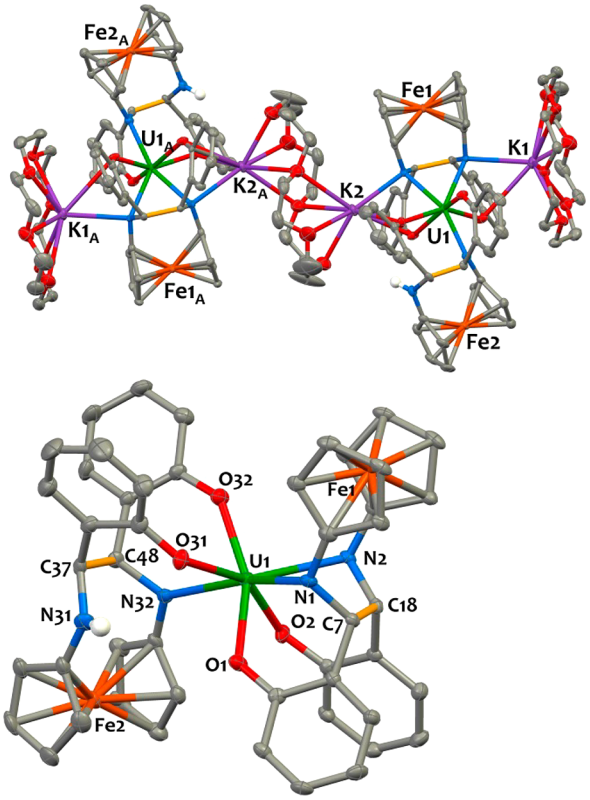

Figure 9. Ortep diagram of the solid-state molecular structure of the $[(K18\text{-}c\text{-}6)_2U(bis\text{-}salfen)(Hbis\text{-}salfen)]_2^{2-}$ dimeric anion in **5** (upper) and of the coordination environment around the uranium ion (lower). Hydrogen atoms, except that of the amino moiety, and interstitial solvent molecules are omitted for clarity. The C−C bonds formed by reduction of the imine moieties of the salfen ligands are represented in yellow. Uranium (green), iron (orange), nitrogen (blue), oxygen (red), potassium (purple), carbon (gray), and hydrogen (white) atoms are represented with 50% probability ellipsoids.

bisphenolate bisamido ligand (bis-salfen; Figure 8). The intraligand reductive coupling of the two imido moieties forms a linker between the two C_5H_5 ligands, yielding an *ansa*-ferrocene derivative. The structure shows that in one of the two bis-salfen ligands one amido group is protonated to give the Hbis-salfen ligand, which acts as a tridentate OON ligand, with the amino group (N32) remaining uncoordinated. The resulting heteroleptic complex is therefore composed of a

DOI: 10.1021/acs.inorgchem.5b00467
Inorg. Chem. 2015, 54, 5774−5783

Table 1. Mean Values of Selected Bond Lengths [Å] in the U(IV) Complexes 3, 5, and 6

compd	3	5	6
U−N	2.664(7)	2.46(6)	2.355(4)
U−O	2.231(9)	2.29(5)	2.24(3)
$C-C_{link}$		1.62(2)	1.586(8)
C−N	1.294(6)	1.471(3)	1.469(11)
U−Fe	4.316(11)	4.3450(2) (Fe1) 5.0419(3) (Fe2)	4.8874(9)
Fe−C	2.041(7)	2.046(17)	2.043(13)

U(IV) cation coordinated by a tetraanionic bis-salfen ligand and a trianionic Hbis-salfen ligand, which is consistent with the overall trianionic charge for the complex. The metrical parameters, given in Table 1, are in agreement with this description. Notably, the $U-N_{amido}$ average bond distance (2.46(6) Å) is shorter by ∼0.2 Å compared to the $U-N_{imino}$ bond distances found in **3** and falls in the range of what was observed in related U(IV) amido complexes.[8a,13] The C−N bond distances are elongated by ∼0.18 Å compared to those of complex **3**, in agreement with the reduction of the imine double C═N bond into amido/amino units.

Detailed analysis of the proton NMR spectrum of the reaction mixture obtained from the reduction of $[U(salfen)_2]$ with KC_8 reveals that this apparently complex pattern can be decomposed into two sets of resonances, one corresponding to the complex two **4-H** and one additional reduced complex with higher solution symmetry identified (see below) as $K_2[U(Hbis-salfen)_2]$ **4-H_2** (Scheme 5). However, their separation proved difficult, preventing the isolation of significant amounts of these species in analytically pure form.

Single crystals of $[K(dibenzo18-c-6)(Py)]_2[U(Hbis-salfen)_2]\cdot py_5$, **6**, were grown upon slow diffusion of hexane into a pyridine solution of the reaction mixture in the presence of dibenzo18-c-6. The solid-state structure consists of an isolated ion pair, and the structure of the $[U(Hbis-salfen)_2]^{2-}$ anion is presented in Figure 10. Selected bond distances are given in Table 1. The uranium(IV) cation lies on a symmetry center and

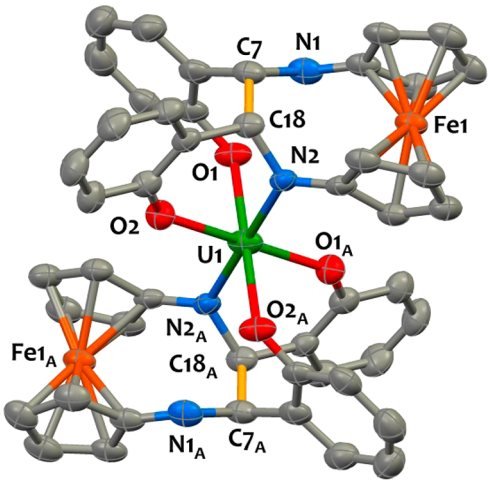

Figure 10. Solid-state molecular structure of the $[U(Hbis-salfen)_2]^{2-}$ anion in $[K(dibenzo18-c-6)(Py)]_2[U(Hbis-salfen)_2]\cdot py_5$ **6**. Hydrogen atoms and solvent molecules are omitted for clarity. The C−C bond formed through the reductive coupling of the imino groups is represented in yellow and uranium (green), nitrogen (blue), oxygen (red), iron (orange) ellipsoids. Selected metrical parameters are reported in Table 1

exhibits a pseudo-octahedral coordination with four phenolate moieties from the Hbis-salfen ligands coordinated in the equatorial plane and two amido moieties bound in a trans configuration. The NMR pattern of **4-H_2** features 18 signals, indicating that the ligands are equivalents on the NMR time scale in agreement with the ligand arrangement found in the solid-state crystal structure of **6**. The value of the distance of the C−C bond formed from the coupling of two imino groups is 1.586(8) Å. The value of the C−C bond distance falls in the range of the ones found in bis-salophen, cyclo-salophen, and bis-napthquinolen ligands formed from reductive coupling of imino groups in tetradentate and tridentate Schiff bases, respectively.[8a,13] Similarly to **5**, the C18−N2 and C7−N1 bond distances (1.476(6) Å and 1.461(5) Å) in **6** are longer than the $C-N_{imino}$ bond distances found in **3** and correspond to C−N simple bonds. The U1−N2 bond distance (2.355(4) Å) is much shorter than the $U-N_{imino}$ bond distances found in **3**, which is consistent with an amido moiety. While N2 is coordinated to the uranium cation, as expected for an amido moiety, the neutral amino nitrogen N1 remains uncoordinated to the metal center. The average value of the U−O bond distances (2.24(3) Å) is in line with those reported for U(IV) phenolate systems.[8a,26] The U···Fe separation (4.8874(9) Å) in **6** is longer than the one in **3**. Finally, the overall K/U ratio is 2, in agreement with a +IV charge for the uranium. Thus, the formula $[U(Hbis-salfen)_2]^{2-}$ where Hbis-salfen is a trianionic tridentate ligand provides a good description of the complex.

These studies indicate that ligand reduction is more favorable than a U(IV) to U(III) process. The complex reduction results in the reductive coupling of the imino moieties of the salfen ligand yielding U(IV) amidophenolate compounds. Metal-mediated intramolecular and intermolecular reductive coupling of the imino group of the tetradentate Schiff-base salophen has been previously reported for U(IV) (Scheme 1),[8a] Ln(III),[14b] and d-block metals.[32] However, the isolated complexes **4-H** and **4-H_2** show that in the reduction of the $[U(salfen)_2]$ complex, the reductive coupling occurs between the imino groups of the same salfen ligand (Scheme 5). Such reactivity is unprecedented, and it is most likely the result of the higher flexibility of the salfen ligand compared to the salophen one.

Mixtures of **4-H** and **4-H_2** were reproducibly obtained from independent syntheses. These species are, respectively, the monoprotonated and the diprotonated analogues of a bis-amido bis-phenolate $[U(bis-salfen)_2]^{4-}$ complex and are probably formed by hydrogen abstraction from the solvent. We previously observed that the amido moieties of the bis-salophen ligand formed upon reductive coupling of the salophen Schiff-base feature a basic character.[14b] In the putative tetraanionic mononuclear $[U(bis-salfen)_2]^{4-}$ species (Scheme 5), resulting from the four-electron reduction of $[U(salfen)_2]$, the octaanionic environment provided at the U(IV) cation by the four phenolates and four amido groups likely results in a high electron density at the metal responsible for the low stability of this species. Unfortunately, efforts to characterize this intermediate so far proved unsuccessful in our hands. Attempts to perform the reduction in the more robust 1,2-dimethoxyethane solvent afforded the same mixture of compounds. Similar results were obtained when replacing KC_8 by K metal. Using a larger number of equivalents of potassium graphite resulted in the formation of intractable mixtures containing **4-H_2** and/or **4-H** together with other unidentified reduction products. When only 2 equiv of KC_8 are

DOI: 10.1021/acs.inorgchem.5b00467
Inorg. Chem. 2015, 54, 5774−5783

used in the reduction, a mixture of unreacted complex **3** and reduced **4-H** and **4-H$_2$** species were obtained.

Interestingly, preliminary studies show that despite the presence of protonated amino groups the electrons stored in the C−C bonds can became available to oxidizing agents. Notably, the addition of 4 equiv of AgOTf to the reaction mixture of **4-H** and **4-H$_2$** led to immediate restoration of the original [U(salfen)$_2$] (Scheme 6). This suggests that the

Scheme 6

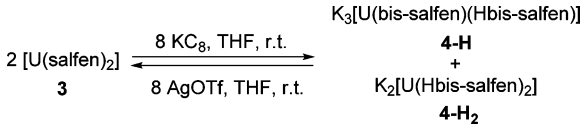

[U(salfen)$_2$] can be used to store four electrons for the reduction of substrates even in the presence of proton sources. This result contrasts with what was previously found for the complex K[Nd(bis-H$_2$salophen)] where the electrons stored in the C−C bond of the protonated bis-salophen ligand are no longer available to oxidizing agents.[14b] Work in progress is directed to investigate the reactivity of the reduced [U(salfen)$_2$] and to probe its ability to transfer the electrons stored in the C−C bond to different oxidizing substrates.

CONCLUSIONS

In summary, a series of heterometallic uranium−iron complexes was synthesized and fully characterized by NMR spectroscopy, single-crystal X-ray diffraction, variable-temperature magnetic measurements, and cyclovoltammetry. The ferrocene-based Schiff-base ligand salfen was shown to be a good platform for stabilizing the three higher oxidation states of uranium (IV, V, and VI). The reduction of the U(IV) bis-ligand complex [U(salfen)$_2$] led to ligand-centered reduction involving the reductive coupling of the imino groups on the Schiff-base ligand. This results in the unprecedented formation of an intramolecular intraligand C−C bond between the two imino groups of a salfen ligand rather than in the interligand C−C bond formation reported previously for tridentate and tetradentate Schiff bases. Such novel reactivity arises from the high flexibility of the ferrocene backbone. We also show that the electrons stored in the C−C bond are available for the oxidation of substrates. Future work will be directed to investigate the reactivity of the reported complexes.

ASSOCIATED CONTENT

Supporting Information

Synthesis information, selected ^{1}H NMR spectra, electrochemistry and magnetism data, and X-ray crystallographic data and files in CIF format. This material is available free of charge via the Internet at http://pubs.acs.org.

AUTHOR INFORMATION

Corresponding Author

*E-mail: marinella.mazzanti@epfl.ch.

Author Contributions

All authors have given approval to the final version of the manuscript.

Notes

The authors declare no competing financial interest.

ACKNOWLEDGMENTS

We thank Stephanie M. Quan and Prof. P. Diaconescu for kindly giving us generous samples of the salfen ligands. We thank C. Lebrun, J.-F. Jaquot, J. Hermle, and P.-A. Bayle for their contribution to the spectroscopic characterizations.

REFERENCES

(1) (a) Graves, C. R.; Kiplinger, J. L. *Chem. Commun.* **2009**, 3831−3853. (b) Graves, C. R.; Scott, B. L.; Morris, D. E.; Kiplinger, J. L. *J. Am. Chem. Soc.* **2007**, *129*, 11914−11915. (c) Arnold, P. L.; Love, J. B.; Patel, D. *Coord. Chem. Rev.* **2009**, *253*, 1973−1978. (d) Natrajan, L.; Burdet, F.; Pecaut, J.; Mazzanti, M. *J. Am. Chem. Soc.* **2006**, *128*, 7152−7153. (e) Hayton, T. W.; Wu, G. *J. Am. Chem. Soc.* **2008**, *130*, 2005−2014. (f) Nocton, G.; Horeglad, P.; Pecaut, J.; Mazzanti, M. *J. Am. Chem. Soc.* **2008**, *130*, 16633−16645.

(2) (a) MacDonald, M. R.; Fieser, M. E.; Bates, J. E.; Ziller, J. W.; Furche, F.; Evans, W. J. *J. Am. Chem. Soc.* **2013**, *135*, 13310−13313. (b) Arnold, P. L.; Patel, D.; Wilson, C.; Love, J. B. *Nature* **2008**, *451*, 315−318. (c) La Pierre, H. S.; Scheurer, A.; Heinemann, F. W.; Hieringer, W.; Meyer, K. *Angew. Chem., Int. Ed.* **2014**, *53*, 7158−7162.

(3) (a) King, D. M.; Liddle, S. T. *Coord. Chem. Rev.* **2014**, *266*, 2−15. (b) La Pierre, H. S.; Meyer, K. In *Progress in Inorganic Chemistry;* Karlin, K. D.; Ed. **2014**; Vol. *58*, pp 303−415. (c) Arnold, P. L. *Chem. Commun.* **2011**, *47*, 9005−9010. (d) Summerscales, O. T.; Cloke, F. G. N.; Hitchcock, P. B.; Green, J. C.; Hazari, N. *Science* **2006**, *311*, 829−831. (e) Frey, A. S. P.; Cloke, F. G. N.; Coles, M. P.; Maron, L.; Davin, T. *Angew. Chem., Int. Ed.* **2011**, *50*, 6881−6883. (f) Thomson, R. K.; Cantat, T.; Scott, B. L.; Morris, D. E.; Batista, E. R.; Kiplinger, J. L. *Nat. Chem.* **2010**, *2*, 723−729. (g) King, D. M.; Tuna, F.; McInnes, E. J. L.; McMaster, J.; Lewis, W.; Blake, A. J.; Liddle, S. T. *Science* **2012**, *337*, 717−720. (h) Karmel, I. S. R.; Fridman, N.; Tamm, M.; Eisen, M. S. *J. Am. Chem. Soc.* **2014**, *136*, 17180−17192. (i) Camp, C.; Pecaut, J.; Mazzanti, M. *J. Am. Chem. Soc.* **2013**, *135*, 12101−12111.

(4) Nocton, G.; Pecaut, J.; Mazzanti, M. *Angew. Chem., Int. Ed.* **2008**, *47*, 3040−3042.

(5) (a) Layfield, R. A. *Organometallics* **2014**, *33*, 1084−1099. (b) Long, J. R.; Meihaus, K. R. *J. Chem. Soc., Dalton Trans.* **2015**, *44*, 2517−2528.

(6) (a) Rinehart, J. D.; Long, J. R. *J. Am. Chem. Soc.* **2009**, *131*, 12558−12559. (b) Mougel, V.; Chatelain, L.; Pecaut, J.; Caciuffo, R.; Colineau, E.; Griveau, J. C.; Mazzanti, M. *Nat. Chem.* **2012**, *4*, 1011−1017. (c) Pereira, L. C. J.; Camp, C.; Coutinho, J. T.; Chatelain, L.; Maldivi, P.; Almeida, M.; Mazzanti, M. *Inorg. Chem.* **2014**, *53*, 11809−11811.

(7) Sessler, J. L.; Melfi, P. J.; Pantos, G. D. *Coord. Chem. Rev.* **2006**, *250*, 816−843.

(8) (a) Camp, C.; Mougel, V.; Horeglad, P.; Pecaut, J.; Mazzanti, M. *J. Am. Chem. Soc.* **2010**, *132*, 17374−17377. (b) Salmon, L.; Thuery, P.; Ephritikhine, M. *J. Chem. Soc., Dalton Trans.* **2004**, 4139−4145. (c) Salmon, L.; Thuery, P.; Ephritikhine, M. *J. Chem. Soc., Dalton Trans.* **2004**, 1635−1643. (d) Arnold, P. L.; Potter, N. A.; Carmichael, C. D.; Slawin, A. M. Z.; Roussel, P.; Love, J. B. *Chem. Commun.* **2010**, *46*, 1833−1835.

(9) Arnold, P. L.; Stevens, C. J.; Farnaby, J. H.; Gardiner, M. G.; Nichol, G. S.; Love, J. B. *J. Am. Chem. Soc.* **2014**, *136*, 10218−10221.

(10) Arnold, P. L.; Potter, N. A.; Magnani, N.; Apostolidis, C.; Griveau, J. C.; Colineau, E.; Morgenstern, A.; Caciuffo, R.; Love, J. B. *Inorg. Chem.* **2010**, *49*, 5341−5343.

(11) (a) Mizuoka, K.; Tsushima, S.; Hasegawa, M.; Hoshi, T.; Ikeda, Y. *Inorg. Chem.* **2005**, *44*, 6211−6218. (b) Takao, K.; Tsushima, S.; Takao, S.; Scheinost, A. C.; Bernhard, G.; Ikeda, Y.; Hennig, C. *Inorg. Chem.* **2009**, *48*, 9602−9604. (c) Mougel, V.; Horeglad, P.; Nocton, G.; Pecaut, J.; Mazzanti, M. *Angew. Chem., Int. Ed.* **2009**, *48*, 8477−8480. (d) Mougel, V.; Horeglad, P.; Nocton, G.; Pecaut, J.; Mazzanti, M. *Chem.—Eur. J.* **2010**, *16*, 14365−14377. (e) Nocton, G.; Horeglad, P.; Vetere, V.; Pecaut, J.; Dubois, L.; Maldivi, P.; Edelstein, N. M.; Mazzanti, M. *J. Am. Chem. Soc.* **2010**, *132*, 495−508. (f) Mougel, V.; Pecaut, J.; Mazzanti, M. *Chem. Commun.* **2012**, *48*, 868−870.

DOI: 10.1021/acs.inorgchem.5b00467
Inorg. Chem. 2015, 54, 5774−5783

(g) Mougel, V.; Horeglad, P.; Nocton, G.; Pecaut, J.; Mazzanti, M. *Chem.—Eur. J.* **2010**, *16*, 14365−14377.
(12) (a) Mougel, V.; Chatelain, L.; Hermle, J.; Caciuffo, R.; Colineau, E.; Tuna, F.; Magnani, N.; de Geyer, A.; Pecaut, J.; Mazzanti, M. *Angew. Chem., Int. Ed.* **2014**, *53*, 819−823. (b) Chatelain, L.; Walsh, J. P. S.; Pecaut, J.; Tuna, F.; Mazzanti, M. *Angew. Chem., Int. Ed.* **2014**, *53*, 13434−13438.
(13) Camp, C.; Andrez, J.; Pecaut, J.; Mazzanti, M. *Inorg. Chem.* **2013**, *52*, 7078−7086.
(14) (a) Cozzi, P. G. *Chem. Soc. Rev.* **2004**, *33*, 410−421. (b) Camp, C.; Guidal, V.; Biswas, B.; Pecaut, J.; Dubois, L.; Mazzanti, M. *Chem. Sci.* **2012**, *3*, 2433−2448.
(15) Diaconescu, P. L. *Comments Inorg. Chem.* **2010**, *31*, 196−241.
(16) (a) Duhovic, S.; Oria, J. V.; Odoh, S. O.; Schreckenbach, G.; Batista, E. R.; Diaconescu, P. L. *Organometallics* **2013**, *32*, 6012−6021. (b) Monreal, M. J.; Carver, C. T.; Diaconescu, P. L. *Inorg. Chem.* **2007**, *46*, 7226−7228. (c) Monreal, M. J.; Diaconescu, P. L. *Organometallics* **2008**, *27*, 1702−1706. (d) Monreal, M. J.; Diaconescu, P. L. *J. Am. Chem. Soc.* **2010**, *132*, 7676−7683. (e) Monreal, M. J.; Khan, S.; Diaconescu, P. L. *Angew. Chem., Int. Ed.* **2009**, *48*, 8352−8355. (f) Monreal, M. J.; Khan, S. I.; Kiplinger, J. L.; Diaconescu, P. L. *Chem. Commun.* **2011**, *47*, 9119−9121. (g) Diaconescu, P. L. *Acc. Chem. Res.* **2010**, *43*, 1352−1363. (h) Shafir, A.; Arnold, J. *J. Am. Chem. Soc.* **2001**, *123*, 9212−9213. (i) Ramos, A.; Otten, E.; Stephan, D. W. *J. Am. Chem. Soc.* **2009**, *131*, 15610−15611. (j) Green, A. G.; Kiesz, M. D.; Oria, J. V.; Elliott, A. G.; Buechler, A. K.; Hohenberger, J.; Meyer, K.; Zink, J. I.; Diaconescu, P. L. *Inorg. Chem.* **2013**, *52*, 5603−5610. (k) Huang, W.; Dulong, F.; Khan, S. I.; Cantat, T.; Diaconescu, P. L. *J. Am. Chem. Soc.* **2014**, *136*, 17410−17413. (l) Wang, X.; Thevenon, A.; Brosmer, J. L.; Yu, I.; Khan, S. I.; Mehrkhodavandi, P.; Diaconescu, P. L. *J. Am. Chem. Soc.* **2014**, *136*, 11264−11267.
(17) Shafir, A.; Fiedler, D.; Arnold, J. *J. Chem. Soc., Dalton Trans.* **2002**, 555−560.
(18) Broderick, E. M.; Thuy-Boun, P. S.; Guo, N.; Vogel, C. S.; Sutter, J.; Miller, J. T.; Meyer, K.; Diaconescu, P. L. *Inorg. Chem.* **2011**, *50*, 2870−2877.
(19) Broderick, E. M.; Diaconescu, P. L. *Inorg. Chem.* **2009**, *48*, 4701−4706.
(20) Carmichael, C. D.; Jones, N. A.; Arnold, P. L. *Inorg. Chem.* **2008**, *47*, 8577−8579.
(21) Avens, L. R.; Bott, S. G.; Clark, D. L.; Sattelberger, A. P.; Watkin, J. G.; Zwick, B. D. *Inorg. Chem.* **1994**, *33*, 2248−2256.
(22) *CrysAlisPro CCD; CrysAlisPro RED ; ABSPACK; CrysAlis PRO;* Agilent Technologies: Yarnton, England, 2010.
(23) Horeglad, P.; Nocton, G.; Filinchuk, Y.; Pecaut, J.; Mazzanti, M. *Chem. Commun.* **2009**, 1843−1845.
(24) Chatelain, L.; Mougel, V.; Pecaut, J.; Mazzanti, M. *Chem. Sci.* **2012**, *3*, 1075−1079.
(25) (a) Burdet, F.; Pecaut, J.; Mazzanti, M. *J. Am. Chem. Soc.* **2006**, *128*, 16512−16513. (b) Krot, N. N.; Grigoriev, M. S. *Russ. Chem. Rev.* **2004**, *73*, 89−100.
(26) Mora, E.; Maria, L.; Biswas, B.; Camp, C.; Santos, I.; Pécaut, J.; Cruz, A.; Carretas, J. M.; Marçalo, J.; Mazzanti, M. *Organometallics* **2013**, *32*, 1409−1422.
(27) Dunitz, J. D.; Orgel, L. E.; Rich, A. *Acta Crystallogr.* **1956**, *9*, 373−375.
(28) Westmoreland, I.; Arnold, J. *Acta Crystallogr., Sect. E* **2006**, *62*, M2303−M2304.
(29) Kindra, D. R.; Evans, W. J. *Chem. Rev.* **2014**, *114*, 8865−8882.
(30) Kaufmann, L.; Breunig, J.-M.; Vitze, H.; Schoedel, F.; Nowik, I.; Pichlmaier, M.; Bolte, M.; Lerner, H.-W.; Winter, R. F.; Herber, R. H.; Wagner, M. *J. Chem. Soc., Dalton Trans.* **2009**, 2940−2950.
(31) (a) Yin, H.; Lewis, A. J.; Williams, U. J.; Carroll, P. J.; Schelter, E. J. *Chem. Sci.* **2013**, *4*, 798−805. (b) Odom, A. L.; Arnold, P. L.; Cummins, C. C. *J. Am. Chem. Soc.* **1998**, *120*, 5836−5837. (c) Baker, R. J. *Coord. Chem. Rev.* **2012**, *256*, 2843−2871. (d) Chomitz, W. A.; Minasian, S. G.; Sutton, A. D.; Arnold, J. *Inorg. Chem.* **2007**, *46*, 7199−7209. (e) Lewis, A. J.; Williams, U. J.; Kikkawa, J. M.; Carroll, P. J.; Schelter, E. J. *Inorg. Chem.* **2012**, *51*, 37−39. (f) Duhovic, S.; Khan, S.; Diaconescu, P. L. *Chem. Commun.* **2010**, *46*, 3390−3392.
(32) (a) Gambarotta, S.; Mazzanti, M.; Floriani, C.; Zehnder, M. *J. Chem. Soc., Chem. Commun.* **1984**, 1116−1118. (b) Solari, E.; Maltese, C.; Franceschi, F.; Floriani, C.; ChiesiVilla, A.; Rizzoli, C. *J. Chem. Soc., Dalton Trans.* **1997**, 2903−2910.

DOI: 10.1021/acs.inorgchem.5b00467
Inorg. Chem. 2015, 54, 5774−5783

ChemPubSoc Europe

DOI: 10.1002/chem.201503637

CHEMISTRY A European Journal Communication

Uranium Chemistry

Heterometallic Fe_2^{II}–U^V and Ni_2^{II}–U^V Exchange-Coupled Single-Molecule Magnets: Effect of the 3d Ion on the Magnetic Properties

Lucile Chatelain,[a, b] Jacques Pécaut,[b] Floriana Tuna,[c] and Marinella Mazzanti*[a]

Abstract: Uranium-based compounds have been put forward as ideal candidates for the design of single-molecule magnets (SMMs) with improved properties, but to date, only two examples of exchange-coupled 3d–5f SMM containing uranium have been reported and both are based on the Mn^{II} ion. Here we have synthesized the first examples of exchange-coupled uranium SMMs based on Fe^{II} and Ni^{II}. The SMM behavior of these complexes containing a quasi linear {M–O=U=O–M} core arises from intramolecular Fe–U and Ni–U exchange interactions combined with the high Ising anisotropy of the uranyl(V) moiety. The measured values of the relaxation barrier (53.9 ± 0.9 K in the UFe_2 complex and of 27.4 ± 0.5 K in the UNi_2 complex) show clearly the dependency on the spin value of the transition metal, providing important new information for the future design of improved uranium-based SMMs.

Actinides, because they combine both high magnetic anisotropy and the possibility of magnetic exchange interactions, open new perspectives in the design of molecular magnets[1] with possible use in the development of memory devices.[2]

Over the last few years, an increasing number of monometallic compounds containing the U^{III} ion,[3] or mono-oxo and dioxo U^V units[4] have been reported to show slow relaxation of purely molecular origin (i.e., single-molecule magnets or SMMs). The highly anisotropic $5f^1$ UO_2^+ uranyl cation has also been demonstrated to be a valuable, and so far unique, building block for the assembly of exchange-coupled uranium-based SMMs and single-chain magnets (SCMs).[4b,c,5] Notably, examples of polymetallic complexes of uranium showing unambiguous magnetic coupling between the metal centers remain rare,[1a,6] but the so-called cation–cation interaction of the uranyl(V) oxo groups with other metal cations provides an efficient pathway for magnetic exchange in homopolymetallic 5f–5f compounds and in 3d–5f and 4f–5f heteropolymetallic assemblies.[6e,f,7]

However, to date, only two examples of discrete polymetallic 3d–5f clusters exhibiting exchange-coupled SMM behavior have been reported and both examples are based on the Mn^{II} ion.[4b,c] The large size and the molecular complexity of the $\{U_{12}Mn_6\}$ wheel-shaped uranyl(V) SMM cluster renders the modulation of the geometry and of the nature of the d ion arduous.[4b] In contrast, we have recently reported a trinuclear $\{U^VMn^{II}_2\}$ SMM compound with a high relaxation barrier that can be assembled in a controlled manner through cation–cation interactions between a uranyl(V) complex[8] and a Mn^{II} ion complexed by a strategically chosen ligand.[4c]

This $\{U^VMn^{II}_2\}$ system appears to be an ideal and so far unique candidate for investigating the effects of the nature of the d block ion (through the replacement of the Mn^{II} ion), and of the overall complex architecture (through ligand replacement) on the magnetic behavior of uranium-based SMMs. However, due to the low stability of the UO_2^+ species, the replacement of the Mn^{II} ion is synthetically challenging as it may lead to disproportionation of uranyl(V).[9] Here we report the synthesis of a series of trinuclear 3d–5f $\{U^VM^{II}_2\}$ (M: Fe, Ni) complexes that were assembled through cation–cation interactions between the UO_2^+ group and the respective 3d cations, complexed with different capping ligands. These compounds are the first examples of exchange-coupled 3d–5f SMMs containing Fe^{II} and Ni^{II}.

A discrete and well-defined trinuclear complex was obtained in reasonable yield (Scheme 1; 43%) from the reaction of $[UO_2(Mesaldien)K]_n$[8] (Mesaldien = *N*,*N*′-(2-aminomethyl) diethylenebis(salicylidene imine)), with two equivalents of the Fe^{II} complex $[Fe(TPA)Cl_2]$ (TPA = tris(2-pyridylmethyl)amine). X-ray diffraction studies revealed the presence of the trinuclear complex $[\{Fe(TPA)Cl\}\{UO_2(Mesaldien)\}\{Fe(TPA)Cl\}]I$ (**UFe_2TPA**) (Figure 1) assembled from the linear cation–cation interactions between two uranyl(V) oxo groups with the two d-block Fe^{II} cations. The presence of the iodide counterion is essential to obtain X-ray quality crystals.

The crystal and molecular structure of the trimer $[\{M(TPA)X\}\{UO_2(Mesaldien)\}\{M(TPA)X\}]^+$ in **UFe_2TPA** is closely related to

[a] L. Chatelain, Dr. M. Mazzanti
Institut des Sciences et Ingénierie Chimiques
Ecole Polytechnique Fédérale de Lausanne (EPFL)
1015 Lausanne (Switzerland)
E-mail: marinella.mazzanti@epfl.ch

[b] L. Chatelain, Dr. J. Pécaut
Université Grenoble Alpes, INAC-SCIB
38000 Grenoble (France)
and
CEA, INAC-SCIB, 38000 Grenoble (France)

[c] Dr. F. Tuna
School of Chemistry and Photon Science Institute
The University of Manchester, Oxford Road
Manchester, M13 9PL (UK)

Supporting information for this article is available on the WWW under http://dx.doi.org/10.1002/chem.201503637.

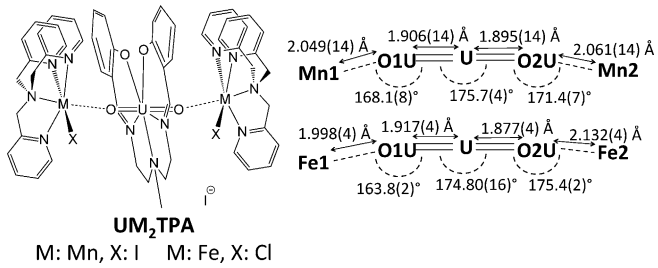

Scheme 1. Drawing of complexes **UFe$_2$TPA** and **UMn$_2$TPA** with associated structural parameters for the UO_2M_2 core.

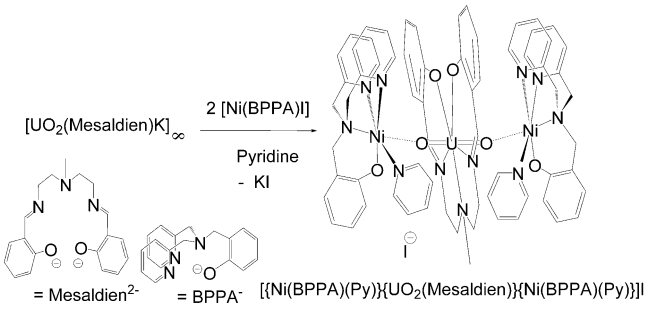

Scheme 2. Synthesis of the trinuclear complex **UNi$_2$BPPA**.

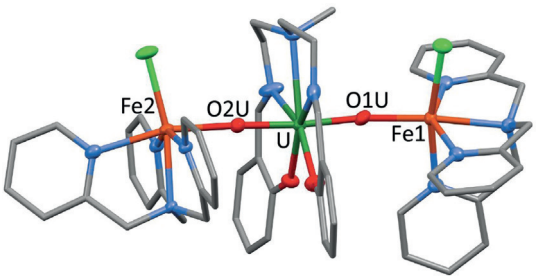

Figure 1. Crystallographic structure of **UFe$_2$TPA**; ligand represented in pipes (hydrogen atoms and iodide couteranion omitted for clarity). Atoms: C (grey), O (red), Fe (orange), N (light blue), Cl (light green) and U (green).

the one found in the previously reported **UMn$_2$TPA** complex.[4c] In particular, in both complexes the arrangement of the three metal ions is almost linear (M-U-M is 173.7667(5)° in **UMn$_2$TPA** and 173.5401(1)° in **UFe$_2$TPA**). Similarly to the Mn^{II} in **UMn$_2$TPA**, the Fe^{II} cation in **UFe$_2$TPA** is hexacoordinated by the four nitrogen atoms of the TPA ligand, one oxygen atoms from the uranyl(V) group, and a coordinated halide anion (Cl^- in **UFe$_2$TPA** and I^- in **UMn$_2$TPA**).

In both complexes, the mean U=O bond lengths lie in the range of the values previously observed for uranyl(V) complexes[4b,c,6e,9–10] (2.06(7) Å in **UFe$_2$TPA** and 2.05(1) Å in **UMn$_2$TPA**[4c]). The mean Fe^{II}—O_{yl} distance (2.07(7) Å) is longer than that found in the only other heteronuclear uranyl(V)–Fe$^{II}_2$ complex (1.946(4) Å) reported.[10d] The values of the intramolecular U–Fe (mean value 3.941(1) Å) and Fe–Fe (7.869(1) Å) distances in **UFe$_2$TPA** are similar to those reported for the mean U–Mn (3.939(5) Å) and Mn–Mn (7.8666(4) Å) distances in **UMn$_2$TPA**. The shortest intermolecular U–U, U–M and M–M distances in **UFe$_2$TPA** (9.8358(4), 9.5228(8) and 7.2977(12) Å) are also comparable to those reported for **UMn$_2$TPA** (10.9469(4), 8.7589(4) and 7.6296(4) Å).[4c]

Attempts to prepare the analogous [{Ni(TPA)X}{UO_2(Mesaldien)}{Ni(TPA)X}]$^+$ trimeric complex led to a mixture of two complexes presenting a different coordination environment for the two nickel ions (see Ni^{II} structure in the Supporting Information). Since the analysis of magnetic data of such mixture of compounds could prove challenging, we have prepared an analogous trimeric compound using the tripodal tetradentate ligand BPPAH (BPPAH = bis(2-picolyl)(2-hydroxybenzyl)amine). The use of this monoanionic capping ligand prevents isomer formation.

The reaction of [UO_2(Mesaldien)K]$_n$[8] with two equivalents of the [M(BPPA)I] (M: Fe, Ni) complexes in pyridine (Scheme 2) affords the stable trinuclear compounds [{Fe(BPPA)(Py)}{UO_2(Mesaldien)}{Fe(BPPA)}]I (**UFe$_2$BPPA**) and [{Ni(BPPA)(Py)}{UO_2(Mesaldien)}{Ni(BPPA)(Py)}]I (**UNi$_2$BPPA**) in 70–84% yield.

The presence of a trimeric structure was confirmed by X-ray diffraction for the Ni^{II} and Fe^{II} complexes (Figures 2 and 3 respectively). In the structure of the **UM$_2$BPPA** complexes, the two [M(BPPA)]$^+$ ions are linked to the uranyl(V) oxo groups through linear cation–cation interactions. Similarly to what is found in the **UM$_2$TPA** complexes, in the **UM$_2$BPPA** complexes the uranium atoms are heptacoordinate with a slightly distorted pentagonal bipyramid geometry by the two uranyl oxygen and the five donor atoms of the Mesaldien^{2-} ligand in the equatorial plane. The environment of the transition metals is different in the **UM$_2$BPPA** compared to the **UM$_2$TPA** ones, but the overall metric parameters of the linear {M–O=U=O–M} core remain similar in all complexes.

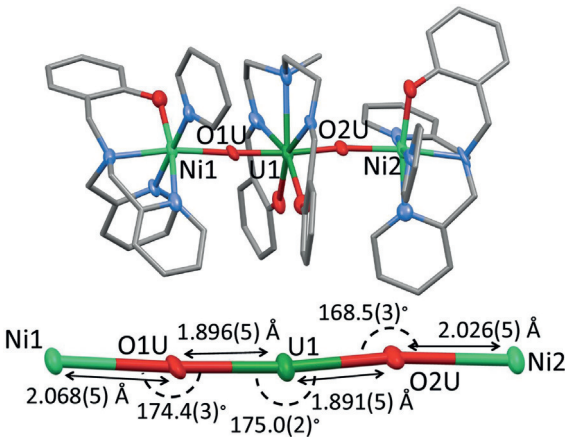

Figure 2. Crystallographic structure of **UNi$_2$BPPA** with hydrogen atoms, iodide couteranion and solvent molecules omitted for clarity and ligand represented in pipes. Atoms: C (grey), O (red), Ni (light green), N (light blue) and U (green).

In **UNi$_2$BPPA** the Ni^{II} ions are both hexacoordinate with a slightly distorted octahedral geometry. In the **UFe$_2$BPPA** trimer the two Fe^{II} cations are in a different coordination environment, one Fe^{II} complex is hexacoordinate with a slightly

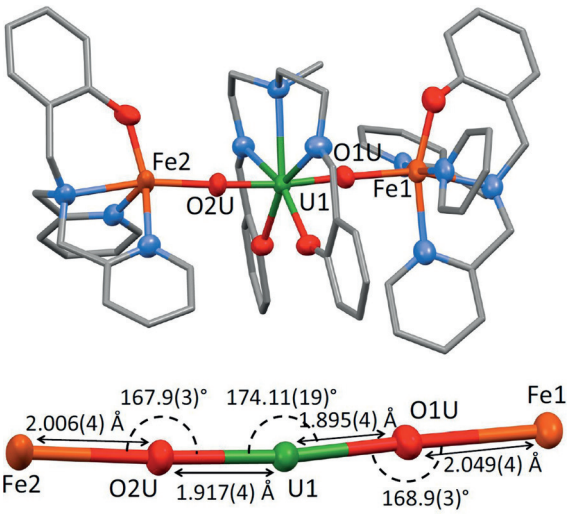

Figure 3. Crystallographic structure of **UFe_2BPPA** with hydrogen atoms, iodide couteranion and solvent molecules omitted for clarity. Atoms: C (grey), O (red), Fe (orange), N (light blue) and U (green).

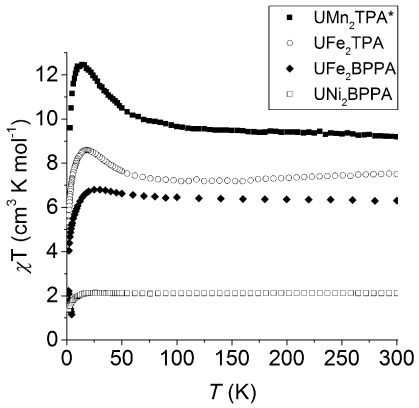

Figure 4. Plots of χT versus T for polycrystalline samples of **UM_2BPPA** and **UM_2TPA** (* from reference [4d]) measured in 0.5 T dc field.

distorted octahedral geometry, whereas the second is pentacoordinate with a distorted square pyramidal geometry. Selected bond lengths and angles are reported in Table S1 in the Supporting Information. The values of the mean M^{II}–O_{yl} (2.03(2) Å for Fe^{II} and 2.05(2) Å for Ni^{II}) distances in the **UM_2BPPA** trimers, of the mean intramolecular U–M distances (3.913(12) Å in **UFe_2BPPA** and 3.9287(9) Å in **UNi_2BPPA)** and of the M–M intramolecular distances (7.8131(16) Å in **UFe_2BPPA** and 7.8522(16) Å in **UNi_2BPPA)** are similar to those found in the **UM_2TPA** complexes. The shortest intermolecular U–U, U–M and M–M distances—10.2602(9), 9.1797(10) and 7.9627(14) Å in **UFe_2BPPA** and 11.148(1), 9.1476(12) and 8.571(2) Å in **UNi_2BPPA**, respectively—are also comparable to those found in the **UM_2TPA** complexes.

The **UM_2TPA** and the **UM_2BPPA** complexes are stable in the solid state and in pyridine or acetonitrile for months under an argon atmosphere. Moreover, ^{1}H proton NMR and ESI/MS studies show that the complexes retain their trimeric structure in solution.

Magnetic susceptibility measurements under a static field (dc) were performed on polycrystalline samples of **UFe_2TPA**, **UFe_2BPPA**, and **UNi_2BPPA** over the temperature range 2–300 K (Figure 4). The χT (χ = molar magnetic susceptibility) values of 7.7 $cm^3 K mol^{-1}$ for **UFe_2TPA**, 6.3 $cm^3 K mol^{-1}$ for **UFe_2BPPA**, and 2.11 $cm^3 K mol^{-1}$ for **UNi_2BPPA** were measured at room temperature. The two values measured for **UFe_2BPPA** and **UNi_2BPPA** are in agreement with the presence of two non-interacting M^{II} ions (Fe: $S=2$, $g_{iso}=2$, $\chi T=3$ $cm^3 K mol^{-1}$, Ni: $S=1$, $g_{iso}=2$, $\chi T=1$ $cm^3 K mol^{-1}$) and one uranium(V) ion (a contribution of 0.32 $cm^3 K mol^{-1}$ has been previously measured for the uranyl(V) ion in the **UCd_2TPA** complex containing the diamagnetic Cd^{II} ion).[4c] Although the χT value at 300 K measured for **UFe_2TPA** is significantly higher, the Fe^{II} contribution estimated for independent ions is in the range of reported experimental values. The χT of the **UFe_2TPA** decreases first with decreasing temperature down to 100 K, then increases, reaching a maximum of 8.66 $cm^3 K mol^{-1}$ at 18 K in **UFe_2TPA** (a maximum of 12.5 $cm^3 K mol^{-1}$ at 12 K was found[4c] for **UMn_2TPA**), and then decreases again to a value of 3.99 $cm^3 K mol^{-1}$ at 2 K. The analysis of the magnetic data previously reported for the **UMn_2TPA** complex had shown the presence of ferromagnetic coupling between the Mn and U centers with a $J=+7.5$ cm^{-1}.[4c] Here, the increase of χT with decreasing temperature also suggests the occurrence of magnetic coupling between the uranium and iron ions in **UFe_2TPA**. Similar behavior is observed for **UFe_2BPPA** with a maximum of 6.8 $cm^3 K mol^{-1}$ at 30 K, while the presence of a maximum is more ambiguous for **UNi_2BPPA**. It should be noted that no evidence of magnetic coupling was found in the previously reported heterometallic uranyl(V)–Fe^{II}_2 complex[10d] suggesting that the {M–O=U=O–M} arrangement is key to the magnetic coupling. For all three complexes, the downturn observed in the χT plot after each maximum is most probably the result of zero-field splitting effects associated with the resulting high-spin ground state.

A divergence between zero-field-cooled (ZFC) and field-cooled (FC) susceptibilities as a function of temperature is observed below 2.1 K for **UFe_2TPA** (see Supporting Information). M(H) data at 1.8–2 K are marked by irreversibility effects but the hysteresis loop collapses on approaching zero field.

The magnetization dynamics for these trinuclear species were investigated by alternating current (ac) magnetic susceptibility measurements as a function of temperature (**UFe_2TPA**: 2.1–5.7 K, **UFe_2BPPA**: 1.8-5 K, **UNi_2BPPA**: 1.8–3.3 K) and frequency ($\nu=0.1$–1400 Hz for **UFe_2TPA** and $\nu=1$–1400 Hz for **UFe_2BPPA** and **UNi_2BPPA**), in a zero dc field (Figure 5 and the Supporting Information).

For all three complexes, the in-phase (χ') and out-of-phase (χ'') components of the ac susceptibility are strongly frequency-dependent at low temperatures and maxima are also observed in $\chi''(T)$. These observations are indicative of slow relaxation of the molecular magnetization, and hence of single molecule magnet (SMM) behavior for all complexes. Semicircular Cole–Cole plots were obtained at fixed temperatures between 2.7 and 4.8 K for **UFe_2TPA** and 1.8 and 2.9 K for **UNi_2BPPA**, which could be fitted to a generalized Debye model[11] with an α parameter in the range of 0.12–0.20 and 0.26–0.40, respec-

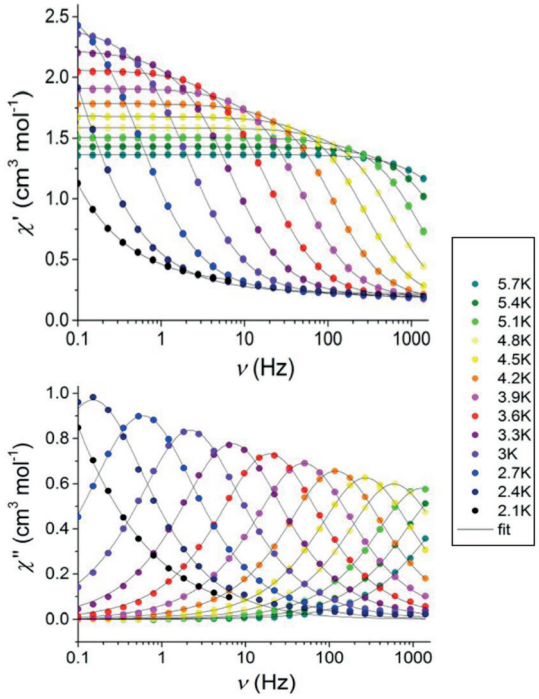

Figure 5. In-phase (top) and out-of-phase (bottom) frequency dependence of **UFe_2TPA** measured at zero dc field and 1.55 G ac field oscillating at frequencies in the range 0.1–1400 Hz. The solid lines correspond to the Debye fits.

tively. Plots of the relaxation time constants τ (determined from $\chi_M''(\nu, T)$) as $\ln(\tau)$ versus T^{-1} are linear above 3.7, 2.4 and 2.3 K for **UFe_2TPA** **UFe_2BPPA** and **UNi_2BPPA**, respectively. Fits to the Arrhenius law $\tau = \tau_0 \exp(\Delta E/k_B T)$ give thermal energy barriers to magnetization relaxation of $\Delta E = 53.9 \pm 0.9$ K with $\tau_0 = 3.40 \times 10^{-9}$ s for **UFe_2TPA**, $\Delta E = 9.0 \pm 1.1$ K with $\tau_0 = 7.82 \times 10^{-6}$ s for **UFe_2BPPA** and $\Delta E = 27.4 \pm 0.5$ K with $\tau_0 = 2.40 \times 10^{-8}$ s for **UNi_2BPPA** (Figure 6 and the Supporting Information). The value of the inversion barrier is significantly lower for the **UFe_2BPPA** trimer compared to the **UFe_2TPA** one. The application of a small dc field of 400 G results in a significant increase of the relaxation barrier ($\Delta E = 35.6 \pm 0.6$ K with $\tau_0 = 3.14 \times 10^{-9}$ s). This phenomenon is usually encountered when quantum tunneling occurs. In this case the occurrence of quantum tunneling in the **UFe_2BPPA** trimer can be assigned to the presence of a different coordination environment of the Fe^{II} cation compared to the **UFe_2TPA**.

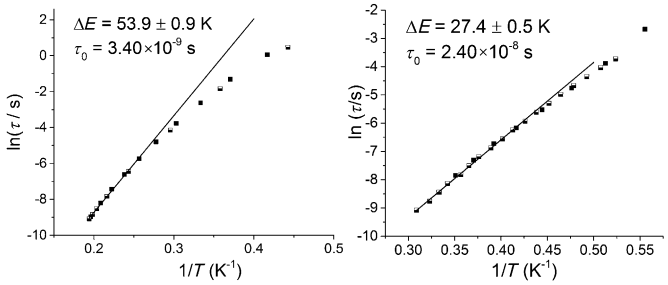

Figure 6. Arrhenius plot displaying T dependence of the relaxation times for **UFe_2TPA** (left) and for **UNi_2BPPA** (right). Black squares indicate that the corresponding relaxation time was extracted from fitting the frequency-dependent ac susceptibility curves with a modified Debye model, whereas half-open squares indicate that the temperature corresponding to the peak maximum in ac curves was measured at constant frequency.

In all three complexes SMM behavior was observed at zero-dc field and originates from magnetic exchange between 3d M^{II} the U^{V} ions. Notably, the analogous uranyl(V) complex **UCd_2TPA** containing the diamagnetic Cd^{II} ion shows weak SMM behavior only under applied dc field.[4c]

The inversion barrier measured for the **UFe_2TPA** is significantly lower than that previously reported for the analogous **UMn_2TPA** complex (81.0 ± 0.5 K with $\tau_0 = 5.02 \times 10^{-10}$).[4c] Since the crystal and molecular structure of the trimer $[\{M(TPA)X\}\{UO_2(Mesaldien)\}\{M(TPA)X\}]^+$ in **UFe_2TPA** is very similar to that of **UMn_2TPA**,[4c] the difference in the SMM behavior can be related to the presence of an overall lower spin for the Fe^{II} complex. The inversion barrier of **UFe_2TPA** is much lower than the one very recently reported for a 3d–4f Fe_2Dy trimer containing the $S = 15/2$ Dy^{III} ion (495 K),[12] but is significantly higher than the value of energy barriers found in large homometallic exchange coupled Fe^{II} clusters (10–44 K).[13] The lower barrier found for the **UNi_2BPPA** trimer can be related to the presence of a $S = 1$ Ni^{II} ion. SMMs based on Ni^{II} clusters remain rare[14] and the inversion barrier measured for **UNi_2BPPA** is significantly higher than the highest barrier found so far (a barrier of 14 K was reported for a nickel(II) cluster).[15]

These results show that the properties of 3d–5f SMMs can be modulated by the nature of the transition metal. Indeed, for the trimers in which the 3d metal adopts an octahedral geometry, the value of the energy barrier is directly correlated to the spin of the ground state and it decreases along the Mn, Fe, Ni series (high spin Mn^{II}: $S = 5/2$; Fe^{II}: $S = 2$; and Ni^{II}; $S = 1$). However, depending of the coordination environment of the 3d metal ion, quantum tunnelling can lead to a reduced value of the inversion barrier.

In conclusion we have synthesized and characterized the first examples of exchange-coupled 3d–5f SMMs containing Fe^{II} and Ni^{II}. The **UNi_2BPPA** complex also provides the first example of a UO_2^{+}–Ni^{2+} cation–cation complex. Moreover, the **UFe_2TPA**, **UFe_2BPPA** and **UNi_2BPPA** trimers are the first examples of unambiguous magnetic coupling between U^{V} and Fe^{II} or Ni^{II} ions. The comparative study of the magnetic properties of the **UM_2TPA** and **UM_2BPPA** complexes unambiguously demonstrates that the SMM behavior of the discrete trinuclear entity arises from the intramolecular exchange interactions between M^{II} and U^{V} ions associated with the large Ising-type anisotropy defined by the O=U=O group.[10b] The effective energy barriers to the reversal of magnetization of 53.9 ± 0.9 K in **UFe_2TPA** and of 27.4 ± 0.5 for **UNi_2BPPA** are large, considering that SMM behavior arising from single-ion effects of the uranium(V) ion is only observed under applied dc field with non-measurable barriers.[4a,c] Moreover, these values can be related to the spin of the d-block metal ions when their coordination environment is equivalent. These studies show that uranyl(V) provides a versatile building block for the assembly of exchange-coupled 3d–5f clusters with tunable geometry, which in turn should bring essential information for the synthesis of

uranium-based SMMs with higher inversion barriers and open hysteresis at higher temperatures.

Acknowledgements

We thank François Jacquot and Colette Lebrun for their help in physicochemical measurement. We thank L. Plassais for the synthesis of the BPPA ligand. We acknowledge support from the EPFL and from the EPSRC UK National EPR Facility. This work benefited from COST Action CM1006-UFEN: European F-Element Network.

Keywords: actinides · cations · magnetic properties · polymetallic complexes · single-molecule magnets · uranium

[1] a) J. D. Rinehart, T. D. Harris, S. A. Kozimor, B. M. Bartlett, J. R. Long, *Inorg. Chem.* **2009**, *48*, 3382 – 3395; b) N. Magnani, *Int. J. Quantum Chem.* **2014**, *114*, 755 – 759; c) J. R. Long, K. R. Meihaus, *Dalton Trans.* **2015**, *44*, 2517 – 2528; d) S. T. Liddle, *Angew. Chem. Int. Ed.* **2015**, *54*, 8604 – 8641; *Angew. Chem.* **2015**, *127*, 8726 – 8764; e) R. A. Layfield, *Organometallics* **2014**, *33*, 1084 – 1099.

[2] D. Gatteschi, R. Sessoli, J. Villain, *Molecular Nanomagnets*, Oxford University Press, Oxford, UK, **2006**.

[3] a) J. D. Rinehart, J. R. Long, *J. Am. Chem. Soc.* **2009**, *131*, 12558 – 12559; b) J. D. Rinehart, K. R. Meihaus, J. R. Long, *J. Am. Chem. Soc.* **2010**, *132*, 7572 – 7573; c) M. A. Antunes, L. C. J. Pereira, I. C. Santos, M. Mazzanti, J. Marcalo, M. Almeida, *Inorg. Chem.* **2011**, *50*, 9915 – 9917; d) J. T. Coutinho, M. A. Antunes, L. C. J. Pereira, H. Bolvin, J. Marcalo, M. Mazzanti, M. Almeida, *Dalton Trans.* **2012**, *41*, 13568 – 13571; e) D. P. Mills, F. Moro, J. McMaster, J. van Slageren, W. Lewis, A. J. Blake, S. T. Liddle, *Nat. Chem.* **2011**, *3*, 454 – 460; f) F. Moro, D. P. Mills, S. T. Liddle, J. Slangeren, *Angew. Chem. Int. Ed.* **2013**, *52*, 3430 – 3433; *Angew. Chem.* **2013**, *125*, 3514 – 3517; g) J. D. Rinehart, J. R. Long, *Dalton Trans.* **2012**, *41*, 13572 – 13574; h) K. R. Meihaus, J. D. Rinehart, J. R. Long, *Inorg. Chem.* **2011**, *50*, 8484 – 8489.

[4] a) D. M. King, F. Tuna, J. McMaster, W. Lewis, A. J. Blake, E. J. L. McInnes, S. T. Liddle, *Angew. Chem. Int. Ed.* **2013**, *52*, 4921 – 4924; *Angew. Chem.* **2013**, *125*, 5021 – 5024; b) V. Mougel, L. Chatelain, J. Pecaut, R. Caciuffo, E. Colineau, J. C. Griveau, M. Mazzanti, *Nat. Chem.* **2012**, *4*, 1011 – 1017; c) L. Chatelain, J. P. S. Walsh, J. Pecaut, F. Tuna, M. Mazzanti, *Angew. Chem. Int. Ed.* **2014**, *53*, 13434 – 13438; *Angew. Chem.* **2014**, *126*, 13652 – 13656; d) S. Carretta, G. Amoretti, P. Santini, V. Mougel, M. Mazzanti, S. Gambarelli, E. Colineau, R. Caciuffo, *J. Phys. Condens. Matter* **2013**, *25*, 486001.

[5] a) V. Mougel, L. Chatelain, J. Hermle, R. Caciuffo, E. Colineau, F. Tuna, N. Magnani, A. de Geyer, J. Pecaut, M. Mazzanti, *Angew. Chem. Int. Ed.* **2014**, *53*, 819 – 823; *Angew. Chem.* **2014**, *126*, 838 – 842; b) L. Chatelain, F. Tuna, J. Pécaut, M. Mazzanti, *Chem. Commun.* **2015**, *51*, 11309 – 11312.

[6] a) O. P. Lam, F. W. Heinemann, K. Meyer, *Chem. Sci.* **2011**, *2*, 1538 – 1547; b) L. P. Spencer, E. J. Schelter, P. Yang, R. L. Gdula, B. L. Scott, J. D. Thompson, J. L. Kiplinger, E. R. Batista, J. M. Boncella, *Angew. Chem. Int. Ed.* **2009**, *48*, 3795 – 3798; *Angew. Chem.* **2009**, *121*, 3853 – 3856; c) P. L. Arnold, G. M. Jones, S. O. Odoh, G. Schreckenbach, N. Magnani, J. B. Love, *Nat. Chem.* **2012**, *4*, 221 – 222; d) R. K. Rosen, R. A. Andersen, N. M. Edelstein, *J. Am. Chem. Soc.* **1990**, *112*, 4588 – 4590; e) L. Chatelain, V. Mougel, J. Pecaut, M. Mazzanti, *Chem. Sci.* **2012**, *3*, 1075 – 1079; f) V. Mougel, P. Horeglad, G. Nocton, J. Pecaut, M. Mazzanti, *Angew. Chem. Int. Ed.* **2009**, *48*, 8477 – 8480; *Angew. Chem.* **2009**, *121*, 8629 – 8632; g) A.-C. Schmidt, F. W. Heinemann, W. W. Lukens, Jr., K. Meyer, *J. Am. Chem. Soc.* **2014**, *136*, 11980 – 11993; h) S. A. Kozimor, B. M. Bartlett, J. D. Rinehart, J. R. Long, *J. Am. Chem. Soc.* **2007**, *129*, 10672 – 10673; i) E. J. Schelter, J. M. Veauthier, J. D. Thompson, B. L. Scott, K. D. John, D. E. Morris, J. L. Kiplinger, *J. Am. Chem. Soc.* **2006**, *128*, 2198 – 2199; j) T. Le Borgne, E. Riviere, J. Marrot, J. J. Girerd, M. Ephritikhine, *Angew. Chem. Int. Ed.* **2000**, *39*, 1647 – 1649; *Angew. Chem.* **2000**, *112*, 1713 – 1715; k) T. Le Borgne, E. Riviere, J. Marrot, P. Thuery, J. J. Girerd, M. Ephritikhine, *Chem. Eur. J.* **2002**, *8*, 774 – 783.

[7] a) P. L. Arnold, N. A. Potter, N. Magnani, C. Apostolidis, J. C. Griveau, E. Colineau, A. Morgenstern, R. Caciuffo, J. B. Love, *Inorg. Chem.* **2010**, *49*, 5341 – 5343; b) P. L. Arnold, E. Hollis, F. J. White, N. Magnani, R. Caciuffo, J. B. Love, *Angew. Chem. Int. Ed.* **2011**, *50*, 887 – 890; *Angew. Chem.* **2011**, *123*, 917 – 920; c) G. Nocton, P. Horeglad, J. Pécaut, M. Mazzanti, *J. Am. Chem. Soc.* **2008**, *130*, 16633 – 16645; d) P. L. Arnold, E. Hollis, G. S. Nichol, J. B. Love, J. C. Griveau, R. Caciuffo, N. Magnani, L. Maron, L. Castro, A. Yahia, S. O. Odoh, G. Schreckenbach, *J. Am. Chem. Soc.* **2013**, *135*, 3841 – 3854.

[8] V. Mougel, J. Pecaut, M. Mazzanti, *Chem. Commun.* **2012**, *48*, 868 – 870.

[9] V. Mougel, P. Horeglad, G. Nocton, J. Pecaut, M. Mazzanti, *Chem. Eur. J.* **2010**, *16*, 14365 – 14377.

[10] a) M. Zegke, G. S. Nichol, P. L. Arnold, J. B. Love, *Chem. Commun.* **2015**, *51*, 5876 – 5879; b) G. Nocton, P. Horeglad, V. Vetere, J. Pecaut, L. Dubois, P. Maldivi, N. M. Edelstein, M. Mazzanti, *J. Am. Chem. Soc.* **2010**, *132*, 495 – 508; c) P. L. Arnold, D. Patel, A. J. Blake, C. Wilson, J. B. Love, *J. Am. Chem. Soc.* **2006**, *128*, 9610 – 9611; d) P. L. Arnold, D. Patel, C. Wilson, J. B. Love, *Nature* **2008**, *451*, 315 – 318; e) T. W. Hayton, G. Wu, *J. Am. Chem. Soc.* **2008**, *130*, 2005 – 2014.

[11] K. S. Cole, R. H. Cole, *J. Chem. Phys.* **1941**, *9*, 341 – 351.

[12] J.-L. Liu, J.-Y. Wu, Y.-C. Chen, V. Mereacre, A. K. Powell, L. Ungur, L. F. Chibotaru, X.-M. Chen, M.-L. Tong, *Angew. Chem. Int. Ed.* **2014**, *53*, 12966 – 12970; *Angew. Chem.* **2014**, *126*, 13180 – 13184.

[13] a) H. Oshio, N. Hoshino, T. Ito, *J. Am. Chem. Soc.* **2000**, *122*, 12602 – 12603; b) A. K. Boudalis, Y. Sanakis, J. M. Clemente-Juan, B. Donnadieu, V. Nastopoulos, A. Mari, Y. Coppel, J.-P. Tuchagues, S. P. Perlepes, *Chem. Eur. J.* **2008**, *14*, 2514 – 2526.

[14] a) A. Bell, G. Aromi, S. J. Teat, W. Wernsdorfer, R. E. P. Winpenny, *Chem. Commun.* **2005**, 2808 – 2810; b) R. Biswas, Y. Ida, M. L. Baker, S. Biswas, P. Kar, H. Nojiri, T. Ishida, A. Ghosh, *Chem. Eur. J.* **2013**, *19*, 3943 – 3953.

[15] G. Aromí, S. Parsons, W. Wernsdorfer, E. K. Brechin, E. J. L. McInnes, *Chem. Commun.* **2005**, 5038 – 5040.

Received: September 10, 2015
Published online on October 28, 2015

JACS
JOURNAL OF THE AMERICAN CHEMICAL SOCIETY
Communication
pubs.acs.org/JACS

Synthesis and Structure of Nitride-Bridged Uranium(III) Complexes

Lucile Chatelain, Rosario Scopelliti, and Marinella Mazzanti*

Institut des Sciences et Ingénierie Chimiques, Ecole Polytechnique Fédérale de Lausanne (EPFL), CH-1015 Lausanne, Switzerland

Supporting Information

ABSTRACT: The reduction of the nitride-bridged diuranium(IV) complex $Cs[\{U(OSi(O^tBu)_3)_3\}_2(\mu\text{-}N)]$ affords the first example of a uranium nitride complex containing uranium in the +III oxidation state. Two nitride-bridged complexes containing the heterometallic fragments $Cs_2[U^{III}\cdots N\cdots U^{IV}]$ and $Cs_3[U^{III}\cdots N\cdots U^{III}]$ have been crystallographically characterized. The presence of two or three Cs^+ cations binding the nitride group is key for the isolation of these complexes. In spite of the fact that the nitride group is multiply bound to two uranium and two or three Cs^+ cations, these complexes transfer the nitride group to CS_2 to afford SCN^- and uranium(IV) disulfide.

Molecular uranium nitrides are attractive synthetic targets because of their potential as precursors to ceramic materials or as efficient molecular catalysts.[1] Notably, uranium(III) mononitride, UN,[2] a solid that is difficult to synthesize and solubilize, has been proposed for alternative nuclear fuels[3] and as an effective catalyst in dinitrogen reduction to ammonia.[4] Moreover, molecular nitride complexes are also important to gain a better understanding of f orbital implication in multiple bonding and covalency in actinide−ligand bonds.[5] Uranium nitride chemistry remains much less developed than the d-block counterparts. In recent years several molecular complexes of uranium have been prepared that contain nitride groups bridging two or more uranium ions[6] or terminal nitride groups.[7] Most of these complexes contain uranium in its +IV oxidation state, with a few systems containing U(V) and U(VI). In spite of their relevance in materials science and catalysis and the anticipated attractive reactivity of uranium(III) nitrides, no molecular uranium(III) nitride complex has been isolated in solution or in the solid state. The isolation of molecular uranium(III) nitrides is essential for investigating the reactivity of the U^{III}−nitride bond, which in turn will lead to convenient routes to nitride materials and the design of molecular catalysts. Here we report the first examples of nitride-bridged complexes containing uranium in the +III oxidation state.

Recently we reported the synthesis and molecular structure of the dinuclear uranium(IV)/uranium(IV) nitride $Cs[\{U(OSi(O^tBu)_3)_3\}_2(\mu\text{-}N)]$ (**1**). This complex remains a rare example[6f,h] of a dinuclear uranium nitride complex featuring a linear $U^{IV}\cdots N\cdots U^{IV}$ fragment (U−N−U angle = 170.2(3)°) and short U−N distances (U1−N1, 2.058(5) Å; U2−N1, 2.079(5) Å) indicative of U−N multiple bonds. Moreover, in complex **1** the Cs^+ cation binds the bridging nitride and six oxygen atoms from the siloxide ligands, affording a unique heterometallic structure. The ability of the $OSi(O^tBu)_3$ ligand to bind to Cs^+, thus stabilizing highly charged species, motivated us to explore the possibility of stabilizing the $U\cdots N\cdots U$ fragment in highly reduced uranium species.

The reduction of complex **1** with 1 equiv or a large excess of Cs^0 in tetrahydrofuran (THF) at −40 °C under argon allowed the synthesis and characterization of the U(III)/U(IV) complex $Cs_2[\{U(OSi(O^tBu)_3)_3\}_2(\mu\text{-}N)]$ (**2**) in 67% yield and the U(III)/U(III) complex $Cs_3[\{U(OSi(O^tBu)_3)_3\}_2(\mu\text{-}N)]$ (**3**) in 77% yield, respectively (Scheme 1). The solid-state molecular

Scheme 1. Synthesis of $Cs_2[\{U(OSi(O^tBu)_3)_3\}_2(\mu\text{-}N)]$ (2) and $Cs_3[\{U(OSi(O^tBu)_3)_3\}_2(\mu\text{-}N)]$ (3)

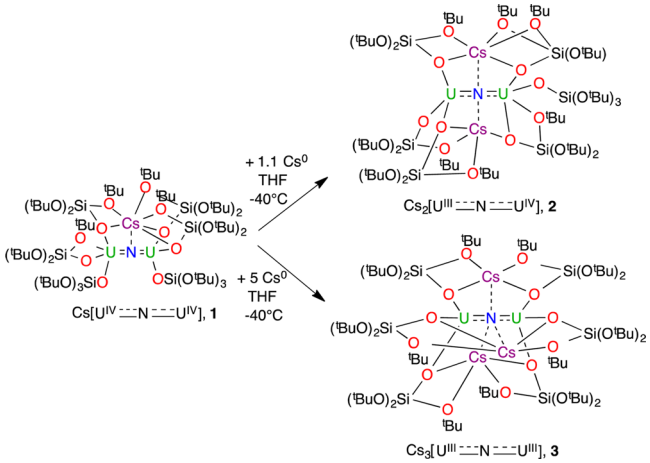

structures of complexes **2** and **3** were determined by single-crystal X-ray diffraction (Figures 1 and 2). In both complexes **2** and **3**, each uranium ion is coordinated by a nitride group and three siloxide oxygens with a pseudotetrahedral geometry. The two U−N distances in complex **3** are equivalent as a result of the twofold crystallographic axis passing through one Cs and the nitride ion. In complex **2** the two U−N distances are similar (Table 1), suggesting the presence of nonlocalized charge.

In all of the complexes **1**−**3**, the Cs^+ cations are bound to the bridging nitride and to the siloxide oxygens. In complex **2**, two Cs^+ cations bind the nitride in an almost linear way (Cs−N−Cs angle =161.8(4)°) with the Cs−N−Cs and the $U\cdots N\cdots U$ fragments located in the same plane and perpendicular to each other. In complex **3**, the three Cs^+ cations bind the nitride to form an irregular triangle located in a plane perpendicular to the $U\cdots N\cdots U$ fragment (Cs−N−Cs angles: 119.1(4),

Received: December 3, 2015
Published: February 5, 2016

DOI: 10.1021/jacs.5b12620
J. Am. Chem. Soc. 2016, 138, 1784−1787

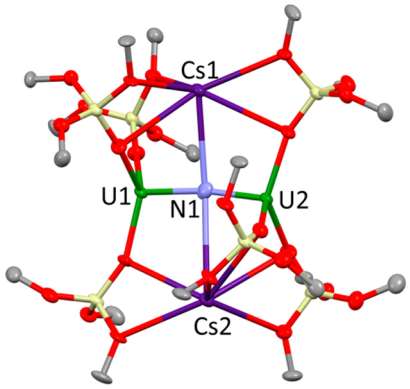

Figure 1. Crystallographic structure of $Cs_2[\{U(OSi(O^tBu)_3)_3\}_2(\mu\text{-}N)]$ (**2**) crystallized from a saturated THF solution. The ellipsoid probability is 50%, and hydrogen atoms, methyl groups, and solvent molecules have been omitted for clarity. Atoms: C (gray), O (red), Si (light yellow), N (light blue), Cs (purple), and U (green).

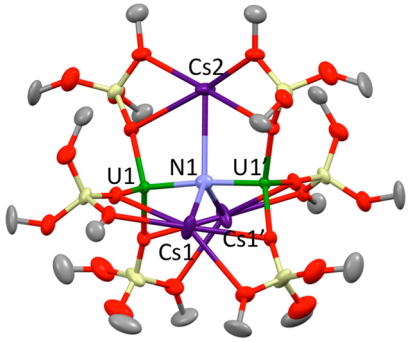

Figure 2. Crystallographic structure of $Cs_3[\{U(OSi(O^tBu)_3)_3\}_2(\mu\text{-}N)]$ (**3**) crystallized from a saturated THF solution. The ellipsoid probability is 50%, and hydrogen atoms, methyl groups, and disorder on Cs2 have been omitted for clarity. Atoms: C (gray), O (red), Si (light yellow), N (light blue), Cs (purple), and U (green).

108.9(3), and 132.0(7)°). The Cs–N distances are longer than those found in an imido-bridged U(IV) complex (mean Cs–N = 3.075(10) Å).[7d]

Complexes **2** and **3** display a linear U---N---U motif with U–N–U angles comparable to that found in complex **1** (Table 1). The U–N distances in complexes **2** and **3** fall in the range 2.081–2.1495 Å and are longer than those found in **1**[6g] and previously reported U(IV)/U(V) nitrides containing the linear U=N=U motif (2.012(16)–2.090(8) Å).[6a,f,h] These distances remain much shorter than U(III)–N single-bond distances (e.g., $U-N_{cyanate}$ = 2.456(7) Å,[8] $U-N_{dinitrogen}$ = 2.401(8)–2.423(8) Å,[9] and $U-N_{amide}$ = 2.320(4) Å in $U[N(SiMe_3)_2]_3$[10]). Longer U–N distances were also found in a U(IV) cluster with a $U_4(\mu_4\text{-}N)$ core (2.271(3)–2.399(5) Å).[6d] This points to the presence of U^{III}–N multiple bonding in **2** and **3**. The mean value of the U–N bond distance in the nitride core increases by about 0.08 Å in the fully reduced $Cs_3[U^{III}---N---U^{III}]$system compared with the $Cs[U^{IV}---N---U^{IV}]$ unit, probably as a result of the presence of additional electrons at the uranium center. Such an increase is similar to the increase in the average U–O bond length (0.09 Å), which can be related to the difference between the ionic radii of U(III) and U(IV) (0.135 Å). A smaller variation (0.03 Å) was observed by Cummins and co-workers in the successive oxidation of a linear U(IV)=N=U(IV) fragment supported by amide ligands to U(V)=N=U(V).[6f] The larger variation observed in the successive reduction of the siloxide complex **1** is at least partly due to the presence of an increasing number of Cs^+ cations binding the nitride group and thus polarizing and reducing the electron density on the U---N---U fragment. Lengthening of U–N bonds upon alkali-metal ion coordination to the N atom has been observed in dinuclear U(IV) imido complexes.[7d]

Complex **2** can be prepared analytically pure and stored in the solid state under argon at −40 °C for several weeks, but it is very reactive and can only be handled in solution at −40 °C. Complex **3** can be obtained analytically pure but decomposes very quickly both in the solid state and in THF solution at −40 °C, yielding mixtures of complexes **2** and **3** and free siloxide ligand. The extremely high reactivities of complexes **2** and **3** are in agreement with the absence in the literature of any molecular nitride compounds containing uranium in the +III oxidation state. The presence of the multidentate siloxide groups capable of binding the Cs^+ cation is key to the isolation of complex **3**. Notably, the reduction of **1** with an excess of Cs^0 in the presence of crown ether 18C6 leads to intractable reaction mixtures containing the free ligand as the only NMR-detectable species. This indicates that when the Cs^+ cation is removed by the crown ether from the coordination pocket formed by the siloxide ligands in **1**, it becomes impossible to isolate the $[U^{III}---N---U^{III}]^{3-}$ species from the reduction of **1**. The proton NMR spectra of complexes **2** and **3** in THF solution show the presence of only one signal for the six siloxide ligands, in agreement with the presence of symmetry-related siloxides. In the case of complex **2**, this can interpreted in terms of the fluxionality of the bound Cs cation. Proton NMR studies showed that the addition of crown ether to complex **2** in THF results in the removal of the bound Cs^+, leading to a significant decrease in the stability. In contrast, the addition of crown ether to complex **3** in THF does not lead to Cs removal.

Significant changes were also observed in the cyclic voltammogram of **1** when the electrochemistry was carried in the presence of 18C6. The cyclic voltammogram of complex **1** measured in THF (see the Supporting Information) shows two irreversible electrochemical events at −2.34 and −0.92 V (vs $[Cp_2Fe]^{0/+}$), corresponding to reduction and oxidation of the complex. The irreversibility of these redox events is probably

Table 1. Comparative Structural Parameters of Complexes 1–3

	$[U^{IV}---N---U^{IV}]$ (**1**)	$[U^{III}---N---U^{IV}]$ (**2**)	$[U^{III}---N---U^{III}]$ (**3**)
U1–N (Å)	2.058(5)	2.099(12)	2.1495(12)
U2–N (Å)	2.079(5)	2.081(12)	
$U-O_{avg}$ (Å)	2.19(3)	2.243(25)	2.282(24)
Cs1–N (Å)	3.393(4)	3.276(12)	3.348(8)
Cs2–N (Å)	–	3.635(12)	3.22(2)
U–N–U (deg)	170.2(3)	169.1(7)	174.2(11)

DOI: 10.1021/jacs.5b12620
J. Am. Chem. Soc. 2016, 138, 1784–1787

due to the important rearrangement of the coordination sphere during the redox processes. After removal of Cs^+, the reduction wave is shifted to lower potential (E_{pc} = −2.43 V), indicating that the reduction of complex **1** is more difficult in the absence of coordinated Cs^+.

Complexes **2** and **3** provide the first examples of isolated molecular nitride complexes containing uranium in the +III oxidation state. These systems are expected to show high reactivity with a wide range of substrates because of the low oxidation state of uranium.[11] Previous reactivity studies of nitride-bridged uranium compounds are limited to a single example in which the U^{IV}=N=U^{IV} fragment reacts as a masked metallonitrene with NaCN.[6f]

Preliminary reactivity studies carried out with CS_2 showed that complexes **2** and **3** can transfer the nitride group to electrophilic substrates in spite of the fact that the nitride group is located in a protective pocket provided by the siloxide ligands and the multimetallic binding by two U and three Cs cations (see figures in the Supporting Information). The reactivity of complexes **2** and **3** with CS_2 is in agreement with a nucleophilic character of the nitride. Notably, the addition of $^{13}CS_2$ at −40 °C in THF to the bridging nitride led to the isolation of the disulfide-bridged diuranium(IV) complex $(Cs(THF))_2[\{U(OSi(O^tBu)_3)_3\}_2(\mu\text{-}S)_2]$ (**4**) in 25% yield (Scheme 2), which

Scheme 2. Reactivities of $Cs_2[\{U(OSi(O^tBu)_3)_3\}_2(\mu\text{-}N)]$ (2) and $Cs_3[\{U(OSi(O^tBu)_3)_3\}_2(\mu\text{-}N)]$ (3) with CS_2

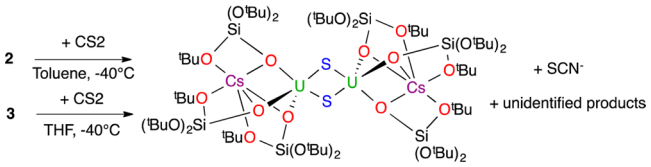

was characterized by X-ray diffraction (see the Supporting Information). ^{13}C NMR monitoring of the reaction mixture allowed the product of nitride transfer to CS_2 to be identified as thiocyanate (SCN^-). The disulfide complex is thus likely to be formed by extrusion of CsSCN from a highly reactive dithiocarbamate intermediate. Proton NMR studies showed that the formation of **4** occurs immediately even at low temperature, and it was not possible to isolate any intermediate. Similar reactivity has been reported for a terminal V(V) nitride, but in that case the decomposition was slower and the dithiocarbamate intermediate was isolated.[12] However, the formation of **4** involves oxidation of the metal center from U(III) to U(IV), and therefore, additional products must be formed that remain unidentified.

In conclusion, here we have expanded the family of molecular uranium nitride complexes to include the +III oxidation state. This has been accomplished by reducing the U(IV) analogue with cesium metal. Structural studies point to the presence of U^{III}−N multiple bonding. Future studies will be directed to further investigation of the nature of the U−N bonding in these systems. The reported reactivity with CS_2 is in agreement with a nucleophilic character of the nitride group. These complexes associating the highly reducing uranium(III) ion to a multiply bonded nitride group provide unprecedented precursors for the discovery of novel reactivity and unusual transformations. We are currently investigating the reactivities of these complexes with various substrates.

■ ASSOCIATED CONTENT

Supporting Information

The Supporting Information is available free of charge on the ACS Publications website at DOI: 10.1021/jacs.5b12620.

Experimental procedures and spectral data (PDF)
Crystallographic data for **4** (CIF)
Crystallographic data for **3** (CIF)
Crystallographic data for **2**·2THF (CIF)

■ AUTHOR INFORMATION

Corresponding Author

*marinella.mazzanti@epfl.ch

Notes

The authors declare no competing financial interest.

■ ACKNOWLEDGMENTS

This work was supported by the Swiss National Science Foundation and by the Ecole Polytechnique Fédérale de Lausanne (EPFL). We thank Euro Solari for carrying out the elemental analyses and for technical support. We thank Marta Falcone for some preliminary experiments.

■ REFERENCES

(1) King, D. M.; Liddle, S. T. *Coord. Chem. Rev.* **2014**, *266-267*, 2−15.
(2) (a) Silva, G. W. C.; Yeamans, C. B.; Sattelberger, A. P.; Hartmann, T.; Cerefice, G. S.; Czerwinski, K. R. *Inorg. Chem.* **2009**, *48*, 10635−10642. (b) Black, L.; Miserque, F.; Gouder, T.; Havela, L.; Rebizant, J.; Wastin, F. *J. Alloys Compd.* **2001**, *315*, 36−41. (c) Green, D. W.; Reedy, G. T. *J. Chem. Phys.* **1976**, *65*, 2921−2922. (d) Andrews, L.; Wang, X. F.; Gong, Y.; Kushto, G. P.; Vlaisavljevich, B.; Gagliardi, L. *J. Phys. Chem. A* **2014**, *118*, 5289−5303.
(3) Streit, M.; Ingold, F. *J. Eur. Ceram. Soc.* **2005**, *25*, 2687−2692.
(4) (a) Haber, F. Ammonia. German patent DE 229126, 1909. (b) Fox, A. R.; Bart, S. C.; Meyer, K.; Cummins, C. C. *Nature* **2008**, *455*, 341−349.
(5) (a) Neidig, M. L.; Clark, D. L.; Martin, R. L. *Coord. Chem. Rev.* **2013**, *257*, 394−406. (b) Kaltsoyannis, N. *Inorg. Chem.* **2013**, *52*, 3407−3413. (c) Hayton, T. W. *Chem. Commun.* **2013**, *49*, 2956−2973.
(6) (a) Evans, W. J.; Kozimor, S. A.; Ziller, J. W. *Science* **2005**, *309*, 1835−1838. (b) Korobkov, I.; Gambarotta, S.; Yap, G. P. A. *Angew. Chem., Int. Ed.* **2002**, *41*, 3433−3436. (c) Todorova, T. K.; Gagliardi, L.; Walensky, J. R.; Miller, K. A.; Evans, W. J. *J. Am. Chem. Soc.* **2010**, *132*, 12397−12403. (d) Nocton, G.; Pecaut, J.; Mazzanti, M. *Angew. Chem., Int. Ed.* **2008**, *47*, 3040−3042. (e) Fortier, S.; Wu, G.; Hayton, T. W. *J. Am. Chem. Soc.* **2010**, *132*, 6888−6889. (f) Fox, A. R.; Arnold, P. L.; Cummins, C. C. *J. Am. Chem. Soc.* **2010**, *132*, 3250−3251. (g) Camp, C.; Pecaut, J.; Mazzanti, M. *J. Am. Chem. Soc.* **2013**, *135*, 12101−12111. (h) Maria, L.; Santos, I. C.; Sousa, V. R.; Marcalo, J. *Inorg. Chem.* **2015**, *54*, 9115−9126.
(7) (a) Thomson, R. K.; Cantat, T.; Scott, B. L.; Morris, D. E.; Batista, E. R.; Kiplinger, J. L. *Nat. Chem.* **2010**, *2*, 723−729. (b) King, D. M.; Tuna, F.; McInnes, E. J. L.; McMaster, J.; Lewis, W.; Blake, A. J.; Liddle, S. T. *Nat. Chem.* **2013**, *5*, 482−488. (c) King, D. M.; Tuna, F.; McInnes, E. J. L.; McMaster, J.; Lewis, W.; Blake, A. J.; Liddle, S. T. *Science* **2012**, *337*, 717−720. (d) King, D. M.; McMaster, J.; Tuna, F.; McInnes, E. J. L.; Lewis, W.; Blake, A. J.; Liddle, S. T. *J. Am. Chem. Soc.* **2014**, *136*, 5619−5622.
(8) Cleaves, P. A.; King, D. M.; Kefalidis, C. E.; Maron, L.; Tuna, F.; McInnes, E. J. L.; McMaster, J.; Lewis, W.; Blake, A. J.; Liddle, S. T. *Angew. Chem., Int. Ed.* **2014**, *53*, 10412−10415.
(9) (a) Cloke, F. G. N.; Hitchcock, P. B. *J. Am. Chem. Soc.* **2002**, *124*, 9352−9353. (b) Roussel, P.; Scott, P. *J. Am. Chem. Soc.* **1998**, *120*, 1070−1071.
(10) Stewart, J. L.; Andersen, R. A. *Polyhedron* **1998**, *17*, 953−958.

DOI: 10.1021/jacs.5b12620
J. Am. Chem. Soc. 2016, 138, 1784−1787

(11) Smith, J. M. *Prog. Inorg. Chem.* **2014**, *58*, 417−470.
(12) Brask, J. K.; Dura-Vila, V.; Diaconescu, P. L.; Cummins, C. C. *Chem. Commun.* **2002**, 902−903.

DOI: 10.1021/jacs.5b12620
J. Am. Chem. Soc. 2016, 138, 1784−1787

A Journal of the Gesellschaft Deutscher Chemiker

Angewandte International Edition Chemie

GDCh

www.angewandte.org

2016–55/12

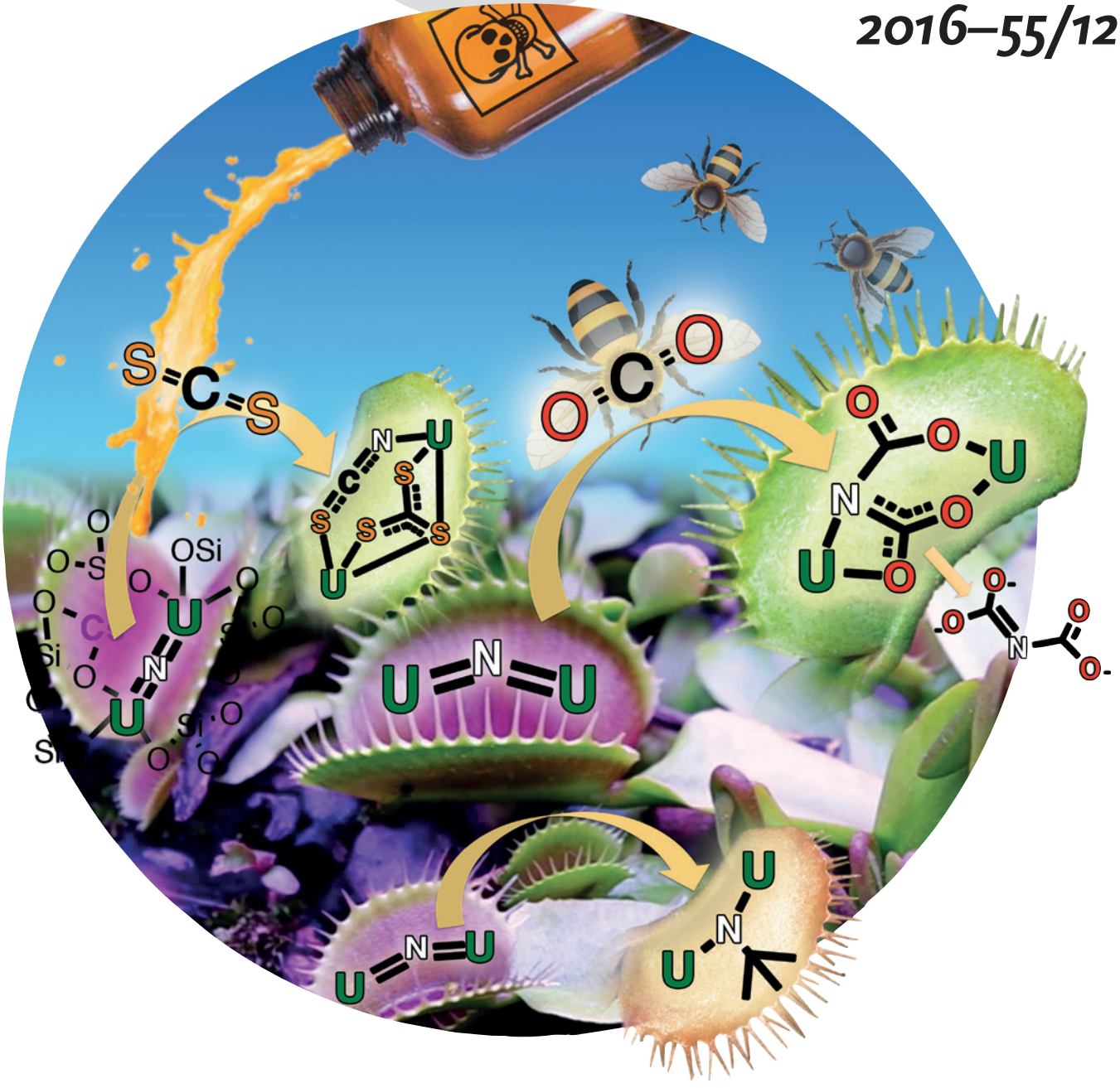

Cover Picture

M. Mazzanti et al.

Nucleophilic Reactivity of a Nitride-Bridged Diuranium(IV) Complex: CO_2 and CS_2 Functionalization

ACIEFS 55 (12) 3831–4102 (2016) · ISSN 1433–7851 · Vol. 55 · No. 12

WILEY-VCH

N–C Bond Formation

International Edition: DOI: 10.1002/anie.201600158
German Edition: DOI: 10.1002/ange.201600158

Nucleophilic Reactivity of a Nitride-Bridged Diuranium(IV) Complex: CO_2 and CS_2 Functionalization

*Marta Falcone, Lucile Chatelain, and Marinella Mazzanti**

Abstract: *Thermolysis of the nitride-bridged diuranium(IV) complex Cs{(μ-N)[U(OSi(O^{t}Bu)$_3$)$_3$]$_2$} (**1**) showed that the bridging nitride behaves as a strong nucleophile, promoting N–C bond formation by siloxide ligand fragmentation to yield an imido-bridged siloxide/silanediolate diuranium(IV) complex, Cs{(μ-N^{t}Bu)(μ-O$_2$Si(O^{t}Bu)$_2$)U$_2$(OSi(O^{t}Bu)$_3$)$_5$}. Complex **1** displayed reactivity towards CS_2 and CO_2 at room temperature that is unprecedented in f-element chemistry, affording diverse N-functionalized products depending on the reaction stoichiometry. The reaction of **1** with two equivalents of CS_2 yielded the thiocyanate/thiocarbonate complex Cs{(μ-NCS)(μ-CS$_3$)[U(OSi(O^{t}Bu)$_3$)$_3$]$_2$} via a putative NCS$^-$/S^{2-} intermediate. The reaction of **1** with one equivalent of CO_2 resulted in deoxygenation and N–C bond formation, yielding the cyanate/oxo complex Cs{(μ-NCO)(μ-O)[U(OSi(O^{t}Bu)$_3$)$_3$]$_2$}. Addition of excess CO_2 to **1** led to the unprecedented dicarbamate product Cs{(μ-NC$_2$O$_4$)[U(OSi(O^{t}Bu)$_3$)$_3$]$_2$}.*

Uranium nitrides are attractive candidates for both stoichiometric and catalytic nitrogen-transfer reactions and small-molecule transformations.[1] Understanding the reactivity of uranium nitrides is also of great interest because of their importance in many fields of science and engineering (e.g., as nuclear fuels).[2] In recent years, an increasing number of molecular nitride compounds of uranium have been prepared and characterized,[2b,3] but their reactivity has remained virtually unexplored. The activation of a C–H bond by a transient terminal uranium nitride, which resulted in the formation of new N–H and N–C bonds, was first reported by Kiplinger and co-workers.[3j] More recently, the two-electron reduction of terminal U^V and U^{VI} nitrides to cyanates by carbon monoxide has also been described.[3n] Although most previously reported uranium nitride complexes contain a bridging nitride, the reactivity of the U=N=U fragment has thus far only been studied for a diuranium(V) complex in which the nitride reacted as a masked metallonitrene to afford a cyanoimide diuranium(IV/IV) complex.[3g]

N–C bond-formation reactions are very important in the construction of value-added chemical compounds, such as amino acids, pharmaceuticals, or agrochemicals,[4] and synthetic methods that use inexpensive and largely available feedstocks, such as carbon dioxide, are particularly desirable.[5] A few examples of N–C bond formation from the reaction of carbon dioxide with activated nitride-bridged complexes[6] or terminal nitride complexes[7] have been reported for transition metals but thus far, the reactivity of molecular nitride compounds of f-block elements with CO_2 has not been investigated.

Herein, we have investigated the ability of a previously described nitride-bridged diuranium(IV) complex, Cs{(μ-N)-[U(OSi(O^{t}Bu)$_3$)$_3$]$_2$} (**1**),[3h] to promote N–C bond formation, and we have studied its reactivity with CO_2 and CS_2. We found that the temperature-induced decomposition of complex **1** induced N–C bond formation by fragmentation of a siloxide ligand. We also report the isolation and characterization of the products obtained from the room-temperature reactions of **1** with CO_2 and CS_2. In these reactions, the bridging nitride group acts as a strong nucleophile, which leads to N–C bond formation yielding cyanate and thiocyanate species and the unprecedented construction of a dicarbamate.

The nitride-bridged diuranium(IV) complex Cs{(μ-N)[U-(OSi(O^{t}Bu)$_3$)$_3$]$_2$} (**1**) is stable in solution at −40 °C for several months but undergoes decomposition at higher temperatures. Notably, the overnight thermolysis of **1** at 80 °C in toluene solution resulted in the complete transformation of **1** to afford a new imido-bridged siloxide/silanediolate diuranium(IV) complex, Cs{(μ-N^{t}Bu)(μ-O$_2$Si(O^{t}Bu)$_2$)U$_2$(OSi(O^{t}Bu)$_3$)$_5$} (**2**), in 65 % yield (Scheme 1). The solid-state crystal structure of **2** was determined by single-crystal X-ray diffraction (Figure 1).

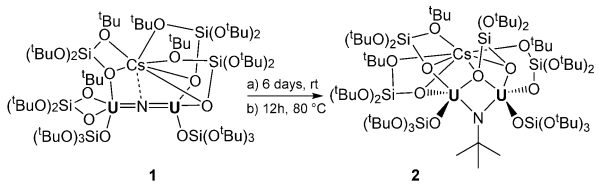

Scheme 1. *tert*-Butyl transfer from a ligand of Cs{(μ-N)[U(OSi-(O^{t}Bu)$_3$)$_3$]$_2$} (**1**) to the bridging nitride to form Cs{(μ-N^{t}Bu)(μ-O$_2$Si-(O^{t}Bu)$_2$)U$_2$(OSi(O^{t}Bu)$_3$)$_5$} (**2**).

The structure of **2** shows the presence of a tris(siloxide) U^{IV} moiety, [U(OSi(O^{t}Bu)$_3$)$_3$], and of a bis(siloxide)/mono(silanediolate) U^{IV} moiety, [U(O$_2$Si(O^{t}Bu)$_2$)(OSi(O^{t}Bu)$_3$)$_2$]. The two uranium ions are bridged by a *tert*-butylimido group and by one of the oxygen atoms of the silanediolate moiety, affording a non-symmetric structure. This result shows that the thermolysis of complex **1** leads to C–O cleavage in one of the siloxide ligands with concomitant transfer of the *tert*-butyl

[*] M. Falcone, L. Chatelain, Dr. M. Mazzanti
Institut des Sciences et Ingénierie Chimiques
Ecole Polytechnique Fédérale de Lausanne (EPFL)
1015 Lausanne (Switzerland)
E-mail: marinella.mazzanti@epfl.ch

Supporting information for this article can be found under http://dx.doi.org/10.1002/anie.201600158.

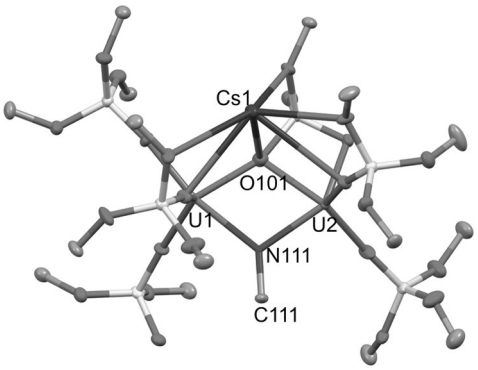

Figure 1. Crystal structure of Cs{(μ-N^{t}Bu)(μ-O_2Si(O^{t}Bu)$_2$)U_2(OSi(O^{t}Bu)$_3$)$_5$} (**2**). Thermal ellipsoids set at 50% probability. Hydrogen atoms and methyl groups were omitted for clarity. Selected bond lengths [Å]: U1–N111 2.300(3), U2–N111 2.398(3), N111–C111 1.461(6), U2–O101 2.223(4), U1–O101 2.323(4), Cs1–O101 3.340(4).

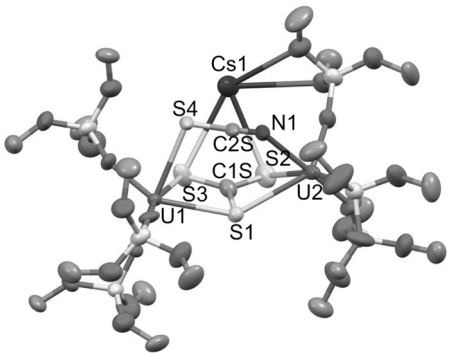

Figure 2. Crystal structure of Cs{(μ-NCS)(μ-CS_3)[U(OSi(O^{t}Bu)$_3$)$_3$]$_2$} (**3a**) in **3**. Thermal ellipsoids set at 50% probability. Hydrogen atoms, methyl groups, and lattice solvent molecules were omitted for clarity. Selected bond lengths [Å] for **3a**: U1–S1 2.9792(18), U1–S4 3.029(4), U1–S3 2.885(3), U2–S1 3.0411(18), U2–S2 2.881(4), U2–N1 2.501(15), S4–C2S 1.639(15), N1–C2S 1.07(2), S1–C1S 1.740(12), S2–C1S 1.682(9), S3–C1S 1.712(10), Cs1–S3 3.525(3), Cs1–S4 4.170(6), Cs1–S2 3.408(3), U2–Cs1 4.7200(9).

group to the nitride, giving a dianionic silanediolate ligand that bridges the two uranium centers. C–O cleavage in a *tert*-butoxysiloxide ligand with concomitant elimination of isobutene has previously been observed in the thermolysis of the diuranium(III) complex [U(OSi(O^{t}Bu)$_3$)$_2$(μ-OSi(O^{t}Bu)$_3$)]$_2$.[8] The strongly nucleophilic character of the bridging nitride in **1** results in the formation of a new N–C bond with the *tert*-butyl group from the siloxide ligand, yielding the *tert*-butylimido bridging group. The *tert*-butylimide bridges the two uranium centers in a non-symmetric fashion with U–N_{imido} bond lengths of 2.300(3) and 2.398(3) Å, which are slightly longer than those found in the few reported examples of dinuclear imido-bridged U^{IV} complexes (2.156(8)–2.378(3) Å).[9]

The high nucleophilic reactivity of the bridging nitride, as evidenced by the slow decomposition of complex **1** at room temperature, inspired us to investigate the reactivity of this complex with the electrophiles CS_2 and CO_2. The addition of two equivalents of CS_2 to **1** resulted in an immediate color change of the solution to green. Storing the solution at −40 °C resulted in the isolation of Cs{(μ-NCS)(μ-CS_3)[U(OSi(O^{t}Bu)$_3$)$_3$]$_2$} (**3**) in 58% yield (Scheme 2).

The solid-state structure of **3** is disordered with an occupancy of 0.85 for the Cs atom in one position (**3a**, Figure 2) and an occupancy of 0.15 in the other position (**3b**; see the Supporting Information). The structure of **3a** consists of a diuranium(IV) complex in which two [U(OSi(O^{t}Bu)$_3$)$_3$] fragments are bridged by a thiocyanate unit and a trithiocarbonate unit that binds the two uranium cations and the cesium

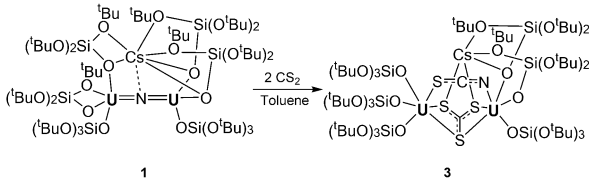

Scheme 2. Reaction of Cs{(μ-N)[U(OSi(O^{t}Bu)$_3$)$_3$]$_2$} (**1**) with CS_2 to form Cs{(μ-NCS)(μ-CS_3)[U(OSi(O^{t}Bu)$_3$)$_3$]$_2$} (**3**).

cation in a μ_3-κ^2:κ^2:κ^2 fashion. The C–S bond lengths (1.740(12), 1.682(9), 1.712(10) Å) are consistent with electronic delocalization of the negative charge over the CS_3^{2-} unit, and are similar to those found in the two other reported uranium trithiocarbonate complexes.[10] The bridging thiocyanate is disordered over two positions: one with N bound to U2 and S bound to U1, and one with N bound to U1 and S bound to U2. Only the structure with N1 bound to U2 is shown in Figure 2.

The U–N bonds (U1–N1 2.501(15) Å, U2–N1 2.62(2) Å) are longer than those reported for terminal N-bound U^{IV} thiocyanate complexes (2.385(4) Å).[11] No examples of uranium complexes containing bridging thiocyanate or S-bound thiocyanate ligands were found in the Cambridge Structural Database.

The ^{13}C NMR spectrum of **3** in [D_8]toluene shows a resonance at $\delta = 124.0$ ppm for the bridging NCS^- ligand and one at 195.8 ppm for the bridging CS_3^{2-} ligand. The ^{13}C NMR spectrum of **3** in [D_6]DMSO shows a resonance at 129.3 ppm that was assigned to the NCS^- anion. The presence of two ν(^{13}CN) stretches at 2006 and 2085 cm^{-1} in the IR spectrum of a sample of **3** that was prepared with $^{13}CS_2$ is consistent with the presence of a bridging thiocyanate ligand.[12]

The addition of an equimolar amount of CS_2 to complex **1** led to a mixture of unreacted complex **3** and an additional species (**a**), which was transformed into **3** after addition of a second equivalent of CS_2. The ^{13}C NMR spectrum in [D_6]DMSO of the residue obtained after drying of the reaction mixture allowed us to confirm the presence of the free NCS^- group. This finding suggests that the formation of the trithiocarbonate- and thiocyanate-bridged complex **3** is most likely the result of the reaction of a sulfide- and thiocyanate-bridged intermediate, "Cs{(μ-NCS)(μ-S)[U(OSi(O^{t}Bu)$_3$)$_3$]$_2$}" (**a**), with a second molecule of CS_2. The formation of a trithiocarbonate-bridged diuranium(IV) complex by the nucleophilic addition of a sulfide-bridged diuranium(IV) complex to CS_2 has previously been described by Meyer et al.[10a] Moreover, the formation of sulfide and

thiocyanate species from the nucleophilic addition of CS_2 to a nitride via a dithiocarbamate intermediate has been described for a terminal V^V nitride.[7b]

Rather different reactivity was observed with CO_2. The addition of three equivalents of CO_2 to **1** in toluene at low temperature (below −70 °C) resulted in an immediate color change to yield a blue solution. Storing the solution at −40 °C gave $Cs\{(\mu\text{-}NC_2O_4)[U(OSi(O^tBu)_3)_3]_2\}$ (**4**) in 72% yield (Scheme 3). Complex **4** is stable in toluene solution at room

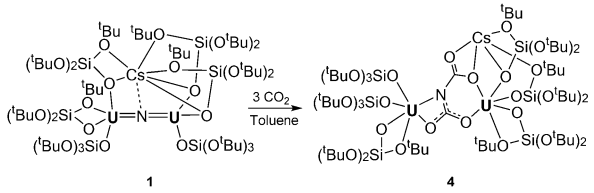

Scheme 3. Reaction of $Cs\{(\mu\text{-}N)[U(OSi(O^tBu)_3)_3]_2\}$ (**1**) with CO_2 to form $Cs\{(\mu\text{-}NC_2O_4)[U(OSi(O^tBu)_3)_3]_2\}$ (**4**).

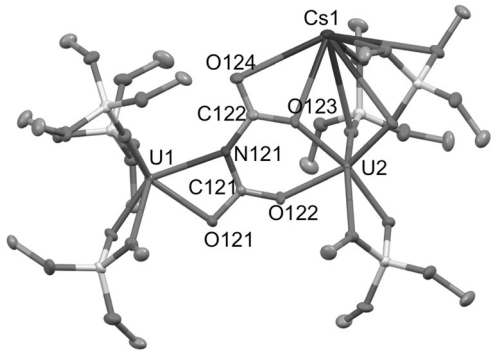

Figure 3. Crystal structure of $Cs\{(\mu\text{-}NC_2O_4)[U(OSi(O^tBu)_3)_3]_2\}$ (**4**). Thermal ellipsoids set at 50% probability. Hydrogen atoms, methyl groups, and solvent molecules were omitted for clarity. Selected bond lengths [Å]: U1–O121 2.360(3), U1–N121 2.467(3), O121–C121 1.292(5), C121–N121 1.347(5), C121–O122 1.282(4), N121–C122 1.396(6), C122–O124 1.229(6), C122–O123 1.317(4), U2–O123 2.252(3), U2–O122 2.283(3), O124–Cs1 3.206(3), O123–Cs1 3.045(3). Torsion angles [°]: O121-C121-N121-C122 178.11, O124-C122-N121-C121 158.03.

temperature for up to two weeks. The solid-state structure of **4** (Figure 3) shows the presence of a unique dicarbamate ligand bridging two $[U(OSi(O^tBu)_3)_3]$ fragments in an asymmetric fashion and a cesium cation. One uranium cation is bound by the nitrogen atom and a carboxylate oxygen atom, while the second uranium cation is bound by two oxygen atoms from two different carbamate units. The $U_2NC_2O_4$ core comprises two fused rings, with one six-membered ring (UOCNCO) and one four-membered ring (UNCO). The two rings share the N–C bond and are arranged in a planar fashion. A carbamate oxygen atom that is not bound to the uranium ion is located above this plane, and it is bound to the Cs cation. The U–N bond length (2.467(3) Å) is longer than those usually found in U^{IV} amide complexes (ca. 2.3 Å)[13] but similar to the U^{IV}–N bond reported for a sterically demanding amide (2.415 Å)[14] and in the range of U–N bond lengths reported for amido-bridged diuranium(IV) complexes (2.4–2.57 Å).[15] The similar values of the O121–C121 and C121–O122 bond lengths (1.292(5) and 1.282(4) Å) are consistent with delocalization of the negative charge. The C122–O124 bond (1.229(6) Å) is shorter than the C122–O123 bond (1.317(4) Å), which suggests a localized C=O bond.

The ^{13}C NMR spectrum of the crude reaction mixture obtained from the reaction of **1** with three equivalents of $^{13}CO_2$ in $[D_8]$toluene only shows one peak at −134.1 ppm, which was assigned to the bridging dicarbamate ligand. This result suggests that complex **4** is the only product formed in this reaction. In contrast, ^1H and ^{13}C NMR studies showed that the addition of smaller amounts of carbon dioxide (1–2 equiv) led to a mixture of **4**, unreacted **1**, and an additional species that cannot be transformed into **4** by the subsequent addition of excess CO_2. X-ray diffraction analysis of crystals obtained from this reaction mixture showed the presence of two co-crystallized complexes, $Cs\{(\mu\text{-}NCO)(\mu\text{-}O)[U(OSi(O^tBu)_3)_3]_2\}$ (**5**; Figure 4) and $Cs_2\{(\mu\text{-}O)_2[U(OSi(O^tBu)_3)_3]_2\}$

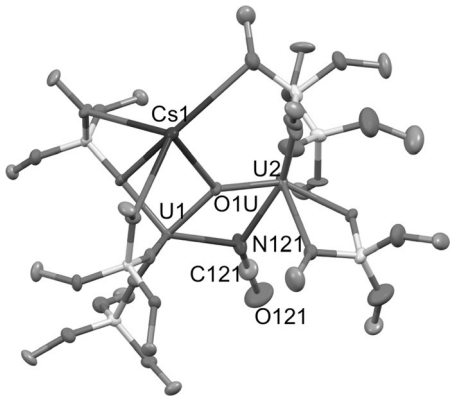

Figure 4. Crystal structure of $Cs\{(\mu\text{-}NCO)(\mu\text{-}O)[U(OSi(O^tBu)_3)_3]_2\}$ (**5**) in $\mathbf{5}\cdot\mathbf{6}_{0.5}$. Thermal ellipsoids set at 50% probability. Hydrogen atoms, methyl groups, and lattice solvent molecules were omitted for clarity. Selected bond lengths [Å] of **5**: U1–N121 2.535(9), U2–N121 2.582(9), U1–O1U 2.118(5), U2–O1U 2.127(5), N121–C121 1.178(2), C121–O121 1.180(2).

(**6**; Figure S27), in a ratio of 1:0.5. The ^{13}C NMR spectrum of these crystals in $[D_6]$DMSO shows the presence of free isocyanate, indicating that NCO^- is released when the crystals are dissolved in DMSO. The structure of **5** shows the presence of two tris(siloxide) U^{IV} moieties that are bridged by an oxo ligand and an N-bound isocyanate. The U–N bonds (2.535(9) and 2.582(9) Å) are longer than those found in terminally bound isocyanates (around 2.3 Å)[11] but similar to those reported for an isocyanatodioxouranate(VI) (2.58(1) Å), in which the cyanate group adopted a similar bridging mode.[16]

The isolation of compound **5** indicates that at substoichiometric ratios of CO_2, the reaction of **1** with CO_2 proceeds with deoxygenation and N–C bond formation to yield the cyanate/oxo complex, which is probably formed via a bridging carbamate intermediate. Analogous reactivity has been reported for a terminal niobium carbamate, which undergoes intramolecular metathesis to afford a terminal oxo complex and free isocyanate, but only after heating at 80 °C.[7c] The

presence of the co-crystallized bis(oxo) complex **6** also suggests that scrambling of the isocyanate and oxo ligands occurs in solution, which is in agreement with the observation of only one peak for this complex in the ^{1}H NMR spectrum of crystals of **5**·**6**$_{0.5}$. In the presence of excess CO_2, the addition of a second equivalent of CO_2 to the monocarbamate intermediate is faster than the isocyanate formation that affords the stable complex **4**.

The formation of a dicarbamate from the reaction of a metal nitride with CO_2 is unprecedented and points to the presence of a highly nucleophilic nitride in complex **1**. Moreover, complexes of the $N(CO_2)_2^{3-}$ ligand have never been reported, which is probably due to the difficulty of preparing the parent triprotic species.[17] Only a few examples of the reactivity of the U–N bond with CO_2 have been previously described. Insertion of CO_2 into U^{III}–N_{amide} or U^{IV}–N_{amide} bonds resulted in the formation of O-bound carbamate complexes of U^{III} or U^{IV} [13c,18] or U^{IV} isocyanate complexes,[19] and the reaction of CO_2 with U^{V} imido complexes led to isocyanate extrusion and formation of a terminal U^{V} oxo complex by multiple metathesis.[18d,20] However, we have herein described the first example of the insertion of CO_2 into a U–$N_{nitride}$ bond. The high reactivity of **1** with electrophiles is in stark contrast to the often inert character of nitride-bridged transition-metal complexes,[21] which require activation of the nitride group for further functionalization,[6] and this result highlights the potential of uranium nitrides in promoting N–C bond-formation reactions. The results presented in this work open up new pathways for the selective synthesis of new organic molecules from metal nitrides and the abundant and inexpensive feedstock CO_2, and demonstrate that nitride functionalization with heteroallenes is readily feasible with uranium. This novel reactivity of uranium nitrides will certainly inspire new approaches to both stoichiometric and catalytic N–C bond-formation reactions.

Acknowledgements

We acknowledge support from the Swiss National Science Foundation and the Ecole Polytechnique Fédérale de Lausanne (EPFL). We thank Euro Solari for carrying out the elemental analyses, Rosario Scopelliti for collecting X-ray data, and Jacques Pécaut for solving the crystal structures.

Keywords: carbon dioxide · carbon disulfide · cyanates · nitrides · uranium

How to cite: *Angew. Chem. Int. Ed.* **2016**, *55*, 4074–4078
Angew. Chem. **2016**, *128*, 4142–4146

[1] a) F. Haber, DE 229126, **1909**; b) A. R. Fox, S. C. Bart, K. Meyer, C. C. Cummins, *Nature* **2008**, *455*, 341–349; c) M. S. Eisen, *Top. Organomet. Chem.* **2010**, *31*, 157–184.

[2] a) G. W. C. Silva, C. B. Yeamans, A. P. Sattelberger, T. Hartmann, G. S. Cerefice, K. R. Czerwinski, *Inorg. Chem.* **2009**, *48*, 10635–10642; b) D. M. King, S. T. Liddle, *Coord. Chem. Rev.* **2014**, *266–267*, 2–15.

[3] a) T. W. Hayton, *Chem. Commun.* **2013**, *49*, 2956–2973; b) W. J. Evans, S. A. Kozimor, J. W. Ziller, *Science* **2005**, *309*, 1835–1838; c) I. Korobkov, S. Gambarotta, G. P. A. Yap, *Angew. Chem. Int. Ed.* **2002**, *41*, 3433–3436; *Angew. Chem.* **2002**, *114*, 3583–3586; d) T. K. Todorova, L. Gagliardi, J. R. Walensky, K. A. Miller, W. J. Evans, *J. Am. Chem. Soc.* **2010**, *132*, 12397–12403; e) G. Nocton, J. Pecaut, M. Mazzanti, *Angew. Chem. Int. Ed.* **2008**, *47*, 3040–3042; *Angew. Chem.* **2008**, *120*, 3082–3084; f) S. Fortier, G. Wu, T. W. Hayton, *J. Am. Chem. Soc.* **2010**, *132*, 6888–6889; g) A. R. Fox, P. L. Arnold, C. C. Cummins, *J. Am. Chem. Soc.* **2010**, *132*, 3250–3251; h) C. Camp, J. Pecaut, M. Mazzanti, *J. Am. Chem. Soc.* **2013**, *135*, 12101–12111; i) L. Maria, I. C. Santos, V. R. Sousa, J. Marcalo, *Inorg. Chem.* **2015**, *54*, 9115–9126; j) R. K. Thomson, T. Cantat, B. L. Scott, D. E. Morris, E. R. Batista, J. L. Kiplinger, *Nat. Chem.* **2010**, *2*, 723–729; k) D. M. King, F. Tuna, E. J. L. McInnes, J. McMaster, W. Lewis, A. J. Blake, S. T. Liddle, *Nat. Chem.* **2013**, *5*, 482–488; l) D. M. King, F. Tuna, E. J. L. McInnes, J. McMaster, W. Lewis, A. J. Blake, S. T. Liddle, *Science* **2012**, *337*, 717–720; m) D. M. King, J. McMaster, F. Tuna, E. J. L. McInnes, W. Lewis, A. J. Blake, S. T. Liddle, *J. Am. Chem. Soc.* **2014**, *136*, 5619–5622; n) P. A. Cleaves, D. M. King, C. E. Kefalidis, L. Maron, F. Tuna, E. J. L. McInnes, J. McMaster, W. Lewis, A. J. Blake, S. T. Liddle, *Angew. Chem. Int. Ed.* **2014**, *53*, 10412–10415; *Angew. Chem.* **2014**, *126*, 10580–10583.

[4] S. D. Roughley, A. M. Jordan, *J. Med. Chem.* **2011**, *54*, 3451–3479.

[5] M. Aresta, A. Dibenedetto, *J. Chem. Soc. Dalton Trans.* **2007**, 2975–2992.

[6] a) S. P. Semproni, P. J. Chirik, *J. Am. Chem. Soc.* **2013**, *135*, 11373–11383; b) S. P. Semproni, P. J. Chirik, *Angew. Chem. Int. Ed.* **2013**, *52*, 12965–12969; *Angew. Chem.* **2013**, *125*, 13203–13207.

[7] a) J. M. Smith, *Prog. Inorg. Chem.* **2014**, *58*, 417–470; b) J. K. Brask, V. Dura-Vila, P. L. Diaconescu, C. C. Cummins, *Chem. Commun.* **2002**, 902–903; c) J. S. Silvia, C. C. Cummins, *J. Am. Chem. Soc.* **2010**, *132*, 2169–2170.

[8] C. Camp, C. E. Kefalidis, J. Pecaut, L. Maron, M. Mazzanti, *Angew. Chem. Int. Ed.* **2013**, *52*, 12646–12650; *Angew. Chem.* **2013**, *125*, 12878–12882.

[9] a) J. G. Brennan, R. A. Andersen, A. Zalkin, *J. Am. Chem. Soc.* **1988**, *110*, 4554–4558; b) J. L. Stewart, R. A. Andersen, *New J. Chem.* **1995**, *19*, 587–595; c) R. C. Schnabel, B. L. Scott, W. H. Smith, C. J. Burns, *J. Organomet. Chem.* **1999**, *591*, 14–23.

[10] a) O. P. Lam, L. Castro, B. Kosog, F. W. Heinemann, L. Maron, K. Meyer, *Inorg. Chem.* **2012**, *51*, 781–783; b) C. Camp, O. Cooper, J. Andrez, J. Pecaut, M. Mazzanti, *J. Chem. Soc. Dalton Trans.* **2015**, *44*, 2650–2656.

[11] C. Camp, N. Settineri, J. Lefevre, A. R. Jupp, J. M. Goicoechea, L. Maron, J. Arnold, *Chem. Sci.* **2015**, *6*, 6379–6384.

[12] M. A. S. Goher, *Collect. Czech. Chem. Commun.* **1977**, *42*, 1478.

[13] a) S. M. Franke, M. W. Rosenzweig, F. W. Heinemann, K. Meyer, *Chem. Sci.* **2015**, *6*, 275–282; b) L. P. Spencer, P. Yang, S. G. Minasian, R. E. Jilek, E. R. Batista, K. S. Boland, J. M. Boncella, S. D. Conradson, D. L. Clark, T. W. Hayton, S. A. Kozimor, R. L. Martin, M. M. MacInnes, A. C. Olson, B. L. Scott, D. K. Shuh, M. P. Wilkerson, *J. Am. Chem. Soc.* **2013**, *135*, 2279–2290; c) J. A. Higgins Frey, G. N. Cloke, S. M. Roe, *Organometallics* **2015**, *34*, 2102–2105.

[14] C. A. P. Goodwin, F. Tuna, E. J. L. McInnes, S. T. Liddle, J. McMaster, I. J. Vitorica-Yrezabal, D. P. Mills, *Chem. Eur. J.* **2014**, *20*, 14579–14583.

[15] a) J. G. Reynolds, A. Zalkin, D. H. Templeton, N. M. Edelstein, *Inorg. Chem.* **1977**, *16*, 599–603; b) J. G. Reynolds, A. Zalkin, D. H. Templeton, N. M. Edelstein, L. K. Templeton, *Inorg. Chem.* **1976**, *15*, 2498–2502.

[16] M. J. Crawford, P. Mayer, H. Noth, M. Suter, *Inorg. Chem.* **2004**, *43*, 6860 – 6862.
[17] R. B. MacMullin, US 43178, **1935**.
[18] a) P. J. Fagan, J. M. Manriquez, S. H. Vollmer, C. S. Day, V. W. Day, T. J. Marks, *J. Am. Chem. Soc.* **1981**, *103*, 2206 – 2220; b) E. M. Matson, P. E. Fanwick, S. C. Bart, *Organometallics* **2011**, *30*, 5753 – 5762; c) A. L. Arduini, J. D. Jamerson, J. Takats, *Inorg. Chem.* **1981**, *20*, 2474 – 2479; d) S. C. Bart, C. Anthon, F. W. Heinemann, E. Bill, N. M. Edelstein, K. Meyer, *J. Am. Chem. Soc.* **2008**, *130*, 12536 – 12546.
[19] C. Camp, L. Chatelain, C. E. Kefalidis, J. Pécaut, L. Maron, M. Mazzanti, *Chem. Commun.* **2015**, *51*, 15454 – 15457.
[20] A.-C. Schmidt, F. W. Heinemann, L. Maron, K. Meyer, *Inorg. Chem.* **2014**, *53*, 13142 – 13153.
[21] B. A. MacKay, M. D. Fryzuk, *Chem. Rev.* **2004**, *104*, 385 – 401.

Received: January 6, 2016
Published online: February 23, 2016

